2007

Gas-liquid mass transfer in an external airlift loop reactor for syngas fermentation

Samuel T. Jones
Iowa State University

Gas-liquid mass transfer in an external airlift loop reactor for syngas fermentation

by

Samuel T. Jones

A dissertation submitted to the graduate faculty

in partial fulfillment of the requirements for the degree of

DOCTOR OF PHILOSOPHY

Co-majors: Mechanical Engineering; Biorenewable Resources and Technology

Program of Study Committee:
Theodore J. Heindel, Major Professor
Robert C. Brown
Gerald M. Colver
Alan A. Dispirito
Jacqueline V. Shanks

Iowa State University

Ames, Iowa

2007

TABLE OF CONTENTS

LIST OF FIGURES

LIST OF TABLES

NOMENCLATURE

Abbreviations

ALR	Airlift loop reactor
BC	Bubble column
BCR	Bubble column reactor
CSTR	Continuous stirred tank reactor
CV	Closed vent
EALR	External airlift loop reactor
OV	Open vent
KCl	Potassium chloride

Roman Symbols

a_L	Gas-liquid interfacial area per unit liquid volume	(cm^{-1})
A	Aerator plate open area ratio	(%)
Abs	Absorption value	(-)
A_d	Downcomer cross-sectional area	(cm^2)
AR	Reactor downcomer to riser cross-sectional area ratio	(-)
A_r	Riser cross-sectional area	(cm^2)
Av	Camera f-stop	(-)
C	Molar concentration	(µM)
C^*	Gas-Liquid interface equilibrium molar concentration	(µM)

C_E	Uncorrected molar concentration from the oxygen electrode	(μM)
C_G	Gas phase molar concentration	(μM)
C_{Gi}	Gas phase interface molar concentration	(μM)
C_L	Liquid phase molar concentration	(μM)
C_{Li}	Liquid phase interface molar concentration	(μM)
C_{Lss}	Steady state liquid phase molar concentration	(μM)
C_o	Steady state concentration at t = 0	(μM)
C_p	Myoglobin concentration	(μM)
ΔC	Molar concentration gradient	(μM)
d_e	Distance between the conductivity electrodes	(cm)
d_m	Oxygen electrode membrane thickness	(mm)
D	Diffusivity	($cm^2\ s^{-1}$)
D_L	Liquid film diffusivity	($cm^2\ s^{-1}$)
D_m	Oxygen electrode membrane diffusivity	($cm^2\ s^{-1}$)
DR	Dilution ratio	(-)
E_D	Eddy diffusivity	
F	Volumetric flow rate	($cm^3\ s^{-1}$)
G_G	Volumetric gas flow rate	($cm^3\ s^{-1}$)
GTR	Molar gas mass transfer rate	(μM s^{-1})
Δh_d	Distance between the manometer ports on the reactor	(cm)
Δh_m	Manometer liquid height change	(cm)

H	Height above the aerator plate	(cm)
H_v	Unaerated liquid height above the aerator plate	(cm)
$\tilde{H}$	Henry's Constant	(-)
J_A	Molar flux	(kmoles cm^{-2} s^{-1})
k	Mass transfer coefficient	(cm s^{-1})
k_G	Gas film mass transfer coefficient	(cm s^{-1})
k_L	Liquid film mass transfer coefficient	(cm s^{-1})
k_La	Overall volumetric mass transfer coefficient based on liquid film	(s^{-1})
K	Conductivity electrode constant	(-)
K_L	Overall mass transfer coefficient based on liquid film	(cm s^{-1})
M	Molarity	(moles L^{-1})
n	Exponent	(-)
ΔP	Pressure gradient	(cm H_2O)
ΔP_o	Liquid hydrostatic head when $U_G = 0$	(cm H_2O)
qX	Microbial gas conversion rate	(kmoles cm^{-3} s^{-1})
s	Surface renewal rate	(s)
SS	Percent of saturated carbon monoxide spectrum	(%)
t	time	(s)
t_c	Circulation time	(s)
t_e	Exposure time	(s)
t_p	Time between the conductivity electrode signal peaks	(s)

Tv	Camera shutter speed	(s)
U_G	Superficial gas velocity	(cm s^{-1})
U_L	Superficial liquid velocity	(cm s^{-1})
U_{Ld}	Downcomer superficial liquid velocity	(cm s^{-1})
U_{Lr}	Riser superficial liquid velocity	(cm s^{-1})
V_L	Interstitial liquid velocity (linear velocity)	(cm s^{-1})
V_{Ld}	Downcomer interstitial liquid velocity (linear velocity)	(cm s^{-1})
V_{Lr}	Riser interstitial liquid velocity (linear velocity)	(cm s^{-1})
Vol_G	Total reactor dispersed gas volume	(cm^3)
Vol_L	Total reactor unaerated liquid volume	(cm^3)
Vol_S	Sample volume in cuvette	(µL)
Vol_T	Total liquid volume in cuvettes	(mL)
x_c	Circulation path length	(cm)
Δx	Film thickness	(cm)

Greek Symbols

ε	Overall gas holdup	(-)
ε_d	Downcomer gas holdup	(-)
ε_m	Protein extinction coefficient	(μM^{-1} cm^{-1})
ε_r	Riser gas holdup	(-)
π	pi	(-)

ρ_G	Gas phase density	(kg cm^{-3})
ρ_L	Liquid phase density	(kg cm^{-3})
τ_d	Oxygen electrode lag time	(s)
τ_d	Reactor gas phase residence time	(s)
τ_e	Oxygen electrode time constant	(s)

ABSTRACT

Converting biomass to useful products through synthesis gas (syngas) fermentation has the potential to replace petroleum based products with biobased ones; however, these process are limited in their application. One of the most significant limiting steps in syngas fermentations is the gas-liquid mass transfer in the bioreactor due to the low solubilities of the major syngas components, CO and H_2. Hence, to explore possible solutions for over coming the gas-liquid mass transfer barrier, a non-traditional external airlift loop reactor is considered. This study evaluates the hydrodynamics and gas-liquid mass transfer rates in an external airlift loop reactor with an area ratio of 1:16 operating under different conditions. Two downcomer configurations are investigated consisting of the downcomer vent open or closed to the atmosphere. Experiments for these two configurations are carried out over a range of superficial gas velocities (U_G) from U_G = 0.5 to 20 cm/s using three aeration plates with open area ratios of 0.66, 0.99 and 2.22%. These results are compared to a bubble column operating under similar conditions. Water quality variations are also investigated over the same range of U_G with the downcomer open to the atmosphere. Experimental results show that the gas holdup in the riser does not vary significantly with a change in the downcomer configuration or bubble column operation, while a considerable variation is observed in the downcomer gas holdup. Gas holdup in both the riser and downcomer are found to increase with increasing superficial gas velocity. Test results also show that the maximum gas holdup for the three aeration plates is similar, but that the gas holdup trends are different. The superficial liquid velocity is found to vary considerably for the two

downcomer configurations. However, for both cases, the superficial liquid velocity is a function of the superficial gas velocity and/or the flow condition in the downcomer. These observed variations are independent of the aerator plate open area ratio. Gas-liquid mass transfer results indicate that mass transfer rates do vary for oxygen and carbon monoxide gas species. Gas-liquid mass transfer rates are observed to increase linearly with U_G in the presence of a surfactant and to increase similarly to riser gas holdup with U_G for deionized water and ionic solutions. The gas-liquid mass transfer rates are relatively unaffected by the reactor configuration. The results also show that the addition of a surfactant or ionic compounds has a significant effect on mass transfer, where the surfactant restricts gas-liquid mass transfer and the ionic compounds enhance gas-liquid mass transfer.

ACKNOWLEDGEMENTS

This material is based upon work supported by the Natural Resources Conservation Service, U.S. Department of Agriculture, under Agreement No. NRCS 68-3475-3-151. Any opinions, findings, conclusions, or recommendations expressed herein are those of the authors and do not necessarily reflect the views of the USDA.

The author acknowledges all the members of his program of study committee, especially Dr. Theodore Heindel for his valuable insight, support, patience, and friendship that have been generously given over the past several years.

The author also wishes to acknowledge Dr. Mark Hargrove and the undergraduate students who have assisted with this project.

Finally, thanks must be given to my wife and family for their love, encouragement, patience, and sacrifice.

CHAPTER 1: INTRODUCTION

1.1 Motivation

Materials and energy derived from biomass offer an alternative to conventional petroleum sources that would support national economic growth, national security, and reduce national dependence on imported petroleum sources. Currently, the popular method for converting biomass to energy, specifically ethanol, is the sugar to ethanol process. Another method that may be used to convert biomass to energy and other useful compounds is the thermochemical process. The thermochemical process relies on gasifying biomass to create synthesis gas (syngas) which is primarily a mixture of gaseous hydrogen, carbon monoxide, and carbon dioxide. Syngas may be converted biologically or chemically to compounds that can be used to displace traditional petroleum based compounds.

The biological approach to converting syngas to useful products relies on using microorganisms to metabolize the carbon monoxide and hydrogen to compounds that can be used as a feedstock for biopolymers. However, because of the very low aqueous solubilities of carbon monoxide and hydrogen, syngas fermentations are limited by the low gas-liquid mass transfer rates. Hence, if the gas-liquid mass transfer road block can be removed, syngas fermentations could become the preferred method for converting biomass to petroleum substitutes.

The use of mechanically agitated reactors in biological applications have been extensively studied over the past several decades and are widely used in some industrial

settings. However, these bioreactors have been found to have mixing characteristics that may adversely affect cell growth [1-6]. Thus, there is great interest in using pneumatically agitated bioreactors for processes such as syngas fermentation. Like mechanically agitated bioreactors, pneumatically agitated bioreactors have been studied over the last several decades; however, these bioreactors have not received as much attention and are not used as extensively in commercial applications. The design of pneumatically agitated bioreactors, unlike their mechanically agitated counter parts, varies widely and, as a result, the hydrodynamic and mass transfer characteristics of these bioreactors are often system dependent, hindering their wide spread implementation. To facilitate their use, a better understanding of reactor hydrodynamics and gas-liquid mass transfer characteristics is needed.

1.2 Objectives

This research will focus on investigating transport phenomena in an external airlift loop reactor related to oxygen and carbon monoxide uptake in liquid media. This will be accomplished by completion of the following objectives:

Objective 1: Review the literature related to transport phenomena in airlift loop reactors to understand hydrodynamic and gas-liquid mass transfer fundamentals for this reactor type.

Objective 2: Measure gas holdup and liquid velocity to explore the hydrodynamics in an external airlift loop reactor with a downcomer to riser area ratio of 1:16.

2a: Study how reactor hydrodynamics vary with volumetric flow rate by altering the operational mode of the external airlift loop reactor.

2b: Assess the affect of aerator plate open area ratio on fluid dynamics for the operating conditions studied in 2a above.

2c: Evaluate the influence of water quality on hydrodynamics for the conditions considered in 2a and 2b above.

Objective 3: Simplify the bioassay method used to quantify dissolved carbon monoxide concentration.

Objective 4: Measure and compare the gas-liquid volumetric mass transfer rates for an external airlift loop reactor using the dynamic gassing out method for oxygen (with a dissolved oxygen electrode) and carbon monoxide (with a bioassay).

4a: Quantify how the gas-liquid volumetric mass transfer rate varies with the operational mode of the external airlift loop reactor.

4b: Determine the affect of aerator plate open area ratio on gas-liquid mass transfer for the operating conditions in 4a above.

4c: Consider the impact of water quality on gas-liquid mass transfer rates by studying and quantify how water quality impacts mass transfer for the conditions studied in 4a and 4b above.

Objective 5: Compare the gas-liquid mass transfer data for oxygen and carbon monoxide and verify methods used to estimate one from the other.

The remainder of this dissertation expands on the above objectives. Chapter 2 reviews airlift loop reactor hydrodynamics, the factors known to affect hydrodynamics, the methods used to measure gas-liquid mass transfer, and the factors known to impact gas-liquid mass transfer with an emphasis being placed on the external airlift loop reactors. Chapter 3 addresses the methods and equipment used to quantify reactor hydrodynamics and gas-liquid mass transfer rates. Chapter 4 presents and discusses selected gas holdup, superficial liquid velocity, and gas-liquid mass transfer results. Chapter 5 briefly summarizes the trends and conclusions presented in Chapter 4 and well as presents some suggestions for future work.

CHAPTER 2: LITERATURE REVIEW

This chapter is composed of four major sections. The first section reviews bioreactor applications and types with a focus on external airlift loop reactors. The second section presents the fundamental terminology related to airlift loop reactors. The third section discusses airlift loop reactor performance. The fourth section reviews methods used to measure gas-liquid mass transfer rates.

2.1 Bioreactors

A reactor in the most general form is simply defined as a vat or tank for chemical reaction. Reactors used in modern industrial settings vary from simple tanks, where two or more chemicals are allowed to react, to more complex systems with agitators, baffles, static mixers, heat coils, cooling jackets, etc. to facilitate the production of a desired product.

The term bioreactor has been coined to describe a special class of reactors used in biological processes. Like reactors, bioreactors vary in shape, size, and complexity depending on the requirements of the application. For example, bioreactors may be as simple as an ensilaging bag used to ferment and store biomass, to as complex as a chemostat used to culture artificial tissues and organs. Regardless of the design and application, most bioreactors fall into one of three general categories: (i) a simple tank reactor, (ii) an agitated tank reactor, and (iii) a flow reactor. The focus of this work deals with the agitated reactor.

2.1.1 Applications

Bioreactors are used in many industrial applications around the world and thus it is not feasible here to discuss all the possible applications. Suffice it to say that these applications vary from simple sugar fermentations to very complex processes that cultivate human tissue. As the world continues to move toward to a bioeconomy, bioreactor applications will continue to increase. Of particular interest in this work is the use of bioreactors to convert biomass to energy and other useful commodities that will eventually replace petroleum based products through a process called syngas fermentation.

2.1.2 Types

While the sparged stirred tank reactor is still the most common industrial reactor, it is not always the best reactor for microbial cultivation [2]. Hence, there is a large array of bioreactors currently in use. Rather than try to describe all the various sparged reactor designs that may exist, only the three basic sparged reactor types will be discussed here: continuous stirred tank, bubble column, and airlift loop reactors (Figure 2.1).

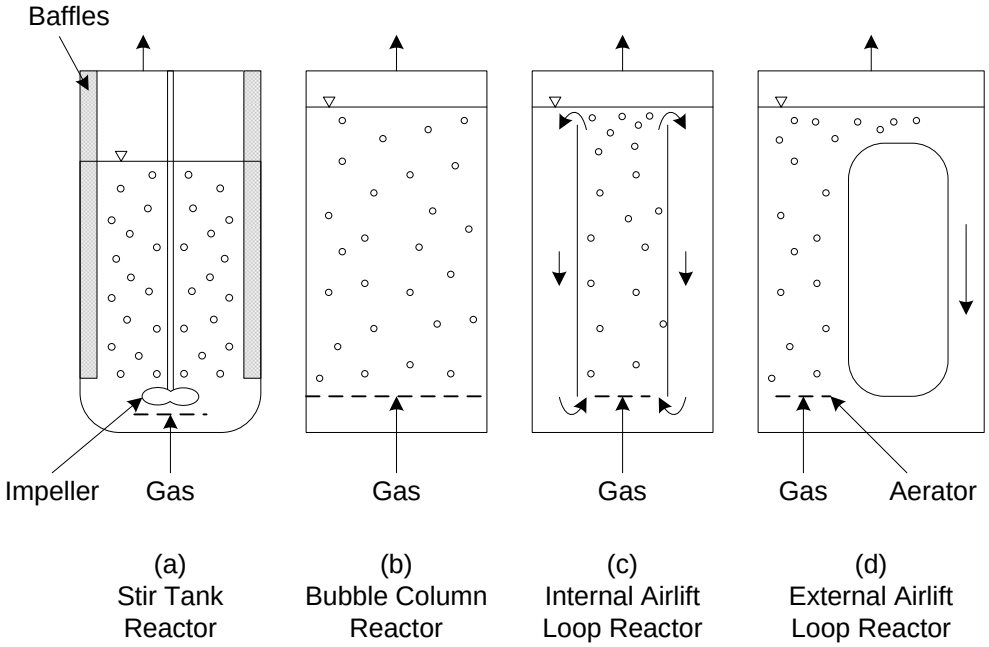

Figure 2.1: Basic sparged reactor types commonly used for industrial and biochemical applications.

2.1.2.1 Continuous Stirred Tank Reactor (CSTR)

The continuous stirred tank reactor (CSTR) is defined as an agitated vessel with the continuous addition and removal of mass and energy [7]. The main virtues of a CSTR are that they are highly flexible, have high overall mass transfer rates, are easily scaled up, and can be treated as ideal systems [4]. Due to these virtues, CSTRs have been widely studied and are commonly used in industrial applications.

A schematic of a CSTR is shown in Figure 2.1a. Most CSTRs are cylindrical with a height to diameter ratio greater than or equal to 2:1 [4, 5]. Although some CSTRs do have multiple agitators to enhance mixing, the typical CSTR is equipped with a single mechanical agitator located near the bottom of the reactor. To prevent solid body rotation of the contents

in the reactor, CSTRs are fitted with baffles. A gas sparger is placed below the impeller for aeration. Sparger design in CSTRs is usually not considered critical as long as the sparger diameter is less than the impeller diameter as the agitator speed largely determines gas bubble size and dispersion. Some CSTRs are also fitted with either cooling coils or a heating jacket for temperature sensitive processes.

While CSTRs are widely used, they do have intrinsic limitations that make them unsuitable for many microbial applications. First, sparger flooding limits the gas throughput. Second, the degree of agitation required to provide sufficient gas-liquid mass transfer for microbial growth may cause damage to the microorganisms passing through the high shear impeller zone [2]. Third, the mechanical energy needed to achieve the desired mixing and mass transfer rate is high, resulting in low power efficiencies as well as the need for a heat sink to remove heat due to mechanical energy dissipation [2, 8]. Fourth, the sterility of the CSTR is hard to maintain over long periods due to the complex mechanical seals needed for the impeller shaft. Fifth, the aeration zone is confined to the impeller region when the media is highly viscous, which is commonly encountered in microbial fermentations [2, 8]. Finally, due the complexity of CSTRs, they are more expensive and less robust than bubble columns and airlift loop reactors. Due to these shortcomings, much attention has been on and continues to be given to, finding more suitable bioreactor designs.

2.1.2.2 Bubble Column Reactor (BCR)

The bubble column reactor (BCR) in its simplest form is a vertical column that is pneumatically agitated. Pneumatic agitation produces ascending bubbles that cause random mixing within the BCR. The degree of mixing and the resulting fluid flow regime encountered in a BCR are mainly determined by pneumatic sparging and only slightly affected by reactor design. BCR designs vary greatly in shape, height, diameter, and sparger configuration. BCRs may also be fitted with internals to alter mixing and mass transfer rates. The main advantages associated with BCRs are that they are suitable for low viscosity media, are energy efficient, may provide a low shear mixing environment, and do not have a mechanical agitator. Due to their simple design and low cost, BCRs are widely used in the chemical industry.

Figure 2.1b shows a simple schematic of a BCR. Most BCRs are cylindrical in shape and built with a height to diameter ratio greater than 2:1; however, square and other unusual shaped BCRs do exist [4]. Typically, BCRs have a single sparger located near the bottom of the reactor. Exact sparger design may vary from a single orifice to a series of equally space orifices to a porous plate depending on the application. Some specific applications also employ the use of internal diffusers to aide in the reduction of bubble coalescence.

Even though BCRs are simple and inexpensive to build, their application in microbial fermentations is limited. First, due to their lack of flexibility, BCR design is application specific and only works over a narrow range of gas flow rates because of bubble coalescence and broth foaming problems [8]. Second, BCRs may have recirculation zones that provide

inadequate mass transfer to sustain microbial growth and result in microbial activity reduction or death [2]. Third, the narrow range of possible gas flow rates limit BCR mixing and mass transfer rates. Consequently, during the last several decades, much attention has been given to BCR modifications [3]. One such modification is the airlift loop reactor.

2.1.2.3 Airlift Loop Reactor (ALR)

The airlift loop reactor (ALR) is a modified BCR that covers a wide range of pneumatic contacting devices characterized by a defined fluid circulation path within the ALR [6, 9-11]. Like BCRs, ALRs are pneumatically agitated by compressed gas and have numerous designs. Unlike BCRs, the major liquid flow patterns in ALRs are defined by the reactor design. Typically, ALRs consist of a fluid pool divided into two individual zones, one of which is sparged by gas, resulting in gassed and ungassed zones that have different bulk densities [2]. This difference in bulk density causes the fluid circulation pattern typical of ALRs. The main advantages of ALRs over BCR are improved mixing, higher mass transfer rates (in some instances), a broader range of gas flow rates, a defined fluid flow pattern, and the ability to handle more viscous fluids.

ALRs are divided into two major classes based upon their structure: (1) the internal ALR (Figure 2.1c); and (2) the external ALR (Figure 2.1d) [2, 4, 6, 8, 12]. The internal ALR resembles a BCR with the addition of a draught tube or a baffle. The external ALR (Figure 2.1d), on the other hand, consists of two pipes connected at the top and bottom to form a loop. The design for both types of ALRs can be further modified allowing for variations in

liquid flow, mixing, mass transfer rates, bubble coalescence, and bubble disengagement. Some of the geometric modifications are schematically shown in Figure 2.2.

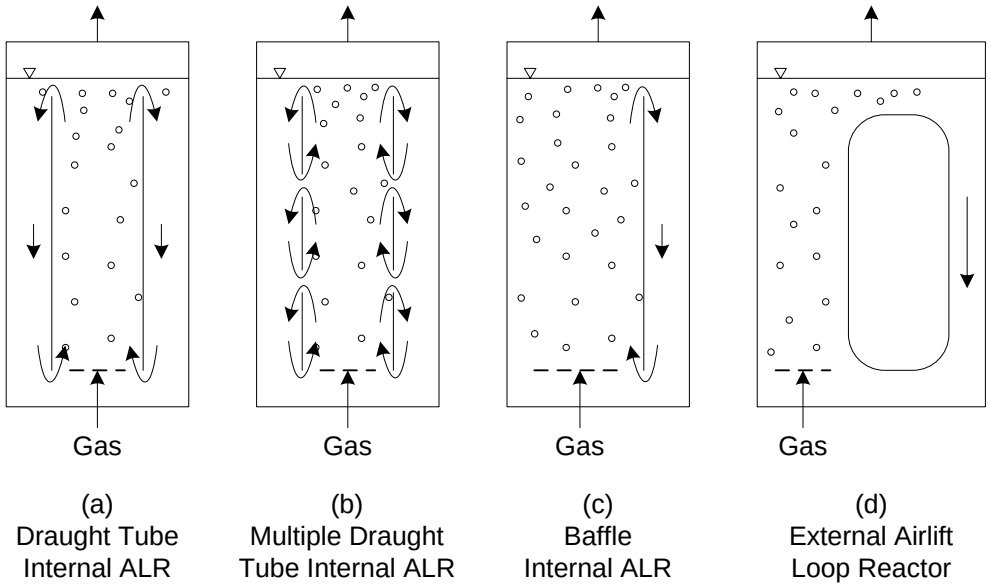

Figure 2.2: Internal and external loop reactor configurations common encountered in the literature.

Weiland and Onken [9] indicated that of the ALRs shown in Figure 2.2, the external loop reactors and the internal loop reactors with concentric draft tubes were most often used for single cell protein production. While the remaining internal loop split shaft and thin channel reactors were often used for wastewater treatment.

ALRs offer several advantages over conventional bioreactors [13]. First, the ALR design is simple (similar to a BCR) and has no moving mechanical parts. Second, the energy required for agitation enters the system with the gas. Third, the shear stresses imposed by turbulent mixing are low, which is important for cells that are shear sensitive. Fourth, scale up from pilot-plant data is relatively simple.

Regardless of the basic configuration, all ALRs are comprised of four distinct sections (Figure 2.3) [2, 6, 14, 15]:

Riser: The riser is the main component of the ALR and is the section that defines the overall mixing and gas-liquid mass transfer rates of the ALR. The gas sparger is usually located at the bottom of this section, and the flow of gas, liquid, and solids (if present) is predominantly an upward co-current multiphase flow. This section has the lowest fluid bulk density and is where most of the gas-liquid mass transfer takes place.

Downcomer: The downcomer section runs parallel to the riser and is connected to it at both the top and bottom. The fluid bulk density in the downcomer is higher than the bulk density in the riser. Flow in the downcomer is in the opposite direction of the riser flow; a result of the density difference that exists between these sections. The gas holdup (volumetric gas fraction) in this section is related to the riser gas holdup and is mostly a function of the ALR design.

Base: The base is the section that connects the bottom of the riser to the downcomer and in most cases contains the sparger. Most ALR designs employ a very simple connection zone between the riser and downcomer where the primary goal is promoting fluid circulation. The gas sparger is typically located in the base, either just below the lower connector as a plate sparger of some type, or just above the lower connector as a single orifice nozzle, a multiple orifice ring sparger, or a multiple orifice spider sparger. Little attention has been given to how the design of the base affects the overall reactor behavior in the literature. Most consider the base design to be of little influence on ALR

performance; however, some of the more recent work indicate this philosophy may be flawed [6].

Gas Separator: The gas separator section connects the top of the riser to the downcomer and allows for liquid circulation and gas disengagement. Fluid residence time in the gas separator varies with gas separator design and influences the gas holdup in both the downcomer and riser. The gas separator design has been widely studied and is considered one of the key ALR components [14].

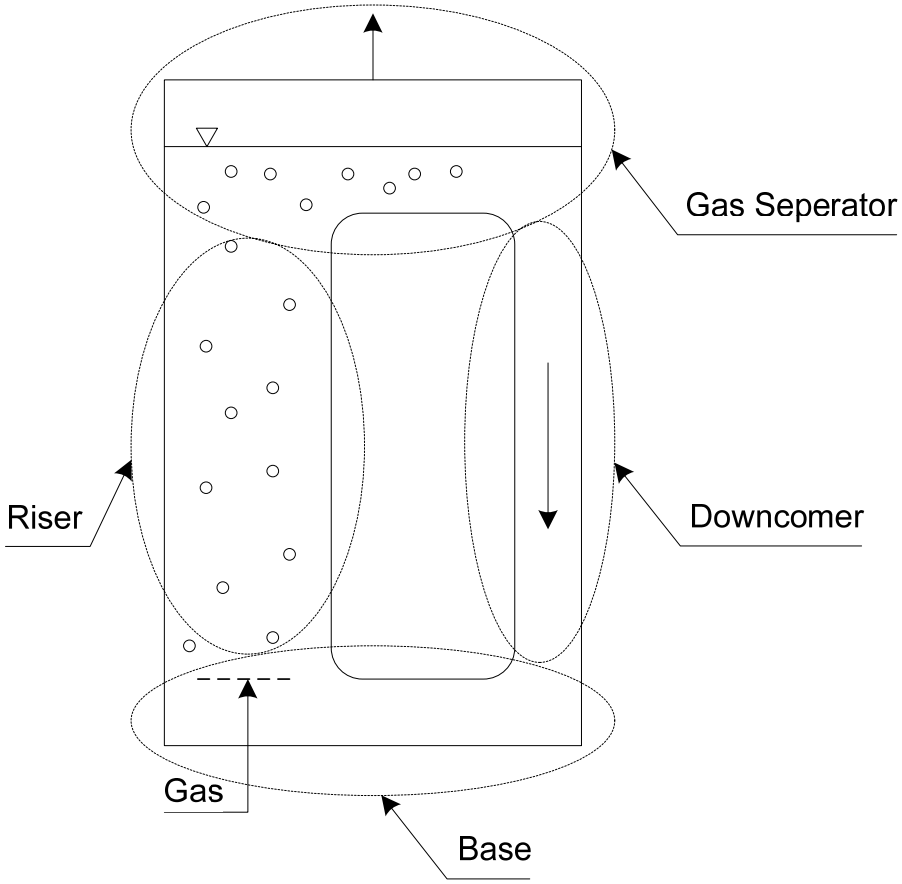

Figure 2.3: External airlift loop reactor schematic showing the four basic reactor sections.

Although ALRs are thought to be an improvement over BCRs, they still have limitations. First, the ALR, like the BCR, is not suitable for highly viscous fluids. Second, all ALRs have a minimum volume that must be maintained to ensure consistent fluid circulation within the reactor. Third, ALR design is usually reactor and application specific, limiting individual ALR usefulness to processes with minimal changes in the operating parameters because after the initial geometric parameters are set at design time, the gas velocity is the only remaining adjustable parameter [15].

ALRs do offer several advantages over CSTRs and BCRs, [2, 4, 5]. First, when compared to CSTRs, their simple construction is a distinct advantage. Since there are usually no moving mechanical parts, these reactors have no need for seals and bearings, thus reducing the danger of contamination. Second, the dual functioning injection gas provides both aeration and agitation, promoting energy efficiency. Third, when compared to BCRs, ALRs have the advantage of having a fixed circulation path which provides an increased capacity for heat and mass transfer and longer gas-liquid contact times. Fourth, the ALR is superior to BCRs and CSTRs as it provides a lower shear stress environment due to the directionality of the liquid flow. Fifth, depending on the geometric configuration, the ALR may allow for much higher gas throughputs when compared to BCRs and CSTRs.

2.1.3 Selection

All three bioreactor types have been successfully used for a variety of applications. To help in reactor selection for a particular application, the following rules of thumb have

been suggested to assist in the selection of the appropriate bioreactor and are based on specific reactor advantages and disadvantages [4]:

- For media with a viscosity greater than 0.1 $N \cdot s \cdot m^{-2}$, a CSTR is recommended.
- A CSTR is recommended in pilot plant operations that require flexibility in viscosity and mass transfer rates because BCRs and ALRs do not offer enough operational flexibility.
- For large scale (50-500 m^3) low viscosity fermentations, BCRs are recommended because they are the cheapest to build and operate.
- For *very* large scale (200-10,000 m^3) low viscosity fermentations, ALRs are recommended because they permit local and controlled substrate addition.
- For shear-sensitive cultures of low viscosity, BCRs or ALRs are recommended as pneumatic agitation can provide the low fluid shear.
- For large scale (>500 m^3) high viscosity fermentations, it was indicated that there are no good reactors because CSTRs have mechanical problems at this size and pneumatically agitated reactors do not function properly with highly viscous media.

The discussion presented hereafter will focus on using an ALR for syngas fermentation. The decision to select an ALR for this work was not based solely upon the above listed criteria, but more so with the intent to understand the baseline mixing and mass transfer rates associated with this particular ALR and to identify characteristic mixing and mass transfer rate properties for future enhancement work.

2.2 Airlift Reactor Fundamentals

The analysis and description of the hydrodynamic and gas-liquid mass transfer behavior for ALRs usually involve the use of parameters such as gas velocity, gas holdup, superficial liquid velocity, and mixing [16]. These parameters were reported by Weiland [17] to be determined by complex interactions between buoyancy, inertia, friction, and hydrostatic pressure. Due to the large degree of interaction between these parameters, the definition of ALR behavior is often quite complex. Chisti and Moo-Young [18] described the hydrodynamics of multiphase systems as being the controlling influence on heat and mass transfer, and thus, a thorough understanding of how these parameters affect ALR operation is a necessity. This section will address the definition of these and other parameters as they relate to ALRs.

2.2.1 Superficial Gas Velocity

Superficial gas velocity (U_G) as defined in the literature is dependent upon the cross sectional area of the riser and the volumetric inlet gas flow rate according to:

$$U_G = \frac{G_G}{A_r} \tag{2.1}$$

where G_G is the volumetric gas flow rate and A_r is the riser cross sectional area. However, other definitions of U_G are used when comparing U_G for internal ALRs and BCRs where A_r may be replaced with the overall reactor cross sectional area.

2.2.2 Gas Holdup

The volumetric gas fraction in a multiphase dispersion is known as gas holdup or gas void fraction [2, 5, 19]. The overall gas holdup (ε) is given by:

$$\varepsilon = \frac{Vol_G}{Vol_G + Vol_L} \tag{2.2}$$

where Vol_G is the gas dispersion volume and Vol_L is the liquid/slurry volume. Individual riser and downcomer gas holdups, ε_r and ε_d, respectively, are commonly reported and can be algebraically related to the overall gas holdup via [2]:

$$\varepsilon = \frac{A_r \cdot \varepsilon_r + A_d \cdot \varepsilon_d}{A_r + A_d} \tag{2.3}$$

where A_d is the downcomer cross sectional area.

The importance of gas holdup is multifaceted. Gas holdup determines the gas phase residence time in the liquid phase, and in conjunction with bubble size, it helps determine the gas-liquid mass transfer rate [1, 13]. Gas holdup is also important as the total reactor volume must be large enough to accommodate the aerated liquid volume for the range of desired operating conditions [18]. Though mainly dependant upon fluid properties and gas velocity. Gas holdup has a very complex relationship with superficial liquid velocity in ALRs, were the two are often functions of one another.

Onken and Weiland [10] showed that gas holdup was strongly dependent on superficial liquid velocity. When the superficial liquid velocity was low, as in a BCR, gas holdup values were observed to be the highest. When the superficial liquid velocity increased, gas holdup decreased. They attributed the decrease in gas holdup to an

acceleration of the gas phase by the moving liquid phase. Gavrilescu and Tudose [11], Bello et al. [20], Russell [16], Choi and Lee [21], and Merchuk [22], as well as many others, reported a similar effect of superficial liquid velocity on gas holdup. Wang et al. [23] demonstrated that the relationship between gas holdup and superficial liquid velocity exists regardless of reactor size, where they compared a mini ALR (~16 mL) to large-scale ALRs (6.5 to 60 L).

Bello et al. [24] in a comparison of similar sized internal and external ALRs and a BCR, discussed how gas holdup varied between the three. It was observed that the riser gas holdup for the BCR and internal the ALR were very similar, but the gas holdup for external ALR was significantly lower and depended upon the reactor downcomer to riser area ratio. The downcomer gas holdup for the internal and external ALRs was significantly different, ranging between 0 to 50% and 80 to 95% of the riser gas holdup, respectively. The large difference in gas holdup was attributed to geometric variations.

Changes in fluid properties, such as viscosity, surface tension and ionic strength were reported to have a slight effect on gas holdup [2]. Note, however, that Gavrilescu and Tudose [11] indicated that liquid property variations had a stronger influence on gas holdup in smaller systems.

2.2.3 Slip Velocity

The gas bubble velocity relative to the liquid velocity through which it is moving is called the slip velocity. The slip velocity is one of the main parameters that determine the

gas volume in the system. However, the slip velocity is seldom discussed in the literature in regard to ALRs; instead, more attention is given to the superficial liquid velocity and gas holdup, which are functions of the slip velocity.

2.2.4 Mixing Time

Mixing time is defined as the time required to achieve a specified quality of mixing after the addition of some feed [13, 25]. An understanding of this parameter is very important in fermentation processes as there is a risk that cell damage may occur if local additive concentrations exceed permissible levels. In continuous reactors the mixing time is commonly expressed as the residence time and used extensively as a key parameter in ALR modeling.

2.2.5 Superficial Liquid Velocity

The liquid circulation in an ALR for a given reactor geometry, fluid type, and superficial gas velocity is determined by the difference in riser and downcomer gas holdup. The difference in riser and downcomer gas holdup creates a hydrostatic pressure difference between the bottom of the riser and the bottom of the downcomer, which in turn acts as the driving force for liquid circulation. A mean circulation velocity U_{Lc} is defined as [1]:

$$U_{Lc} = \frac{x_c}{t_c} \tag{2.4}$$

where x_c is the circulation path length and t_c is the average circulation time for one complete circulation.

However, liquid circulation is not commonly used as a characteristic parameter for gas-liquid contactors. The superficial liquid velocity in the riser (U_{Lr}) or downcomer (U_{Ld}) are more commonly used as they are more meaningful and allow for direct comparison of liquid circulation rates in vessels of varying sizes. The superficial liquid velocity is different from the true linear velocity because the liquid flow occupies only a portion of the flow channel. The riser and downcomer linear velocity (V_L) and superficial velocity (U_L) are related as follows [2]:

$$V_{Lr} = \frac{U_{Lr}}{1-\varepsilon_r} \tag{2.5}$$

and

$$V_{Ld} = \frac{U_{Ld}}{1-\varepsilon_d} \tag{2.6}$$

While the superficial liquid velocity is a function of riser and downcomer gas holdup, it also influences these holdups. In order to change the superficial liquid velocity in an ALR, the geometry of the reactor must be altered or the gas velocity must be changed. In some cases, a throttling device may be installed somewhere in the reactor loop to regulate the superficial liquid velocity, independent of the superficial gas velocity [26].

The superficial liquid velocity has been shown to be a distinct function of the superficial gas velocity [27]. In addition, it has been shown that the superficial liquid velocity rate of growth with superficial gas velocity was very rapid at low superficial gas velocities, but eventually the superficial liquid velocity reached an asymptotic value. The

relationship between these two velocities is affected by the area ratio, where smaller downcomer areas cause the asymptotic value to be reached at a lower superficial gas velocity. This suggests that the airlift effect is significantly reduced as the downcomer area is reduced.

From an operational stand point, the superficial liquid velocity is what sets an ALR apart from a BCR. For example, BCRs typically have only a low fixed local superficial liquid velocity as shown in Figure 2.4, while ALRs may have an overall superficial liquid velocity over an order of magnitude higher. In fact, if the superficial liquid velocity becomes too high, it may adversely affect overall mass transfer rates as gas residence times become too short [14, 28]. The superficial liquid velocity has been shown to influence most of the other hydrodynamic and mass transfer parameters, including the mean gas phase residence time, bubble size, overall mass transfer rates, and mixing time [25]. Accordingly, the superficial liquid velocity is reported as one of the key parameters in ALR design and scale-up [13].

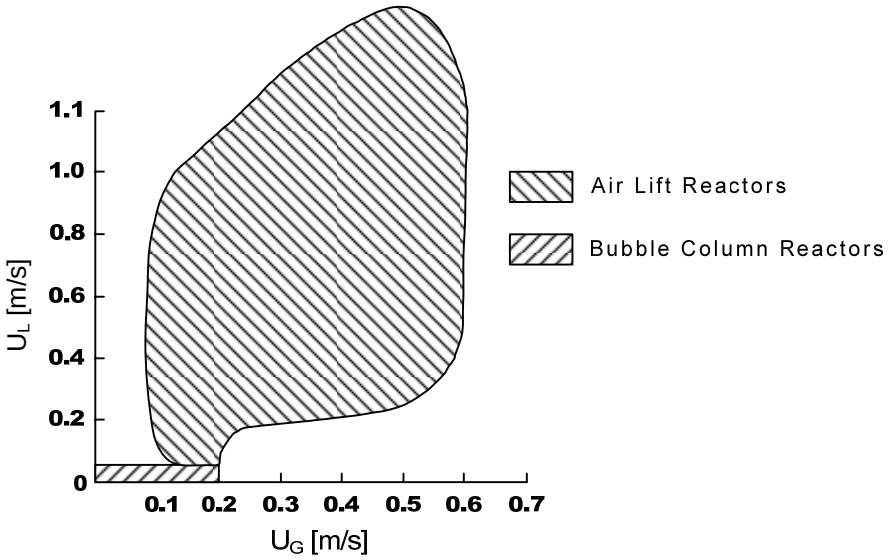

Figure 2.4: Possible operating conditions for BCRs and ALRs, adopted from Merchuk [22].

2.2.6 Flow Regimes

The multiphase flow hydrodynamics in gas-liquid contactors have a controlling influence on both the interphase and bulk transport phenomena. Typically, the hydrodynamics in ALRs are characterized by four flow regimes identified in Figure 2.5 [3, 18, 29, 30]:

Homogeneous (Bubbly) flow: At low gas inputs, gas bubbles rise nearly vertically with little interaction. This is known as the unhindered bubble, homogeneous, or bubbly flow regime. This regime is also characterized by a nearly uniform radial distribution of equally size bubbles [30].

Transitional flow: As the gas flow increases, bubbles begin to interact and may eventually coalesce. This forms the transitional flow regime that bridges the homogeneous and turbulent flow regimes.

Heterogeneous (Turbulent) flow: Heterogeneous flow occurs when bubble-bubble interactions become common, leading to large bubble formation. Large bubble formation in this flow regime is typically very random in which bubble size varies widely. This regime is also known as the turbulent or churn-turbulent flow regime.

Slug flow: Slug flow, an extreme heterogeneous flow regime condition, occurs at very high gas velocities with large bubble formation. The size and frequency of the large bubbles in this regime increase with gas flow. The large bubbles may have diameters approaching the tube diameter in small diameter columns.

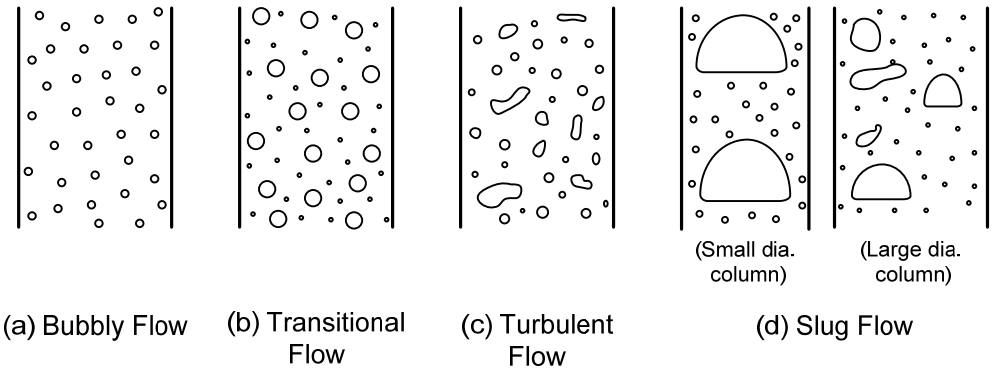

Figure 2.5: Typical hydrodynamic flow regime encountered in ALRs, adopted from Chisti and Moo-Young [18].

The volumetric gas flow rate range for a particular flow regime largely depends upon the reactor riser diameter, area ratio, effective reactor height, sparger design, superficial liquid velocity, and fluid properties [3, 18]. Identification of these flow regimes is very important for biological applications, as it is most desirable to operate in the homogeneous condition to prevent regions of high shear, which can be detrimental in some biological fermentations [31]. Also, from a gas-liquid mass transfer stand point, is it desirable to

operate in the homogeneous and transitional flow regimes to prevent slugging, where large bubbles reduce gas-liquid contact time and contact area, creating a poor gas-liquid mass transfer environment.

2.2.7 Area Ratio

One of several defining characteristics for ALRs is the ratio of riser and downcomer cross sectional areas. The area ratio for a specific ALR is typically defined as follows:

$$AR = \frac{A_d}{A_r} = \frac{\text{Downcomer Cross Sectional Area}}{\text{Riser Cross Sectional Area}} \tag{2.7}$$

The area ratio (AR) is significant for many reasons. AR is used as a key dimensionless parameter for ALR comparison and scale-up. It is also used for modeling purposes to predict gas holdup, superficial liquid velocity, and mass transfer, as well as being used in calculations to relate superficial liquid velocity and gas holdup in the riser and downcomer.

2.2.8 Overall Gas-Liquid Mass Transfer Coefficient

The transfer of gas from the gas phase to a microorganism suspended in a multiphase medium must take place along a certain pathway. Figure 2.6 schematically describes the general transport route. As shown in Figure 2.6, eight resistances to gas mass transfer may exist [32]:

(1) in the gas film inside the bubble

(2) at the gas-liquid interface

(3) in the liquid film at the gas-liquid interface

(4) in the bulk liquid

(5) in the liquid film surrounding the cell

(6) at the liquid-cell interface

(7) the internal resistance

(8) at the site of the biochemical reaction

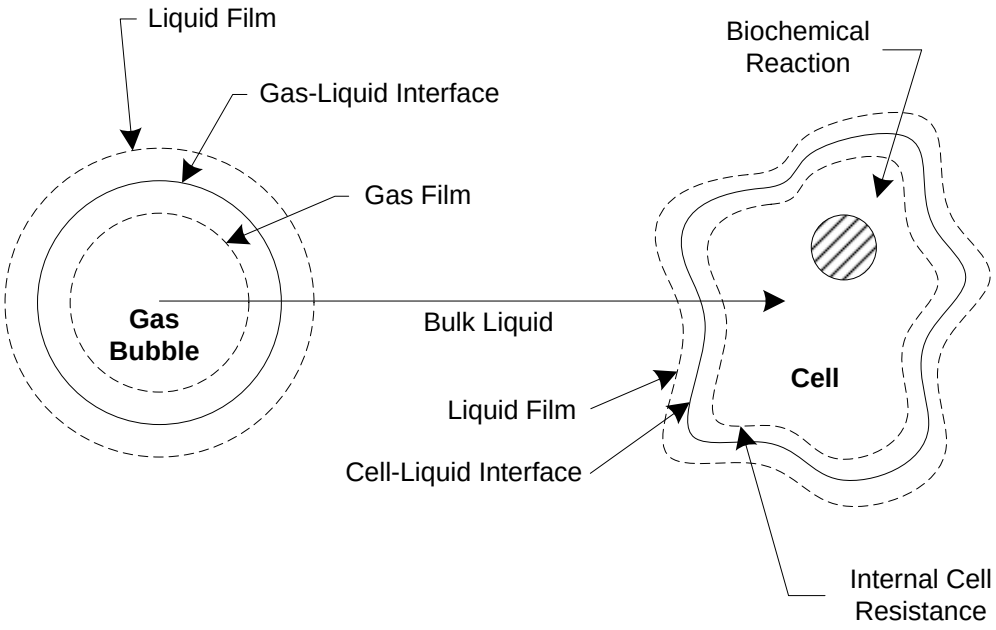

Figure 2.6: Mass transfer resistances encountered in gas-liquid dispersions containing active cells, adapted from Chisti [2].

It should be noted that all resistances are purely physical except for the last one and that not all mass transfer resistances may be significant for a given system. Many of the resistances may be neglected in most bioreactors except for those around the gas-liquid

interface [2, 32]. Thus, the transport problem is greatly simplified to a gas-liquid interfacial mass transfer problem.

To further simplify the transport problem, the two-film theory developed in 1923 by Whitman is commonly used as a starting point for understanding mass transfer across a phase boundary [2, 33-35]. According to the two-film model, the mass transfer resistance across the gas-liquid interface can be characterized by two thin films, one for each of the phases in contact with the interface, which itself is assumed to offer no resistance to mass transfer. Fluid motion in each of the thin films is assumed stagnant, which, if true, means that transport in the films occurs solely by molecular diffusion. Thus, at steady state, a linear concentration gradient exists allowing the molar flux (J_A), to be related to the molar concentration gradient (ΔC), in the respective film and the film thickness (Δx), using Fick's First Law:

$$J_A = \frac{D}{\Delta x}\Delta C \tag{2.8}$$

where D is the molecular diffusion in the film. The ratio of $D/\Delta x$ is known as the overall mass transfer coefficient, k.

Equation (2.8) may be rewritten for the gas and liquid films as follows:

$$J_A = k_G\left(C_G - C_{Gi}\right) \tag{2.9}$$

$$= k_L\left(C_{Li} - C_L\right) \tag{2.10}$$

where k_G and k_L are the gas and liquid film mass transfer coefficients, respectively, and C_G, C_{Gi}, C_{Li}, and C_L are the molar concentrations in the gas phase, gas phase interface, liquid

phase interface, and the liquid phase concentrations, respectively. This pair of equations can be further reduced as the interfacial concentrations are assumed to be in equilibrium. The resulting mass flux equation may be expressed in terms of the overall concentration driving force as follows:

$$J_A = K_L\left(C^* - C_L\right) \tag{2.11}$$

where K_L is the overall mass transfer coefficient based on the liquid film and C^* is the equilibrium gas concentration in the liquid. C^* is related to C_G using Henry's law [36]:

$$C_G = \tilde{H}C^* \tag{2.12}$$

where $\tilde{H}$ is Henry's constant. It can also be shown that [2]

$$\frac{1}{K_L} = \frac{1}{k_L} + \frac{1}{\tilde{H}k_G} \tag{2.13}$$

Equation (2.13) may be further reduced as well. For sparingly soluble gases such as oxygen, carbon monoxide, and hydrogen, $\tilde{H}$ is much greater than unity. Furthermore, k_G is typically much greater than k_L [2] and the gas film thickness is much smaller than the liquid film thickness. For these conditions, the second term on the right of Equation (2.13) becomes negligible leaving:

$$\frac{1}{K_L} \approx \frac{1}{k_L} \tag{2.14}$$

This implies that nearly all the resistance to mass transfer for a sparingly soluble gas occurs in the liquid side film at the gas-liquid interface. In other words, mass transfer is liquid-film controlled.

For gas-liquid systems, the assumption that mass transfer in the liquid film is only by diffusion is not always representative of actual conditions because turbulent eddies can penetrate this film. Additionally, the assumption that mass transfer is constant with time may not be applicable to gas-liquid systems involving transient conditions. Thus, other mass transfer models may be more appropriate for mobile gas-liquid interfaces. These include the penetration theory developed by Higbie, the surface renewal and random surface renewal theories of Danckwarts, the film-penetration theory of Toore and Marchello, and boundary layer theory [2, 33-35]. Detailed reviews of these theories may be found in texts detailing mass transfer across a phase boundary [33-35]. All of these models can be used to relate transport flux to a concentration difference and an overall mass transfer coefficient. The liquid side mass transfer coefficient can be estimated using each of the models as follows:

$$k_L = \frac{D_L}{\Delta x} \qquad \text{(two-film theory)} \qquad (2.15)$$

$$k_L = \sqrt{\frac{4D_L}{\pi t_e}} \qquad \text{(penetration theory)} \qquad (2.16)$$

$$k_L = \sqrt{D_L s} \qquad \text{(surface renewal theory)} \qquad (2.17)$$

$$k_L = \sqrt{\frac{D_L}{\pi t_e}}\left(1 + 2\sum_{i=1}^{i=\infty} e^{-\left(i^2 L^2\right)/(D_L t_e)}\right) \qquad \text{(film-penetration theory)} \qquad (2.18)$$

$$k_L \approx (D_L + E_D) \qquad \text{(boundary layer theory)} \qquad (2.19)$$

In bioreactors the fluid properties and operating temperature more or less fix the gas diffusivity through a liquid (D_L). Hence any change to k_L must be accomplished by changing the liquid film thickness (Δx), the exposure time (t_e), the surface renewal rate (s), or the eddy

diffusivity (E_D), all of which are functions of the reactor hydrodynamics. However, the direct calculation of k_L using Equations (2.15) - (2.19) is nearly impossible due to the inability to accurately quantify film thickness, exposure time, surface renewal rates, and eddy diffusivity in a bioreactor. Although k_L may not be directly calculated using one of the above equations, it is generally proportional to $(D_L)^m$ where m may vary from ½ to 1 depending on the mechanism of mass transfer that dominates for the given physical and hydrodynamic conditions [2, 33-35].

The mass transfer rate and molar flux are related by:

$$\frac{dC_L}{dt} = a_L J_A \tag{2.20}$$

where a_L is the interfacial area per unit liquid volume. By combining Equations (2.11), (2.14), and (2.20), the gas-liquid mass transfer rate may be written as:

$$\frac{dC_L}{dt} = k_L a_L \left(C^* - C_L\right) \tag{2.21}$$

In practice, a_L = a and $k_L a_L$ is lumped together to form as a single term ($k_L a$) due to the complexities involved in calculating either term individually. The overall volumetric mass transfer coefficient ($k_L a$) is typically determined experimentally using Equation (2.21) and gas concentration verses time data for a given bioreactor. A discussion of the methods used to experimentally measure gas concentration with respect to time for transient conditions is presented later in Section 2.4.1.

Once an experimental value for $k_L a$ has been determined for a specific gas in a gas-liquid contactor, it may be used to determine the $k_L a$ for another gas species in a similar

system. The estimation of k_La for a gas species based upon data for another gas species must be done using the proper transformation techniques based upon the best available mass transfer theory for a given system. The equation used to transform k_La from species *A* to species *B* is [2, 33]:

$$(k_La)_B = (k_La)_A \left(\frac{D_{LB}}{D_{LA}} \right)^n \tag{2.22}$$

where n ranges from ½ to 1 depending on the mass transfer theory used. Typically, for the two-film theory n = 1, for the penetration, surface renewal, and film-penetration theories n = ½, and for the boundary layer theory n = ⅔. In applying this transformation, care must be taken to ensure that all factors such as fluid type, temperature, flow rate, location, depth, pressure, and so on remain constant for species B if the transformation is to be even remotely accurate. Note that Equation (2.22) is based upon theoretical relationships that may or may not represent the system under consideration. In fact, the use of Equation (2.22) has been observed to lead to large discrepancies [2]. Finally, the k_La as shown in Equation (2.21) is a scalar and should therefore be independent of the direction of the concentration driving force, meaning that k_La for desorption and adsorption should be equal for similar conditions.

2.3 Airlift Reactor Performance

Investigators have reported that the performance of ALRs depend on geometric parameters as well as operational conditions [21, 26, 37]. Siegel and Robinson [15] suggested that geometric factors such as reactor height, aspect ratio, downcomer to riser area

ratio, base diameter, and gas separator define ALR operation and influence pressure drop around the reactor loop. Likewise, Bentifraouine et al. [38, 39] identified seven similar parameters that when changed, modify ALR performance: (i) the gas and liquid physical properties, (ii) the downcomer to riser area ratio, (iii) the top and bottom horizontal connector geometries, (iv) the gas separator design, (v) the non-aerated liquid height, (vi) the reactor height, and (vii) the gas sparger design. As all of these parameters have been found to affect ALR operation in some fashion, they will be discussed in one of the following sections on height, area ratio, gas separator, gas sparger, internals, and fluid property effects.

2.3.1 Height

When considering ALR height effects, two heights are usually considered. The first is the effective reactor height which refers to the distance from the base to the gas separator. The second is the unaerated liquid height in the reactor which refers to the distance from the base to the top of the liquid in the riser.

Bentifraouine et al. [39] used an external ALR to study changes in the effective reactor height. In this work the effective reactor height varied between 1 to 1.6 meters. As the height increased, the superficial liquid velocity was observed to significantly increase. The increase in superficial liquid velocity was attributed to an increase in the hydrostatic pressure difference between the riser and downcomer. As the superficial liquid velocity increased, the gas phase residence time was reported to decrease, resulting in a reduction in

gas holdup. Chisti [2] and Russell et al. [16] reported the same trend in similar studies with an internal ALR.

In contrast, Snape et al. [40] found that as the effective reactor height was increased, the gas holdup increased. This change in behavior from that reported earlier was attributed to dissimilar hydrodynamic conditions in the reactors studied. Although gas holdup was shown to change with the effective reactor height, the superficial liquid velocity remained unchanged for the effective reactor heights studied by Snape et al. [40].

Bentifraouine et al. [38, 39] also considered how changing the unaerated liquid height affected overall gas holdup and superficial liquid velocity while maintaining a constant effective reactor height. When the unaerated liquid height was less than the effective reactor height, the superficial liquid velocity increased and the gas holdup decreased as the unaerated liquid height increased. On the other hand, when the unaerated liquid height was equal to or greater than the effective reactor height, gas holdup and superficial liquid velocity were independent of unaerated liquid height. Snape et al. [40] also studied the relationship between unaerated liquid and effective reactor height and reported that liquid height changes did not affect ALR operation; however, the unaerated liquid height was always greater than the effective reactor height in their study.

In a review of previously published research, Siegel and Merchuk [28] discussed how ALR height influenced overall mass transfer coefficients. The overall mass transfer coefficient was reported to increase as the effective reactor height increased. The increase in

the overall mass transfer coefficient was thought to be due to the longer gas phase residence time in the reactor. Nakanoh and Yoshida [41] reported a similar trend.

2.3.2 Gas Separator

The importance of the gas separator has been neglected by many, while it is claimed by some to be one of the most important geometric factors influencing ALR operation [14]. The degree of bubble disengagement in the gas separator was shown to be a key consideration as the gas separator directly affects the superficial liquid velocity and gas holdup in an ALR. The three most common gas separators considered in the literature are shown in Figure 2.7. The tank separator is commonly used for both internal and external ALRs and has been extensively studied, while the tube and vented tube gas separators are used exclusively in external ALRs.

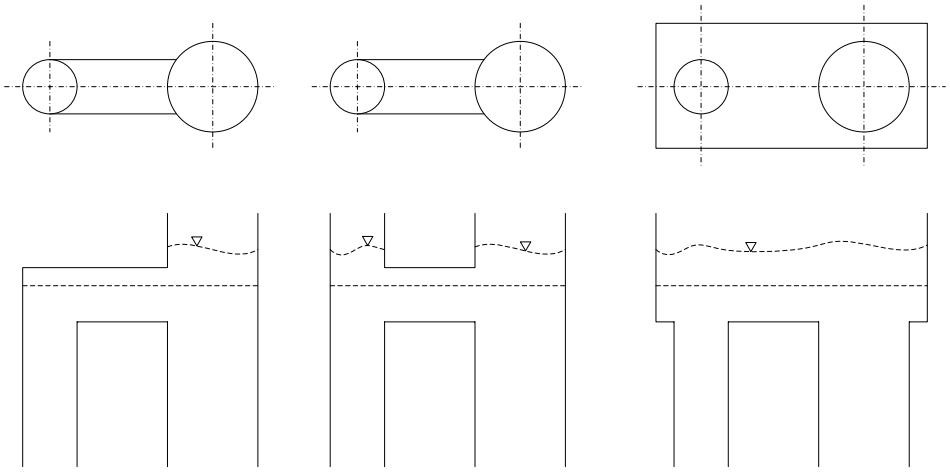

Figure 2.7: Gas separators commonly encounter in external airlift loop reactors.

2.3.2.1 Tank Separator

Seigel et al. [42] compared many tank gas separator configurations and showed that decreasing the fluid residence time in the gas separator increased downcomer gas holdup and reduced superficial liquid velocity. In that study, the fluid residence time in the gas separator was altered by changing the size of the separator and by changing the unaerated liquid height. They concluded that, until a critical fluid volume in the gas separator was reached, the liquid level played a predominant role in controlling gas recirculation and superficial liquid velocity. Once the critical fluid volume in the gas separator was reached, the separator size no longer dominated flow characteristics. Therefore, increasing the gas separator volume can decrease k_La, but an increase in aerated liquid volume creates a balancing effect that can be used to optimize a reactor performance.

Using a different tank gas separator, Al-Masry [43] studied the effect of changing the fluid volume in the gas separator. The fluid volume in the separator was increased from 0 to 37% of the total reactor volume to determine its influence on gas holdup and superficial liquid velocity. Gas holdup and superficial liquid velocity were found to only be affected by the separator fluid volume when it was in the range of 0 to 11% of the total reactor volume. Further increases in the fluid volume had little, if any, influence on gas holdup and superficial gas velocity. Similarly, Choi [44] found that varying the unaerated liquid height in the tank separator had the same effect. As the unaerated liquid height was varied from 0 to 8 cm, gas holdup and superficial liquid velocity were observed to change as noted by Al-Masry [43], after which any further increases in the liquid height did not result in any

significant gas holdup or superficial liquid velocity changes. Al-Masry [45] reported similar results in a subsequent study using a smaller ALR. However, in this new study, the volume in the liquid separator was found to affect gas holdup and superficial liquid velocity as the volume ranged from 0 to 30% of the total reactor volume. Thus, the reactor volume and ALR area ratio were found to influence how the gas holdup and superficial liquid velocity reacted to gas separator effects.

Experiments by Merchuk et al. [46] revealed that the design of the gas separator was an important factor affecting mass transfer rates. Their study revealed that as the gas separator volume increased, the overall mass transfer coefficient decreased. This trend was not observed at low superficial gas velocities, but became pronounced as superficial gas velocity increased. As discussed earlier, superficial liquid velocity was shown to increase as the gas separator volume grew; thus, this decreased the gas-liquid contact and reduced the overall mass transfer coefficient as the gas separator volume increased.

These studies indicate that the fluid residence time in the gas separator can be manipulated to control gas recirculation, superficial liquid velocity, gas holdup, and overall mass transfer coefficients.

2.3.2.2 Tube Separators

Bentifraouine et al. [38] modified a tube gas separator by adding vents to it and exploring how this affected ALR operation. They reported that when the vents were closed, perfect gas separation was not achieved and gas buildup occurred in the horizontal connector

creating a resistance to liquid flow. For this case, they also saw that beyond a critical value of superficial gas velocity, the superficial liquid velocity peaked and then decreased. Choi [47] and Siegel et al. [28] reported for similar reactor configurations that superficial liquid velocity was restricted in tube gas separators without a vent. The decrease in superficial liquid velocity reported by both authors was due to the air buildup in the tube connector that reduced the open cross-sectional area of the tube connector; thus, changing the effective downcomer to riser area ratio. Additionally, these authors observed that the size of the gas buildup in the horizontal connector grew rapidly and then collapsed, causing the superficial liquid velocity to surge in a periodic fashion.

When the tube connector was vented however, Bentifraouine et al. [38] reported a drastic change in the tube gas separator performance. In this case, the superficial liquid velocity continued to increase as the superficial gas velocity increased and a local maximum was not observed. Likewise, Choi [47] reported that for identical conditions, the superficial liquid velocity was higher in an ALR with a vented tube gas separator than in an unvented one. Both studies also reported that gas holdup was lower for the ALR with the vented tube separator.

Increasing the horizontal connector length in a tube separator was observed to have two competing effects [21]. As the horizontal connecter length was increased, the fluid residence time in the gas separator increased and the downcomer gas holdup decreased causing an increase in the superficial liquid velocity. The frictional losses were also observed to increase causing a decrease in the superficial liquid velocity. In general, the

decrease in superficial liquid velocity due to frictional losses was smaller than the increase caused by changes in the downcomer gas holdup. Hence, an overall increase in the superficial liquid velocity in the ALR was observed as the horizontal connector length was extended. It is plausible, however; that at some point, an increase in connector length will cause the frictional losses to dominate, resulting in a superficial liquid velocity reduction. Moreover, the riser and downcomer gas holdups and the overall mass transfer coefficient were found to decrease as the connector length was extended [47].

2.3.3 Area Ratio

The downcomer to riser area ratio has been reported to be the geometric parameter having the most influence on liquid flow patterns in ALRs [11, 37, 48]. Weiland [17] studied the effect of downcomer to riser area ratio using internal ALRs and found that changing the downcomer to riser area ratio affected gas holdup, liquid circulation velocity, mass transfer, and mixing time. They reported that no optimal area ratio existed and that the area ratio influence was process specific. Subsequently, it was suggested that restriction valves be placed in the downcomer to provide operational flexibility.

The downcomer to riser area ratio was shown to influence the hydrodynamics of an external ALR in two ways [48]. For a given superficial gas velocity and riser area, increasing the downcomer area lowered the resistance to flow in the downcomer, leading to an increase in superficial liquid velocity with no change in the hydrodynamic driving force. The downcomer to riser ratio also influenced the overall friction factor in the ALR, and

changes in riser and downcomer diameters were observed to directly affect the hydrodynamic driving force and liquid circulation. An increase in the downcomer to riser area ratio resulted in a higher superficial liquid velocity. Merchuk [27], Bello et al. [24], and Choi and Lee [21] observed that as the downcomer area was increased, the superficial liquid velocity increased too. Popovi and Robison [26] reported a similar trend where a change in the downcomer to riser area ratio from 0.11 to 0.44 resulted in a four-fold increase in superficial liquid velocity.

Bendjaballah et al. [49] illustrated the effect of changing the area ratio in a study that utilized a restriction valve in the downcomer where the flow field was changed from completely unobstructed to completed blocked in incremental steps. Results of this work showed that gas holdup varied only slightly as the valve was closed from 100% open to 40% open, but a significant change was observed as the valve was closed further. In addition, the superficial liquid velocity was shown to decrease as the valve was closed.

The overall mass transfer coefficient in ALRs was observed to increase as the downcomer to riser area ratio decreased [11, 21, 24, 43, 50]; this increase was attributed to a superficial liquid velocity decrease and gas holdup increase. In another study, Choi [47] observed the same trend; however, the decrease in the overall mass transfer coefficient was small.

2.3.4 Gas Sparger

In general, the influence of sparger type is rather complex and is mostly a function of fluid properties. The sparger plays a role in the resulting ALR bubble size and gas holdup,

which can be influenced by fluid coalescence. Thus, sparger design may play an important role in overall reactor design depending on the specific fluid properties.

As reported in the literature, bubble formation in an ALR can be accomplished by means of a variety of gas spargers, typically classified as either static or dynamic [18]. Dynamic spargers consist of injector nozzles and venturies that rely on the kinetic energy of a liquid jet to disperse the gas. Figure 2.8 shows some typical dynamic spargers use in BCRs and ALRs [2, 51]. Dynamic spargers are complex in design, require the use of a pumping device, and have areas of high shear. Because of this, they are not commonly used in bioreactors. Static spargers, on the other hand, consist of perforated plates on tubes that are cheap to make and operate. Most static spargers reported in the literature can be divided in to four main categories (Figure 2.9): single orifice nozzles, perforated plates, perforated rings/pipes, and porous plates. Single orifice nozzles and perforated plates and pipes have been reported to be the least expensive to install and operate, while porous plates have been reported to be more expensive, prone to blockage, and have higher operating costs [18]. Of the static sparger types, the perforated plate is normally used in bioreactor applications, although the porous plate has been used [19].

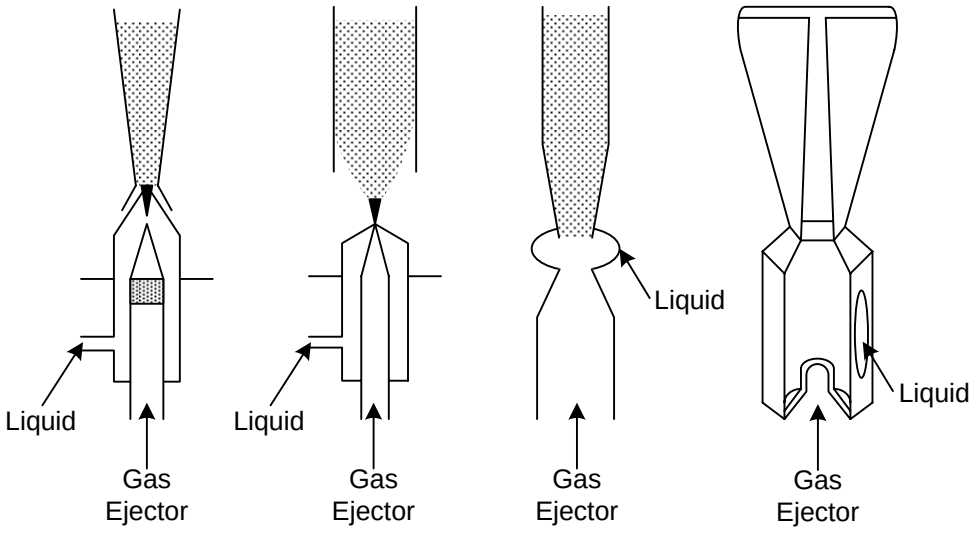

Figure 2.8: Dynamic gas spargers commonly used in pneumatic gas-liquid reactors, adopted from van Dam-Mieras et al. [51].

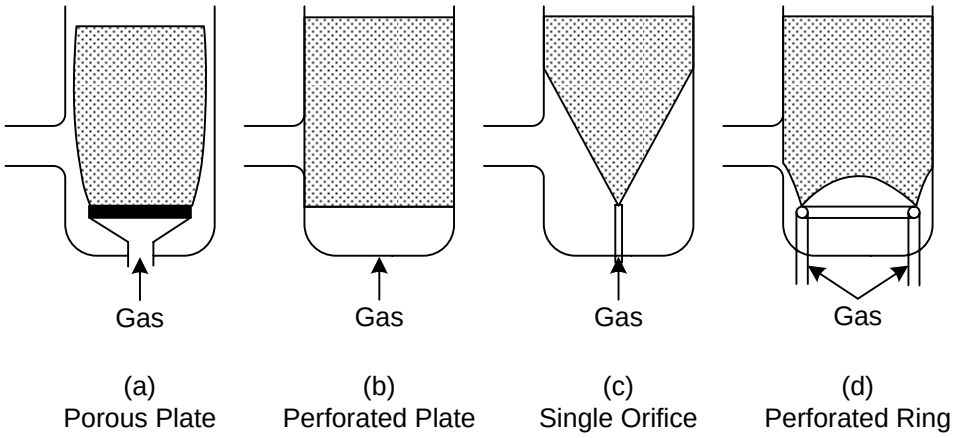

Figure 2.9: Static spargers commonly encounter in pneumatic gas-liquid reactors, adapted from van Dam-Mieras et al. [51].

Two important elements of sparger design are orifice size and open area ratio [27]. These are reported to be significant as they determine the initial size and number of bubbles in the reactor. Nonetheless, the significance of sparger design for coalescing fluids is often disputed in the literature. Sparger orifice size and number have been reported by some to significantly influence ALR hydrodynamics [27, 40, 52]. However, there are others that

insist that the number and size of orifices does not affect ALR hydrodynamics [2, 22, 31, 53], claiming that the effect of sparger design on ALR hydrodynamics was tied to other design considerations. For non-coalescing fluids, however, there seems to be a consensus in the literature that sparger design is important because the initial ALR bubble size is preserved as the bubbles rise up the reactor [18].

In addition to orifice size and open area ratio, Merchuk et al. [46] indicated that the ability of a sparger to evenly distribute gas through all the orifices was a key consideration in sparger design. They suggested that a Weber number (based on orifice diameter) greater than two guarantees the sparger's ability to evenly distribute gas. If the Weber number was less than two, they indicated that care must be taken to ensure that weeping does not occur at inactive orifices.

In a study that compared ten single orifice nozzles and perforated plates, it was found that reactor hydrodynamics were only slightly affected at low superficial gas velocities [53]. Onken and Weiland [10] also reported that gas sparger type had little influence on ALR gas holdup. However, Merchuk [27] and Bendjaballah et al. [49] compared a single orifice sparger to a perforated plate and showed a significant difference in gas holdup. They found that gas holdup increased differently with superficial gas velocity for single and multiple orifice spargers, and that the magnitude of superficial liquid velocity only varied with superficial gas velocity. Snape et al. [40] also observed that gas holdup was a function of gas sparger design for gas spargers having an equal open area ratio with different orifice

diameters. Variations in gas holdup were ascribed to the flow regime transition point happening at different superficial gas velocities due to initial bubble size.

For a fixed orifice diameter, Vasconcelos et al. [54] found gas holdup to be dependent on the superficial gas velocity. However, as the orifice diameter was increased from 0.5 to 3 mm for a constant superficial gas velocity, gas holdup decreased due to the generation of larger bubbles, which resulted in a higher terminal bubble rise velocity and a shorter residence time in the riser.

Siegel and Merchuk [28] found that, for coalescing fluids, porous plate spargers performed much better than orifice type spargers at low gas rates, but that as the gas flow rate increased, the performance dropped off due to increased bubble coalescence at the plate surface. In a comparison of porous and perforated plates at low superficial gas velocities, Lin et al. [52] reported that porous plates provided a more uniform radial bubble distribution than perforated plates.

Chisti and Moo-Young [18] evaluated the effected of sparger location on ALR hydrodynamics and found that when the sparger was located at the base of the riser, as is typically done in BCRs, the recirculating fluid flow from the downcomer caused an uneven gas distribution and resulted in a higher concentration of gas bubbles along the opposite side of the riser (Figure 2.10a). To improve the bubble distribution in the reactor base, they proposed that the gas sparger be located just inside the riser and that the base be filled with inert material to prevent dead zones (Figure 2.10b). Merchuk et al. [46] also reported that the

size and shape of the base connector played an important role in ALR behavior, where if the base connector was small in size, it restricted liquid flow and increased gas holdup.

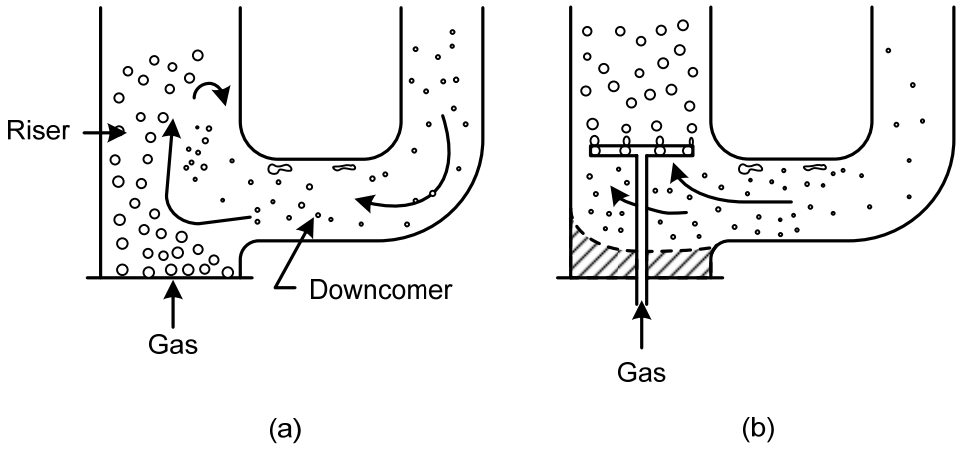

Figure 2.10: Fluid flow patterns observed in external airlift loop reactors for two reactor base styles, adopted from Chisti [2].

Siegel et al. [42] studied sparger location effects and considered the effect of moving the sparger further up the riser. They found that raising the level of the gas sparger above a critical point decreased riser gas holdup. Most of the gas holdup change, however, was attributed to the unaerated region below the sparger and not to flow changes above the sparger. On the other hand, when the sparger was below the critical point, there was no reported affect on gas holdup. Furthermore, they reported that sparger configuration and orifice size did not influence gas holdup or superficial liquid velocity.

Some researchers have considered the addition of a second sparger to the downcomer as a method of providing additional control over ALR flow characteristics and increasing overall mass transfer rates [42]. In this type of system, fresh gas was also introduced near the downcomer entrance to decrease the time that the fermentation process was gas starved in the

downcomer. As a result, the superficial liquid velocity was sharply reduced throughout the reactor causing a subsequent increase in gas holdup, even though the gas throughput in the reactor was not increased. However, the use of an additional sparger in the downcomer also presented some operational challenges because if the difference between the liquid and gas velocities in the downcomer were too small, an unstable flow condition was created where the direction of fluid flow oscillated. To overcome the oscillation, higher liquid velocities had to be maintained.

Miyahara et al. [53] also compared the overall mass transfer coefficients for multiple sparger designs. Although they reported that ALR hydrodynamics did not vary for their experimental conditions, the overall mass transfer rates varied significantly. A perforated plate, which had the smallest orifice diameter, exhibited a much higher overall mass transfer coefficient when compared to a single orifice nozzle for similar operating conditions. The difference in overall mass transfer coefficients for the various gas spargers was noted to be more pronounced at lower superficial gas velocities.

2.3.5 Internals

Auxiliary internals such as impellers [1], projecting baffles [55-57] and static mixers [58, 59] have been the subject of some study, with the intent to improve mixing and mass transfer while limiting bubble coalescence. In general, it has been shown that these devices can enhance gas holdup and mass transfer while either reducing or enhancing mixing, depending on the internal [18]. The introduction of static mixers has two important roles in

mass transfer enhancement: (i) bubble redispersion and (ii) increased interfacial turbulence during bubble coalescence and redispersion [60].

Partitioning plates and baffles have been reported to improve mass transfer, increase gas holdup, and decrease liquid circulation [55-57]. Much of the improvement in mass transfer was the result of smaller bubble sizes and uniform gas holdup throughout the system. The overall mass transfer coefficient also increased with the number of partitioning plates [55].

Nikakhtari and Hill [58, 59] modified an ALR by adding a section of structured packing. The addition of packing increased gas holdup by up to 37% and decreased the superficial liquid velocity by nearly 53%. The lower superficial liquid velocity and higher gas holdup increased mass transfer by nearly a factor of four when compared to a similar ALR without packing. They also reported there was no significant change in operating costs for the packed bed ALR relative to the unpacked ALR. Chisti et al. [61] likewise studied mass transfer enhancement in different liquids using static mixers. They also reported that the overall mass transfer rate was higher when an internal packing was used.

A mechanically agitated internal ALR was used by Chisti and Jauregui-Haza [62] to evaluate the effect of additional mixing. The mechanical agitator was found to increase gas holdup and mass transfer as the impeller speed increased. In view of the improvements to gas holdup and mass transfer, the use of impellers did come at a cost to the overall energy efficiency of the system. Hence, the mechanically agitated ALRs may be well suited only for certain applications where low energy efficiency is acceptable.

2.3.6 Liquid Phase Properties and Hydrodynamics

Liquid phase properties such as ionic strength, surface tension, and viscosity have been reported by many to have a significant affect on ALR operation [9, 40, 63]. However, the degree to which liquid phase properties influence ALR operation varies widely depending on operating conditions and reactor geometry. Onken and Weiland [63], as well as others [20, 64], showed that while physical properties greatly influence BCR operation, ALR operation was not affected to the same degree.

Weiland and Onken [25] reported that experiments with different electrolytes without liquid circulation showed that the gas holdup increased with electrolyte concentrations until a critical ionic strength was achieved. At which point, the maximum inhibition of bubble coalescence was reached. Zahradnik et al. [65] also investigated the addition of various salt solutions to the liquid phase in a BCR. The effect of adding salt solutions on gas holdup depended upon reactor flow regime. For heterogeneous flow regimes, gas holdup was only slightly affected, but for the homogeneous flow regime, significant variations in gas holdup were observed. Weiland and Onken [25] reported a maximum change in gas holdup at a critical salt concentration. In a study of electrolyte concentration on bubble coalescence, Prince and Blanch [66] indicated that salts inhibit bubble coalescence by retarding the thinning of the bubble film making the bubble film more rigid. Consequently, gas holdup increased with the addition of electrolytes to pure media.

Onken and Weiland [63] also studied the affect of liquid properties on gas holdup in an ALR by adding sugar, 2-propanol, or sodium chloride to the liquid phase in the following

percentages: sugar at 34.7 wt% and 51.8 wt%; 2-propanol at 1.65 vol% and 4.90 vol%; and sodium chloride at 0.1M and 0.4M. Gas holdup as a function of superficial gas velocity was then observed to be nearly identical for pure water and water containing sodium chloride, while gas holdup varied between pure water and water containing sugar and 2-propanol. The gas holdup for water with sugar and 2-propanol was slightly higher than pure water, with the largest difference noted at low superficial gas velocities. In a comparison between BCR and ALR reactors using pure water and a sodium chloride solution, Bello et al. [20] reported a similar trend in which the gas holdup data was generally about 10% higher for the 0.15M sodium chloride solution. McManamey et al. [64] observed slight changes in gas holdup with electrolyte concentration in an external ALR.

Nicol and Davidson [67] investigated the effect of n-octanol and bovine serum albumen addition to the fluid phase and reported a change in bubble size due to a suppression of bubble coalescence. However, they reported no change in overall gas holdup when these surfactants were added.

Snape et al. [40] used saccharose and various salts to evaluate how different additives changed the fluid phase behavior. The saccharose solutions had little affect on gas holdup at the lowest gas flow rates, while exhibiting a slight affect at higher gas flow rates. Unlike gas holdup, superficial liquid velocity varied significantly with saccharose concentration for all considered flow rates. The addition of saccharose solutions also altered the superficial liquid velocity trends with an increasing gas flow rate. As the gas flow rate increased, the superficial liquid velocity increased faster and exhibited a local maximum under some

operating conditions. The experimental data for the various salt solutions again showed that gas holdup only increased slightly with the addition of salt up to a critical salt concentration, at which point no further affect was reported. The one exception was at high electrolyte concentrations, where the addition of salt had a tendency to reduce gas holdup. Gas holdup was also reported to be independent of ionic strength and type of electrolyte for ALRs containing electrolyte solutions. Finally, salt addition was reported to dampen the sparger design influence on gas holdup for a given gas flow rate.

In an earlier study by Snape et al. [68], various sugar solutions were used to study gas holdup and superficial liquid velocity changes as a function of gas flow rate. For low gas flow rates, the effect of sugar concentration on gas holdup was negligible. At high gas flow rates, low sugar concentrations increased gas holdup and higher sugar concentrations lowered gas holdup. The superficial liquid velocity, however, was found to be influenced by sugar concentration at low gas flow rates where as the sugar concentration was increased, the superficial liquid velocity increased slightly until a local maximum was observed, after which the superficial liquid velocity decreased with further increases in the sugar concentration.

2.3.7 Liquid Phase Properties and Mass Transfer

The addition of surface active agents to pure water systems may enhance or reduce overall mass transfer coefficients and complicate gas-liquid mass transfer [69]. Surface active agents (surfactants) are believed to accumulate at the gas-liquid interface lowering

surface tension, reducing interfacial renewal, and reducing gas diffusion in the liquid [70]. This effect causes bubbles to behave like solid particles resulting in much lower transport rates [71]. The addition of small amounts of organic additives is believed to retard the expansion and compression of the bubble surface reducing the interfacial overall mass transfer coefficient. Organic additives may also prevent bubble coalescence, increase the number of bubbles, and in turn increase the overall mass transfer coefficient [69]. In general, the mass transfer rate may increase or decrease in the presence of organic additives while it always decreases in the presence of antifoam agents [54, 69, 72-74].

In an attempt to explain the effect of surfactants on gas-liquid systems, Russo et al. [70] reported the following trends:

(1) For a given contaminant concentration, gas-liquid interfaces with high renewal rates have higher overall mass transfer rates.

(2) For a given flow regime, higher contaminant concentrations result in lower mass transfer rates.

(3) At higher renewal rates, the variation due to different contaminant concentration was smaller than the variation at lower renewal rates, indicating that more turbulent flow regimes can offset contaminant concentration effects.

2.3.7.1 Organic Additives and Electrolytes

Sarding et al. [75] evaluated surfactant effects on mass transfer in a bubble column reactor using three surfactants types: cationic, non-ionic, and anionic. Their results showed

that the surfactant type and concentration had a direct affect on mass transfer. The magnitude of the overall mass transfer coefficients obtained from their work is summarized as follows: cationic (lowest), non-ionic, anionic, and pure water (highest).

The addition of sugar to water was shown to drastically reduce the overall mass transfer coefficient as the sugar concentration increased [63]. However, in the same study, the addition of sodium chloride and 2-propanol to water caused a significant increase in the overall mass transfer coefficient. 2-propanol provided more mass transfer enhancement than sodium chloride. The change in mass transfer with respect to 2-propanol concentration was small, while increasing the sodium chloride concentration resulted in a larger change in overall mass transfer coefficient. Likewise, Bello et al. [20], in a comparison between pure water and a sodium chloride solution, reported that the overall mass transfer coefficient was about 10% higher in a 0.15M sodium chloride solution.

The effect of adding propanol, benzoic acid, isoamyl alcohol, and carboxymethylcellulose was evaluated by Muthukumar [69]. At all concentrations, the propanol and benzoic acid had the effect of increasing mass transfer, while isoamyl alcohol and carboxymethylcellulose reduced mass transfer. The increase in mass transfer for propanol and benzoic acid was thought to be a result of bubble coalescence inhibition resulting in a larger interfacial area due to the addition of these additives. The reduction in mass transfer by the addition of isoamyl alcohol was thought to be a result of isoamyl alcohol not spreading evenly in the bubble surface causing interfacial blockage. The observed reduction in mass transfer for carboxymethylcellulose was attributed to the increased fluid

phase viscosity. Muthukumar concluded that the behavior of additives was rather complex because different trends were observed with different additives.

2.3.7.2 Antifoam Agents

Al-Masry [74] showed that the addition of antifoam agents to a pure water reduced gas holdup at all concentrations studied (0 to 100 ppm). The most severe reduction occurred at relatively low concentrations, whereas further increases in the antifoam concentration lead to gas holdup values approaching pure water values. It was also noticed that the bubbles produced in the presence of antifoam were larger than those found in pure water due to enhanced bubble coalescence. The liquid circulation velocity appeared to be unaffected by the addition of antifoam; however, the overall mass transfer coefficient, like gas holdup, was severely affected. For all antifoam concentrations considered, the overall mass transfer coefficient was nearly 50% lower than that of pure water.

In another study, the addition of antifoam agents was shown to have a strong affect on mass transfer [54]. As the antifoam concentration was increased from 0 to 10 ppm, the overall mass transfer coefficient abruptly dropped to less than half its original value. Further increases in the antifoam agent had little, if any, effect on the overall mass transfer coefficient. Vasconcelos et al. [54] attributed this behavior to the assumption that material accumulated at the bubble interface causing the bubble interface to change from mobile to rigid. In separate studies, Kawase and Moo-Young [71] and Al-Masry and Dukkan [73]

reported that the addition of antifoaming agents dramatically decreased mass transfer rates, in some cases by as much as 50%.

2.3.7.3 Fibers

Chisti and Moo-Young [18] evaluated the effect of adding Solka Floc cellulose fiber in low concentrations to the liquid phase of an ALR. As the cellulose concentration varied from 0 to 3 wt%, the resulting overall mass transfer coefficient declined dramatically. Cellulose addition was also noted to significantly affect how the overall mass transfer coefficient responded to changes in the superficial gas velocity.

2.3.8 Solid Particles

Hwang and Lu [76] evaluated the effect of adding small solid particles to a gas-liquid system. The addition of 2.4 mm polystyrene particles significantly affected mass transfer rates in an internal ALR. The overall mass transfer coefficient decreased dramatically as the solid concentration increased and was attributed to a lower gas holdup and a change in the degree of mixing caused by the addition of solid particles. Similarly, Muthukumar [69] saw the same trend in an external ALR when 3.5 mm polystyrene and nylon particles were added to a pure water system. Muthukumar concluded that the decrease in overall mass transfer coefficient with increasing solids loading was due to the reduction in interfacial area.

Gourich et al. [77] considered the effect of adding 750 μm polystyrene particles to a gas-liquid system. They found that the addition of solid particles showed an initial 25%

reduction in mass transfer. Solid loading beyond 5 wt% had a negligible affect on the mass transfer rate. Conversely, they noted that the addition of solid particles had a slight influence on gas holdup. The riser gas holdup initially increased and then decreased slightly as the solid loading increased. Dhaouadi et al. [78] observed that gas holdup in an external ALR with 90 μm glass beads was about the same as that of a similar system without glass beads. However, the superficial liquid velocity was observed to decrease significantly with the addition of the glass beads.

In a similar study using 12 nm solid particles, Wen et al. [79] discovered that gas holdup in the riser decreased with an increase in solid loading. The authors speculated that the gas holdup reduction was due to the solid particles restricting the effective flow area for the gas and liquid phases, causing a reduction in the gas residence time. Likewise, the overall mass transfer coefficient decreased as the solid concentration increased, and this effect was attributed to the possibility that solid particles increase bubble coalescence.

Conversely, Kluytmans et al. [80] found that the overall mass transfer coefficient increased with the addition of 30 μm carbon particles in a bubble column. The overall mass transfer coefficient for pure water was reported the be nearly the same as when the particles were added for gas velocities up to 6 cm/s, at which point the overall mass transfer coefficient for pure water began to be noticeably lower. The authors of this work attributed the increase in mass transfer for this system to the possibility that the carbon particles increased turbulence. Kluytmans et al. [81] reported that the addition of carbon particles also resulted in an increase in gas holdup much like when electrolytes are added to pure gas-liquid

systems. The results of these works are in direct contrast to what has been reported in airlift reactors for mass transfer, indicating that the significant differences may exist depending upon the type of solid additive.

Dhaouadi et al. [78] listed the following mechanisms as possible explanations for the variation in hydrodynamics due to the addition of solid particles:

(1) Solid particles may increase bubble coalescence producing larger bubbles that move faster.

(2) Particulate systems may be more turbulent, generating smaller bubbles with lower rise velocities.

(3) Particles may act to increase fluid viscosity and density, causing an increase in the superficial liquid velocity and a decrease in the bubble rise velocity.

(4) Solid particles in the bubble wake stabilize the bubble flow allowing for faster bubble rise velocities and loading to a reduced gas holdup.

2.3.9 Performance Summary

Mass transfer data in the literature for ALR varies a great deal and is sometimes contradictory. This is due to the wide range of reactors studied and the techniques used to study them. Merchuk [14]; however, reported that most researchers are in agreement on the following points:

(1) The physical and chemical properties of the liquid phase have a small, but significant affect on mass transfer rates in ALRs, especially when compared to BCR.

(2) The overall mass transfer rate generally increases with increasing superficial gas velocity.

(3) For a given superficial gas velocity, an increase in superficial liquid velocity generally results in a lower mass transfer rate.

(4) Taller ALRs tend to have a higher mass transfer rate than shorter ones.

(5) Cocurrent gas flow in the downcomer tends to have a higher mass transfer rate than stagnant or no gas flow in the downcomer.

(6) The aeration efficiency of ALRs remains relatively constant for increasing mass transfer rate and superficial gas velocity compared to BCRs and CSTRs, which typically show a decrease in aeration efficiency as mass transfer rate and superficial gas velocity increase.

(7) A change from homogeneous to heterogeneous flow in ALRs typically leads to a decrease in mass transfer rate.

As discussed above, factors influencing gas-liquid mass transfer are often related and quite complex. Benyahia et al. [82], Merchuk and Gluz [6], Merchuk et al. [83], Heijen and Van't Riet [19], and Chisti [2] suggested how these factors might be related. Figure 2.11 is a compilation of how the suggested operating and design variables influence transport parameters. Figure 2.11 also illustrates how complex the relationships are for factors affecting gas-liquid mass transfer.

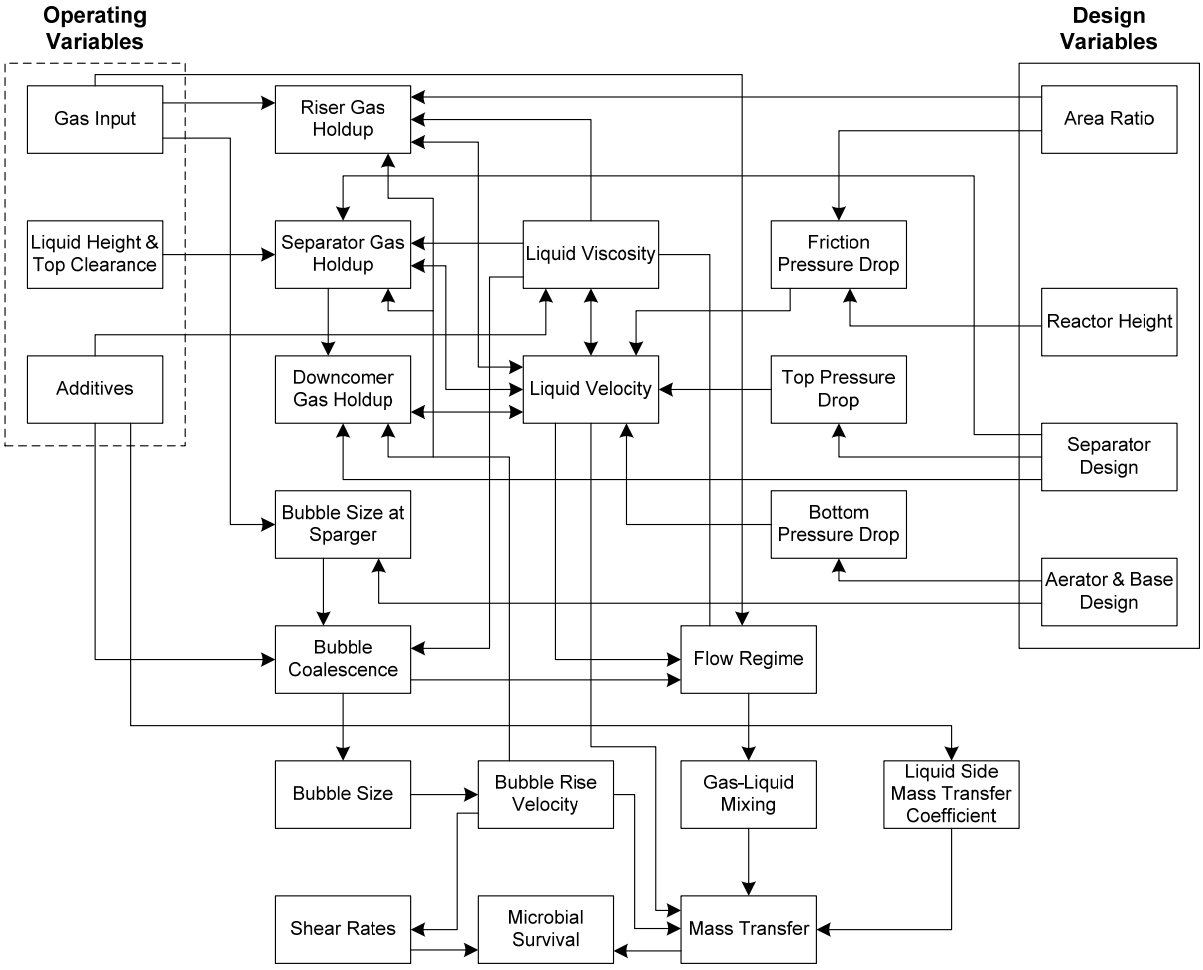

Figure 2.11: Diagram showing the relationship between design and operating variables and their effect on airlift loop reactor performance, compiled from the literature [2, 6, 19, 82, 83].

Onken and Weiland [10] reported that like gas holdup, mass transfer rates in ALRs are lower than those observed in similar BCRs due to the effect of superficial liquid velocity on the gas phase residence time. The addition of compounds which reduced bubble coalescence may increase overall mass transfer coefficients by a factor of two when compared to pure water; however, the increase in overall mass transfer coefficients was much smaller than those observed in BCRs, which were reported to be nearly six-fold for similar

conditions. The lower overall mass transfer coefficients for ALRs were still acceptable because ALRs can be operated at much higher gas velocities than BCRs, allowing them to operate over a wide range of gas flow rates to achieve much higher overall mass transfer coefficients.

2.4 Dissolved Oxygen Measurement Techniques

There are several techniques used to determine the dissolved oxygen content of a fluid. In practice, five general methods exist: chemical, volumetric, tubing, optodes, and the electrochemical electrode [51, 84]. This section will discuss these methods and some of their limitations and uses. The majority of this section, however, will focus on electrochemical electrodes as they are the most common.

2.4.1 Chemical Method

In the chemical method, a sample is taken from the reactor and the dissolved oxygen concentration is determined off line using a titrimetric method. The use of chemical methods for systems that have rapidly changing dissolved oxygen content is limited because these methods are laborious, slow, and prone to error if done incorrectly.

The most widely used chemical method is the Winkler method (iodometric method) developed by Lajos Winkler in 1888 [85]. The Winkler method is considered to be the most reliable and precise titrimetric procedure for dissolved oxygen analysis.

This method involves several steps which include: First, adding a divalent manganese solution followed by a strong alkali to a sample in a gas tight container; this causes the dissolved oxygen to oxidize an equivalent amount of manganese ions to hydroxide. Second, an acid is added to convert the hydroxide to iodine. Third, the solution is titrated with a thiosulfate solution in the presence of a starch indicator to determine the number of iodine molecules in solution. The number of measured iodine molecules is proportional to the number of dissolved oxygen molecules in the original sample as shown by:

$$1 \text{ mole of } O_2 \rightarrow 4 \text{ moles of } Mn(OH)_3 \rightarrow 2 \text{ moles of } I_2 \qquad (2.23)$$

As with any analytical method, the success of the Winkler method is highly dependent upon how the sample is collected and prepared. Care must be taken during all steps of the analysis to ensure that oxygen is neither introduced nor lost from the sample. Furthermore, care must be taken to ensure that the sample is free of contaminants because they may oxidize the iodide or reduce the iodine, problems commonly encountered with fermentation broths. Wilkin et al. [86] stated that the Winkler method is the most accurate and precise of all methods for determining dissolved oxygen concentrations, but that it is also the most challenging technique to master and the most time consuming.

Other chemical methods such as the NADH oxidation and phenylhydrazine oxidation have been employed to determine dissolved oxygen content [51], but are limited in use.

2.4.2 Volumetric Method

The volumetric method is simple and robust in principle, but rather inaccurate in practice. This method relies on the conversion of dissolved oxygen to carbon dioxide which is then driven out of solution. As the carbon dioxide is driven out of solution, it is collected and its volume determined at a known pressure and temperature. Then using the ideal gas law and an elemental balance for the oxygen to carbon dioxide reaction, the oxygen concentration is determined. While simple in theory and nearly unaffected by other compounds that might be in the sample, this method, like the chemical method, is slow and lacks the sensitivity needed for dynamic biological applications [51].

2.4.3 Tubing Method

The tubing method consists of using a very small diameter thin walled tube of semi-permeable material that is immersed in a fermentation broth [51, 87]. A slow stream of oxygen free carrier gas is pumped through the immersed tube, and allowed to absorb oxygen from the fermentation broth by diffusion. The concentration of oxygen in the exit gas stream is then measured using a gas analyzer or electrode. This method is strongly influenced by the tubing type, length, diameter, carrier gas flow rate, wall thickness, temperature, and the mixing characteristics within the reactor vessel. Due to the many factors that may influence the operation of this method, extensive calibration is required. The tubing method has been shown to have response times of two to ten minutes [87]. However, despite the long

response times and the need for extensive calibration, this method can be very accurate, robust, and withstand repeated sterilization cycles.

2.4.4 Optode Method

A recent development for the measurement of gaseous and dissolved oxygen has been the introduction of the photometric transducer or optode [88]. Many types of optodes exist, of these the fluorescence quenching optode is the most widely used for oxygen measurements [87].

Optodes for oxygen sensing are constructed using an immobilized flurophore (a special dye) attached directly to the end of an optic fiber. When excited by a reference light wave, the flurophore will emit another light wave having a different wavelength with an intensity that depends on the quencher concentration. Thus when the quencher is oxygen, the intensity of the emitted light is proportional to the dissolved oxygen concentration.

These relatively new sensors show great promise as they can be used in very harsh environments, do not consume oxygen, are very small, are very sensitive to oxygen concentration changes, and are not prone to time response issues common to other methods [87-92]. However, a few drawbacks like ambient light interactions and photo bleaching are currently preventing their widespread use.

2.4.5 Electrochemical Electrode Method

In 1950, Leland Clark developed the membrane coated dissolved oxygen electrodes that have become one of the most important process instruments for aerobic fermentations. Normally, the membrane used with these electrodes is only gas permeable and impermeable to most ions such as those used in the electrolyte solution, thus these electrodes do not disturb the biological process. For this reason, and the fact that dissolved oxygen electrodes are relatively easy to use, they are very popular and widely used in industry. Today most all oxygen electrodes can be classified as either polarographic or galvanic.

Both of these electrodes are based on the reduction of oxygen at the cathode, which is negatively polarized with respect to the anode. While these electrodes are similar in construction and operation, the main difference between the two is the source of the needed polarization voltage. Polarographic electrodes are typically charged with a negative voltage of 0.75 volts by an external source, while galvanic electrodes utilize a negative 0.75 volt potential created by the use of dissimilar metals.

It is important to note that both the polarographic and galvanic electrodes measure the oxygen tension of the medium in which they are placed [5]. So when an electrode is placed in a liquid, it does not measure dissolved oxygen, but rather the dissolved oxygen partial pressure, which is proportional to oxygen tension in the fluid. It is necessary to know the oxygen solubility, pressure, and temperature of the fluid medium in order to determine the exact dissolved oxygen concentration.

2.4.5.1 Polarographic Electrodes

Polarographic electrodes usually contain a platinum or gold cathode, a silver/silver chloride anode, and a potassium chloride electrolyte. Figure 2.12a shows a schematic representation of a polarographic electrode. When the anode of the electrode is polarize by an external power supply, the following reactions take place at the surface of the electrode [51, 87, 93]:

$$\begin{aligned} &\text{cathode:} && O_2 + 2H_2O + e^- \rightarrow H_2O_2 + 2OH^- \\ &&& H_2O_2 + 2e^- \rightarrow 2OH^- \\ &\text{anode:} && Ag + Cl^- \rightarrow AgCl + e^- \\ &\text{overall:} && 4Ag + O_2 + 2H_2O + 4Cl^- \rightarrow 4AgCl + 4OH^- \end{aligned} \tag{2.24}$$

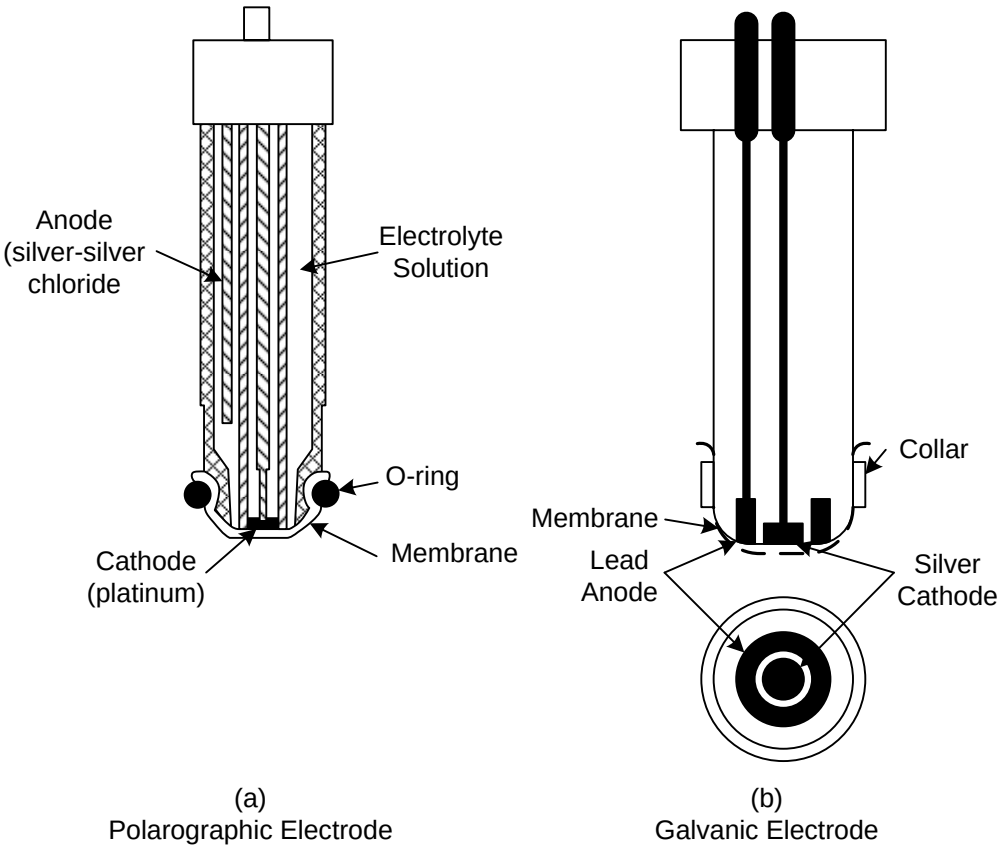

Figure 2.12: Schematics showing the typically construction of polarographic and galvanic electrodes, adopted from Linek [94].

The potassium chloride electrolyte solution between the membrane and probe tip provides the chloride ion needed for the above reactions. Since chloride ions are consumed over time with this type of probe, it is necessary to periodically replace the electrolyte solution. Due to the reactions that take place at the electrode surface, a voltage dependant current is created that can be related to the oxygen partial pressure as shown in the polarogram (current vs. voltage diagram) in Figure 2.13. The rate at which the current producing reaction takes place at the electrode surface in the plateau region shown in Figure 2.13 is limited by the diffusion rate of dissolved oxygen through the membrane and electrolyte, Figure 2.14 [51, 93, 94]. Since these reactions are very quick, the diffusion rate is a function of the bulk fluid oxygen concentration. As shown in Figure 2.13, when the correct polarization voltage is selected for a particular electrode, the current output is linear with respect to dissolved oxygen concentration. Care must be taken to ensure that the voltage is not too high to prevent the formation of hydrogen peroxide due to water electrolysis as this will increase the current generation. On the other hand, if the voltage is too low, the current response will be nonlinear. Care must also be taken to ensure that the reaction at the electrode is sufficiently fast to prevent the built up of hydrogen peroxide that may promote hydrogen peroxide diffusion from the electrode tip. If hydrogen peroxide diffuses away, the electrode reaction stoichiometry will be altered. Likewise, it has been shown that the accumulation of OH^- ions also retards the probe reaction rates [93]. Thus, it can be concluded that a careful balance must be achieved to ensure proper electrode

operation, however, on a positive note, this balance is relatively easy to achieve and maintain in practice.

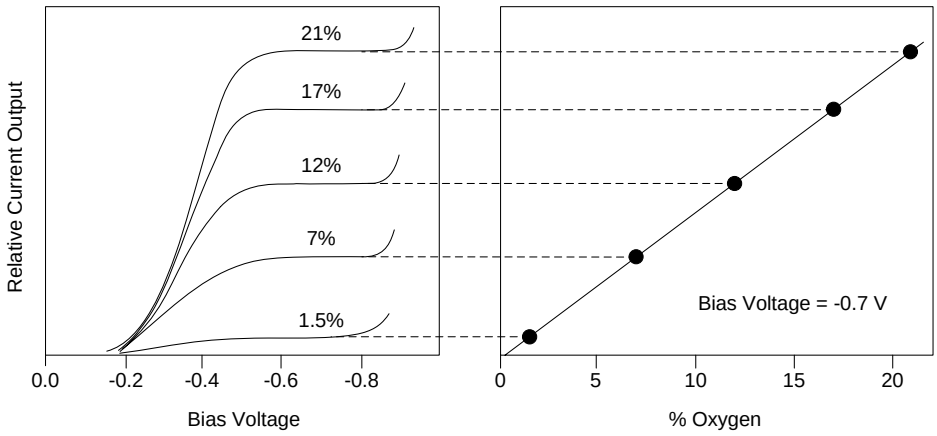

Figure 2.13: Typical polarographic electrode polarogram, adopted from Lee and Tsao [95].

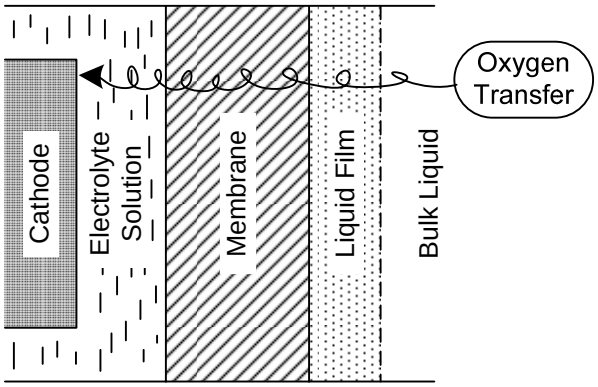

Figure 2.14: The typical oxygen transport path encountered at an electrode tip.

2.4.5.2 Galvanic Probes

In contrast to the polarographic electrode, a galvanic probe utilizes an anode of zinc, lead, or cadmium and a cathode of silver or gold, where a silver cathode and lead anode are the most common [93]. Figure 2.12b shows a schematic representation of a typical galvanic probe. The electrochemical reactions that take place at the probe surface are [51, 87, 93]:

$$\begin{aligned} &\text{cathode:} \quad O_2 + 2H_2O + 4e^- \rightarrow 4OH^- \\ &\text{anode:} \quad Pb \rightarrow Pb^{2+} + 2e^- \\ &\text{overall:} \quad 2Pb + O_2 + 2H_2O \rightarrow 2Pb(OH)_2 \end{aligned} \tag{2.25}$$

Like the polarographic probe, the galvanic probe is constrained by the rate limiting step of oxygen diffusion across the probe membrane. Thus, the current output of the probe is linearly related to the dissolved oxygen concentration in the bulk fluid.

2.4.5.3 Electrochemical Electrode Time Constant

Despite their fundamental differences, both electrochemical electrodes presented above operate on the same basic principles, where the electrode behavior can be predicted using a simplified electrode model with the following assumptions [95]:

(1) The cathode is well polished and the membrane is placed over the cathode surface to minimize the thickness of the electrolyte layer, allowing the electrolyte layer to be neglected in the mathematical model.

(2) The liquid around the probe is well mixed so that the oxygen partial pressure at the membrane surface is the same as in the bulk fluid.

(3) The electrochemical reaction at the surface of the electrode is much faster than oxygen diffusion through the membrane.

(4) Oxygen diffusion occurs only in one direction, perpendicular to the probe.

These assumptions lead to the development of the so called one layer model [95, 96]. A schematic representation of the one layer model is shown in Figure 2.15a where oxygen diffusion to the electrode surface is only a function of the membrane layer. Under steady

state conditions for the above simplifications, Fick's First Law describes oxygen diffusion from the bulk fluid to the membrane surface, showing that the electrode current output is linearly related to bulk fluid oxygen partial pressure. However, in application, the above over simplifications can rarely be used.

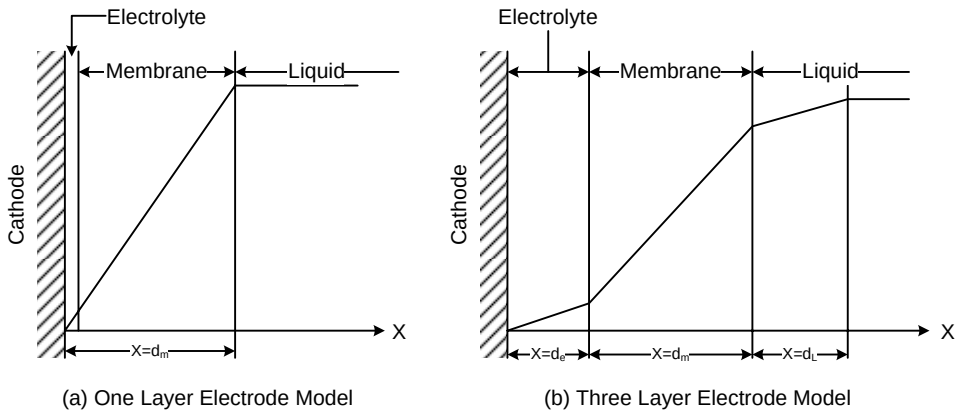

Figure 2.15: One and three layer electrode models used to estimate electrode time constants, adopted from Linek [94].

Although the one layer model is an over simplification of actual conditions, its application to the case where the oxygen partial pressure is allowed to change with time illustrates how electrode properties affect transient dissolved oxygen measurements. Fick's Second Law is needed to describe the unsteady state diffusion in the membrane, and shows that the diffusion coefficient of the membrane directly determines how fast an electrode will respond to a step change in the oxygen partial pressure [95-97]. Lee and Tsao [95] showed mathematically that the electrode time response, for the one layer model, depends on the electrode time constant defined as:

$$\tau_e = \frac{\pi^2 D_m}{d_m^2} \tag{2.26}$$

where D_m is the membrane diffusion constant and d_m is the membrane thickness. A large τ_e results in a fast probe response, which means that the membrane is either very thin or it has a high D_m. On the other hand, a small τ_e indicates that the membrane is impermeable to oxygen or that the membrane is too thick. Since electrode stability relies on membrane controlled diffusion, a compromise between electrode response and stability is required.

As stated earlier, the one layer model is an over simplification of actual conditions typically observed and hence, a three layer model is typically employed. This model accounts for the effects of the electrolyte and the stagnant boundary layer as shown in Figure 2.15b [95-97]. While the three layer model is more suited to quantifying the electrode response to transient conditions, it only provides the foundation for determining the electrode response constant due to the many factors listed in the literature that may affect it. Electrode design aspects like membrane type, membrane thickness, cathode surface area, electrolyte, and electrode style all profoundly affect the behavior of the electrode response to oxygen partial pressure. Likewise, bulk fluid properties such as fluid type, viscosity, temperature, total pressure, oxygen partial pressure, fluid velocity, and solid loading can also affect electrode dynamics.

2.4.5.4 Electrochemical Electrode Response Time (τ_e)

Due to the complexity involved in estimating the probe time constant, most investigators opt to measure the electrode response time to a step change in the oxygen

partial pressure. Typically, the electrode response time is defined as the time it takes the electrode to indicate 63% of the total change in dissolved oxygen concentration [5, 97-99]. There are several experimental procedures described in the literature for obtaining the τ_e to stepwise concentration changes [93].

Procedure 1: The electrode is placed at the output of a three way valve and the interchange of fluids having different oxygen concentrations takes place when the valve is turned.

Procedure 2: The electrode is placed in a tube and the concentration change is produced by starting and stopping the flow of liquid saturated with air. While the flow of liquid is stopped, the concentration of oxygen in the liquid near the electrode decreases due to the chemical reaction at the electrode. The decrease in concentration will continue until nearly all the oxygen near the electrode is consumed. When this near steady state condition is reached, liquid flow is restarted causing a jump in the oxygen concentration near the electrode surface. This method is limited for use with electrodes that have a large cathode, i.e., ones that consume oxygen rapidly.

Procedure 3: The electrode is transferred between two vessels having liquids of different oxygen concentrations that are well mixed and thermostatically controlled.

Procedure 4: The electrode is transferred from air to a sulfite solution by inclining a vessel such that the probe, initially in air, is immersed in the sulfite solution.

Procedure 5: The electrode is rapidly transferred from a pure nitrogen environment to a vessel containing a liquid saturated with air. The liquid and hydrodynamic conditions in

the test vessel should be the same as those in which the electrode will be used after calibration.

Procedure 6: The electrode is placed in a closed vessel containing a liquid saturated with oxygen and a stirrer. The stepwise concentration change is then facilitated by introducing a compound that immediately consumes all of the dissolved oxygen.

Regardless of the procedure used to find τ_e, care must be taken to ensure that the hydrodynamic conditions around the electrode during the time response test closely resemble those of the process in which the probe will be used, and that the step change is as rapid as possible.

To achieve reasonably accurate overall mass transfer values, a τ_e much smaller than $1/k_La$ is recommended [4, 98] as problems occur when this is not the case. Thus, in practice there are three conditions of interest [100].

(1) $\tau_e << 1/k_La$: In this range, the response time of the electrode is much smaller than the dynamic oxygen concentration change in the reactor and the electrode is suitable for monitoring changes in oxygen concentration with small error.

(2) $\tau_e \approx 1/k_La$: In this range, the response time is of the same order of magnitude as the reactor response time and considerable errors may be encounter when calculating overall mass transfer coefficients. However, since this case is commonly encountered, models have been developed that account for this error.

(3) $\tau_e >> 1/k_La$: In this range, the response time is much larger than that of the reactor and the use of electrodes to monitor changes in oxygen concentration is not suitable.

2.4.5.4.1 Electrochemical Electrode Response Models

Most oxygen measuring electrodes used in biological processes have response times that range from 3 to 100 seconds [4, 100], which may result in the need to correct oxygen concentration data depending on the reactor dynamics. Many models have been developed to correct for τ_e and are discussed in great detail in the literature [2, 4, 93-95, 97-113]. Lee and Luk [110] and Sobotka et al. [97] provide a good review of these model corrections. A selection of these models is presented below starting with the simplest and finishing with a few of the more popular complex models.

2.4.5.4.2 Models that Neglect the Electrode Dynamic Response

Van't Riet [114] and Gaddis [100] suggest that if τ_e is less than three seconds, the overall mass transfer coefficient can be accurately measured without model correction. Hence, assuming ideal mixing and insignificant gas phase concentration changes, the overall mass transfer coefficient may be calculated from:

$$\frac{C^* - C_L}{C^* - C_o} = \exp\left(-k_L a \cdot t\right) \tag{2.27}$$

However, Van't Riet [114] also cautioned that considerable corrections have to be made to coefficients calculated using this method if the gas residence time in the reactor is much greater than $1/k_La$. These corrections were reported to greatly reduce the accuracy of Equation (2.27). Linek et al. [106, 115] also reported that the use of this model to relate experimental data to overall mass transfer coefficients would lead to an under estimation of k_La for air systems in which nitrogen transport is neglected, and that this model is really only

sufficient for steady state signals and marginally acceptable in the extreme case when oxygen concentration changes are much slower than τ_e.

2.4.5.4.3 Models Considering Membrane Diffusion

The following model has been used when assuming that the electrode response is a first order lag function, the liquid and gas phases are perfectly mixed, there is negligible nitrogen diffusion, and the interfacial area and oxygen concentration in the gas phase are constant [2, 112, 116, 117]:

$$\frac{C^* - C_L}{C^* - C_o} = \frac{(e^{-k_L a \cdot t} - k_L a \cdot \tau_e \cdot e^{-t/\tau_e})}{(1 - k_L a \cdot \tau_e)} \tag{2.28}$$

In general τ_e represents all the diffusional properties of the measurement system in the model [97]. As with the previous model, the adequacy of this model depends on the ratio of τ_e and $1/k_La$. When τ_e is much less than $1/k_La$, Equation (2.28) reduces to Equation (2.27) and the resulting error associated with neglecting τ_e has been reported to be small [41, 100, 118]. This model is again subject to the same errors and limitations as the previous one, especially if nitrogen transport is neglected.

Linek et al. [93], however, suggested a different approach using a very sophisticated model in which the electrode time constant plays a major role. Rather than solve the model explicitly to determine k_La, they suggested that since the electrode signal is most distorted during the initial response, one could find k_La by removing the distorted portion of the signal

and using the remaining response and Equation (2.27) to find k_La. The proper application of this technique is discussed in detail in the literature [93, 119].

If the system being studied can be assumed to have a perfectly mixed liquid phase and a constant oxygen concentration in the gas phase, Tobajas and Garcia-Calvo [101] suggested that the following model be used to determine k_La:

$$\frac{C^* - C_L}{C^* - C_0} = \frac{1}{1-m}\left[1 - \exp\left(\frac{-m \cdot t}{\tau_e}\right) - m\left(1 - \exp\left(\frac{-t}{\tau_e}\right)\right)\right] \tag{2.29}$$

where m is defined as

$$m = \frac{k_L a \cdot \tau_e}{1-\varepsilon} \tag{2.30}$$

and ε is the gas holdup.

2.4.5.4.4 Models Considering Membrane Diffusion and Time Delay

Lopez et al. [103] and Vardar [99] suggested that, when the electrode dynamic response was first order with a time delay, the following model be used to correct the dissolved oxygen concentration data:

$$C_L(t - \tau_d) = C_E(t) + \tau_e \frac{dC_E(t)}{dt} \tag{2.31}$$

where C_E is the recorded electrode concentration and τ_d is dead time. The dead time, τ_d, represents the time from the beginning of the concentration step change to the beginning of the change in the electrode signal. Once the concentration data is corrected for the electrode dynamic response, Equation (2.27) was used to determine k_La.

Sobotka et al. [97], on the other hand, suggested that the following relationship be used to find k_La using the electrode data:

$$\frac{C^* - C_L}{C^* - C_o} = \frac{1}{1 - k_L a \cdot \tau_e}\left[\frac{1}{1 - k_L a \cdot \tau_d}\exp\left(-k_L a \cdot t\right) - \frac{k_L a \cdot \tau_e^2}{t_e - t_d}\exp\left(-t/\tau_e\right) + \left(\left(1 - k_L a \cdot \tau_e\right) - \frac{1}{1 - k_L a \cdot \tau_d} + \frac{k_L a \cdot \tau_e^2}{\tau_e - \tau_d}\right)\exp\left(-t/\tau_d\right)\right] \quad (2.32)$$

When $\tau_d << \tau_e$, Equation (2.32) reduces to Equation (2.28), and when $\tau_d << \tau_e << 1/k_La$, Equation (2.32) reduces to Equation (2.27).

2.4.5.4.5 Models Considering Membrane and Liquid Film Diffusion

These models are quite complex as they are second order in nature and the solution to these models require numerical analysis or a method of moments due to their complexity [97]. Linek et al. [93], Ruchti et al. [102], and Dang et al. [120] suggested that while these models are more complex and involved, their solutions are much superior to any first order model. However, due to there complexity, they are typically not used and the reader is referred to the literature for more information concerning these models.

2.4.5.4.6 Models Considering a Membrane Diffusion Model

Sobotka et al. [97] claimed that the empirical time delay models previously described do not properly consider the physical nature of the electrode response. Instead, they insisted that models based upon Fick's Second Law are superior and encouraged their use to more

accurately model system dynamics. In their review, they presented many of the different diffusional models that have been developed and discussed their usefulness.

As has been shown by a review of just a few of the models presented in the literature, the use of electrochemical electrodes to accurately determine k_La can be complicated due to internal instrument dynamics as well as system dynamics. Hence, as implied by Tribe et al. [98] and others [93, 95, 97, 110, 121], the proper selection of an electrode and method for evaluating its signal will greatly impact the accuracy of the experimental results.

2.5 Dissolved Carbon Monoxide Measurement

This section will review the bioassay technique employed by Riggs [122], Kapic [123], and Ungerman [124] to measure dissolved carbon monoxide concentrations in a bioreactor. Note that, unlike dissolved oxygen measurements where electrodes are available, no dissolved carbon monoxide electrodes are currently on the market.

In the bioassay, a sample is taken from the reactor and the dissolved carbon monoxide concentration is determined off line using a protein binding method. The use of the bioassay is limited, much like the chemical methods for determining dissolved oxygen concentrations, because this method is laborious, slow, and prone to error if done incorrectly.

The method involves several steps which include: First, preparing a myoglobin protein solution that is free of dissolved oxygen and carbon monoxide. Second, the myoglobin protein solution is added to a sample in a gas tight container; this causes the dissolved carbon monoxide to bind to the myoglobin. Third, the change in the absorbance

spectrum (400 to 700 nm) of the sample after the protein solution is measured. The change in the absorbance spectrum is proportional to the number of dissolved carbon monoxide molecules in the original sample.

As with any analytical method, the success of the bioassay is highly dependent upon how the samples are collected and prepared. Care must be taken during all of the steps of the analysis to ensure that oxygen is not allowed to bind with myoglobin and that all measurements are carried out very carefully [122]. Furthermore, care must be taken to ensure that small gas bubbles are not entrained in the samples when they are collected as this leads to errors [123]. Although difficult to use, the bioassay technique, once mastered, may be successfully used to accurately measure dissolved carbon monoxide concentrations.

2.6 Determining k_La

For two phase gas-liquid systems, it has been shown that the gas mass transfer rate (GTR) can be described by:

$$GTR = \frac{dC_L}{dt} = k_L a\left(C^* - C_L\right) = a \cdot J_A \tag{2.33}$$

where C^* and C_L are the equilibrium gas concentration at the gas-liquid interface and the dissolved gas concentration in the liquid phase, respectively.

In bioreactors, dC_L/dt, C^*, and C_L can all be measured directly. However, as stated earlier, k_L and a are not so easily measured, so it is common to report the product of k_La. This product is commonly called the overall volumetric mass transfer coefficient and has units of s^{-1}.

The most widely used methods for determining k_La in bioreactors will be presented next [2, 4, 97, 125]. Prior to presenting these methods, it is important to realize that Equation (2.33) was derived using the assumptions of having well mixed gas and liquid phases, so that k_La can be assumed constant over the entire gas-liquid system. These assumptions, however, are not always applicable to the system being evaluated and further modeling of the gas-liquid system may be needed.

2.6.1 Gas Balance Method

The gas balance method can only be used in a gas consuming system. Typically, this method is applied to a fermentation run where all the variables except k_La are measured. The gas concentration and the entering and exiting gas stream flow rates are monitored using a gas analyzer and mass flow rate meters. Using this information, the GTR can be calculated from [4]:

$$GTR = \frac{F_i \cdot C_i - F_o \cdot C_o}{V_L} \tag{2.34}$$

where F is the respective gas flow rate, C is the respective gas concentration, and V_L the liquid volume. Once the GTR is known using Equation (2.33), k_La can be calculated.

The gas balance method is claimed by Doran [5, 126] to be the most reliable method for determining k_La. However, this method requires the precise measurement of the gas inlet and outlet concentrations and flow rates. Since the difference between inlet and outlet conditions is typically very small, the accuracy of this method is determined in large part by

the accuracy of the instrumentation [51, 126]. The instrumentation cost for this method is often high and usually only justified in situations where expensive gas monitoring equipment is also needed for process control.

This method is also limited by the underlying assumption that the gas phase is constant throughout the bioreactor. For large systems where the gas concentration may vary widely from inlet to outlet, gas phase modeling is required to accurately estimate GTR and k_La [4].

2.6.2 Dynamic Method

The dynamic method involves measuring the dissolved gas concentration as a function of time for a step change in the inlet gas concentration. Like the gas balance method, this method can be applied to an actual fermentation or it can be applied to systems containing no microorganisms. Due to its versatility and ease of use, this method is widely used and discussed in the literature [2, 4, 5, 51, 97, 127]. As a result, many variations of this method exist of which a select few are discussed in more detail below.

2.6.2.1 Biological Dynamic Method

The biological dynamic method is applied to actual fermentations using a step change in inlet gas concentration, where the change in dissolved gas concentration in the bulk fluid is recorded. The step change is initiated in one of several ways that will be discussed in more detail below. This method consists of three primary steps. First, the system is brought to an

initial steady state condition. Second, the inlet gas step change is initiated and the change in dissolved gas concentration is recorded. Typically, the dissolved gas concentration is reduced to a point just above the critical gas concentration needed to prevent cell death and/or an irreversible change in cell behavior [127]. Third, after a period of time the inlet gas concentration is returned to its original state and the change in gas concentration is recorded as the system moves back to the original steady state condition. Figure 2.16 illustrates the typical dissolved gas concentration profile obtained using the dynamic method.

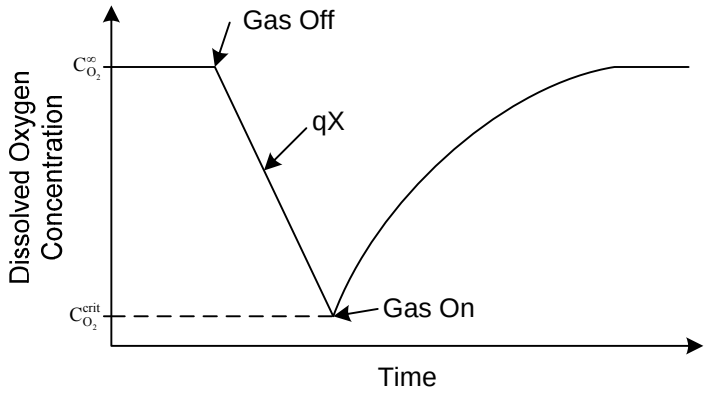

Figure 2.16: Typical dissolved oxygen concentration variation with time for the biological dynamic method, adopted from Blanch and Clark [127].

The system mass balance for the dynamic method is as follows:

$$\frac{dC_L}{dt} = k_L a\left(C^* - C_L\right) - qX \tag{2.35}$$

where qX is the microbial gas consumption rate. If the gas phase disengages quickly from the liquid, then the transport term disappears in the above relationship and it reduces to:

$$\frac{dC_L}{dt} = -qX \tag{2.36}$$

This equation can be used to find qX assuming the microbial uptake of the gas is unaffected by stopping aeration. k_La is calculated using the overall system mass balance and does not require previous knowledge of qX, as qX can be replaced in equation (2.35) with the following expression [5]:

$$qX = k_La\left(C^* - C_{Lss}\right) \tag{2.37}$$

where C_{Lss} is the dissolved gas concentration at steady state. Equation (2.35) then reduces to the following equation and can be directly solved for k_La:

$$\frac{dC_L}{dt} = k_La\left(C_{Lss} - C_L\right) \tag{2.38}$$

The instruments used in obtaining the liquid gas concentration data for this method depend on the gas required for the fermentation. For processes that utilize oxygen, typically an oxygen electrode is used, although in rare situations another dissolved oxygen measuring technique may be used. If an oxygen electrode is used, care must be taken to properly account for the probe dynamics as discussed earlier in Section 2.4.5 [2, 4]. For processes that utilize other gasses such as hydrogen or carbon monoxide, specialized measuring instruments or techniques must be employed. For example, dissolved carbon monoxide concentration data can be obtained using the bioassay presented earlier in Section 2.5.

Blanch [127] reported that the biological dynamic method is commonly used in both large and small scale equipment, primarily due to the fact that sterilizable oxygen probes permit the finding of k_La during a fermentation without significantly upsetting the system.

2.6.2.2 Non-Biological Dynamic Method

This method is similar to the biological dynamic method in that it employs the use of an inlet gas concentration step change, though it differs from the previous method as the system either has microorganisms that have been killed, had cell respiration blocked, or does not have any microorganisms present [51]. Commonly, this method is used for systems that contain no microorganisms at all [30, 97, 114].

The non-biological dynamic method begins by first removing the dissolved gas being studied from the vessel by (i) aerating the system with an inert gas such as nitrogen, (ii) using a vacuum to cause the dissolved gas to come out of solution, or (iii) adding a chemical compound to consume the dissolved gas. Once the dissolved gas has been removed, the system is then aerated and the change in gas concentration is recorded until steady state is reached.

Without cell respiration, the overall mass balance for the biological dynamic method simplifies from Equation (2.35) to Equation (2.33). k_La is then evaluated by integrating this relationship and plotting $\ln[(C^*-C_L)/(C^*-C_o)$ vs. t, where k_La is the slope of the resulting line or by curve fitting the data with a non-linear regression software package.

This method is reported to offer accurate results if the system being studied does not vary significantly from the actual system containing respiring microorganisms [51]. However, the accuracy of the results obtained using this method were reported to depend on the procedure used to initiate the concentration step change and electrode dynamics (if a dissolved oxygen electrode is used) [4, 109, 115, 128, 129].

2.6.2.3 Variations of the Inlet Step Change

While variations for each of the dynamic methods have been reported in the literature, the variation of greatest importance seems to be in how to initiate the change in the dissolved gas concentration. The remainder of this section will review the most popular techniques used to instigate a step change in the inlet gas concentration.

2.6.2.4 Gas Off/On or Startup

The gas off/on technique is used primarily for fermentations that have actively respiring cells. In such fermentation systems, the dynamic method is applied by turning the gas flow off and allowing the cells to deplete the dissolved gas until the critical gas concentration is reached and then the gas is turned back on (Figure 2.16).

One of the main advantages of using this technique is that the gas-liquid mass transfer is not affected by alternating the gas species, which has been reported to affect the calculation of k_La values [130]. Another advantage is the low cost associated with this technique as it requires no additional equipment. However, this method has a couple of limitations that must also be realized. First, this method must be done quite rapidly and with extreme care to ensure that cell respiration is not affect by the change in dissolved gas concentration. Second, when the gas is turned off and then on again, the system hydrodynamics are altered. Consideration must also be given to the time needed to once again reach steady state hydrodynamic behavior because if the startup time nears or exceeds the length of the experiment, then the method can not be used for calculating k_La [125]. For

example, in the extreme case when vessels are very large or have a height greater than one meter, the time to reestablish steady state gas holdup conditions may be larger than the characteristic k_La, resulting in inaccurate k_La estimates that are not representative of normal operation [4].

2.6.2.5 Gassing Out or Gassing In

Since dynamic methods are usually quite sensitive to the starting conditions of the experiment, a gas switching technique is used to eliminate hydrodynamic changes. The gassing out technique is one of the most widely used techniques for the dynamic method when a simulated fermentation broth is used. This technique, as the name implies, begins by aerating with one gas and then switching at $t = 0$ to a second gas. For example, in an air-water system, the system may first be aerated with air until the water is completely saturated, and then aerated with nitrogen to replace the oxygen in solution (Figure 2.17). A wide variety of gas pairs have been used in the application of this technique in the literature, though air-nitrogen is the most common gas pair.

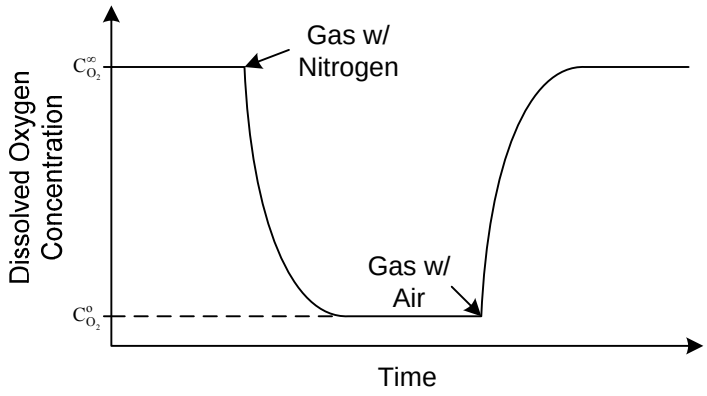

Figure 2.17: Typical dissolved oxygen concentration variation with time for the non-biological dynamic method, adapted from Blanch and Clark [127].

Van't Riet [4] reported that when deoxygenation with nitrogen was followed by an aeration switch, the average gas phase residence time (τ_g) must be considered as the gas phase concentration was no longer constant over the entire test. Van't Riet defined τ_g as:

$$\tau_g = \frac{H_v}{U_G}\left(\frac{\varepsilon}{1-\varepsilon}\right) \tag{2.39}$$

where H_v is the unaerated liquid height in the vessel, U_G is the superficial gas velocity, and ε is the gas holdup. If τ_g is the same order of magnitude as $1/k_La$, then the assumption of a constant gas phase concentration used to derive Equation (2.35) is no longer valid [97]. Models to correct for this behavior have been proposed by Dunn and Einsele [131] and Dang et al. [120]. These models have been reported to be only useful over a narrow range of conditions [4]. Linek et al. [130] reported that interphase nitrogen transport may significantly influence k_La estimations. Linek et al. [128] indicated that errors in k_La estimation due to nitrogen transport can be as high as 25% for large k_La. However, they also indicated that for low k_La values commonly encountered, the error due to nitrogen transport

may be negligible. Stenberg and Andersson [132] found that the change from nitrogen to air had a small, but significant, affect on k_La measurement, but this error was smaller than other observed experimental errors.

Lopez et al. [103] and Chang et al. [113] suggested that a gas pair of air and oxygen-enriched air be used to improve this technique by eliminating the need for pure nitrogen. Lopez et al. showed that k_La values measured with this technique closely matched those obtained for the gas off/on technique. Kim and Chang [111] indicated that the difference in inlet oxygen concentrations for this technique must be at least 20% in order to minimize errors.

2.6.2.6 Pressure Step

Another widely used form of the dynamic method is the pressure step technique where the gas concentration is changed by suddenly increasing or decreasing the system pressure. The system pressure is typically changed by a small amount, for example from 15 to 20 kPa, by the addition of gas into the reactor head space. The sudden pressure change is believed to instantaneously change the gas concentration in the gas phase throughout the vessel independently of system hydrodynamics.

The use of the pressure step technique was found by Blazej et al. [116] and Linek et al. [106] to be more accurate (by up to 60% for systems with noncoalescing liquids) in determining k_La values than the more popular gassing out technique. This increase in accuracy was attributed to model short comings related to the washing out of one gas by

another for systems with noncoalescing liquids. The k_La values for the gassing out and pressure step methods where found to be similar under some operating conditions. Linek et al. [109, 133] also reported that there was no difference in k_La values when gassing with air or pure oxygen, indicating that nitrogen transport was not a factor. They also reported that experimental results for this technique only match those from the gas off/on method for small values of k_La.

2.6.2.7 Non-Ideal Pressure Step

The non-ideal pressure step technique is slightly different from the pressure step technique. The difference in the two is that in the pressure step technique, the pressure change is considered instantaneous or ideal. In the non-ideal pressure step technique, however, the pressure step is actually achieved by throttling the exit gas stream to cause a pressure buildup, where the time lag for the pressure step depends on the gas flow rate and the vessel size. Linek et al. [128] compared this technique to the pressure step technique and reported that results from the two techniques agreed very well.

2.6.2.8 Concentration Step

The concentration step technique is a rarely used technique that deoxygenates the liquid phase by the addition of a small amount of a chemical compound like sulfite without interrupting aeration. This technique should not be confused with the chemical sorption methods as only a small amount of the compound is added with the intent of causing a

dissolved gas concentration step change. For this method to work properly, the system must be well mixed to ensure uniform dissolved gas concentrations. Also, care must be taken to ensure that the chemical compound being added does not alter the hydrodynamics or enhance mass transfer rates.

2.6.2.9 Dynamic Method Drawbacks

The dynamic methods are significantly affected by several factors:

(1) These methods assume that both the gas and liquid phases are well mixed. However, if either one of these phases is anything other than well mixed, which is often the case, especially for large or tall vessels, k_La accuracy decreases [127].

(2) Since air is commonly used for experimental purposes, the effect of simultaneous oxygen and nitrogen transport may affect the accuracy of experimentally determined k_La values [125, 128, 130, 132].

(3) Changing from one steady state to another, where the gas phase residence times are significant, will cause the k_La estimate to be inaccurate. This is especially true when the time to move from steady state conditions is of the same magnitude as $1/k_La$ [114, 125].

(4) The rapid change in dissolved oxygen concentrations with time may lead to oxygen electrode outputs that are not directly related to the instantaneous oxygen concentration unless the output is conditioned to adjust for electrode dynamics [114]. Tribe et al. [98] showed that neglecting electrode probe response time, while using

any of the dynamic measurement methods, would cause errors in k_La estimates, regardless of how much smaller τ_e is compared to $1/k_La$. They indicated that proper accounting for the electrode dynamics is needed for reliable measurements.

A comparison of methods done by Poughon et al. [126] concluded, without explanation, that the use of the dynamic method always results in an under prediction of k_La when compared to other methods, such as the gas balance and chemical sorption methods.

2.6.3 Chemical Sorption Methods

These methods are based on a chemical reaction between the absorbed gas and a chemical that is added to the liquid phase. Four of these methods will be presented here, although many others exist. The sulfite oxidation, hydrazine, and peroxide methods are applicable to systems studying oxygen transport, while the carbon dioxide absorption method, like its name implies, is for measuring dissolved carbon dioxide.

2.6.3.1 Sulfite Oxidation Method

The sulfite oxidation method is based on the oxidation of sulfite to sulfate in the presence of a catalyst, where dissolved oxygen is consumed by the reaction:

$$Na_2SO_3 + \tfrac{1}{2}O_2 \xrightarrow{\text{catalyst}} Na_2SO_4 \qquad (2.40)$$

Thus, to make this method work, the bulk fluid has to have a high concentration of sulfite and catalyst prior to aeration. Once aeration begins, any oxygen that dissolves into the fluid phase is immediately consumed by the sulfite reaction and the rate of sulfite oxidation

is proportional to k_La. Since the bulk fluid oxygen concentration remains at zero, k_La is given by:

$$-\frac{dC_{sulfite}}{dt} \approx k_L a \cdot C^* \tag{2.41}$$

The sulfite concentration in the bulk fluid is followed by taking liquid samples over a given time interval. The samples are then quenched with excess iodine and back titrated with thiosulfate to determine the residual iodine concentration and, subsequently, the sample sulfite concentration [97]. Then knowing the sulfite concentration change with time, Equation (2.41) can be used to determine k_La.

Chisti [2] and Blanch [127] reported that this technique had severe limitations. First, there is a need for expensive high purity chemicals. Second, the chemical reaction produces a highly ionic fluid that is non-coalescing. Third, sample analysis is often slow and tedious [97]. Fourth, the sulfite oxidation rate is very sensitive to fluid properties and impurities, thus the reaction rate depends on the type of catalyst used, its concentration, trace metals, temperature, and fluid pH. Hence, k_La determination requires that the reaction conditions be carefully controlled, the sulfite concentration kept sufficiently high, and excess of catalyst must be present in the bulk fluid to ensure that oxidation occurs in the bulk fluid and not at the gas-liquid interface [2]. Gogate and Pandit [125] indicated that this method is not suitable for use in systems using pure oxygen because bubble size in the system changes dramatically by the high chemical reaction rate. Van't Riet [114] also reported that the reaction rate constant can vary in unknown ways and that this method should be avoided.

2.6.3.2 The Hydrazine Method

The steady state hydrazine (N_2H_4) method makes use of the following reaction [2]:

$$N_2H_4 + O_2 \rightarrow N_2 + H_2O \tag{2.42}$$

This method uses a steady flow of hydrazine into an aerated reactor. The dissolved oxygen concentration is then followed by an oxygen electrode. The intent of this method is to introduce hydrazine into the system at a rate equal to k_La which, when accomplished, keeps the electrode signal at a constant level. The rate at which hydrazine is consumed is equal to k_La.

The reaction in Equation (2.42) does not form ionic species, therefore the system hydrodynamics are not affected during the course of the test, unlike the sulfite oxidation method. [2].

2.6.3.3 Peroxide Method

The peroxide method is based on the following chemical reaction where oxygen is produced in the reactor liquid:

$$2H_2O_2 \xrightarrow{\text{catalase}} 2H_2O + O_2 \tag{2.43}$$

The oxygen is transferred to a carrier gas that is used to transport the oxygen out of the system. Under steady state conditions, the oxygen production is equal to the oxygen transfer rate. To calculate the oxygen transfer rate, only the peroxide inlet flow rate and concentration, liquid volume, carrier gas flow rate, and dissolved oxygen concentrations are needed at steady state conditions. This method uses catalase enzymes that are known to

enhance foam formation and alter the gas bubble diameter which is a severe limitation when considering the use of the method [125].

2.6.3.4 Carbon Dioxide Absorption Method

Another commonly employed chemical technique is the absorption of carbon dioxide into a mild alkaline or an appropriately buffered solution [134]. The carbon dioxide method is similar in principle and procedure to the sulfite oxidation method. Chisti [2] indicated that the limitations for this method where similar to those of the sulfite oxidation method.

2.7 Summary

Hydrodynamics of EALRs have been extensively studied in the last three decades. This has led to improvements in EALR design and created a knowledge base useful in understanding how design and operating parameters may influence EALR operation (e.g., Figure 2.11). However, there remains a need to further understand these relationships because each EALR has unique characteristics that affect gas-liquid mass transfer and system hydrodynamics. Additionally, a significant effort has been put into understanding how to accurately measure oxygen gas-liquid mass transfer rates. While much has been suggested on this subject, most of which is contradictory, past work provides useful information about the pros and cons of the most common methods used to determine oxygen gas-liquid mass transfer that can be used in developing an appropriate measurement technique for any given situation. Furthermore, it was found that very little work has been completed to develop

techniques for measuring gas-liquid mass transfer rates for gas species other than oxygen. The goal of this work is to build upon the existing knowledge base and to further develop the understanding of EALR transport theory needed to promote the future use of EALRs in bioprocessing applications.

CHAPTER 3: EQUIPMENT AND EXPERIMENTAL METHODS

This chapter describes the experimental equipment and methods used in this research. It is divided into nine sections: external airlift loop reactor setup, visual flow observations, gas holdup measurement, superficial liquid velocity measurement, dynamic gassing method, dissolved oxygen measurement, dissolved carbon monoxide measurement, k_La determination, and measurement uncertainty.

3.1 External Airlift Loop Reactor Setup

The bioreactor used in this research (Figure 3.1) is a custom made external airlift loop reactor (EALR). A schematic representation of this reactor is shown in Figure 3.2. The EALR consists of two main parts, a 2.4 m cast acrylic riser with a 10.2 cm ID, and a 2.4 m cast acrylic downcomer with a 2.5 cm ID, giving the EALR an aspect ratio (AR) of 1:16. The downcomer and riser sections are connected with two 13.3 cm cast acrylic tubes with 2.5 cm ID located at H = 5 and H = 127 cm, where H is the height above the aerator plate. The location of the top connector tube fixes the EALRs effective reactor height at H_e = 127 cm (12.5 column diameters).

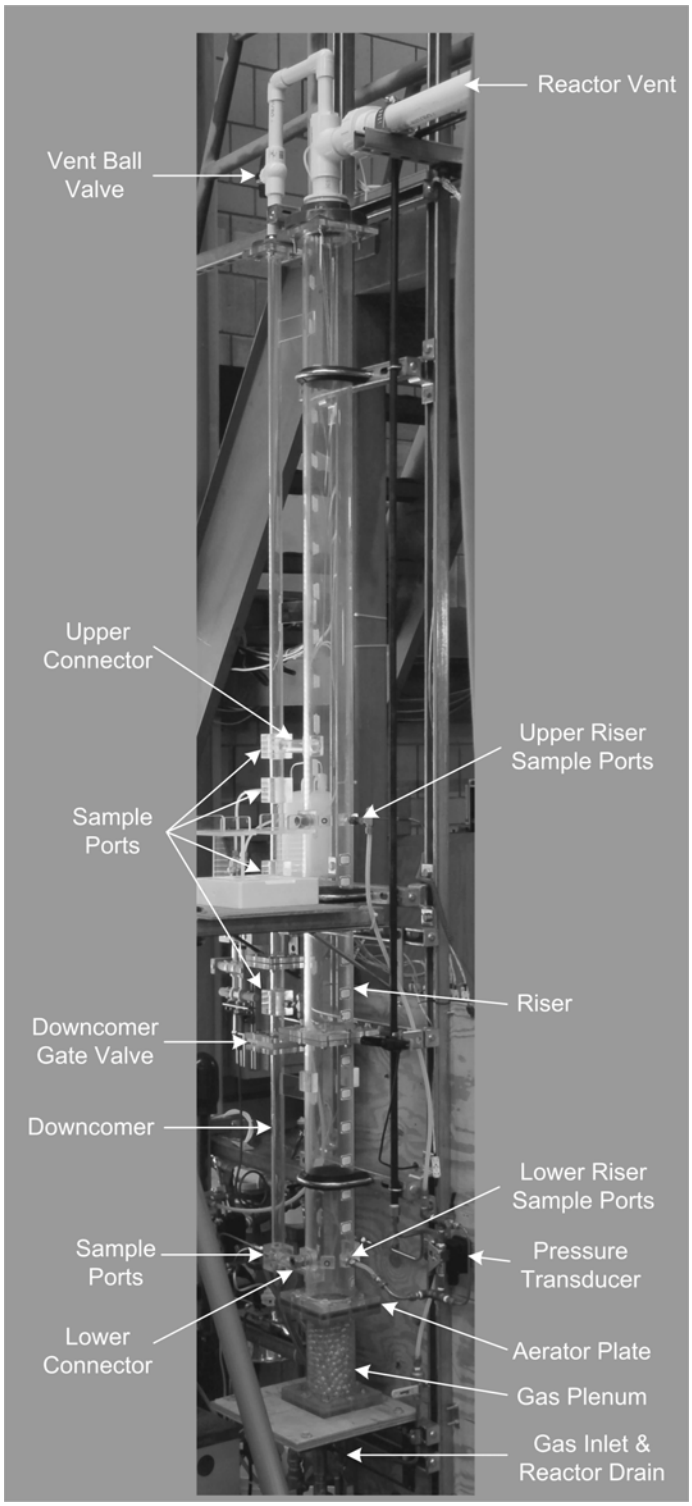

Figure 3.1: External airlift loop reactor used in this study.

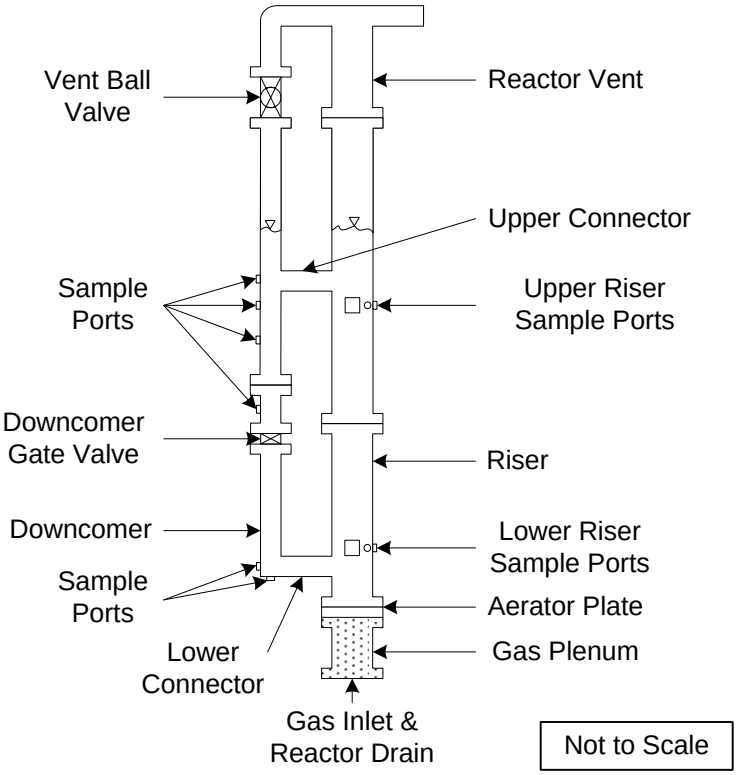

Figure 3.2: Schematic representation of the external airlift loop reactor showing the key components.

A gas plenum is located beneath the aerator plate and filled with large glass beads (i.e., marbles) to promote uniform gas distribution through the aerator plate into the riser. The top of the riser and downcomer sections are joined together with a ball valve as they enter the reactor vent; this allows for the possibility of gas flow out of the downcomer. A gate valve is installed in the middle of the downcomer section so that when closed, the EALR approximates a semi-batch BCR.

The EALR is fitted with 14 sample ports of which eight are in the riser and six are in the downcomer. The sample ports in the riser are located at H = 10.2 and 110.5 cm with 4 ports at each height, one each on the front, back and side of the EALR with the last port

located between the front and side port (Figure 3.3). The front ports are 2.5 cm in diameter and used for dissolved carbon monoxide samples. The side and back ports are 1.1 cm in diameter and are used for measuring temperature and pressure. The ports located between the front and side ports are 0.1 cm in diameter and used for measuring the dissolved oxygen partial pressure. The sample ports on the downcomer are located at H = 5.0, 67.2, 97.8, 108, and 127.0 cm with 2 ports at 67.2 cm. These ports are 1.1 cm in diameter and are used for measuring conductivity (H = 98.7 and 67.2 cm), pressure (H = 5.0 and 67.2 cm), and injecting salt tracers (H = 108 cm). The EALR is also fitted with three other ports, one on the bottom of the downcomer and two on the bottom of the riser that are used for filling and draining the EALR with water and for introducing aeration gas.

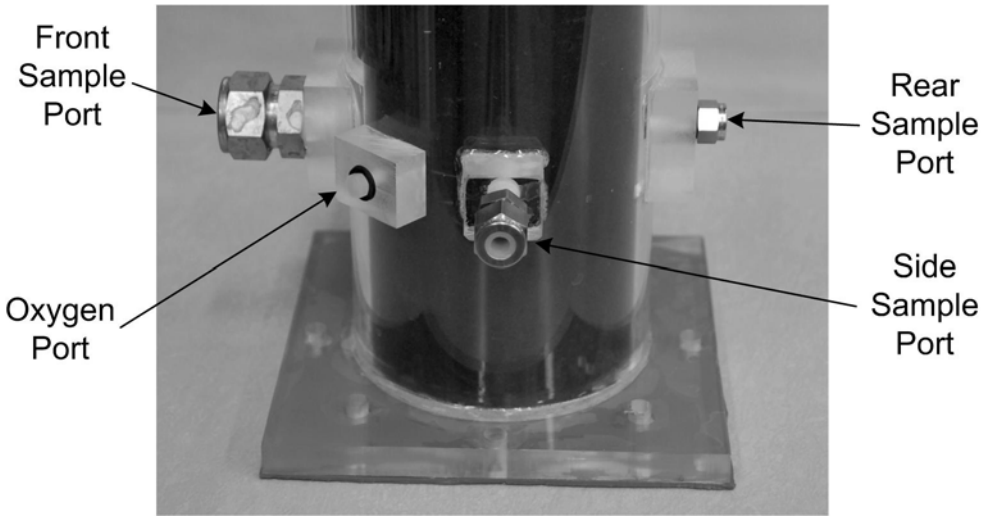

Figure 3.3: Close up view of the external loop airlift reactor riser showing the layout of the sample ports on the riser.

The EALR is aerated with compressed gas from one of several sources depending on the test. Compressed air is supplied by the Iowa State University physical plant. Prior to

use, the air is filtered to remove moisture, oil, and debris. Ninety-nine percent pure compressed nitrogen and carbon monoxide are purchased in 255 cubic feet cylinders from the Iowa State University Chemistry Stores and connected to the gas delivery system using the appropriate gas cylinder regulators. The compressed gas lines are connected to the EALR gas plenum via a pressure regulator, two gas mass flow meters, and a needle valve (Figure 3.4). The pressure regulator is used to maintain a constant working pressure of ~22 psi across the mass flow meters. The first gas mass flow meter is an Aalborg model GFM37S meter with a flow range of 0 to 30 L/min and the second is an Aalborg model GFM471S meter with a flow range of 0 to 100 L/min. These meters are connected to the pressure regulator and needle valve with ball valves such that the small and large meters can be used to measure low (0 to 30 L/min) and high (30 to 100 L/min) inlet gas velocities, respectively. The needle valve is used to adjust the inlet volumetric gas flow rate from 0 to 100 L/min, which corresponds to a superficial gas velocity range of 0 to 20 cm/sec.

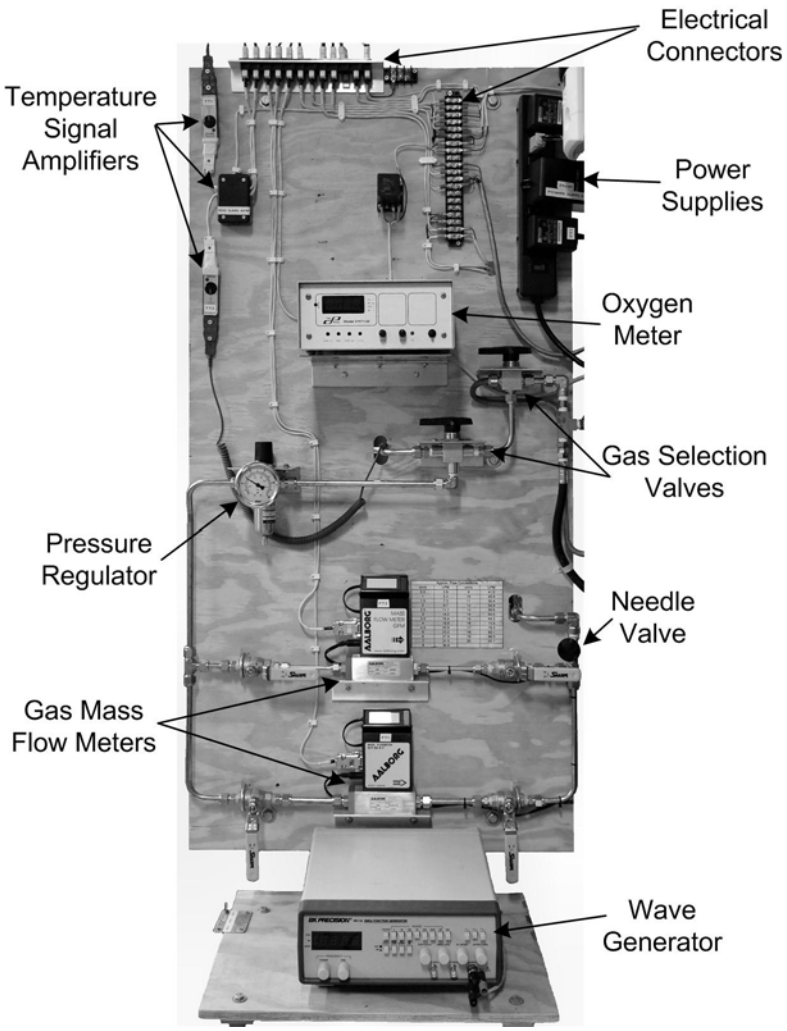

Figure 3.4: Experimental instrumentation panel.

3.1.1 Data Acquisition System

The data acquisition system is composed of a personal computer, a National Instruments 6030E E series multifunction data acquisition card, National Instruments SCB-68 shielded connector block, National Instruments LabView 7.0 data acquisition software, several 24 VDC power supplies, a temperature amplifier, and various other electrical components.

The data acquisition system is used to monitor and record EALR parameters such as temperature, riser pressures, conductivity, volumetric gas flow rates, and dissolved oxygen partial pressure. The system is also used to control the salt tracer injector and to provide test timing. At the heart of the data acquisition system are several software programs written with LabView 7.0. These programs are used to automate the data collection process to reduce test taking time and to improve data repeatability.

3.1.2 Working Fluid/Water Quality

Water is the primary working fluid used in the reactor. The water used in this work includes unconditioned tap water, deionized tap water, and treated deionized tap water. The unconditioned tap water is used in the initial tests to observe visual fluid flow patterns and reactor hydrodynamics. The deionized and treated deionized tap is used to study gas-liquid mass transfer and reactor hydrodynamics, and is maintained at 20 °C. The pure deionized water is studied to eliminate ionic compounds that were shown in Sections 2.3.6 and 2.3.7 to significantly affect gas-liquid mass transfer rates and hydrodynamics. The treated deionized water is then studied to understand how mass transfer and hydrodynamics are affected by inorganic compounds and surfactants. The deionized water treatments include (i) adding 5.11 gm of potassium chloride (KCl) per liter of water to create a 0.07 M KCl solution, (ii) adding 1.34 gm dibasic sodium phosphate (Na_2HPO_4), 0.77 gm monobasic potassium phosphate (KH_2PO_4), 0.5 gm sodium bicarbonate ($NaHCO_3$), and 2.5 gm ammonium sulfate ($[NH_4]_2SO_4$) per liter water to create a 0.04 M nitrosomonas solution (typical inorganic

fermentation media), and (iii) adding an unknown surfactant species and concentration. (Note: the addition of the surfactant was unknown at the time of testing and therefore little is known about the surfactant concentration or composition; however, the results for tests using this media justify their inclusion.)

The reactor is filled to a liquid height of 142.2 cm (14 column diameters) for all tests preformed as part of this work.

3.1.3 Aerator Plates

Gas is injected at the riser base through the gas plenum using one of three 11.4 cm circular stainless steel aerator plates having open area ratios A = 0.62, 0.92, 2.22% (Figure 3.5). Each plate has 1 mm diameter holes that are uniformly distributed over the entire plate area, where the change in open area is accomplished by changing the number of uniformly distributed holes (Table 3.1).

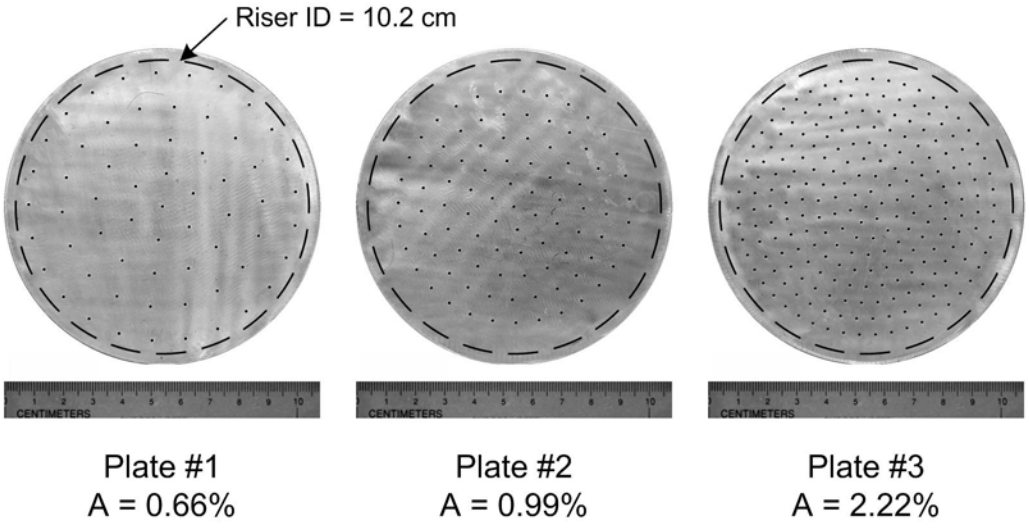

Figure 3.5: Aerator plates used in the external airlift loop reactor.

Table 3.1: The aerator plate open area ratios and corresponding 1 mm orifice count used in the external airlift loop reactor.

	Open Area Ratio	Orifice Diameter	Number of Orifices
Plate #1	0.62%	1 mm	62
Plate #2	0.92%	1 mm	95
Plate #3	2.22%	1 mm	224

3.1.4 Superficial Gas Velocity

The EALR is operated using a superficial gas velocity (U_G) that ranges between 0.5 to 20 cm/s. Table 3.2 shows which U_G were used in the different experiments performed as part of this work.

Table 3.2: The superficial gas velocities used this work.

	Tap Water		Deionized and Treated Water[a]			Treated Water[b]	
U_G (cm/s)	Visual Observations	Hydrodynamic	Hydrodynamic	Oxygen Mass Tranfer	Carbon Monoxide Mass Transfer	Oxygen Mass Tranfer	Carbon Monoxide Mass Transfer
0.5	X	X	X	X		X	X
1.0	X	X					
1.5	X	X					
2.0	X	X	X	X	X	X	X
2.5	X	X					
3.0	X	X					
3.5	X	X					
4.0	X	X	X	X		X	X
4.5	X	X					
5.0	X	X					
6.0	X	X	X	X	X	X	X
7.0	X	X					
8.0	X	X	X	X		X	X
9.0	X	X					
10.0	X	X	X	X	X		
11.0	X	X					
12.0	X	X	X	X		X	X
13.0	X	X					
14.0	X	X	X	X	X		
15.0	X	X					
16.0	X	X	X	X		X	X
17.0	X	X					
18.0	X	X	X	X			
19.0	X	X					
20.0	X	X	X	X		X	X

a The treated water in these tests includes the 0.07 M KCl and 0.04 M Nitrosomonas solutions.

b The water in this test is the deionized water containing a surfactant.

3.1.5 Reactor Modes of Operation

The EALR is operated in one of three operational modes (open vent mode, closed vent mode, and bubble column mode) set by closing and opening the gate valve in the downcomer and the ball valve in the reactor vent (Figure 3.1 and Figure 3.2). The open vent mode (OV mode) is set by opening the gate valve in the downcomer and the ball valve in the reactor vent (Figure 3.6a) allowing the aeration gas to exit the reactor via both the riser and downcomer vents. The closed vent mode (CV mode) is set by opening the downcomer gate valve and closing the ball valve in the reactor vent (Figure 3.6b) only allowing the aeration gas to exit the reactor through the riser vent. The bubble column mode (BC mode) is achieved by closing both the gate valve in the downcomer and the ball valve in the reactor vent (Figure 3.6c) allowing the aeration gas to exit only through the riser vent and further restricting the system hydrodynamics by removing the fixed fluid circulation path through the downcomer.

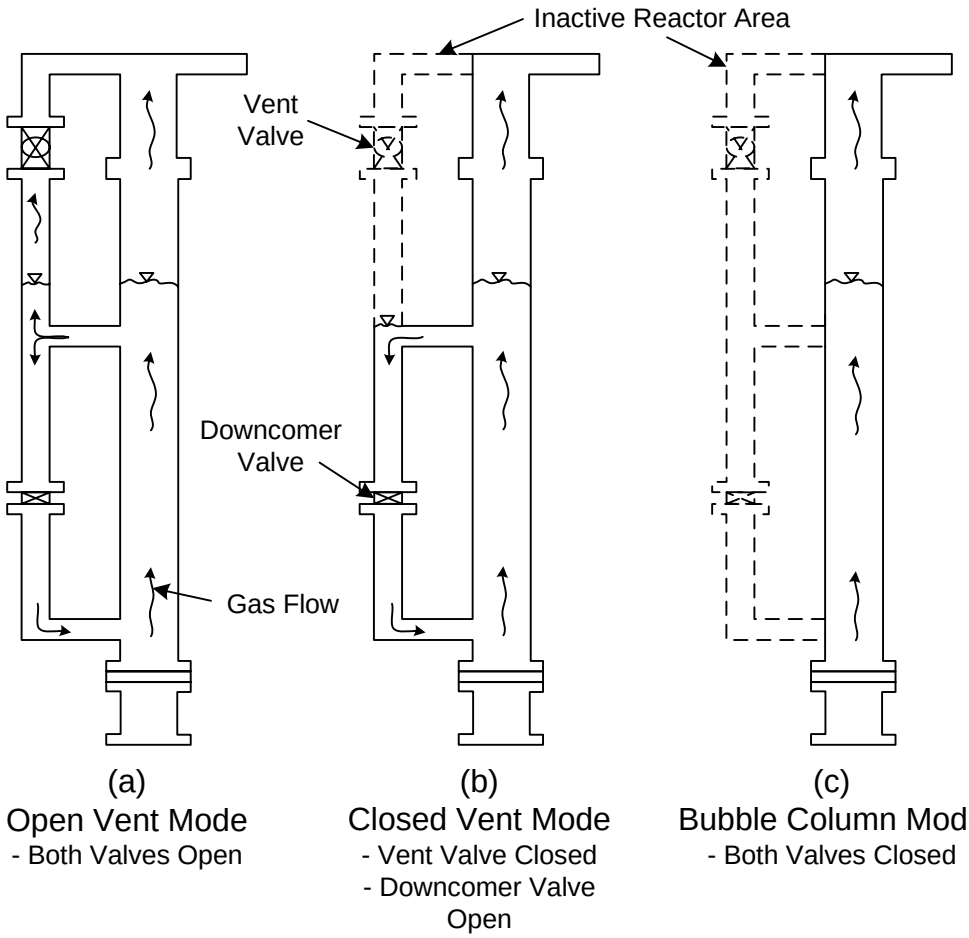

Figure 3.6: Schematic representation of the external airlift loop reactor illustrating the three possible operational modes; open vent mode, closed vent mode, and bubble column mode.

3.2 Visual Flow Observations

Changes in operation mode and inlet superficial gas velocity alter the observable flow patterns in the EALR. The changes in observed flow patterns are quantified using high speed digital photography.

3.2.1 Visual Flow Observation – Experimental Setup

A Nikon digital SLR camera (D50) equipped with a Tamron zoom lens (AF18-200mm F/3.5-6.3 XR Di II) is used to capture still images of the fluid flow patterns. The camera is placed ~60 cm in front of the upper or lower tube connector. Attached to the camera is a remote flash unit (Minolta 132PX) that is synced with the camera shutter. The flash is used to provide back lighting for the picture using a light diffuser made from vellum and acrylic. The diffuser is placed directly behind the upper or lower tube connecter and the remote flash is located at the upper edge of the diffuser. Additional fore lighting is provided by a 250 watt halogen work light placed ~90 cm below the camera. In order to freeze the moving gas bubbles in the EALR, the camera is set to operate at its quickest shutter speed (Tv = 1/4000 sec) with the f-stop set nearly wide open (Av = 20).

3.2.2 Visual Flow Observation – Method

To collect the desired pictures to document the liquid flow behavior in the upper and lower tube connector, the flowing method is used. With the camera and equipment setup and ready to go, the EALR is filled with water to H = 142.2 cm. The aeration gas is turned on and set to the desired inlet superficial gas velocity. Flow conditions in the EALR are allowed to reach steady state by letting the EALR operate for two minutes, and then three pictures are taken at 30 second intervals. This procedure is then repeated for the next operating condition.

Photographs documenting the fluid flow behavior in the upper and lower tube connectors are taken for all three modes of operation and for inlet superficial gas velocities as shown in Table 3.2 for a total 432 photographs. The water used for this test is unconditioned tap water.

3.3 Gas Holdup Measurement

Gas holdup in the riser and downcomer are two of three hydrodynamic parameters tracked during this research. Gas holdup is related to the pressure drop in the reactor by assuming that the acceleration effects are negligible [2]. Thus the total pressure drop in the reactor corresponds to the hydrostatic head.

3.3.1 Riser Gas Holdup (ε_r)

Gas holdup in the riser section (ε_r) is measured between the upper and lower ports on the riser (H = 10.2 and 110.5 cm) using one of two methods. For the tap water tests, two pressure transducers are used to measure the local pressure head at the upper and lower ports (Dwyer Instruments, Inc. models 673-2 and 673-3). These transducers provide a 4 to 20 mA output signal that is proportional to hydrostatic head (cm H_2O) when excited by a 24 VDC power supply. The output signal of the transducers is followed by the data acquisition system.

Average riser pressures are computed from measurements taken over a two second interval at a sampling frequency of 1000 Hz. For each operating condition 100 average riser

pressures are collected and stored to a data file. Following each experimental test the pressure data is used to calculate the overall average riser pressure difference (ΔP). ε_r is then calculated using the following relationship derived in Appendix A:

$$\varepsilon_r = 1 - \frac{\Delta P}{\Delta P_o} \tag{3.1}$$

where ΔP_o is the liquid hydrostatic head when $U_G = 0$ cm/s.

For all other tests, a single differential pressure transducer (Cole-Parmer model U-68071-54) is used to measure the differential pressure between the lower and upper ports on the riser. This transducer likewise provides a 4 to 20 mA output signal that is proportional to the differential hydrostatic head when excited by a 24 VDC power supply. The output of the transducer is followed by the data acquisition system.

The average riser differential pressure is computed from measurements taken over a 0.1 second interval at a sampling frequency of 1000 Hz. For each operating condition at least 1200 average riser differential pressures are collected and stored to a data file. Following each experimental test the differential pressure data is used to calculate the overall average riser differential pressure difference (dP_r). ε_r is then calculated using the following relationship derived in Appendix A:

$$\varepsilon_r = \frac{dP_r}{\Delta h_r} \tag{3.2}$$

where Δh_r is the distance between the riser ports used by the differential pressure transducer.

3.3.2 Downcomer Gas Holdup (ε_d)

Gas holdup in the downcomer section (ε_d) is measured using one of two methods. For the tap water tests an inclined U-tube manometer is used while for all other tests a differential pressure transducer identical to the one on the riser is used to determine downcomer gas holdup.

The inclined U-tube manometer is connected to the downcomer at H = 5.0 and 67.2 cm or at H = 5.0 and 97.8 cm for CV and OV mode, respectively. The change in height of the water columns in the manometer is recorded by hand. For each operating condition the number of collected samples varied depending on U_G and the mode of operation as shown in Table 3.3 (due to the magnitude of the water column vibration in the manometers). At the conclusion of each test, the average height change (Δh_m) is calculated and used to determine ε_d using the following relationship:

$$\varepsilon_d = \frac{\rho_L}{\rho_L - \rho_G} \frac{\Delta h_m}{\Delta h_d} \tag{3.3}$$

where ρ_L is the liquid density, ρ_G is the gas density, and Δh_d is the distance between the downcomer ports used by the manometer.

Table 3.3 Number of samples taken to determine downcomer gas holdup.

Operation Mode	U_G (cm/s)	# Samples
Open Vent Mode	0.5 - 2.0	5
Open Vent Mode	2.5 - 9.0	10
Open Vent Mode	10 - 20	20
Closed Vent Mode	0.5 - 20	10
Bubble Column Mode	N/A	N/A

The downcomer differential pressure transducer is connected in place of the inclined U-tube manometer and connected to the downcomer at H = 5.0 and 67.2 cm. Data collection and processing to determine the downcomer gas holdup using the differential pressure transducer uses the same method outlined in Section 3.3.1 for riser gas holdup where Δh_r in Equation (3.2) is replaced with Δh_d.

3.4 Superficial Liquid Velocity Measurement

The superficial liquid velocity (U_L) is the remaining hydrodynamic parameter tracked in this research. Since U_L can not be directly measured, it is determined from a knowledge of the linear liquid velocity (V_L) and gas holdup. Like gas holdup, U_L and V_L have both riser and downcomer components, yet the riser superficial liquid velocity (U_{Lr}) is the parameter of greatest interest and the one commonly reported in the literature.

The determination of riser and downcomer U_L is often accomplished using a tracer technique or specially calibrated flow meters and mathematical relationships to convert the measurable V_L to U_L (see Section 3.4.4). The tracer techniques commonly used to determine V_L are based on determining the time it takes for a given tracer to travel a set distance. For this work, a potassium chloride salt tracer was selected and conductivity electrodes are used to measure the time it takes an injection of the salt solution to travel past two fixed locations [2, 4, 37, 48, 135, 136].

3.4.1 Test Equipment

To employ the tracer method in this research, the following equipment is used: (i) a salt solution injector, (ii) two conductivity electrodes, (iii) a function generator, and (iv) the data acquisition system.

The salt solution injector shown in Figure 3.7 consists of two 10 mL syringes, an air solenoid, four one-way valves, and a salt solution reservoir (not shown). The injector is powered by an air cylinder with a 1.3 cm maximum stoke that is capable of instantaneously injecting the salt solution into the EALR. The air cylinder is activated by an air solenoid valve controlled via the data acquisition system. The syringes in the injector serve two functions. One of the syringes is used to deliver ~2 mL of the salt solution to the injection port on the EALR and the other syringe is used to remove an equivalent volume of liquid from the riser of the EALR. The action of these two syringes is simultaneous and prevents any change in the overall liquid volume in the EALR during velocity measurement.

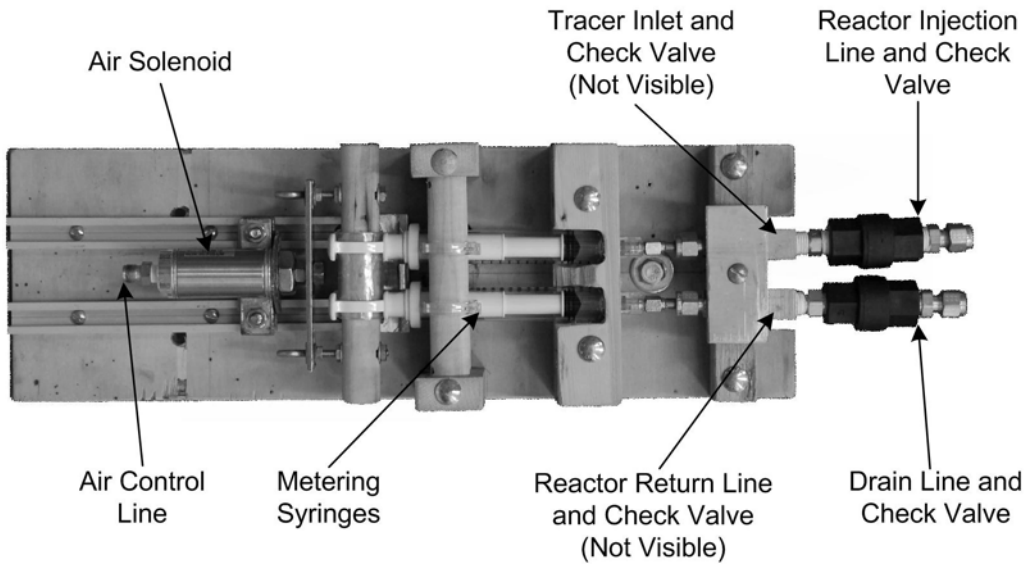

Figure 3.7: Salt solution injector used to measure the linear velocity in the downcomer.

The conductivity electrodes (Figure 3.8) are supplied by Microelectrodes, Inc. These electrodes are custom built to have similar response properties and dimensions compatible with the EALR. The conductivity electrodes both have a 0.6 cm outside diameter and equal electrode constants (K = 1.0). The output of the electrodes is proportional to the ability of the ions in the liquid to conduct an electric current. Therefore, an increase in the concentration of conducting ions will result in an increase in the electrode output signal. A BK Precision function generator (model 4011A 5Mz function generator) provides the AC current needed to power the electrodes (a 5 kHz square wave). The output signal of the electrodes is followed by the data acquisition system.

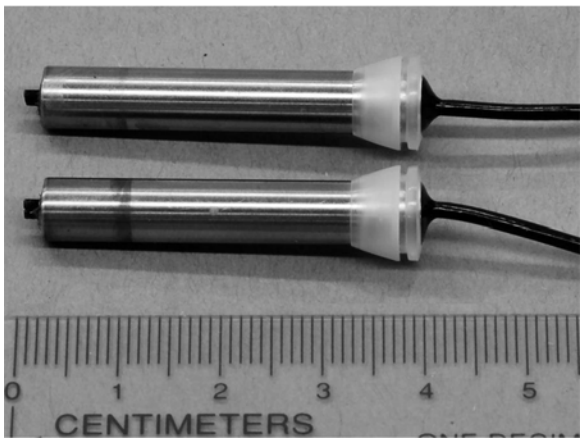

Figure 3.8: Microelectrode, Inc. miniature conductivity electrodes.

3.4.2 Test Reagents

The salt solution used as the chemical tracer in this method is a 0.34 M potassium chloride solution. The salt used in this test is a 99.9% pure potassium chloride obtained from Fisher Scientific. The salt solution is prepared by adding 100 g potassium chloride to four

liters of deionized water. The salt and water are mixed and stored in the salt solution reservoir.

3.4.3 Linear Velocity Measurement

The experimental method to determine the average linear liquid velocity in the downcomer (V_{Ld}) is as follows. Before an experiment is initiated, the salt solution reservoir is filled. The EALR is filled to H = 142.2 cm. The gas is turned on and the gas flow rate is set to the desired operating point and run for approximately two minutes to ensure steady state conditions. Once steady flow is achieved, data collection is initiated. Data is collected by first injecting two milliliters of the salt solution into the downcomer at the injector port and simultaneously withdrawing two milliliters of liquid at the base of the riser using the injector. Second, the concentration response at each of the conductivity electrodes is then followed for 10 seconds using the data acquisition system set to sample the electrode outputs at 50 kHz (Figure 3.9). Third, the time interval between the conductivity peaks (t_p) is determined using LabView 7.0 (National Instruments data acquisition software). To obtain t_p, the steady state and peak conductivities are estimated for both electrode responses using signal processing functions built into LabView. The steady state and peak conductivities are then used to identify a 10% of steady state conductivity threshold for each electrode response. t_p is then found as the time between the points where the rising electrode responses cross the conductivity thresholds (Figure 3.9). The sampling frequency used to follow the electrode signal allows t_p to be resolved with an accuracy of ±0.0001 seconds. Using the

measured t_p and the known distance between the conductivity electrodes (d_e), V_{Ld} is determined by:

$$V_{Ld} = \frac{d_e}{t_p} \tag{3.4}$$

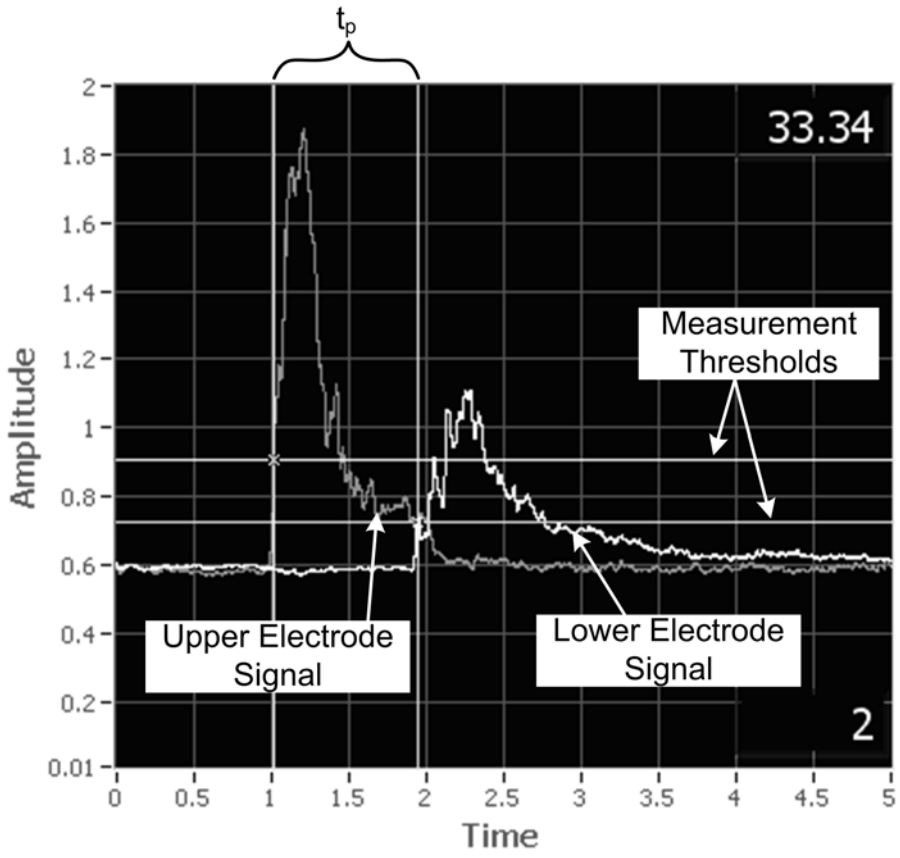

Figure 3.9: Typical conductivity electrode responses used to find the linear velocity.

The use of two identical conductivity electrodes eliminates the need to consider the response time of the electrodes [2, 137]. The data collection steps are repeated 50 times. At the completion of the 50 injections, the EALR is drained, rinsed, and refilled with fresh water. The data collection process is repeated three times for each gas velocity of interest using a randomly generated testing sequence.

3.4.4 Superficial Liquid Velocity Calculations

The superficial liquid velocity in the downcomer (U_{Ld}) and riser (U_{Lr}) are calculated from the following analytical relationships [2]:

$$U_{Ld} = (1-\varepsilon_d)\overline{V}_{Ld} \tag{3.5}$$

$$U_{Lr} = AR \cdot U_{Ld} \tag{3.6}$$

where $\overline{V}_{Ld}$ is the average of 50 V_{Ld} data points taken for the gas velocity of interest and ε_d is the corresponding downcomer gas holdup.

3.5 Dynamic Gassing Out Method

In order to determine gas-liquid mass transfer rates, there has to be a change in the steady state gas concentration, which in turn causes the dissolved gas concentration to change. The change in dissolved gas concentration then is used to determine mass transfer rates. To accomplish a step change in the EALR gas concentration, one of the many methods presented earlier in the literature review may be used. This work uses the dynamic gassing out method to provide the needed gas concentration step change. Two variations of this method are used depending on the gas species being studied.

3.5.1 Basic Dynamic Gassing Out Method

The basic dynamic gassing out method utilizes two gas species, air and pure nitrogen (realizing that air is technically a mixture of several gas species). The application of this method involves using one or more repetitions of the following five step cycle.

(1) The system is brought to a steady state operating condition where air is used as the sparging gas species.

(2) Once the air steady state condition has been obtained and maintained for several minutes, the sparging gas is switched to nitrogen and the system is allowed to progress to a nitrogen steady state condition.

(3) The system is allowed to reach the new steady state condition and is kept at this state for a several minutes.

(4) Next the sparging gas is changed back to air and the system allowed to return to its initial steady state condition.

(5) After steady state is once again achieved, it is maintained for several minutes.

Figure 3.10 shows the dissolved gas concentration in the liquid phase and denotes the basic dynamic gassing out method.

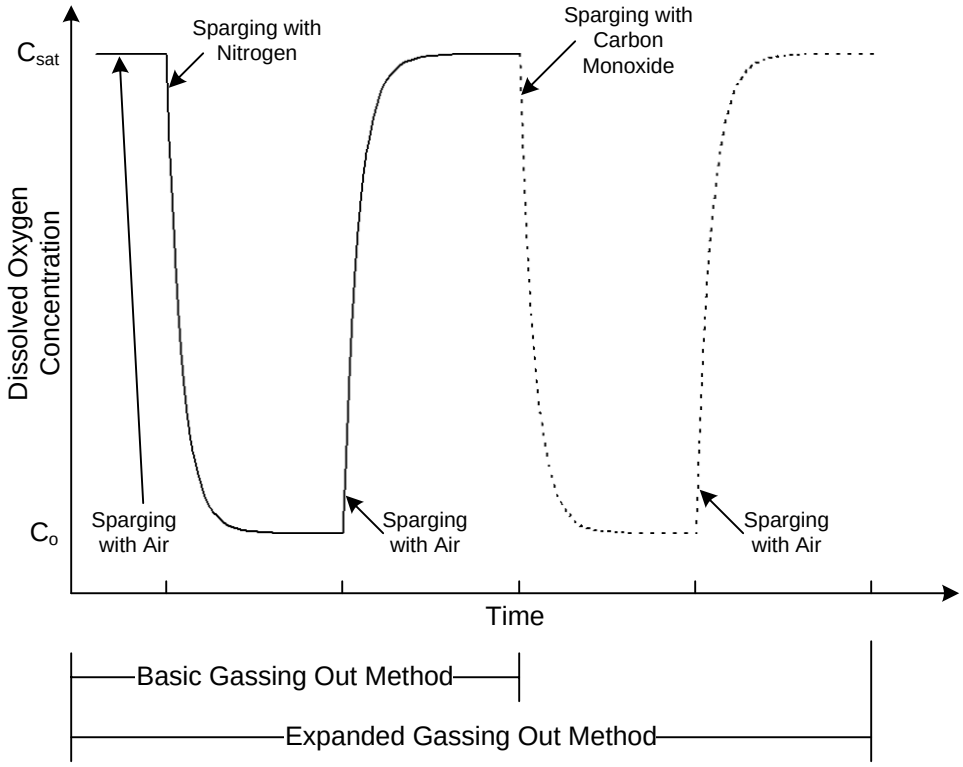

Figure 3.10: Generic dissolved oxygen concentration as a function of time for the basic and the extended gassing out methods.

3.5.2 Expanded Dynamic Gassing Out Method

The extended dynamic gassing out method is similar to the basic dynamic gassing out method with the addition of another gas species, pure carbon monoxide. The application of this method involves adding four steps to the end of the five step cycle used in the basic dynamic gassing method. First, the basic dynamic gassing out method is completed as described above using air and nitrogen. After the 2nd air steady state has been maintained for a short length of time, the sparging gas is switched to pure carbon monoxide and the system is allowed to shift to a new steady state condition. This steady state condition is maintained for several minutes, and then the sparging gas is once again switched back to air. The system

is now allowed to shift back to the air steady state condition where it is once again held for several minutes. Figure 3.10 also depicts the dissolved gas concentration in the liquid phase for the expanded dynamic gassing out method.

3.5.3 Dynamic Gassing Out Method – Step Time

The length of time associated with each of the steps in the two dynamic gassing out methods varies with the inlet superficial gas velocity and is experimentally determined to ensure that steady state conditions are achieved. Typically, 10 minutes is required to reach steady state for U_G = 0.5 cm/s while only 1.5 minutes is needed when U_G = 20 cm/s.

3.6 Dissolved Oxygen Measurement

The dynamic gassing out method is employed to measure the dissolved oxygen as a function of time. A review of this method may be found in Section 2.6.2.

3.6.1 Experimental Equipment

Dissolved oxygen concentrations are measured using a Diamond General Development Corp. 730 mini Clark-style oxygen electrode (Figure 3.11). The mini oxygen electrode measures 3.2 cm long by 3.2 mm in diameter. The cathode is an exposed section of 0.1 mm pure platinum wire in a fused glass seal and the anode is the silver electrode body coated with a chloride layer. The electrode has a polyethylene membrane that is sealed with an o-ring over a drop of electrolyte solution on the electrode tip. The oxygen electrode is connected to a Cole Parmer benchtop dissolved oxygen meter (model 01971-00) that supplies

the polarization voltage and measures the electrode output current. The electrode current, which is proportional to the dissolved oxygen partial pressure, is converted to a percent of saturation by the meter and output as a 4 to 20 mA signal. The oxygen meter output is followed with the data acquisition system.

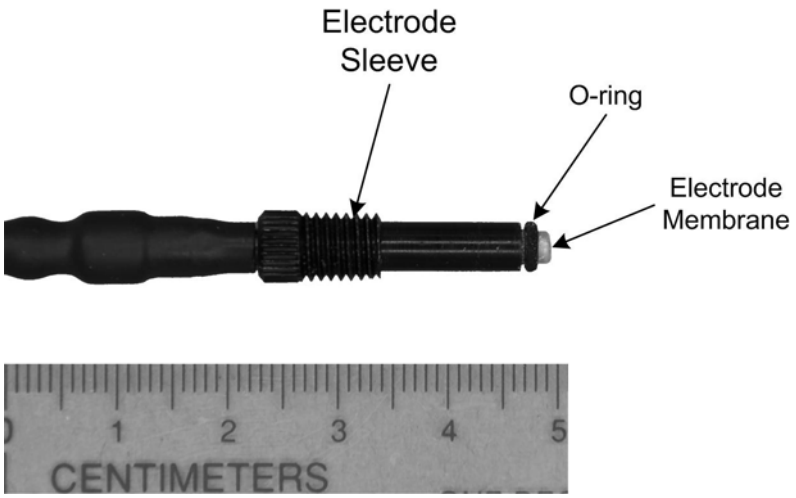

Figure 3.11: Diamond General Development Corp. dissolved oxygen electrode.

3.6.2 Electrode Preparation

The oxygen electrode output current depends on the electrolyte layer thickness, electrolyte purity, the electrode tip condition, the polarizing voltage, the oxygen permeability of the membrane, and the oxygen partial pressure in the bulk fluid. As all but the last one of these factors is related to electrode physical condition, the condition and setup of the oxygen electrode is of great importance.

3.6.2.1 Electrode Electrolyte

The electrolyte solution used with this oxygen electrode is a ~50% saturated potassium chloride solution. The electrolyte solution is prepared using 100 mL of deionized water and 15 g of pure potassium chloride. Since purity is more critical than concentration, a new electrolyte solution is prepared on a weekly basis and stored in an air tight container.

3.6.2.2 Electrode Maintenance

Electrode maintenance of some sort is performed on a daily basis, using the equipment shown in Figure 3.12. The type of maintenance performed depends on a visual inspection of the electrode and the behavior of the output signal. Each day the electrode tip is inspected to ensure that the electrode tip is a dull gray/brown color which indicates that the chloride layer is still intact. If the electrode tip is another color, typically white, the electrode must be cleaned and reconditioned, see Section 2.4.5 for more details. Usually the tip color is the proper color and only requires reconditioning about every two weeks depending on the amount of use. The electrode is also visually inspected to see if the membrane has any visible tears or if air bubbles exist within the electrolyte solution. If a tear or air bubble exists, the membrane and electrolyte are replaced. Also, if the output of the electrode for a known steady state condition is noticed to be inconsistent with expected results, or if the signal is observed to drift significantly over a short time period, the electrode membrane and electrolyte are replaced.

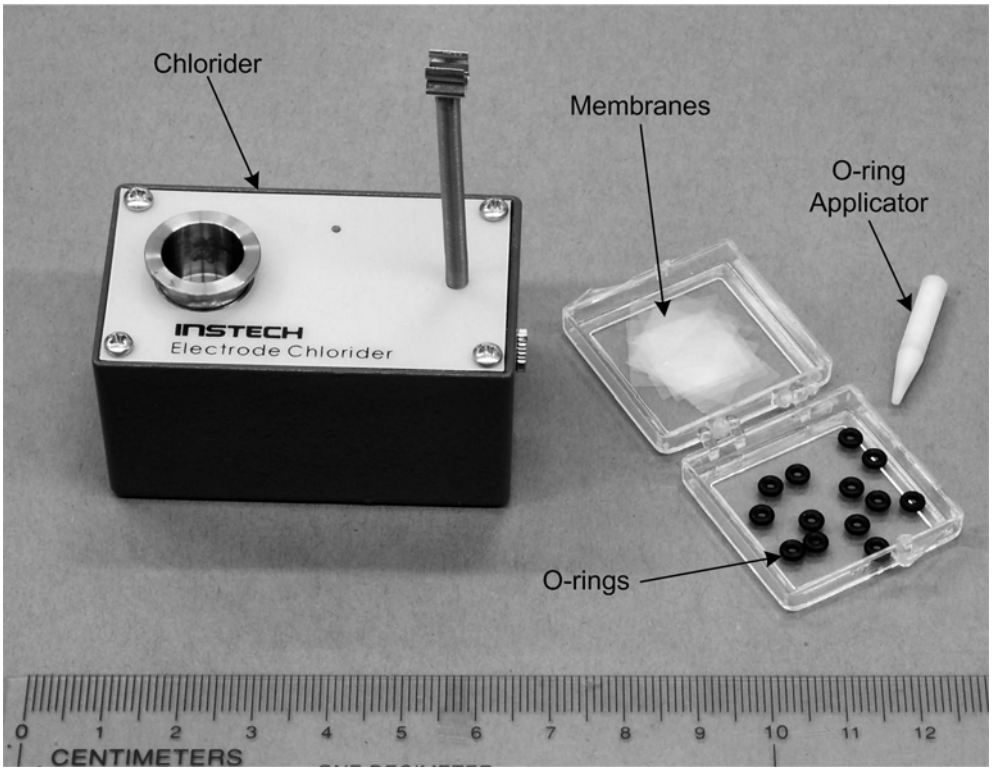

Figure 3.12: Electrode chlorider, o-ring applicator, membranes, and o-rings used to maintain the oxygen electrode.

Assuming that the chloride layer is intact, the electrode is prepared for service using the following steps. First, the electrode is disconnected from the meter and the existing o-ring and membrane removed. Second, the electrode is cleaned using deionized water, inspected, and dried. Third, the tip of the electrode is dipped into the electrolyte solution and a drop of solution is allowed to form on the tip. Fourth, using the o-ring installation tool, a new membrane is placed over the drop of electrolyte solution and sealed in place with an o-ring (Figure 3.13). Fifth, the newly installed membrane and electrolyte are checked for tears and air bubbles, if either are present, this procedure must be repeated. Finally, the electrode

is reconnected to the meter and allowed to polarize. Once the output signal has stabilized, indicating that the electrode is properly polarized, it is ready for use.

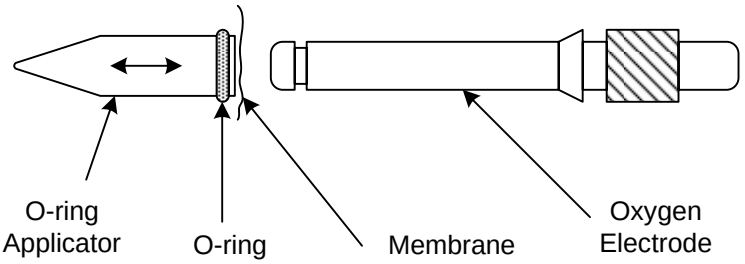

Figure 3.13: Installing a new membrane with the o-ring applicator.

3.6.2.3 Electrode Meter Setup

The Cole Parmer oxygen meter (Figure 3.14) provides the negative 0.75 V polarizing voltage necessary to use the oxygen electrode. The meter is also used to measure and scale the electrode output current. The output signal of the electrode is scaled using a two point method where meter readings of 0 and 6.0 ppm are set to represent steady state conditions for liquid saturated with nitrogen and air, respectively. The data acquisition system is then used to normalize the meter output so that the recorded data represents oxygen concentrations ranging from 0 to 100 percent.

Figure 3.14: Cole Parmer oxygen meter.

3.6.2.4 Electrode Reconditioning

Reconditioning of the electrode tip is periodically needed to restore the chloride layer on the anode of the electrode. The electrode is reconditioned using the Diamond General Development Corp. 3004 chlorider/maintenance kit (Figure 3.12). First, the electrode is unplugged from the oxygen meter. Second, the o-ring and membrane are removed from the electrode and the electrode is cleaned with ammonia to remove the remaining chloride layer and other impurities until the electrode tip is a shiny silver color. Occasionally, a Scotch-Brite pad is used to remove stubborn spots. Third, the electrode tip is inspected to ensure that the face of the electrode is flat. If the tip is not flat, emery polishing paper is used to flatten the tip. Fourth, the electrode is cleaned with deionized water. Fifth, using the 3004 chlorider with a four molar potassium chloride solution, a new chloride layer is applied to the tip as shown in Figure 3.15.

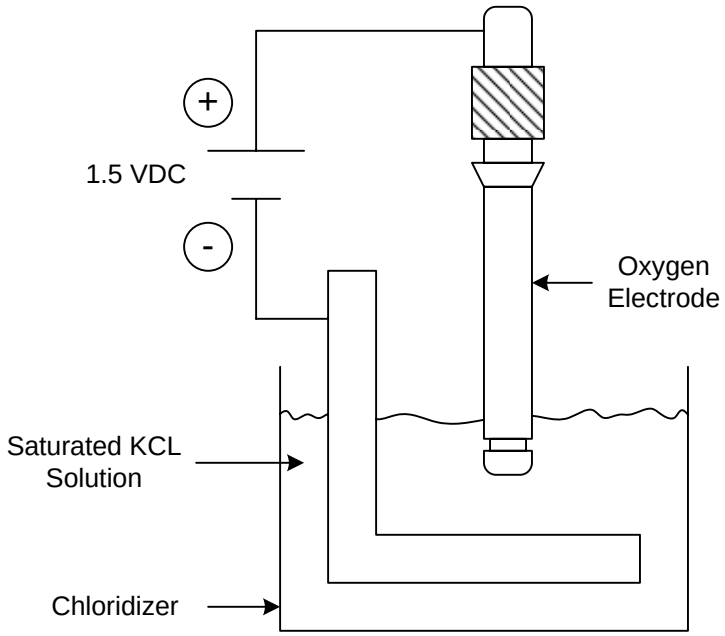

Figure 3.15: Schematic showing how the chloride layer is applied to the oxygen electrode.

3.6.2.5 Electrode Time Constant

The time constant of this electrode depends on the time required to establish the various oxygen gradients in the electrolyte. This depends primarily on the permeability of the membrane, the mobility of oxygen in the bulk fluid, and the electrolyte layer. To increase the electrode response time, a thin membrane with a high oxygen diffusion constant is needed; however, under these conditions stirring artifacts will be exaggerated. Therefore, it is preferable to use a 0.025 mm thick polyethylene membrane as this is a reasonable compromise between signal strength, time constant, and stirring artifacts, as well as being readily available in the form of sandwich bags. The thickness of the electrolyte behind the membrane is important to the electrode response time and is affected by two factors: (i) the flatness of the electrode surface near the cathode and (ii) proper membrane installation to

ensure that there are no creases in the membrane, no air bubble under the membrane, and minimal membrane stretching. The membrane manufacturer indicated that if these considerations are observed, the electrode time constant should be about four seconds.

Experimental determination of the electrode time constant is completed at the beginning and end of each day and recorded for later use in determining mass transfer coefficients. The water used to find the time constant is the same as the water used in the mass transfer tests. The water is put into two clean containers that are both well stirred and sparged with air or nitrogen (Figure 3.16). The water in each of the containers is sparged for several minutes prior to use to ensure that steady state gas concentrations exist in each. With steady state established, the oxygen electrode is placed in the first container, the one sparged with nitrogen, until the electrode output has stabilized at a zero percent oxygen concentration. The electrode is then rapidly moved to the other container, the one sparged with air, and the electrode response with time recorded. Once the electrode output stabilizes at 100% oxygen, it is rapidly moved back to the previous container and the electrode response recorded again. This procedure is repeated three times. Using the collected data, the electrode time constant is then calculated as the time it takes the output signal to move from 0 to 63 or 100 to 37 percent oxygen concentration depending on if the electrode is moved from a container being sparging with nitrogen to one sparged with air or vise versa.

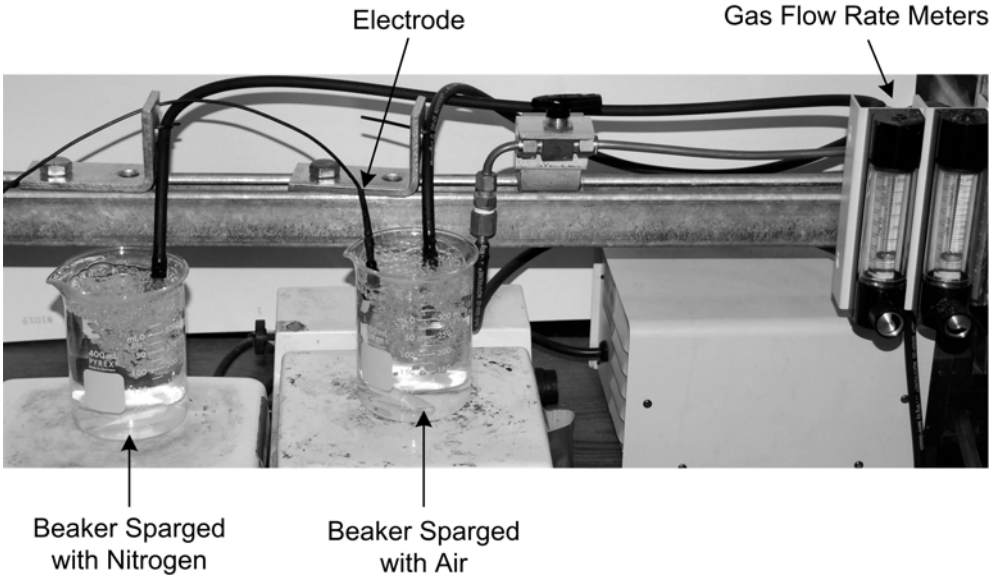

Figure 3.16: Apparatus used to determine the electrode time constant.

3.6.3 Gas Flow Rates

Prior to the use of either one of the dynamic gassing methods, the pressure regulators for each sparging gas are adjusted to ensure that volumetric flow rates for each gas are identical. First, the air flow rate is set by adjusting the pressure regulator to ~22 psi and the needle valve (Figure 3.4) to the desired flow rate. Next, using the gas selector valves, the gas species is changed to nitrogen (Figure 3.4). The nitrogen flow rate is set to match the air flow rate by adjusting the pressure regulator on the nitrogen cylinder. Next the carbon monoxide flow rate is set following the same procedure used for the nitrogen. Once the follow rates are set all the gases are turned off.

3.6.4 Dissolved Oxygen Concentration Measurement

Determining the dissolved oxygen concentration as a function of time for various operating conditions is initiated by filling the EALR to a height of H = 142.2 cm with water that has been conditioned as outlined in Section 3.1.2, and setting the inlet gas flow rate to the desired setting as specified in Section 3.1.4. Then, using either the basic or the expanded dynamic gassing out method and the oxygen electrode, the dissolved oxygen concentration change with time is recorded. The data acquisition system used to collect the data is set to gather oxygen concentration data at a rate of one kilohertz and to calculate the average oxygen concentration every tenth of a second. Measurements are taken three times for each condition listed in Table 3.2.

3.7 Dissolved Carbon Monoxide Measurement

This section describes the technique for measuring pure dissolved carbon monoxide in water to calculate k_La values. Like the dissolved oxygen measurements, carbon monoxide concentration changes in the liquid phase are initiated by filling the EALR to a height of H = 142.2 cm with preconditioned water using the expanded dynamic gassing out method. However, a dissolved carbon monoxide electrode, like a dissolved oxygen electrode, does not exist. Therefore, dissolved carbon monoxide concentrations are determined using a bioassay that is performed with liquid samples withdrawn from the EALR.

3.7.1 Safety

Since carbon monoxide is odorless and lethal in high doses, extreme care is taken to prevent carbon monoxide poisoning. The compressed carbon monoxide gas cylinders are stored in a special cabinet that is vented to outside of the building. The vent of the EALR is also connected to the same exhaust system to prevent carbon monoxide buildup in the lab. The lab space is also equipped with two Nigthhawk (model KN-COPP-3) and one Crowson Gasmater (TXgard-IS+) carbon monoxide sensors that have alarms set to go off if a leak is detected. In addition, the EALR and piping are periodically checked with a hand held sensor to ensure that there are no gas leaks.

3.7.2 Equipment and Reagents

Dissolved carbon monoxide concentration measurements are made using an Ocean Optics ChemUSB2-VIS-NIR spectrophotometer (Figure 3.17). The spectrophotometer measures light absorption in the 350 to 1000 nm wavelength range and has an optical resolution of approximately one nanometer.

Figure 3.17: Ocean Optics USB2000 spectrophotometer.

Samples are prepared and scanned in 1.5 mL polystyrene disposable cuvettes (Figure 3.18) that have a 10 mm path length. These cuvettes are usable for wavelengths ranging from 340 to 800 nm. The cuvettes also have polystyrene caps to reduce contamination.

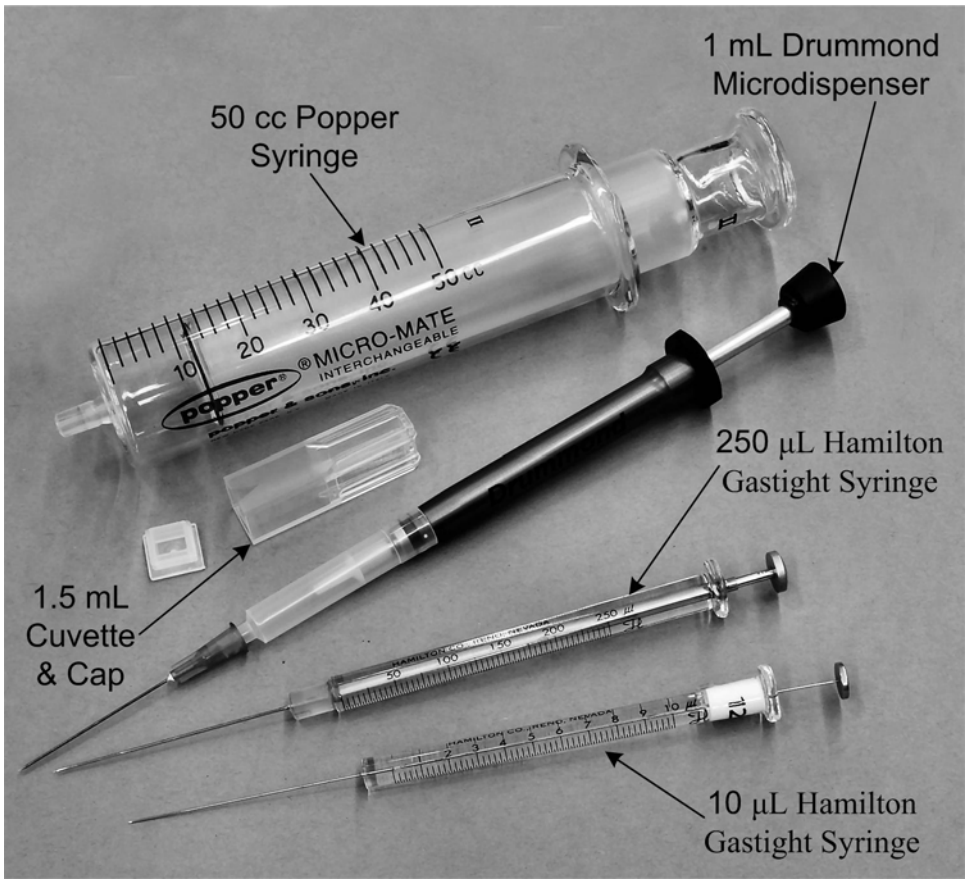

Figure 3.18: Syringes and cuvette used in the bioassay.

Syringes used for liquid sample collection are gastight high performance 10 μL syringes (Figure 3.18) from Hamilton (model 1701). The needles are cemented into this type of syringe.

Several other syringes (Figure 3.18) are used for bioassay solution preparation. The test solution is prepared in a 50 mL glass syringe from Popper & Sons, Inc (model micro-mate 5059). This syringe is capped with a rubber septum from Sigma-Aldrich (model Z100722) to limit solution contamination. A gastight high performance 250 mL syringe from Hamilton (model 1725) is used to meter the protein solution. Test samples are prepared

using a Drummond Scientific Company 1 mL fixed volume microdispenser (model 3-000-390). This microdispenser has a replaceable bore and plunger and is fitted with a disposable 23 gauge needle.

Myoglobin used in the dissolved carbon monoxide concentration measurements is purchased from Sigma-Aldrich (product number M1882) and derived from horse heart. The myoglobin comes as an essentially salt free lyophilized powder at least 90% pure that must be stored at minus 20 degrees Celsius.

The buffer solution used to dilute the protein solution is prepared from common lab chemicals obtained from Iowa State University Chemistry Stores. Since these chemical are common and easy to obtain, their specifics are not presented.

3.7.3 Liquid Samples Collection

Before collecting the liquid samples, 19 ten microliter syringes are numbered from 0 to 15 and SS1 to SS3 and cleaned with deionized water. The syringes are all inserted into the upper carbon monoxide sampling port as shown in Figure 3.19. Syringe tip location is set by making sure that the bottom of the syringe barrel is flush with the outer edge of the sampling port. This allows for a consistent sampling location. Prior to introducing carbon monoxide into the EALR, a single sample is taken with syringe #0 to measure the carbon monoxide concentration at time, $t = 0$. Transient samples are then withdrawn every five or ten seconds, depending on the operating conditions, after carbon monoxide is introduced into the EALR.

Three additional samples are taken after the system has reached steady state prior to switching the sparging gas from carbon monoxide to air.

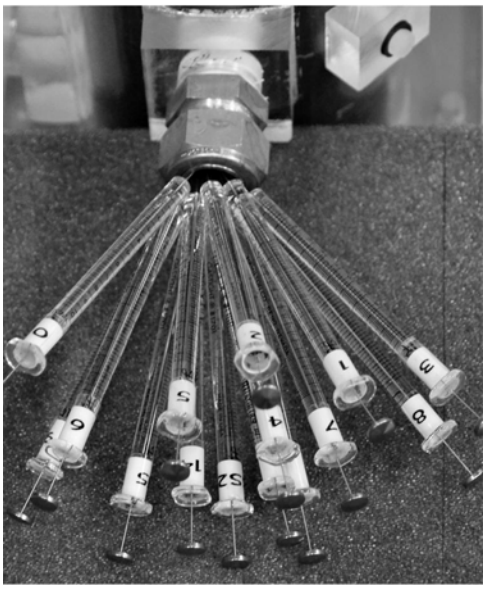

Figure 3.19: **S**ample syringes inserted in the external airlift loop reactor for liquid sample collection.

3.7.4 Reagent Preparation

The bioassay used to determine the dissolved carbon monoxide concentration uses three solutions. The procedure for preparing these three solutions will be presented in the next three sections.

3.7.4.1 Buffer Solution Preparation

The buffer solution used to prepare all of the other solutions is a 0.1 M potassium phosphate pH 7.0 buffer. This solution is prepared by adding 3.3 g of dibasic potassium phosphate powder and 11.0 g of monobasic potassium phosphate powder to 1 L of deionized

water. The pH of the solution is adjusted with either potassium hydroxide or o-phosphoric acid to set the pH at 7.0.

3.7.4.2 Myoglobin Solution Preparation

The myoglobin solution is prepared from the myoglobin powder purchased from Sigma-Aldrich. One gram of myoglobin powder is dissolved in approximately 25 mL of the buffer solution. To increase the shelf life of the myoglobin solution, the solution is run through a dialysis separation process for 24 hours and then spun down in a centrifuge to remove impurities. The solution is separated into 1 mL containers and frozen until needed.

3.7.4.3 Identifying the Concentrated Myoglobin Solution Concentration

Prior to testing, the myoglobin solution is thawed and the myoglobin concentration determined to aid in preparing the test solution. The goal in preparing the test solution is to obtain a peak absorption value near Abs = 1.5 for the saturated oxygen sample (Figure 3.20). This peak occurs at 409 nm for myoglobin.

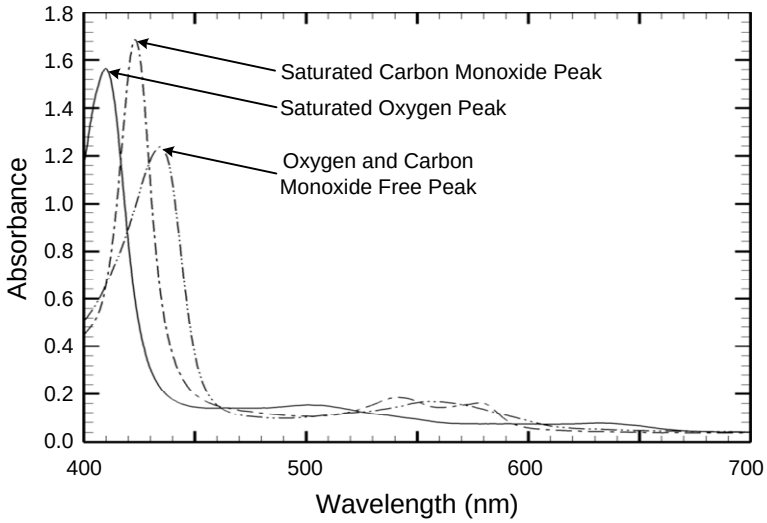

Figure 3.20: **R**eference absorbance spectrums.

The concentration is determined by putting 1 mL the buffer solution into a cuvette and adding 1 μL of protein. The absorbance is measured and more protein is added in 1 μL increments until the peak absorbance is near 1.5 (Figure 3.20). Once the peak absorbance reaches Abs ≈ 1.5, the myoglobin concentration (C_p) and the dilution ratio (DR) are determined from:

$$C_p = \frac{\text{Abs}}{\lambda \cdot \varepsilon_m} \tag{3.7}$$

$$\text{DR} = \frac{\text{microliters of myoglobin solution}}{\text{milliliters of buffer solution}} \tag{3.8}$$

where Abs is the absorption value, λ is the path length of the cuvette, and ε_m is the extinction coefficient. For horse heart myoglobin, ε_m is reported to be 188 $\mu M^{-1}cm^{-1}$ [138].

3.7.4.4 Test Solution Preparation

The test solution used to analyze the liquid samples is prepared just prior to use as the myoglobin solution is temperature sensitive and its exposure to room temperatures must be minimized. The test solution is prepared by pipetting 1 mL of buffer solution for every sample being analyzed into the 50 mL syringe. A typical test uses 20 mL of buffer solution. Then, using the previously calculated dilution ratio, an appropriate amount of myoglobin solution is added to the test solution using the 250 μL syringe. The mixture is gently mixed and a 1 mL is set aside to determine the "oxy" spectrum, see Section 3.7.5. Finally, a small amount of sodium dithionite (N_a2SO_4) is added to neutralize all the dissolved oxygen and the oxygen bonded to the myoglobin.

3.7.5 Bioassay – Measuring Absorbance Spectrums

All measurements are carried out in 1 mL of test solution in the 1.5 mL cuvettes. The sample set aside during test solution preparation is placed in the spectrophotometer and scanned. The measured spectrum is recorded and saved as the "oxy" spectrum. Likewise, the "deoxy" spectrum is determined by scanning a cuvette containing only test solution, this spectrum corresponds to a sample containing no carbon monoxide. In a similar fashion, the "saturated CO" spectrum is found by saturating the solution in a cuvette with an excess amount of carbon monoxide to ensure that all the myoglobin is bound to a carbon monoxide molecule. The resulting spectrum corresponds to the maximum amount of dissolved carbon

monoxide that can be detected without increasing the protein concentration in the test solution.

The liquid samples are analyzed after the three reference spectrums have been determined. After the test solution has been placed in the cuvette, a 10 μL liquid sample is injected into the cuvette and the cuvette capped. The cuvette is gently mixed by inverting the cuvette several times and then scanned. This process is repeated for each of the acquired liquid samples. The resulting spectra will follow the trend shown in Figure 3.21, where an increase in the amount of dissolved carbon monoxide results in the peaks of the spectra initially shifting down and to the left and then up and to the left. Errors may occur in these measurements because of gas bubbles becoming entrained in the liquid sample when it is drawn; thus, care must be taken to ensure that the syringes are clean and properly located in the sample port.

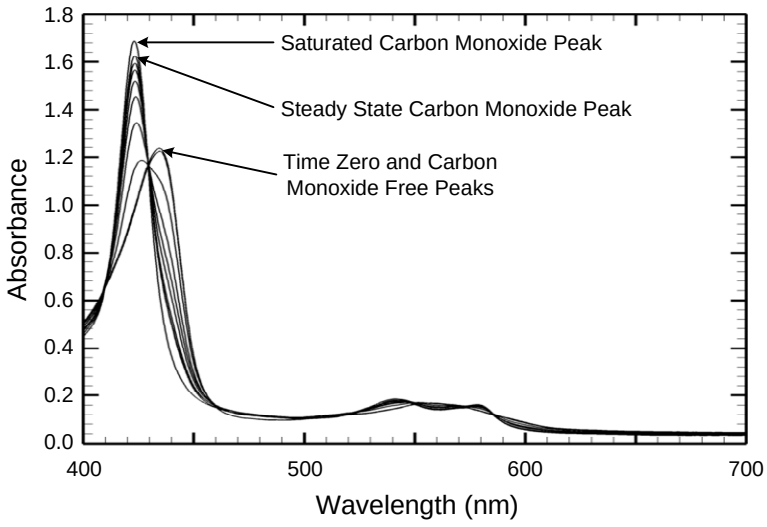

Figure 3.21: Absorbance spectra progression from carbon monoxide free state to a carbon monoxide saturated state.

3.7.6 Bioassay – Spectral Fitting

Quantification of the spectra is achieved by loading the spectra data files into JMP 6.0 to fit the liquid sample spectra between the "deoxy" and "saturated" spectra. The software package uses a least squares fitting routine that outputs a percent similarity to each of the reference spectra. This output data is then used to determine the carbon monoxide concentration (C_{CO}) with time as a percent of the steady state concentration using the following relationship:

$$C_{CO} = \left(C_p\right)\left(SS\right)\left(\frac{Vol_T}{Vol_S}\right) \tag{3.9}$$

where C_p is the myoglobin concentration in the test solution, SS is the percentage of the steady state concentration exported from JMP 6.0, Vol_T is the total liquid volume in the cuvette, and Vol_S is the dissolve carbon monoxide liquid sample volume.

3.8 Volumetric Mass Transfer Coefficient (k_La) Determination

In order to determine k_La using the concentration versus time data, several assumptions are made about the system dynamics, the gas and liquid concentrations, and the electrode dynamics. The simplest model assumes:

(1) the reactor is modeled as a batch reactor (no liquid flow into or out of the EALR),

(2) the liquid phase is well mixed,

(3) the liquid phase gas concentration change is first order,

(4) the gas phase mole concentrations are constant (no startup effects), and

(5) the electrode dynamics are negligible ($\tau_e << 1/k_La$).

These assumptions allow for the use of the following model as discussed Section 2.4.5.4.2:

$$C(t) = C^* - \left(C^* - C_o\right)\exp\left(-k_L a \cdot t\right) \tag{3.10}$$

where C(t) is the gas concentration as a function of time, C^* is the equilibrium gas concentration in the liquid, and C_o is the initial dissolved gas concentration in the liquid. However, the application of this model is usually limited by the fifth assumption, as electrode dynamics are not always negligible. Thus, the following model is typically used [2, 112, 116, 117] which accounts for electrode dynamics across a wider range of operating conditions:

$$C(t) = C^* - \left(C^* - C_o\right)\frac{\left(\exp^{-k_L a \cdot t} - k_L a \cdot \tau_e \cdot \exp^{-t/\tau_e}\right)}{\left(1 - k_L a \cdot \tau_e\right)} \tag{3.11}$$

where τ_e is the electrode time constant.

When τ_e is much smaller than $1/k_La$, τ_e in Equation (3.11) goes to zero resulting in Equation (3.10) and the electrode dynamics may be neglected, as is the case in Figure 3.22 where τ_e and $1/k_La$ equal 2.3 and 120.5 seconds, respectively. As illustrated in Figure 3.22, both Equations (3.10) and (3.11) fit the experimental data very well. If the difference between τ_e and $1/k_La$ becomes small, then τ_e can no longer be neglected as shown in Figure 3.23. In this case τ_e has approached the same order of magnitude as $1/k_La$, causing Equation (3.10), which neglects τ_e, to under predict k_La and to not fit the experimental data any more (Figure 3.23). Equation (3.11), on the other hand, when fit to the experimental data still provides an adequate fit. Likewise, if the difference between τ_e and $1/k_La$ continues to

decrease as shown in Figure 3.24, the under estimation of k_La and the error in predicting the experimental data using Equation (3.10) increases. Similarly, the use of Equation (3.11) to estimate k_La for conditions represented in Figure 3.24, where τ_e and $1/k_La$ are the same order of magnitude, begins to show signs that Equation (3.11) is initially under estimating the dissolved oxygen concentration and then slightly overestimating the dissolved oxygen concentration, indicating that Equation (3.11) has a limited ability to correctly account for electrode dynamics. Since the data in Figure 3.24 represents conditions in the EALR having the highest observed k_La, it is felt that Equation (3.11) adequately accounts for electrode dynamics for the range of conditions expected in this work; therefore, it will be used to estimate the oxygen gas-liquid mass transfer rates from the collected dissolved oxygen concentration data. The dissolved carbon monoxide concentration data, on the other hand, does not need to be adjusted for electrode dynamics so Equation (3.10) will be used to calculate carbon monoxide k_La. It is worth noting that if oxygen k_La are much higher than those reported in this work, then either another method of accounting for electrode dynamics or an electrode with a faster time constant would be required.

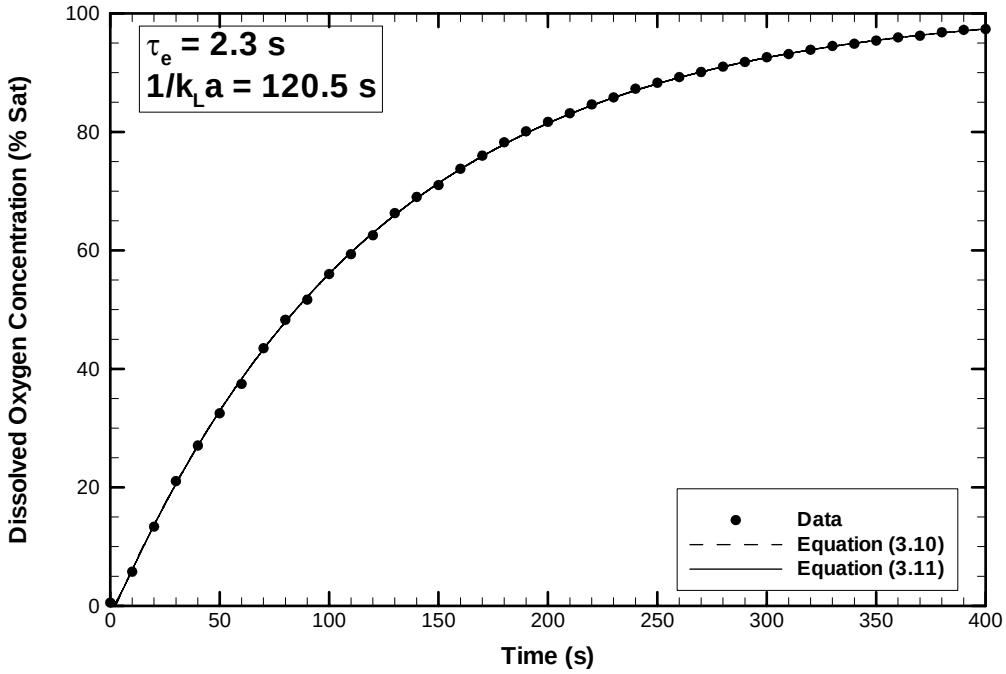

Figure 3.22: An illustration of how Equations (3.10) and (3.11) fit the experimental data when $\tau_e << 1/k_La$.

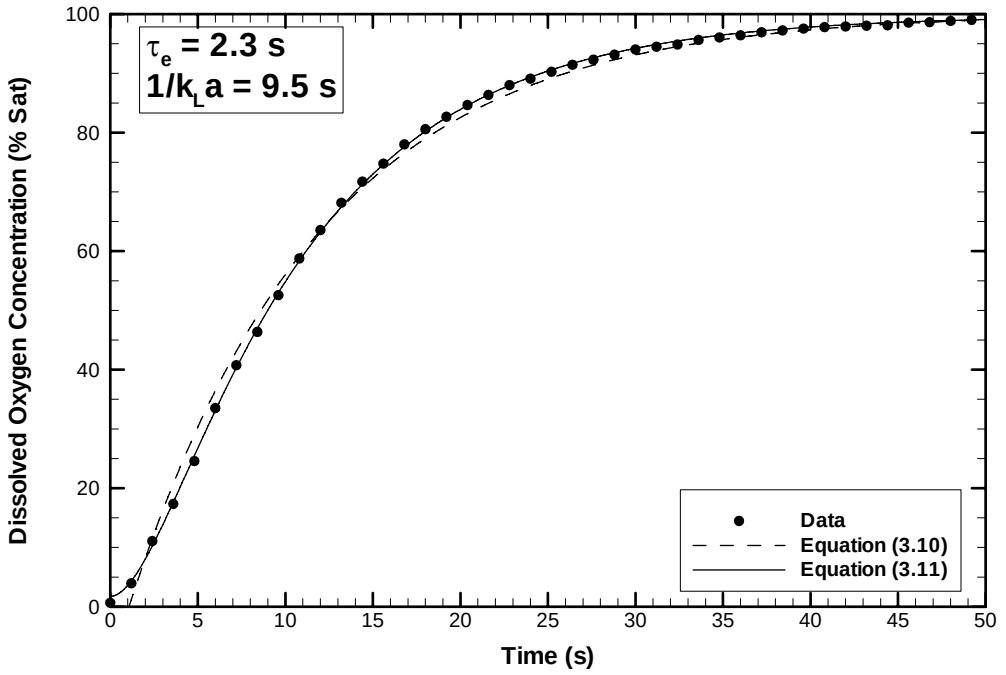

Figure 3.23: An illustration of how Equations (3.10) and (3.11) fit the experimental data when the difference between τ_e and$1/k_La$ is about one order of magnitude.

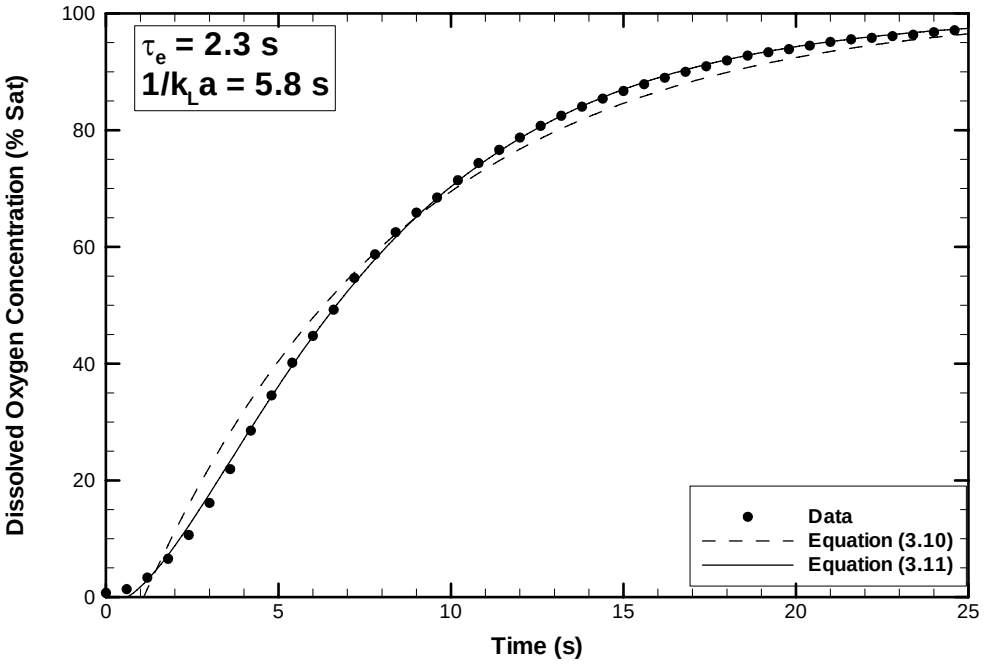

Figure 3.24: An illustration of how Equations (3.10) and (3.11) fit the experimental data when the difference between τ_e and$1/k_La$ is less than one order of magnitude.

A statistical software package, JMP 6.0 (SAS Institute Inc.), equipped with a nonlinear fitting routine is used to determine k_La using the carbon monoxide and oxygen concentration data and Equations (3.10) and (3.11), respectively. The resulting k_La values found using this fitting software are best fit values where initial values for C_o and C^* are not specified. Figure 3.25 and Figure 3.26 illustrate the results of the fitting equations (3.10) and (3.11) to the experimental data for carbon monoxide and oxygen, respectively. (Note that C_o is less than zero for the carbon monoxide test as the carbon monoxide data is not normalized to account for the reactor response lag time.

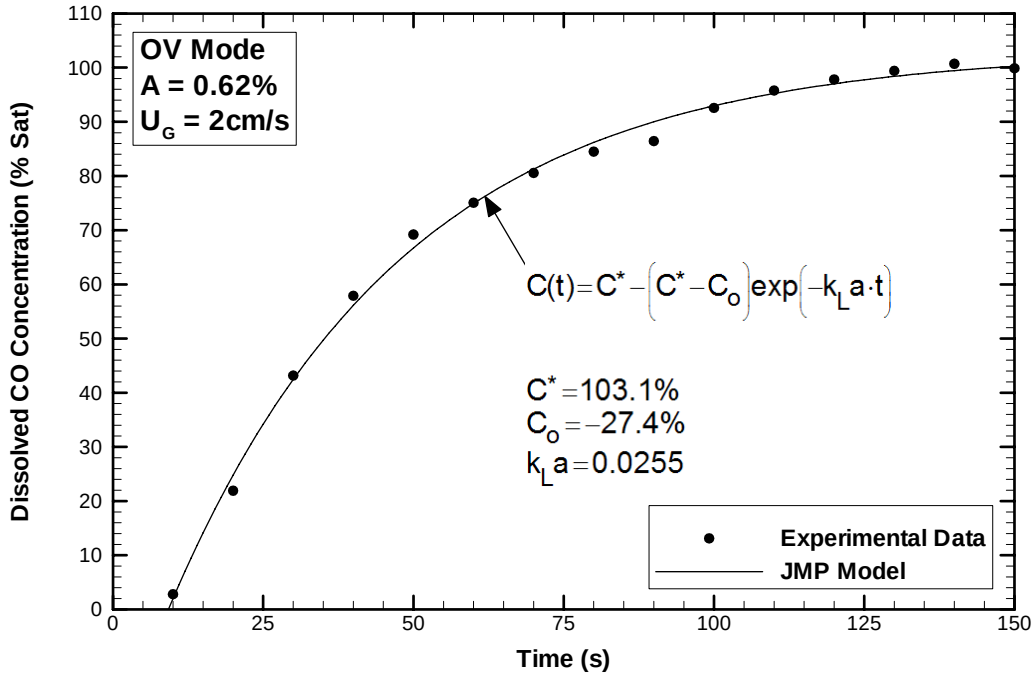

Figure 3.25: Typical dissolved carbon monoxide data and the corresponding k_La value found using a nonlinear fitting routine to Equation (3.10).

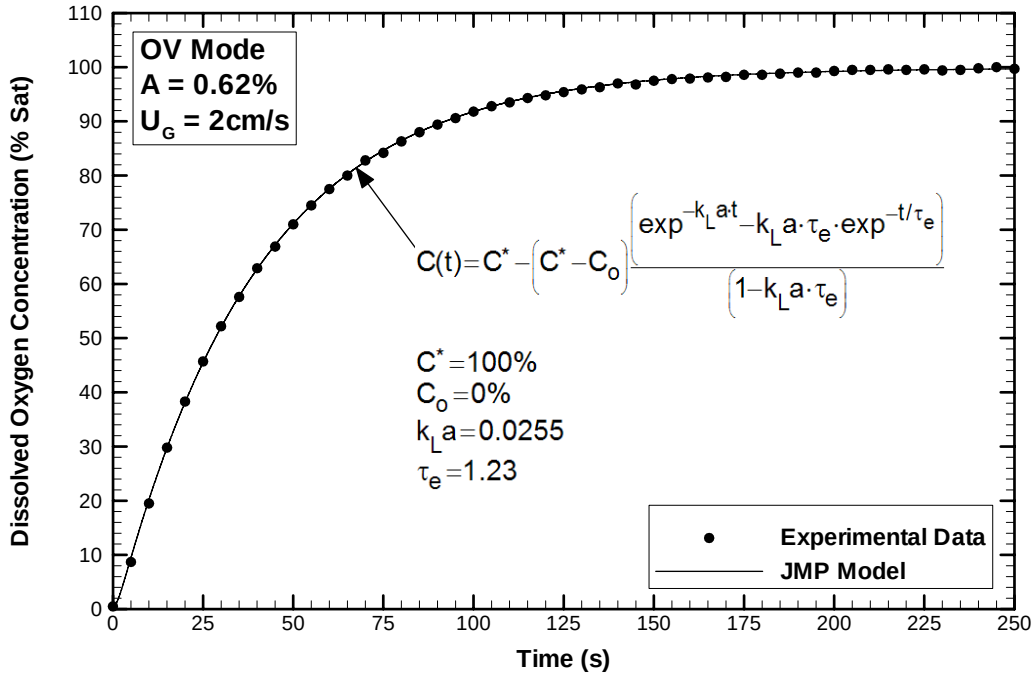

Figure 3.26: Typical dissolved oxygen data and the corresponding k_La value found using a nonlinear fitting routine to Equation (3.11).

3.9 Measurement Uncertainty

Measurement uncertainties are estimated following the methods provided by Figliola and Beasley [139]. The typical uncertainties associated with U_G and V_d are ±1 to 5% and ±1 to 8%, respectively, with the larger uncertainties corresponding to the lowest velocity measurements. The absolute gas holdup uncertainty is estimated to approximately ±0.001 to 0.015. The uncertainty associated with riser superficial liquid velocity is estimated to be about ±1.5 to 3.1%. The uncertainty associated with the gas-liquid mass transfer coefficients is more ambiguous than the other measures due to measurement uncertainties and uncertainties introduced when using JMP to statistically determine k_La values for the collected data. Thus, it is estimated that the oxygen k_La values have uncertainty of ±3 to 10%, where the lowest uncertainties are associated with lower k_La values. The uncertainty associated with the carbon monoxide k_La values is estimated to be ±5 to 10% depending on the operating conditions.

3.10 Summary

The equipment and methods described in this chapter were used to evaluate the EALR hydrodynamic and gas-liquid mass transfer characteristics, the results of which are in the next chapter.

CHAPTER 4: RESULTS

This chapter presents and discusses the experimental results collected as part of this work, and is divided into four sections: visual observations, gas holdup, liquid velocity, and gas-liquid mass transfer results. Note: The lines connecting data points in the figures presented in this chapter are to aid in data presentation and do not represent trends unless otherwise noted.

4.1 Visual Observations

This section discusses the visual flow observations completed with the methods outlined in Section 3.2. This presentation is divided into two subsections and presents only a sampling of the data to illustrate the observed trends. A complete presentation of the photographs acquired for the visual observations is included in Appendix B. Some of the photographs presented in this section are accompanied with hand generated sketches to assist in illustrating the observations being made.

The flow conditions in the EALR are observed for OV and CV modes using an aerator plate open area ratio of A = 0.62% as the superficial gas velocity is increased from 0 to 20 cm/s using the U_G listed for this experiment in Table 3.2. The working fluid for these tests is unconditioned tap water.

4.1.1 Upper Connector Region Visual Observations

The fluid flow pattern in the EALR is very simple for the OV mode at U_G = 0.5 cm/s, Figure 4.1. The gas bubble distribution in the riser appears to indicate that at this condition

the EALR is operating in the homogeneous flow regime. Also, at this condition a small amount of gas is seen to enter the upper connector and exit the reactor through the top of the downcomer. The remainder of the downcomer is gas free at this operating condition.

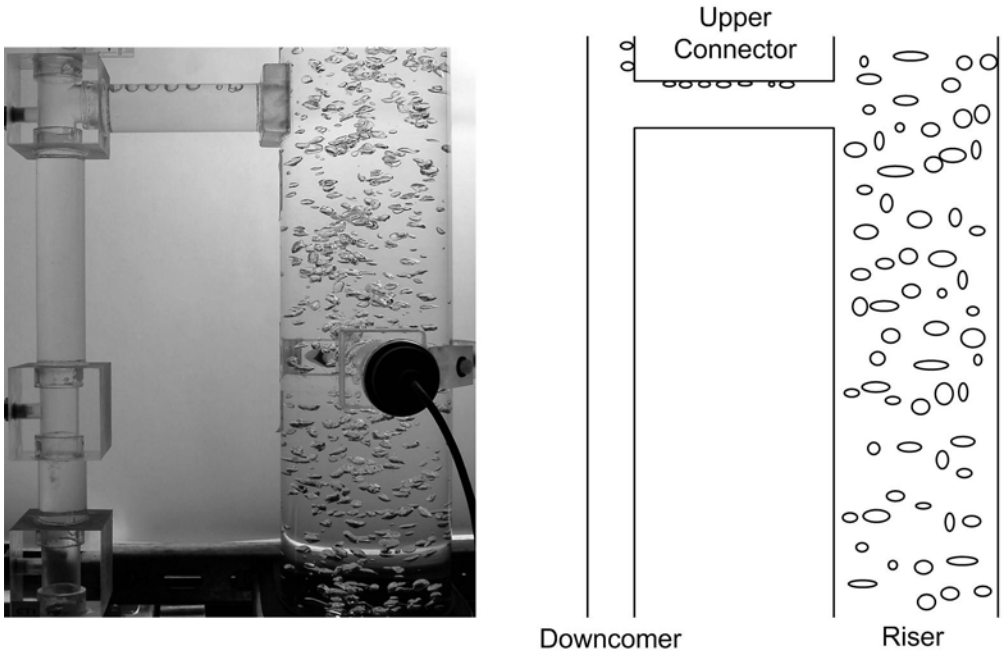

Figure 4.1: External airlift loop reactor flow behavior at the upper connector for open vent mode and U_G = 0.5 cm/s.

As the superficial gas velocity is increased from U_G = 0.5 to 3.5 cm/s, the conditions in the reactor resemble those shown in Figure 4.1 with the exception that the bubble density in the riser increases and gas holdup in the downcomer is no longer absent, Figure 4.2. The liquid momentum in the reactor increases as U_G increases and is responsible for carrying gas bubbles down into the downcomer.

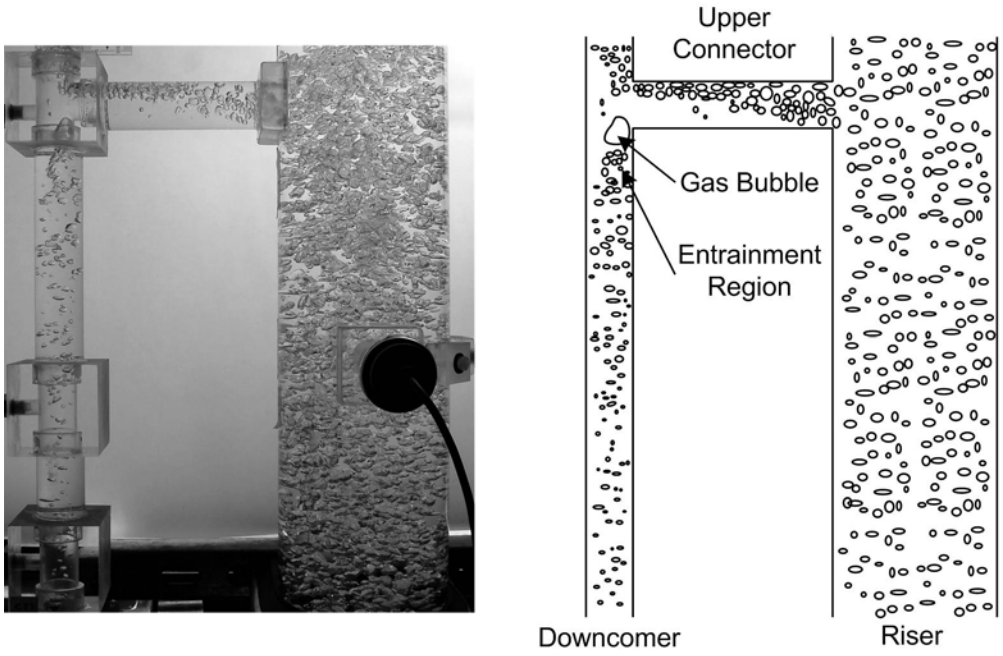

Figure 4.2: External airlift loop reactor flow behavior at the upper connector for open vent mode and U_G = 3.5 cm/s.

At $U_G \approx 3.5$ cm/s, as shown in Figure 4.2, a stationary gas bubble begins to form at the point where the downcomer and upper connector meet. The formation of this stationary gas bubble occurs because of the increase in liquid momentum causing the fluid to separate from the downcomer wall as it travels around the elbow.

When U_G is further increased from $3.5 \lesssim U_G \lesssim 10.0$ cm/s, the diameter and length of the stationary gas bubble is observed to grow, the apparent bubble density in the riser increases, and the flow regime is noted to progress from the homogeneous regime through the transition regime to the heterogeneous regime; these observations are shown in Figure 4.3. Also in this range, the gas pulled into the downcomer is separated from the liquid phase as it moves around the stationary gas bubble and then is re-entrained into the liquid phase in the entrainment region just below the gas bubble (see Figure 4.3 and Figure 4.4).

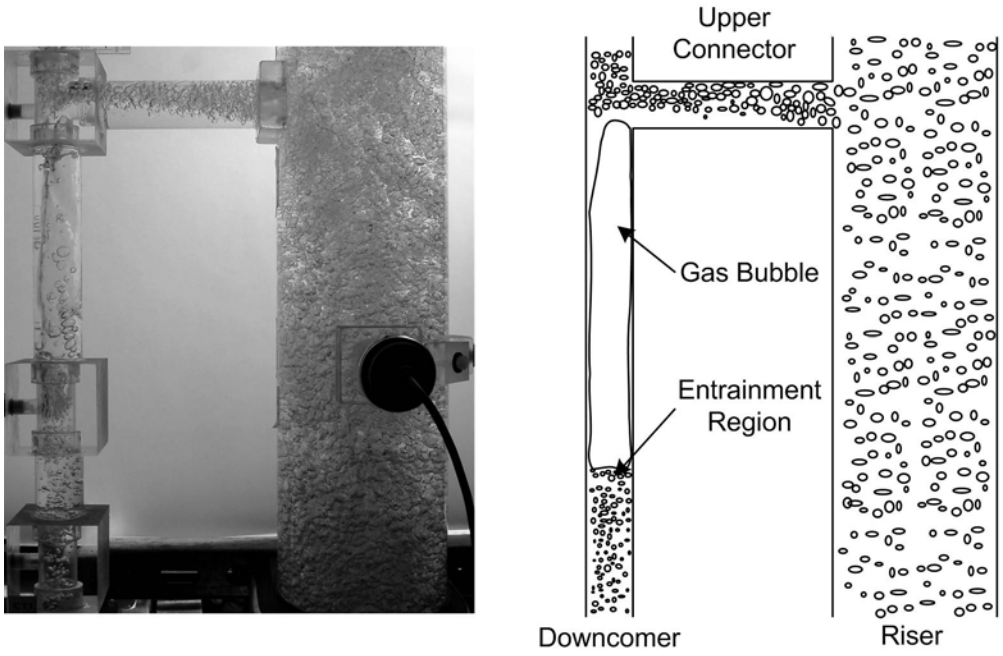

Figure 4.3: External airlift loop reactor flow behavior at the upper connector for open vent mode and U_G = 10.0 cm/s.

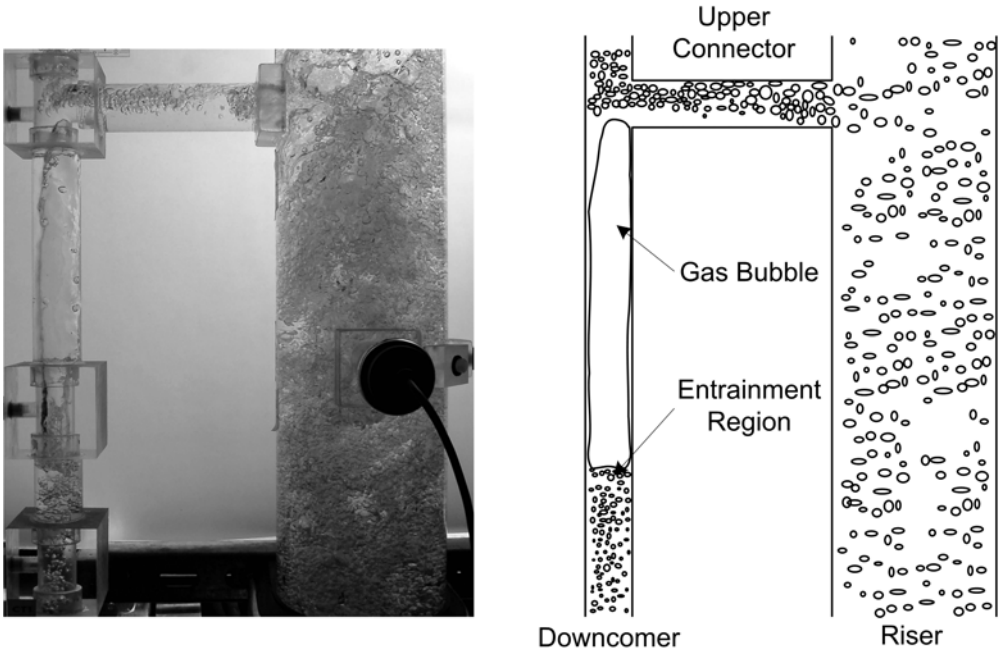

Figure 4.4: External airlift loop reactor flow behavior at the upper connector for open vent mode and U_G = 20.0 cm/s.

As U_G is further increased to 20 cm/s, the mean length and diameter of the stationary gas bubble appears to be independent of U_G. Although, the mean length of the stationary gas bubble does not noticeably change, the length is observed to rapidly oscillate around the mean. The cause of this rapid oscillation in size is thought to be due in part to the rate of gas entrainment below the stationary gas bubble and the periodic escape of gas up the downcomer.

As shown in Figure 4.5, when the EALR is operated in the CV mode, a large gas pocket forms in the upper connector as soon as gas is sparged into the reactor at $U_G = 0.5$ cm/s, the lowest U_G considered. This gas pocket is relatively small at $U_G = 0.5$ cm/s, but grows very quickly to its maximum size with only a slight increase in U_G. Once the maximum gas pocket size is obtained, no sustainable size change is observed over the remaining U_G range. A stationary gas bubble also forms just below the upper connector in the downcomer (Figure 4.5); however, unlike the OV mode, the stationary gas bubble forms at $U_G = 0.5$ cm/s. As U_G increases, the stationary gas bubble diameter grows until it is nearly equal to the inside diameter of the downcomer. Once the stationary gas bubble growth ceases, the bubble length increases as U_G increases to $U_G \approx 7.0$ cm/s, Figure 4.6. For $U_G \gtrsim 7.0$ cm/s the bubble length appears to be independent of U_G; this is revealed by comparing the bubble lengths in Figure 4.6 ($U_G = 7.0$ cm/s) and Figure 4.7 ($U_G = 20.0$ cm/s), which are very similar.

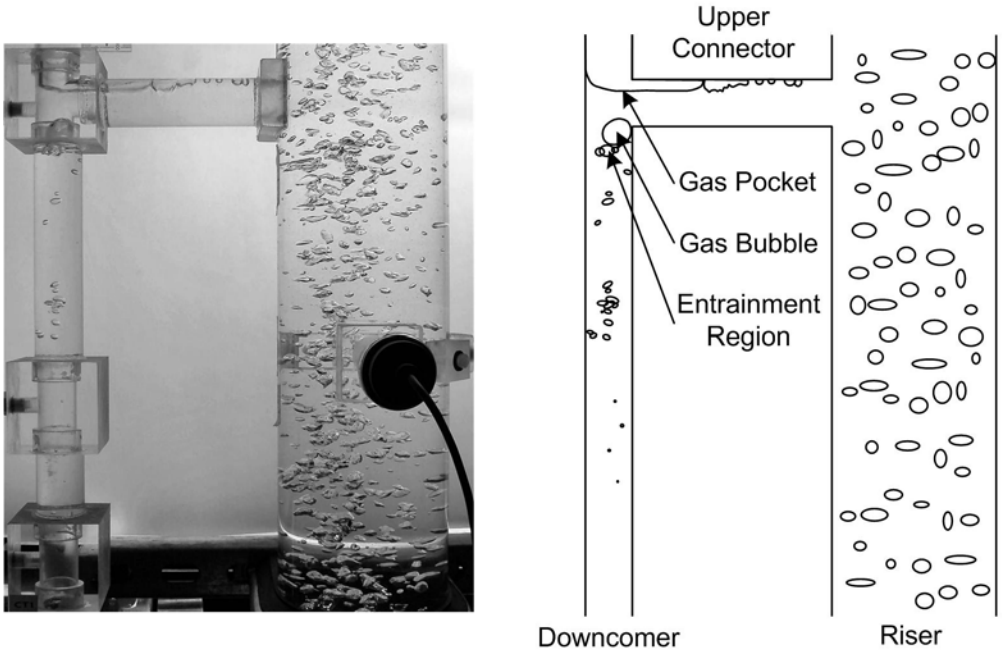

Figure 4.5: External airlift loop reactor flow behavior at the upper connector for closed vent mode and U_G = 0.5 cm/s.

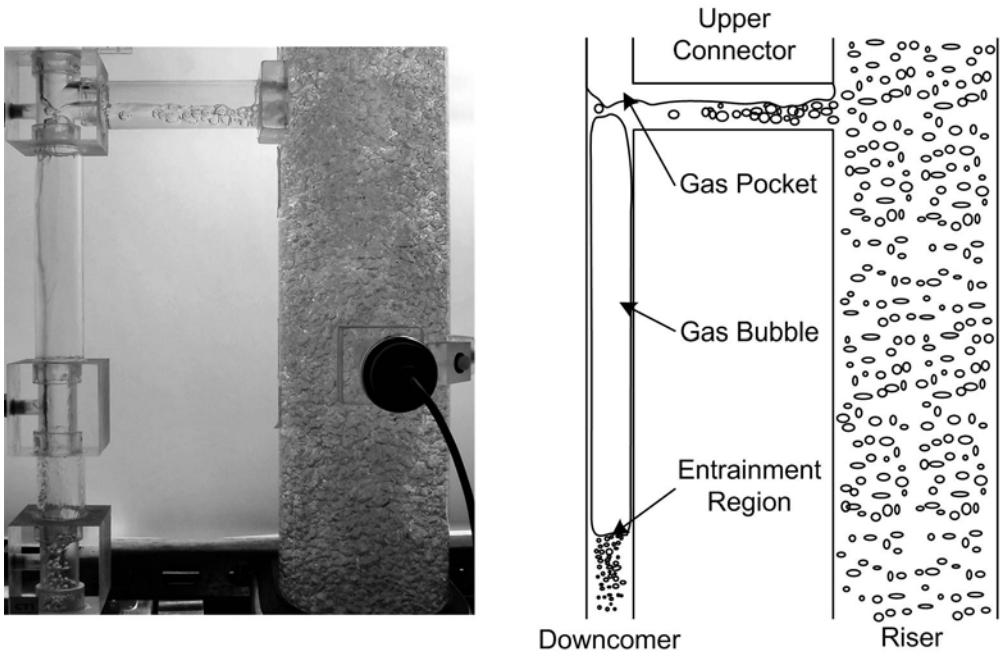

Figure 4.6: External airlift loop reactor flow behavior at the upper connector for closed vent mode and U_G = 7.0 cm/s.

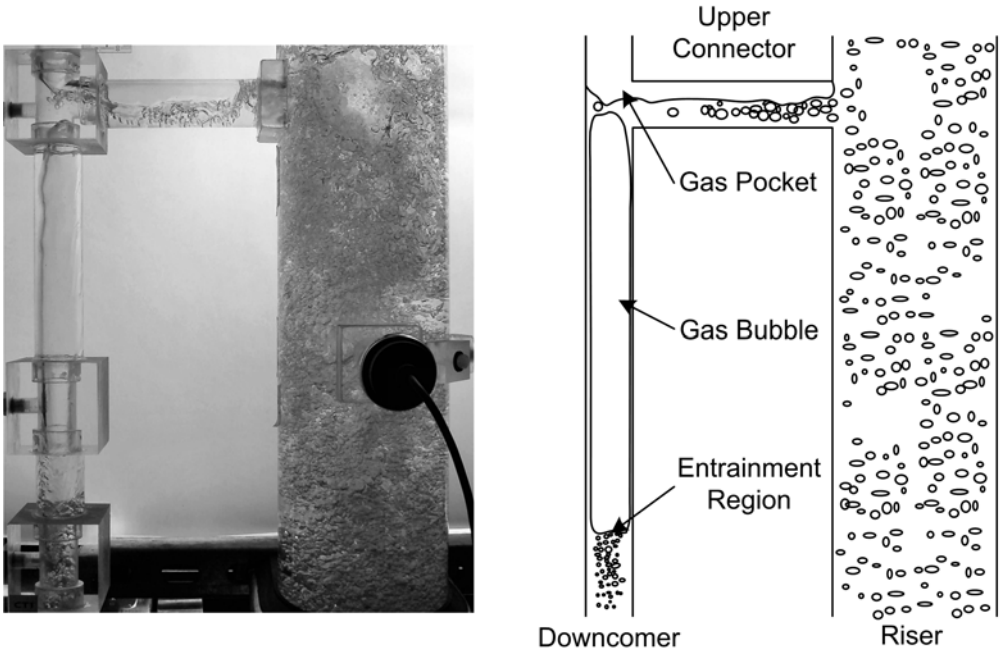

Figure 4.7: External airlift loop reactor flow behavior at the upper connector for closed vent mode and U_G = 20.0 cm/s.

Visual observations also indicate that the liquid below the gas pocket is free of entrained gas as it enters the downcomer over the entire U_G range, indicating that gas separation occurs as the gas-liquid mixture moves through the horizontal connector, similar trends have been reported by others [21, 28]. In the entrainment region below the gas bubble, surface aeration is noted, and is observed to increase as U_G increases. The surface aeration at this location causes some of the gas in the gas bubble to be entrained into the liquid; however, the degree of gas entrainment is small. Most of the small bubbles entrained at this point stay close to the entrainment region while some very small bubbles (estimated to be < 0.5 mm in diameter) are found throughout the downcomer. At $U_G \lesssim 3.5$ cm/s, very few, if any gas bubbles are present in the downcomer. When $U_G \gtrsim 3.5$ cm/s, the number and size of

small bubbles in the downcomer does increase; although, the average gas holdup in the downcomer is not measurable using pressure measurements for the U_G studied.

4.1.2 Visual Observations – Bottom of the Downcomer

The fluid flow in the lower region of the downcomer is remarkably different from that seen in the upper connector and corresponds very well with the gas holdup data. The fluid flow in this region is always downward, and the bubbles (when present) are carried by the fluid from the top of the downcomer through the imaging region to the base of the EALR.

When the EALR is operated in the OV mode, the flow in the lower downcomer is noted to be single phase for $U_G \lesssim 2.0$ cm/s (Figure 4.8a). Once $U_G \gtrsim 2.0$ cm/s, the flow begins to transition from single phase flow to two phase flow (Figure 4.8b). As shown in Figure 4.8b through Figure 4.8d when U_G is further increased, the fluid flow remains two phase where the bubble density changes significantly for $2.0 \lesssim U_G \lesssim 8.0$ cm/s. When $U_G \gtrsim 8.0$ cm/s, the bubble density increases slightly, if at all.

The visual observations in the downcomer for the CV mode are significantly different from those found for the OV mode. As shown in Figure 4.9, the relative bubble size for all U_G is very small when compared to similar conditions for the OV mode. The bubble density appears to change linearly with U_G; however, the overall gas holdup for this operating mode, as will be discussed in Section 4.2, is so small that it can not be measured with the given equipment to verify this trend.

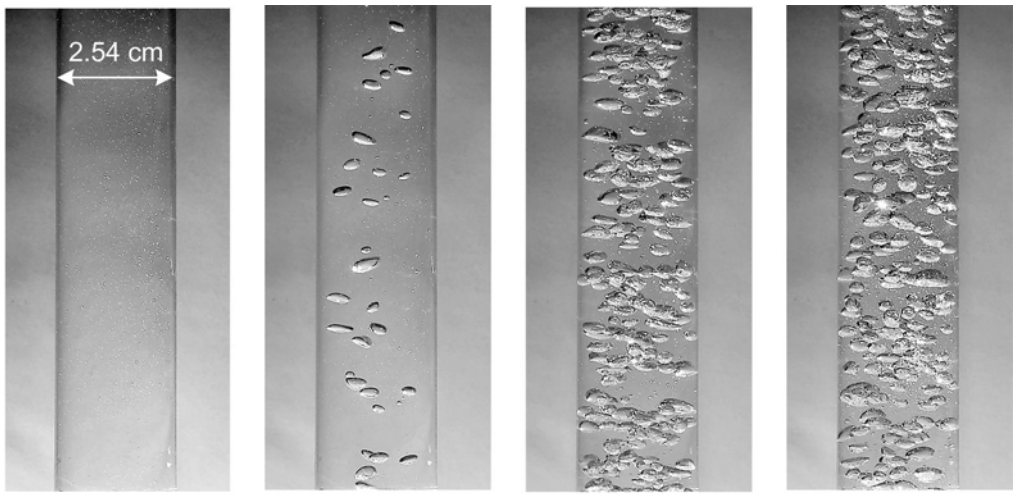

Figure 4.8: External loop reactor flow behavior and gas holdup in the bottom of the downcomer for open vent mode.

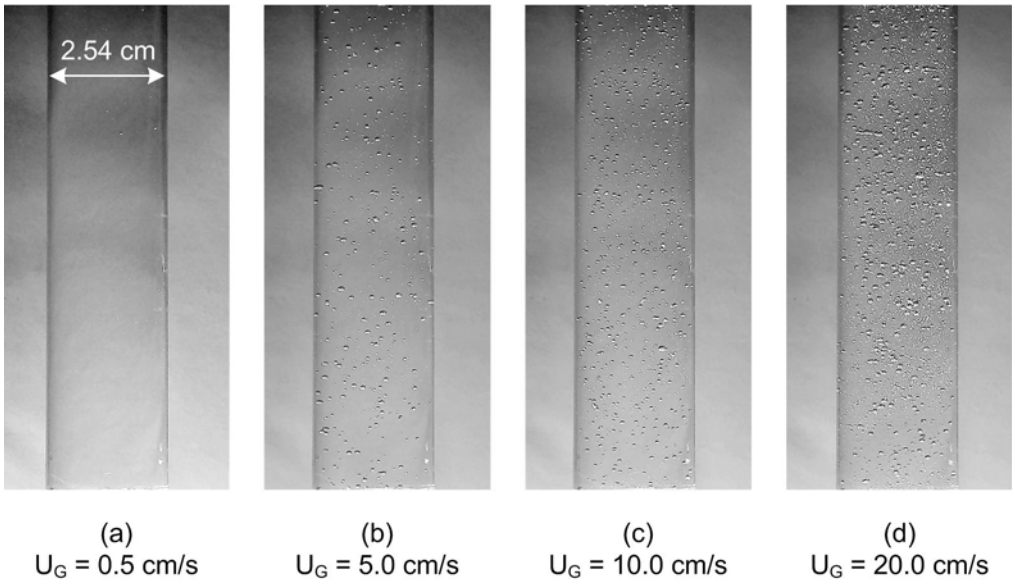

Figure 4.9: External loop reactor flow behavior and gas holdup in the bottom of the downcomer for closed vent mode.

4.2 Gas Holdup

This section presents and discusses the gas holdup data collected for the EALR. The gas holdup data will be presented using four sub-sections: (i) tap water gas holdup, (ii)

deionized water gas holdup, (iii) KCl solution and nitrosomonas solution gas holdup, and (iv) tap water gas holdup correlations. The data presented in this section is a portion of the gas holdup data collected and chosen to illustrate the general trends observed. All of the gas holdup data is presented for each condition in Appendix C.

4.2.1 Tap Water Gas Holdup

The effect of aeration plate open area ratio on gas holdup is shown in Figure 4.10 when the EALR is operated as a bubble column (BC mode). The open area ratio has a negligible effect on gas holdup at low U_G ($U_G \lesssim 5.0$ cm/s) where the corresponding bubble column flow regime is homogeneous. At medium U_G (5.0 cm/s $\lesssim U_G \lesssim$ 12.0 cm/s), where the bubble column flow is in the transition regime, gas holdup behavior is found to deviate among the three plates. In the transition regime, when A < 1%, gas holdup increases with increasing gas flow until a local maxima is achieved, decreases slightly, and then begins to converge as U_G continues to increase into the heterogeneous flow regime. In the case when A = 2.22%, the gas holdup trend deviates from that with A < 1% in the transition and heterogeneous flow regimes and continually increases with increasing U_G. Similar trends have also been reported for a 15.2 cm ID semi-batch bubble column using similar aerator plates [140].

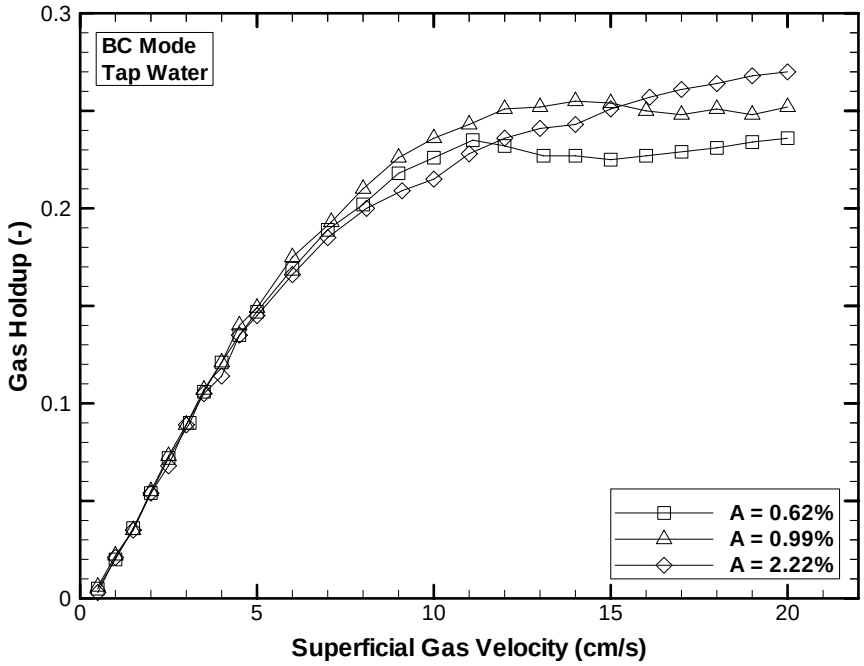

Figure 4.10: Gas holdup using different aeration plates when the external airlift loop reactor is operated in bubble column mode.

To further study the effect of U_G on gas holdup in the EALR, the reactor is operated in the OV and CV modes and compared to the BC mode. The effect of EALR operational mode on gas holdup is shown in Figure 4.11 for A = 0.62%. When $U_G \lesssim 3.5$ cm/s, the operational mode has a negligible effect on riser gas holdup, ε_r. When $U_G \gtrsim 3.5$ cm/s, there appear to be slight differences in ε_r, but this variation is small, and in some cases, the degree of variation is not more than the expected measurement error. It is apparent that aside from minor variations in magnitude, ε_r is, at most, a weak function of EALR operational mode for the given reactor geometry. Similar results are observed for A = 0.99 and 2.22%.

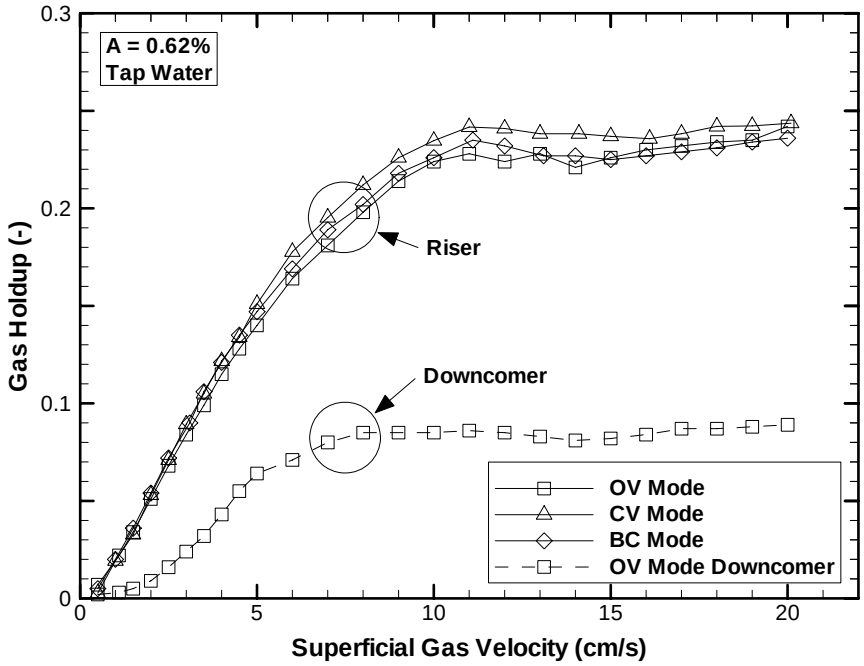

Figure 4.11: Effect of external airlift loop reactor operation mode on gas holdup for A = 0.62%.

Note that the downcomer gas holdup, ε_d, is only shown for the OV mode in Figure 4.11 because ε_d is negligible when the EALR is operated in the CV mode and nonexistent for the BC mode. For $U_G < 2$ cm/s, $\varepsilon_d \approx 0$, which agrees with visual observations made at these operating conditions. When $2 \lesssim U_G \lesssim 10$ cm/s, ε_d increases sharply with increasing U_G. Further increases in U_G result in no change in ε_d. Note that for most cases, ε_d is approximately three times smaller than ε_r for the OV mode and $\varepsilon_d \approx 0$ for the CV mode.

Figure 4.12 shows the effect of aeration plate open area ratio on gas holdup for the OV mode of operation. The ε_r trends between aeration plates for the OV mode are similar to the variations observed when the EALR is operated in BC mode. Figure 4.12 also shows no significant variation in ε_d for the different aeration plates considered in this study.

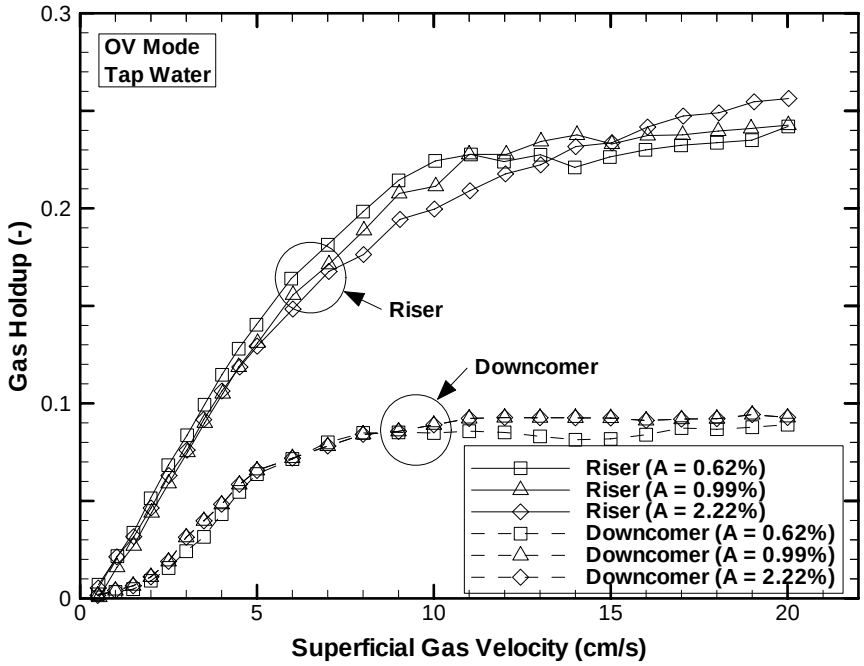

Figure 4.12: Aerator plate open area ratio effect on gas holdup for open vent mode external airlift loop reactor operation.

4.2.2 Deionized Water Gas Holdup

The effect of EALR mode of operation and aerator plate open area ratio on gas holdup is shown Figure 4.13 and Figure 4.14 when deionized water is used as the working fluid. The change in ε_r with U_G for the deionized water (Figure 4.13) closely resembles the trends observed for tap water with a few slight differences. First, it appears that ε_r for the CV mode of operation more closely resembles the BC mode of operation for deionized water than it did for tap water. Second, the locations of the local ε_r maximum and minimum appear to occur at higher U_G for deionized water versus tap water, indicating that the onset of slugging in the heterogeneous flow regime in the riser is delayed from $U_G \approx 10$ cm/s for tap water to $U_G \approx 12$ cm/s for deionized water. Third, the OV mode ε_d response to increasing U_G

resembles more closely the ε_r response for the deionized water than it did for the tap water, where there is a more pronounced local ε_d maximum at $U_G \approx 10$ cm/s and a greater decline in ε_d for $U_G > 14$ cm/s. Likewise when the gas holdup responses in Figure 4.14 are compared to those in Figure 4.12, most of the observed differences are small. The one exception is a notable difference in the ε_d response to U_G when A = 2.22% where ε_d for the deionized water case is shown to be completely independent of U_G for $U_G > 8$ cm/s, a trend that is not seen for any other operating conditions. The gas holdup results for tap water and deionized water show that, albeit minor, differences in both riser and downcomer gas holdup do not appear to be significantly affected by removing compounds from the tap water when it is deionized. This suggests that from a hydrodynamic stand point, there is little benefit associated with using deionized water over tap water.

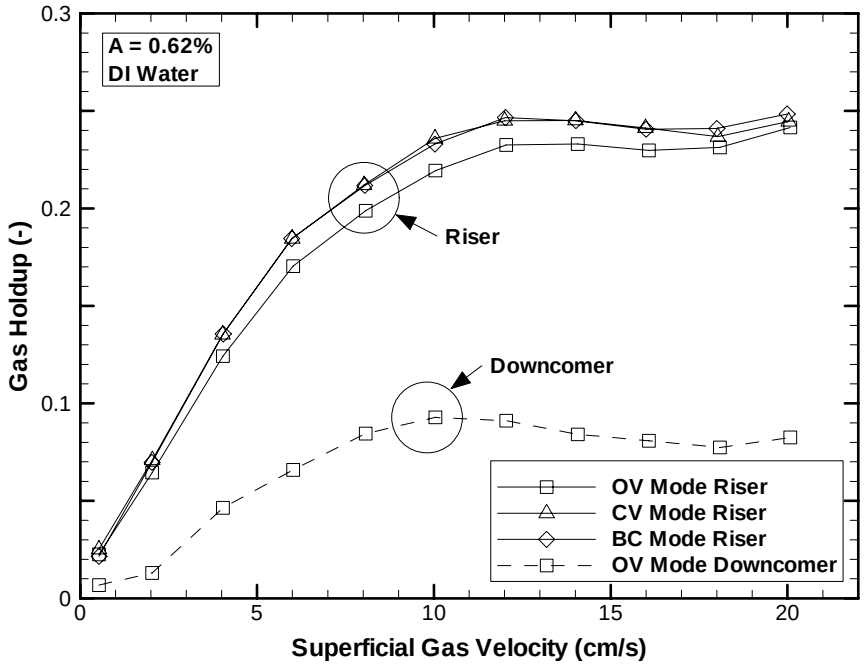

Figure 4.13: Gas holdup as a function of superficial liquid velocity and external airlift loop reactor operation using deionized water when A = 0.62%.

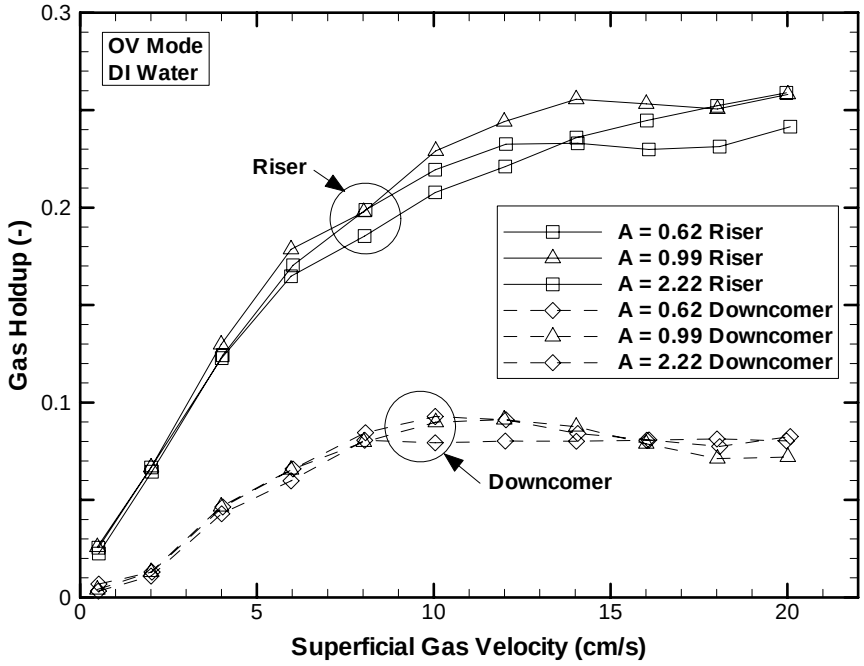

Figure 4.14: Gas holdup as a function of superficial liquid velocity and aerator plate open area using deionized water for the OV mode of external airlift loop reactor operation.

4.2.3 KCl Solution and Nitrosomonas Solution Gas Holdup

Water containing salt and inorganic compounds are known to influence riser and downcomer gas holdup in EALRs, see Section 2.3.6. To determine how gas holdup is affected by these types of compounds, riser and downcomer gas holdup is measured in the EALR using a 0.07 M KCl solution and a 0.04 M nitrosomonas solution and compared to tap and deionized water gas holdup results (Figure 4.15).

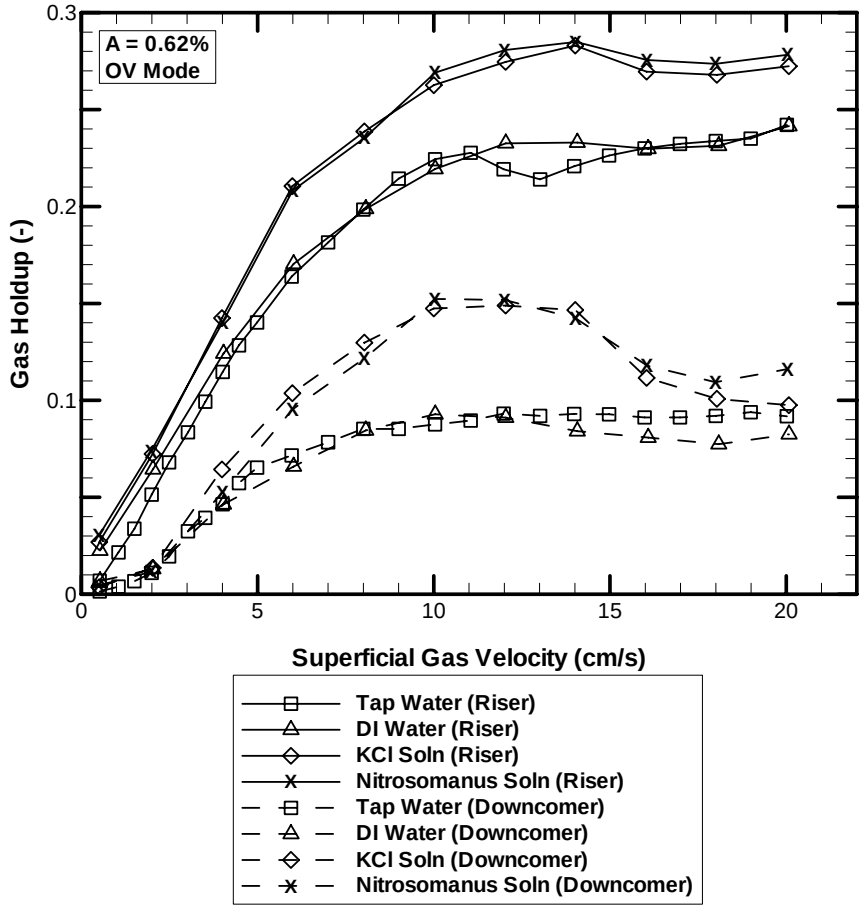

Figure 4.15: Gas holdup as a function of superficial liquid velocity and fluid type for the OV mode external airlift loop reactor where A = 0.62%.

Figure 4.15 shows that the riser and downcomer gas holdup for the KCl and nitrosomonas solutions are nearly identical for all U_G studied. The observed riser gas holdup response with increasing U_G for these two solutions is similar to that observed for both tap and deionized water, with the exception that the riser gas holdup values were higher and that the onset of heterogeneous flows appears to occur later at $U_G \approx 14$ cm/s. While the riser gas holdup mostly differs in magnitude, the downcomer gas holdup includes the increase in magnitude as well as increasing differently with U_G. The downcomer gas holdup local maxima for the KCl and nitrosomonas solutions are more pronounced than those observed for tap and deionized water. Visual observations noted during these two tests also indicate that ε_d significantly increases with the addition of the ionic compounds. The gas bubble size in the riser appears to be smaller also, suggesting that bubble coalescence is reduced by the addition of the ionic compounds. Similar trends have been observed by others [9, 20, 25, 40, 65-67, 81, 141] (see Section 2.3.6).

4.2.4 Gas Holdup Correlations

Sections 4.2.1 through 4.2.3 present gas holdup data for all three reactor flow regimes; however, the literature related to EALRs, unlike BCRs, typically only consider gas holdup data in the homogeneous and transitional flow regimes. Therefore only the gas holdup collected for superficial gas velocities less than $U_G \leq 10$ cm/s will be used to show how this reactor compares to other EALRs having different downcomer to riser cross-

sectional areas (AR), as flow conditions greater than U_G = 10 cm/s are typically heterogeneous in this EALR.

The gas holdup data collected for this particular EALR is compared with literature correlations and plotted in Figure 4.16. The selected correlations, listed in Table 4.1, were developed for varying EALR configurations having ARs that ranged from 0.11 to 1.0, and were reported by the corresponding authors to fit their data with correlation coefficients greater than 0.96. The predicted ε_r corresponds to predictions using the respective correlations from the literature and the measured ε_r corresponds to the tap water ε_r data from this study. If the correlation correctly predicted the experimental data, the symbols in Figure 4.16 would fall on the x = y line. Figure 4.16 shows that correlations #5 through #7 represent the data very well for gas holdup values above $\varepsilon_r \approx 0.07$ while correlations #1 to #4 exhibit up to a 20% disparity for the same range of ε_r values. There is at least a 20% disparity at lower gas holdups for correlations #1 to #7 and the disparity between the data and correlation #8 is never less than ~30%. The fact that most of the correlations presented here for other EALRs do not fit the current data very well reinforces the idea that most empirical scale up equations for EALRs are not generally applicable to other EALRs, especially if there are significant geometric or operating differences. However, it is evident from these correlations that the data can be characterized by:

$$\varepsilon_r = \alpha U_G^{\beta} \tag{4.1}$$

where α and β are empirically determined for specific EALR configurations. In fact, many of the correlations shown in Table 4.1 are in this form, where α is a combination of empirically determined geometric parameters and constants; however, it is evident from the many differing correlations that α has yet to be sufficiently identified in terms of physical parameters, suggesting that Equation (4.1) is sufficient at this time for predicting ε_r. Figure 4.17 shows how well the measured ε_r was predicted using Equation (4.1). In the homogeneous flow regime ($0.5 \lesssim U_G \lesssim 5$ cm/s) the values for α and β are 0.022 and 1.17, respectively, and in the transitional flow regime ($5 \lesssim U_G \lesssim 10$ cm/s) α and β were found to equal 0.059 and 0.58, respectively (Table 4.2). While the determined values are slightly different from those proposed by Chisti [2] and Merchuk [22], these new coefficients, when used with Equation (4.1), fit the data within ±15%.

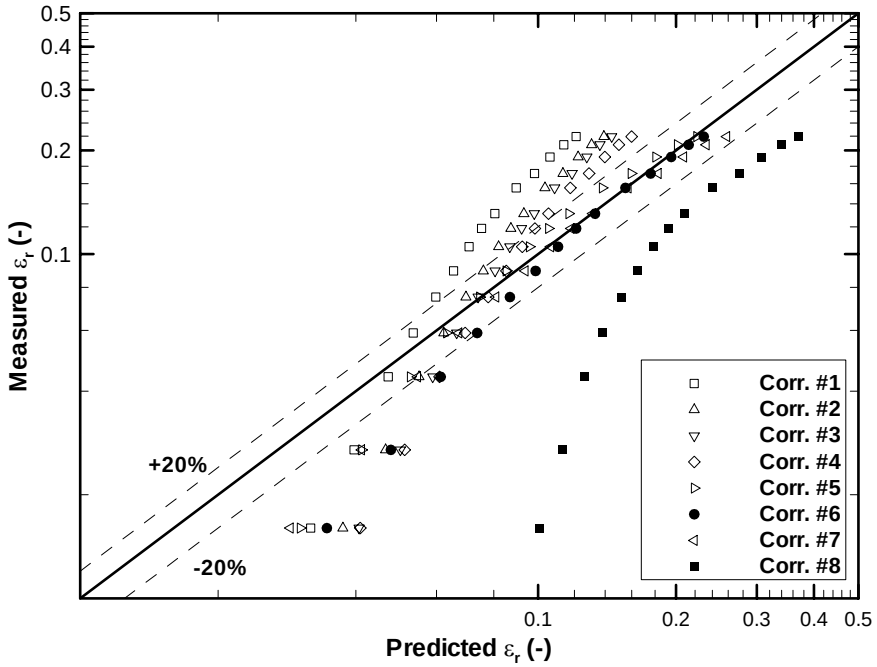

Figure 4.16: Variation in riser gas holdup correlations used to predict gas holdup in an external airlift loop reactor. See Table 4.1 for correlation legend.

Table 4.1: Summary of the correlations selected from the literature relating gas holdup to superficial gas velocity and external airlift loop reactor geometries and used in Figure 4.16.

No.	Reference	Gas Holdup Correlation	Superficial Gas Velocity (m/s)	A_d/A_r (-)	Other[a]
1	Merchuk 1986	$\varepsilon_r = 0.047 U_G^{0.59}$	0.002 - 0.5	?	
2	Choi 2000	$\varepsilon_r = 0.2447\left(\frac{A_d}{A_r}\right)^{-0.2779} U_G^{0.5616} h^{-0.0130}$	0.02 - 0.18	0.11 - 0.53	$0.04 < h < 0.20$
3	Choi 2001	$\varepsilon_r = 0.431 U_G^{0.580}\left(\frac{A_d}{A_r}\right)^{-0.040}\left(\frac{L_c}{L_h}\right)^{-0.042}$	0.02 - 0.18	0.11 - 0.53	$0.1 < L_c/L_h < 0.5$
4	Chisti 1989	$\varepsilon_r = 0.65\left(1+\frac{A_d}{A_r}\right)^{-0.258} U_G^{0.603}$	0.026 - 0.21	0.25 - 0.44	
5	Bentifraouine et al. 1997	$\varepsilon_r = 2 U_G^{0.88}\left(1-0.97 U_{Lr}^{0.49}\right)$	0.002 - 0.06	?	$0.0 < U_{Lr} < 0.2$
6	Hills 1976	$\varepsilon_r = U_G / \left(0.21+1.35(U_G+U_{Lr})\right)^{0.93}$	0.4 - 3.2	1	$0.0 < U_{Lr} < 2.5$
7	Chisti 1989	$\varepsilon_r = 2.4 U_G^{0.97}$	0.026 - 0.21	0.25 - 0.44	
8	Bello et al. 1985	$\varepsilon_r = 0.16\left(\frac{U_G}{U_{Lr}}\right)^{0.57}\left(1+\frac{A_d}{A_r}\right)$	0.005 - 0.1	0.11 - 0.69	

[a] h, unaerated liquid height in the gas/liquid separator (m); L_c/L_h, downcomer/riser connector length to height ratio (-); U_{Lr}, riser superficial liquid velocity (m/s).

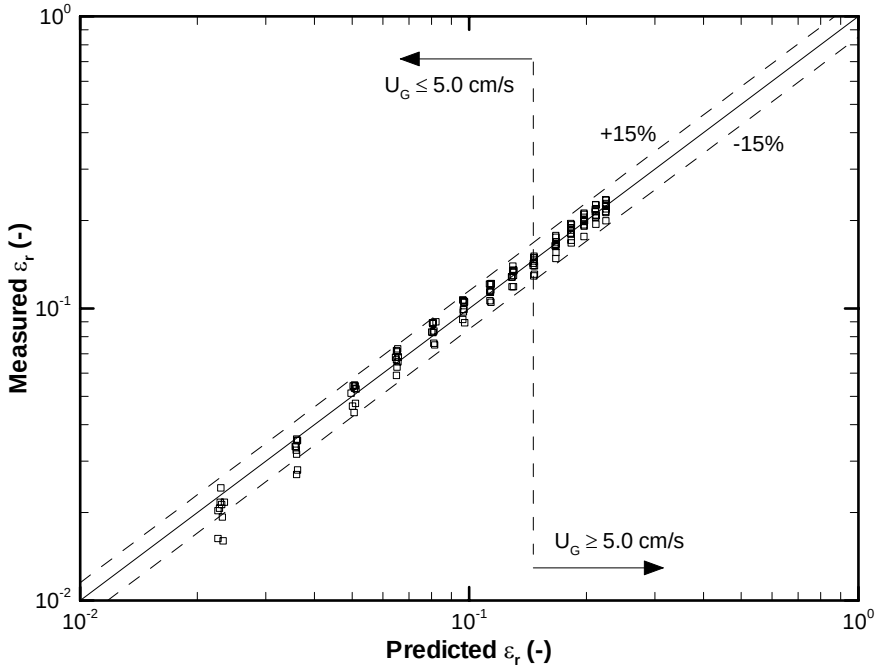

Figure 4.17: Parity plot of the tap water riser gas holdup correlation expressed by Equation (4.1) using the coefficients and exponents shown in Table 4.2.

Table 4.2: Tap water riser gas holdup correlation coefficients and exponents for Equation (4.1) shown in Figure 4.17.

Superficial Gas Velocity (cm/s)	α	β
0.5 – 5.0	0.022	1.17
5.0 – 10	0.059	0.58

4.3 Liquid Velocity

This section presents the results of the liquid velocity tests. Like gas holdup, the liquid velocity is measured for unconditioned tap water, deionized tap water, a KCl solution, and a nitrosomonas solution. This section is divided into three sub-sections covering (i) tap water liquid velocity, (ii) deionized water, KCl solution, and nitrosomonas solution liquid velocity, and (iii) tap water liquid velocity correlations. The first sub-section about the tap water data includes an in depth look at liquid velocity, its dependence on gas holdup, and its relationship to operating conditions, while the second sub-section compares and contrasts the tap water liquid velocity data with the deionized water, KCl solution, and nitrosomonas solution data. All of the liquid velocity data is presented for each condition in Appendix C.

4.3.1 Tap Water Liquid Velocity

The bulk density difference of the two vertical columns in an EALR provides the driving force for liquid circulation (i.e., U_{Lr} and U_{Ld}). At steady state conditions, the driving force is balanced by reactor flow losses due to fluid friction and changes in reactor geometry [2, 21, 137, 142, 143]. Thus, as the difference between ε_r and ε_d increases with increasing U_G, the driving force must also increase due to bulk density changes associated with

changing gas holdup, creating a potential for U_{Lr} to increase. However, in practice, U_{Lr} may increase or decrease with U_G depending on how the reactor flow losses change with U_G. Hence, U_{Lr} can be considered largely a function of U_G and reactor geometry.

The effect of U_G on U_{Lr}, as a function of aerator plate open area ratio and mode of operation, is shown in Figure 4.18. The aerator plate open area ratio has a minimal effect on U_{Lr} for both modes of operation. When the EALR is operated in the OV mode, U_{Lr} increases to a local maximum and then decreases sharply as U_G increases, and eventually becomes independent of U_G. Therefore, three liquid flow regimes are identified for the OV mode of operation: (i) unrestricted flow, (ii) restricted flow, and (iii) fully restricted flow.

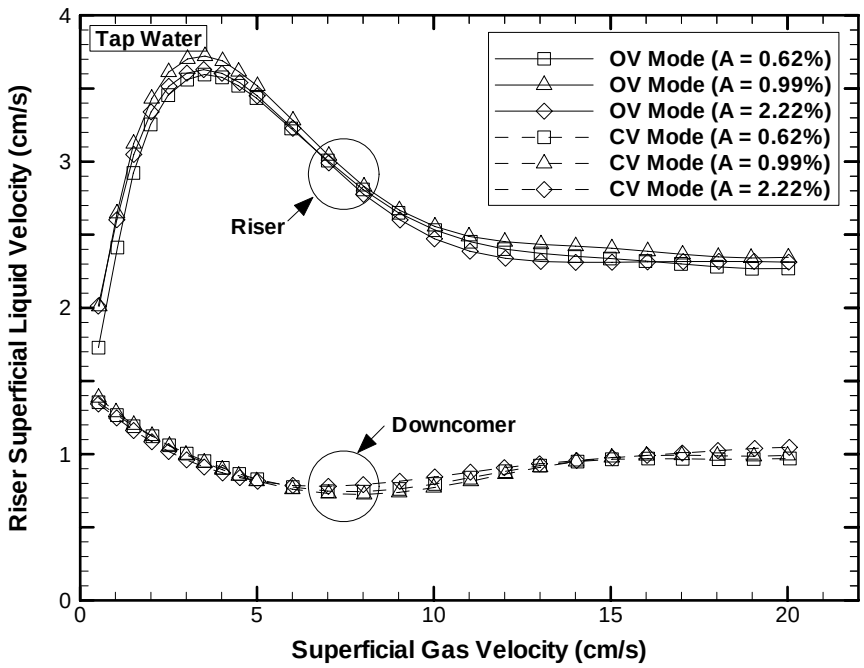

Figure 4.18: Aerator plate open area ratio and mode of operation effects on riser superficial liquid velocity.

In the unrestricted flow regime, U_{Lr} increases sharply with increasing U_G. This initial increase in U_{Lr} corresponds to the rapid rise in ε_r and a much smaller rise in ε_d (Figure 4.12). Hence, when $U_G \lesssim 3.5$ cm/s, U_{Lr} is primarily a function of the bulk density difference; this observation agrees with the experimental results presented by others [18, 21, 24, 48, 144].

When the bulk density difference ($\varepsilon_r - \varepsilon_d$) is plotted as a function of U_{Lr} (Figure 4.19), the relationship between the driving force and liquid circulation becomes evident. As a result, Figure 4.19 is useful in identifying the liquid flow regimes and their transition points. Figure 4.19 shows that the shift from the unrestricted flow regime to the restricted flow regime occurs at $U_{Lr} \approx 3.7$ cm/s, which roughly corresponds to the point where bubble formation is observed in the downcomer. As noted earlier, stationary gas bubble formation in the top of the downcomer begins at $U_G \approx 3.5$ cm/s.

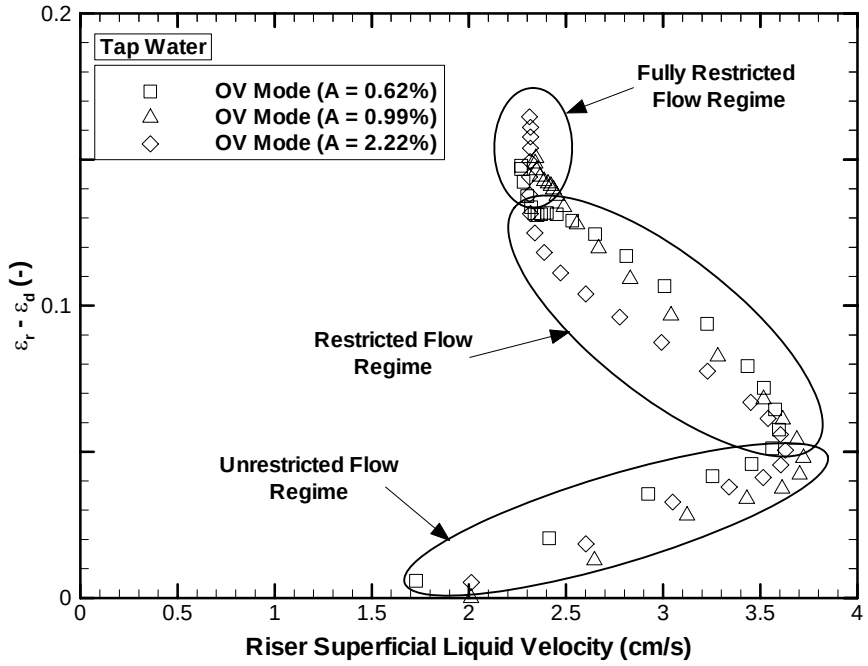

Figure 4.19: Relationship between driving force ($\varepsilon_r - \varepsilon_d$) and superficial liquid velocity as a function of aerator plate open area ratio for the open vent mode external airlift loop reactor operation.

Increasing U_G in the restricted flow regime results in a decrease in U_{Lr}. Figure 4.19 also shows that U_{Lr} decreases in this regime as the bulk density difference increases, which is contrary to the observations made for the unrestricted flow regime. Hence, when U_{Lr} is a function of the flow losses, geometry, and driving force, the flow losses are considered to dominate in this flow regime. The dominance of the flow losses in this regime is attributed to stationary gas bubble growth in the downcomer, which causes the flow losses to increase rapidly with increasing in U_G. Initially, as the stationary gas bubble begins to grow ($3.5 \lesssim U_G \lesssim 5$ cm/s), the effective AR decreases, creating a choked flow condition in the downcomer that corresponds to the U_{Lr} local maximum shown in Figure 4.18. Furthermore, as U_G continues to increase (5 cm/s $\lesssim U_G \lesssim 10$ cm/s), the bubble length increases until it

reaches a maximum length at $U_G \approx 10$ cm/s. Stationary gas bubble length change in this regime is a result of an increase in the bulk density difference and the initial flow restriction in the downcomer due to liquid separation from the downcomer wall. Hence, even though the driving force increases, the flow losses increase faster with U_G causing U_{Lr} to decrease. Essentially, the downcomer flow has become choked.

As shown in Figure 4.18, U_{Lr} continues to decrease with increasing U_G due to stationary gas bubble development and growth until a maximum stationary gas bubble size is reached. This transition is easily identified in Figure 4.19 and occurs when the driving force becomes independent of U_{Lr} (≈ 2.3 cm/s), which corresponds to roughly $U_G = 10$ cm/s. Under these conditions, the liquid flow in the downcomer is fully choked and the EALR hydrodynamics are similar to those of a bubble column.

When the EALR is operated in the CV mode, the U_{Lr} trends as a function of U_G are limited to the later two flow regimes discussed for the OV mode operation (Figure 4.20). As discussed in the hydrodynamic observations, a gas pocket forms immediately in the horizontal connection for the lowest U_G and a stationary gas bubble forms in the downcomer soon after as U_G is increased, causing the EALR to operate in the restricted flow regime. It is worth noting that even though ε_d exists for this mode of operation, the magnitude is so small that it can not be measured with any degree of accuracy, and thus is considered negligible. The driving force for the CV mode of operation becomes solely a function of ε_r, unlike the OV mode where the driving force is a function of the difference between ε_r and ε_d.

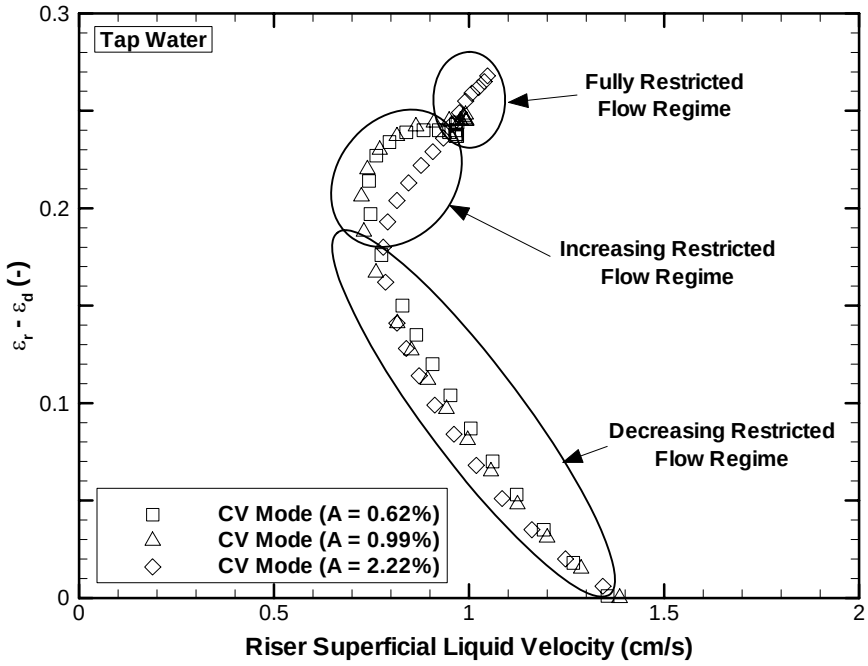

Figure 4.20: Relationship between driving force ($\varepsilon_r - \varepsilon_d$) and superficial liquid velocity as a function of aerator plate open area ratio for the closed vent mode external airlift loop reactor operation.

For the CV mode of operation shown in Figure 4.20, the restricted flow regime is separated into a decreasing and increasing restricted flow regimes. Initially, as U_G increases, the fluid flow is characterized as decreasing restricted flow where, as shown in Figure 4.18, U_{Lr} decreases with increasing U_G. This decrease in U_{Lr} continues until a local minimum is reached at $U_G \approx 7$ cm/s, which corresponds to $\varepsilon_r \approx 0.18$ (Figure 4.11). The decrease in U_{Lr} in this regime is again attributed to the development and growth of the stationary gas bubble in the downcomer. Once the minimum U_{Lr} is reached, U_{Lr} begins to increase with increasing U_G, switching the flow regime to the increasing restricted flow regime. In this flow regime, U_{Lr} continues to increase with U_G and ε_r until $U_G \approx 14$ cm/s and $\varepsilon_r \approx 0.24$. It is important to note that the stationary gas bubble growth is observed to be relatively constant as U_G

increases through both restricted flow regimes, indicating that for the decreasing restricted flow regime, flow losses initially exceed the increase in the driving force. This effect then reverses as the flow regime changes to increasing restricted flow, indicating that in this regime, the driving force is larger than the flow losses.

As shown in Figure 4.18, U_{Lr} is independent of aerator plate open area ratio; however, the onset of the fully restricted flow regime for the CV mode is influenced by the aerator plate open area ratio. The shift from the increasing restricted flow regime to the fully restricted flow regime occurs at $U_G \approx 13$ cm/s for $A < 1\%$. For $A = 2.22\%$, the transition into the fully restricted flow regime occurs at $U_G \approx 19$ cm/s, but more data with $U_G > 20$ cm/s is needed to fully understand the transition location for the CV mode of operation when $A = 2.22\%$. As discussed for the open vent mode of operation, U_{Lr} in the fully restricted flow regime is independent of U_G.

4.3.2 Deionized Water, KCl Solution, and Nitrosomonas Solution Liquid Velocity

The riser superficial liquid velocity as a function of aerator open area ratio and U_G when deionized water is used in place of tap water is shown in Figure 4.21. Figure 4.21 shows that the U_{Lr} change with increasing U_G is similar to that shown in Figure 4.18 for tap water. As with tap water, U_{Lr} is dependent on EALR mode of operation and not a function of aerator plate open area ratio. When U_{Lr} data for tap water and deionized water are direct compared as shown in Figure 4.22, it is seen that there is no significant difference in U_{Lr} for

$U_G < 8.0$ cm/s; however, for $U_G > 8.0$ cm/s differences in U_{Lr} are noted where U_{Lr} is higher for deionized water. The increase in U_{Lr} when $U_G > 8.0$ cm/s is attributed to the shift in the local ε_r maximum and the lower ε_d for deionized water compared to tap water.

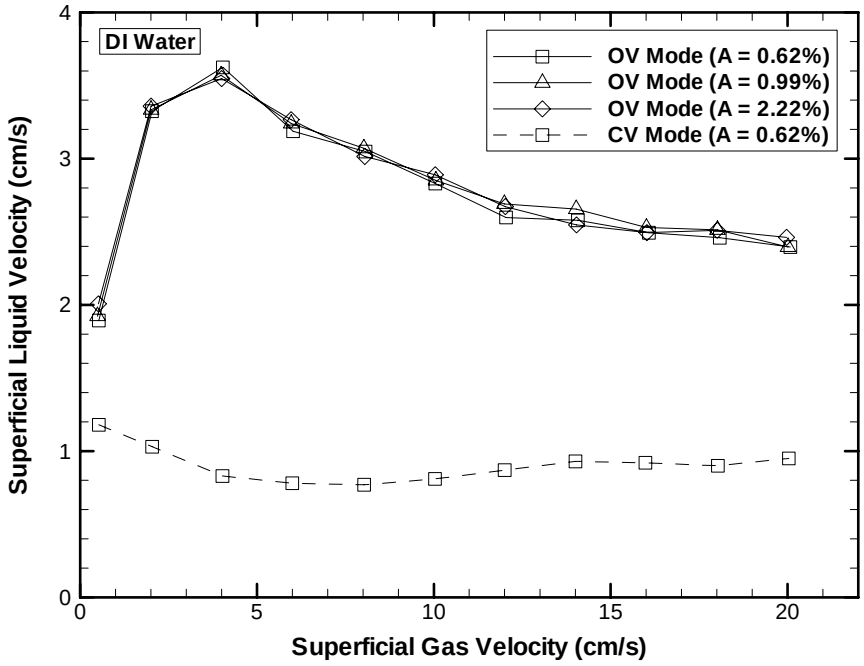

Figure 4.21: Aerator plate open area ratio and mode of operation effects on riser superficial liquid velocity for deionized water.

Figure 4.22 also shows that U_{Lr} for the KCl and nitrosomonas solutions changes with U_G much like U_{Lr} did for tap water, however, the response is somewhat different. For $U_G < 2.0$ cm/s, there is no observable difference in U_{Lr} for any of the liquid media considered. As U_G increases from 2 cm/s to 10 cm/s, a considerable difference in U_{Lr} is noted. For the nitrosomonas solution U_{Lr} initial behaves like tap and deionized water, but then dramatically drops to a local minimum at $U_G \approx 10$ cm/s and then converges back to U_{Lr} values observed for tap water. Similarly, U_{Lr} for the KCl solution also declines dramatically

like that seen for the nitrosomonas solution; however, the local maximum at $U_G \approx 4$ cm/s is much lower for the KCl solution than for all of the other media types. Otherwise the KCl solution U_{Lr} behaves much like the nitrosomonas solution U_{Lr} where the slight difference in behaviors that occur between $10 \lesssim U_G \lesssim 16$ cm/s are due to magnifications of the minor differences in ε_d that get magnified when U_{Lr} is calculated using Equations (3.5) and (3.6).

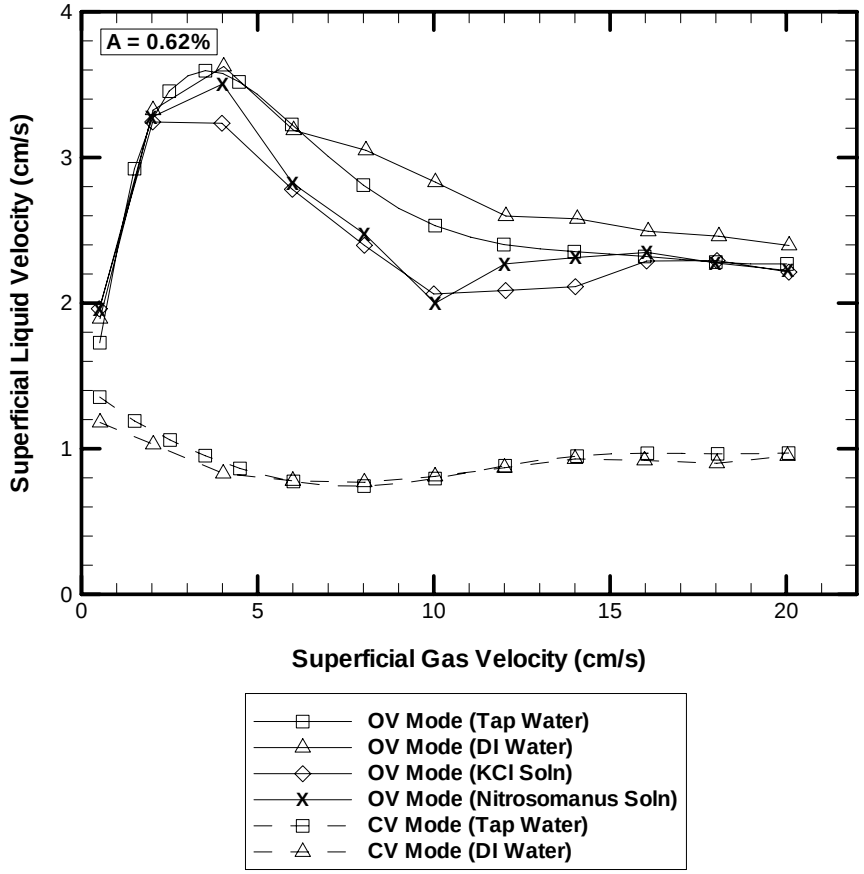

Figure 4.22: Liquid medium and mode of operation effects on riser superficial liquid velocities for A = 0.62%.

Figure 4.22 shows that there is no significant change in U_{Lr} due to liquid phase properties for the CV mode of operation. This similarity in the U_{Lr} response does not follow

the trends observed for the OV mode of operation where U_{Lr} changed with changes in ε_r and ε_d. The lack of a change in the CV mode U_{Lr} with fluid types indicates that this mode of operation is dominated by flow restrictions in the upper horizontal connector and downcomer. Since the tap water and deionized water results showed no real change, the CV mode of operation tests were not completed using the KCl and nitrosomonas solutions as no significant change in U_{Lr} is expected.

4.3.3 Tap Water Liquid Velocity Correlations

Figure 4.23 compares the tap water U_{Lr} data for this work to the U_{Lr} values reported in the literature for EALRs with similar geometries and ARs that vary from 0.04 to 1.0 [11, 21, 22, 37]. The magnitude of U_{Lr} for the current study is similar to that reported in these works for EALRs with an A_d/A_r ratio smaller than 0.11; however, the response of U_{Lr} with increasing U_G is much different due to the unique flow conditions observed in this EALR. Therefore, any attempt to predict U_{Lr} for this reactor using the published correlations failed due to the changing liquid flow regimes in this reactor (Section 4.3.1). However, as suggested by Gavrilescu and Tudose [11] the U_{Lr} data for the current study is a function of U_G with a power-law dependence in the form:

$$U_{Lr} = \alpha U_G^{\beta} \tag{4.2}$$

where, as explained by Gavrilescu and Tudose [11], α and β are not constant for the entire range of U_G. The exponent β was reported to be dependent on U_G while α depends on the reactor geometry. Thus, for this EALR α is best described by:

$$\alpha = \varphi\left(\varepsilon_r - \varepsilon_d\right)^{\gamma} \tag{4.3}$$

where $(\varepsilon_r - \varepsilon_d)$ accounts for the driving force within the EALR which is a function of the flow restriction in the downcomer.

Using the empirically determined coefficients listed in Table 4.3, the predicted U_{Lr} values are compared to the measured U_{Lr} data points in Figure 4.24. The proposed correlation as shown in Figure 4.24 predicts the experimental data with an error of less than 10%.

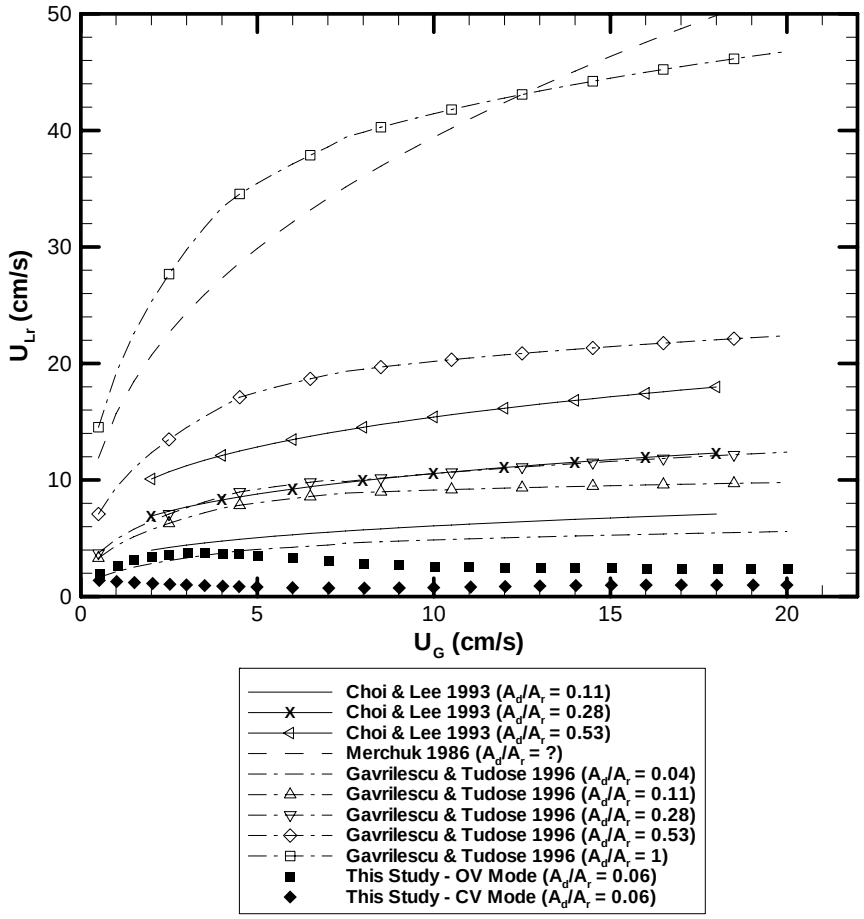

Figure 4.23: Riser superficial liquid velocity in external airlift loop reactors as a function of superficial gas velocity for reactors with similar geometric configurations and downcomer to riser cross sectional area ratios that range from 0.04 to 1.0.

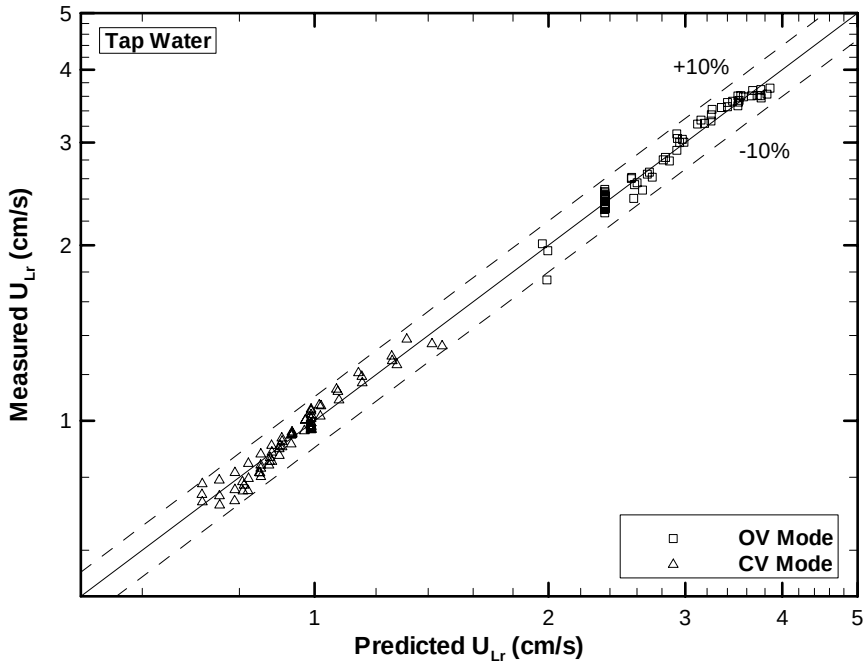

Figure 4.24: Parity plot of the U_{Lr} correlation expressed by Equations (4.2) and (4.3).

Table 4.3: Riser superficial liquid velocity correlation coefficients and exponents for Equations (4.2) and (4.3) shown in Figure 4.24.

Mode of Operation	Superficial Gas Velocity (cm/s)	β	φ	γ
Open Vent Mode	0.5 – 3.5	0.054	0.09	0.219
Open Vent Mode	3.5 – 12	-0.079	0.01	-0.359
Open Vent Mode	12 – 20	0.0	0.024	0.0
Closed Vent Mode	0.5 – 8	-0.388	0.003	0.069
Closed Vent Mode	8 – 15	0.576	0.029	0.0
Closed Vent Mode	15 – 20	0.0	0.01	0.0

4.4 Gas-Liquid Mass Transfer

This section presents the gas-liquid mass transfer results for the EALR. This section will be presented in three sub-sections (i) oxygen gas-liquid mass transfer, (ii) carbon monoxide gas-liquid mass transfer, and (iii) gas-liquid mass transfer correlations. The data presented in this section are tabulated in Appendix D.

4.4.1 Oxygen Gas-Liquid Mass Transfer

Figure 4.25 shows the oxygen k_La as both a function of U_G and EALR mode of operation for A = 0.62% and deionized water. The oxygen k_La for all three modes increases with U_G nearly the same way as ε_r did for similar operating conditions (Figure 4.11). The oxygen k_La for all three modes of operation shown in Figure 4.25 initially increases with U_G until the flow regime in the reactor approaches the heterogeneous flow regime at about $U_G \approx 10$ cm/s, at which point a local maximum in oxygen mass transfer is observed. For $U_G > 10$ cm/s, the oxygen mass transfer begins to decline with increasing U_G until a local minimum is reached somewhere between $14 \lesssim U_G \lesssim 16$ cm/s, at which point oxygen k_La begins to slightly increase with U_G. This decrease and then slight increase in k_La for $U_G > 10$ cm/s is believed to be a result of gas slugging within the EALR that significantly reduces the gas bubble interfacial surface area available for gas-liquid mass transfer.

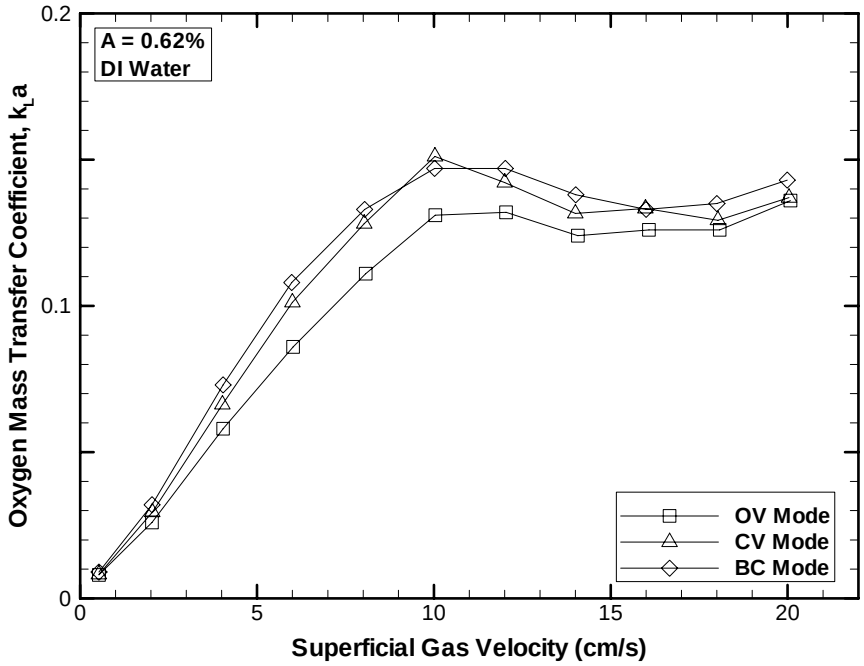

Figure 4.25: Oxygen volumetric mass transfer coefficient shown as a function of U_G and external airlift loop reactor mode of operation for A = 0.62% and deionized water.

Just as with ε_r, there appears to be little difference in the measured oxygen k_La values for the BC and CV modes of operation, and a slight difference between the measured oxygen k_La values for the OV mode of operation and the other two modes of operation. When the observed lower k_La and ε_r are compared for the OV mode of operation, it becomes apparent that k_La is significantly influenced by factors that also effect ε_r. Similarly, oxygen k_La as a function of aerator plate open area ratio and U_G (Figure 4.26) again behaves like ε_r (Figure 4.14) for similar operating conditions where the only major difference is that the maximum oxygen k_La occurs at a lower U_G.

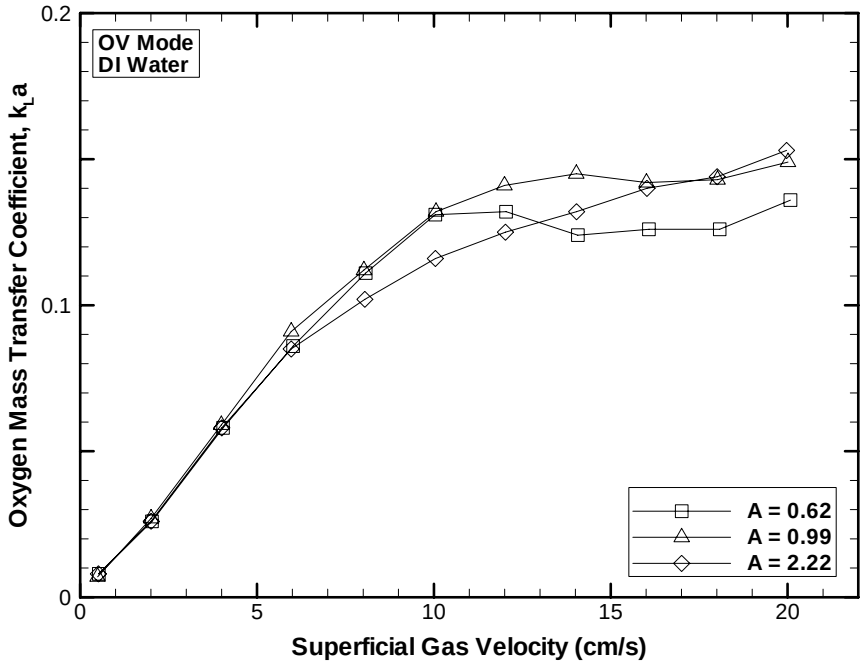

Figure 4.26: Oxygen volumetric mass transfer coefficient shown as a function of U_G and aerator plate open area ratio for external airlift loop reactor open vent mode of operation and deionized water.

The results presented in Figure 4.25 and Figure 4.26 show that EALR mode of operation and aerator plate open area ratio in and of themselves do not impact gas-liquid mass transfer rates, but that gas-liquid mass transfer rates are most notably impacted by changes in ε_r. Since gas-liquid mass transfer appears to be independent of most operating conditions and primarily a function of U_G, it is concluded that gas-liquid mass transfer is primarily a function of gas holdup for deionized water.

Since most biological applications do not use just deionized water, additional oxygen mass transfer tests are completed using a 0.07M KCl solution and a 0.04M nitrosomonas solution for A = 0.62% and the OV vent mode of operation. The observed k_La values for the KCl and nitrosomonas solutions are presented in Figure 4.27 and compared to those observed

for deionized water with and without a surfactant. For the KCl and nitrosomonas solutions, the oxygen k_La increases with U_G for the entire range of U_G considered except when $U_G = 16$ and 18 cm/s for the nitrosomonas solutions. The measured oxygen k_La values for these two solutions are only slightly greater than those observed using deionized water for $U_G < 10$ cm/s while being much greater for $U_G > 10$ cm/s. The magnitude of this observed difference between the oxygen k_La values for $U_G < 10$ cm/s is expected and is very similar to results presented in the literature [20, 63, 69, 80] and discussed in Section 2.3.7. However, the magnitude of the observed difference in oxygen k_La values between the deionized water and KCl or nitrosomonas solutions for $U_G > 10$ cm/s is much larger than expected and greater than anything presented in the reviewed literature in Section 2.3.7. One possible explanation for this large discrepancy between the measured data and the results reviewed in the literature is that most of the results presented in the literature review are for conditions representing the homogeneous and transitional flow regimes in the riser, whereas this study includes k_La data in the heterogeneous flow regime ($U_G > 10$ cm/s). Yet, this is not the primary factor influencing the observed difference in k_La values for the deionized water and the KCl and nitrosomonas solutions. In fact, the difference is believed to be largely due the hydrodynamic conditions that exist in the EALR for $U_G > 10$ cm/s.

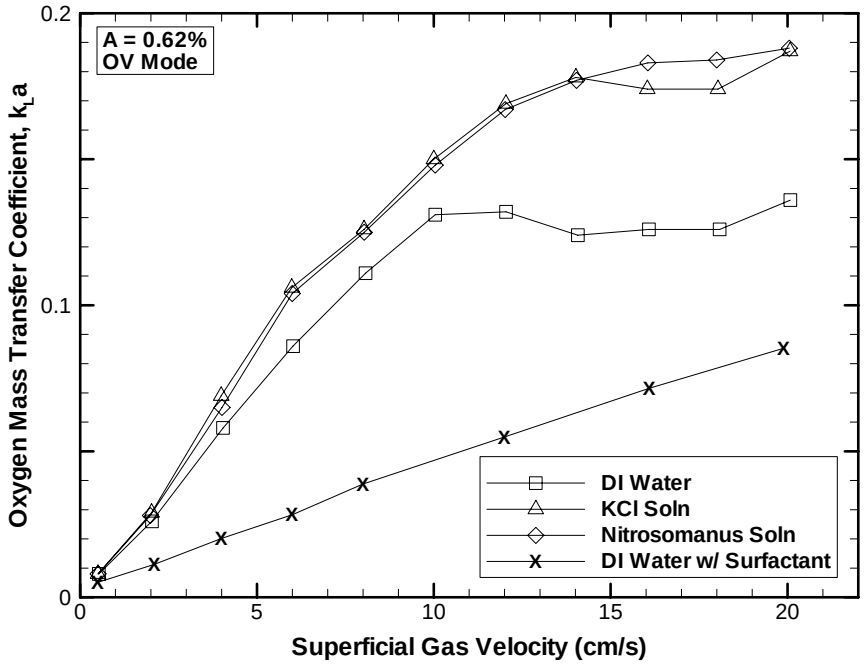

Figure 4.27: Oxygen volumetric mass transfer coefficient shown as a function of U_G and fluid type for A = 0.62% and external airlift loop reactor open vent mode of operation.

When $U_G > 10$ cm/s, ε_r is noted to be independent of U_G suggesting that k_La should likewise be independent of U_G, assuming of course, that k_La is a function of ε_r for all operating conditions. However, this supposition assumes that the bubble interfacial surface area increases proportionally with increasing ε_r, which is not entirely true in the heterogeneous flow regime because large bubbles form that have diameters approaching the same order of magnitude as the riser diameter. Hence, in the heterogeneous flow regime, ε_r may remain constant while the bubble interfacial surface area declines. This explains why k_La generally decreases when ε_r is relatively constant for deionized water and $U_G > 10$ cm/s.

In the case of the KCl and nitrosomonas solutions, another trend is observed, where k_La continues to increase with U_G even though ε_r remains constant. As before, large bubbles

are present in the riser, which reduces the effective bubble interfacial surface area, but the presence of inorganic compounds for these two test conditions is believed to inhibit formation of these large bubbles to a certain extent, while aiding in the formation of very small bubbles as the large bubbles form and break up. Thus, even though there are large bubbles present, it is believed that the presence of the more numerous smaller bubbles allows the k_La values to continue to increase with U_G in the heterogeneous flow regime, which is not observed when deionized water is considered.

Figure 4.27 also shows oxygen k_La data collected using deionized water containing an unknown surfactant. The data collected for the deionized water having the surfactant is the result of an unexpected contaminant being introduced into the water during the first set of deionized water tests. Even though this contamination happened accidentally and the exact water quality is unknown, the results of these tests were highly repeatable as shown Figure 4.28. Therefore, it is felt that the data gathered under these circumstances is not completely useless and may provide some useful insight. In fact, the oxygen k_La in this case is observed to increase in a linear fashion with U_G when the surfactant is present while not varying significantly with operational mode (Figure 4.28), indicating that k_La is primarily a function of U_G for this condition. As an aside, attempts to exactly reproduce the accidental conditions were unsuccessful; although, a few of the attempts using trace amounts of dish soap approached the data shown in Figure 4.28, indicating that dish soap was the probable contaminant.

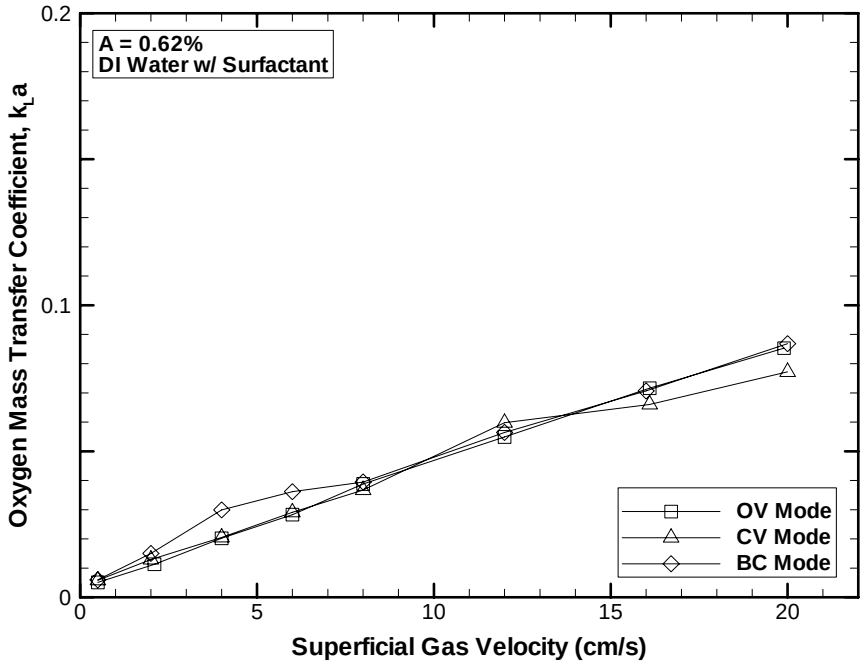

Figure 4.28: External airlift loop reactor volumetric oxygen mass transfer rate as a function of superficial gas velocity and mode of operation for A = 0.62%.

This linear relationship between k_La and U_G is much different from those observed previously for the deionized water, the KCl solution, and the nitrosomonas solution (Figure 4.27) where k_La is a function of U_G and ε_r. The difference in the observed trends is thought, in part, to be a result of the surfactant creating a more rigid bubble surface that increases the liquid film mass transfer resistance. The addition of the surfactant is also believed to increase the bubble surface tension and leads to an increase in the initial bubble size at the aerator plate [141]. However, the exact cause of the reduction in k_La is unknown due to the fact that the exact composition of the surfactant is unidentifiable.

4.4.2 Carbon Monoxide Gas-Liquid Mass Transfer

Carbon monoxide k_La data is collected simultaneously with oxygen k_La for a limited number of tests as listed in Table 3.2. The carbon monoxide k_La data is limited to $U_G < 14$ cm/s for most of the tests due to errors associated with being unable to collect the liquid samples faster than once every three seconds. Figure 4.29 shows the carbon monoxide k_La as a function of both U_G and EALR mode of operation for A = 0.62% and deionized water. The carbon monoxide k_La is found to be independent of EALR mode of operation. Like the oxygen k_La values, the carbon monoxide k_La values increase with increasing U_G for $U_G < 10$ cm/s. For $U_G > 10$ cm/s, it appears that carbon monoxide k_La may become independent of U_G; however, due to the number of data points above $U_G > 10$ cm/s, this trend is not verifiable. Carbon monoxide k_La also differs slightly, if at all, with aerator plate open area ratio as shown in Figure 4.30, much like the oxygen k_La in Figure 4.26, while maintaining the same general relationship with U_G. Similarly, the carbon monoxide k_La shown in Figure 4.31 for the different fluid types again resembles the oxygen k_La data shown in Figure 4.27, where the measured k_La is highest for the KCl and nitrosomonas solutions and lowest for the deionized water having a surfactant. These results suggest that gas-liquid mass transfer for carbon monoxide and oxygen are influenced similarly by operating conditions in the EALR.

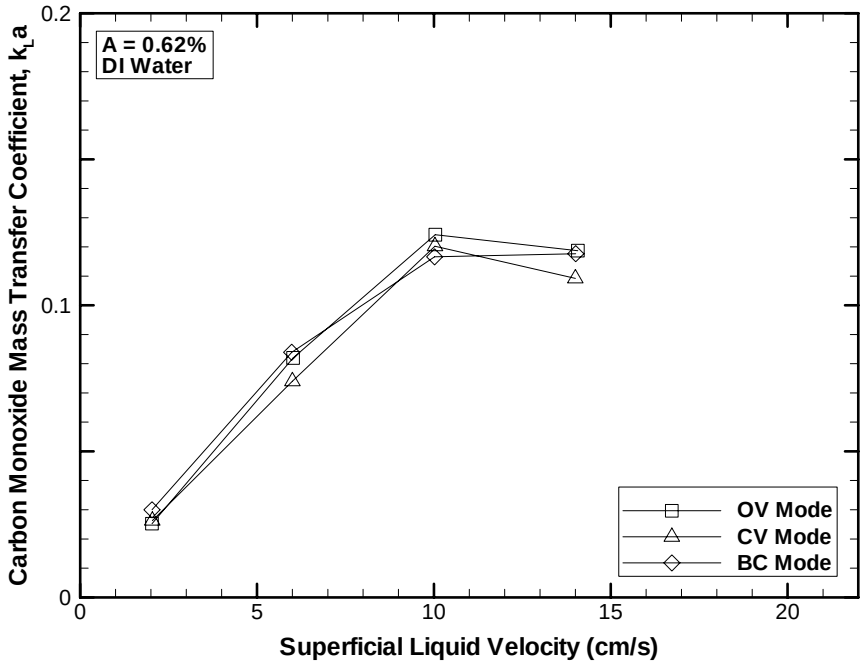

Figure 4.29: Carbon monoxide volumetric mass transfer coefficient shown as a function of U_G and external airlift loop reactor mode of operation for A = 0.62% and deionized water.

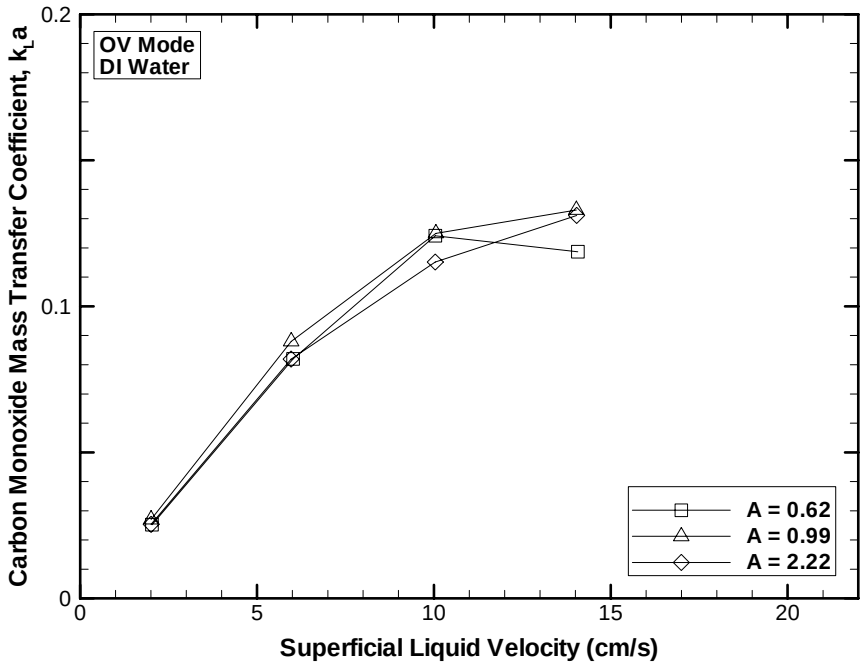

Figure 4.30: Carbon monoxide volumetric mass transfer coefficient shown as a function of U_G and aerator plate open area ratio for external airlift loop reactor open vent mode of operation and deionized water.

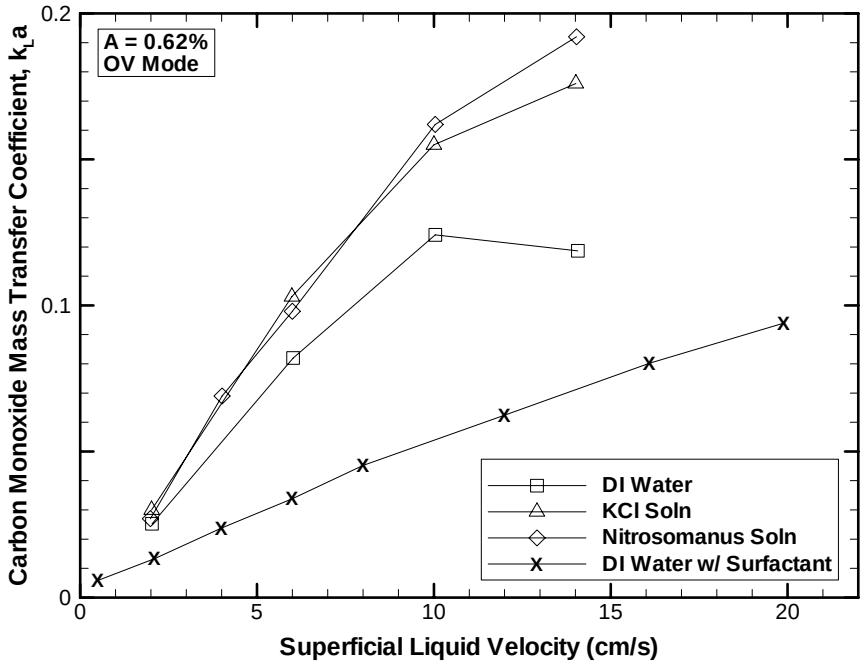

Figure 4.31: Carbon monoxide volumetric mass transfer coefficient shown as a function of U_G and fluid type for A = 0.62% and external airlift loop reactor open vent mode of operation.

4.4.3 Oxygen and Carbon Monoxide Gas-Liquid Mass Transfer Comparison

The theoretical relationship between oxygen and carbon monoxide k_La values shown in Figure 4.32 is based upon the discussion presented in Section 2.2.8 where the carbon monoxide k_La is related to oxygen k_La by [2, 33]:

$$\left(k_La\right)_{CO} = \left(k_La\right)_{O_2}\left(\frac{D_{CO}}{D_{O_2}}\right)^n \tag{4.4}$$

where D_{CO} and D_{O2} equal 2.17 and 2.35 cm^2/s [145], respectively, and n is equal to 0.5 to 1.0 depending on the model used to represent gas-liquid mass transfer. This theoretical relationship suggests that carbon monoxide k_La should always be less than oxygen k_La and that the difference between predicted values for the mass transfer models is less than 10%.

The data collect in this study does not fully support this theoretical relationship. In fact, the observed relationships between oxygen and carbon monoxide mass transfer in this work suggest that the use of these models may be somewhat limited depending on the operating environment.

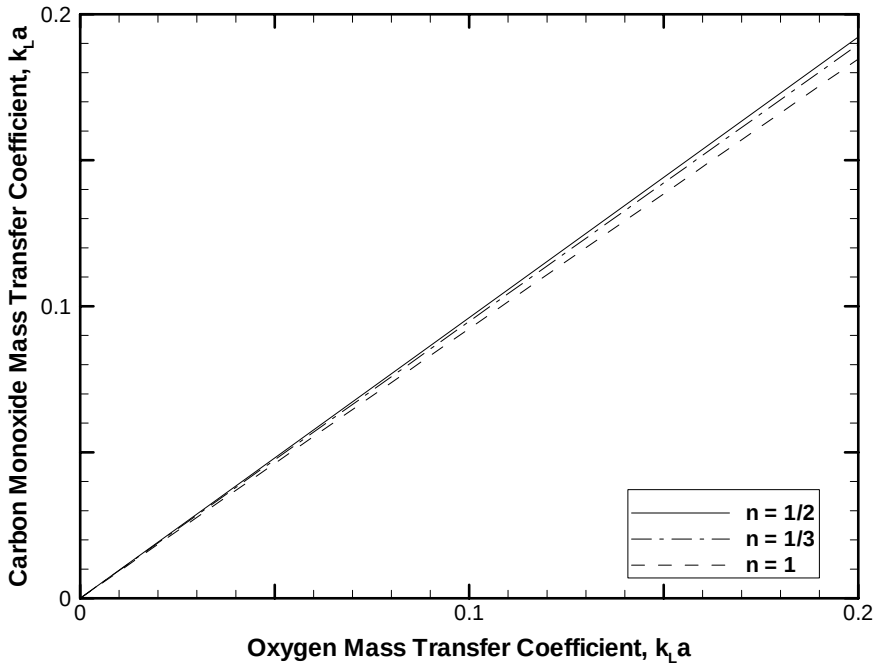

Figure 4.32: The theoretical relationship between oxygen and carbon monoxide mass transfer coefficients based upon the mass transfer models presented in Section 2.2.8.

A comparison of the oxygen and carbon monoxide $k_L a$ for the OV mode of operation using deionized water is shown in Figure 4.33. An empirical fit of Equation (4.4) to determine the value of n that best represents the data shown in Figure 4.33 indicates that n = 0.54 for these three test conditions. This implies that the penetration, surface renewal, or film-penetration model best describes the relationship between oxygen and carbon monoxide mass transfer for these three test conditions. However, this empirical fit only considers 12

data points; hence, it could be argued that any of the models presented in Section 2.2.8 are appropriate.

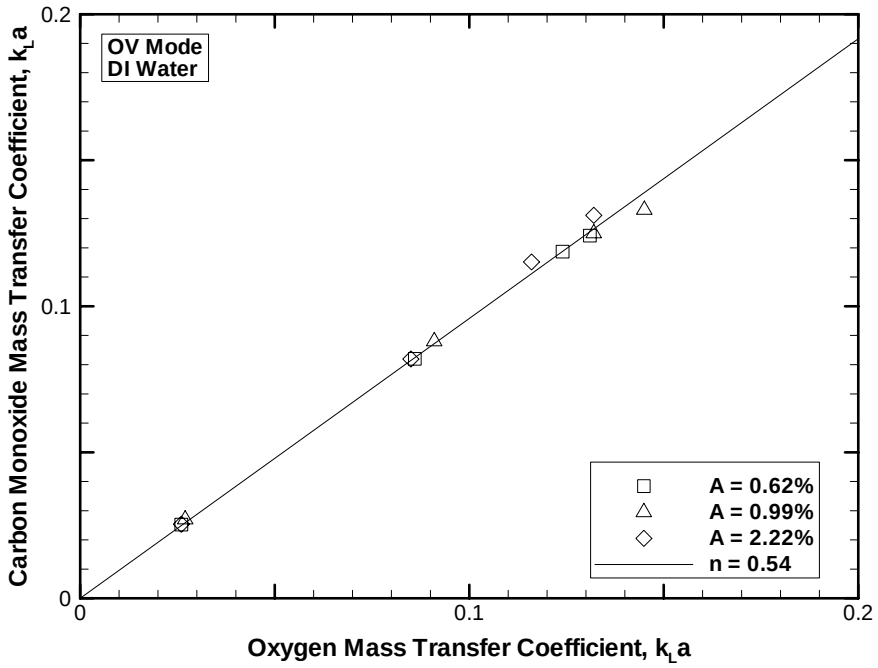

Figure 4.33: A comparison of carbon monoxide and oxygen gas-liquid mass transfer data for the open vent mode of external loop airlift reactor using deionized water showing how Equation (4.4) fits the data when n = 0.54.

When the k_La values are compared for the CV and BC modes of operation and A = 0.62% using deionized water, a slightly different trend is observed and shown in Figure 4.34. For these two conditions the carbon monoxide k_La is much lower than suggested by the theoretical relationships. Again, using Equation (4.4) to characterize the data presented in Figure 4.34, n = 2.72, a value much higher than those suggested by the mass transfer models.

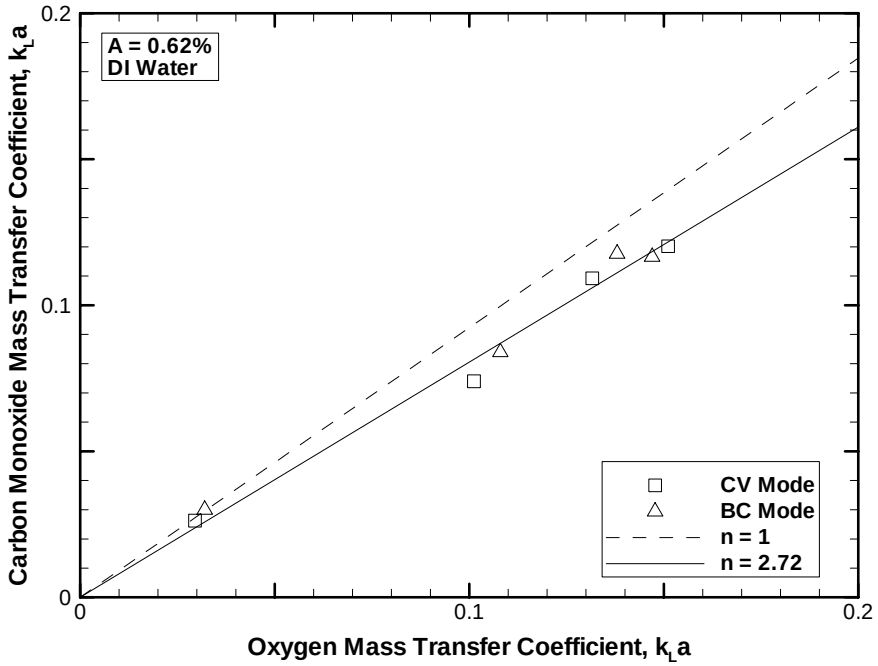

Figure 4.34: A comparison of carbon monoxide and oxygen gas-liquid mass transfer data for A = 0.62% using deionized water showing how Equation (4.4) fits the data when n = 2.72.

Furthermore, a comparison of the k_La data collected using the KCl and nitrosomonas solutions indicate that carbon monoxide k_La are slightly higher than expected (Figure 4.35). For these two conditions, n = -0.41 when Equation (4.4) is fit to the data, suggesting that the addition of inorganic compounds increases carbon monoxide mass transfer when compared to oxygen mass transfer. Likewise, Figure 4.36 shows that the addition of a surfactant to deionized water has a similar but more pronounced effect. The addition of the surfactant results in n = -1.11 for the three test conditions considered. Thus, the three fluid conditions presented in Figure 4.35 and Figure 4.36 indicate that the addition of additives to deionized water may be a method to increase carbon monoxide mass transfer relative to oxygen mass transfer.

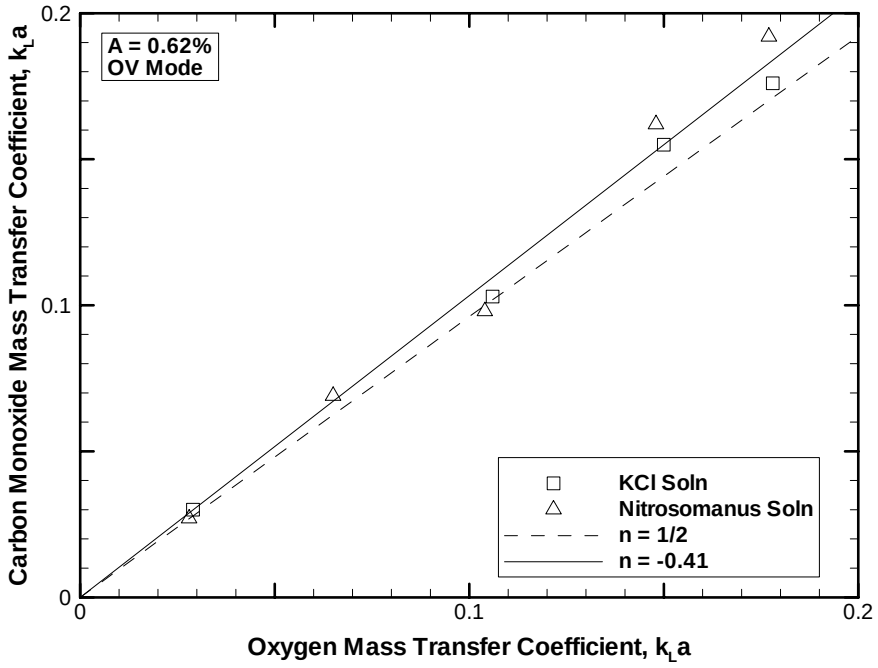

Figure 4.35: A comparison of carbon monoxide and oxygen gas-liquid mass transfer data for A = 0.62% using the KCl and nitrosomonas solutions showing how Equation (4.4) fits the data when n = -0.41.

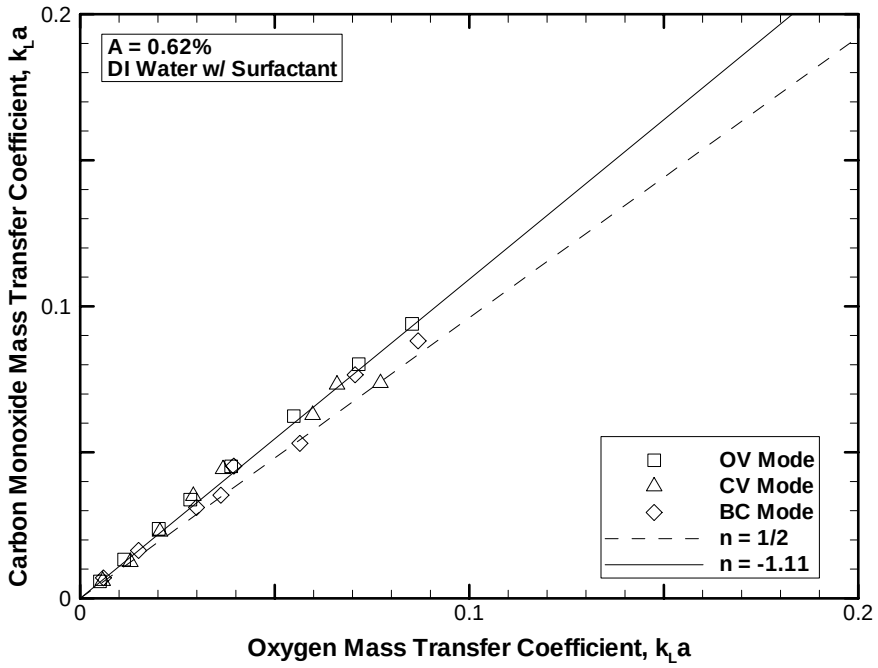

Figure 4.36: A comparison of carbon monoxide and oxygen gas-liquid mass transfer data for A = 0.62% using the deionized water with a surfactant showing how Equation (4.4) fits the data when n = -1.11.

Figure 4.33 through Figure 4.36 show that the value of n may vary depending on the operating conditions that exist in the EALR; however, if Equation (4.4) is fit to the k_La data for all of the test conditions, n = 0.53. So if all of the data are considered together, it would appear as if the penetration, surface renewal, or film-penetration models accurately predict carbon monoxide gas-liquid mass transfer. However, the error associated with using Equation (4.4) with all of the data where $n \approx 0.5$ is ±25% (Figure 4.37). This would imply that the data collected is either quite erroneous or that the proposed models are not properly accounting for some important parameters that are selectively influencing gas-liquid mass transfer. It is felt that the later is probably the case as all of the data included in this comparison are very repeatable. One such possible parameter that could be of considerable importance is the negative ionic charge associated of carbon monoxide molecules and its relationship with compounds residing at the liquid bubble film. Another such parameter that might be of importance is molecular size and shape of the two molecules being compared. Finally, the use of molecular diffusivities may not accurately represent the differing modes of molecular mass transfer in turbulent conditions. Whatever the case may be, it is believed that relating the diffusivities for oxygen and carbon monoxide does not sufficiently describe the actual relationship between oxygen and carbon monoxide gas-liquid mass transfer in highly turbulent conditions where mass transfer is not purely molecular diffusion.

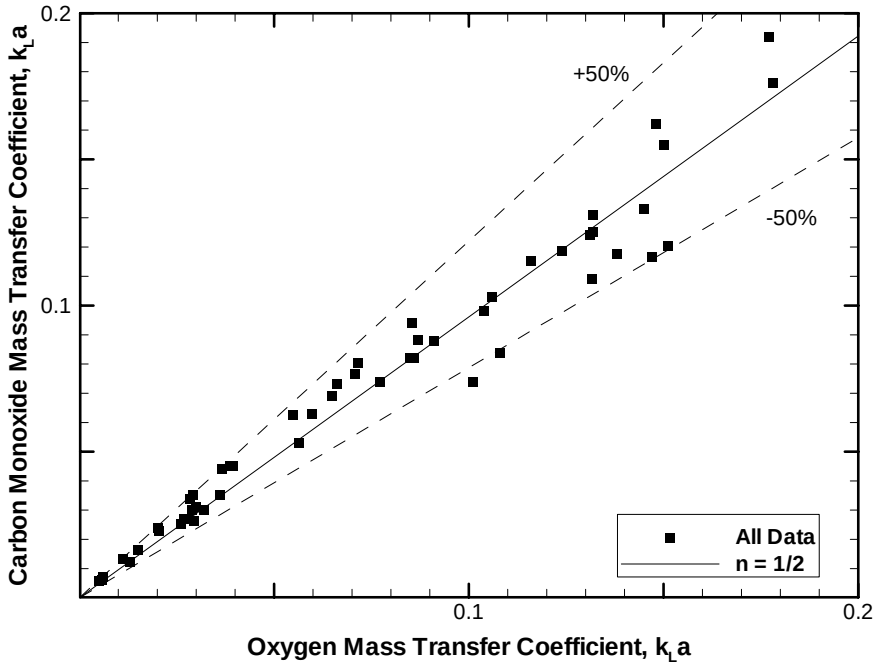

Figure 4.37: A comparison of carbon monoxide and oxygen gas-liquid mass transfer data showing how Equation (4.4) fits the data when n = 0.5.

4.4.4 Gas-Liquid Mass Transfer Correlations

Finally, when all of the mass transfer data as a whole are considered as a function of U_G, two distinct trends are observed. First, the k_La data for all conditions, except those involving the surfactant, seem to respond to U_G in a fashion similar to ε_r. Second, the k_La data collected for the conditions involving the surfactant respond to U_G in a linear fashion (Figure 4.28).

If all of the k_La data except that involving the surfactant are plotted as a function of ε_r, as shown in Figure 4.38, an interesting relationship is observed. Figure 4.38 shows that k_La and ε_r are nearly linearly related; however, upon closer inspection, it is apparent that these two parameters have a power law relationship represented by:

$$k_L a = \alpha \varepsilon_r^{\beta} \tag{4.5}$$

where α and β equal 0.95 and 1.34, respectively. The predicted $k_L a$ using Equation (4.5) are compared to the measured values in Figure 4.39. The observed $k_L a$ are predicted by Equation (4.5) with an error of approximately ±10%. Now if the $k_L a$ data for the remaining test condition containing the surfactant is considered, a linear relationship relating $k_L a$ to U_G of the following form is obtained:

$$k_L a_{CO} = \alpha k_L a_{O_2} \tag{4.6}$$

where α equals 1.12.

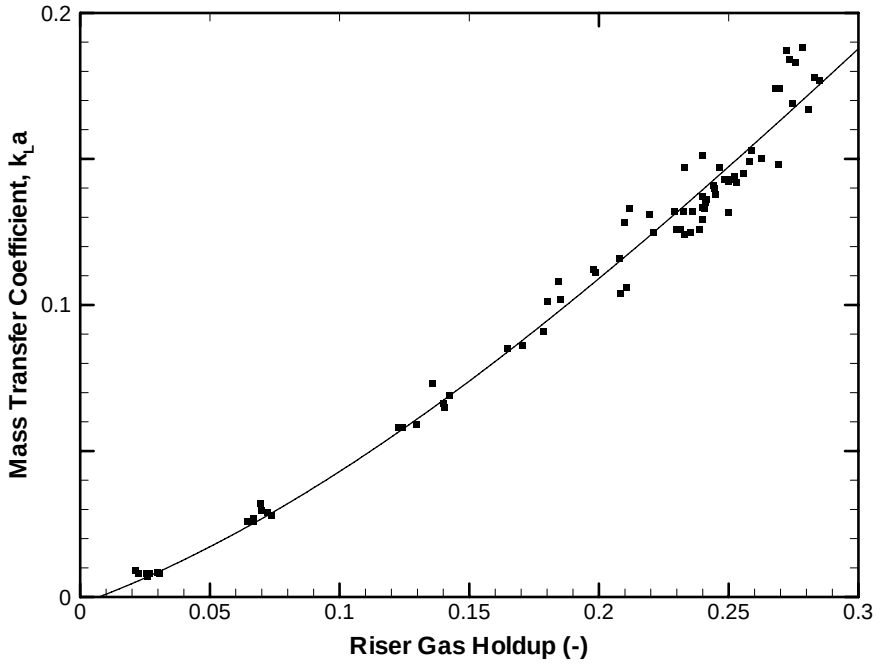

Figure 4.38: Mass transfer coefficients plotted as a function of riser gas holdup for all test conditions expect for those containing the surfactant.

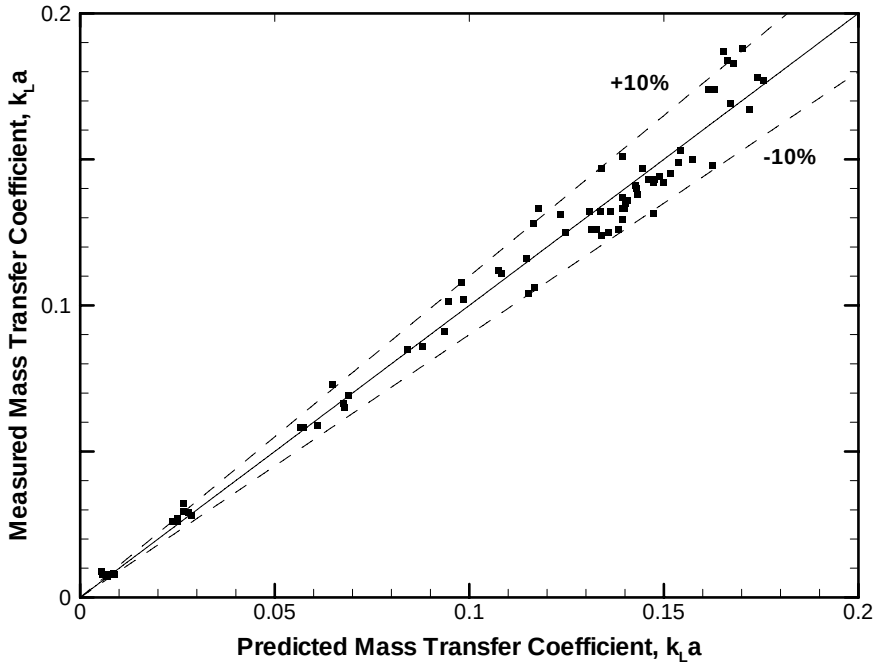

Figure 4.39: Mass transfer coefficients predicted by Equation (4.5).

When considering the two different k_La responses to U_G, it is easiest to consider how the liquid side mass transfer coefficient (k_L) and the interfacial surface area (a) each contribute to the overall measured k_La [71]. For the simplest condition, where the working fluid in the EALR is just deionized water, the resistance to mass transfer due to the liquid film is considered constant, implying that k_L must be independent of U_G. Hence, if k_La increases with increasing U_G, the interfacial surface area must also be increasing with U_G, which makes sense because for the deionized water condition, ε_r and k_La both increase with U_G in a similar fashion. This implies that the interfacial area part of k_La is dominant, indicating that mass transfer is largely a function of convective transport when only deionized water is studied.

For the more complicated conditions where the working fluid is the KCl or nitrosomonas solution, similar conclusions may be drawn. This time while k_L is still independent of U_G, it can not be considered equal to the k_L for the deionized water, in fact the addition of inorganic substances is believed to increase the resistance to gas diffusion [70] resulting in a lower k_L. Conversely though, the addition of inorganic compounds reduces bubble coalescence causing an increase in ε_r and interfacial area. When these two effects are considered together, the resulting k_La may increase or decrease. In this study, the addition of the inorganic compounds results in the measured k_La and ε_r values being higher than those observed with deionized water, but since the relationship between k_La and ε_r is similar to that observed for deionized water (Figure 4.39), it is again concluded that the interfacial area part of k_La is dominant and that mass transfer is largely a function of convective transport.

For the remaining condition involving the addition of a surfactant to the deionized water, k_L once again is considered independent of U_G and different from that for the deionized water. As before, k_La is observed to increase with U_G, but with a linear relationship to U_G instead of a power-law relationship with ε_r, indicating that an increase in the interfacial area with an increase in ε_r no longer has the same affect on mass transfer. Hence, it is thought that the surfactant in the deionized water causes mass transfer in this case to be diffusion limited.

CHAPTER 5: CONCLUSIONS AND RECOMMENDATIONS

5.1 Conclusions

An extensive literature review was presented in Chapter 2. This review demonstrated the complexity of the relationship between geometric and operating parameters and their influence on EALR hydrodynamics and gas-liquid mass transfer, where Figure 2.11 attempted to illustrate these complex relationships. This review also presented a brief summary of the major reactor types commonly encountered in bioprocessing applications, including some rules of thumbs typically used in choosing a reactor type for a specific application. Likewise, techniques used to determine gas-liquid mass transfer were discussed along with methods used to measure dissolved gas concentrations for dynamic systems, where the pros and cons of these methods were assessed.

Gas holdup and liquid superficial velocity results were presented for an external airlift loop reactor with three modes of operation (open downcomer vent, closed downcomer vent, and bubble column modes) for a range of aerator plate open areas ratios (A = 0.62, 0.99, and 2.22%) and superficial gas velocities ($U_G \leq 20$ cm/s) using tap water, deionized water, 0.07 M KCl solution, and 0.04 M nitrosomonas solution. Geometric changes due to flow restrictions and mode of operation significantly affected the fluid flow hydrodynamics in the EALR. Riser gas holdup was observed to be independent of aerator plate open area ratio and mode of operation. Downcomer gas holdup was only significant when the EALR was operated with an opened downcomer vent (OV mode). Both riser and downcomer gas

holdup were observed to vary with fluid type, where the highest gas hold values were observed for the KCl and nitrosomonas solutions. Three liquid flow regimes were identified from the riser superficial liquid velocities: (i) unrestricted flow, (ii) restricted flow, and (iii) fully restricted flow regimes. For open and closed vent downcomer operation (OV and CV mode), riser superficial liquid velocity was independent of aerator plate open area ratio, and strongly dependent on the mode of operation. For open and closed downcomer vent operation (OV and CV mode), riser superficial liquid velocity was a function of superficial gas velocity in the unrestricted and restricted flow regimes, and independent of superficial gas velocity in the fully restricted flow regime.

Riser gas holdup and liquid velocity were correlated to the superficial liquid velocity using relationships suggested by Chisti [2]and Gavrilescu and Toduse [11], respectively. The developed correlations predicted the measured riser gas holdup and superficial liquid velocities within ±15% and ±10%, respectively.

The bioassay method used to quantify dissolved carbon monoxide concentrations in CSTRs presented and used by Riggs [122], Kapic [123], and Ungerman [124] was simplified and updated in Section 3.7. Major changes to the bioassay included a new method for preparing the test solution (Section 3.7.4.4) to reduce measurement errors and the use of JMP 6.0 (SAS Institute Inc.) to perform spectral fitting using a least squares method, and k_La estimation using a nonlinear model fitting routine. These changes, when implemented, reduced the complexity of the bioassay, making it more user friendly and reducing the time required for sample analysis; however, additional work is needed to increase the sampling

frequency from a maximum of one sample every three seconds to much faster rate such as one sample per every half second.

Gas-liquid mass transfer results were presented for an external airlift loop reactor with three modes of operation for aerator plate open area ratios of A = 0.62, 0.99, and 2.22% and a range of superficial gas velocities ($U_G \leq 20$ cm/s) using deionized water, 0.07 M KCl solution, 0.04 M nitrosomonas solution, and deionized water with a surfactant. Changes in reactor mode of operation did not influence gas-liquid mass transfer rates. The gas-liquid mass transfer rates for the deionized water, the KCl solution, and the nitrosomonas solution were proportional to changes in gas holdup and increased with superficial gas velocity, while the gas-liquid mass transfer rates for deionized water with the surfactant were proportional to changes in U_G. The gas-liquid mass transfer rates for the KCl and nitrosomonas solutions had a similar magnitude and were significantly greater than those observed for deionized water, while the gas-liquid mass transfer rates for the deionized water with surfactant were much lower than those measured for the deionized water.

Attempts to estimate gas-liquid mass transfer rates for different gas species using experimental data, gas-liquid diffusivities, and gas-liquid transport theory did not agree with the experimental data collected for carbon monoxide and oxygen for all of the conditions studied. While the gas-liquid transport theory provided an approximation of the measured values, the data indicated that this theory did not properly account for all the factors that may influence gas-liquid mass transfer (Figure 4.37). It is believed that these models fail to account for differences in gas properties other than diffusivities that might enhance or reduce

the ability of a gas molecule from penetrating the bubble liquid film. It is believe that accounting for properties like molecular charge, size, shape, etc. might improve the ability of the proposed theoretical models to predict carbon monoxide gas-liquid mass transfer rates from oxygen gas-liquid mass transfer data.

5.2 Recommendations

As synthesis gas is a mixture of multiple gases, a study should be conducted to assess the effect that a mixture of gases may have on gas-liquid mass transfer rates.

Microbial fermentation systems not only contain water, but nutrients, salts, microorganisms, and biological byproducts. This study considered deionized water and deionized water with selected inorganic compounds; however, more work should be completed to fully understand the effects of these other solutes on gas-liquid mass transfer and system hydrodynamics.

An investigation into different reactors configurations, including stirrers, different geometries, particles, and porous aerator plates, should be performed to determine the best possible configuration for maximizing the gas-liquid mass transfer rate.

Additional work should be completed to understand the complex relationship between gas-liquid mass transfer rates for differing gas species so that mass transfer rates may be accurately estimated using one of the theoretical models with some sort of adaptation.

The bioassay used to measure dissolved carbon monoxide concentrations should be further improved to increase its sampling rate. Additionally, an electrode of some sort,

similar to a dissolved oxygen electrochemical or optode based electrode, should be developed and used in place of the bioassay.

REFERENCES

[1] Blenke, H., 1979, Loop Reactors, in *Advances in Biochemical Engineering/Biotechnology*, T.K. Ghose, A. Fiechter, and N. Blakebrough, Editors, Vol. 13: 121-214.

[2] Chisti, M.Y., 1989, *Airlift Bioreactors*, Elsevier Applied Biotechnology Series, Elsevier Applied Science, London.

[3] Joshi, J.B., V.V. Ranade, S.D. Gharat, and S.S. Lele, 1990, Sparged Loop Reactors, *The Canadian Journal of Cemical Engineering*, 68(10): 705-741.

[4] Van't Riet, K., and J. Tramper, 1991, *Basic Bioreactor Design*, Marcel Dekker, Inc, New York, New York.

[5] Doran, P.M., 1995, *Bioprocess Engineering Principles*, Academic Press, London; San Diego.

[6] Merchuk, J.C., and G. Gluz, 1999, Bioreactors, Air-Lift Reactors, in *Bioprocess Technology: Fermentation, Biocatalysis, and Bioseperation*, M.C. Flickinger and S.W. Drew, Editors, John Wiley & Sons: New York, Vol. 1: 320-352.

[7] Laska, M.E., and C.L. Cooney, 1999, Bioreactors, Continuous Stirred-Tank Reactors, in *Bioprocess Technology: Fermentation, Biocatalysis, Biosperation*, M.C. Flickinger and S.W. Drew, Editors, John Wiley & Sons: New York, Vol. 1: 353-371.

[8] Shuler, M.L., and F. Kargi, 2002, *Bioprocess Engineering Basic Concepts*, 2nd ed, Prentice Hall, Upper Saddle River, NJ.

[9] Weiland, P., and U. Onken, 1981, Differences in the Behaviour of Bubble Columns and Airlift Loop Reactors, *German Chemical Engineering*, 4(3): 174-181.

[10] Onken, U., and P. Weiland, 1980, Hydrodynamics and Mass Transfer in an Airlift Loop Fermentor, *Applied Microbiology and Biotechnology*, 10(1-2): 31-40.

[11] Gavrilescu, M., and R.Z. Tudose, 1996, Effects of Downcomer-to-Riser Cross Sectional Area Ratio on Operation Behavior of External-Loop Airlift Bioreactors, *Bioprocess Engineering*, 15: 77-85.

[12] Atkinson, B., and F. Mavituna, 1983, *Biochemical Engineering and Biotechnology Handbook*, 2nd ed, Sockton Press, New York.

[13] Merchuk, J.C., 1985, Hydrodynamics and Hold-up in Air-Lift Reactors, in *Encyclopedia of Fluid Mechanics*, N.P. Cheremisinoff, Editor, Gulf Publishing Company: Houston, Texas, Vol. 3 (Gas-Liquid Flows): 1485-1511.

[14] Merchuk, J.C., and M.H. Siegel, 1988, Air-Lift Reactors in Chemical and Biological Technology, *Journal of Chemical Technology and Biotechnology*, 41: 105-120.

[15] Siegel, M.H., and C.W. Robinson, 1992, Applications of Airlift Gas-Liquid-Solid Reactors in Biotechnology, *Chemical Engineering Science*, 47(13-14): 3215-3229.

[16] Russell, A.B., C.R. Thomas, and M.D. Lilly, 1994, Influence of Vessel Height and Top-Section Size on the Hydrodynamic Characteristics of Airlift Fermentors, *Biotechnology and Bioengineering*, 43(1): 69-76.

[17] Weiland, P., 1984, Influence of Draft Tube Diameter on Operation Behaviour of Airlift Loop Reactors, *German Chemical Engineering*, 7(6): 374-385.

[18] Chisti, M.Y., and M. Moo-Young, 1987, Airlift Reactors: Characteristics, Applications, and Design Considerations, *Chemical Engineering Communication*, 60: 195-242.

[19] Heijnen, J.J., and K. Van't Riet, 1984, Mass Transfer, Mixing and Heat Transfer Phenomena in Low Viscosity Bubble Column Reactors, *Chemical Engineering Journal and the Biochemical Engineering Journal*, 28(2): 21-42.

[20] Bello, R., Ade, C.W. Robinson, and M. Moo-Young, 1980, Mass Transfer and Liquid Mixing in External-Circulation-Loop Contactors, *Advances in Biotechnology, Proceedings of the 6th international fermentation symposium*, London, Canada: Pergamon Press, pp. 547-552.

[21] Choi, K.H., and W.K. Lee, 1993, Circulation Liquid Velocity, Gas Holdup and Volumetric Oxygen Transfer Coefficient in External-Loop Airlift Reactors, *Journal of Chemical Technology and Biotechnology*, 56: 51-58.

[22] Merchuk, J.C., 1986, Gas Hold-up and Liquid Velocity in a Two-Dimensional Air Lift Reactor, *Chemical Engineering Science*, 41(1): 11-16.

[23] Wang, S., Y. Arimatsu, K. Koumatsu, K. Furumoto, M. Yoshimoto, K. Fukunaga, and K. Nakao, 2003, Gas Holdup, Liquid Circulating Velocity and Mass Transfer Properties in a Mini-Scale External Loop Airlift Bubble Column, *Chemical Engineering Science*, 58(15): 3353-3360.

[24] Bello, R., Ade, C.W. Robinson, and M. Moo-Young, 1985, Gas Holdup and Overall Volumetric Oxygen Transfer Coefficient in Airlift Contactors, *Biotechnology and Bioengineering*, 27: 369-381.

[25] Weiland, P., and U. Onken, 1981, Fluid Dynamics and Mass Transfer in an Airlift Fermenter with External Loop, *German Chemical Engineering*, 4(1): 42-50.

[26] Popovic, M., and C.W. Robinson, 1988, External-Circulation-Loop Airlift Bioreactors: Study of the Liquid Circulating Velocity in Highly Viscous Non-Newtonian Liquids, *Biotechnology and Bioengineering*, 32(7): 301-312.

[27] Merchuk, J.C., and Y. Stein, 1981, Local Hold-up and Liquid Velocity in Air-Lift Reactors, *AIChE Journal*, 27(3): 377-388.

[28] Siegel, M.H., and J.C. Merchuk, 1988, Mass Transfer in Rectangular Air-Lift Reactor: Effects of Geometry and Gas Recirculation, *Biotechnology and Bioengineering*, 32: 1128-1137.

[29] Nicol, R.S., and J.F. Davidson, 1988, Gas Hold-up in Circulating Bubble Columns, *Chemical Engineering Research & Design*, 66(2): 152-158.

[30] Abashar, M.E., U. Narsingh, A.E. Rouillard, and R. Judd, 1998, Hydrodynamic Flow Regimes, Gas Holdup, and Liquid Circulation in Airlift Reactors, *Industrial and Engineering Chemistry Research*, 37: 1251-1259.

[31] Vial, C., E. Camarasa, S. Poncin, G. Wild, N. Midoux, and J. Bouillard, 2000, Study of Hydrodynamic Behavior in Bubble Coulmns and External Loop Airlift Reactors through Analysis of Pressure Fluctuations, *Chemical Engineering Science*, 55: 2957-2973.

[32] Moo-Young, M., and H.W. Blanch, 1981, Design of Biochemical Reactors Mass Transfer Criteria for Simple and Complex Systems, in *Advances in Biochemical Engineering*, Springer Verlag, Berlin, West Germany, Vol. 19: 1-69.

[33] Thibodeaux, L.J., 1995, *Environmental Chemodynamics*, 2nd ed, Environmental Science and Technology, John Wiley & Sons, Inc., New York.

[34] Sherwood, T.K., R.L. Pigford, and C.R. Wilke, 1975, *Mass Transfer*, 1st ed, Mcgraw-Hill Chemical Engineering Series, McGraw-Hill, New York.

[35] Coulson, J.M., and J.F. Richardson, 1999, *Coulson & Richardson's Chemical Engineering*, Vol. 1, Butterworth-Heinemann, Oxford; Boston.

[36] Incropera, F.P., and D.P. DeWitt, 1996, *Fundamentals of Heat and Mass Transfer*, 4th ed, Wiley, New York.

[37] Bello, R.A., C.W. Robinson, and M. Moo-Young, 1984, Liquid Circulation and Mixing Characteristics of Airlift Contactors, *The Canadian Journal of Chemical Engineering*, 62(10): 573-577.

[38] Bentifraouine, C., C. Xuereb, and J.-P. Riba, 1997, Effect of Gas Liquid Separator and Liquid Height on the Global Hydrodynamic Parameters of an External Loop Airlift Contactor, *Chemical Engineering Journal*, 66: 91-95.

[39] Bentifraouine, C., C. Xuereb, and J.-P. Riba, 1997, An Experimental Study of the Hydrodynamic Characteristics of External Loop Airlift Contactors, *Journal of Chemical Technology and Biotechnology*, 69: 345-349.

[40] Snape, J.B., J. Zahradnik, M. Fialova, and N.M. Thomas, 1995, Liquid-Phase Properties and Sparger Design Effects in an External-Loop Airlift Reactor, *Chemical Engineering Science*, 50(20): 3175-3186.

[41] Nakanoh, M., and F. Yoshida, 1983, Transient Characteristics of Oxygen Probes and Determination of k_La, *Biotechnology and Bioengineering*, 25(6): 1653-1654.

[42] Siegel, M.H., J.C. Merchuk, and K. Schugerl, 1986, Air-Lift Reactor Analysis: Interrelationships between Riser, Downcomer, and Gas-Liquid Separator Behavior, Including Gas Recirculation Effects, *AIChE Journal*, 32(10): 1585-1596.

[43] Al-Masry, W., 1999, Effect of Liquid Volume in the Gas-Seperator on the Hydrodynamics of Airlift Reactors, *Journal of Chemical Technology and Biotechnology*, 74: 931-936.

[44] Choi, K.H., 2002, Effect of Unaerated Liquid Height on Hydrodynamic Characteristics of an External-Loop Airlift Reactor, *Chemical Engineering Communications*, 189(1): 23-39.

[45] Al-Masry, W.A., 2004, Influence of Gas Separator and Scale-up on the Hydrodynamics of External Loop Circulating Bubble Columns, *Chemical Engineering Research and Design*, 82(3): 381-389.

[46] Merchuk, J.C., N. Ladwa, A. Cameron, M. Bulmer, and A. Pickett, 1994, Concentric-Tube Airlift Reactors: Effects of Geometrical Design on Performance, *AIChE Journal*, 40(7): 1105-1117.

[47] Choi, K.H., 2001, Hydrodynamic and Mass Transfer Characteristics of External-Loop Airlift Reactors without an Extension Tube above the Downcomer, *Korean Journal of Chemical Engineering*, 18(2): 240-246.

[48] Gavrilescu, M., and R.Z. Tudose, 1995, Study of the Liquid Circulation Velocity in External-Loop Airlift Bioreactors, *Bioprocess Engineering*, 14: 33-39.

[49] Bendjaballah, N., H. Dhaouadi, S.M. Poncin, N., J. Hornut, and G. Wild, 1999, Hydrodynamics and Flow Regimes in External Loop Airift Reactors, *Chemical Engineering Science*, 54: 5211-5221.

[50] Wongsuchoto, P., T. Charinpanitkul, and P. Pavasant, 2003, Bubble Size Distribution and Gas-Liquid Mass Transfer in Airlift Contactors, *Chemical Engineering Journal*, 92(1-3): 81-90.

[51] van Dam-Mieras, M.C.E., W.H. de Jue, J. de Vries, B.R. Currell, J.W. James, C.K. Leach, and R.A. Patmore, 1992, "Operational Modes of Bioreactors." Elsevier Science & Technology Books: San Diego.

[52] Lin, J., M. Han, T. Wang, T. Zhang, J. Wang, and Y. Jin, 2004, Influence of the Gas Distributor on Local Hydrodynamic Behavior of an External Loop Airlift Reactor, *Chemical Engineering Science*, 102: 51-59.

[53] Miyahara, T., H. Hamanaka, T. Umeda, and Y. Akagi, 1999, Effect of Plate Goemetry on Characterisitcs of Fluid Flow and Mass Transfer in External-Loop Airlift Bubble Column, *Journal of Chemical Engineering of Japan*, 32(5): 689-695.

[54] Vasconcelos, J.M.T., J.M.L. Rodrigues, S.C.P. Orvalho, S.S. Alves, R.L. Mendes, and A. Reis, 2003, Effect of Contaminants on Mass Transfer Coefficients in Bubble Column and Airlift Contactors, *Chemical Engineering Science*, 58(8): 1431-1440.

[55] Tsuge, H., S. Otatsume, K. Kobayashi, K. Terasaka, M. Hayasaki, and H. Kobayashi, 2004, Liquid Circulation and Mass Transfer in an External-Loop Airlift Reactor with Partitioning Plates, *Journal of Chemical Engineering of Japan*, 37(8): 941-946.

[56] Vorapongsathorn, T., P. Wongsuchoto, and P. Pavasant, 2001, Performance of Airlift Contactors with Baffles, *Chemical Engineering Journal*, 84(3): 551-556.

[57] Zhang, T., J. Wang, T. Wang, J. Lin, and Y. Jin, 2005, Effect of Internal on the Hydrodynamics in External-Loop Airlift Reactors, *Chemical Engineering and Processing*, 44: 81-87.

[58] Nikakhtari, H., and G.A. Hill, 2005, Hydrodynamic and Oxygen Mass Transfer in an External Loop Airlift Bioreactor with a Packed Bed, *Biochemical Engineering Journal*, 27: 138-145.

[59] Nikakhtari, H., and G.A. Hill, 2005, Volatile Organic Chemical Mass Transfer in an External Loop Airlift Bioreactor with a Packed Bed, *Industrial and Engineering Chemistry Research*, 44(24): 9299-9306.

[60] Tudose, R.Z., and M. Gavrilescu, 1999, Static Mixing, in Fermentation Process, in *Bioprocess Technology: Fermentation, Biocatalysis, and Bioseperation*, M.C. Flickinger and S.W. Drew, Editors, John Wiley and Sons: New York, Vol. 5: 2486-2501.

[61] Chisti, Y., M. Kasper, and M. Moo-Young, 1990, Mass Transfer in External-Loop Airlift Bioreactors Using Static Mixers, *Canadian Journal of Chemical Engineering*, 68(1): 45-50.

[62] Chisti, Y., and U.J. Jauregui-Haza, 2002, Oxygen Transfer and Mixing in Mechanically Agitated Airlift Bioreactors, *Biochemical Engineering Journal*, 10(2): 143-153.

[63] Onken, U., and P. Weiland, 1980, Liquid Velocity as an Important Design Parameter for Airlift Loop-Fermentors, *Advances in Biotechnology, Proceedings of the 6th international fermentation symposium*, London, Canada: Pergamon Press, pp. 559-564.

[64] McManamey, W.J., D.A.J. Wase, S. Raymahasay, and K. Thayanithy, 1984, Influence of Gas Inlet Design on Gas Hold-up Values for Water and Various Solutions in a Loop-Type Air-Lift Fermenter, *Journal of Chemical Technology and Biotechnology, Biotechnology*, 34B(3): 151-164.

[65] Zahradnik, J., M. Fialova, F. Kastanek, K.D. Green, and N.H. Thomas, 1995, The Effect of Electrolytes on Bubble Coalescence and Gas Holdup in Bubble Column Reactors, *Chemical Engineering Research & Design, Transactions of the Institute of Chemical Engineers, Part A*, 73(A3): 341-346.

[66] Prince, M.J., and H.W. Blanch, 1990, Transition Electrolyte Concentrations for Bubble Coalescence, *AIChE Journal*, 36(9): 1425-1429.

[67] Nicol, R.S., and J.F. Davidson, 1988, Effect of Surfactants on the Gas Hold-up in Circulating Bubble Columns, *Chemical Engineering Research & Design*, 66(2): 159-164.

[68] Snape, J.B., M. Fialova, J. Zahradnik, and N.H. Thomas, 1992, Hydrodynamic Studies in an External Loop Airlift Reactor Containing Aqueous Electrolyte and Sugar Solutions, *Chemical Engineering Science*, 47(13-14): 3387-3394.

[69] Muthukumar, K., and M. Velan, 2006, Volumetric Mass Transfer Coefficients in an Internal Loop Airlift Reactor with Low-Density Particles, *Journal of Chemical Technology and Biotechnology*, 81(4): 667-673.

[70] Rosso, D., D.L. Huo, and M.K. Stenstrom, 2006, Effects of Interfacial Surfactant Contamination on Bubble Gas Transfer, *Chemical Engineering Science*, 61(16): 5500-5514.

[71] Kawase, Y., and M. Moo-Young, 1990, The Effect of Antifoam Agents on Mass Transfer in Bioreactors, *Bioprocess and Biosystems Engineering*, 5(4): 169-173.

[72] Kawase, Y., 1990, Liquid Circulation in External-Loop Airlift Bioreactors, *Biotechnology and Bioengineering*, 35(5): 540-546.

[73] Al-Masry, W.A., and A.R. Dukkan, 1997, Role of Gas Disengagement and Surface Active Agents on Hydrodynamic and Mass Transfer Characteristics of Airlift Reactors, *Chemical Engineering Journal*, 65(3): 263-271.

[74] Al-Masry, W.A., 1999, Effects of Antifoam and Scale-up on Operation of Bioreactors, *Chemical Engineering and Processing*, 38(3): 197-201.

[75] Sardeing, R., P. Painmanakul, and G. Hebrard, 2006, Effect of Surfactants on Liquid-Side Mass Transfer Coefficients in Gas-Liquid Systems: A First Step to Modeling, *Chemical Engineering Science*, 61(19): 6249-6260.

[76] Hwang, S.-J., and W.-J. Lu, 1997, Gas-Liquid Mass Transfer in an Internal Loop Airlift Reactor with Low Density Particles, *Chemical Engineering Science*, 52(5): 853-857.

[77] Gourich, B., N. El Azher, M. Soulami Bellhaj, H. Delmas, A. Bouzidi, and M. Ziyad, 2005, Contribution to the Study of Hydrodynamics and Gas-Liquid Mass Transfer in a Two- and Three-Phase Split-Rectangular Airlift Reactor, *Chemical Engineering and Processing*, 44(10): 1047-1053.

[78] Dhaouadi, H., S. Poncin, J. Hornut, and G. Wild, 2006, Solid Effects on Hydrodynamics and Heat Transfer in External Loop Airlift Reactor, *Chemical Engineering Science*, 61: 1300-1311.

[79] Wen, J.P., X.Q. Jia, and W. Feng, 2005, Hydrodynamic and Mass Transfer of Gas-Liquid-Solid Three-Phase Internal Loop Airlift Reactors with Nanometer Solid Particles, *Chemical Engineering and Technology*, 28(1): 53-60.

[80] Kluytmans, J.H.J., B.G.M. van Wachem, B.F.M. Kuster, and J.C. Schouten, 2003, Mass Transfer in Sparged and Stirred Reactors: Influence of Carbon Particles and Electrolyte, *Chemical Engineering Science*, 58(20): 4719-4728.

[81] Kluytmans, J.H.J., B.G.M. Van Wachem, B.F.M. Kuster, and J.C. Schouten, 2001, Gas Holdup in a Slurry Bubble Column: Influence of Electrolyte and Carbon Particles, *Industrial and Engineering Chemistry Research*, 40(23): 5326-5333.

[82] Benyahia, F., L. Jones, S. Petit, and D. Plantaz, 1996, Mass Transfer Studies in Pneumatic Reactors, *Chemical Engineering & Technology*, 19(5): 425-431.

[83] Merchuk, J.C., N. Ladwa, A. Cameron, M. Bulmer, I. Berzin, and A.M. Pickett, 1996, Liquid Flow and Mixing in Concentric Tube Air-Lift Reactors, *Journal of Chemical Technology and Biotechnology*, 66(2): 174-182.

[84] Carroll, J.J., 1991, What Is Henry's Law? *Chemical Engineering Progress*, 87(9): 48-52.

[85] Standard methods for the examination of water and wastewater 21st Ed, 2005, 4500-O Oxygen (Dissolved), New York: American Public Health Association, American Water Works Association, & Water Pollution Control Federation, 4.136-4.143.

[86] Wilkin, R.T., M.S. McNeil, C.J. Adair, and J.T. Wilson, 2001, Field Measurement of Dissolved Oxygen: A Comparison of Methods, *Ground Water Monitoring and Remediation*, 21(4): 124-132.

[87] Turner, A.P.F., and S.F. White, 1999, Process Monitoring, in *Encyclopedia of Process Technology: Fermentation, Biocatalysis, and Bioseperation*, M.C. Flickinger and S.W. Drew, Editors, John Wiley: New York, Vol. 4: 2056-2070.

[88] Koeneke, R., A. Comte, H. Juergens, O. Kohls, H. Lam, and T. Scheper, 1999, Fiber Optic Oxygen Sensors for Use in Biotechnology, Environmental, and Food Industries, *Chemical Engineering and Technology*, 22(8): 666-671.

[89] Zuber, N., and J.A. Findlay, 1965, Average Volumetric Concentration in Two Phase Flow Systems, *Journal of Heat Transfer*, 87: 453-468.

[90] Glazer, B.T., A.G. Marsh, K. Stierhoff, and G.W. Luther III, 2004, The Dynamic Response of Optical Oxygen Sensors and Voltammetric Electrodes to Temporal Changes in Dissolved Oxygen Concentrations, *Analytica Chimica Acta*, 518(1-2): 93-100.

[91] Terasaka, K., D. Hullmann, and A. Schumpe, 1998, Mass Transfer in Bubble Columns Studied with an Oxygen Optode, *Chemical Engineering Science*, 53(17): 3181-3184.

[92] Kohls, O., and T. Scheper, 2000, Setup of a Fiber Optical Oxygen Multisensor-System and Its Applications in Biotechnology, *Sensors and Actuators, B: Chemical*, 70(1-3): 121-130.

[93] Linek, V., J. Sinkule, and V. Vacek, 1985, Dissolved Oxygen Probes, in *Comprehensive Biotechnology*, Pergamon Press, Oxford, Engl, Vol. 4: 363-394.

[94] Linek, V., 1988, *Measurement of Oxygen by Membrane-Covered Probes: Guidelines for Applications in Chemical and Biochemical Engineering*, Ellis Horwood Series in Analytical Chemistry, Halsted Press, New York.

[95] Lee, Y.H., and G.T. Tsao, 1979, Dissolved Oxygen Electrodes, *Advances in Biochemical Engineering*, 13: 35-86.

[96] Aiba, S., M. Ohashi, and S.Y. Huang, 1968, Rapid Determination of Oxygen Permeability of Polymer Membranes, *Industrial and Engineering Chemistry, Fundamentals*, 7(3): 497-502.

[97] Sobotka, M., A. Prokop, I.J. Dunn, and A. Einsele, 1982, Review of Methods for the Measurement of Oxygen Transfer in Microbial Systems, *Annual Reports on Fermentation Processes*, 5: 127-210.

[98] Tribe, L.A., C.L. Briens, and A. Margaritis, 1995, Determination of the Volumetric Mass Transfer Coefficient (k_La) Using the Dynamic 'Gas out-Gas in' Method: Analysis of Errors Caused by Dissolved Oxygen Probes, *Biotechnology and Bioengineering*, 46(4): 388-392.

[99] Vardar, F., and M.D. Lilly, 1982, The Measurement of Oxygen-Transfer Coefficients in Fermentors by Frequency Response Techniques, *Biotechnology and Bioengineering*, 24(7): 1711-1719.

[100] Gaddis, E.S., 1999, Mass Transfer in Gas-Liquid Contactors, *Chemical Engineering and Processing*, 38(4-6): 503-510.

[101] Tobajas, M., and E. Garcia-Calvo, 2000, Comparison of Experimental Methods for Determination of the Volumetric Mass Transfer Coefficient in Fermentation Processes, *Heat and Mass Transfer/Waerme- und Stoffuebertragung*, 36(3): 201-207.

[102] Ruchti, G., I.J. Dunn, and J.R. Bourne, 1981, Comparison of Dynamic Oxygen Electrode Methods for the Measurement of k_La, *Biotechnology and Bioengineering*, 23(2): 277-290.

[103] Lopez, J.L., E.M. Rodriguez Porcel, I. Oller Alberola, M.M. Ballesteros Martin, J.A. Sanchez Perez, J.M. Fernandez Sevilla, and Y. Chisti, 2006, Simultaneous Determination of Oxygen Consumption Rate and Volumetric Aoxygen Transfer Coefficient in Pnuematically Agitated Airlift Bioreactors, *Industrial and Engineering Chemistry Research*, 2006: 1167-1171.

[104] Linek, V., J. Sinkule, and V. Vacek, 1981, Oxygen Electrode Dynamics: Three-Layer Model - Chemical Reaction in the Liquid Film, *Biotechnology and Bioengineering*, 25(5): 1401-1418.

[105] Linek, V., J. Sinkule, and P. Benes, 1992, Critical Assessment of the Dynamic Double-Response Method for Measuring k_La. Experimental Elimination of Dispersion Effects, *Chemical Engineering Science*, 47(15-16): 3885-3894.

[106] Linek, V., J. Sinkule, and P. Benes, 1991, Critical Assessment of Gassing-in Methods for Measuring k_La in Fermentors, *Biotechnology and Bioengineering*, 38(4): 323-330.

[107] Linek, V., P. Benes, and V. Vacek, 1979, Oxygen Probe Dynamics in Flowing Fluids, *Industrial & Engineering Chemistry, Fundamentals*, 18(3): 240-245.

[108] Linek, V., P. Benes, and V. Vacek, 1984, Experimental Study of Oxygen Probe Linearity and Transient Characteristics in the High Oxygen Concentration Range, *Journal of Electroanalytical Chemistry and Interfacial Electrochemistry*, 169(1-2): 233-257.

[109] Linek, V., P. Benes, and V. Vacek, 1989, Dynamic Pressure Method for k_La Measurement in Large-Scale Bioreactors, *Biotechnology and Bioengineering*, 33(11): 1406-1412.

[110] Lee, Y.H., and S. Luk, 1983, Aeration, *Annual Reports on Fermentation Processes*, 6: 101-147.

[111] Kim, D.J., and H.N. Chang, 1989, Dynamic Measurement of k_La with Oxygen-Enriched Air During Fermentation, *Journal of Chemical Technology and Biotechnology*, 45(1): 39-44.

[112] Freitas, C., and J.A. Teixeira, 2001, Oxygen Mass Transfer in a High Solids Loading Three-Phase Internal-Loop Airlift Reactor, *Chemical Engineering Journal*, 84(1): 57-61.

[113] Chang, H.N., B. Halard, and M. Moo-Young, 1989, Measurement of k_La by a Gassing-in Method with Oxygen-Enriched Air, *Biotechnology and Bioengineering*, 34(9): 1147-1157.

[114] Van't Riet, K., 1979, Review of Measuring Methods and Results in Nonviscous Gas-Liquid Mass Transfer in Stirred Vessels, *Industrial & Engineering Chemistry, Process Design and Development*, 18(3): 357-364.

[115] Linek, V., V. Vacek, and P. Benes, 1987, Critical Review and Experimental Verification of the Correct Use of the Dynamic Method for the Determination of Oxygen Transfer in Aerated Agitated Vessels to Water, Electrolyte Solutions and Viscous Liquids, *Chemical Engineering Journal and the Biochemical Engineering Journal*, 34(1): 11-34.

[116] Blazej, M., J. Annus, and J. Markos, 2004, Comparison of Gassing-out and Pressure-Step Dynamic Methods for k_La Measurement in an Airlift Reactor with Internal Loop, *Chemical Engineering Research and Design*, 82(10): 1375-1382.

[117] Fuchs, R., D.D.Y. Ryu, and A.E. Humphrey, 1971, Effect of Surface Aeration on Scale-up Proceedures for Fermentation Process, *Industrial & Engineering Chemistry Process Design and Development*, 10(2): 190-196.

[118] Merchuk, J.C., and R. Yunger, 1990, Role of the Gas-Liquid Separator of Airlift Reactors in the Mixing Process, *Chemical Engineering Science*, 45(9): 2973-2975.

[119] Linek, V., 1972, Determination of Aeration Capacity of Mechanically Agitated Vessels by Fast Response Oxygen Probe, *Biotechnology and Bioengineering*, 14(2): 285-289.

[120] Dang, N.D.P., D.A. Karrer, and I.J. Dunn, 1977, Oxygen Transfer Coefficients by Dynamic Model Moment Analysis, *Biotechnology and Bioengineering*, 19(6): 853-865.

[121] Keitel, G., and U. Onken, 1981, Errors in the Determination of Mass Transfer in Gas-Liquid Dispersions, *Chemical Engineering Science*, 36(12): 1927-1932.

[122] Riggs, S.S., 2004, *Carbon Monoxide and Hydrogen Mass Transfer in a Stirred Tank Reactor*, MS Thesis, Iowa State University, Ames, IA.

[123] Kapic, A., 2005, *Mass Transfer Measurements for Syngas Fermentation*, MS Thesis, Iowa State University, Ames, IA.

[124] Ungerman, A.J., 2006, *Mass Transfer Enhancement for Syngas Fermentation*, MS Thesis, Iowa State University, Ames, IA.

[125] Gogate, P.R., and A.B. Pandit, 1999, Survey of Measurement Techniques for Gas-Liquid Mass Transfer Coefficient in Bioreactors, *Biochemical Engineering Journal*, 4(1): 7-15.

[126] Poughon, L., D. Duchez, J.F. Cornet, and C.G. Dussap, 2003, k_La Determination: Comparative Study for a Gas Mass Balance Method, *Bioprocess and Biosystems Engineering*, 25(6): 341-348.

[127] Blanch, H.W., and D.S. Clark, 1996, *Biochemical Engineering*, M. Dekker, New York.

[128] Linek, V., P. Benes, J. Sinkule, and T. Moucha, 1993, Non-Ideal Pressure Step Method for k_La Measurement, *Chemical Engineering Science*, 48(9): 1593-1599.

[129] Linek, V., and J. Sinkule, 1990, Comments on Validity of Dynamic Measuring Methods of Oxygen Diffusion Coefficients in Fermentation Media with Polarographic Oxygen Electrodes, *Biotechnology and Bioengineering*, 35(10): 1034-1041.

[130] Linek, V., F. Benes, and F. Hovorka, 1981, Role of Interphase Nitrogen Transport in the Dynamic Measurement of the Overall Volumetric Mass Transfer Coefficient in Air-Sparged Systems, *Biotechnology and Bioengineering*, 23(2): 301-319.

[131] Dunn, I.J., and A. Einsele, 1975, Oxygen Transfer Coefficients by the Dynamic Method, *Journal of Applied Chemistry and Biotechnology*, 25(9): 707-720.

[132] Stenberg, O., and B. Andersson, 1988, Gas-Liquid Mass Transfer in Agitated Vessels - I. Evaluation of the Gas-Liquid Mass Transfer Coefficient from Transient-Response Measurements, *Chemical Engineering Science*, 43(3): 719-724.

[133] Linek, V., T. Moucha, M. Dousova, and J. Sinkule, 1994, Measurement of k_La by Dynamic Pressure Method in Pilot-Plant Fermentor, *Biotechnology and Bioengineering*, 43(6): 477-482.

[134] Andre, G., M. Moo-Young, and C.W. Robinson, 1981, Improved Method for the Dynamic Measurement of Mass Transfer Coefficient for Application to Solid-Substrate Fermentation, *Biotechnology and Bioengineering*, 23(7): 1611-22.

[135] Fields, P.R., and N.K.H. Slater, 1983, Tracer Dispersion in a Laboratory Air-Lift Reactor, *Chemical Engineering Science*, 38(4): 647-653.

[136] Shah, Y.T., G.J. Stiegel, and M.M. Sharma, 1978, Backmixing in Gas-Liquid Reactors, *AIChE Journal*, 24(3): 369-400.

[137] Bakker, W.A.M., J. Tramper, and C.D. Gooijer, 1993, Hydrodynamics, Mixing, and Oxygen Transfer in the Multiple Air-Lift Loop Reactor, *3rd International Conference on Bioreactor & Bioprocess Fluid Dynamics*, Cambridge, UK: Mechanical Engineering Publications Limited, pp. 49-60.

[138] Antonini, E., and M. Brunori, 1971, *Hemoglobin and Myoglobin in Their Reactions with Ligands*, Frontiers of Biology, ed. A. Neuberger and E.L. Tatum, Vol. 21, North-Holland Research Monographs, Amsterdam-London.

[139] Figliola, R.S., and D.E. Beasley, 2000, *Theory and Design for Mechanical Measurement*, 3rd ed, John Wiley & Sons Inc, New York.

[140] Su, X., and T.J. Heindel, 2005, Effect of Perforated Plate Open Area on Gas Holdup in Rayon Fiber Suspensions, *Journal of Fluids Engineering*, 127(4): 816-823.

[141] Jamialahmadi, M., and H. Muller-Steinhagen, 1990, Effect of Electrolyte Concentration on Bubble Size and Gas Hold-up in Bubble Columns, *Chemical Engineering Research & Design*, 68(2): 202-204.

[142] Chisti, M.Y., B. Halard, and M. Moo-Young, 1988, Liquid Circulation in Airlift Reactors, *Chemical Engineering Science*, 43(3): 451-457.

[143] Di Felice, R., 2005, Liquid Circulation Rates in Two- and Three-Phase External Airlift Reactors, *Chemical Engineering Journal*, 109: 49-55.

[144] Mercer, D.G., 1981, Flow Characteristics of Pilot-Scale Airlift Fermentor, *Biotechnology and Bioengineering*, 23: 2421-2432.

[145] Perry, R.H., and D.W. Green, 1998, *Perry's Chemical Engineers' Handbook, 7th Edition*, 7th ed, ed. D.W. Green and R.H. Perry, McGraw-Hill, New York.

APPENDIX A:

PRESSURE TRANSDUCER DETERMINATION OF FRACTIONAL GAS HOLDUP

This appendix shows how the gas holdup is determined using either a pair of pressure transducers or a single differential pressure transducer.

The pressure transducer setup is shown in Figure A.1, points 1 and 2 represent the two pressure transducers. The hydrostatic pressures (cm H_2O) recorded by the computer at each of the pressure transducers are schematically represented by two liquid manometers in Figure A.1 (dashed lines) and describe mathematically as follows:

$$P_1 = P_{atm} + \rho_L g \Delta h_1 + \rho_L g \Delta h_r \quad \text{A.1}$$

$$P_2 = P_{atm} + \rho_L g \Delta h_2 \quad \text{A.2}$$

$$\Delta P = P_1 - P_2 = \rho_L g \left(\Delta h_1 - \Delta h_2 + \Delta h_r \right) \quad \text{A.3}$$

where the difference between Δh_1 and Δh_2 represents the water displaced by the gas bubbles in the reactor assuming the gas in the reactor is incompressible and at P_{atm}. Thus, when gas holdup is zero Δh_1 and Δh_2 are equal and the initial liquid hydrostatic head (ΔP_o) is defined as:

$$\Delta P_o = P_{1o} - P_{2o} = \rho_L g \Delta h_r \quad \text{A.4}$$

The mean gas holdup (ε) between points 1 and 2 in the reactor (Figure A.1) may be obtained as follows starting with the hydrostatic pressures measured inside the reactor:

$$P_1 = P_{atm} + \rho_d g \Delta h + \rho_d g \Delta h_r \quad \text{A.5}$$

$$P_2 = P_{atm} + \rho_d g \Delta h \quad \text{A.6}$$

$$\Delta P = P_1 - P_2 = \rho_d g \Delta h_r \quad \text{A.7}$$

where ρ_d is defined by:

$$\rho_d = \rho_L (1-\varepsilon) + \rho_G \varepsilon \qquad \text{A.8}$$

Since $\rho_G << \rho_L$, it is neglected, allowing gas holdup to be expressed as:

$$\varepsilon = \frac{(\rho_L - \rho_d)}{\rho_L} = 1 - \frac{\rho_d}{\rho_L} \qquad \text{A.9}$$

Combining equations (A.4), (A.7), and (A.9)

$$\varepsilon = 1 - \frac{\Delta P}{\Delta P_o} \qquad \text{A.10}$$

which is the desired equation.

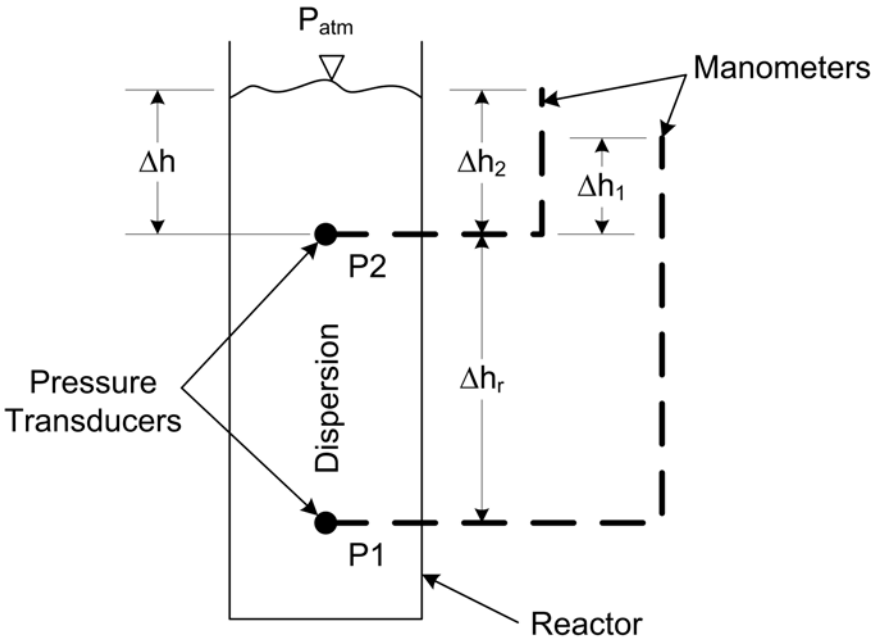

Figure A.1: The pressure transducer setup. (Note: The manometers shown are for illustrative purposes only and do not actually exist on the real system.)

The differential pressure transducer setup is shown in Figure A.2. The mean gas holdup between points 1 and 2 in the reactor (Figure A.2) may be obtained as follows: Because the pressure (ΔP_r) at the differential pressure transducer is equal to the difference between the low and high side pressures, we have:

$$\Delta P_r = \left(P_{atm} + \rho_d g \Delta h + \rho_L g \Delta h_r\right) - \left(P_{atm} + \rho_d g \Delta h + \rho_d g \Delta h_r\right) \quad \text{A.11}$$

$$\Delta P_r = \left(\rho_L g \Delta h_r\right) - \left(\rho_d g \Delta h_r\right) \quad \text{A.12}$$

combining equations (A.9) and (A.12) gives

$$\varepsilon = \frac{\Delta P_r}{\rho_L g \Delta h_r} \quad \text{A.13}$$

or

$$\varepsilon = \frac{dP_r}{\Delta h_r} \quad \text{A.14}$$

which is the desired equation where

$$dP_r = \frac{\Delta P_r}{\rho_L g} \quad \text{A.15}$$

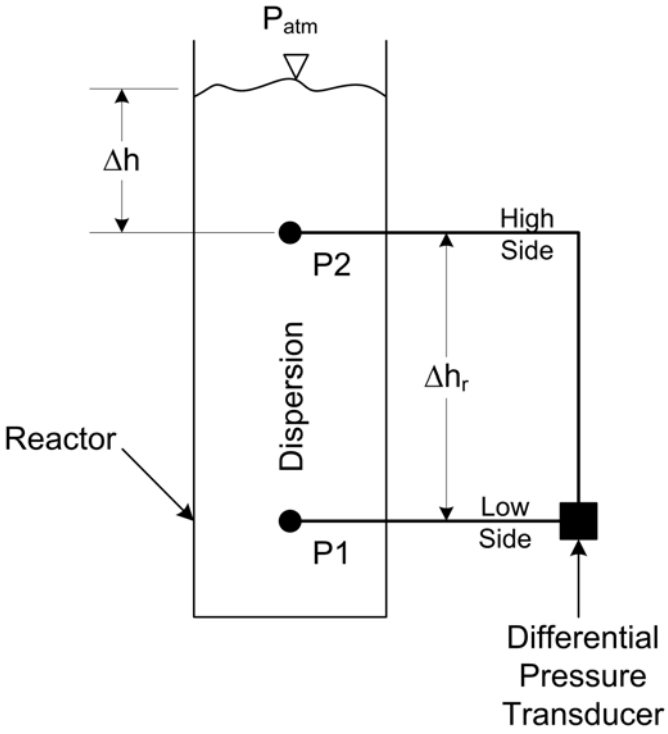

Figure A.2: The differential pressure transducer setup.

APPENDIX B:

DIGITAL IMAGES COLLECTED FOR VISUAL OBSERVATIONS

Appendix B contains the digital images collected and used to visually quantify flow conditions in the EALR for the open and closed vent modes of operation. Images are shown for two locations along the downcomer. First, images taken at the upper horizontal connector are presented for $0.5 < U_G < 20$ cm/s for each aerator plate and mode of operation. Second, images taken just above the lower horizontal connector are presented for similar conditions.

Test Conditions:
A = 0.62%
Open Vent Mode
Upper Horizontal Connector

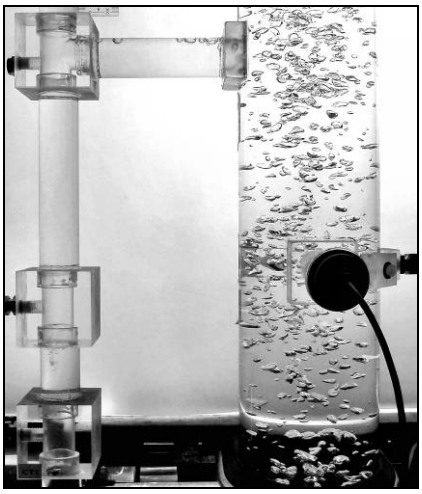
U_G = 0.5 cm/s

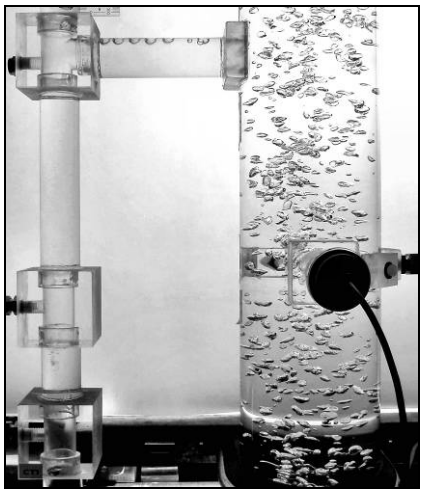
U_G = 0.5 cm/s

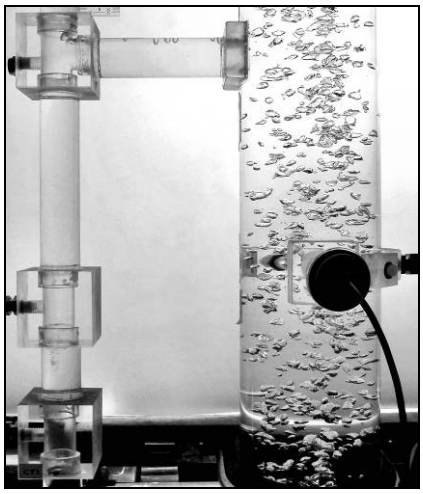
U_G = 0.5 cm/s

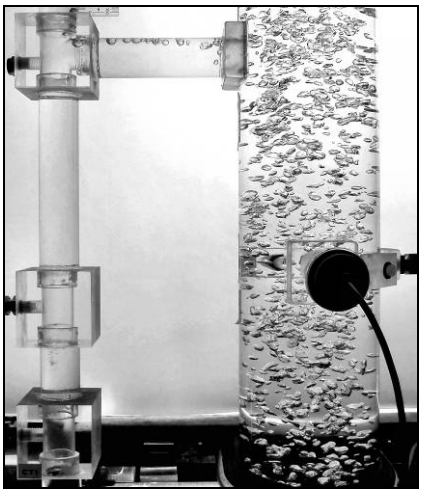
U_G = 1.0 cm/s

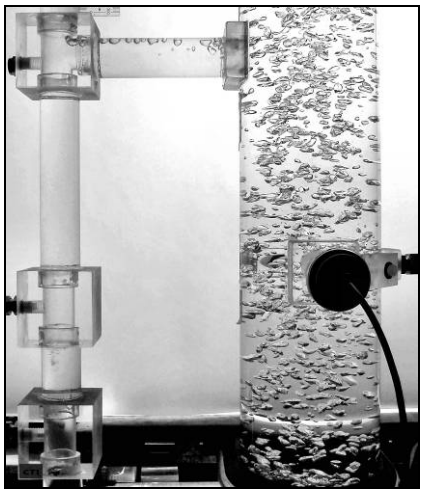
U_G = 1.0 cm/s

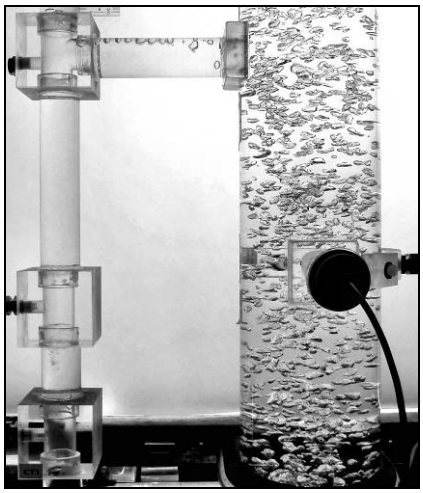
U_G = 1.0 cm/s

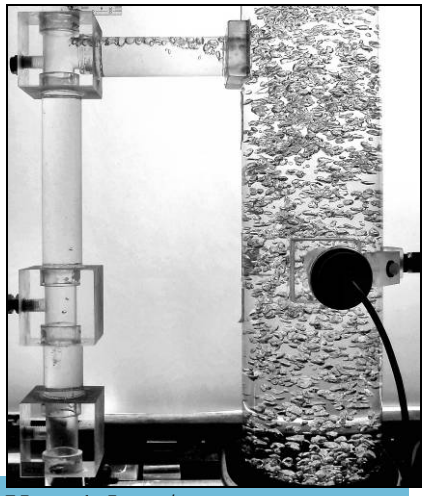
U_G = 1.5 cm/s

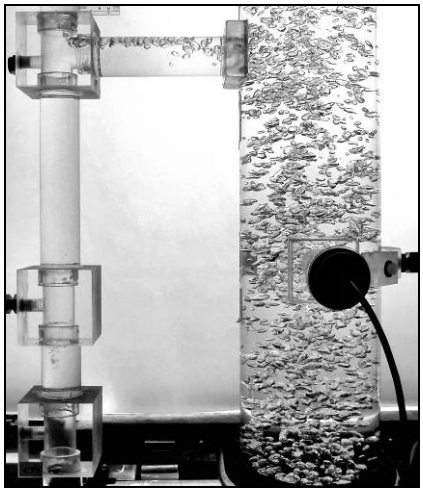
U_G = 1.5 cm/s

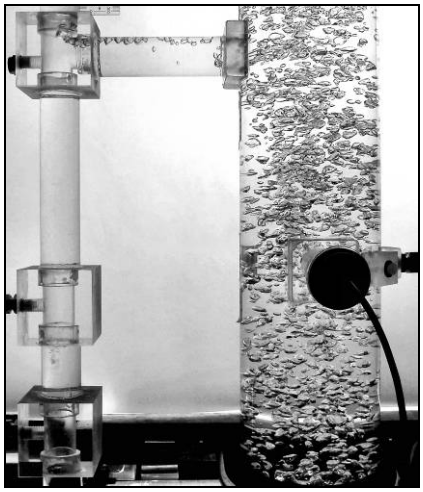
U_G = 1.5 cm/s

Test Conditions:
A = 0.62%
Open Vent Mode
Upper Horizontal Connector

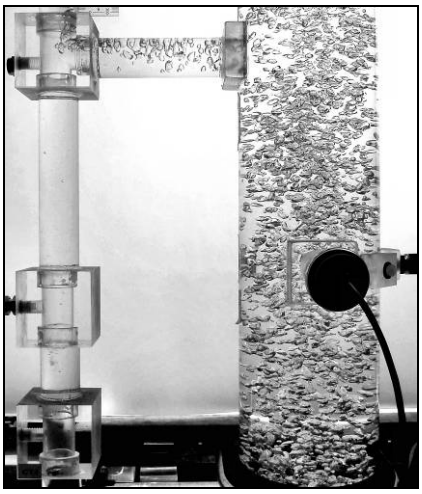
U_G = 2.0 cm/s

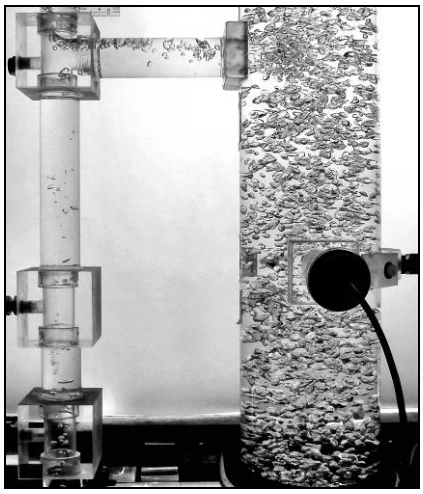
U_G = 2.0 cm/s

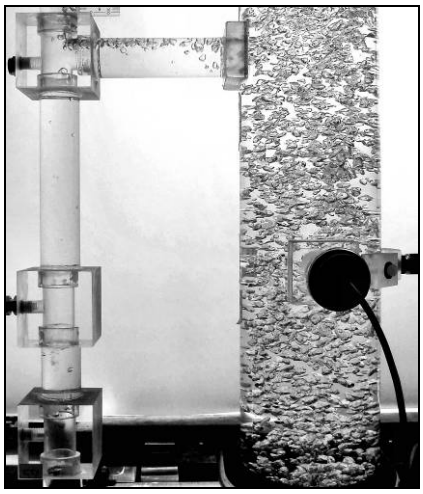
U_G = 2.0 cm/s

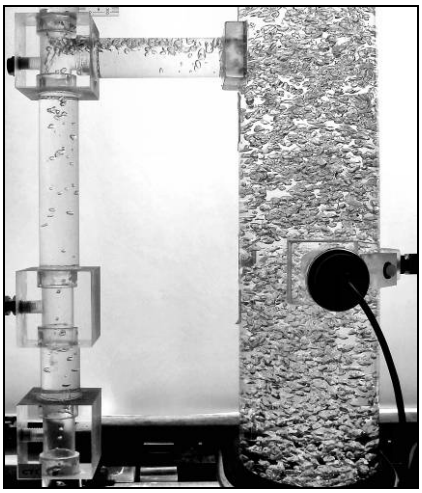
U_G = 2.5 cm/s

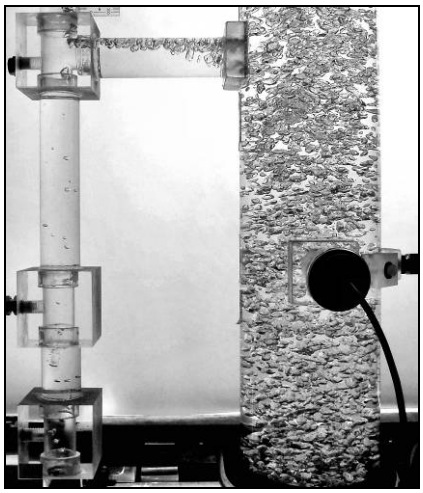
U_G = 2.5 cm/s

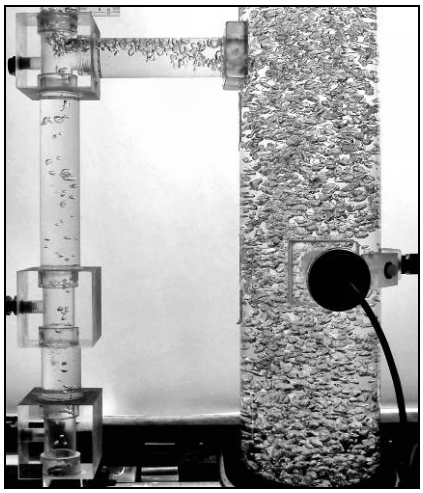
U_G = 2.5 cm/s

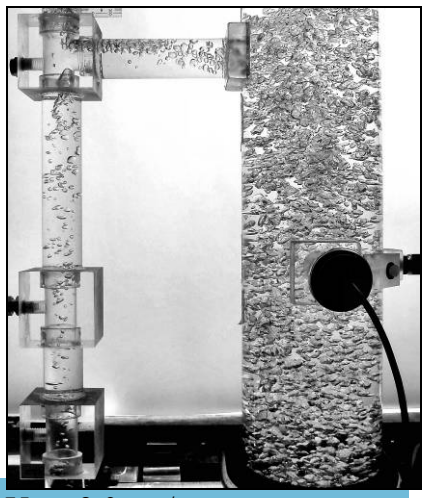
U_G = 3.0 cm/s

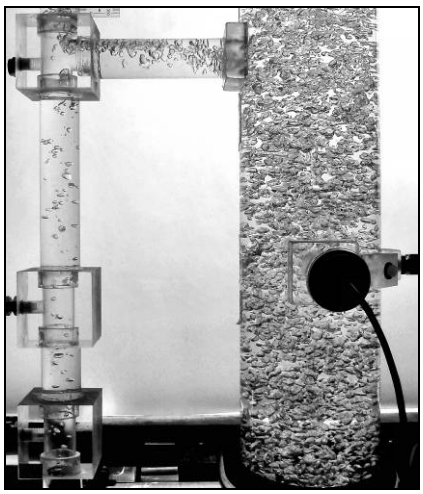
U_G = 3.0 cm/s

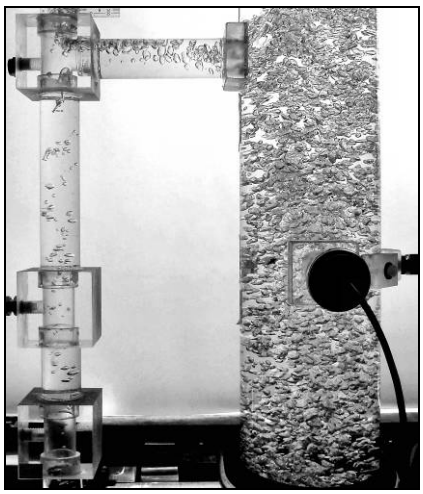
U_G = 3.0 cm/s

Test Conditions:
A = 0.62%
Open Vent Mode
Upper Horizontal Connector

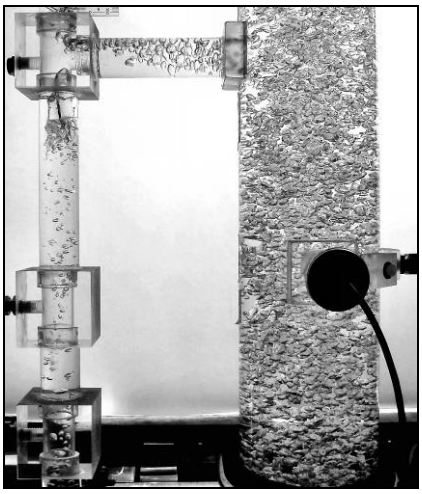
U_G = 3.5 cm/s

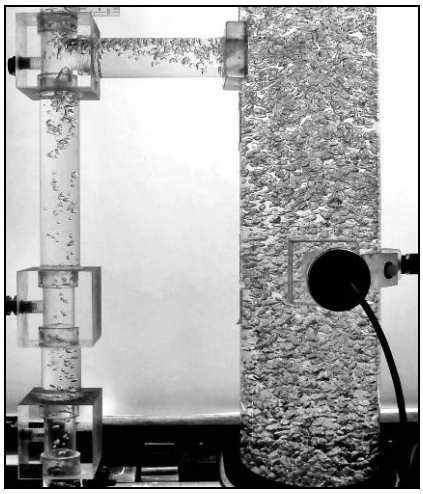
U_G = 3.5 cm/s

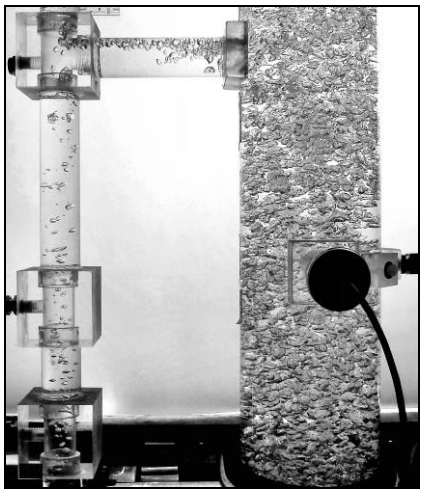
U_G = 3.5 cm/s

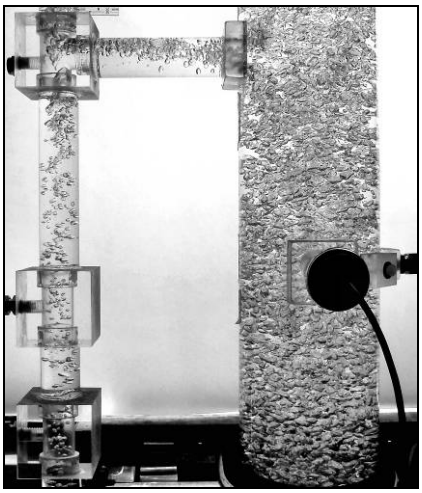
U_G = 4.0 cm/s

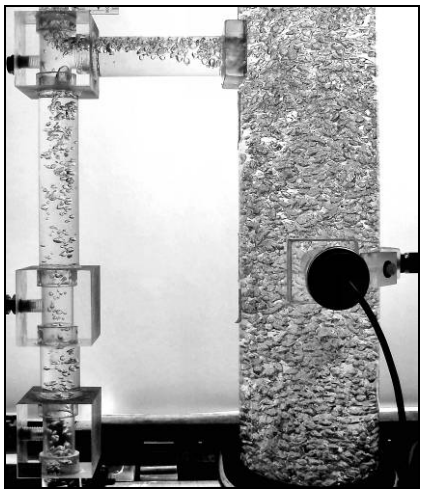
U_G = 4.0 cm/s

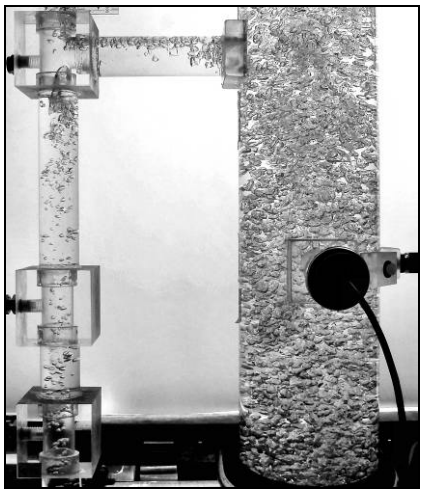
U_G = 4.0 cm/s

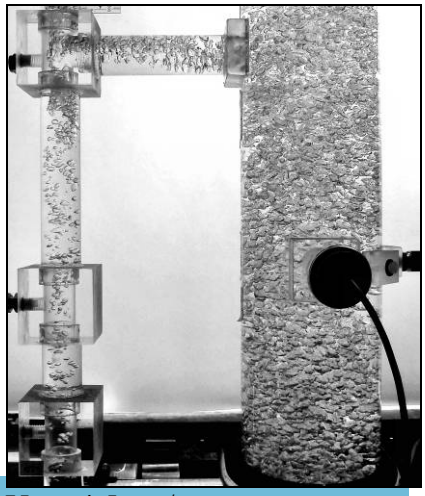
U_G = 4.5 cm/s

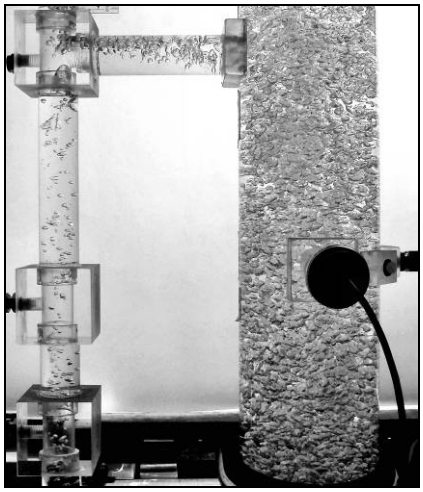
U_G = 4.5 cm/s

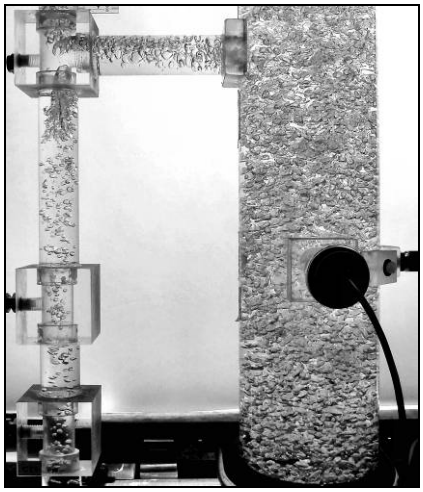
U_G = 4.5 cm/s

Test Conditions:
A = 0.62%
Open Vent Mode
Upper Horizontal Connector

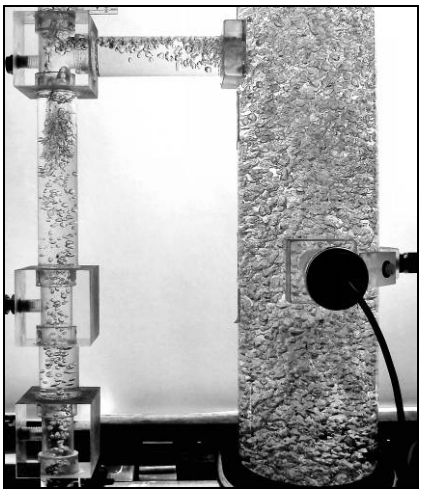
U_G = 5.0 cm/s

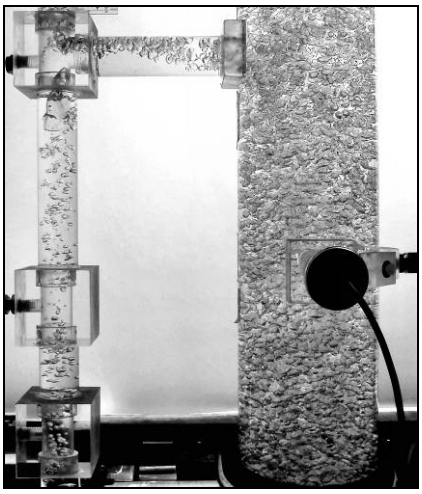
U_G = 5.0 cm/s

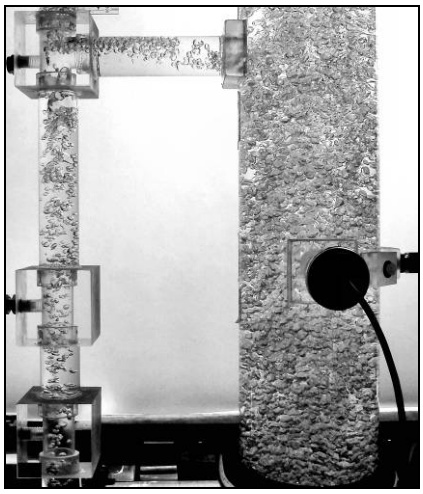
U_G = 5.0 cm/s

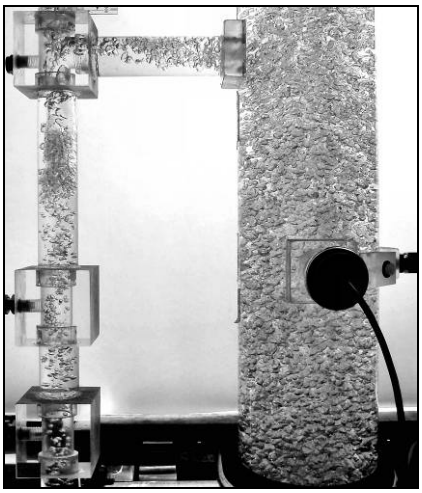
U_G = 6.0 cm/s

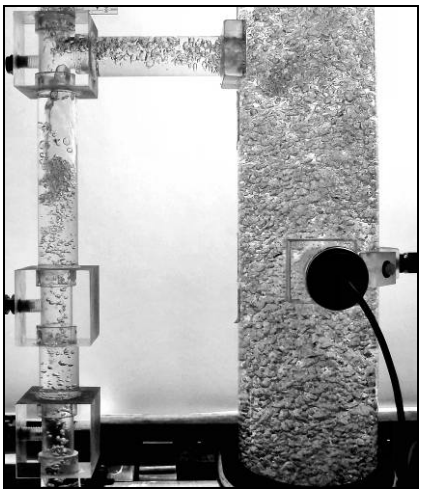
U_G = 6.0 cm/s

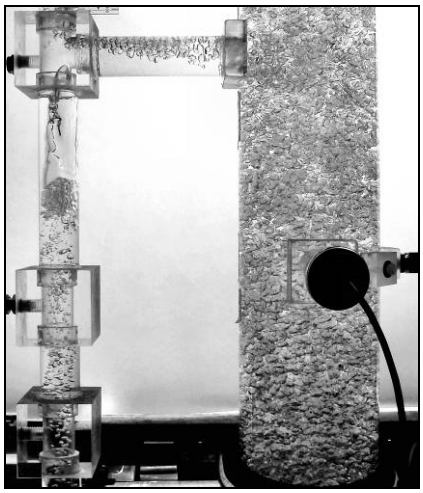
U_G = 6.0 cm/s

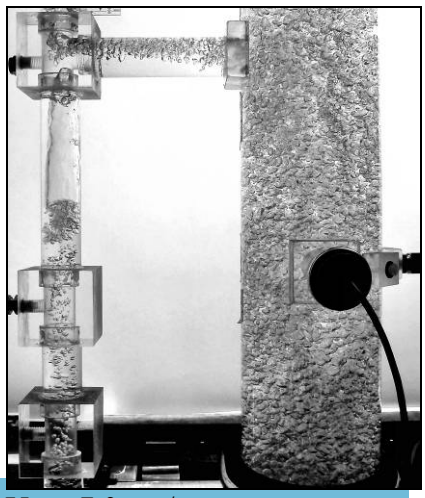
U_G = 7.0 cm/s

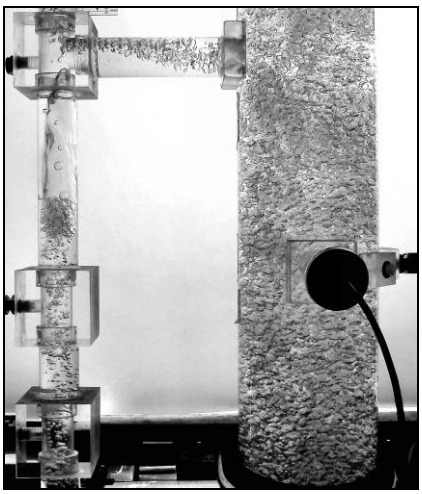
U_G = 7.0 cm/s

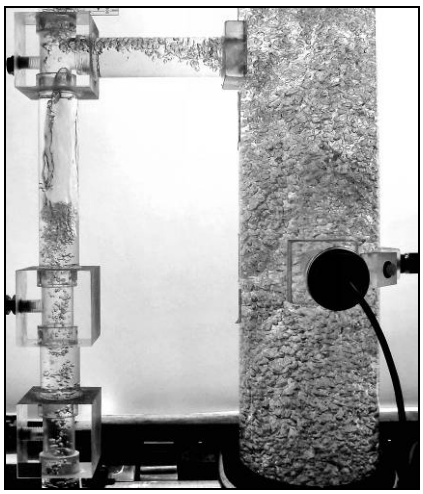
U_G = 7.0 cm/s

Test Conditions:
A = 0.62%
Open Vent Mode
Upper Horizontal Connector

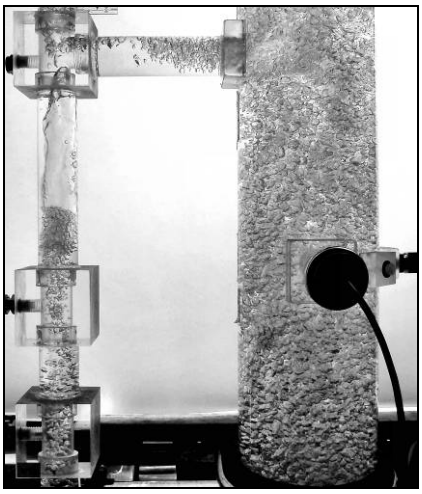
U_G = 8.0 cm/s

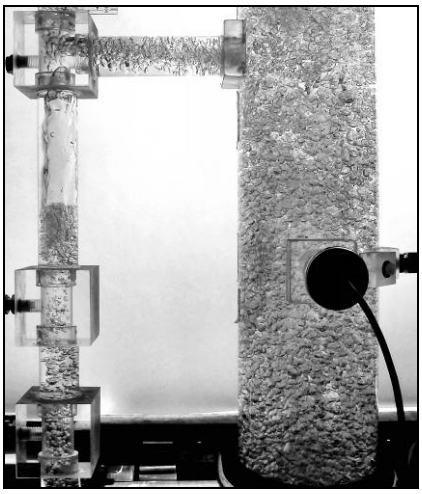
U_G = 8.0 cm/s

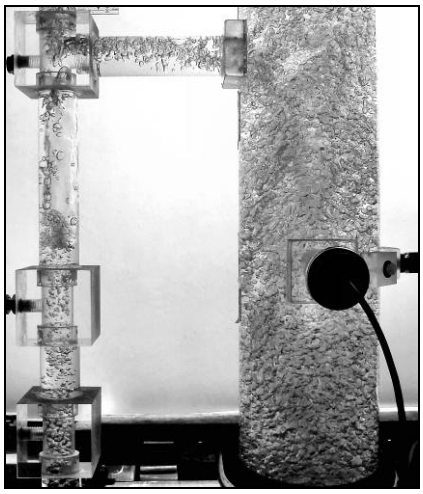
U_G = 8.0 cm/s

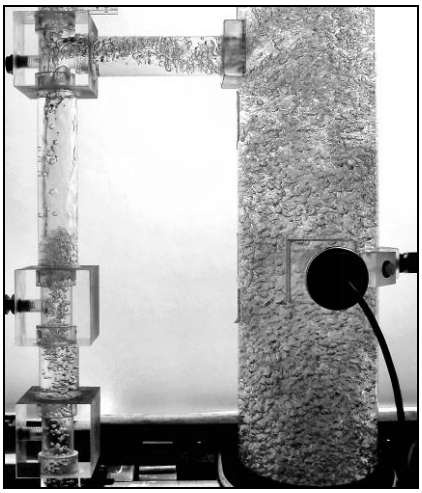
U_G = 9.0 cm/s

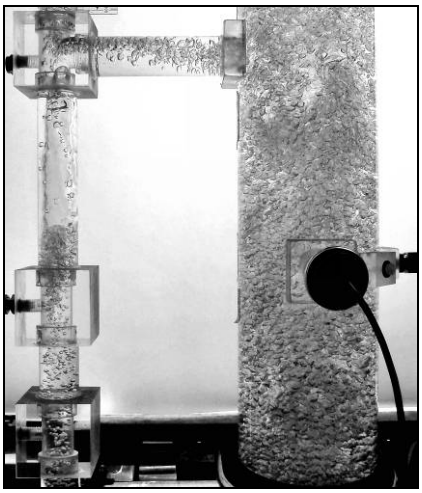
U_G = 9.0 cm/s

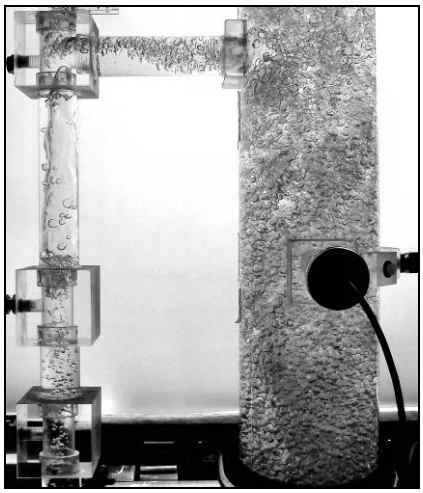
U_G = 9.0 cm/s

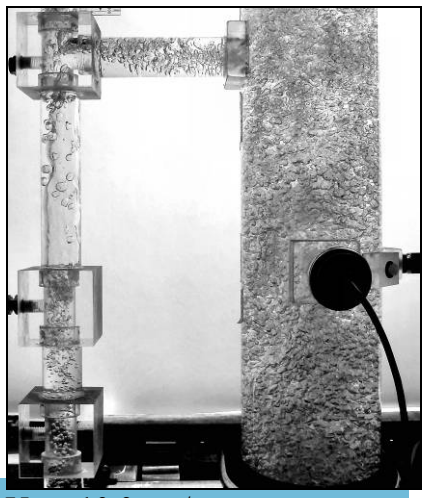
U_G = 10.0 cm/s

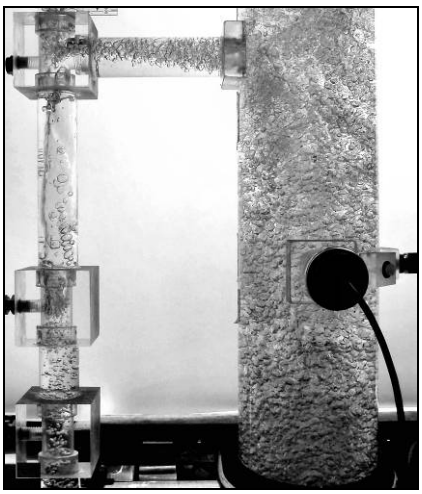
U_G = 10.0 cm/s

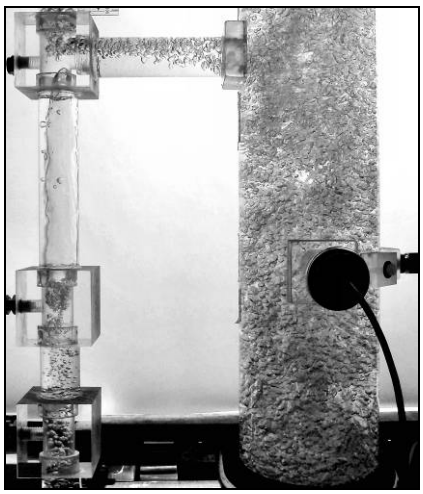
U_G = 10.0 cm/s

Test Conditions:
A = 0.62%
Open Vent Mode
Upper Horizontal Connector

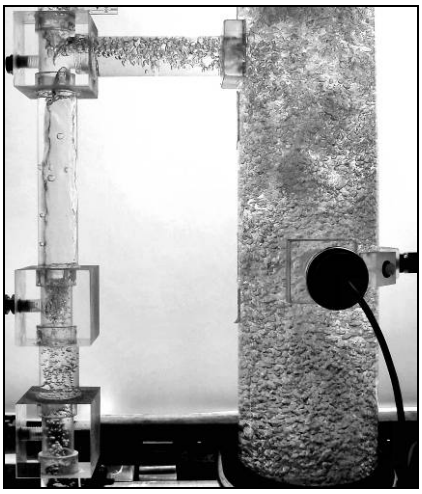
U_G = 11.0 cm/s

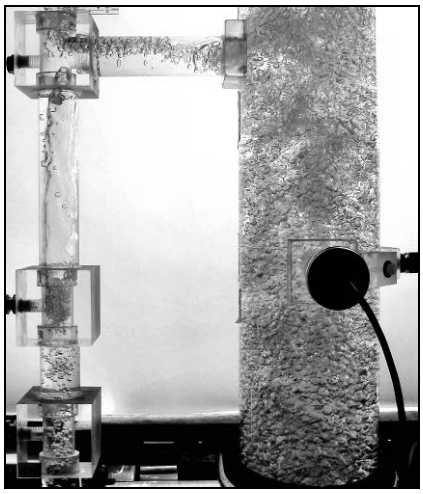
U_G = 11.0 cm/s

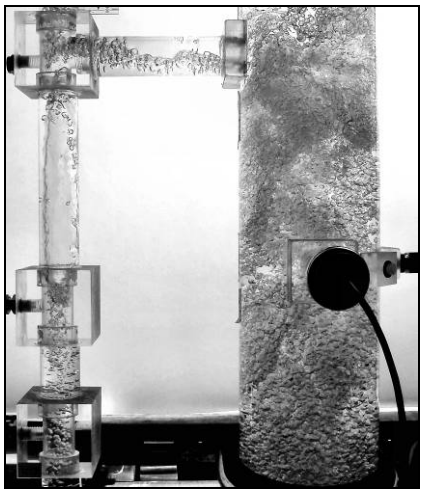
U_G = 11.0 cm/s

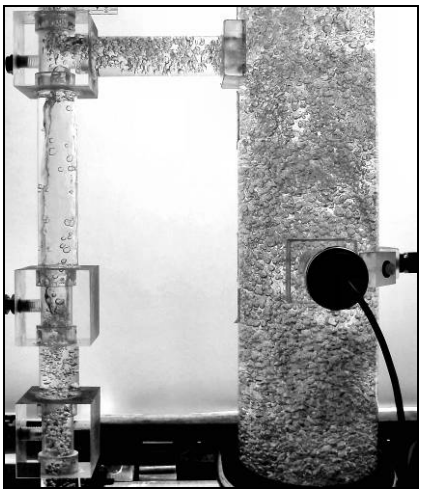
U_G = 12.0 cm/s

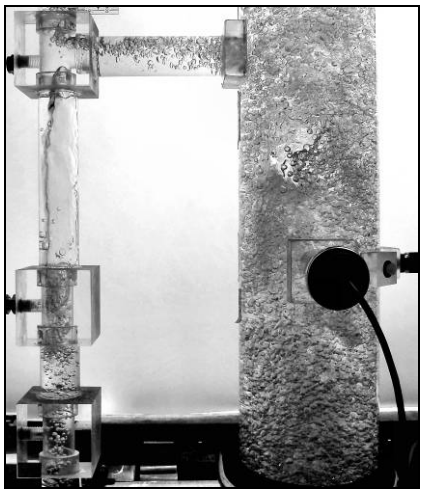
U_G = 12.0 cm/s

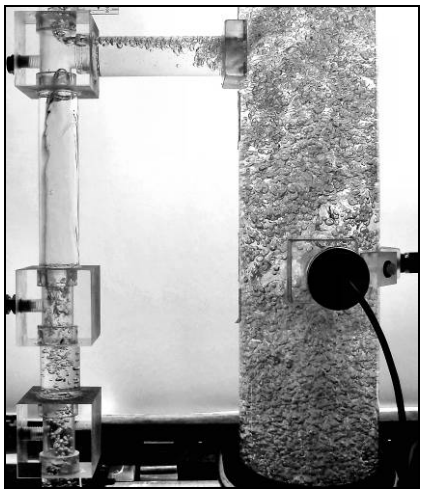
U_G = 12.0 cm/s

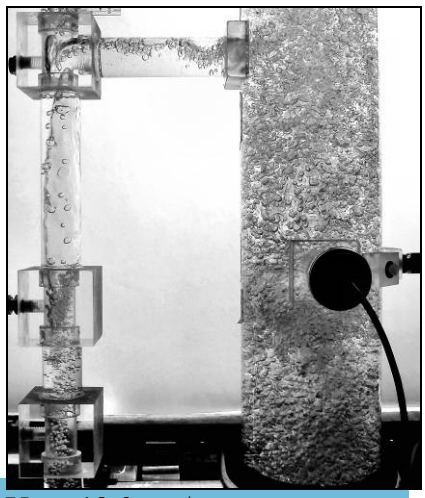
U_G = 13.0 cm/s

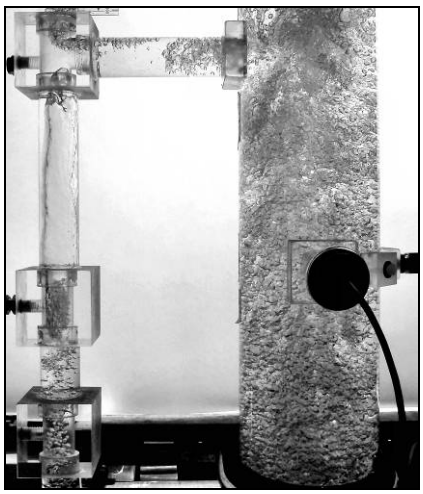
U_G = 13.0 cm/s

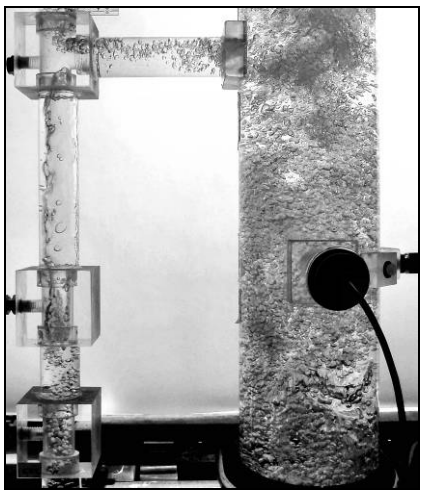
U_G = 13.0 cm/s

Test Conditions:
A = 0.62%
Open Vent Mode
Upper Horizontal Connector

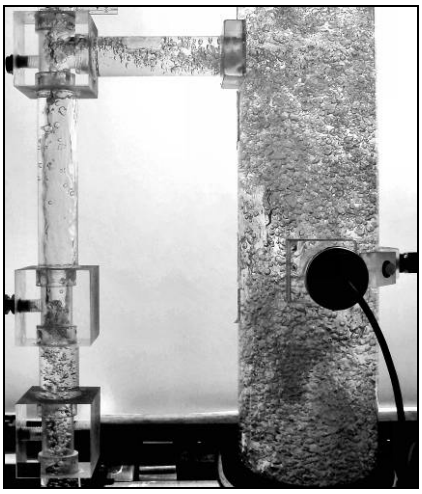
U_G = 14.0 cm/s

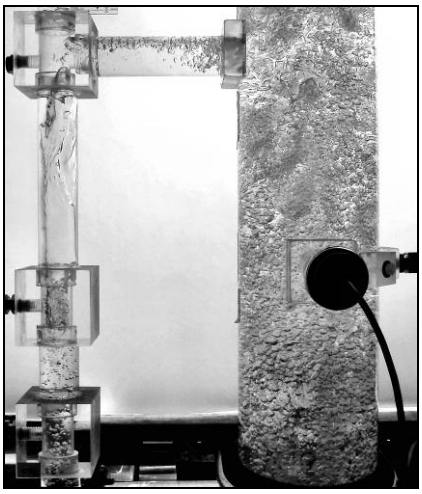
U_G = 14.0 cm/s

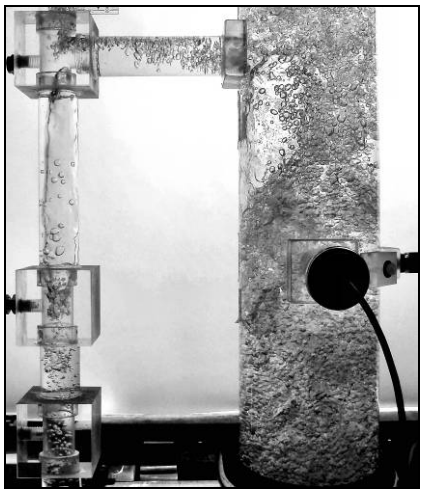
U_G = 14.0 cm/s

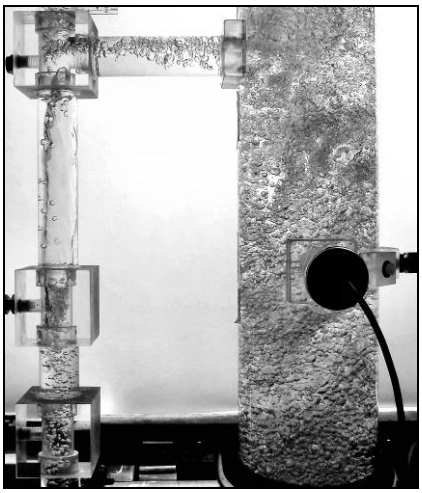
U_G = 15.0 cm/s

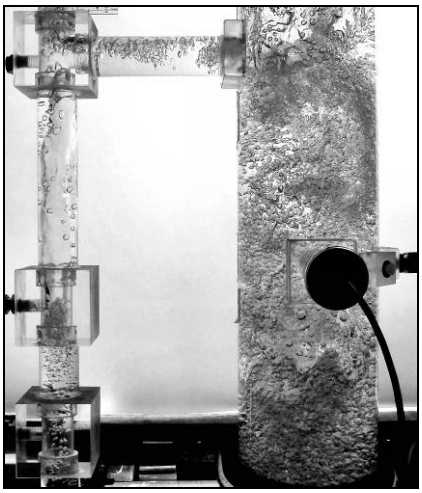
U_G = 15.0 cm/s

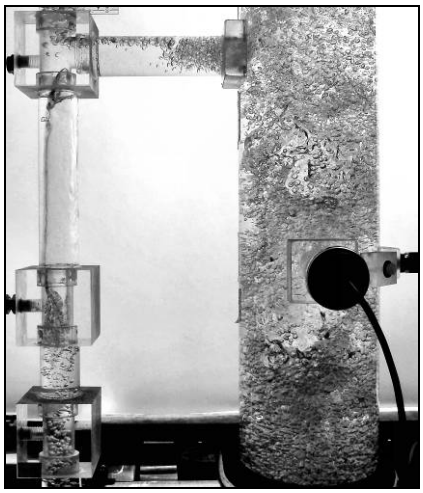
U_G = 15.0 cm/s

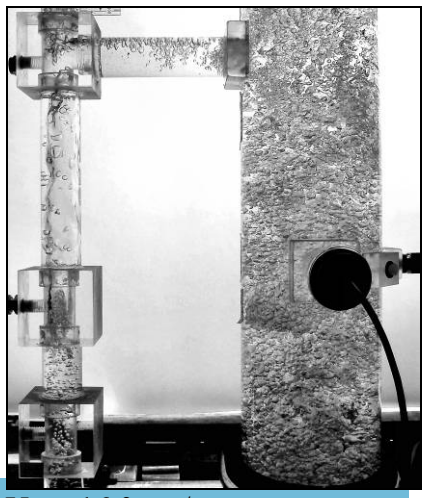
U_G = 16.0 cm/s

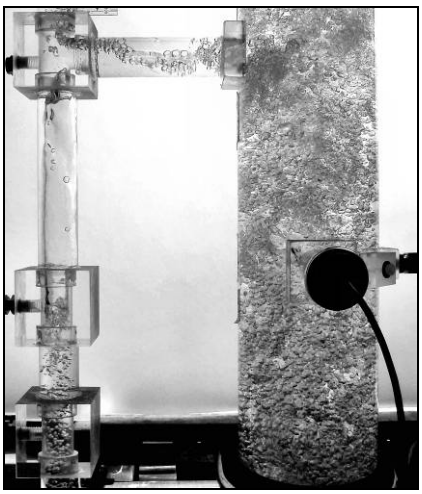
U_G = 16.0 cm/s

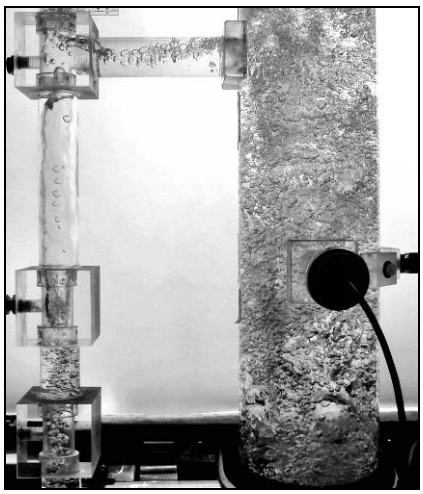
U_G = 16.0 cm/s

Test Conditions:
A = 0.62%
Open Vent Mode
Upper Horizontal Connector

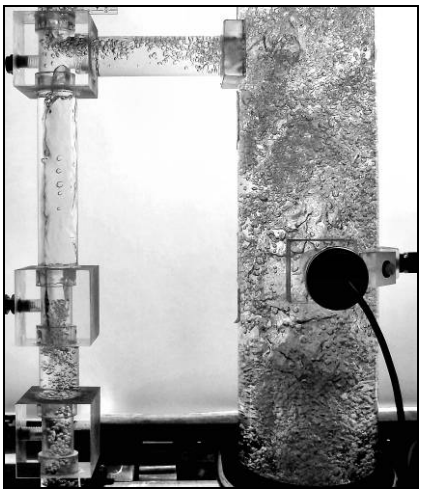
U_G = 17.0 cm/s

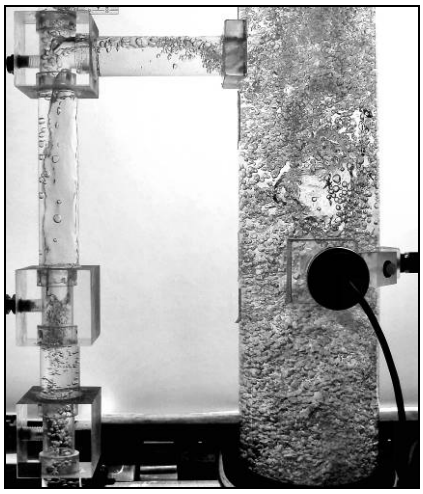
U_G = 17.0 cm/s

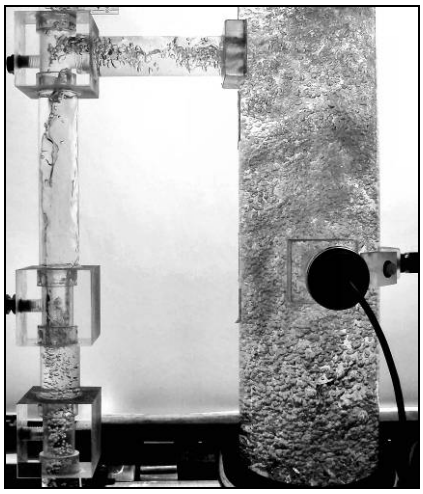
U_G = 17.0 cm/s

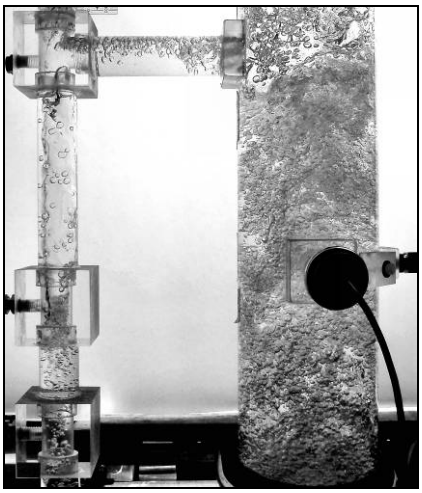
U_G = 18.0 cm/s

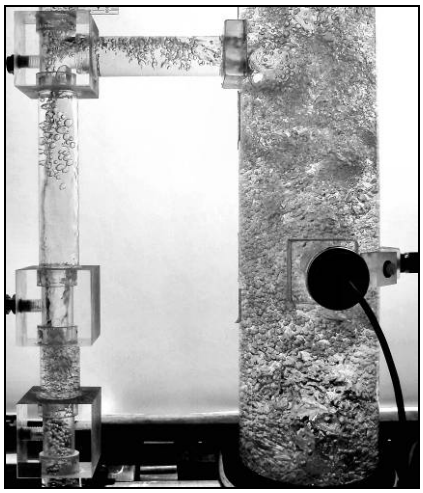
U_G = 18.0 cm/s

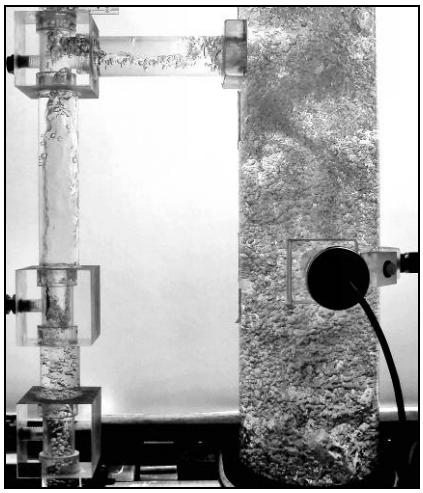
U_G = 18.0 cm/s

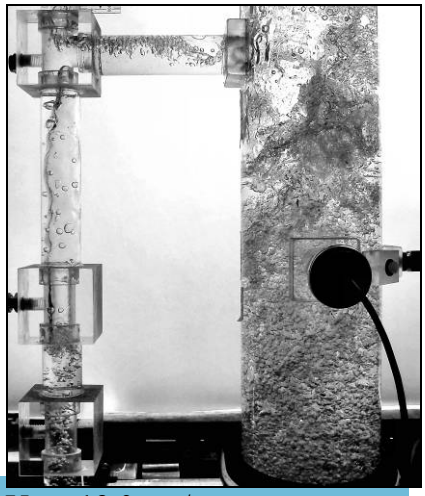
U_G = 19.0 cm/s

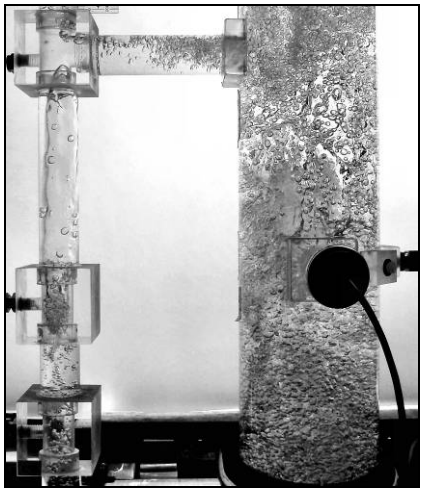
U_G = 19.0 cm/s

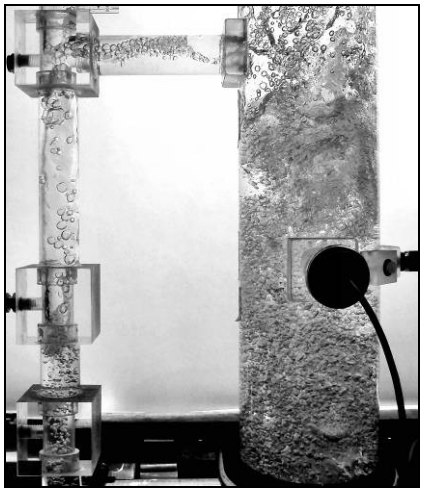
U_G = 19.0 cm/s

Test Conditions:
A = 0.62%
Open Vent Mode
Upper Horizontal Connector

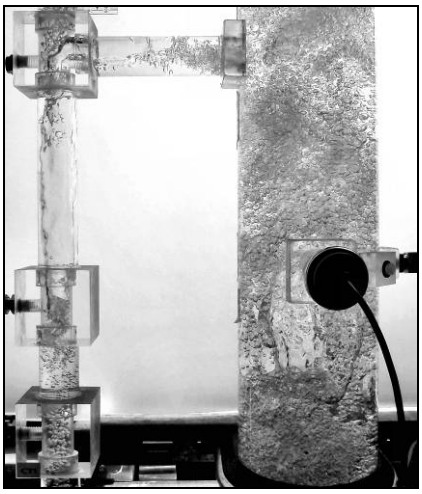
U_G = 20.0 cm/s

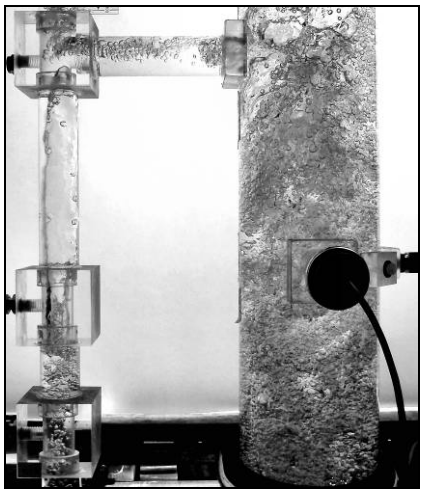
U_G = 20.0 cm/s

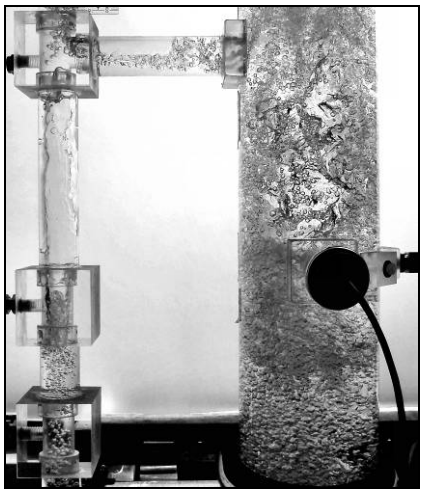
U_G = 20.0 cm/s

Test Conditions:
A = 0.62%
Closed Vent Mode
Upper Horizontal Connector

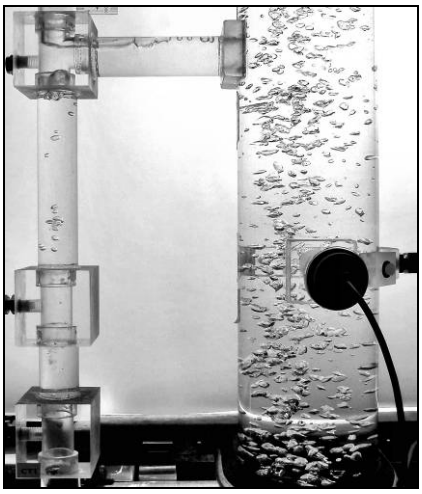
U_G = 0.5 cm/s

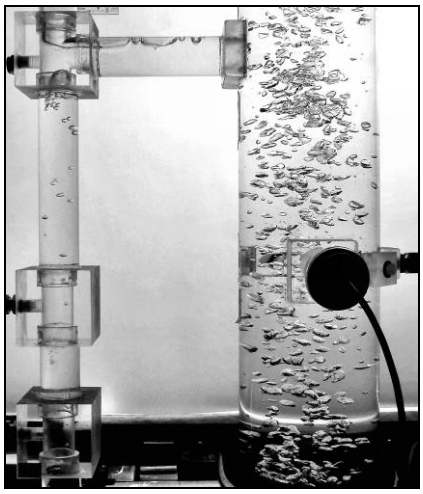
U_G = 0.5 cm/s

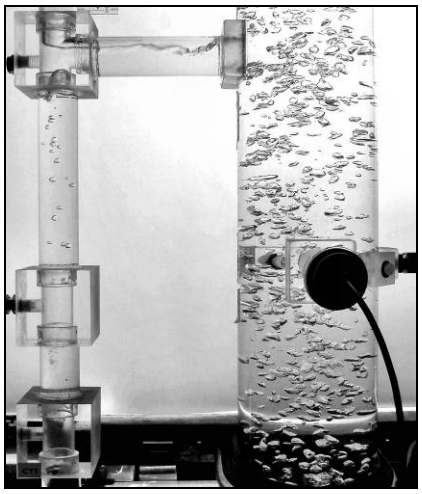
U_G = 0.5 cm/s

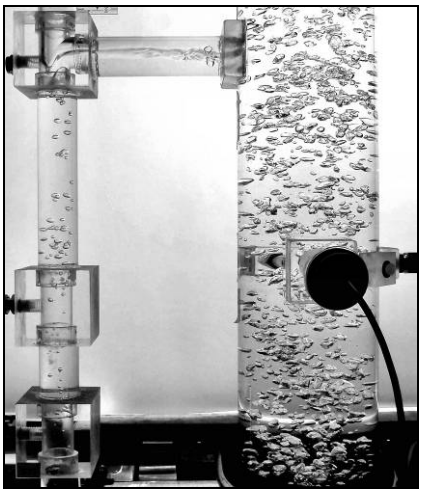
U_G = 1.0 cm/s

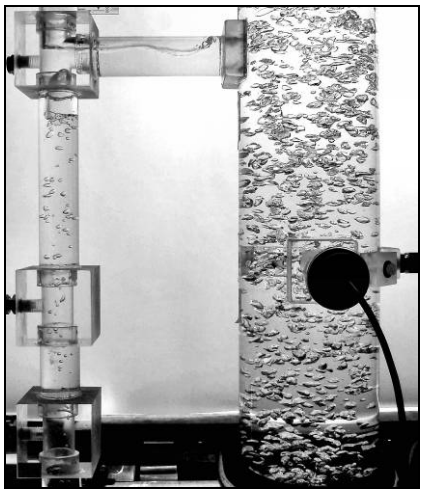
U_G = 1.0 cm/s

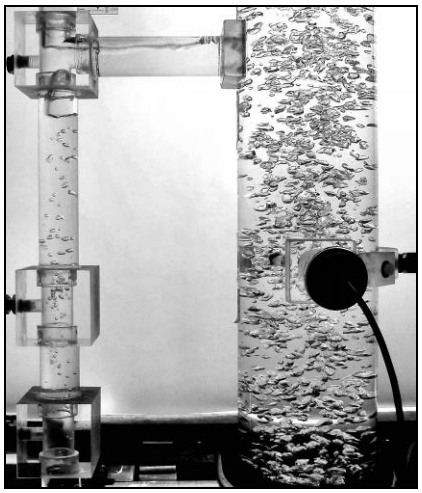
U_G = 1.0 cm/s

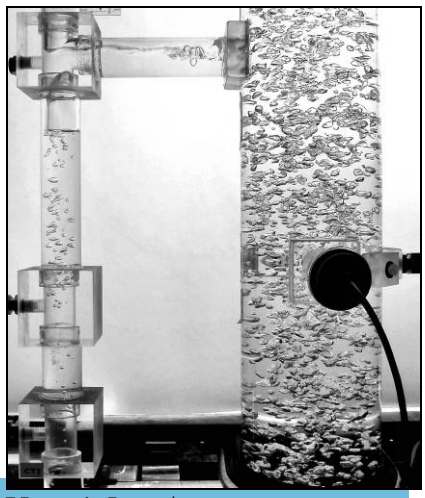
U_G = 1.5 cm/s

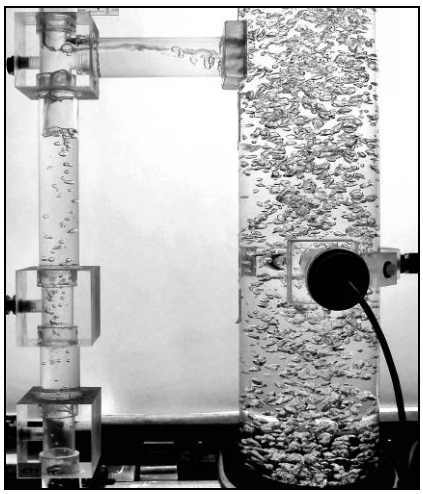
U_G = 1.5 cm/s

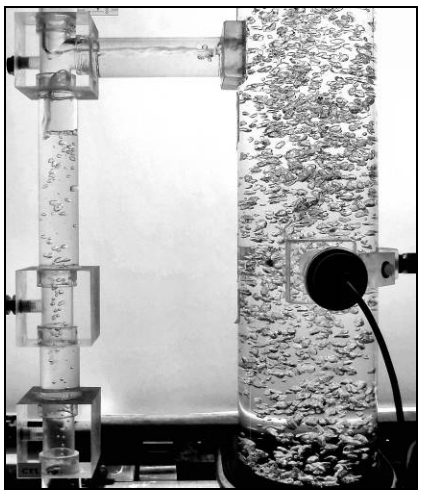
U_G = 1.5 cm/s

Test Conditions:
A = 0.62%
Closed Vent Mode
Upper Horizontal Connector

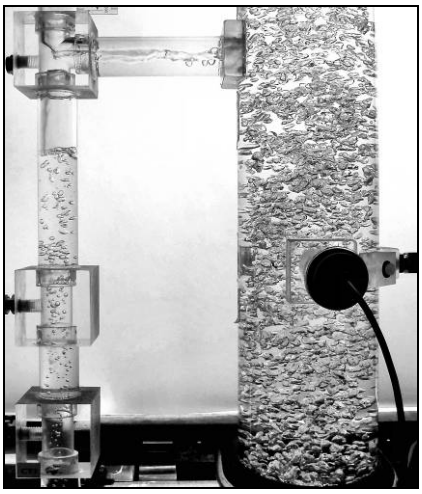
U_G = 2.0 cm/s

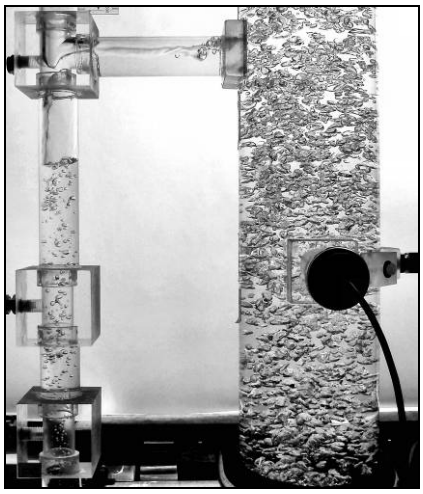
U_G = 2.0 cm/s

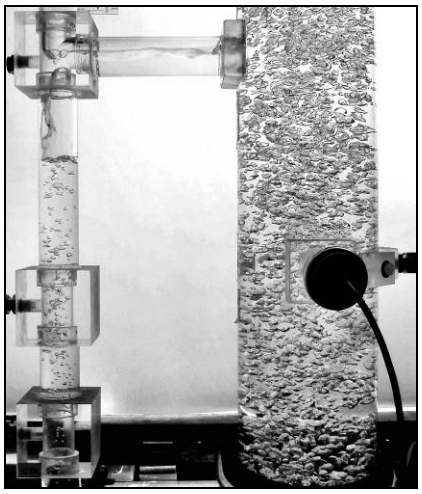
U_G = 2.0 cm/s

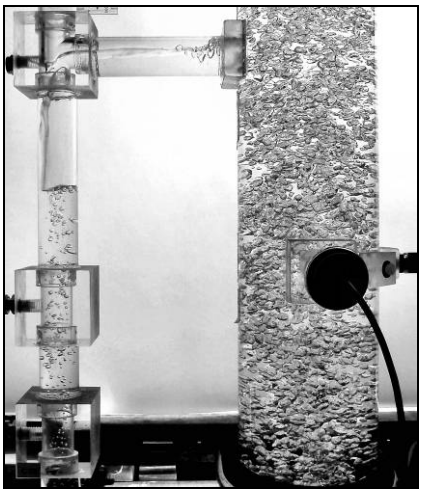
U_G = 2.5 cm/s

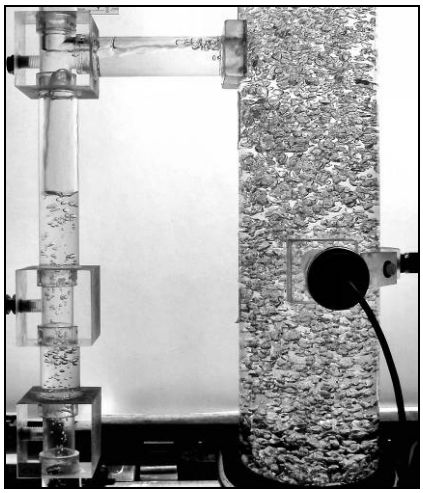
U_G = 2.5 cm/s

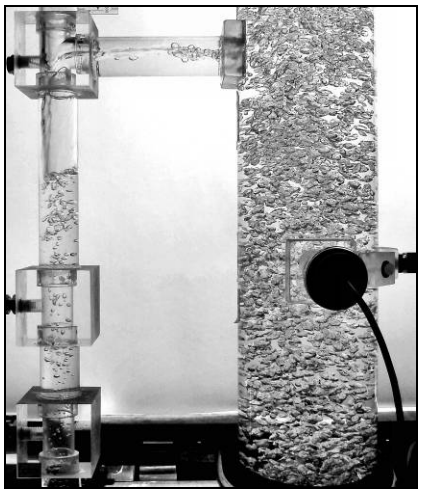
U_G = 2.5 cm/s

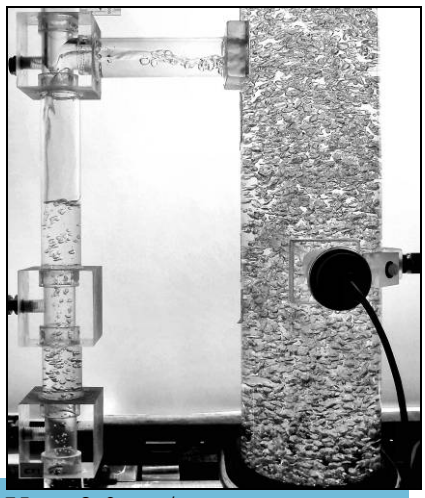
U_G = 3.0 cm/s

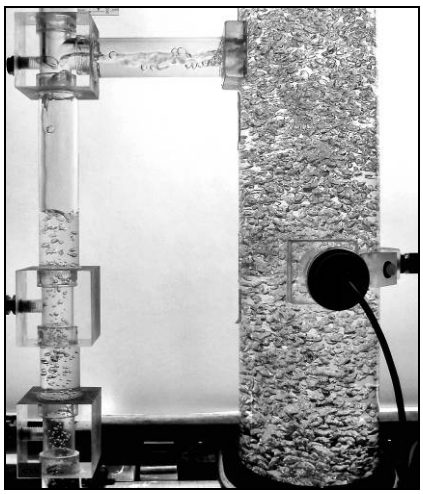
U_G = 3.0 cm/s

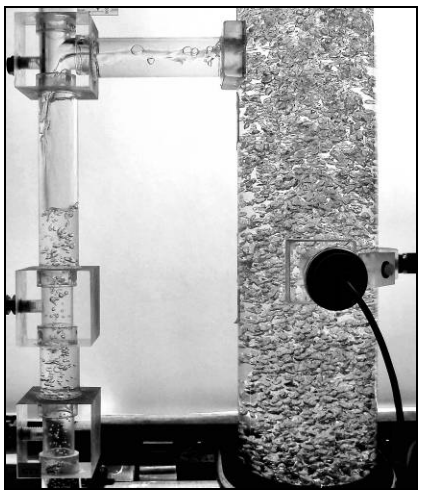
U_G = 3.0 cm/s

Test Conditions:
A = 0.62%
Closed Vent Mode
Upper Horizontal Connector

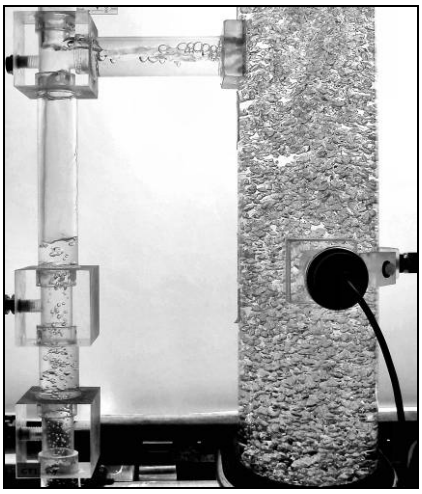
U_G = 3.5 cm/s

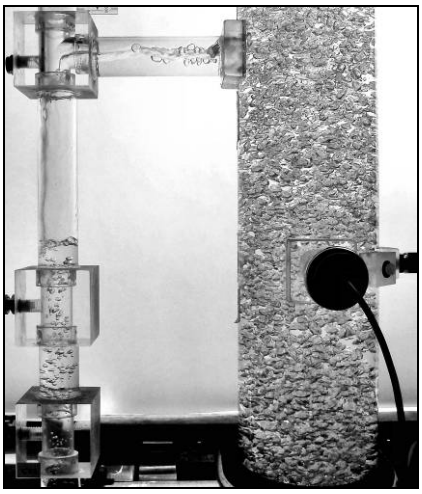
U_G = 3.5 cm/s

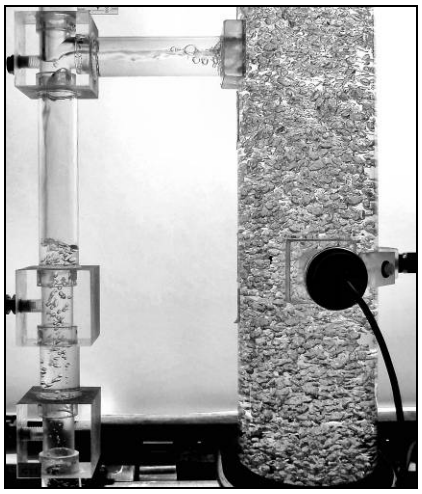
U_G = 3.5 cm/s

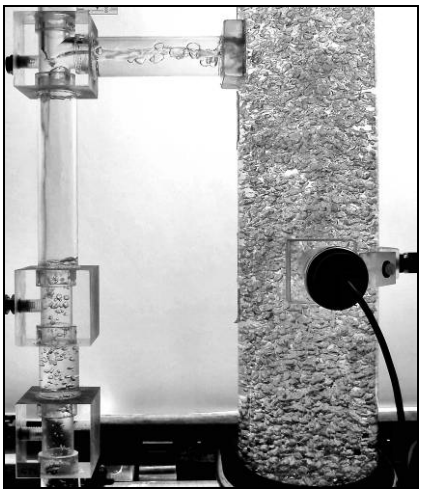
U_G = 4.0 cm/s

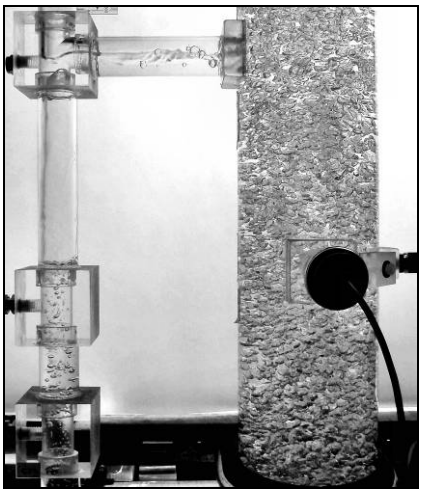
U_G = 4.0 cm/s

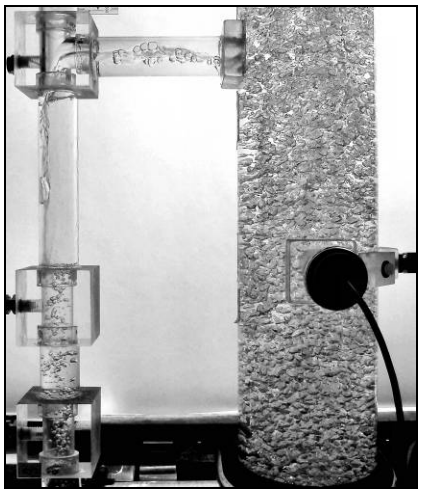
U_G = 4.0 cm/s

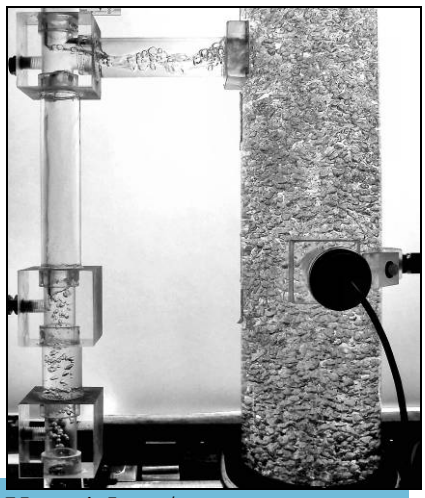
U_G = 4.5 cm/s

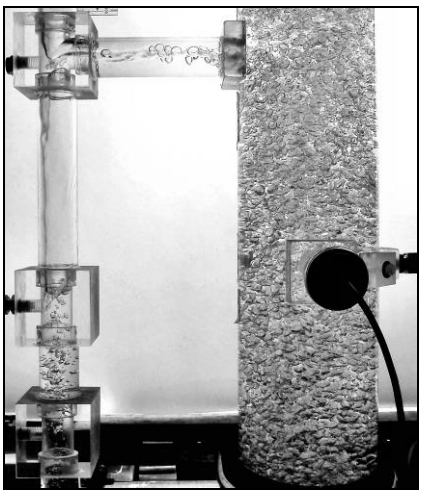
U_G = 4.5 cm/s

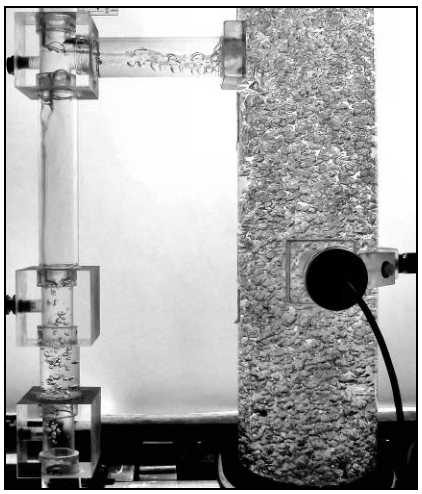
U_G = 4.5 cm/s

Test Conditions:
A = 0.62%
Closed Vent Mode
Upper Horizontal Connector

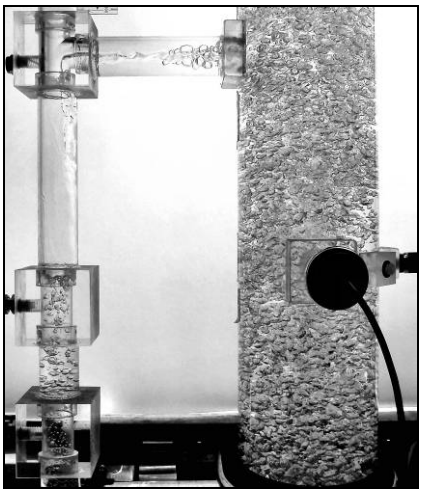
U_G = 5.0 cm/s

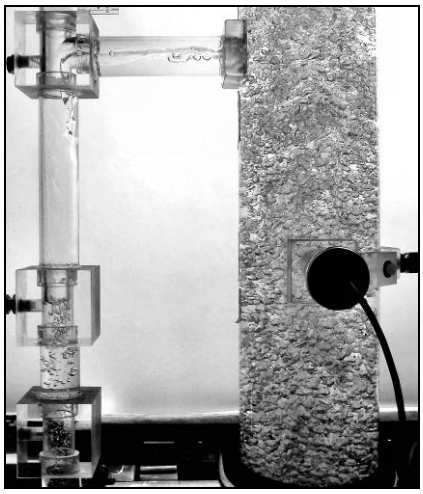
U_G = 5.0 cm/s

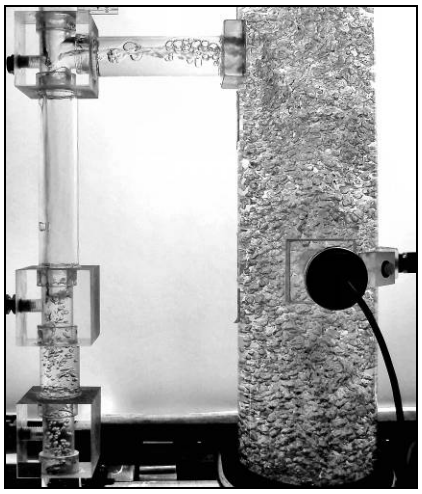
U_G = 5.0 cm/s

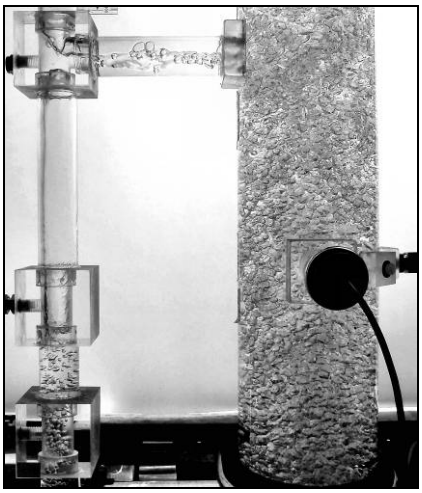
U_G = 6.0 cm/s

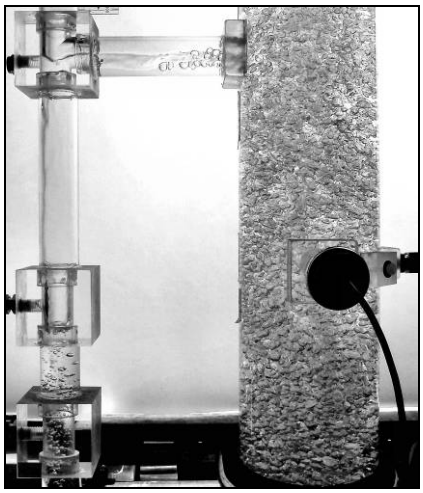
U_G = 6.0 cm/s

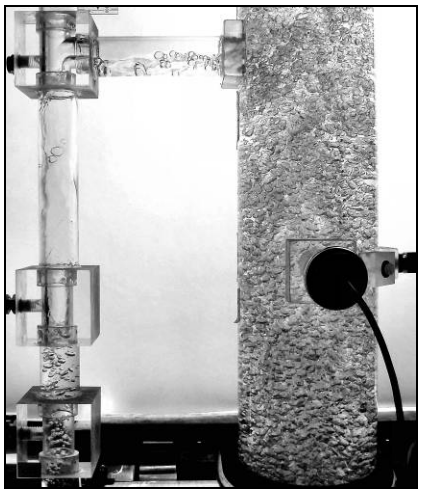
U_G = 6.0 cm/s

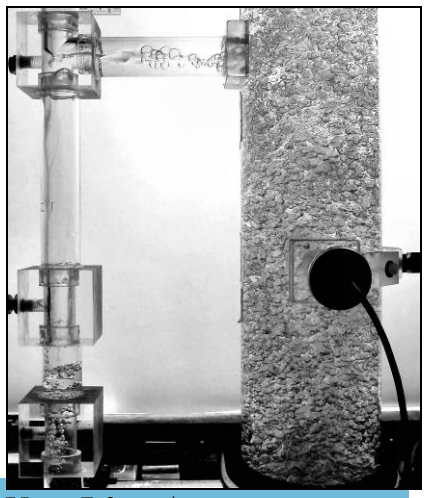
U_G = 7.0 cm/s

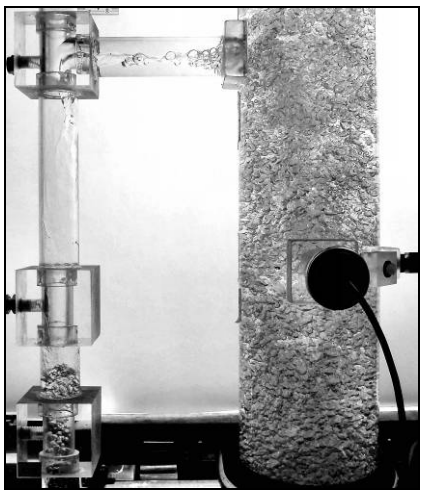
U_G = 7.0 cm/s

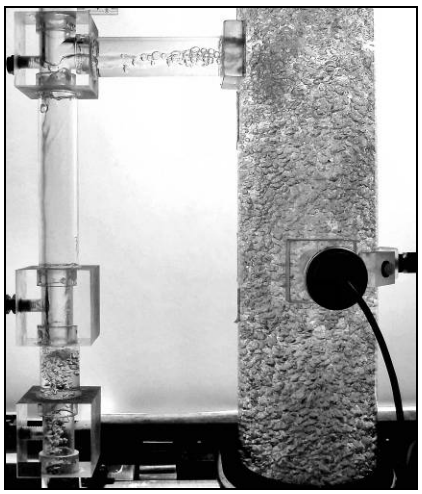
U_G = 7.0 cm/s

Test Conditions:
A = 0.62%
Closed Vent Mode
Upper Horizontal Connector

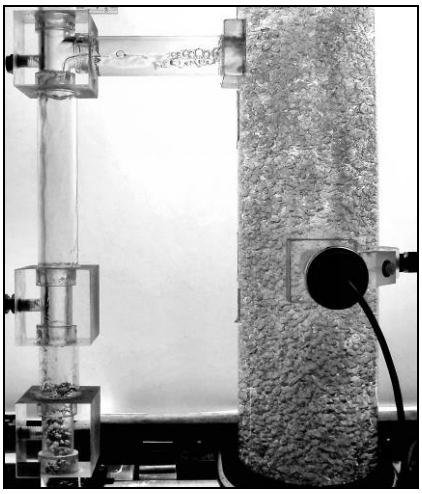
U_G = 8.0 cm/s

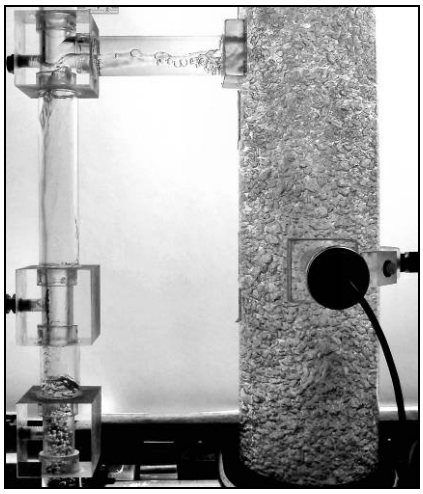
U_G = 8.0 cm/s

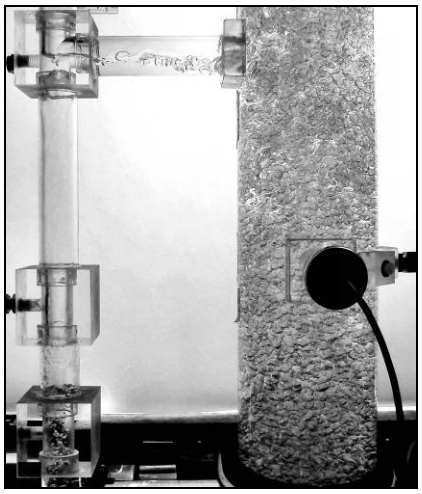
U_G = 8.0 cm/s

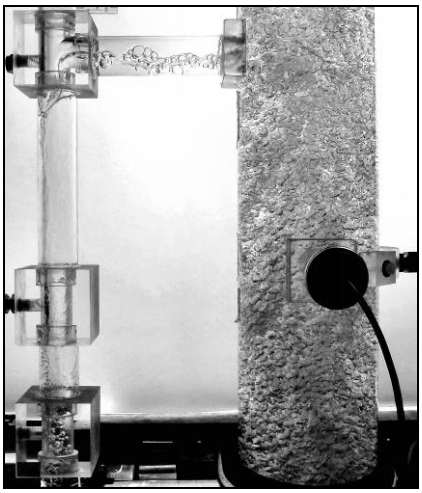
U_G = 9.0 cm/s

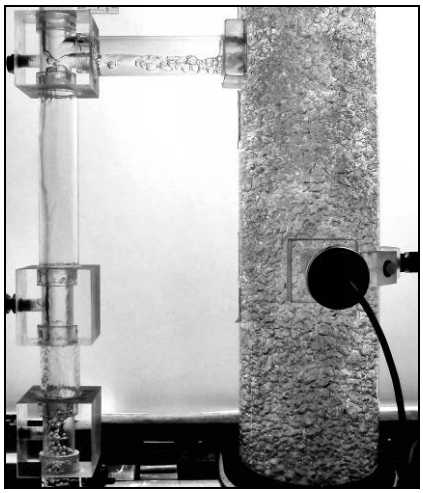
U_G = 9.0 cm/s

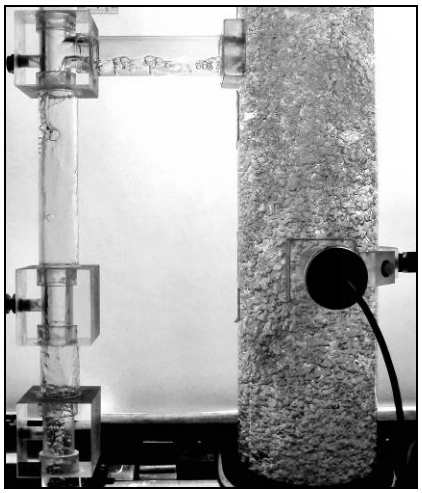
U_G = 9.0 cm/s

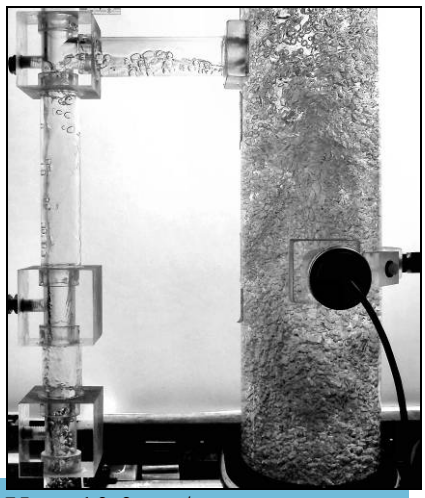
U_G = 10.0 cm/s

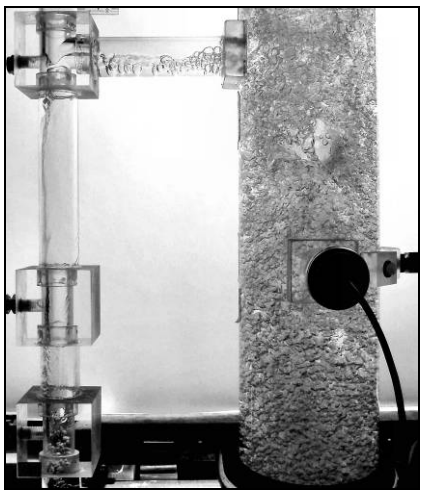
U_G = 10.0 cm/s

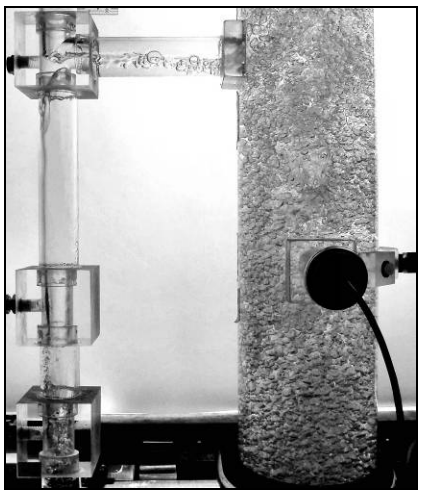
U_G = 10.0 cm/s

Test Conditions:
A = 0.62%
Closed Vent Mode
Upper Horizontal Connector

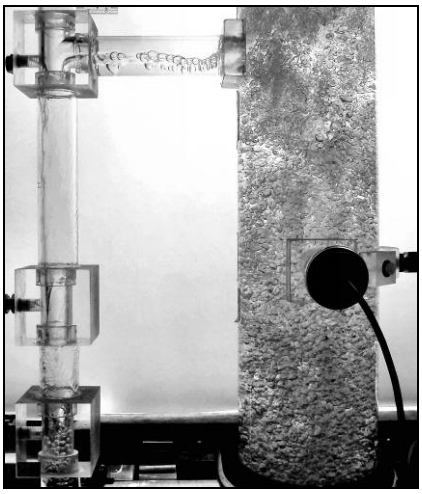
U_G = 11.0 cm/s

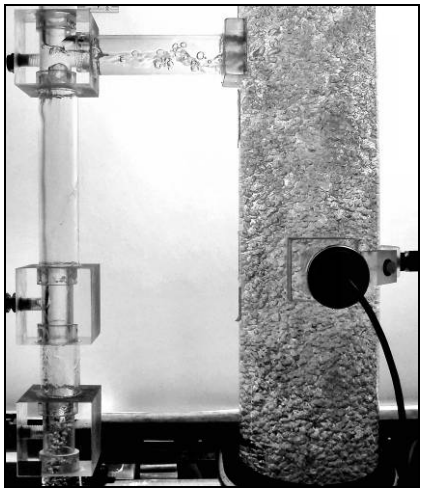
U_G = 11.0 cm/s

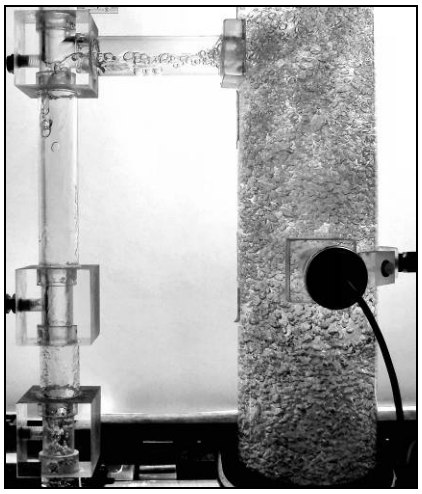
U_G = 11.0 cm/s

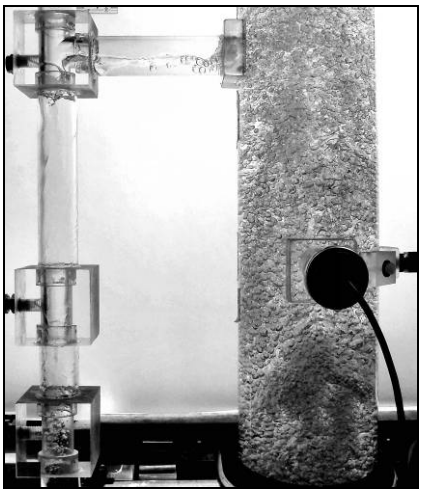
U_G = 12.0 cm/s

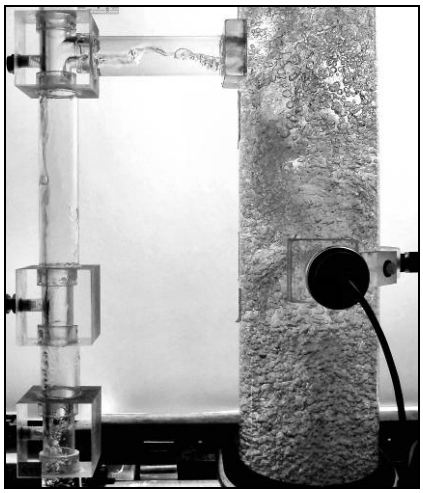
U_G = 12.0 cm/s

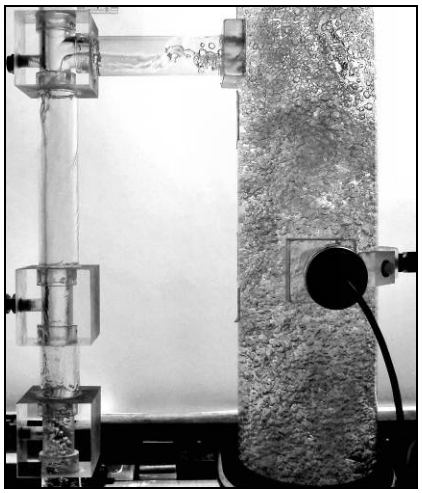
U_G = 12.0 cm/s

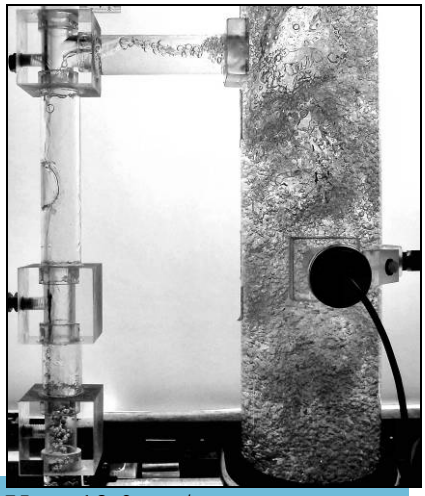
U_G = 13.0 cm/s

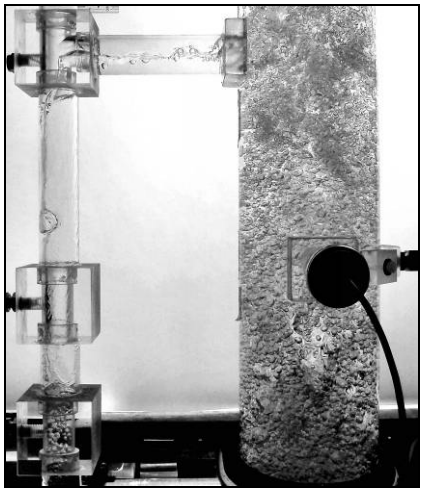
U_G = 13.0 cm/s

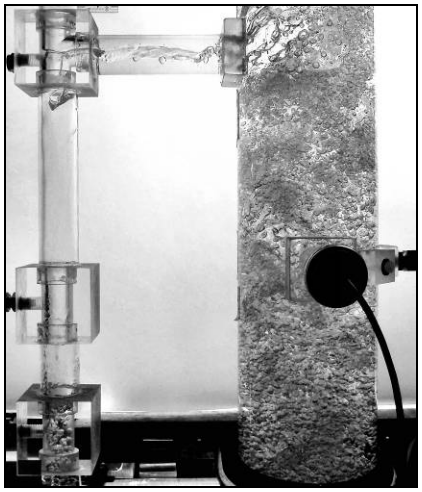
U_G = 13.0 cm/s

Test Conditions:
A = 0.62%
Closed Vent Mode
Upper Horizontal Connector

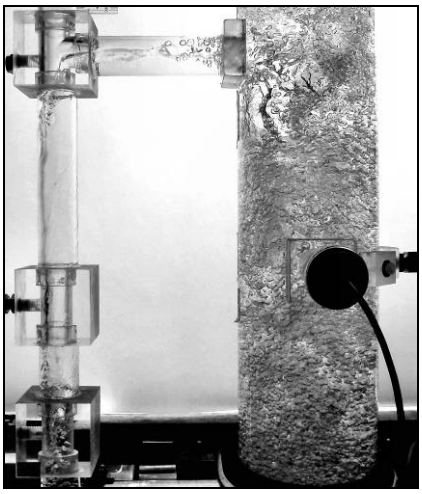
U_G = 14.0 cm/s

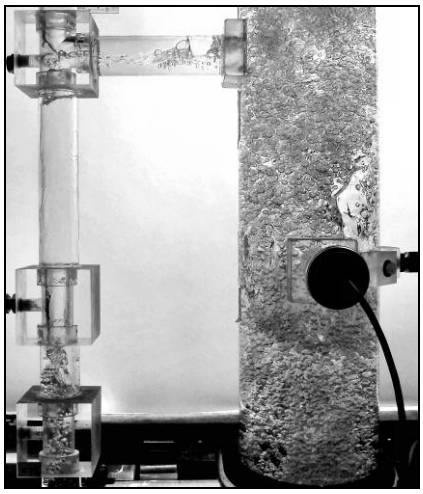
U_G = 14.0 cm/s

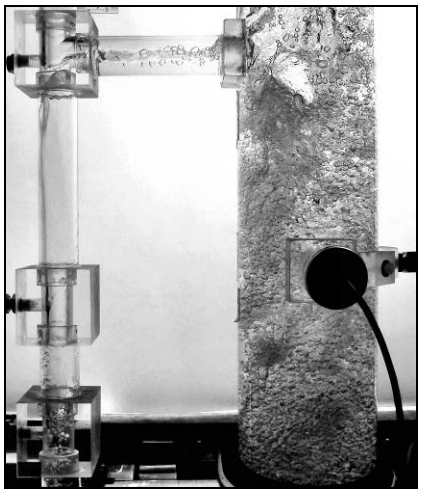
U_G = 14.0 cm/s

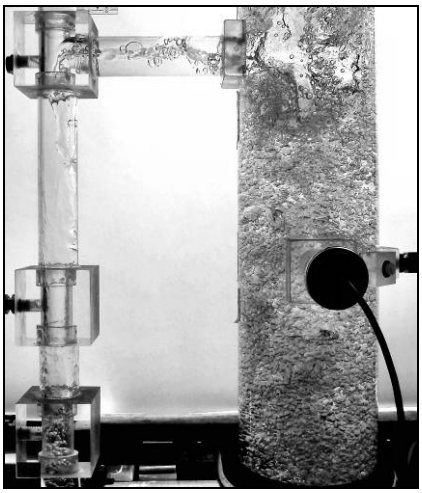
U_G = 15.0 cm/s

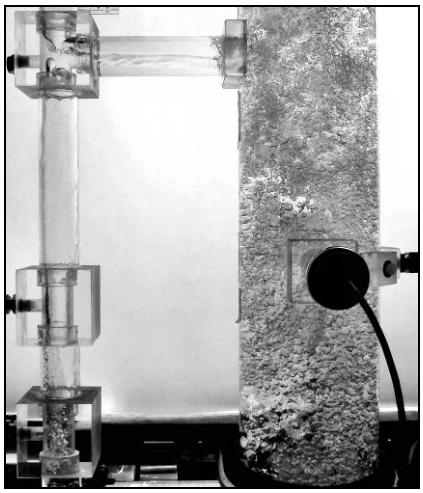
U_G = 15.0 cm/s

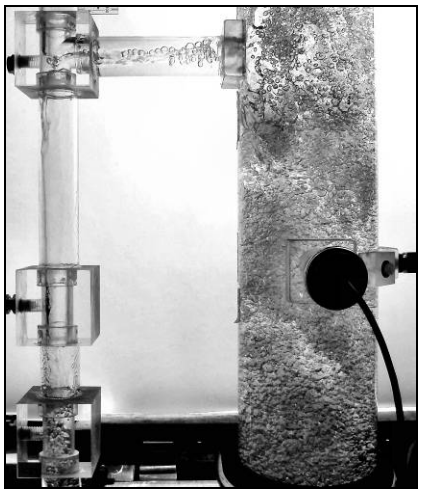
U_G = 15.0 cm/s

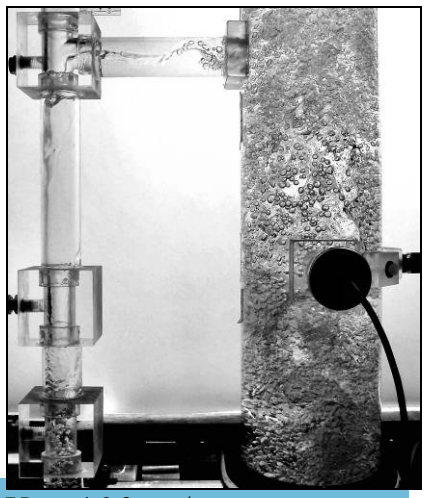
U_G = 16.0 cm/s

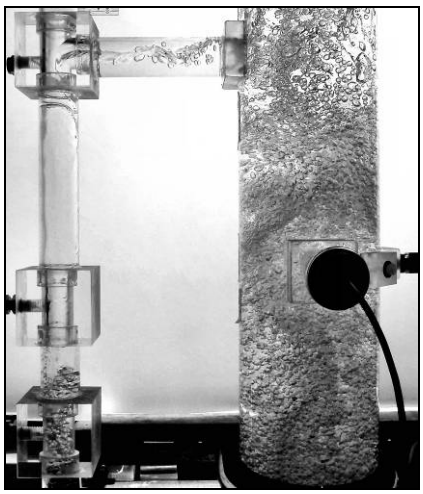
U_G = 16.0 cm/s

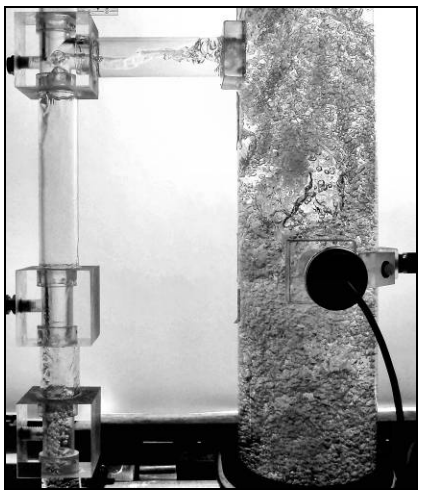
U_G = 16.0 cm/s

Test Conditions:
A = 0.62%
Closed Vent Mode
Upper Horizontal Connector

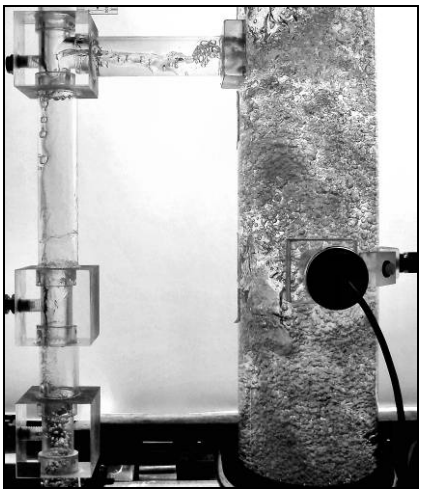
U_G = 17.0 cm/s

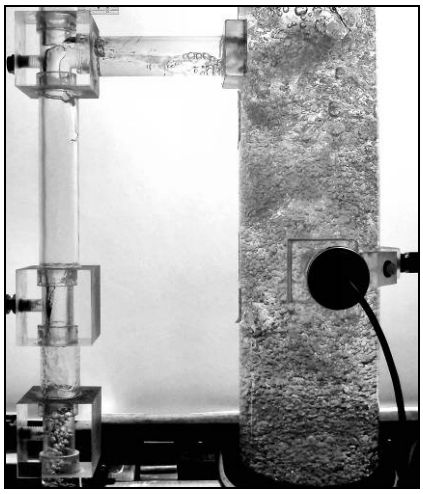
U_G = 17.0 cm/s

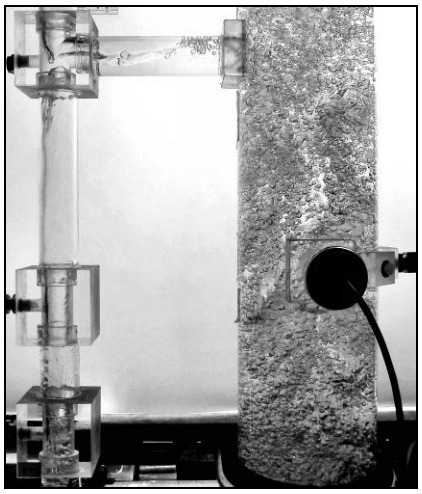
U_G = 17.0 cm/s

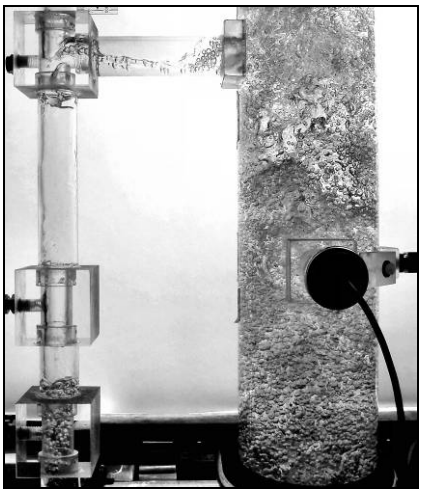
U_G = 18.0 cm/s

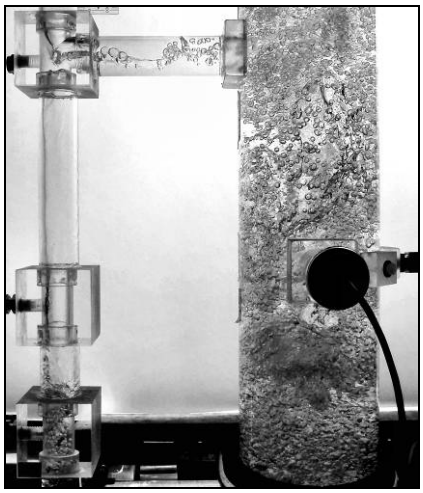
U_G = 18.0 cm/s

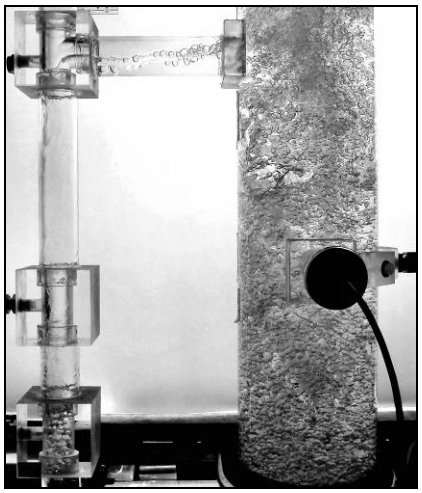
U_G = 18.0 cm/s

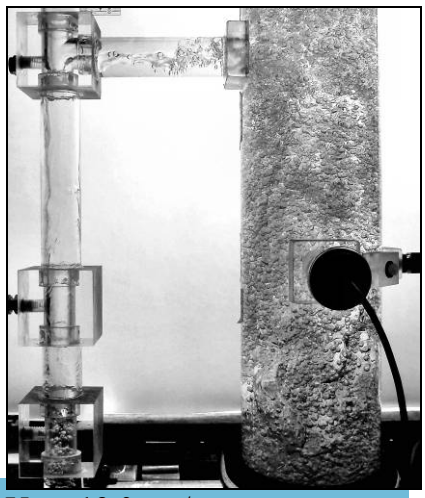
U_G = 19.0 cm/s

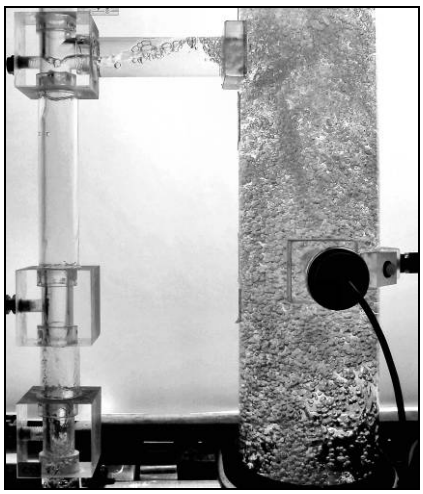
U_G = 19.0 cm/s

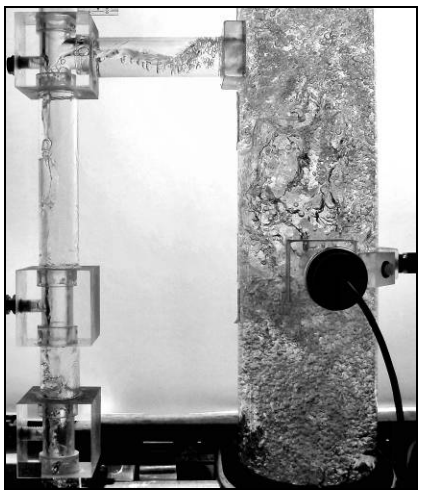
U_G = 19.0 cm/s

Test Conditions:
A = 0.62%
Closed Vent Mode
Upper Horizontal Connector

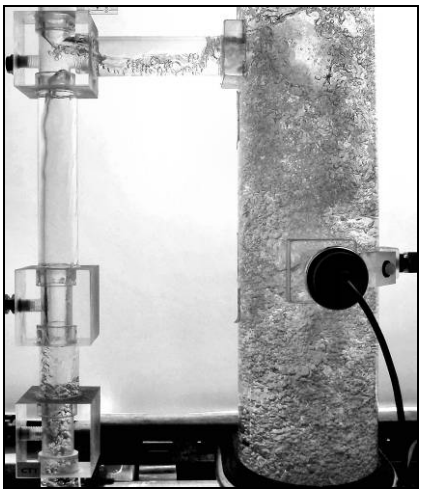
U_G = 20.0 cm/s

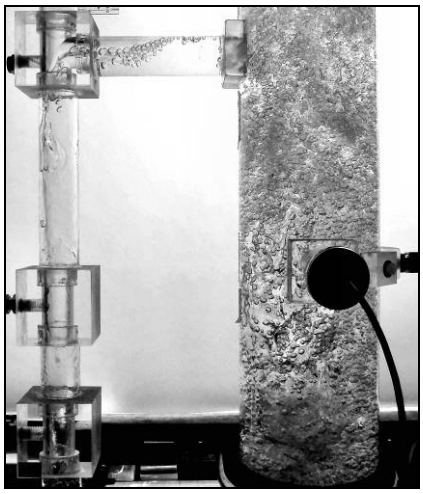
U_G = 20.0 cm/s

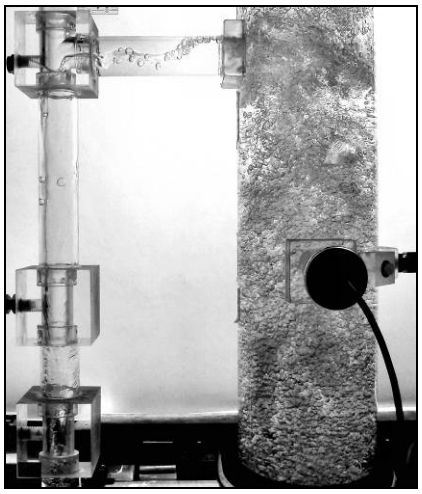
U_G = 20.0 cm/s

Test Conditions:
A = 0.99%
Open Vent Mode
Upper Horizontal Connector

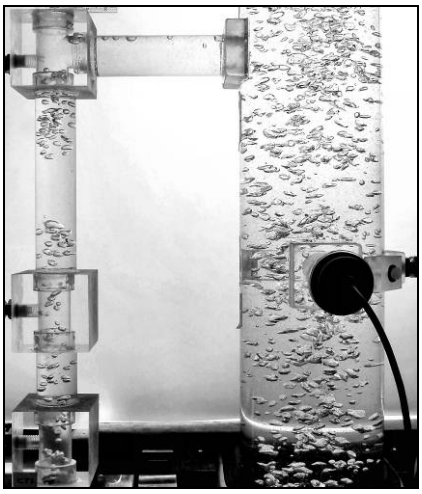
U_G = 0.5 cm/s

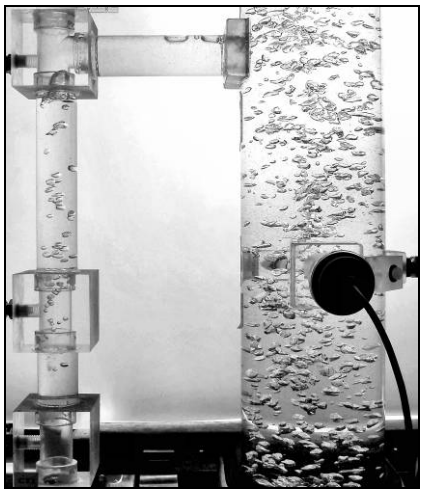
U_G = 0.5 cm/s

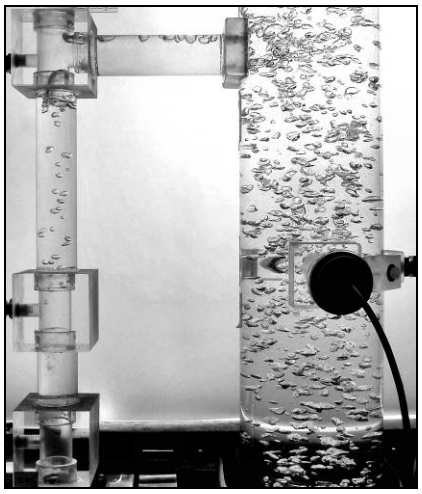
U_G = 0.5 cm/s

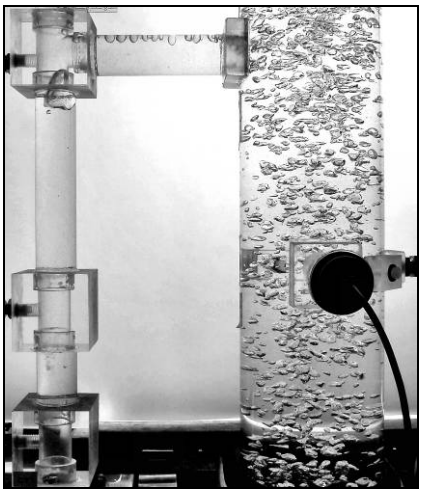
U_G = 1.0 cm/s

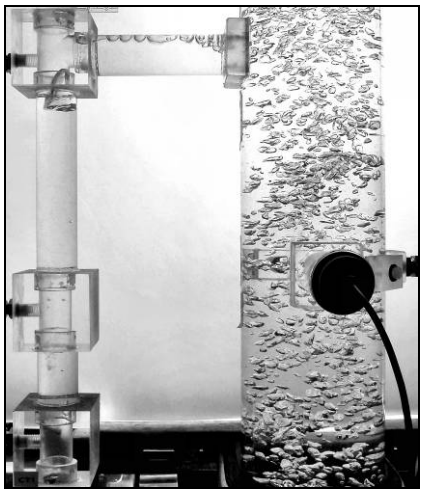
U_G = 1.0 cm/s

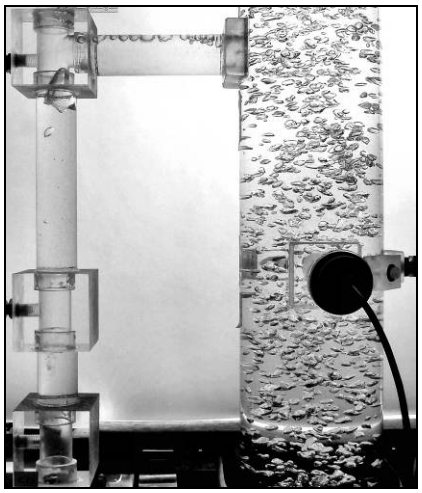
U_G = 1.0 cm/s

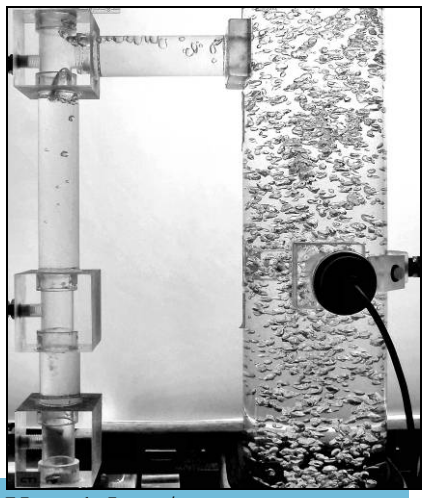
U_G = 1.5 cm/s

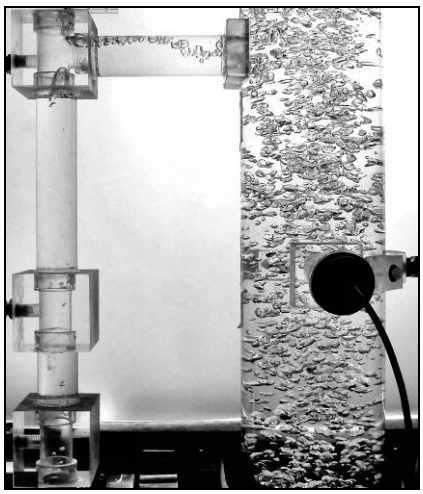
U_G = 1.5 cm/s

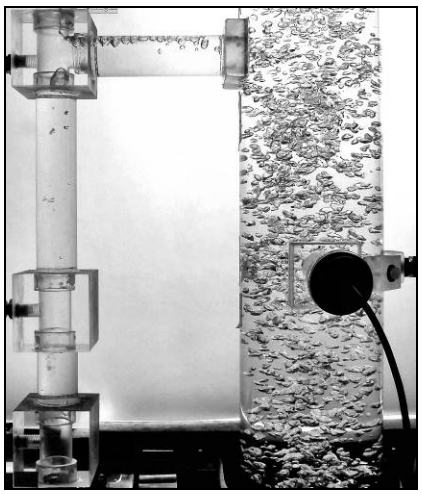
U_G = 1.5 cm/s

Test Conditions:
A = 0.99%
Open Vent Mode
Upper Horizontal Connector

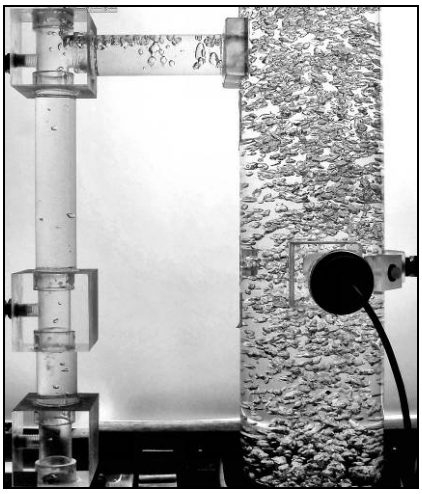
U_G = 2.0 cm/s

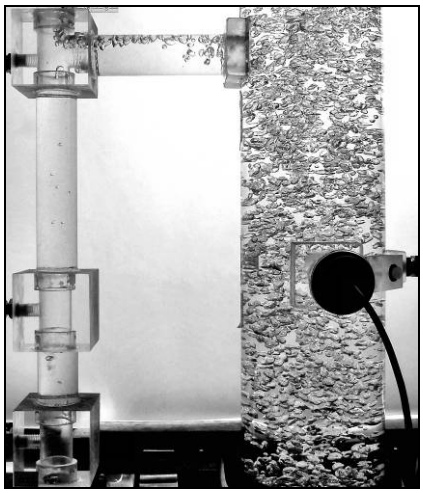
U_G = 2.0 cm/s

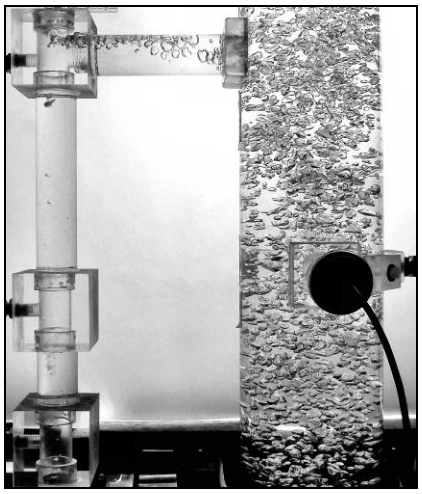
U_G = 2.0 cm/s

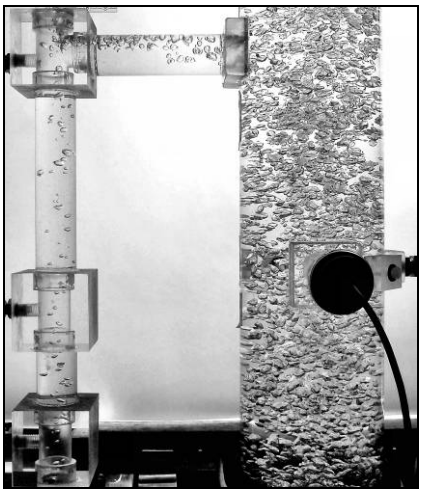
U_G = 2.5 cm/s

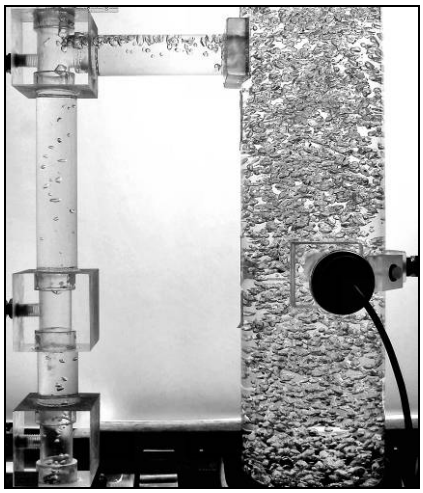
U_G = 2.5 cm/s

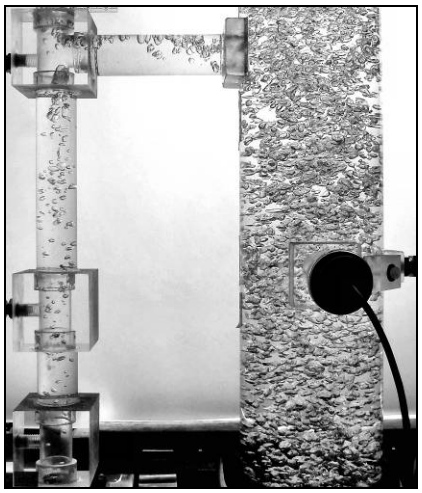
U_G = 2.5 cm/s

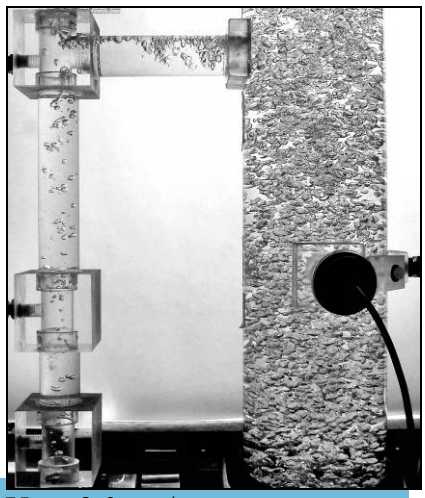
U_G = 3.0 cm/s

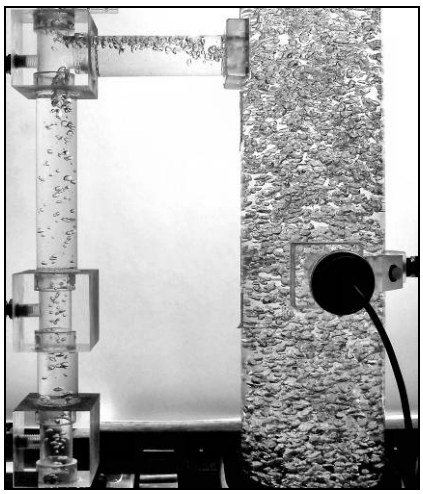
U_G = 3.0 cm/s

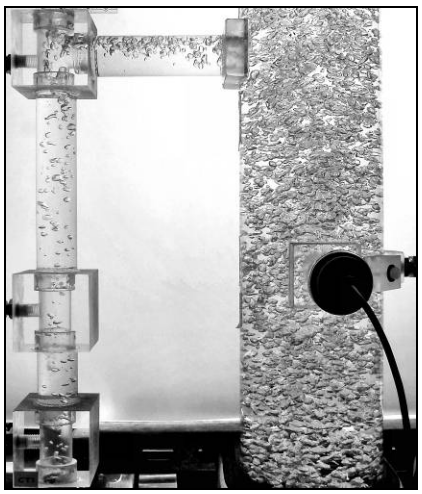
U_G = 3.0 cm/s

Test Conditions:
A = 0.99%
Open Vent Mode
Upper Horizontal Connector

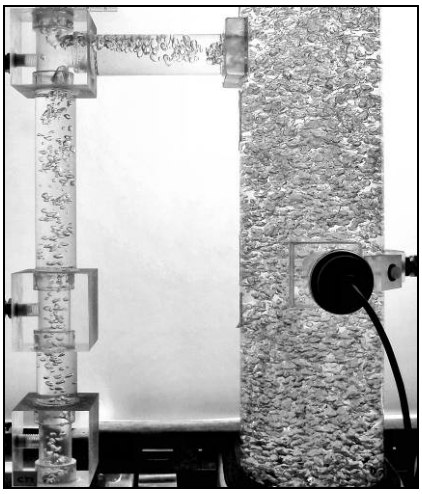
U_G = 3.5 cm/s

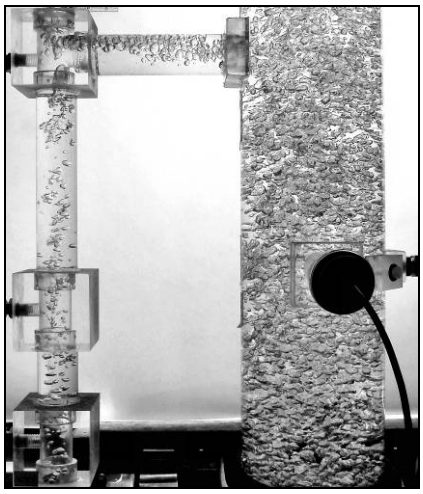
U_G = 3.5 cm/s

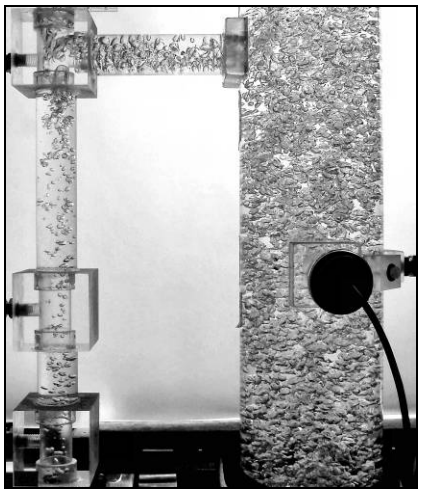
U_G = 3.5 cm/s

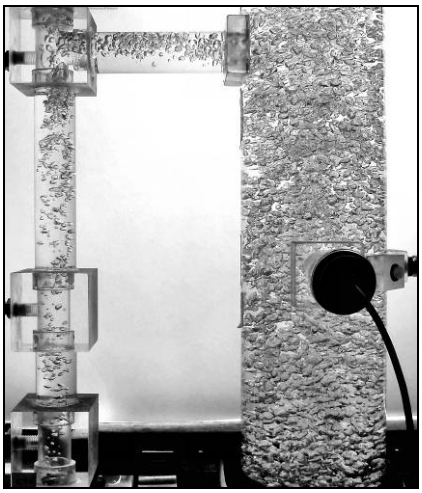
U_G = 4.0 cm/s

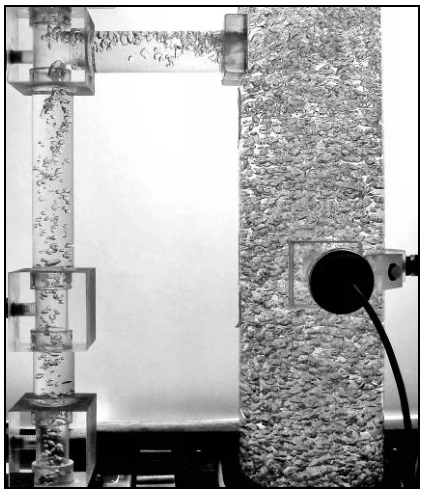
U_G = 4.0 cm/s

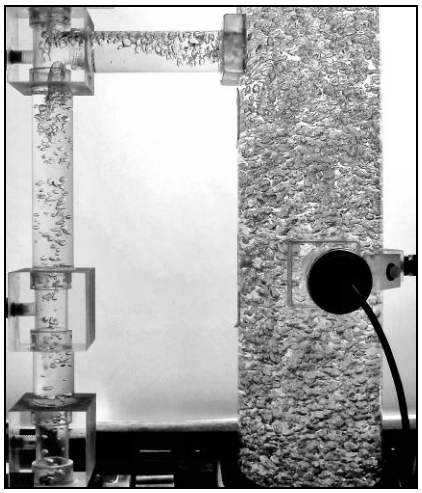
U_G = 4.0 cm/s

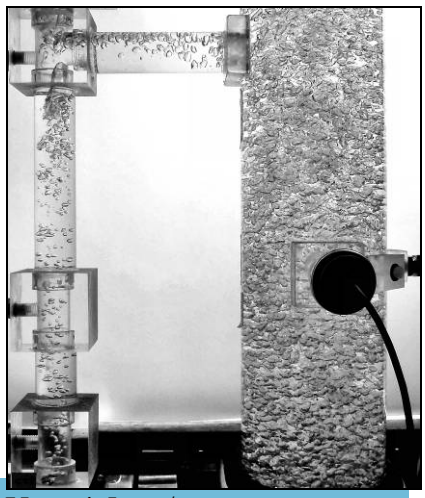
U_G = 4.5 cm/s

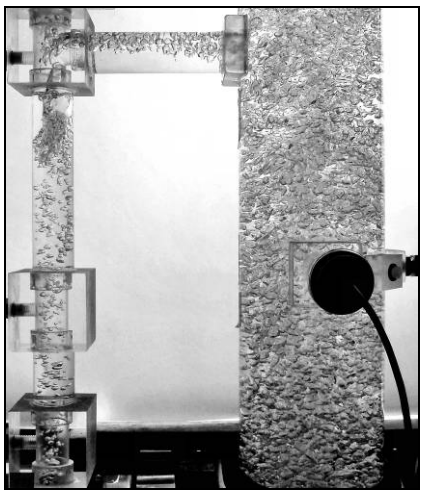
U_G = 4.5 cm/s

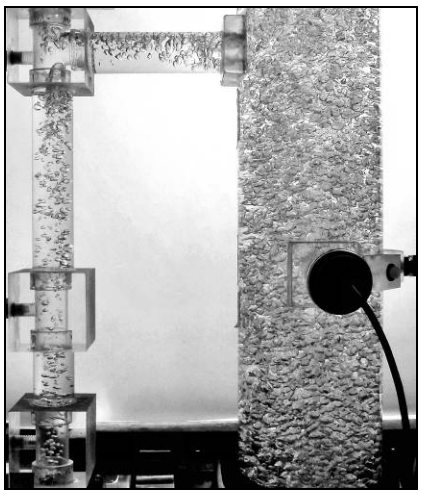
U_G = 4.5 cm/s

Test Conditions:
A = 0.99%
Open Vent Mode
Upper Horizontal Connector

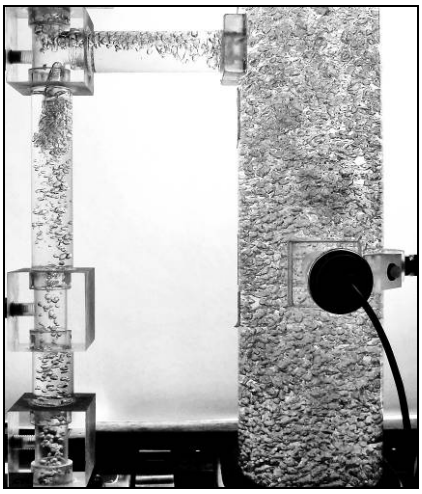
U_G = 5.0 cm/s

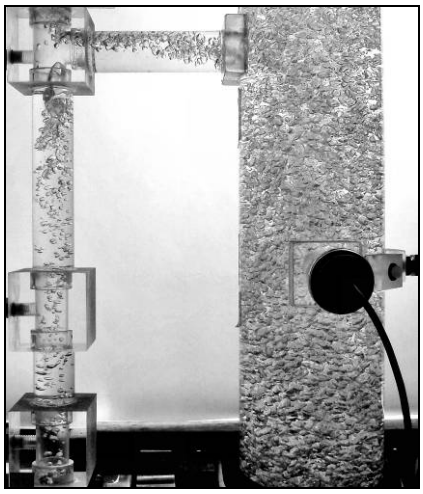
U_G = 5.0 cm/s

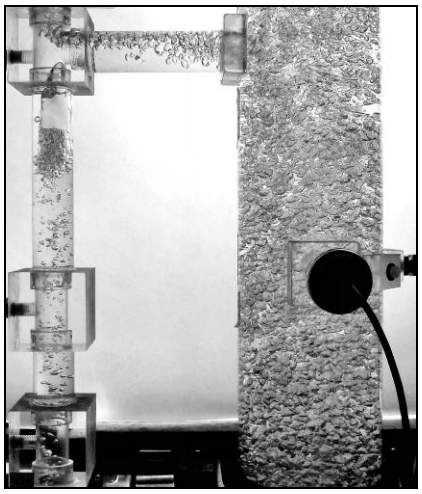
U_G = 5.0 cm/s

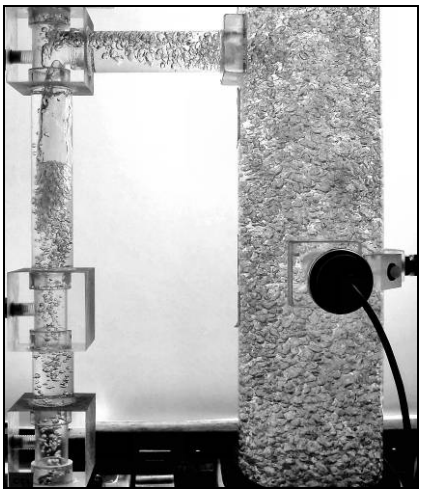
U_G = 6.0 cm/s

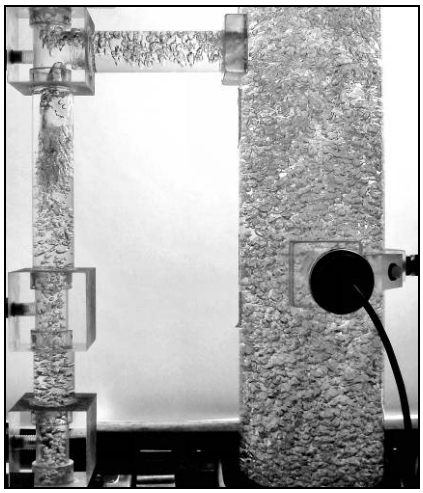
U_G = 6.0 cm/s

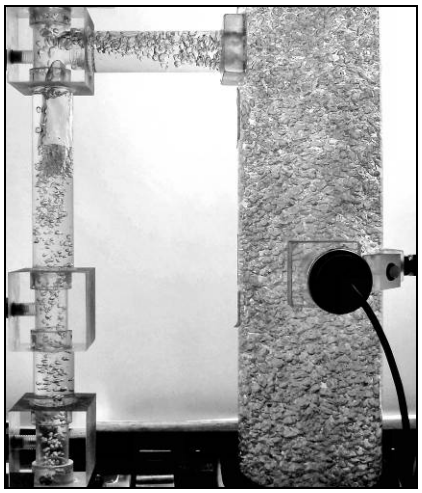
U_G = 6.0 cm/s

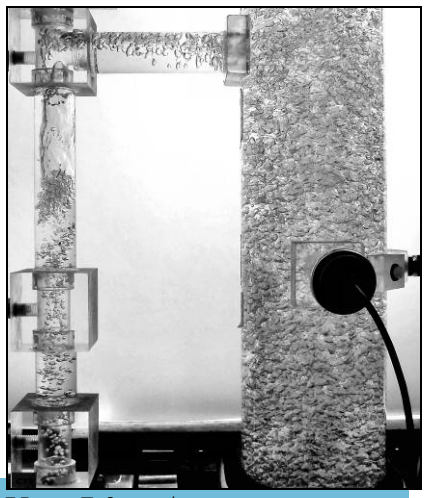
U_G = 7.0 cm/s

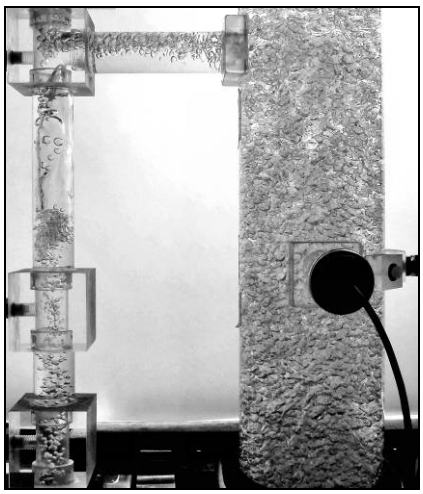
U_G = 7.0 cm/s

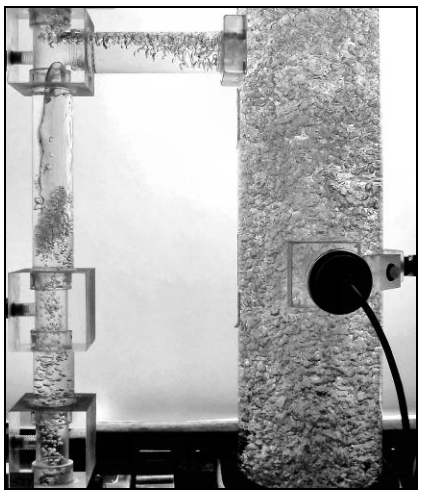
U_G = 7.0 cm/s

Test Conditions:
A = 0.99%
Open Vent Mode
Upper Horizontal Connector

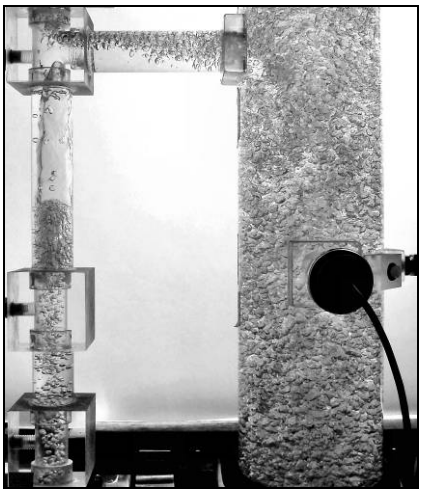
U_G = 8.0 cm/s

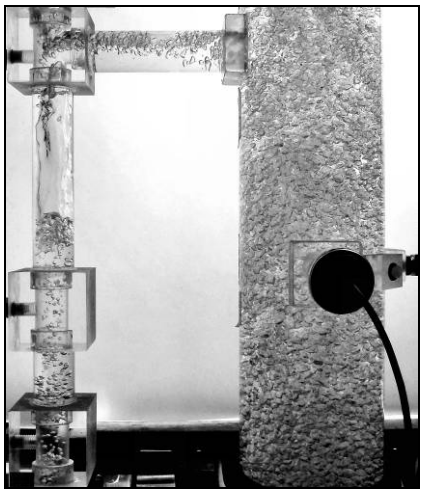
U_G = 8.0 cm/s

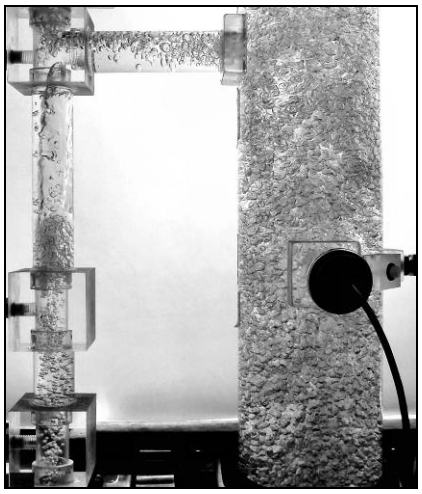
U_G = 8.0 cm/s

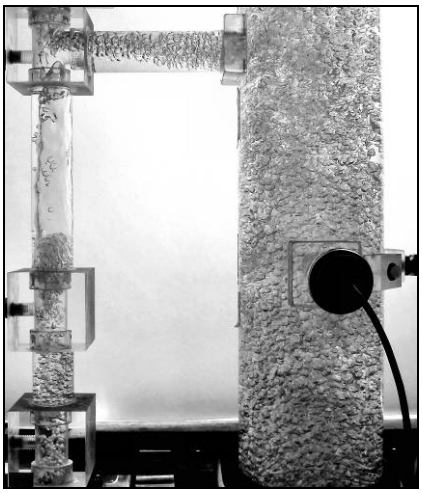
U_G = 9.0 cm/s

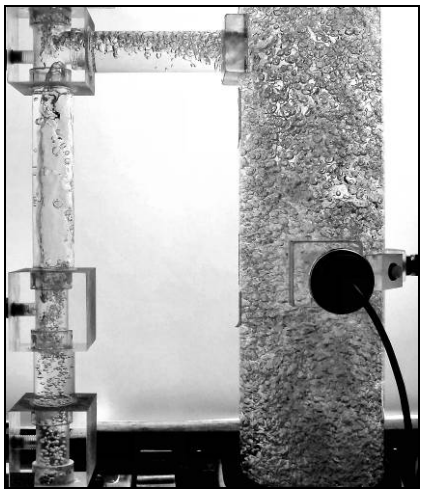
U_G = 9.0 cm/s

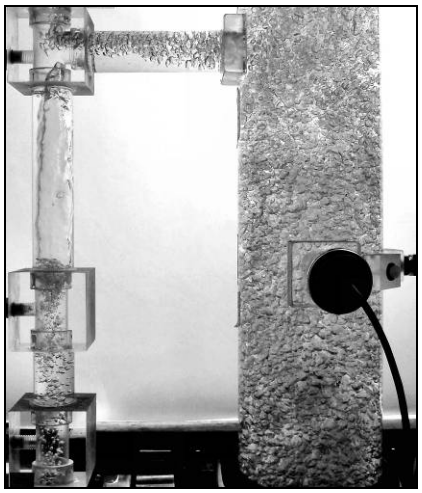
U_G = 9.0 cm/s

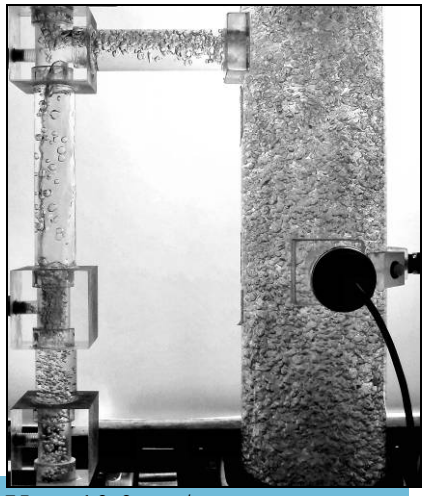
U_G = 10.0 cm/s

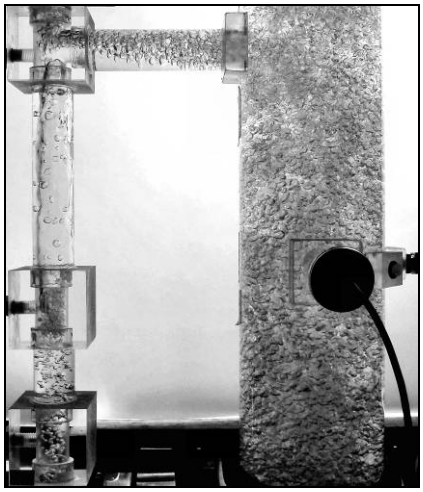
U_G = 10.0 cm/s

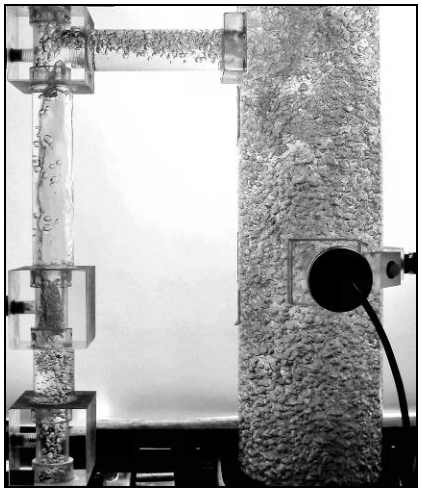
U_G = 10.0 cm/s

Test Conditions:
A = 0.99%
Open Vent Mode
Upper Horizontal Connector

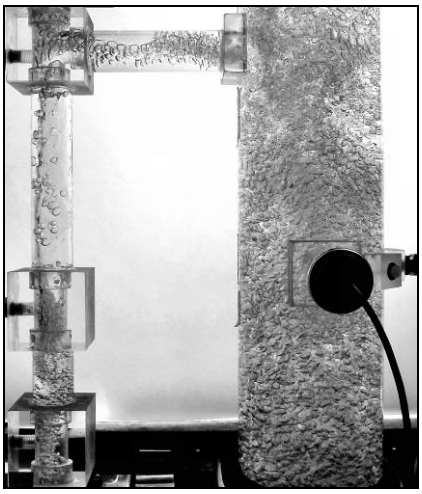
U_G = 11.0 cm/s

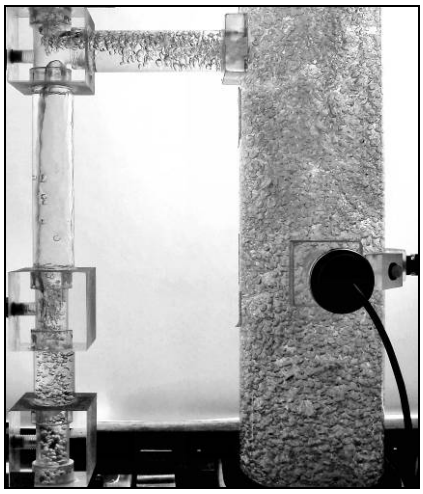
U_G = 11.0 cm/s

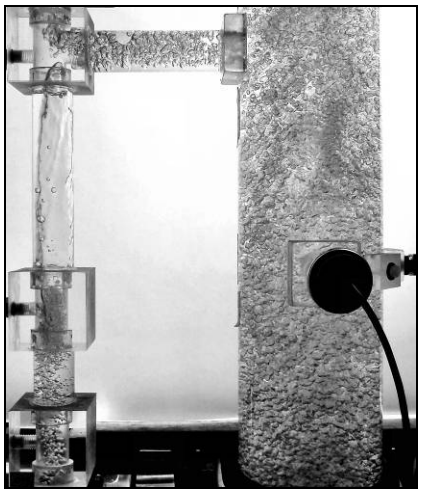
U_G = 11.0 cm/s

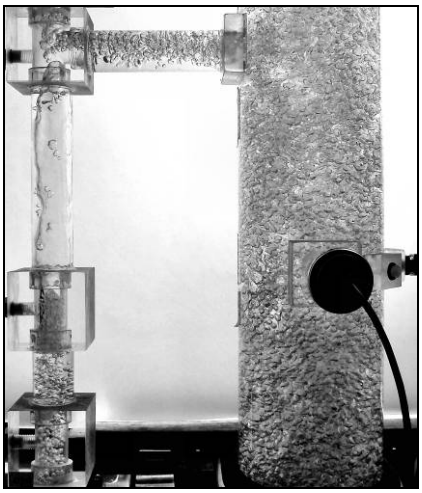
U_G = 12.0 cm/s

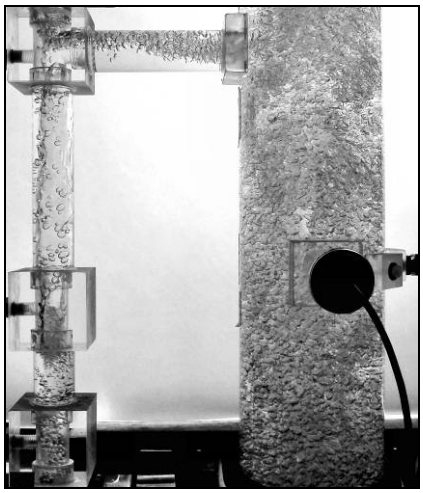
U_G = 12.0 cm/s

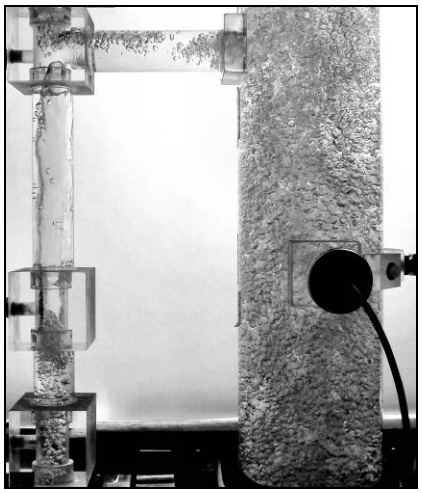
U_G = 12.0 cm/s

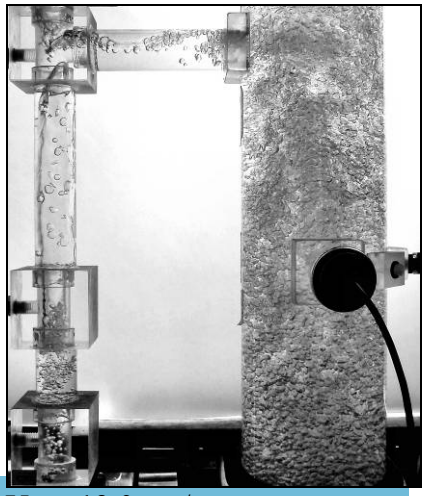
U_G = 13.0 cm/s

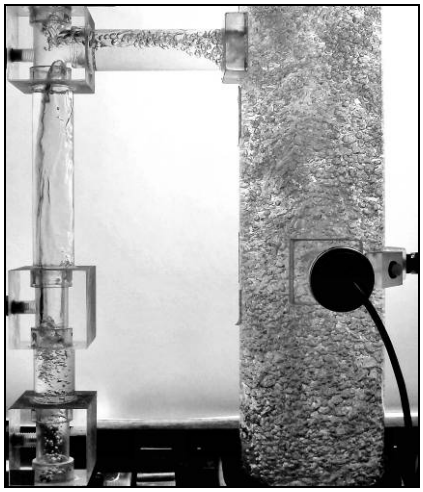
U_G = 13.0 cm/s

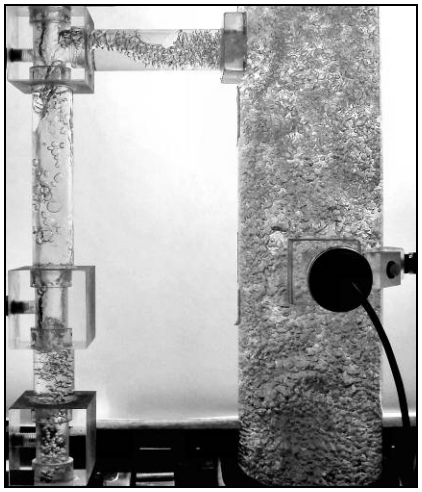
U_G = 13.0 cm/s

Test Conditions:
A = 0.99%
Open Vent Mode
Upper Horizontal Connector

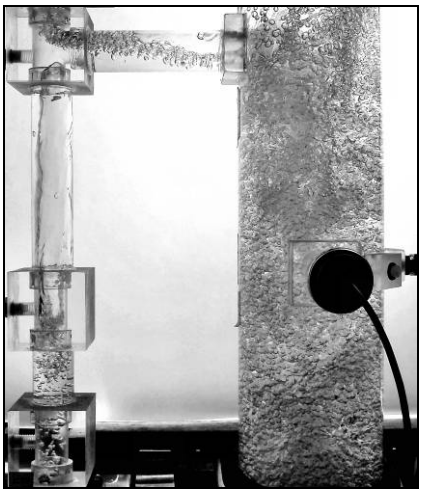
U_G = 14.0 cm/s

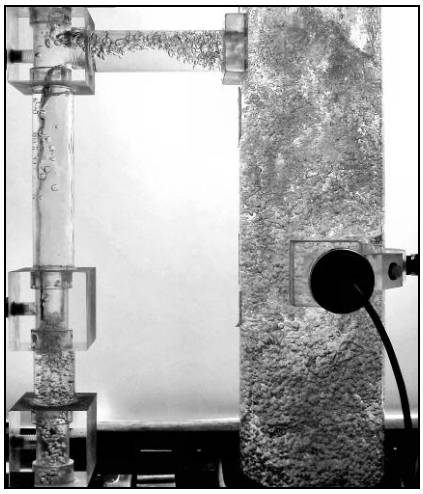
U_G = 14.0 cm/s

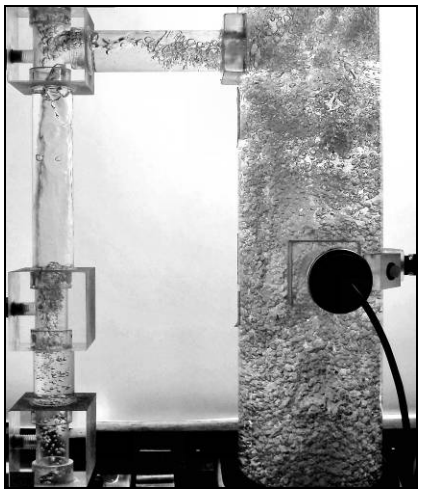
U_G = 14.0 cm/s

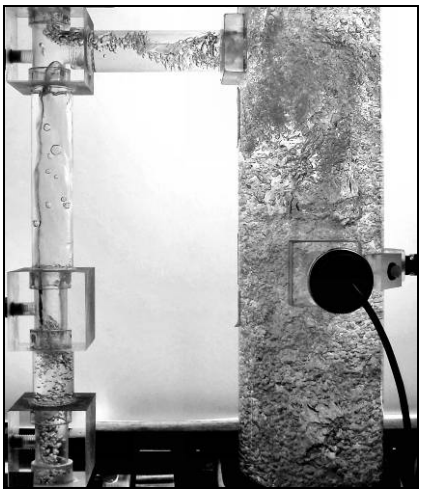
U_G = 15.0 cm/s

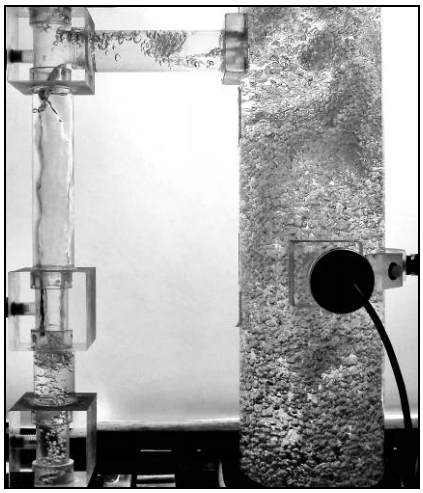
U_G = 15.0 cm/s

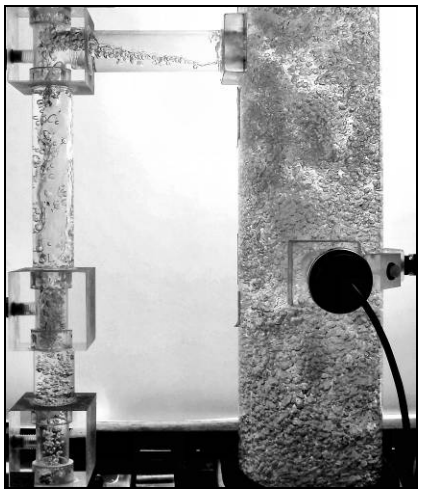
U_G = 15.0 cm/s

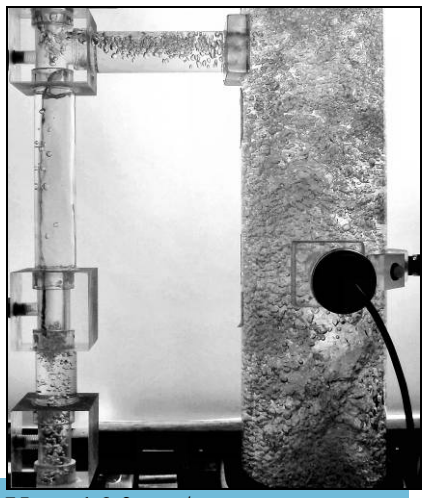
U_G = 16.0 cm/s

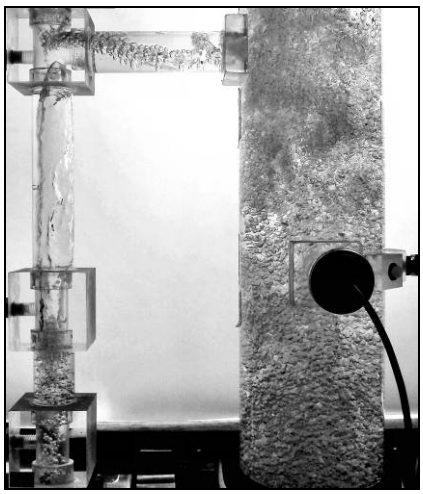
U_G = 16.0 cm/s

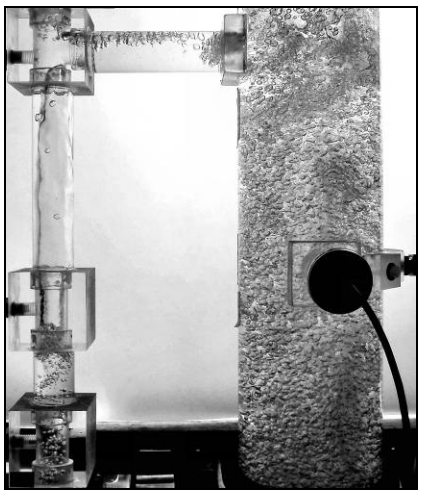
U_G = 16.0 cm/s

Test Conditions:
A = 0.99%
Open Vent Mode
Upper Horizontal Connector

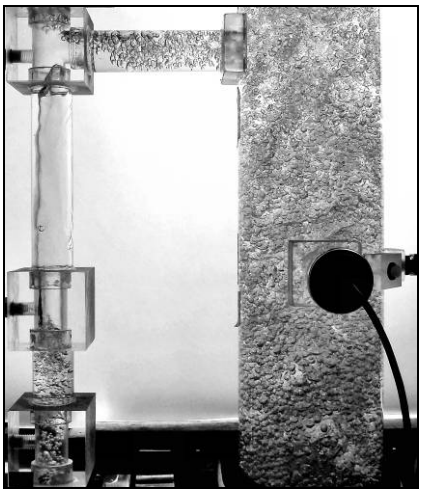
U_G = 17.0 cm/s

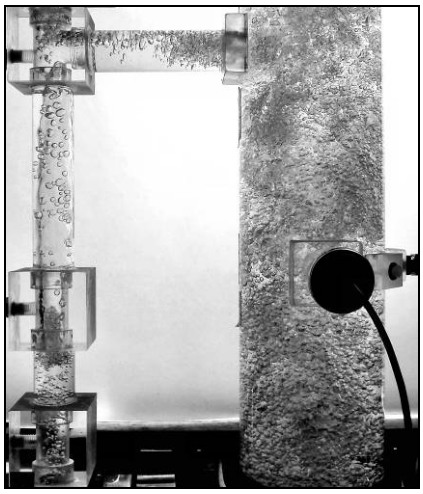
U_G = 17.0 cm/s

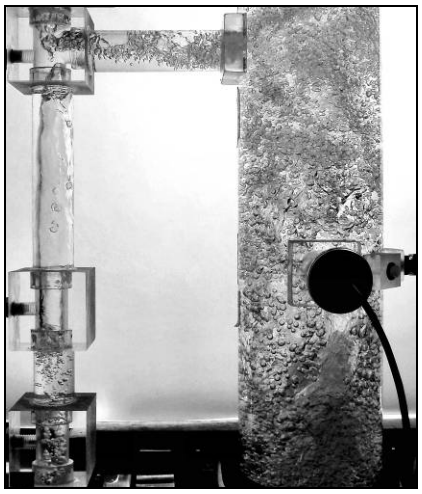
U_G = 17.0 cm/s

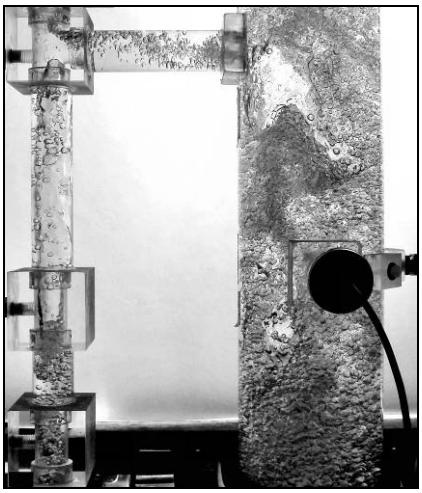
U_G = 18.0 cm/s

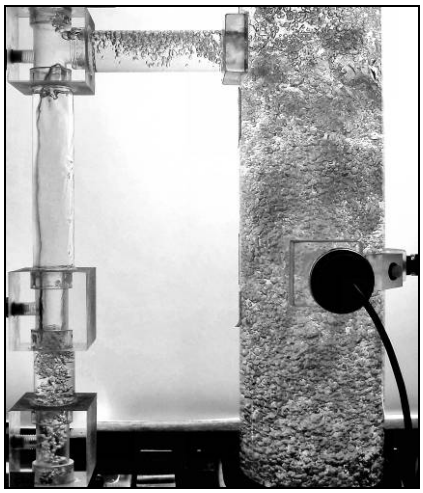
U_G = 18.0 cm/s

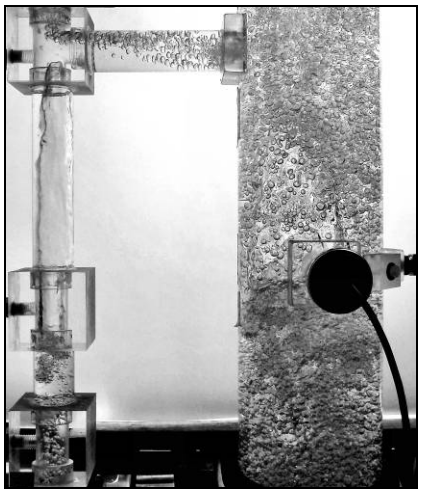
U_G = 18.0 cm/s

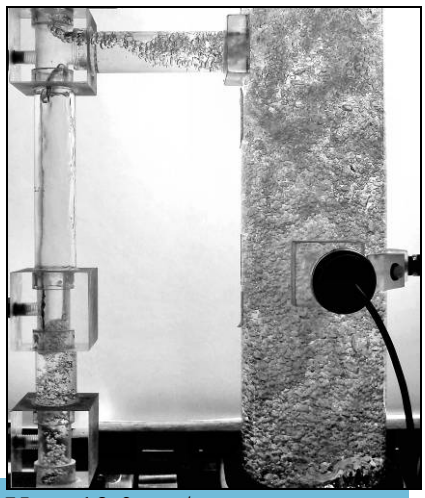
U_G = 19.0 cm/s

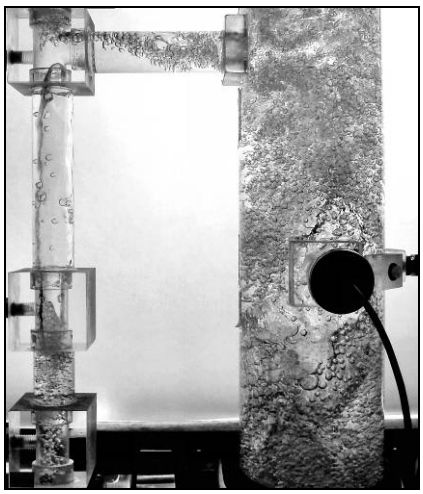
U_G = 19.0 cm/s

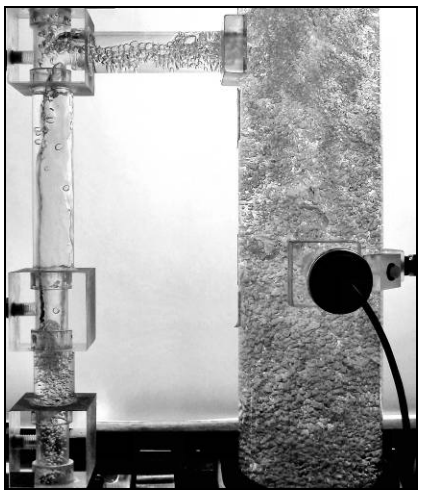
U_G = 19.0 cm/s

Test Conditions:
A = 0.99%
Open Vent Mode
Upper Horizontal Connector

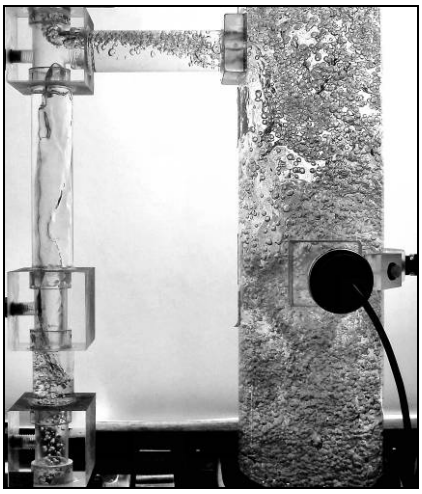
U_G = 20.0 cm/s

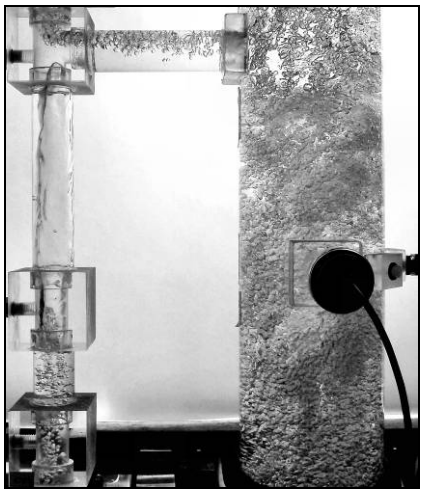
U_G = 20.0 cm/s

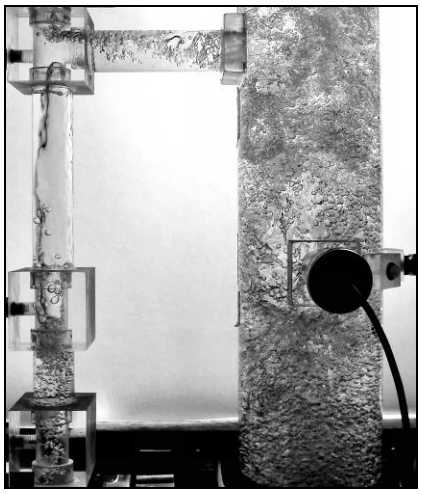
U_G = 20.0 cm/s

Test Conditions:
A = 0.99%
Closed Vent Mode
Upper Horizontal Connector

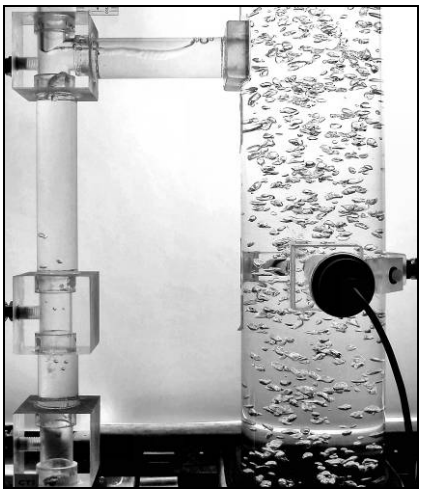
U_G = 0.5 cm/s

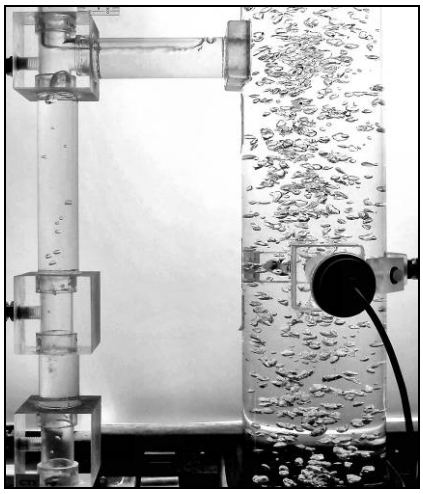
U_G = 0.5 cm/s

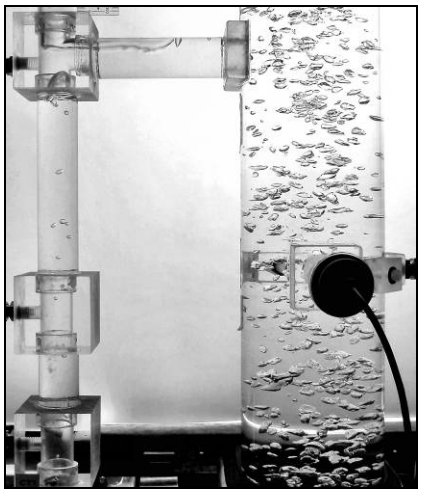
U_G = 0.5 cm/s

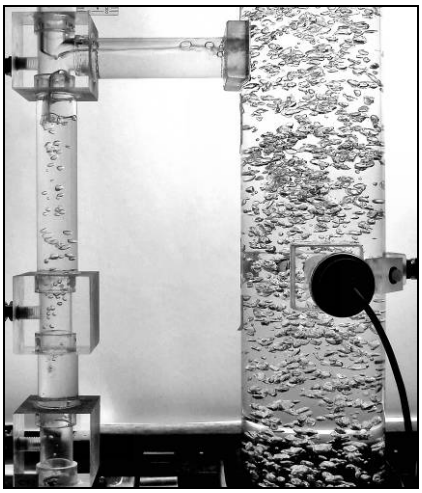
U_G = 1.0 cm/s

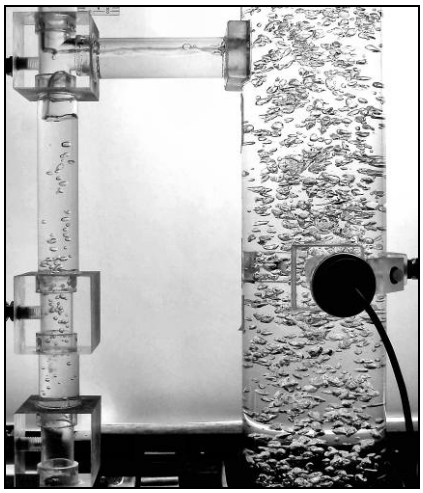
U_G = 1.0 cm/s

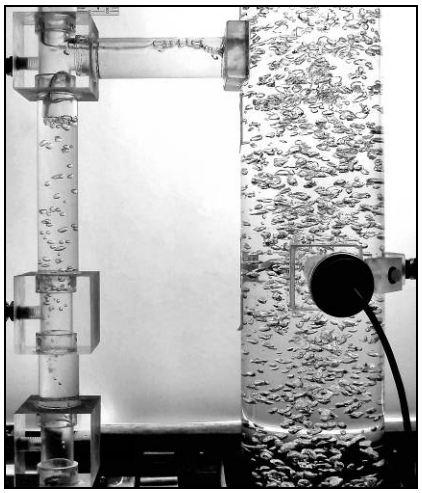
U_G = 1.0 cm/s

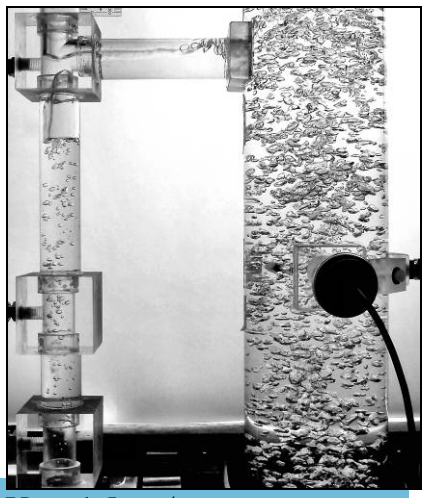
U_G = 1.5 cm/s

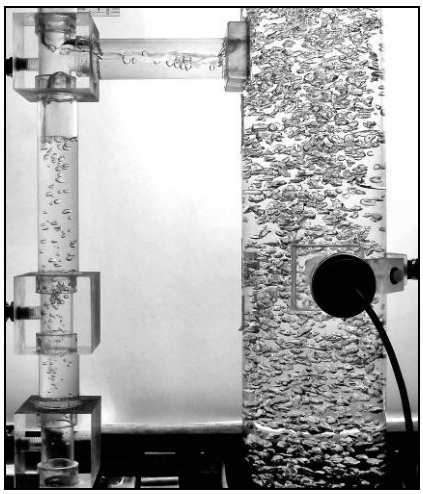
U_G = 1.5 cm/s

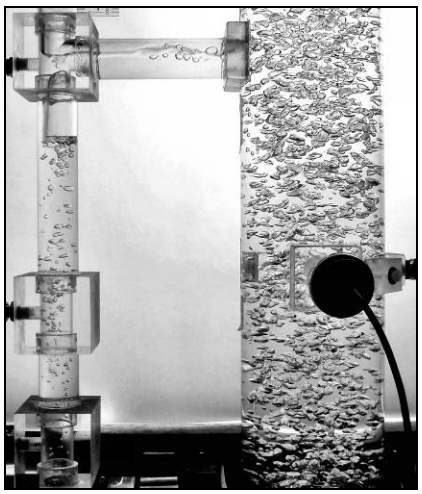
U_G = 1.5 cm/s

Test Conditions:
A = 0.99%
Closed Vent Mode
Upper Horizontal Connector

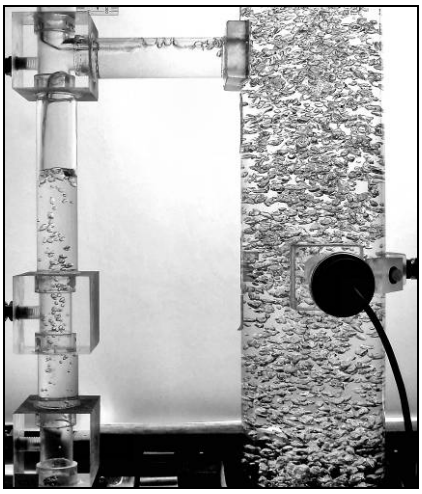
U_G = 2.0 cm/s

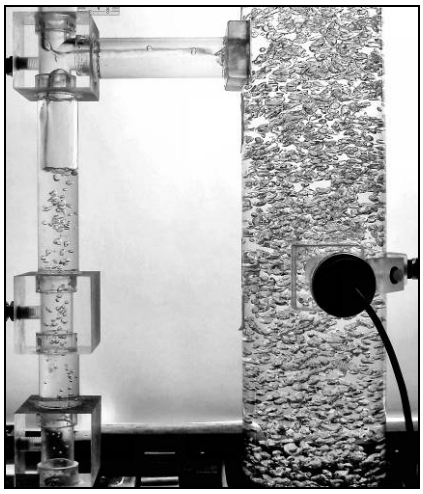
U_G = 2.0 cm/s

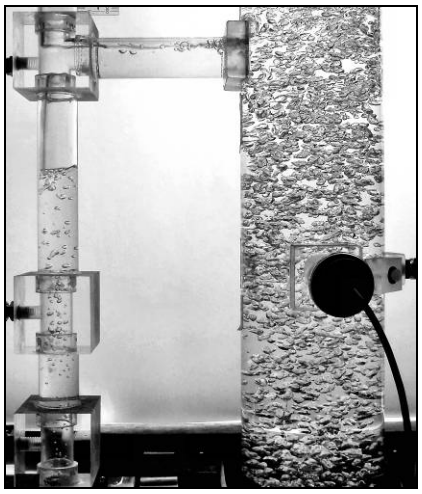
U_G = 2.0 cm/s

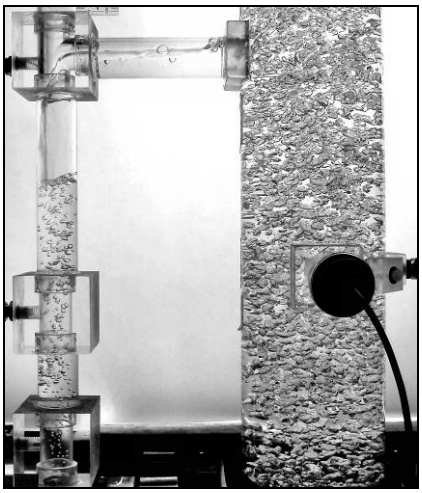
U_G = 2.5 cm/s

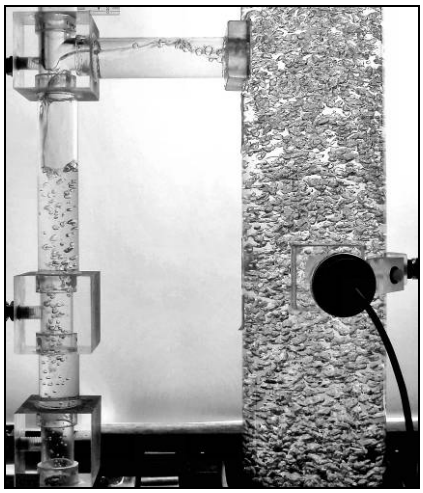
U_G = 2.5 cm/s

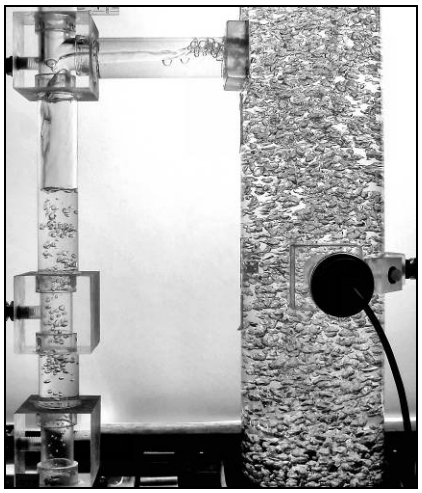
U_G = 2.5 cm/s

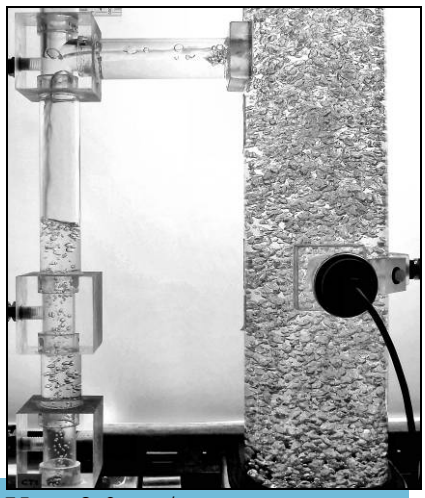
U_G = 3.0 cm/s

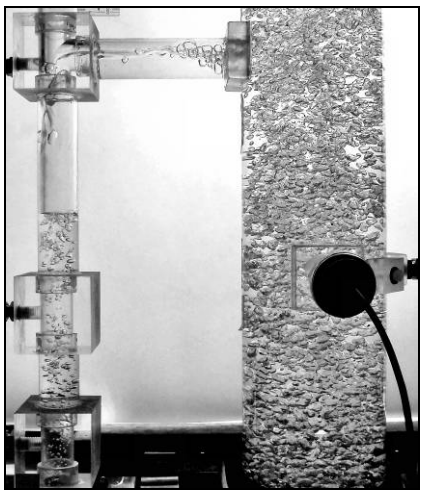
U_G = 3.0 cm/s

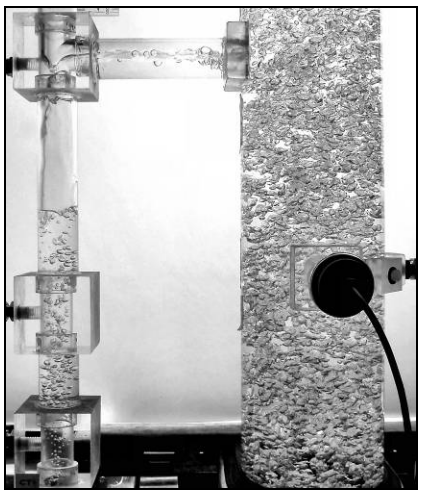
U_G = 3.0 cm/s

Test Conditions:
A = 0.99%
Closed Vent Mode
Upper Horizontal Connector

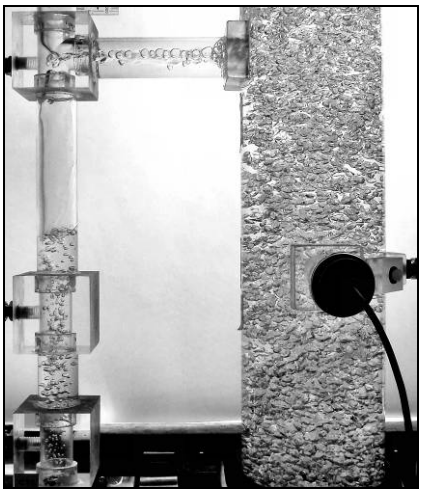
U_G = 3.5 cm/s

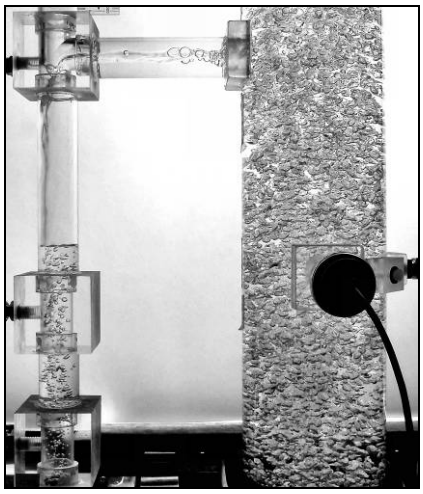
U_G = 3.5 cm/s

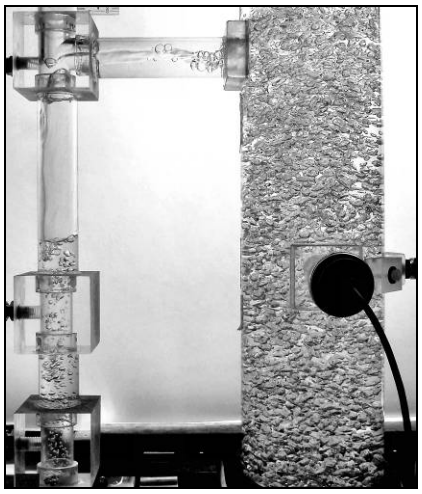
U_G = 3.5 cm/s

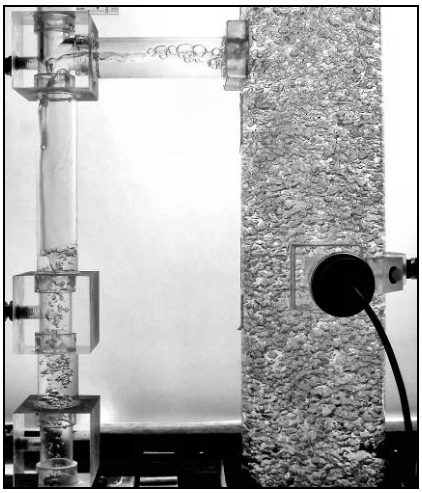
U_G = 4.0 cm/s

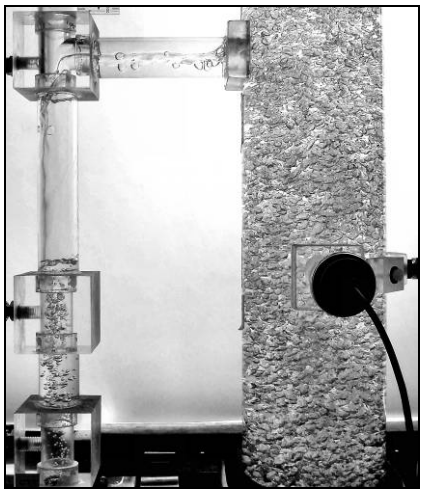
U_G = 4.0 cm/s

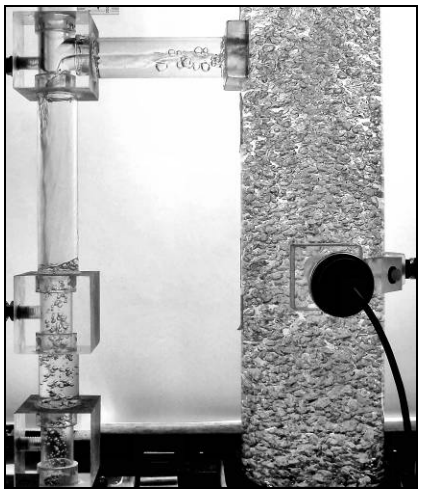
U_G = 4.0 cm/s

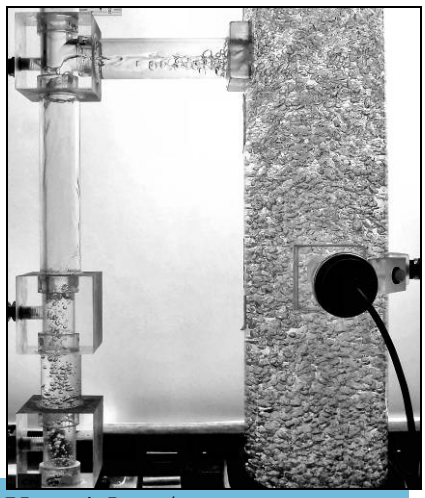
U_G = 4.5 cm/s

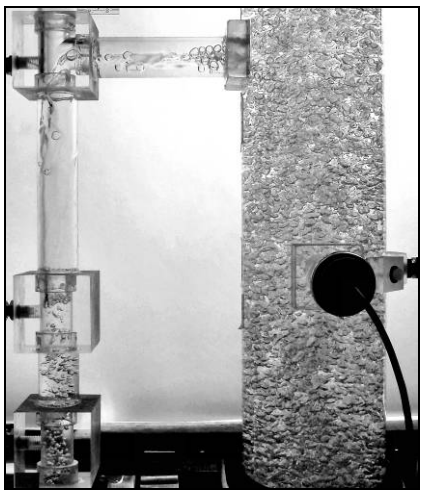
U_G = 4.5 cm/s

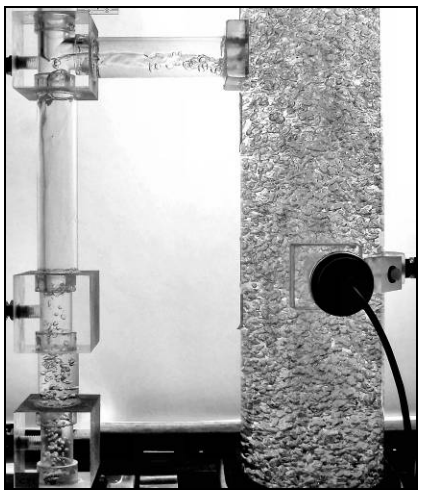
U_G = 4.5 cm/s

Test Conditions:
A = 0.99%
Closed Vent Mode
Upper Horizontal Connector

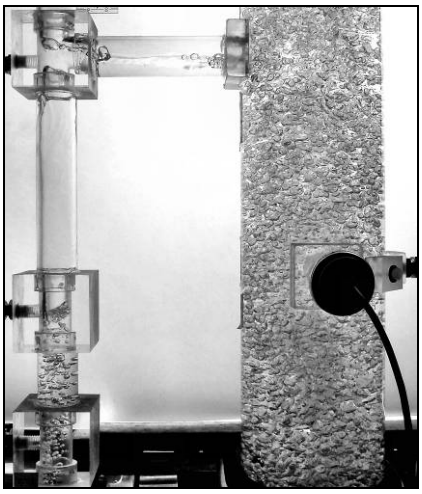
U_G = 5.0 cm/s

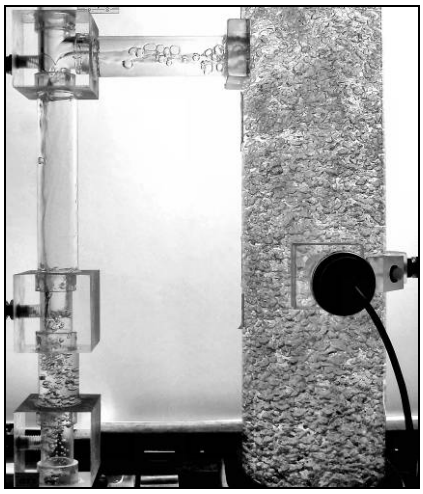
U_G = 5.0 cm/s

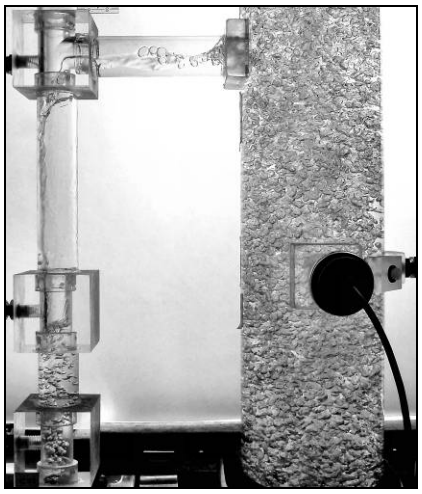
U_G = 5.0 cm/s

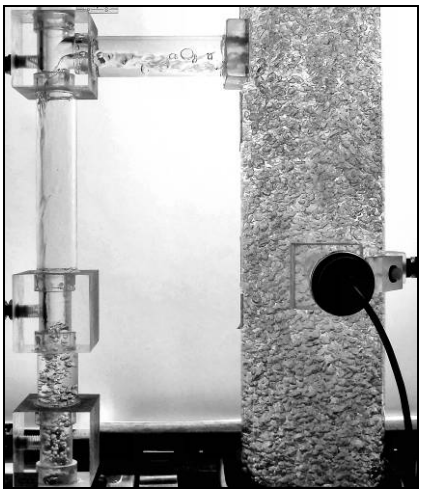
U_G = 6.0 cm/s

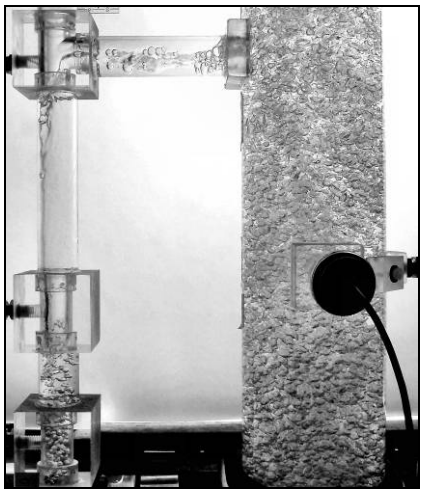
U_G = 6.0 cm/s

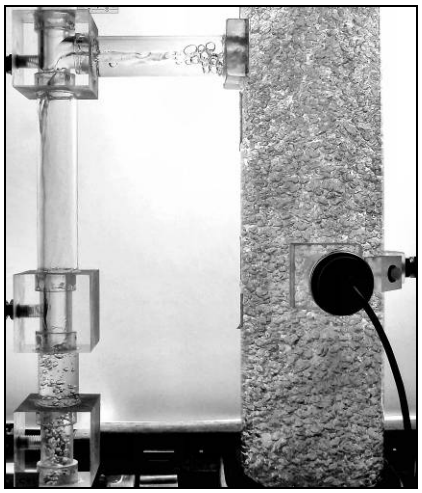
U_G = 6.0 cm/s

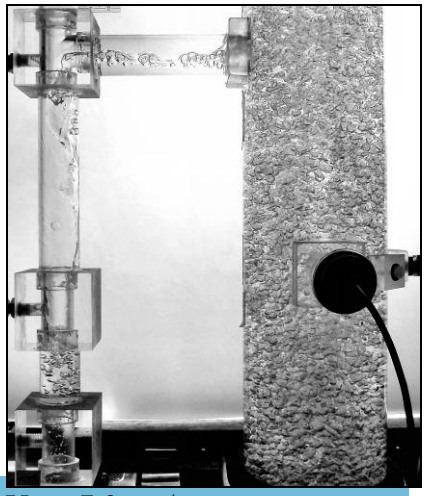
U_G = 7.0 cm/s

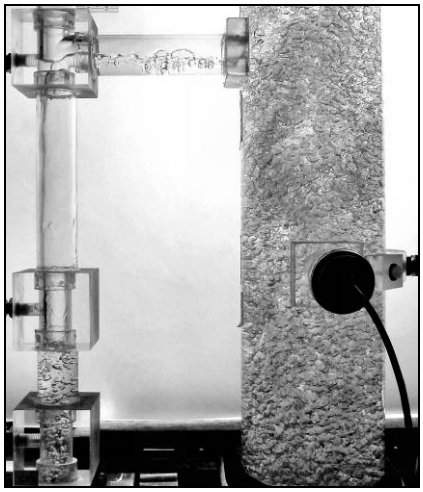
U_G = 7.0 cm/s

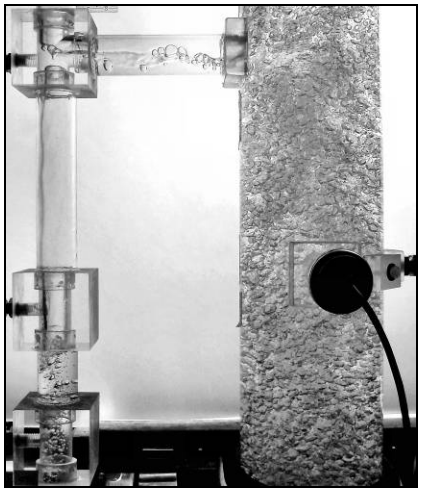
U_G = 7.0 cm/s

Test Conditions:
A = 0.99%
Closed Vent Mode
Upper Horizontal Connector

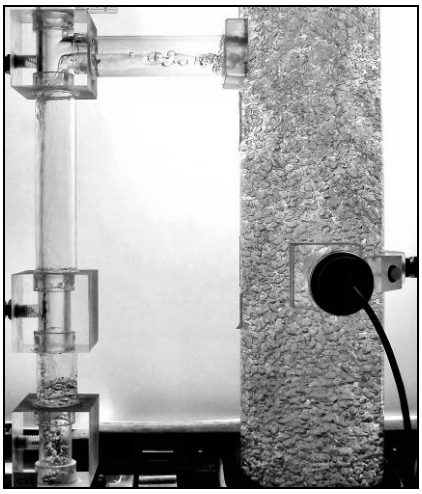
U_G = 8.0 cm/s

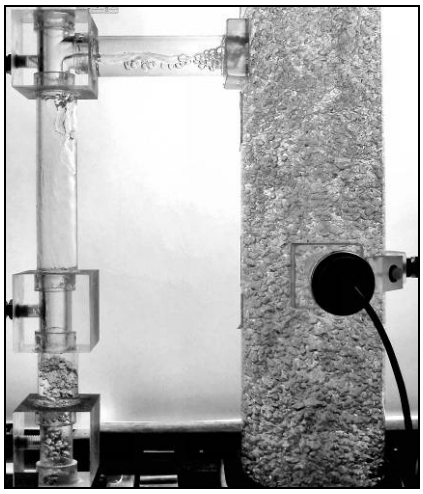
U_G = 8.0 cm/s

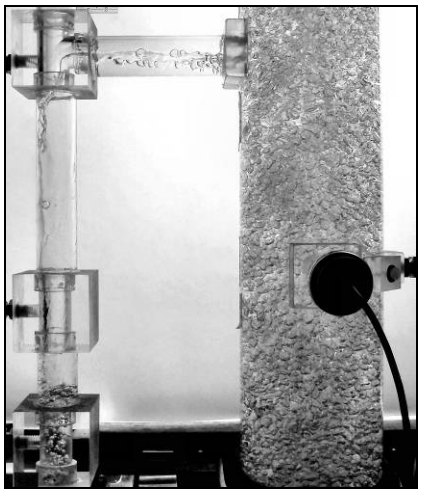
U_G = 8.0 cm/s

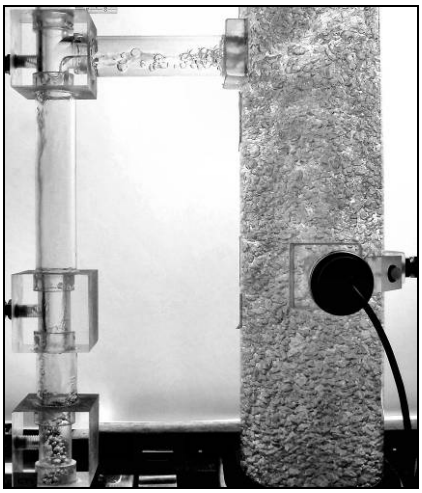
U_G = 9.0 cm/s

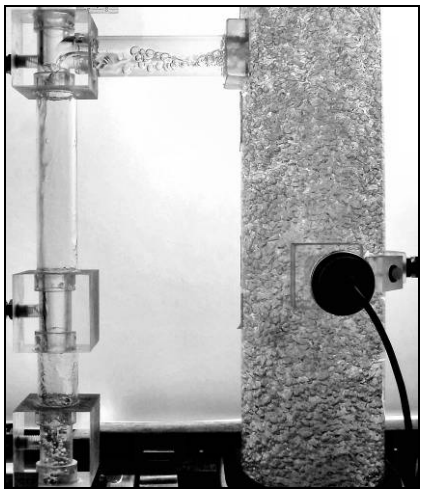
U_G = 9.0 cm/s

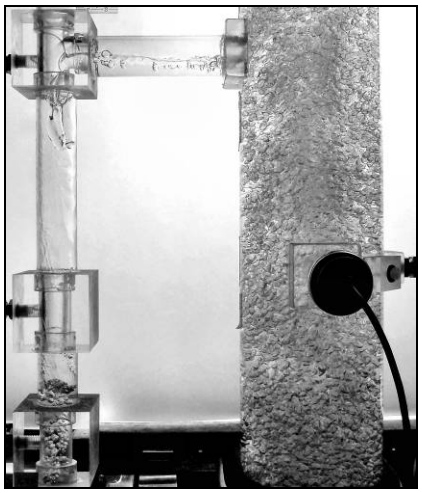
U_G = 9.0 cm/s

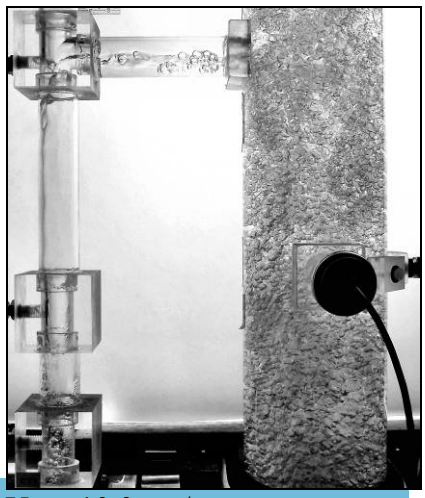
U_G = 10.0 cm/s

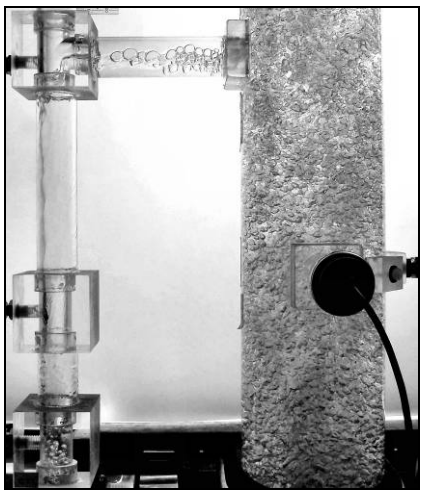
U_G = 10.0 cm/s

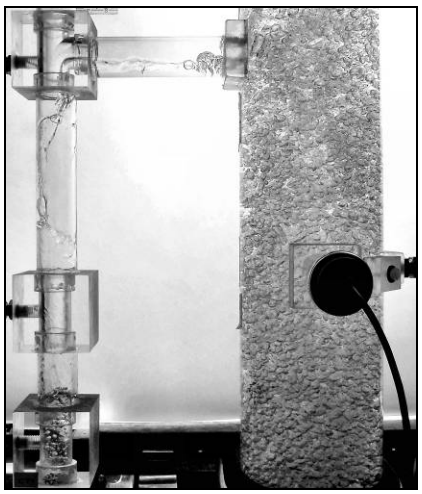
U_G = 10.0 cm/s

Test Conditions:
A = 0.99%
Closed Vent Mode
Upper Horizontal Connector

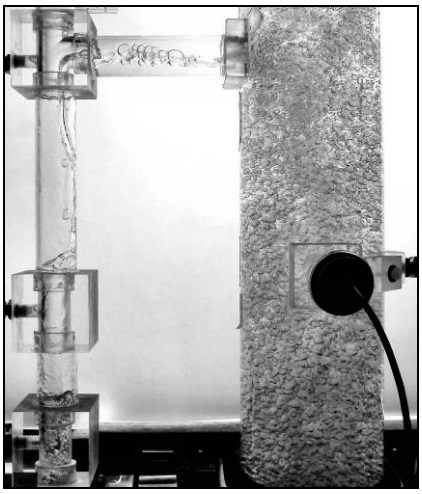
U_G = 11.0 cm/s

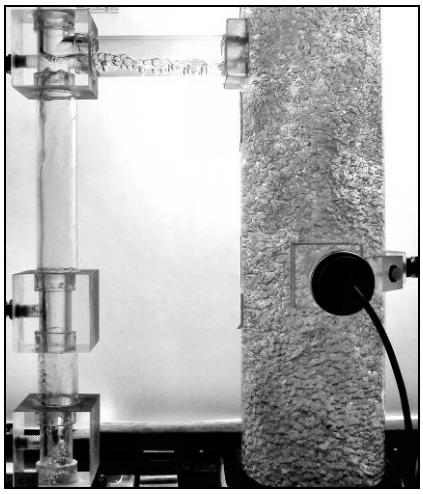
U_G = 11.0 cm/s

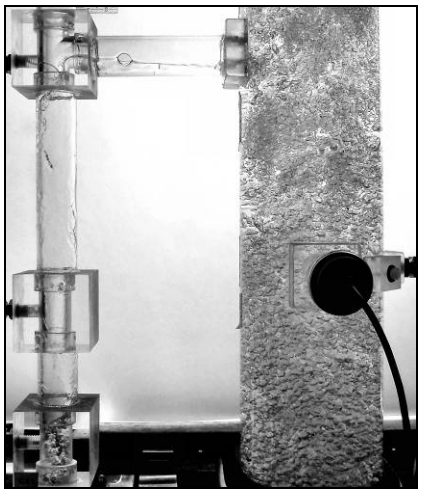
U_G = 11.0 cm/s

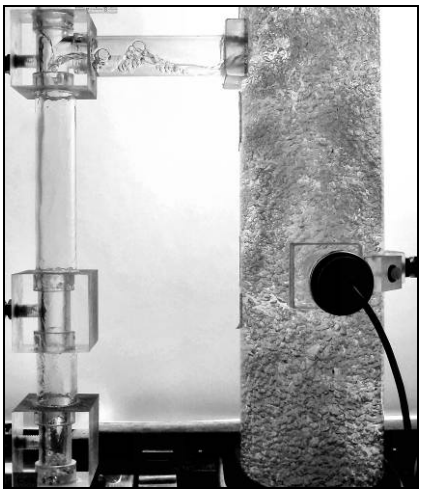
U_G = 12.0 cm/s

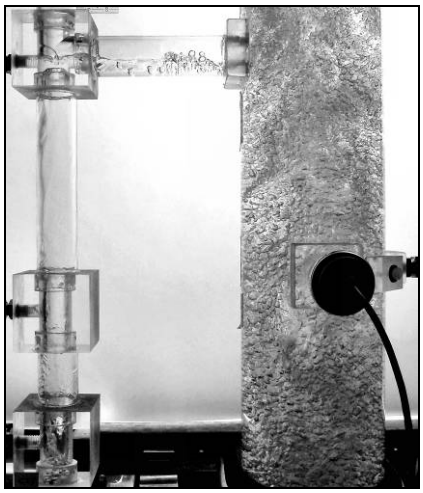
U_G = 12.0 cm/s

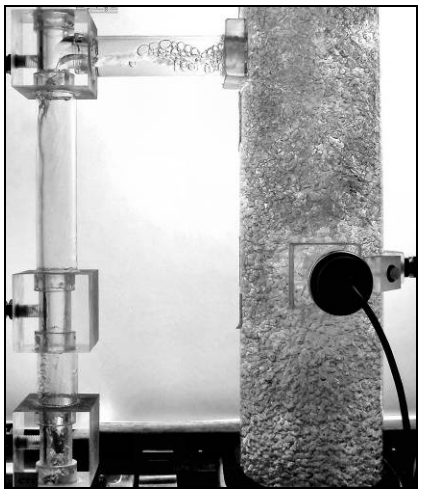
U_G = 12.0 cm/s

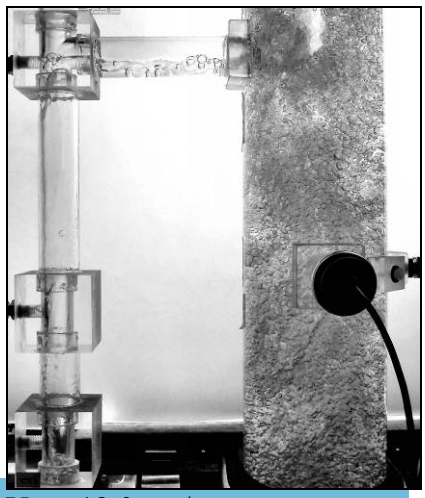
U_G = 13.0 cm/s

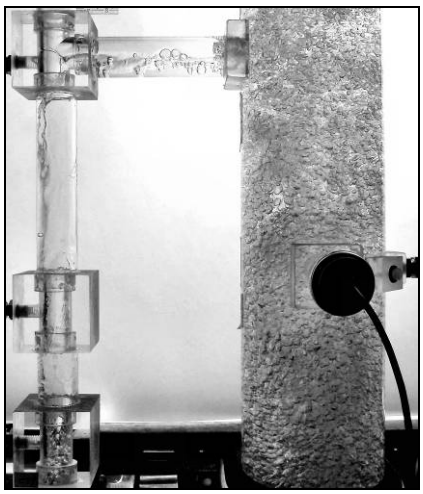
U_G = 13.0 cm/s

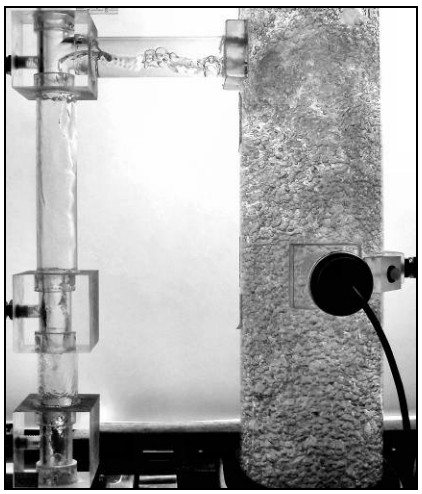
U_G = 13.0 cm/s

Test Conditions:
A = 0.99%
Closed Vent Mode
Upper Horizontal Connector

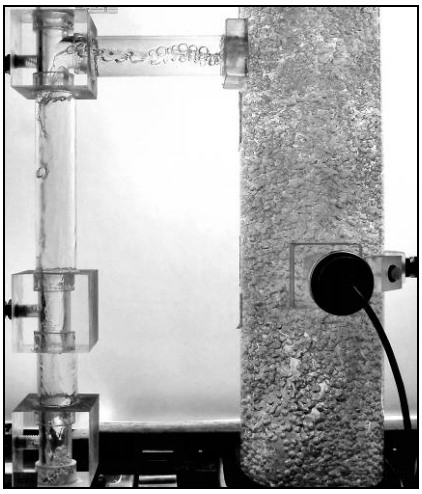
U_G = 14.0 cm/s

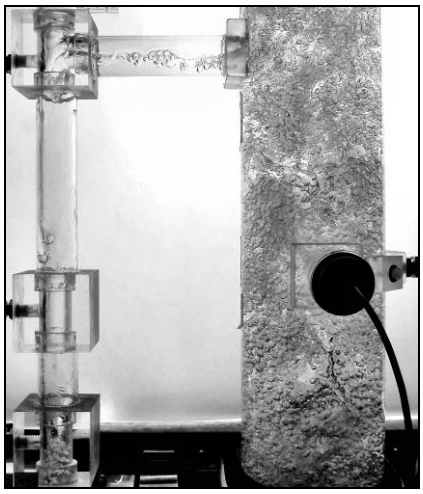
U_G = 14.0 cm/s

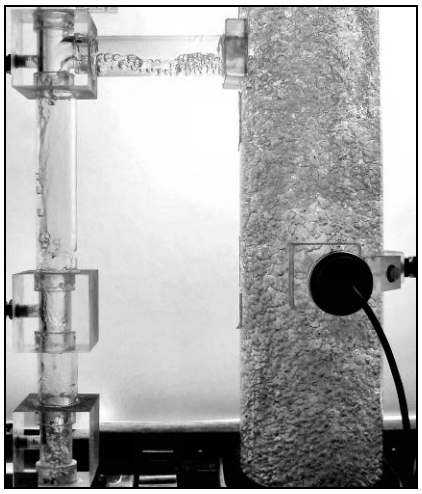
U_G = 14.0 cm/s

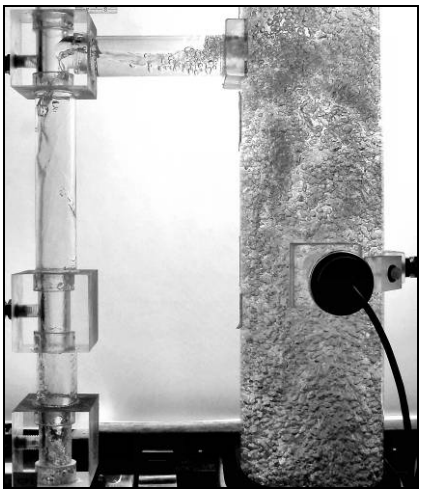
U_G = 15.0 cm/s

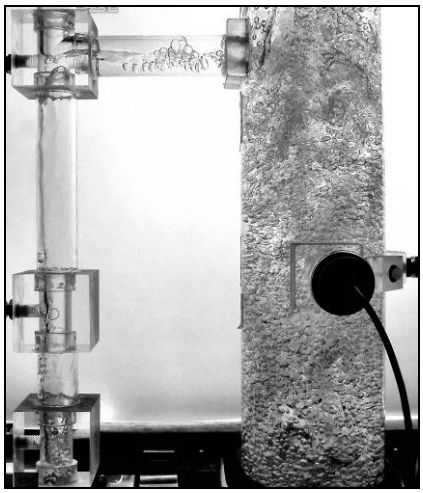
U_G = 15.0 cm/s

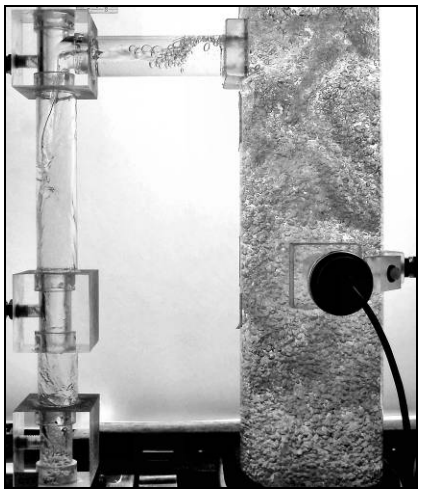
U_G = 15.0 cm/s

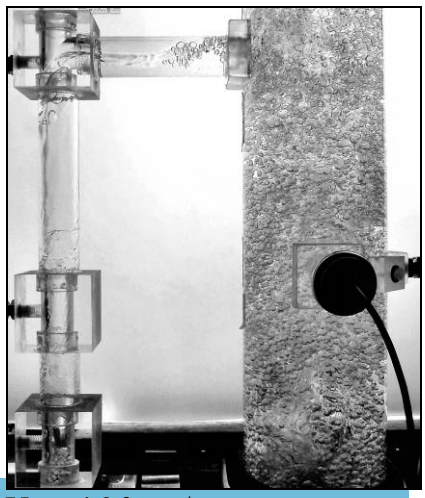
U_G = 16.0 cm/s

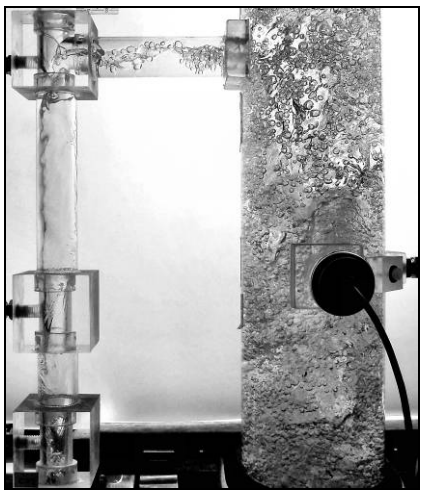
U_G = 16.0 cm/s

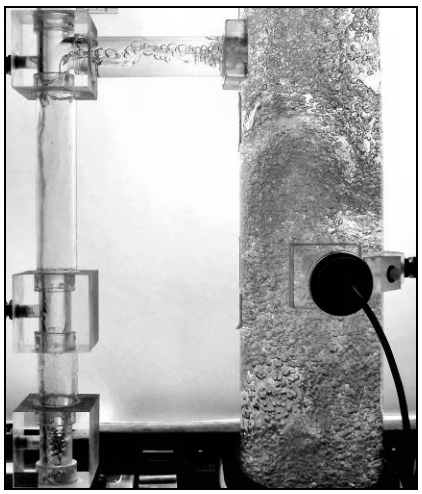
U_G = 16.0 cm/s

Test Conditions:
A = 0.99%
Closed Vent Mode
Upper Horizontal Connector

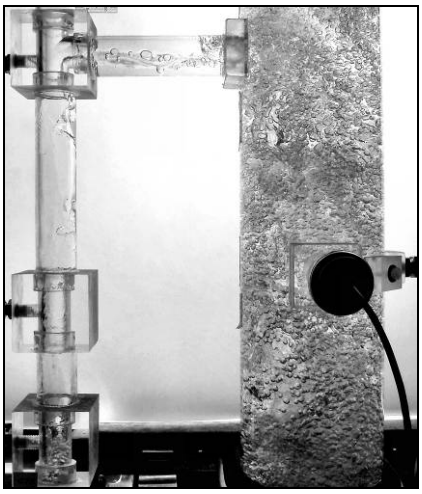
U_G = 17.0 cm/s

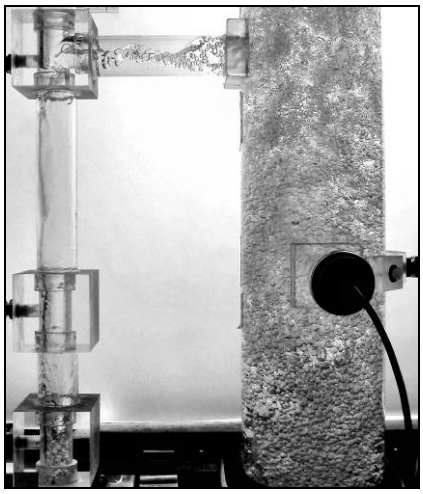
U_G = 17.0 cm/s

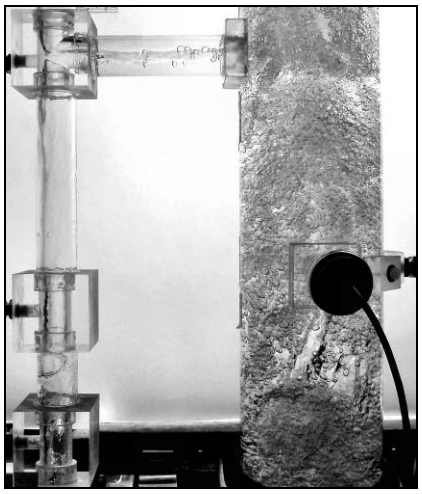
U_G = 17.0 cm/s

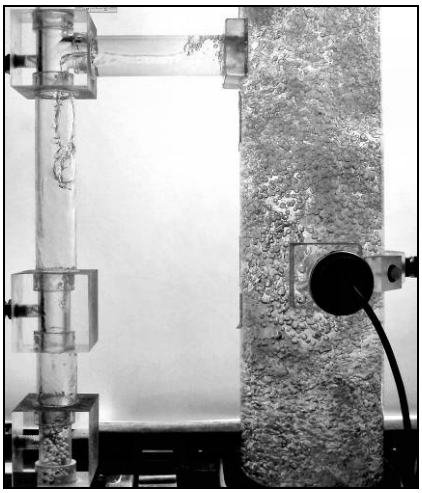
U_G = 18.0 cm/s

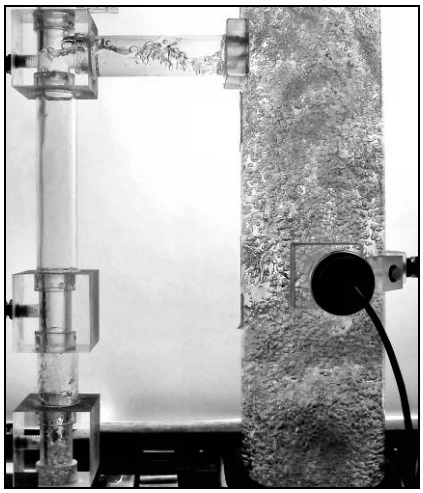
U_G = 18.0 cm/s

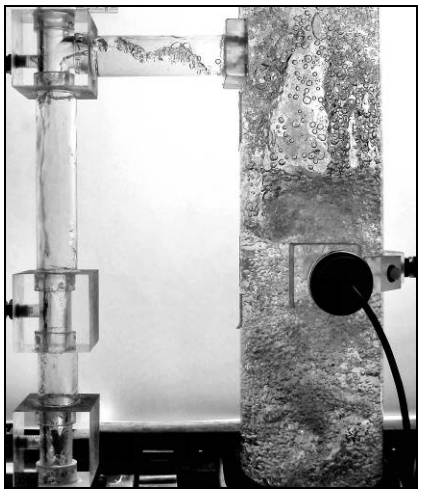
U_G = 18.0 cm/s

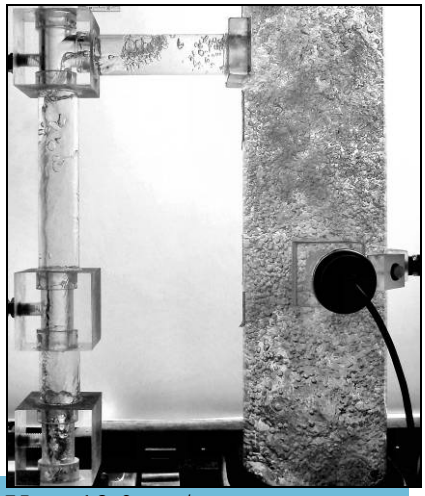
U_G = 19.0 cm/s

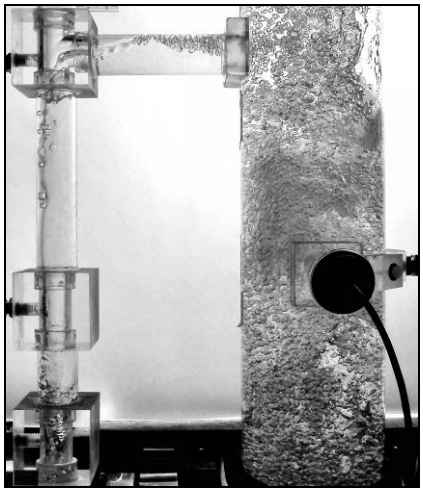
U_G = 19.0 cm/s

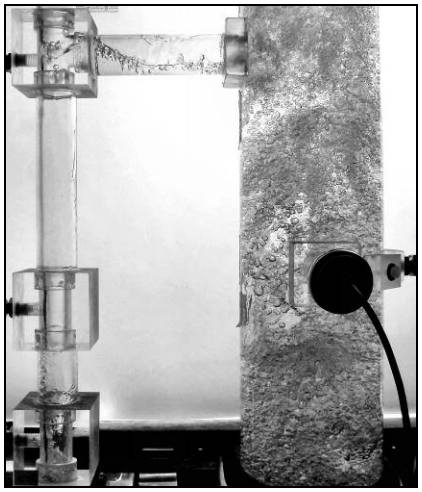
U_G = 19.0 cm/s

Test Conditions:
A = 0.99%
Closed Vent Mode
Upper Horizontal Connector

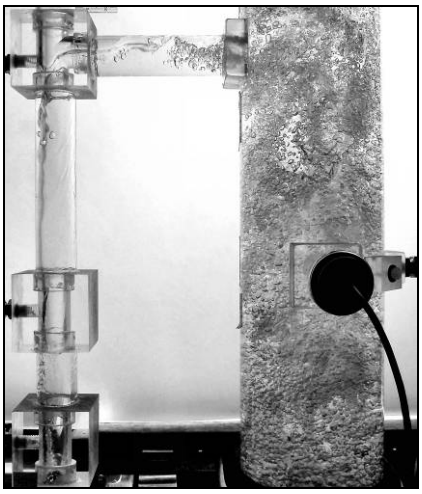
U_G = 20.0 cm/s

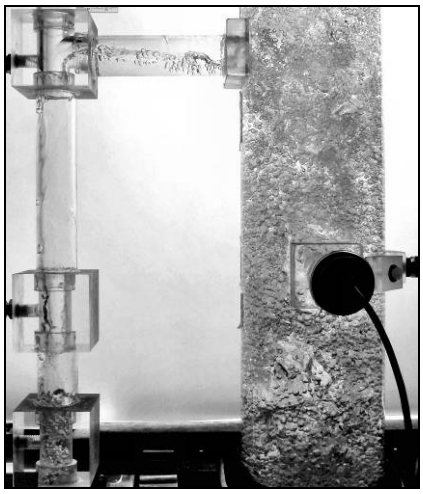
U_G = 20.0 cm/s

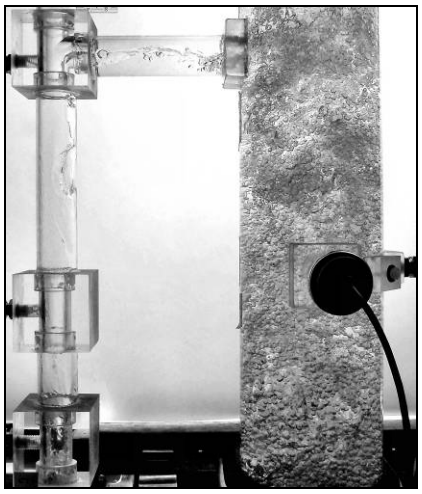
U_G = 20.0 cm/s

Test Conditions:
A = 2.22%
Open Vent Mode
Upper Horizontal Connector

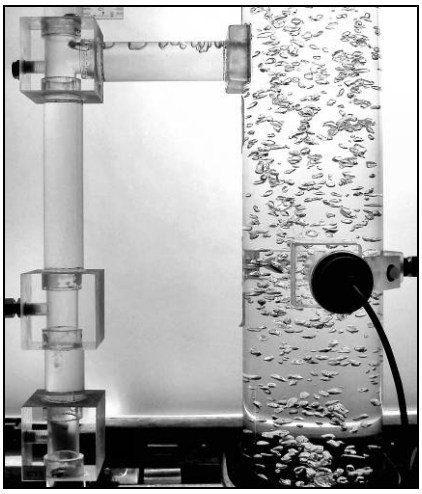
U_G = 0.5 cm/s

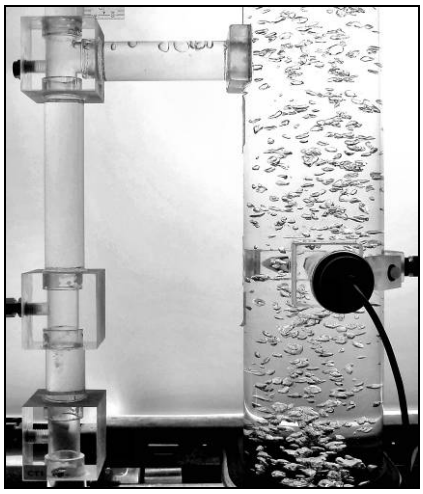
U_G = 0.5 cm/s

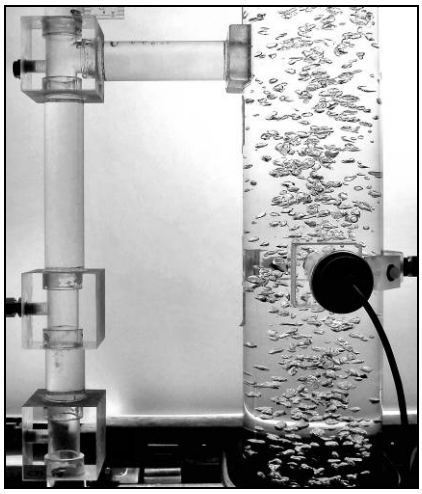
U_G = 0.5 cm/s

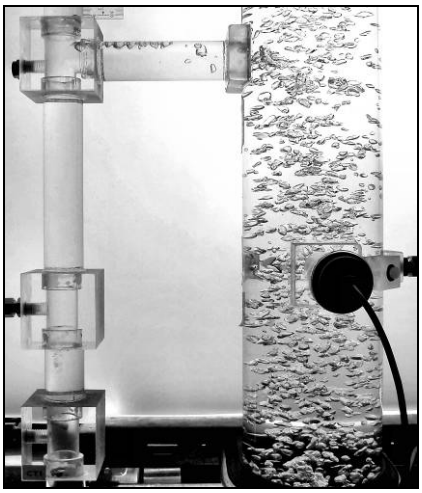
U_G = 1.0 cm/s

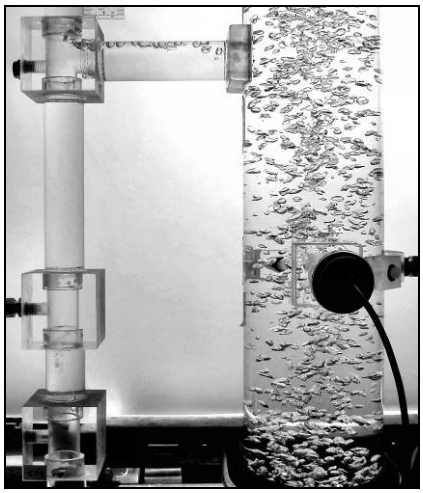
U_G = 1.0 cm/s

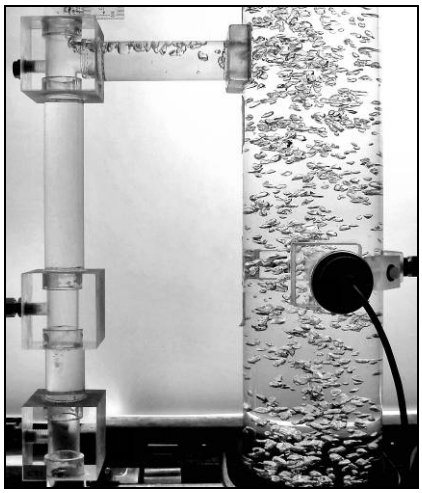
U_G = 1.0 cm/s

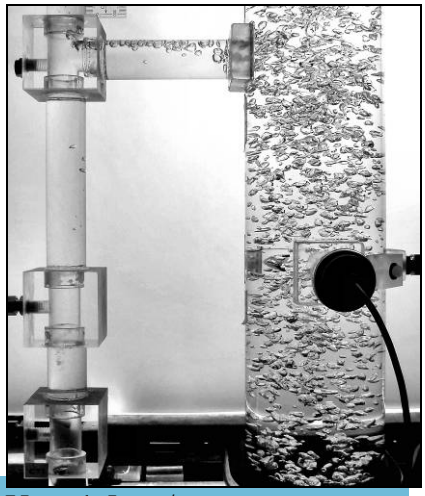
U_G = 1.5 cm/s

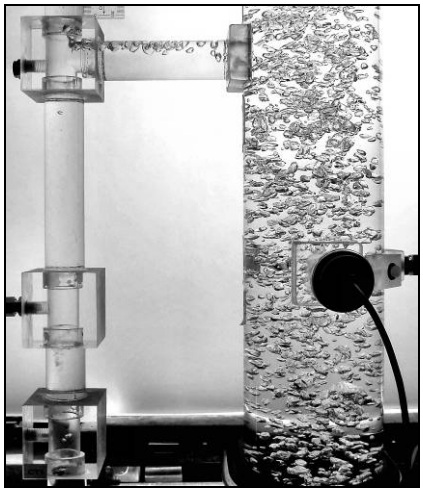
U_G = 1.5 cm/s

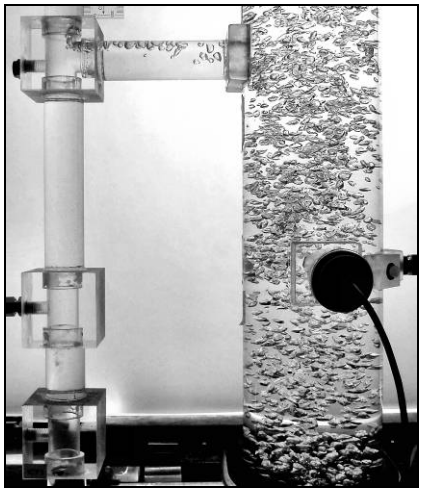
U_G = 1.5 cm/s

Test Conditions:
A = 2.22%
Open Vent Mode
Upper Horizontal Connector

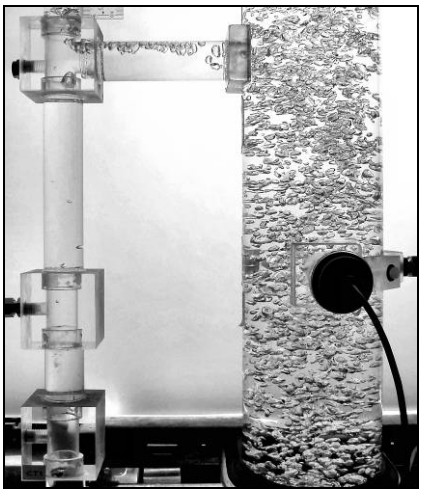
U_G = 2.0 cm/s

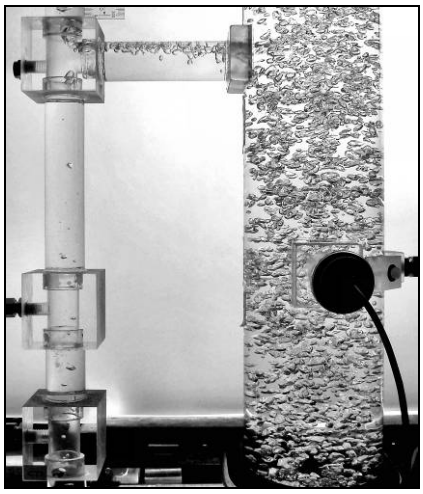
U_G = 2.0 cm/s

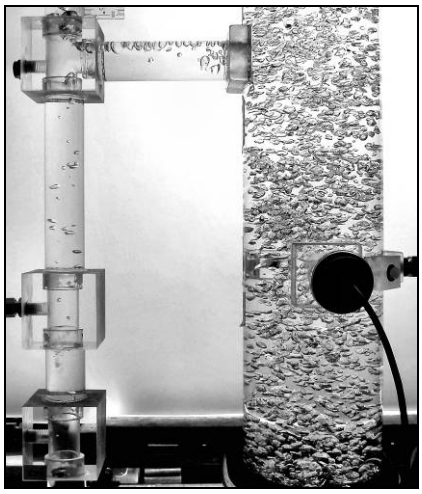
U_G = 2.0 cm/s

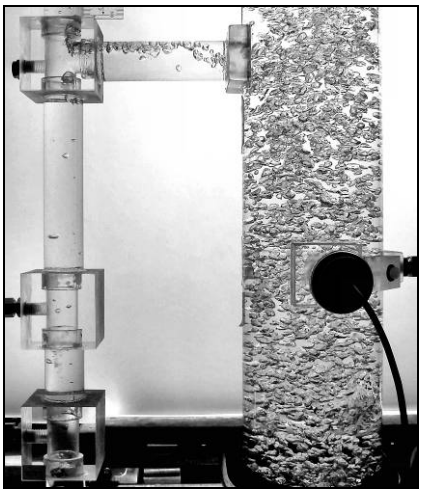
U_G = 2.5 cm/s

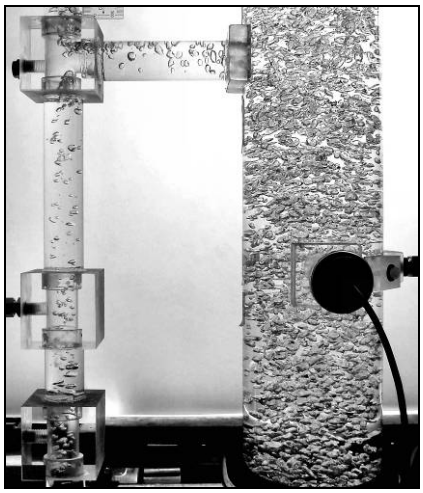
U_G = 2.5 cm/s

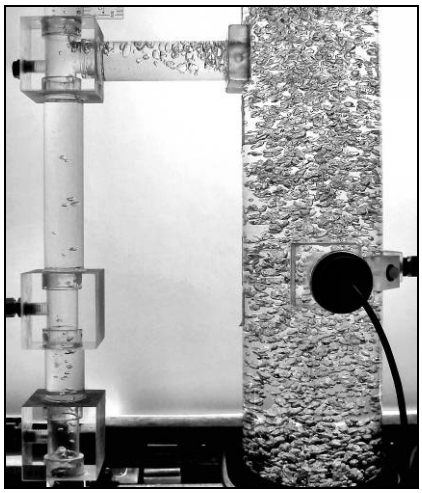
U_G = 2.5 cm/s

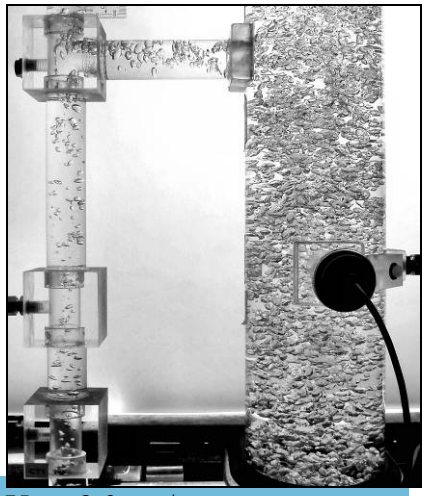
U_G = 3.0 cm/s

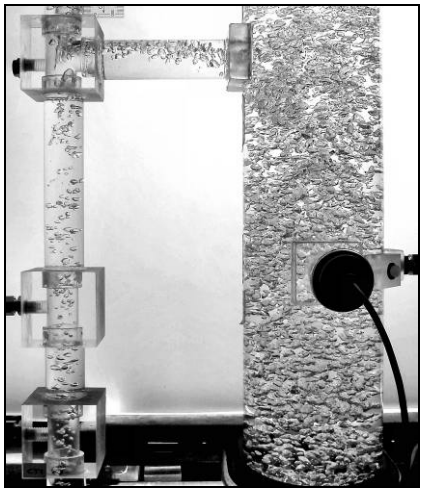
U_G = 3.0 cm/s

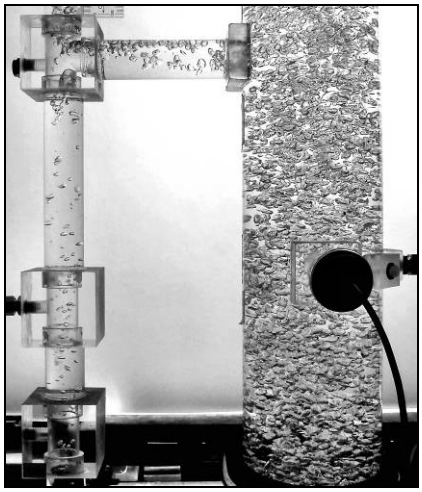
U_G = 3.0 cm/s

Test Conditions:
A = 2.22%
Open Vent Mode
Upper Horizontal Connector

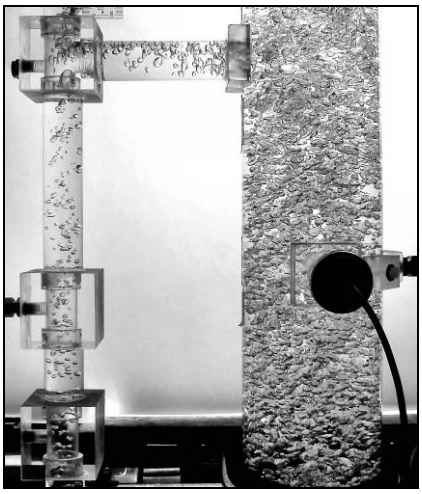
U_G = 3.5 cm/s

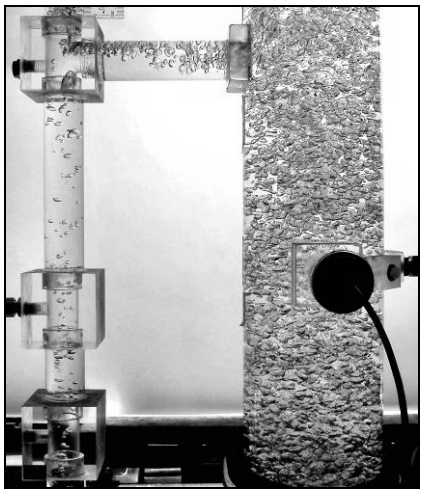
U_G = 3.5 cm/s

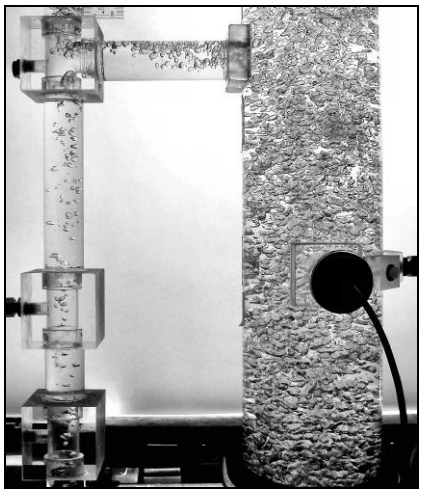
U_G = 3.5 cm/s

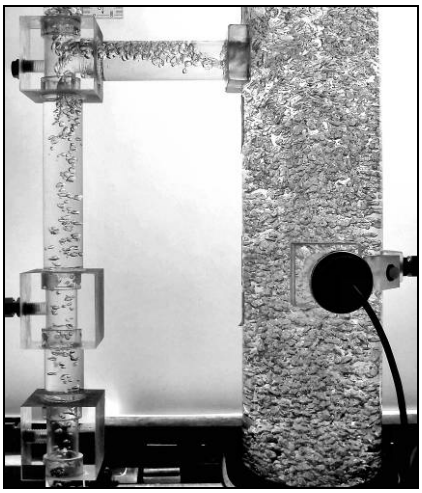
U_G = 4.0 cm/s

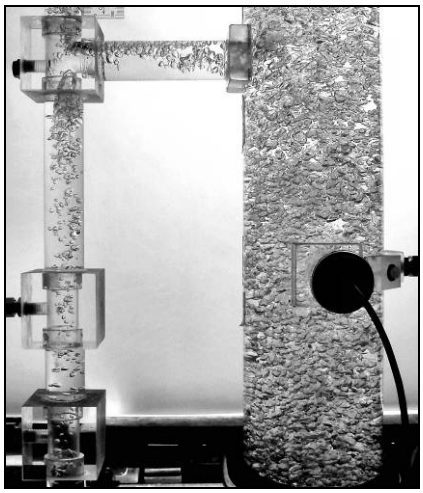
U_G = 4.0 cm/s

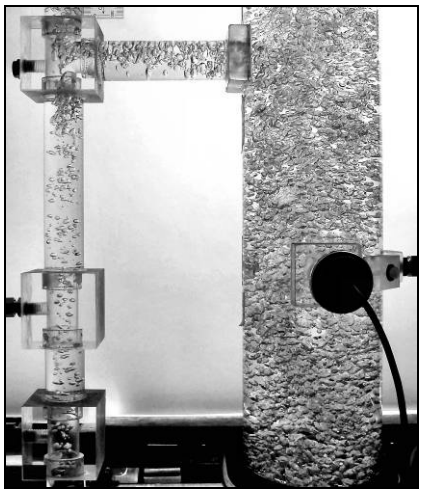
U_G = 4.0 cm/s

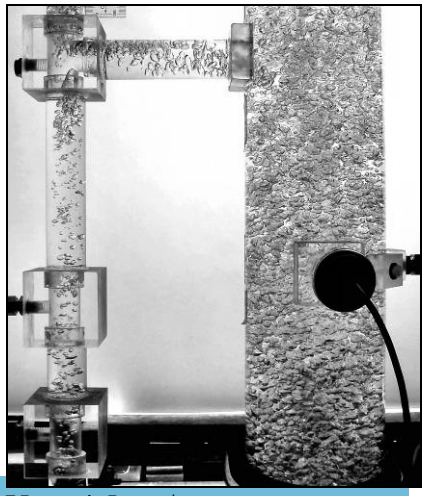
U_G = 4.5 cm/s

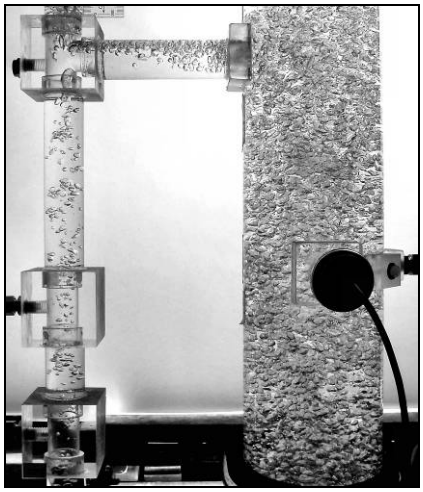
U_G = 4.5 cm/s

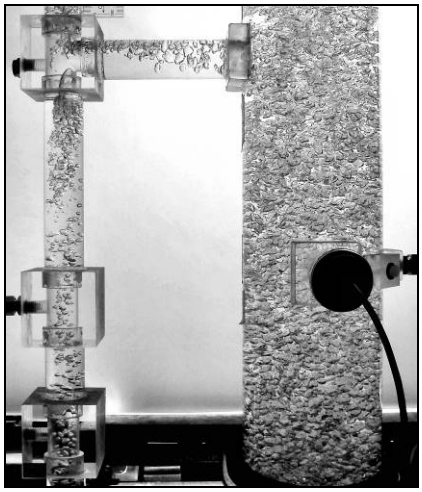
U_G = 4.5 cm/s

Test Conditions:
A = 2.22%
Open Vent Mode
Upper Horizontal Connector

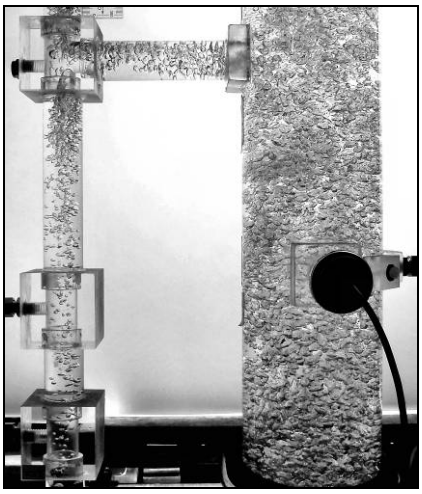
U_G = 5.0 cm/s

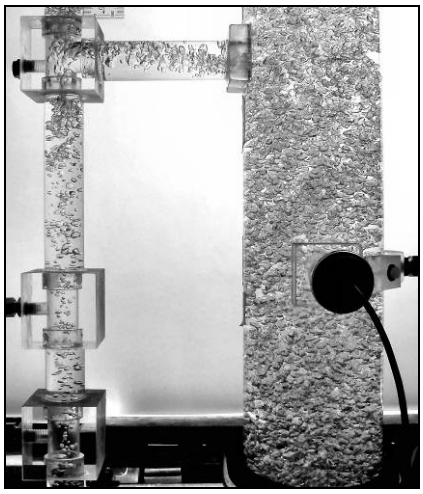
U_G = 5.0 cm/s

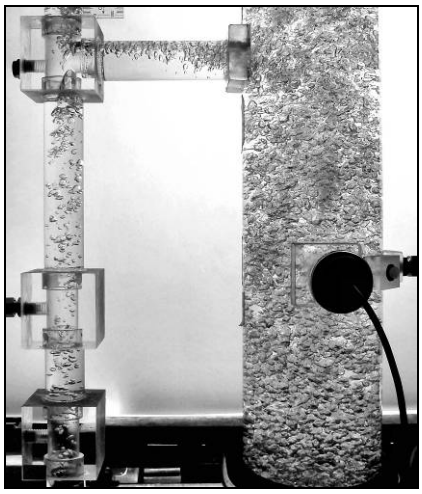
U_G = 5.0 cm/s

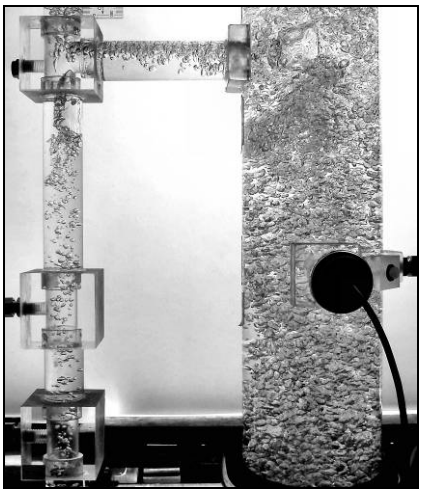
U_G = 6.0 cm/s

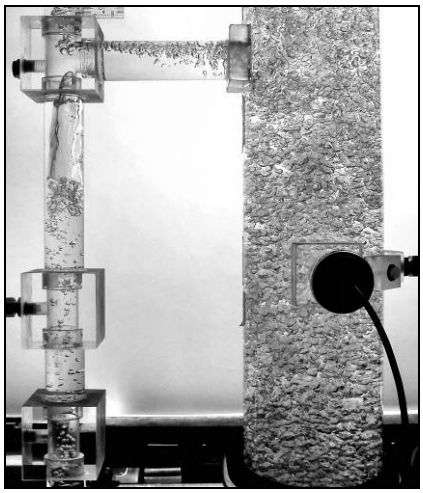
U_G = 6.0 cm/s

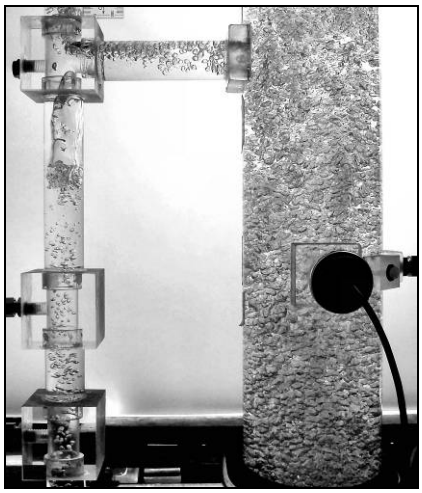
U_G = 6.0 cm/s

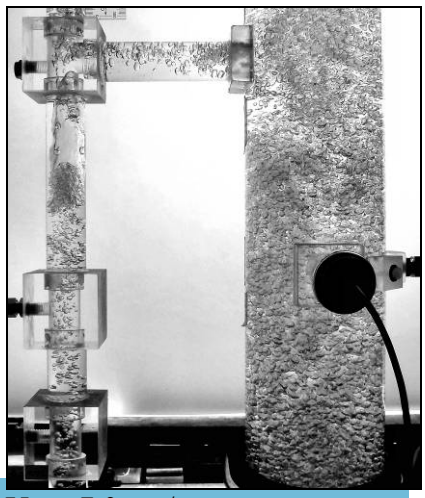
U_G = 7.0 cm/s

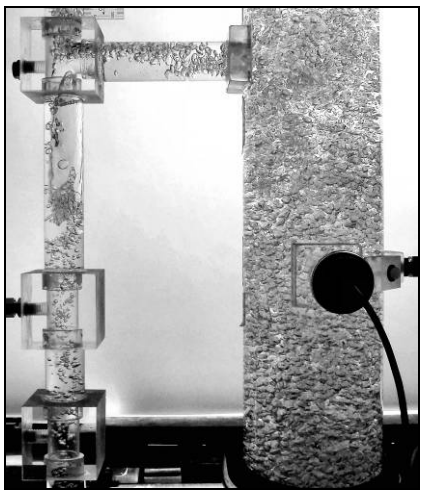
U_G = 7.0 cm/s

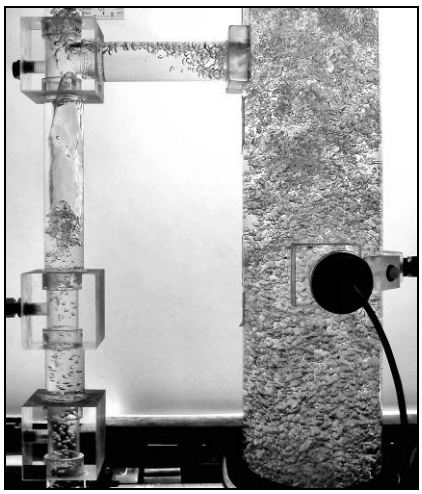
U_G = 7.0 cm/s

Test Conditions:
A = 2.22%
Open Vent Mode
Upper Horizontal Connector

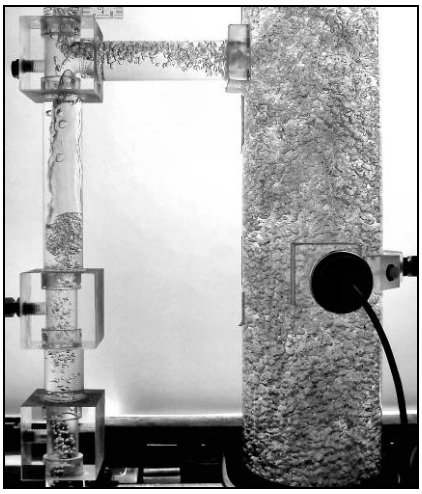
U_G = 8.0 cm/s

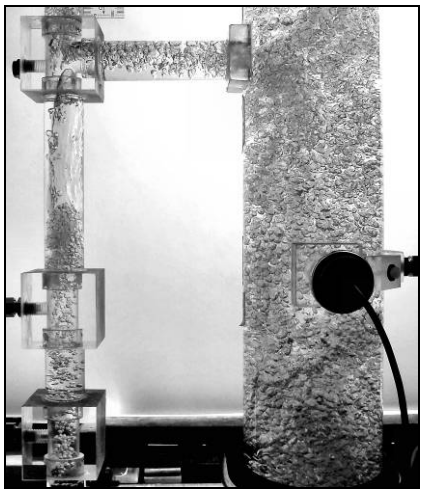
U_G = 8.0 cm/s

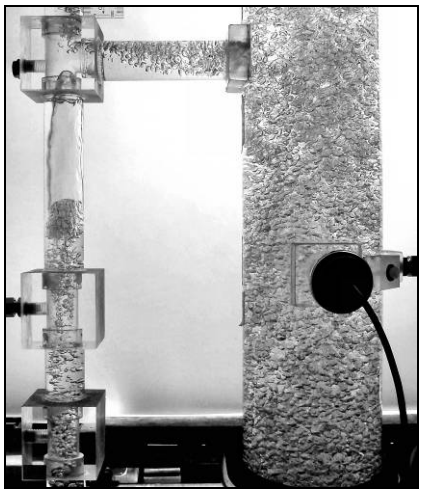
U_G = 8.0 cm/s

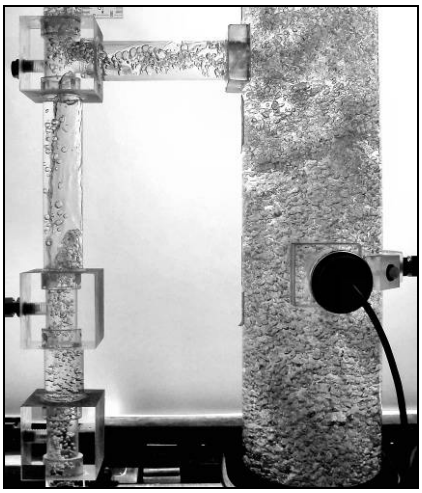
U_G = 9.0 cm/s

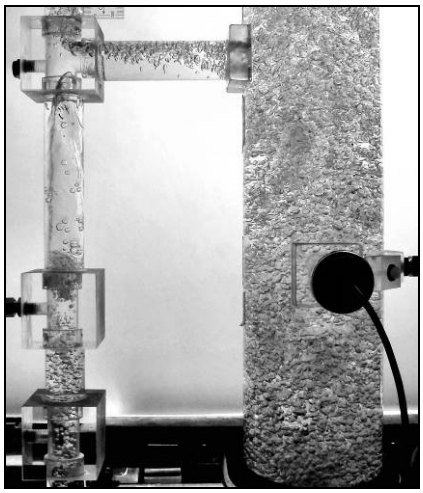
U_G = 9.0 cm/s

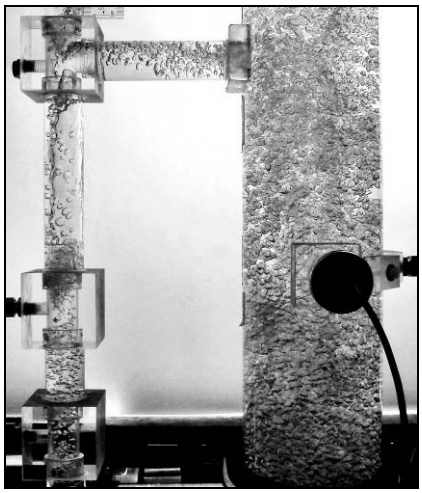
U_G = 9.0 cm/s

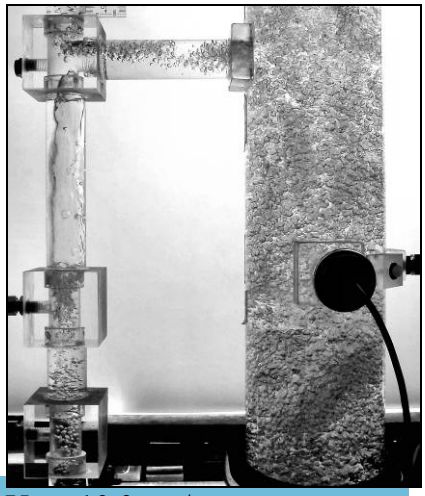
U_G = 10.0 cm/s

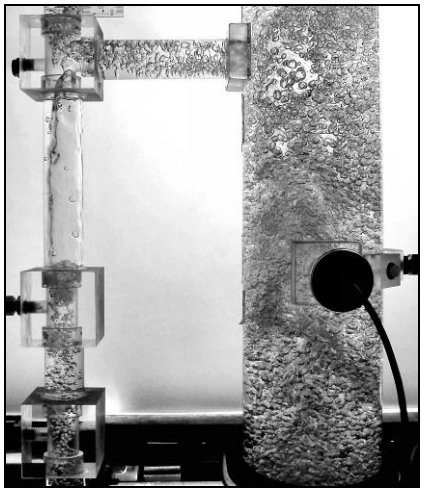
U_G = 10.0 cm/s

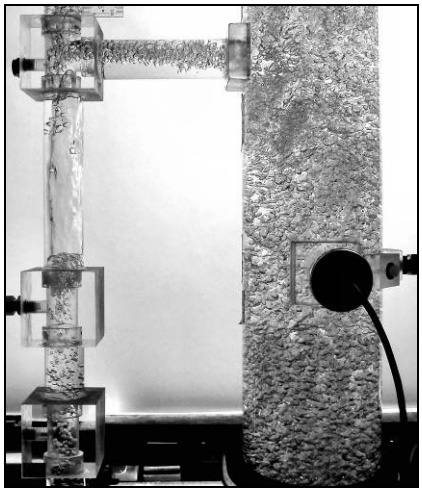
U_G = 10.0 cm/s

Test Conditions:
A = 2.22%
Open Vent Mode
Upper Horizontal Connector

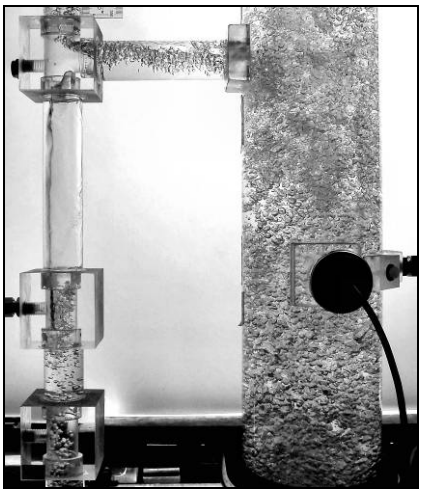
U_G = 11.0 cm/s

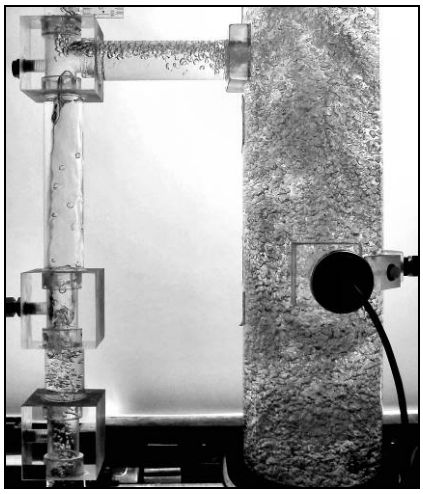
U_G = 11.0 cm/s

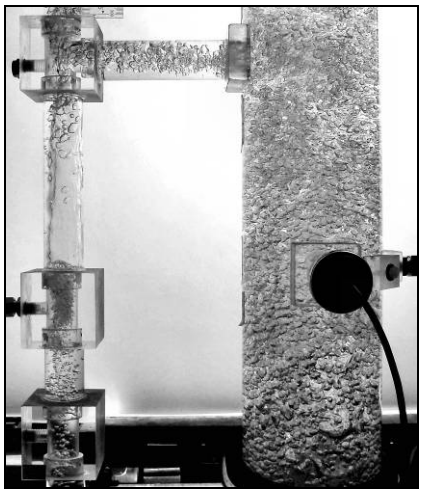
U_G = 11.0 cm/s

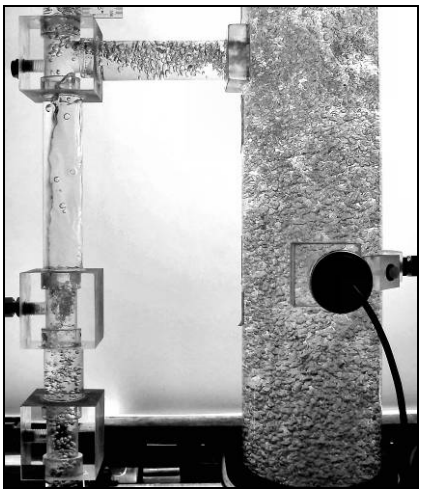
U_G = 12.0 cm/s

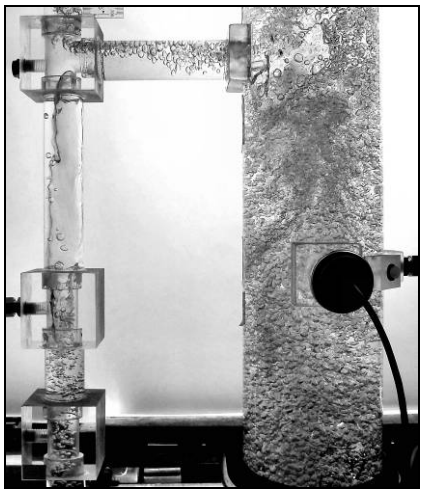
U_G = 12.0 cm/s

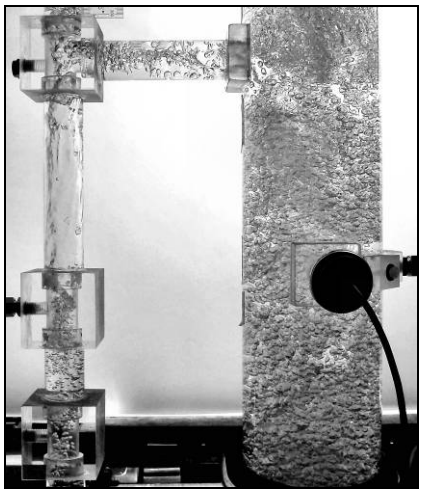
U_G = 12.0 cm/s

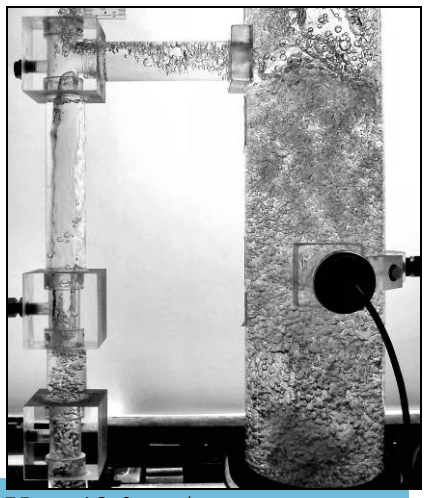
U_G = 13.0 cm/s

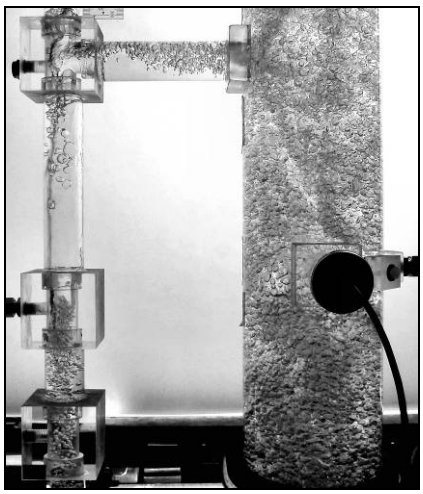
U_G = 13.0 cm/s

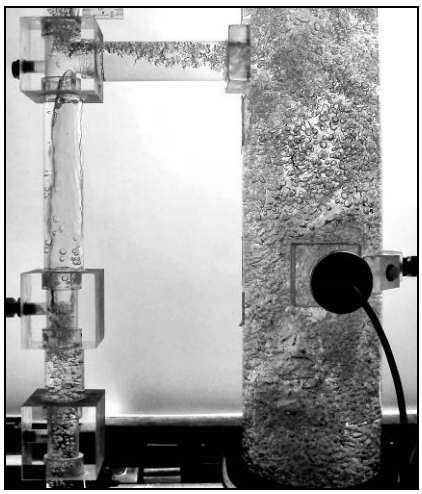
U_G = 13.0 cm/s

Test Conditions:
A = 2.22%
Open Vent Mode
Upper Horizontal Connector

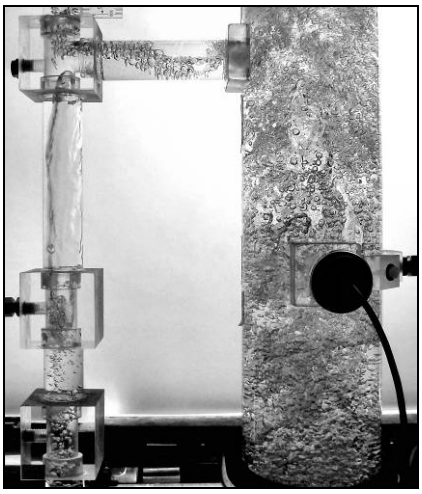
U_G = 14.0 cm/s

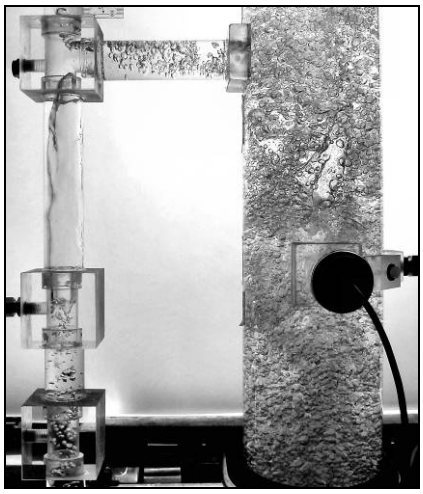
U_G = 14.0 cm/s

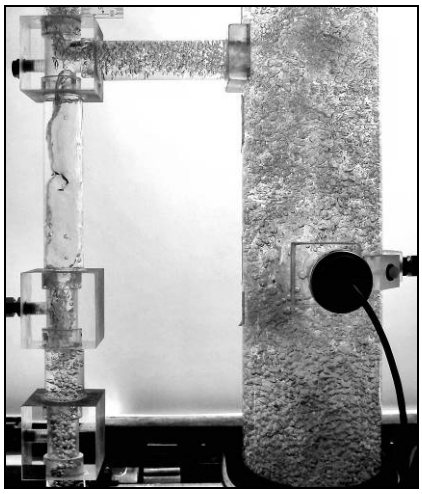
U_G = 14.0 cm/s

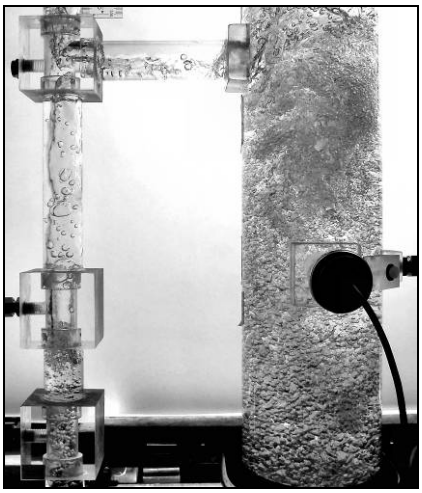
U_G = 15.0 cm/s

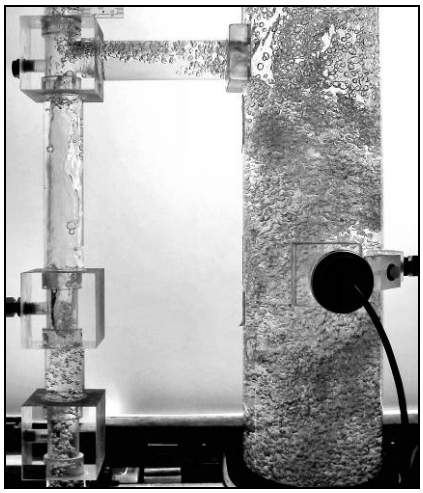
U_G = 15.0 cm/s

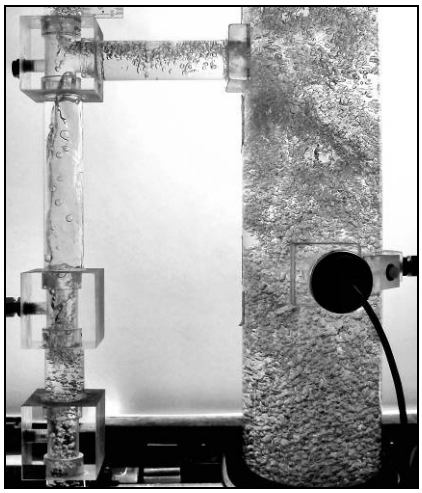
U_G = 15.0 cm/s

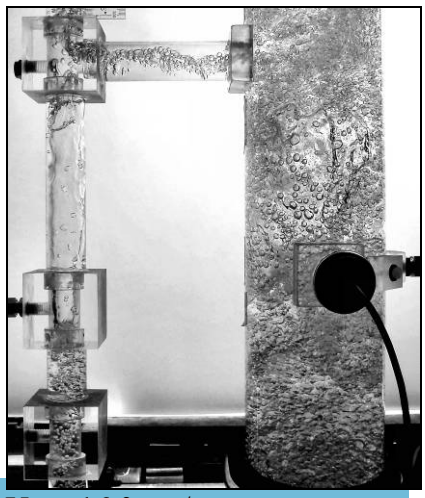
U_G = 16.0 cm/s

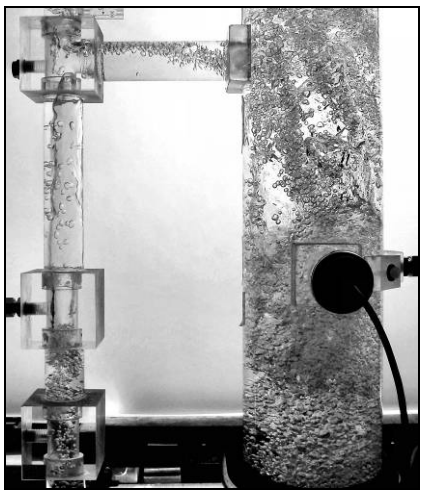
U_G = 16.0 cm/s

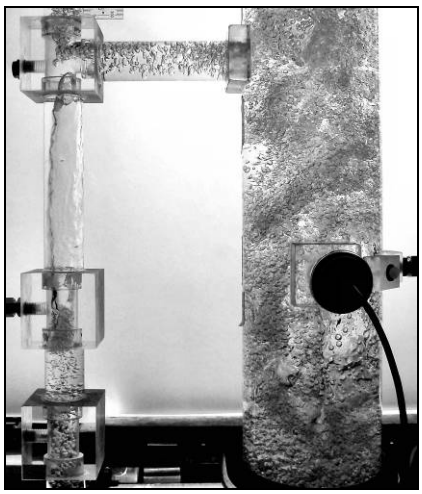
U_G = 16.0 cm/s

Test Conditions:
A = 2.22%
Open Vent Mode
Upper Horizontal Connector

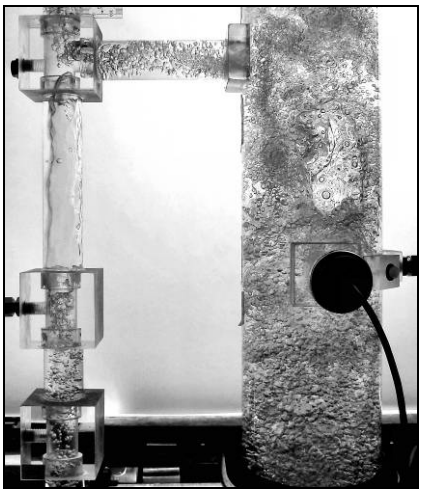
U_G = 17.0 cm/s

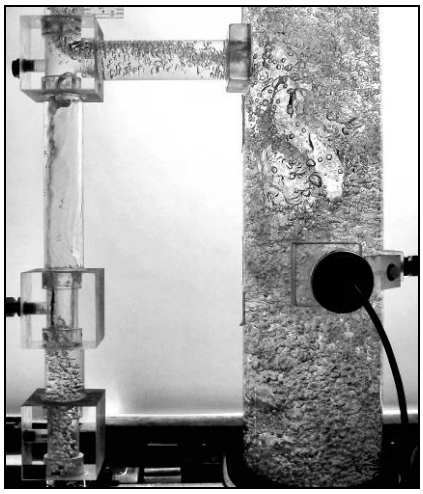
U_G = 17.0 cm/s

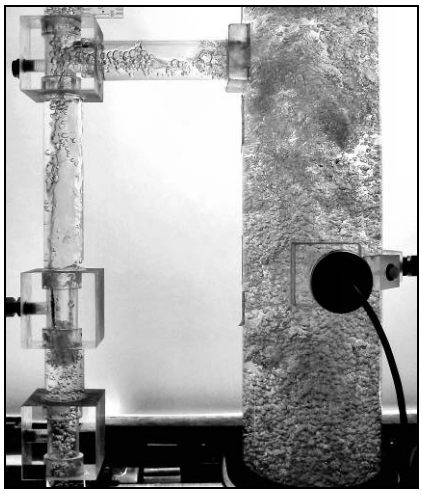
U_G = 17.0 cm/s

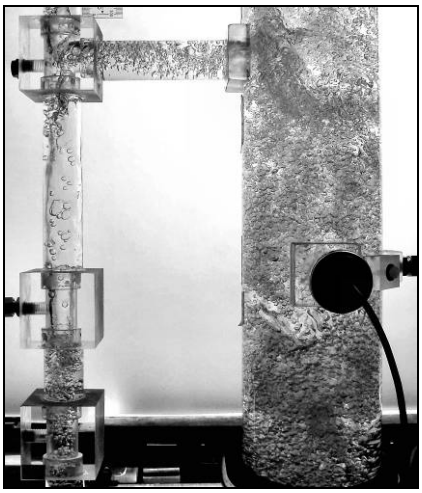
U_G = 18.0 cm/s

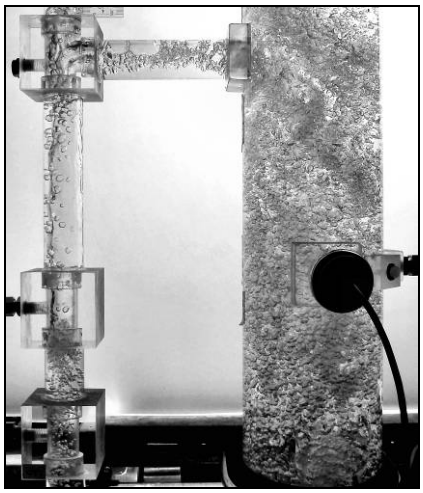
U_G = 18.0 cm/s

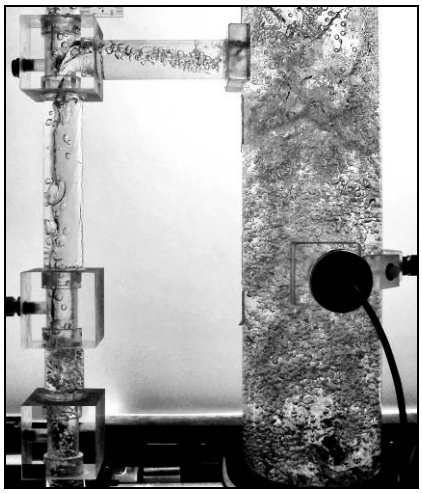
U_G = 18.0 cm/s

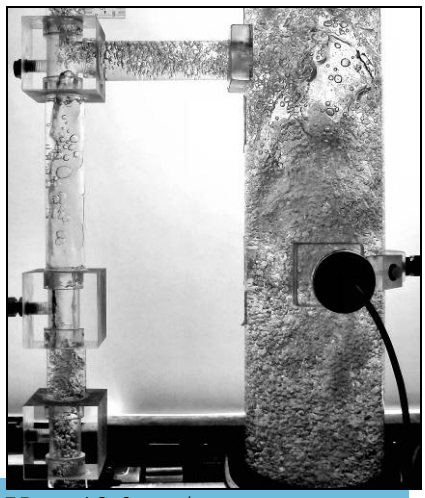
U_G = 19.0 cm/s

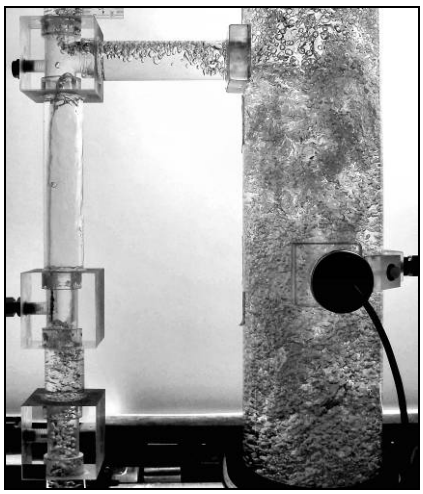
U_G = 19.0 cm/s

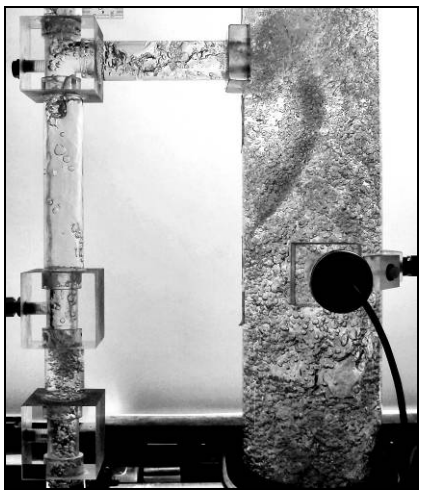
U_G = 19.0 cm/s

Test Conditions:
A = 2.22%
Open Vent Mode
Upper Horizontal Connector

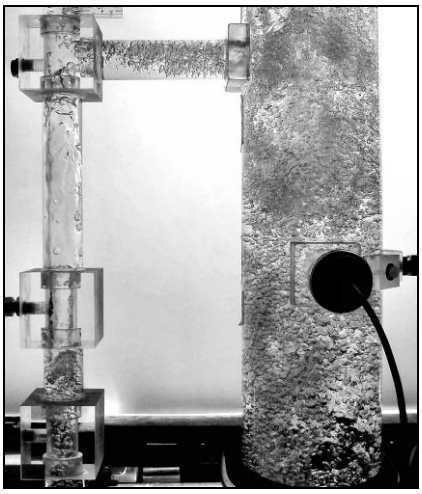
U_G = 20.0 cm/s

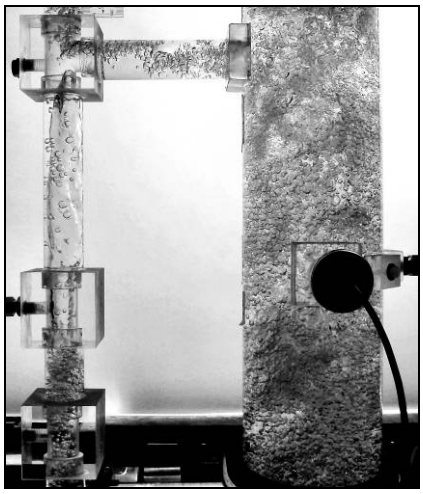
U_G = 20.0 cm/s

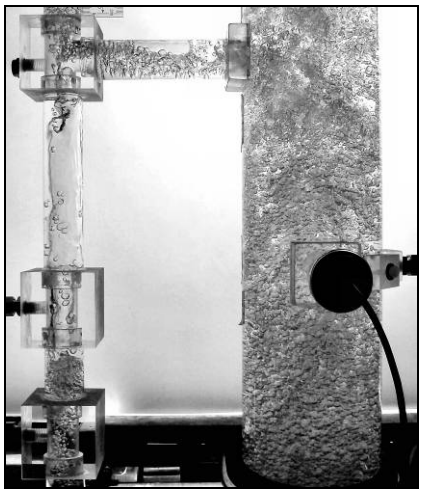
U_G = 20.0 cm/s

Test Conditions:
A = 2.22%
Closed Vent Mode
Upper Horizontal Connector

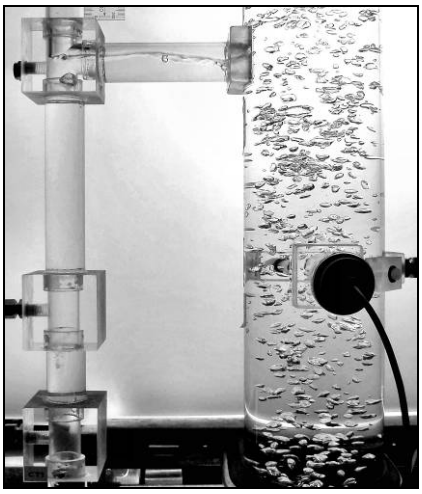
U_G = 0.5 cm/s

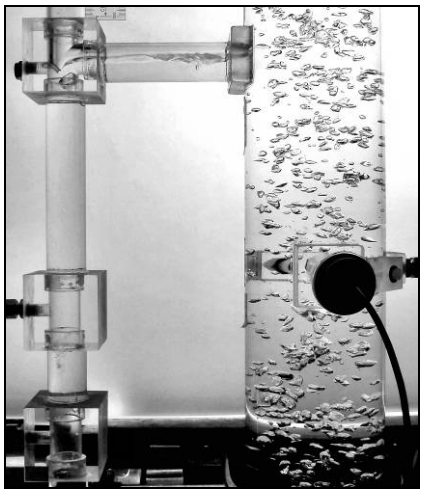
U_G = 0.5 cm/s

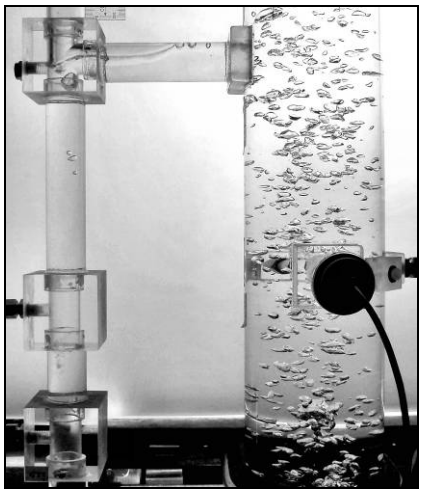
U_G = 0.5 cm/s

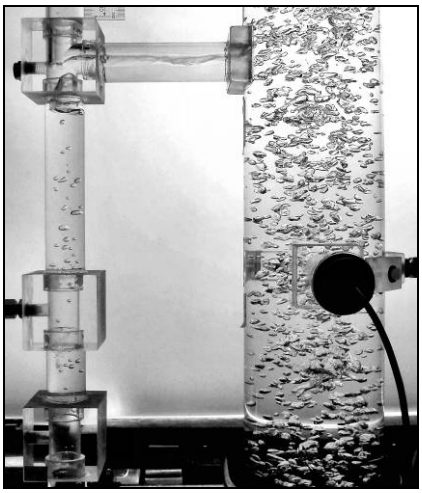
U_G = 1.0 cm/s

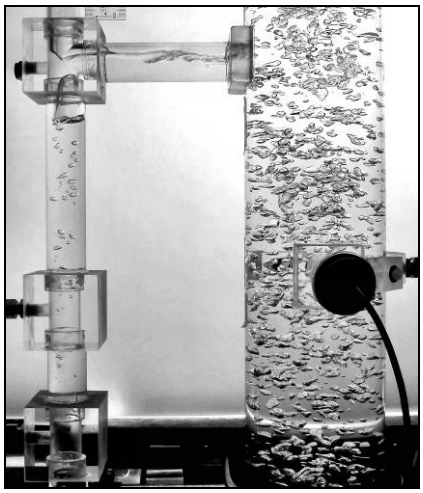
U_G = 1.0 cm/s

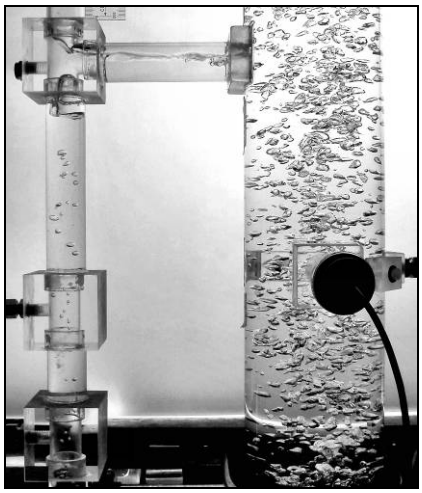
U_G = 1.0 cm/s

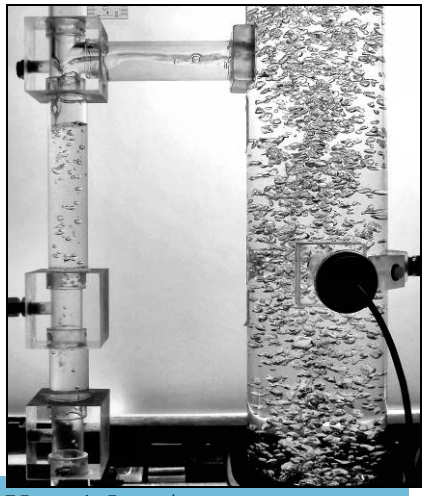
U_G = 1.5 cm/s

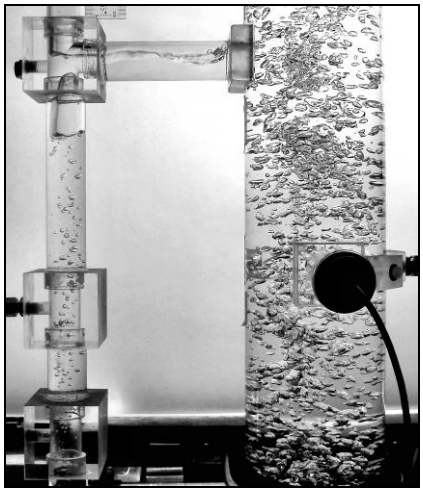
U_G = 1.5 cm/s

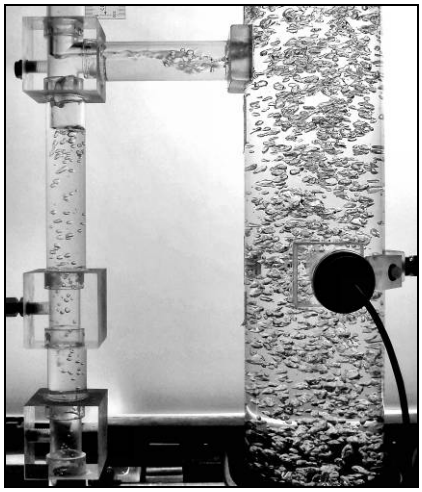
U_G = 1.5 cm/s

Test Conditions:
A = 2.22%
Closed Vent Mode
Upper Horizontal Connector

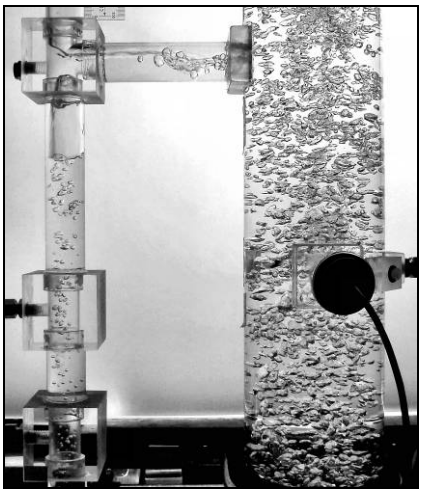
U_G = 2.0 cm/s

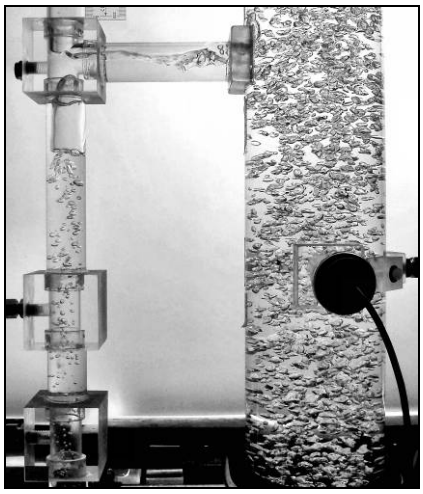
U_G = 2.0 cm/s

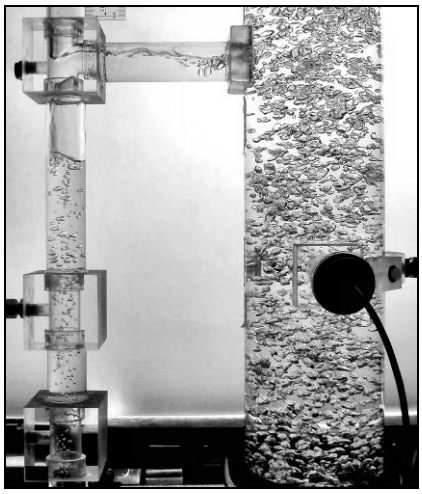
U_G = 2.0 cm/s

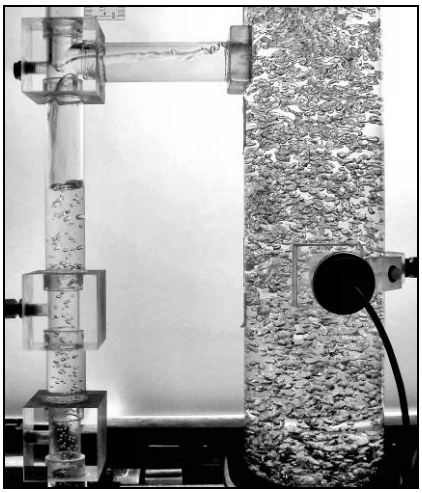
U_G = 2.5 cm/s

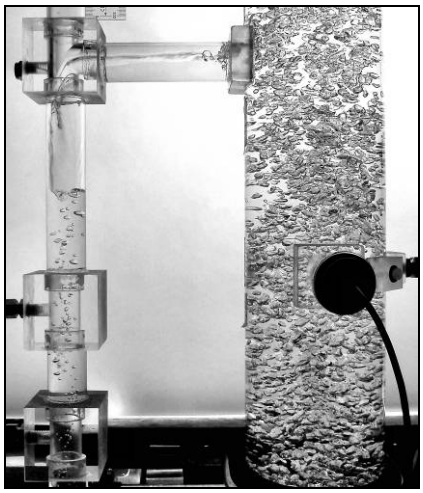
U_G = 2.5 cm/s

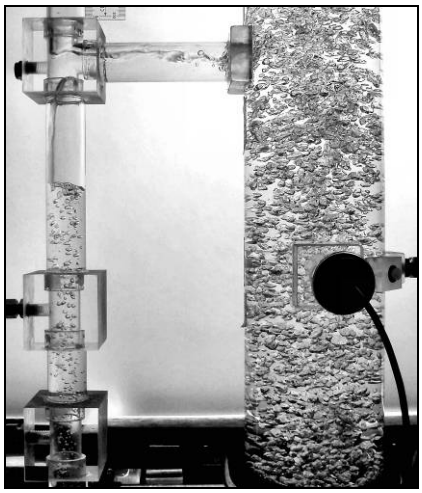
U_G = 2.5 cm/s

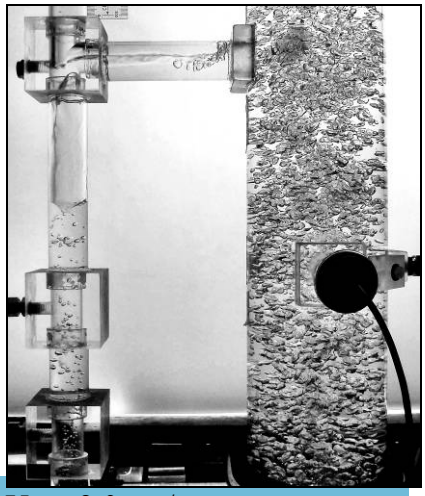
U_G = 3.0 cm/s

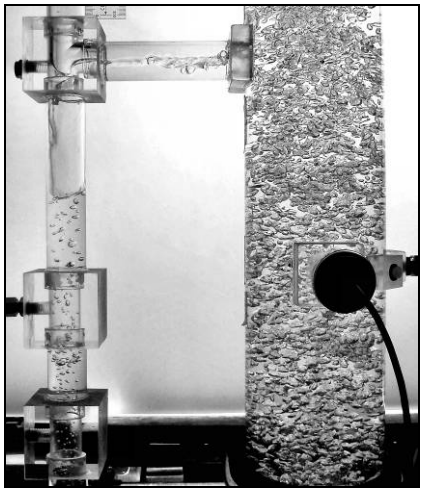
U_G = 3.0 cm/s

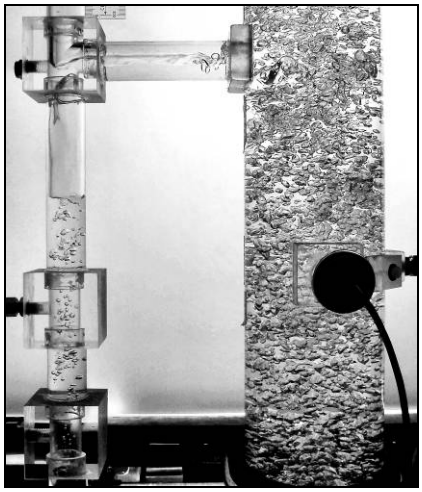
U_G = 3.0 cm/s

Test Conditions:
A = 2.22%
Closed Vent Mode
Upper Horizontal Connector

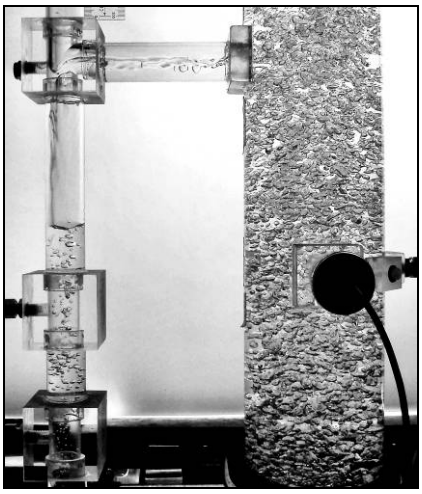
U_G = 3.5 cm/s

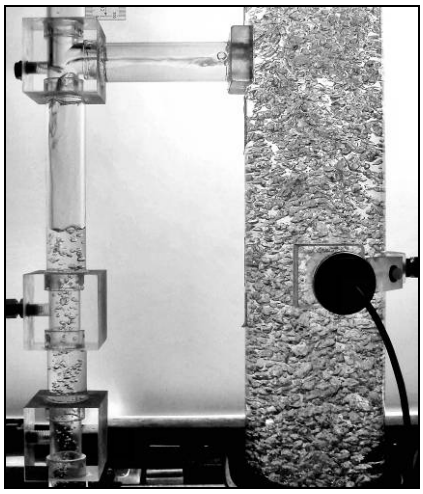
U_G = 3.5 cm/s

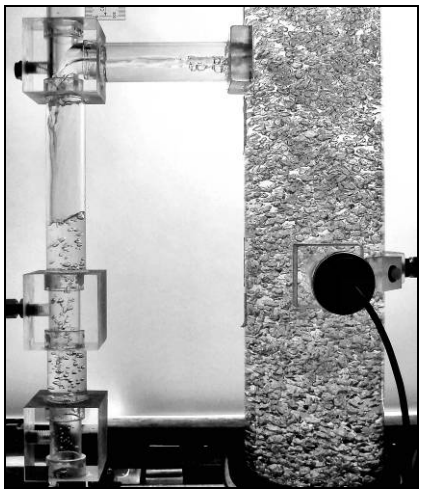
U_G = 3.5 cm/s

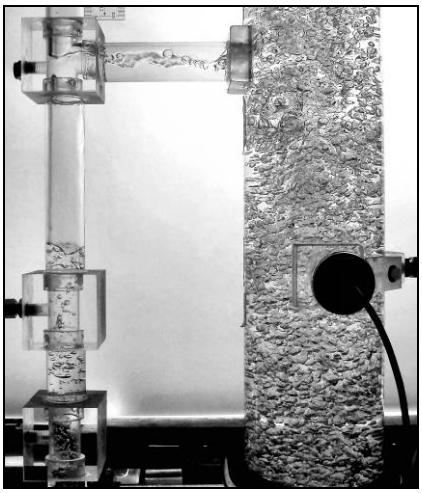
U_G = 4.0 cm/s

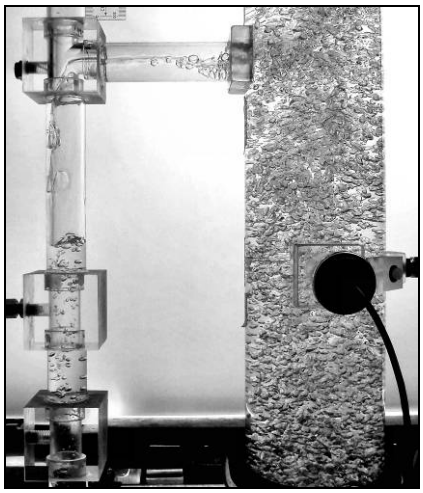
U_G = 4.0 cm/s

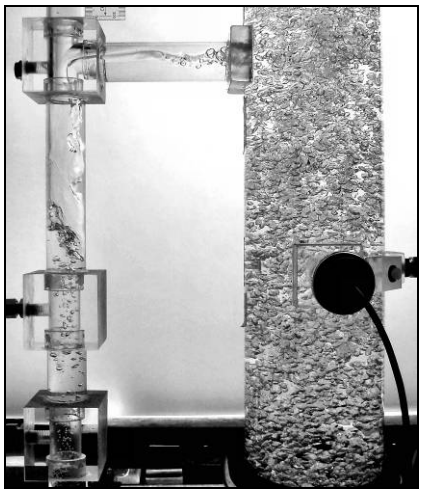
U_G = 4.0 cm/s

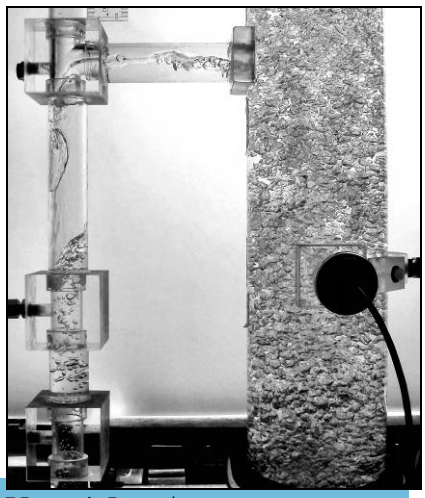
U_G = 4.5 cm/s

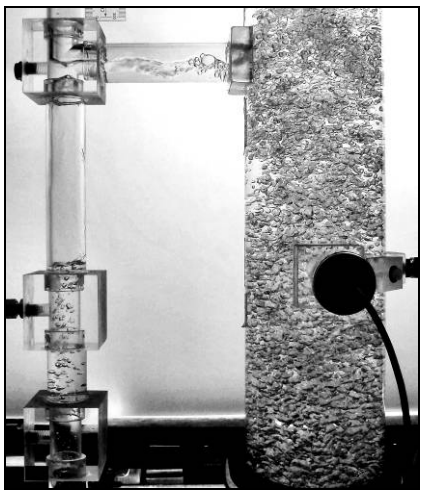
U_G = 4.5 cm/s

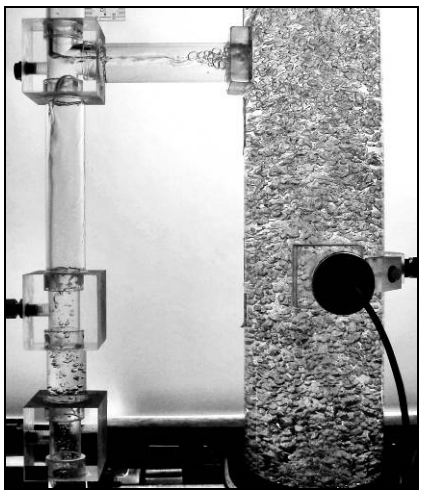
U_G = 4.5 cm/s

Test Conditions:
A = 2.22%
Closed Vent Mode
Upper Horizontal Connector

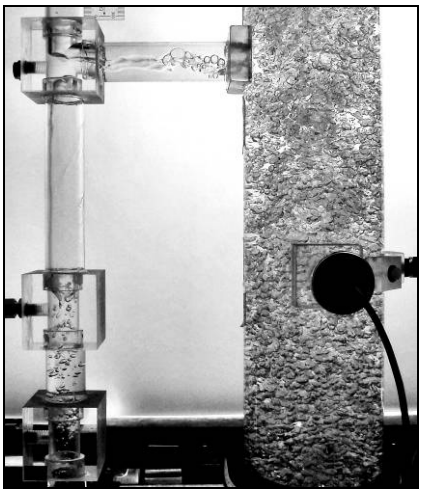
U_G = 5.0 cm/s

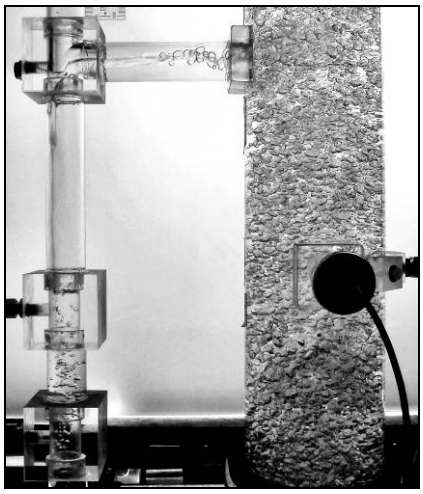
U_G = 5.0 cm/s

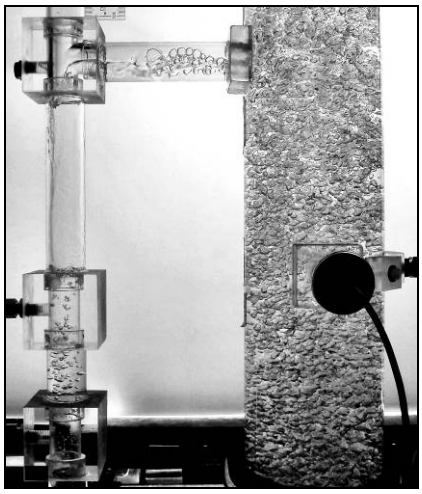
U_G = 5.0 cm/s

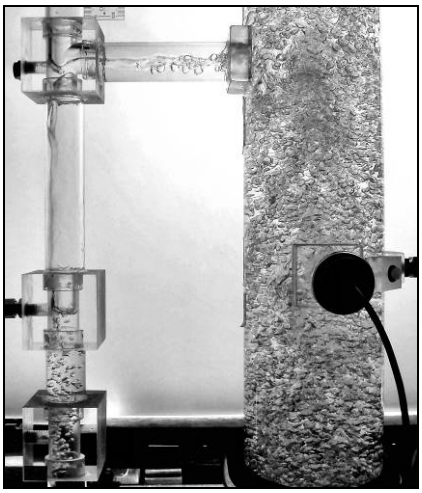
U_G = 6.0 cm/s

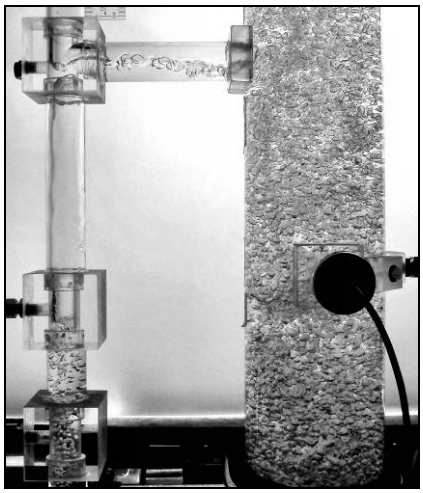
U_G = 6.0 cm/s

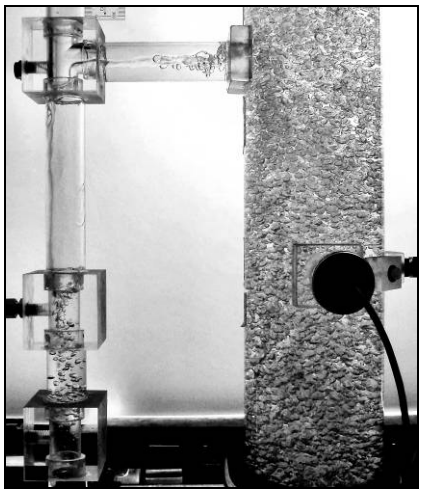
U_G = 6.0 cm/s

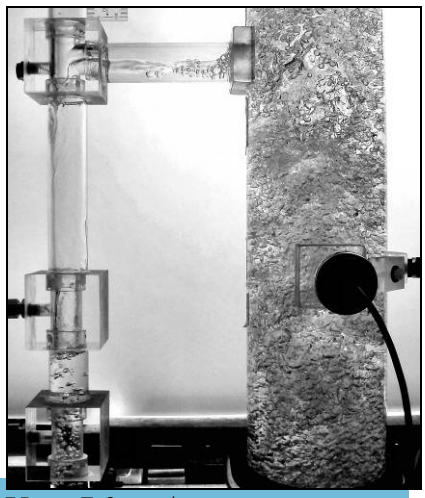
U_G = 7.0 cm/s

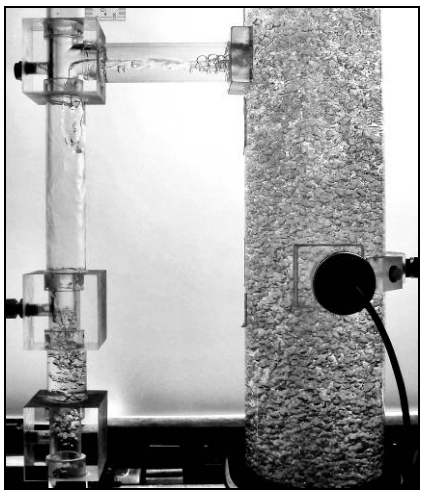
U_G = 7.0 cm/s

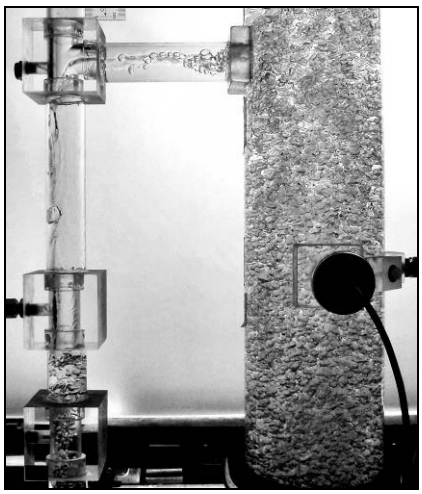
U_G = 7.0 cm/s

Test Conditions:
A = 2.22%
Closed Vent Mode
Upper Horizontal Connector

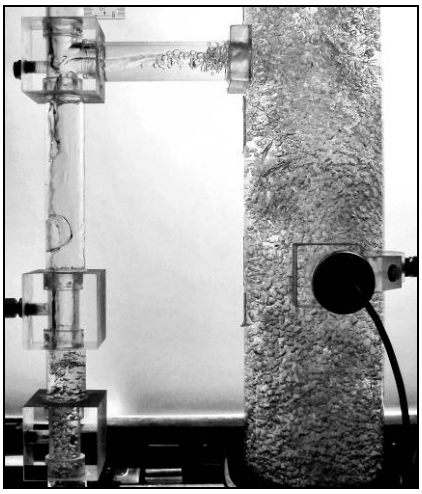
U_G = 8.0 cm/s

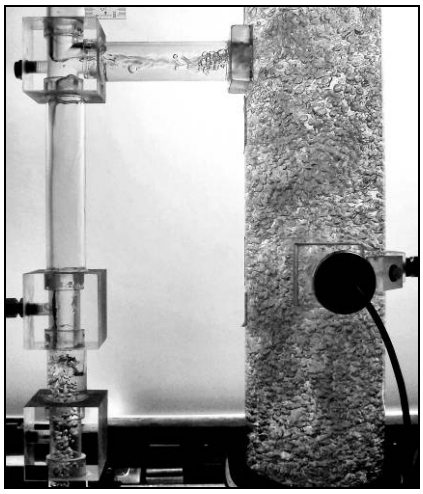
U_G = 8.0 cm/s

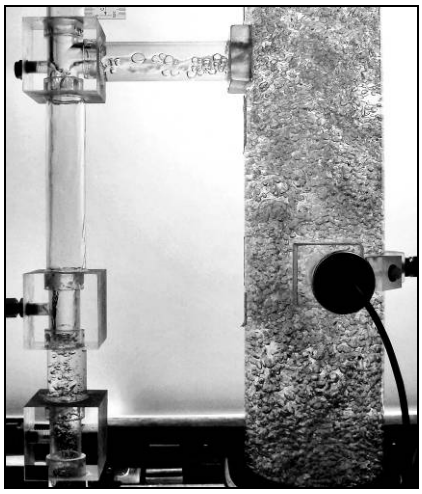
U_G = 8.0 cm/s

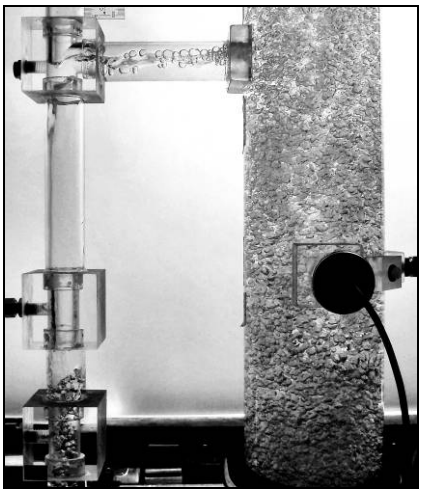
U_G = 9.0 cm/s

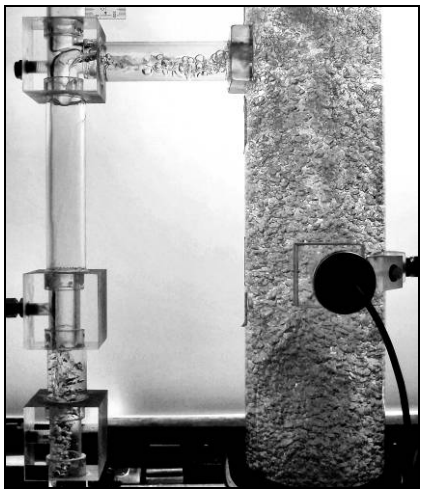
U_G = 9.0 cm/s

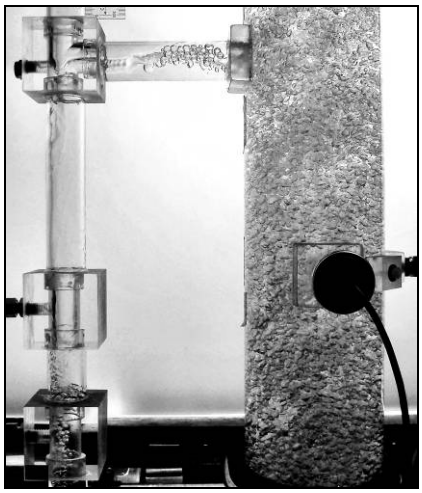
U_G = 9.0 cm/s

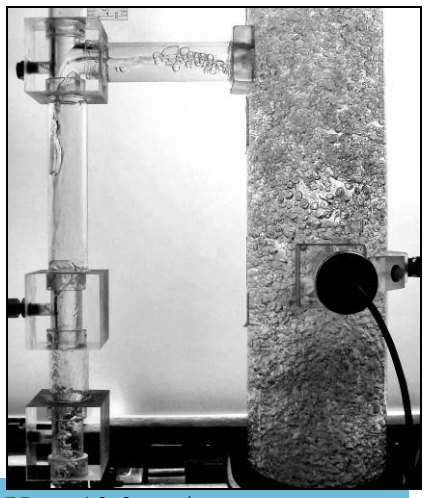
U_G = 10.0 cm/s

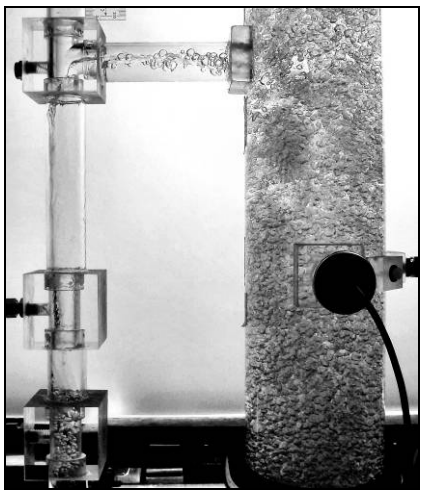
U_G = 10.0 cm/s

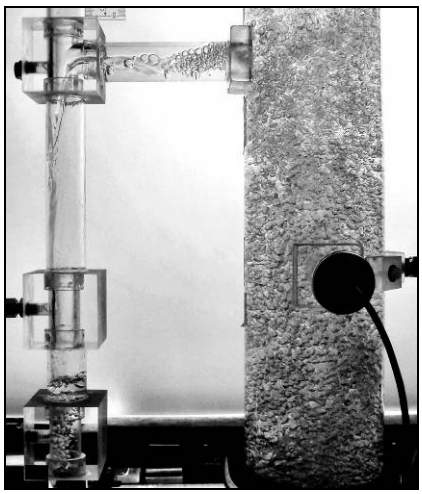
U_G = 10.0 cm/s

Test Conditions:
A = 2.22%
Closed Vent Mode
Upper Horizontal Connector

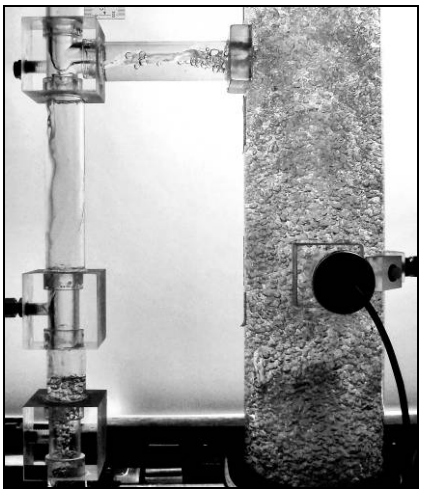
U_G = 11.0 cm/s

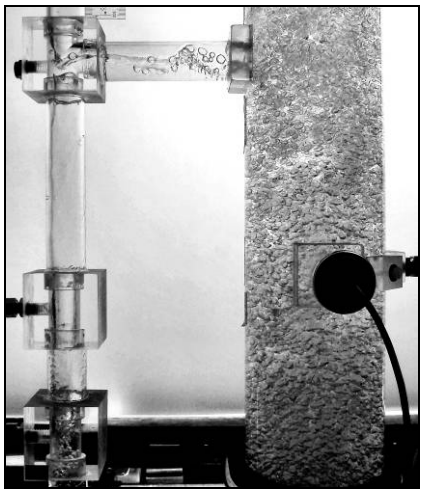
U_G = 11.0 cm/s

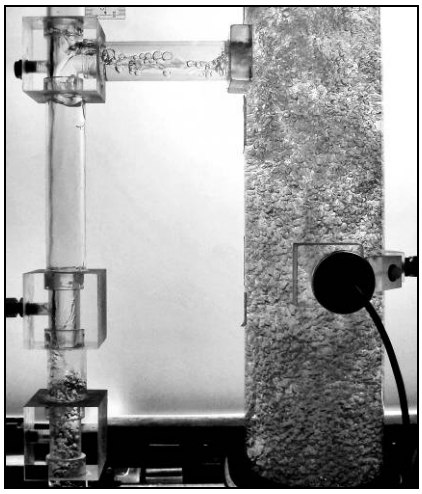
U_G = 11.0 cm/s

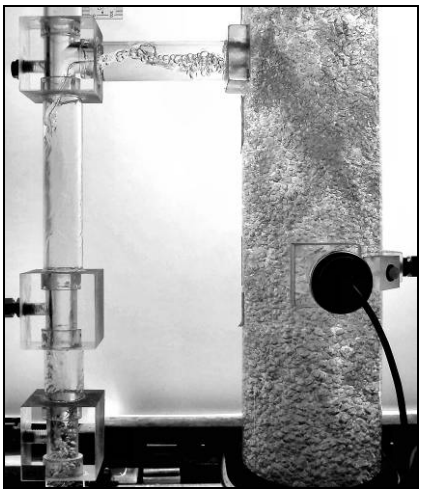
U_G = 12.0 cm/s

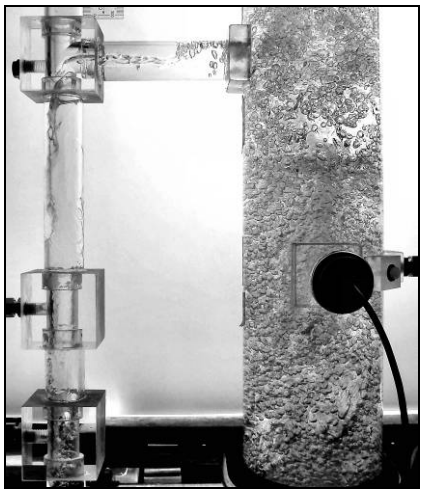
U_G = 12.0 cm/s

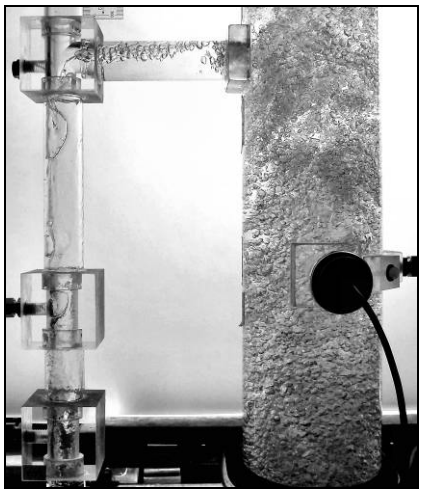
U_G = 12.0 cm/s

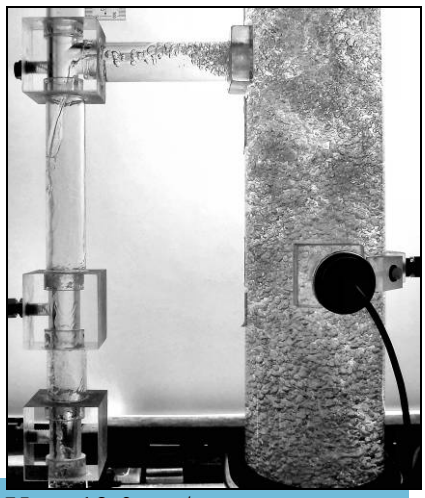
U_G = 13.0 cm/s

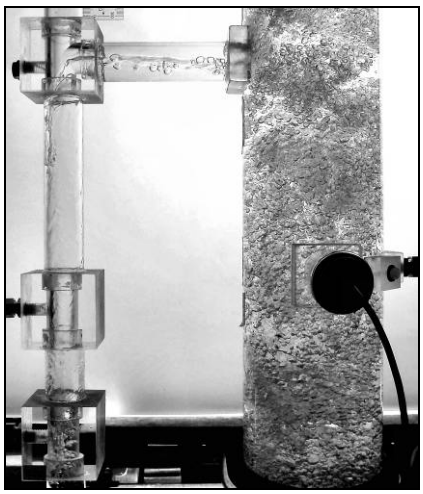
U_G = 13.0 cm/s

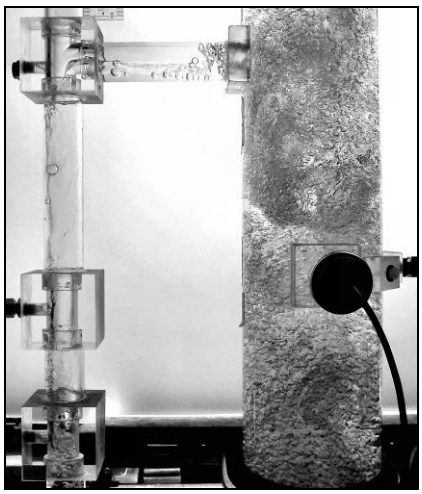
U_G = 13.0 cm/s

Test Conditions:
A = 2.22%
Closed Vent Mode
Upper Horizontal Connector

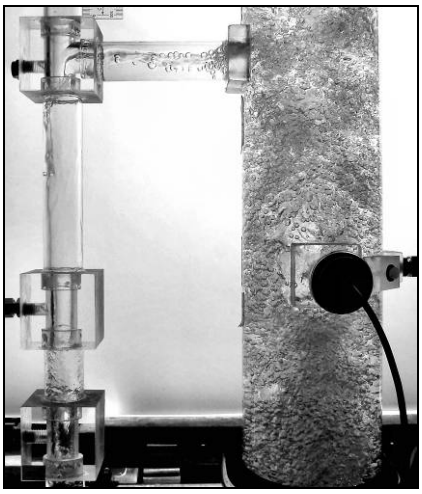
U_G = 14.0 cm/s

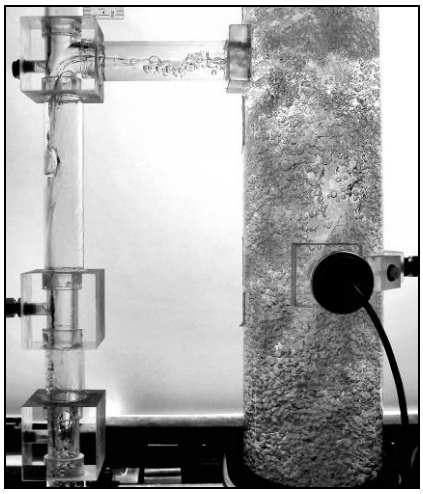
U_G = 14.0 cm/s

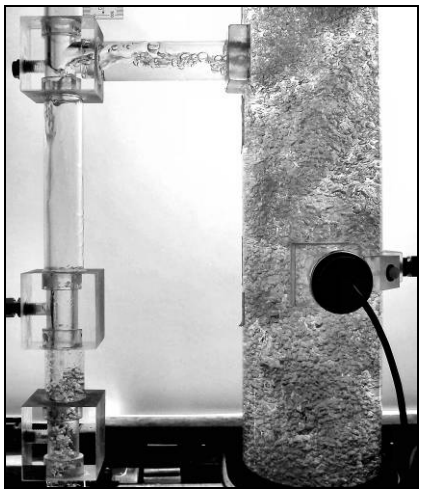
U_G = 14.0 cm/s

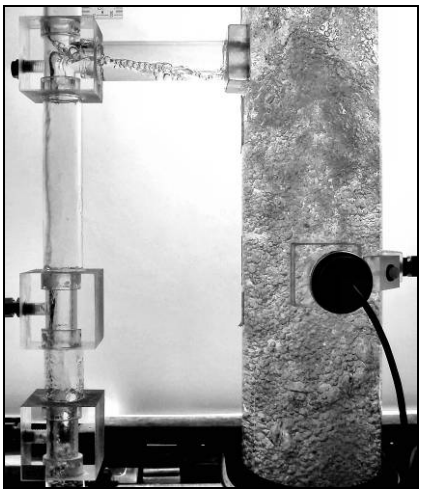
U_G = 15.0 cm/s

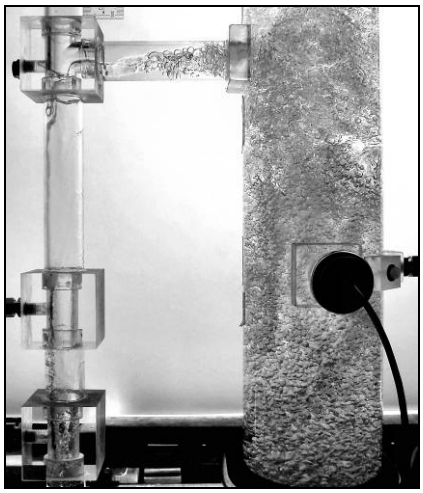
U_G = 15.0 cm/s

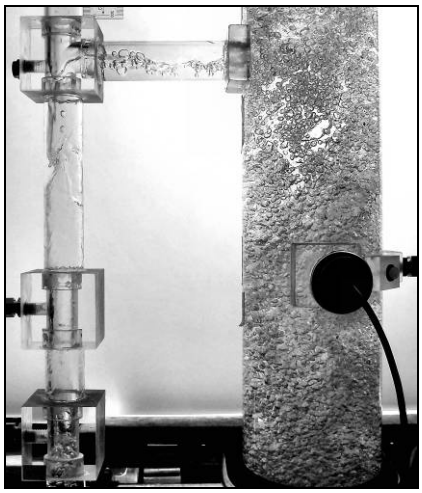
U_G = 15.0 cm/s

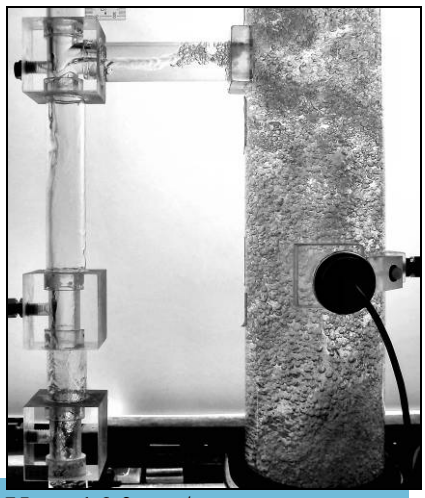
U_G = 16.0 cm/s

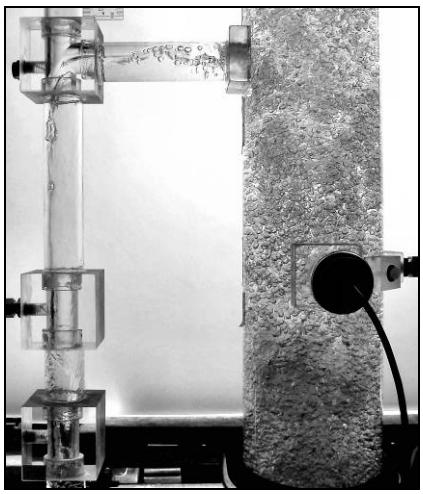
U_G = 16.0 cm/s

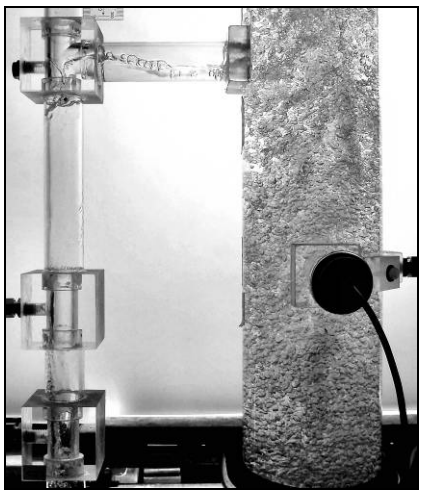
U_G = 16.0 cm/s

Test Conditions:
A = 2.22%
Closed Vent Mode
Upper Horizontal Connector

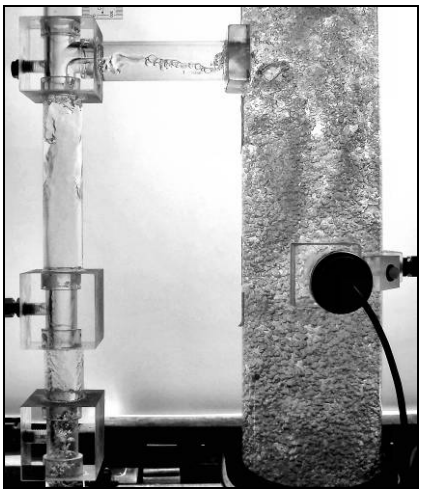
U_G = 17.0 cm/s

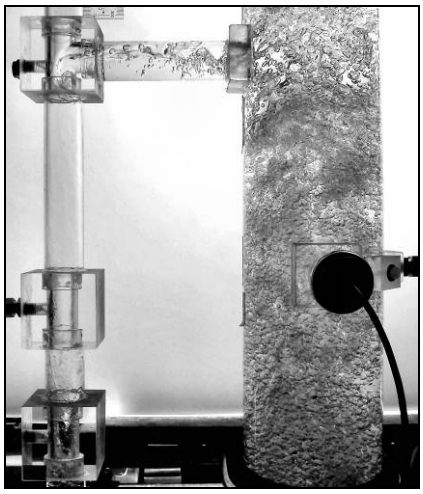
U_G = 17.0 cm/s

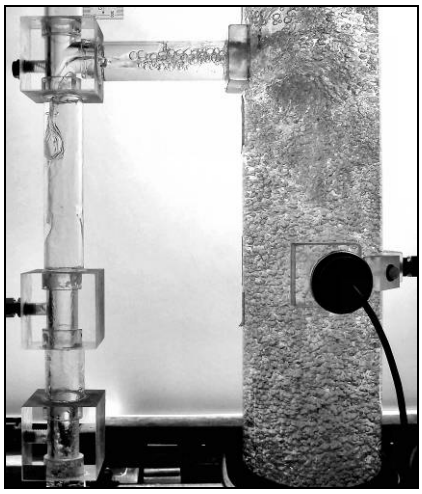
U_G = 17.0 cm/s

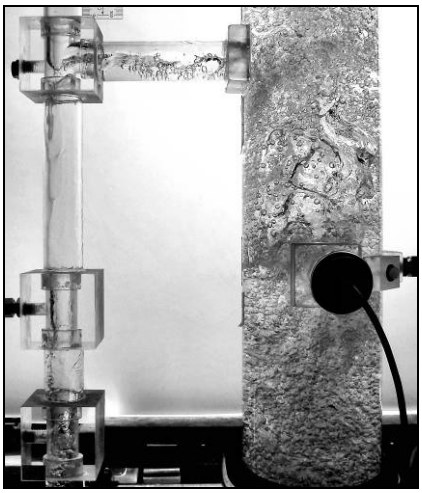
U_G = 18.0 cm/s

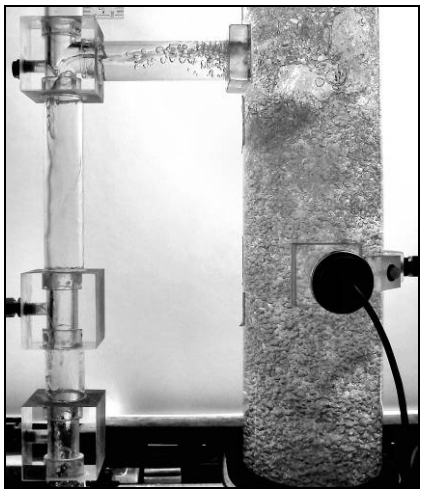
U_G = 18.0 cm/s

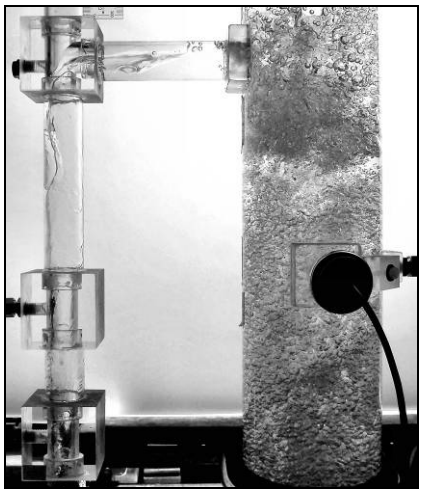
U_G = 18.0 cm/s

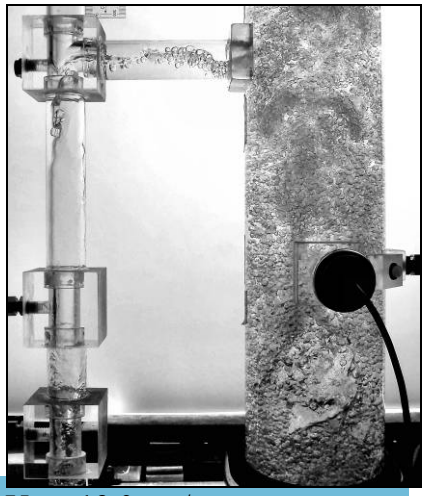
U_G = 19.0 cm/s

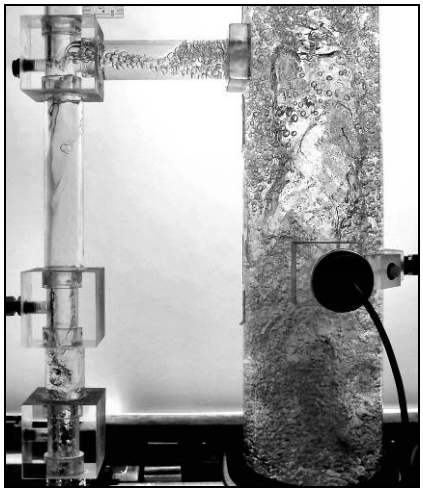
U_G = 19.0 cm/s

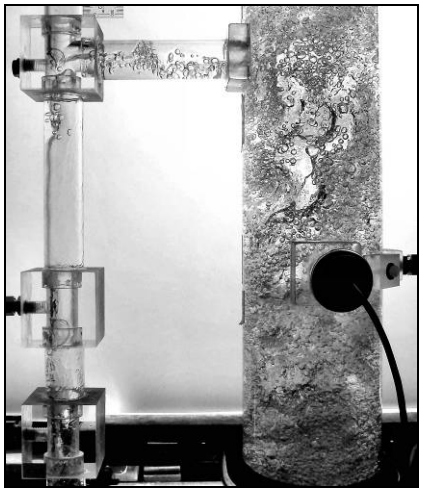
U_G = 19.0 cm/s

Test Conditions:
A = 2.22%
Closed Vent Mode
Upper Horizontal Connector

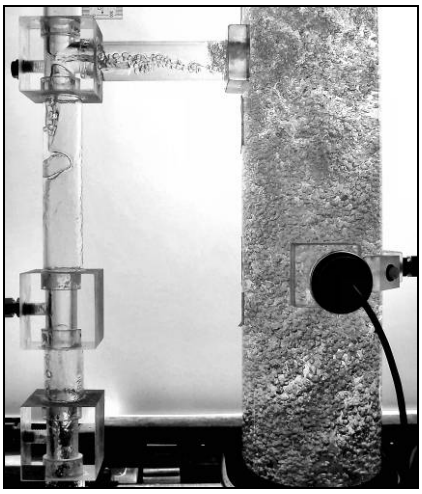
U_G = 20.0 cm/s

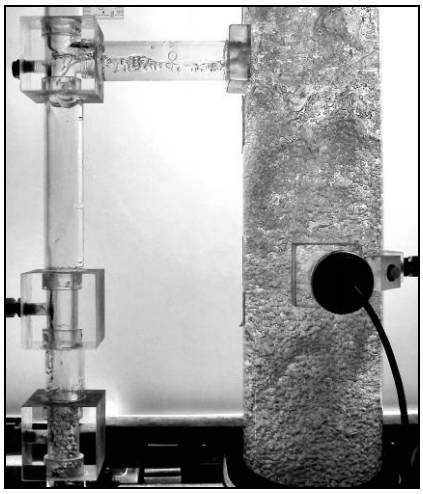
U_G = 20.0 cm/s

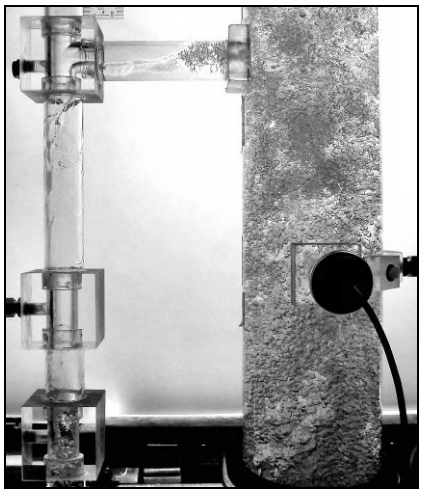
U_G = 20.0 cm/s

Test Conditions:
A = 0.62%
Open Vent Mode
Lower Horizontal Connector

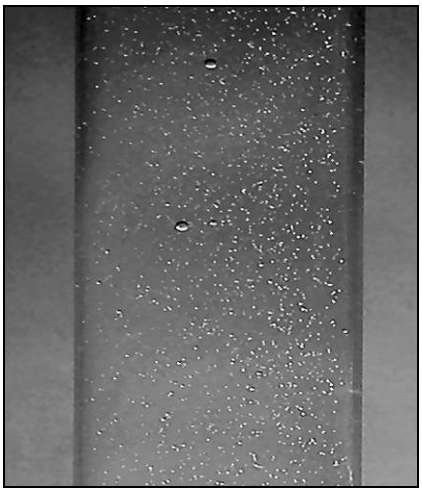
U_G = 0.5 cm/s

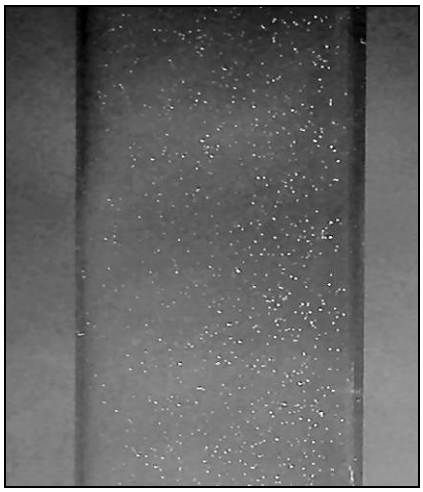
U_G = 1.0 cm/s

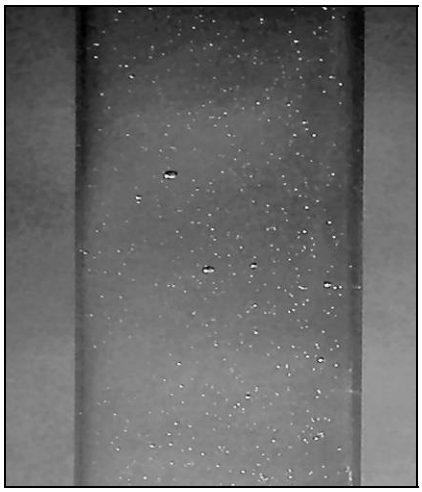
U_G = 1.5 cm/s

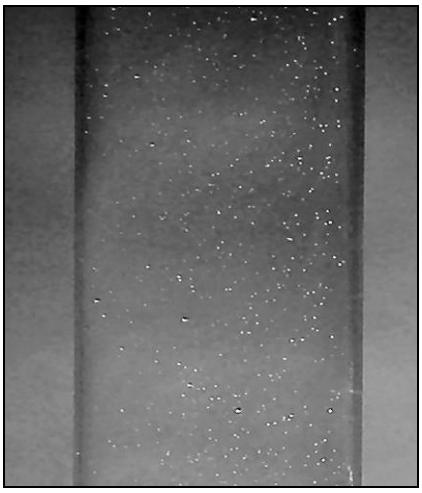
U_G = 2.0 cm/s

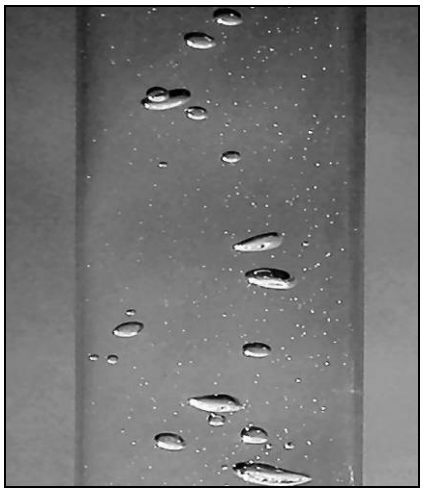
U_G = 2.5 cm/s

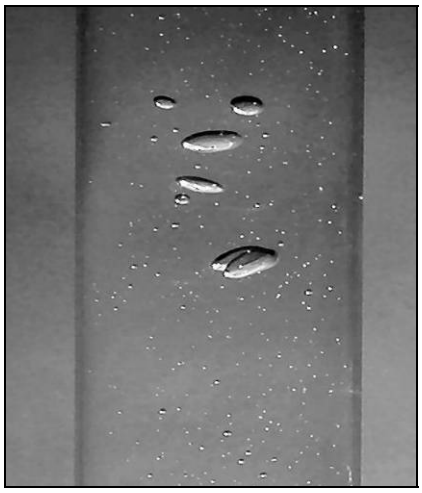
U_G = 3.0 cm/s

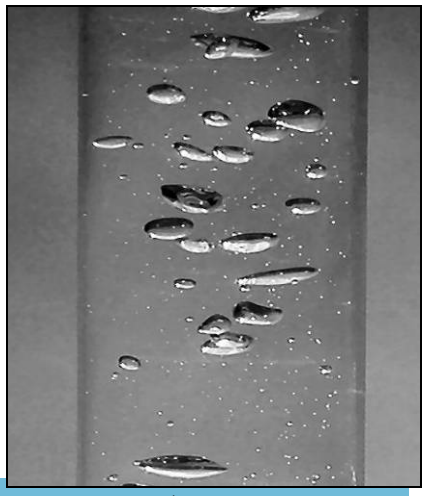
U_G = 3.5 cm/s

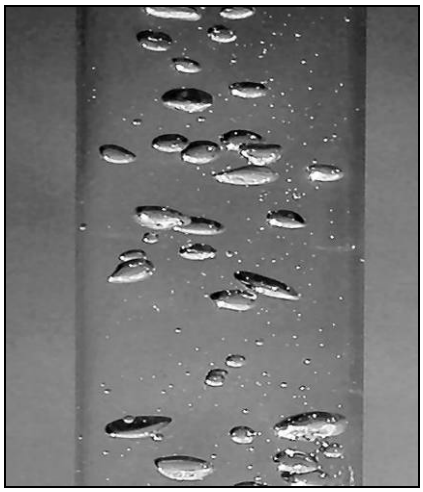
U_G = 4.0 cm/s

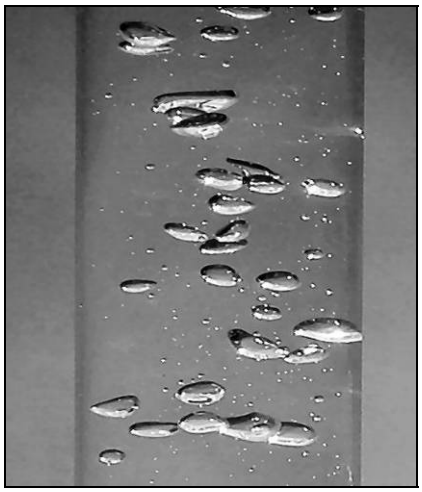
U_G = 4.5 cm/s

Test Conditions:
A = 0.62%
Open Vent Mode
Lower Horizontal Connector

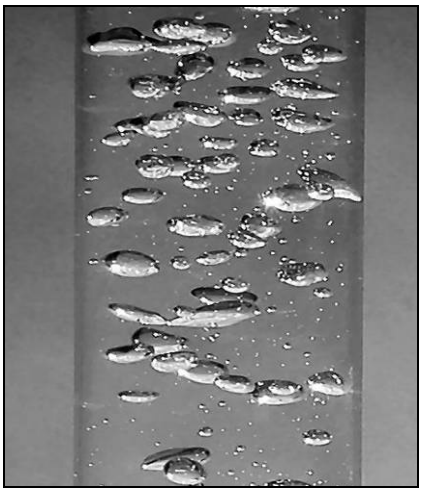
U_G = 5.0 cm/s

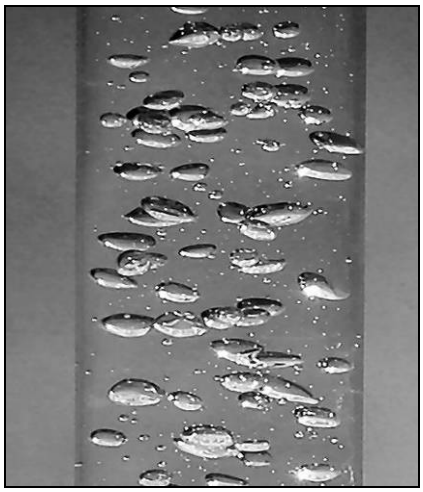
U_G = 6.0 cm/s

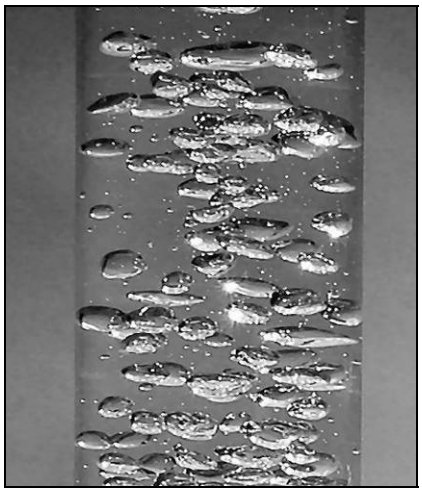
U_G = 7.0 cm/s

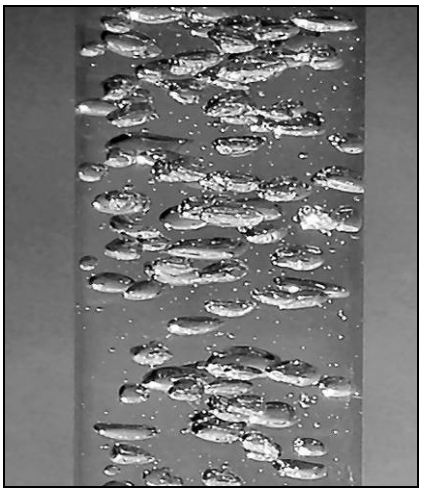
U_G = 8.0 cm/s

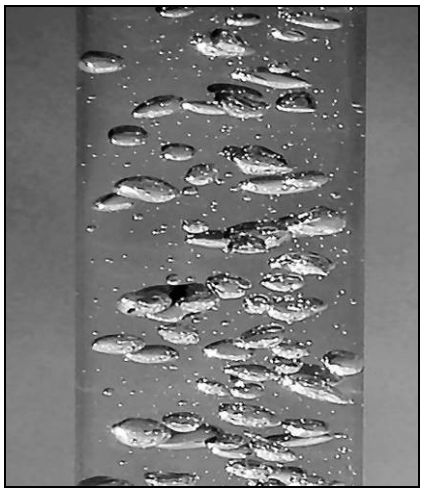
U_G = 9.0 cm/s

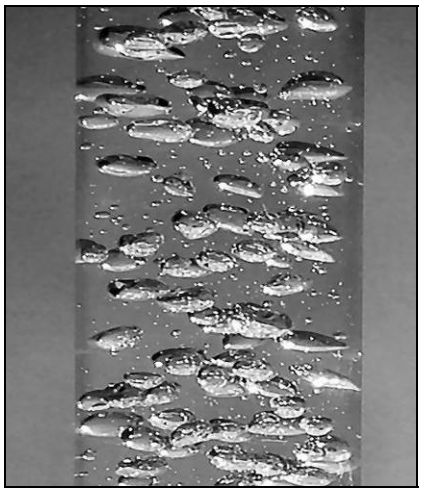
U_G = 10.0 cm/s

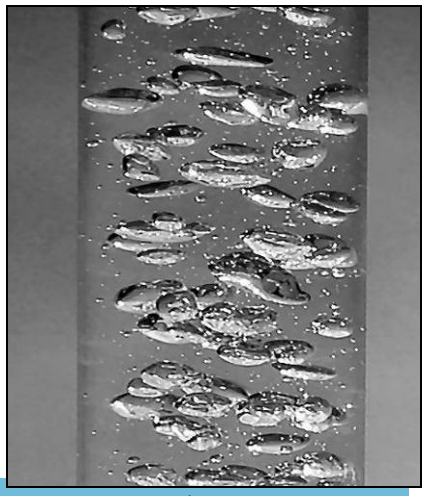
U_G = 11.0 cm/s

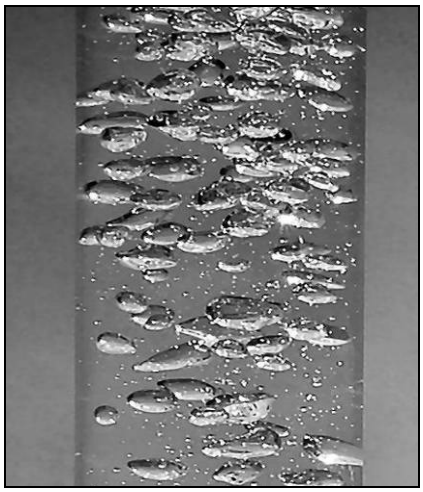
U_G = 12.0 cm/s

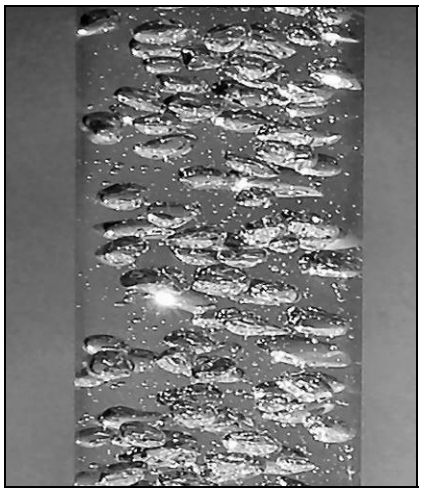
U_G = 13.0 cm/s

Test Conditions:
A = 0.62%
Open Vent Mode
Lower Horizontal Connector

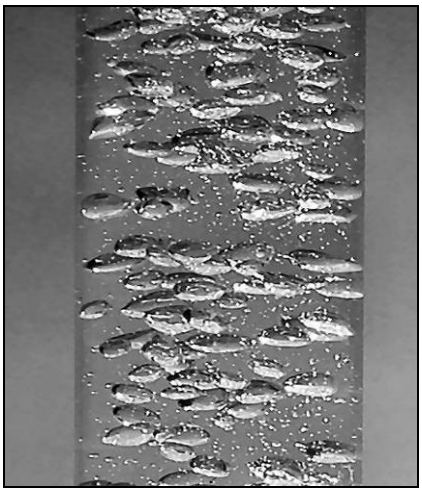
U_G = 14.0 cm/s

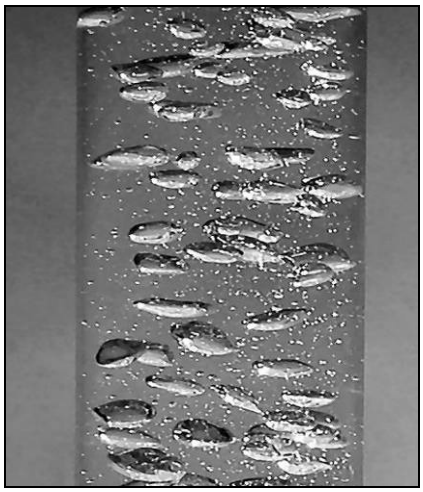
U_G = 15.0 cm/s

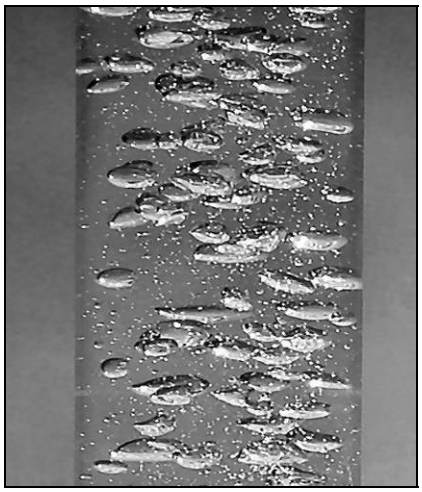
U_G = 16.0 cm/s

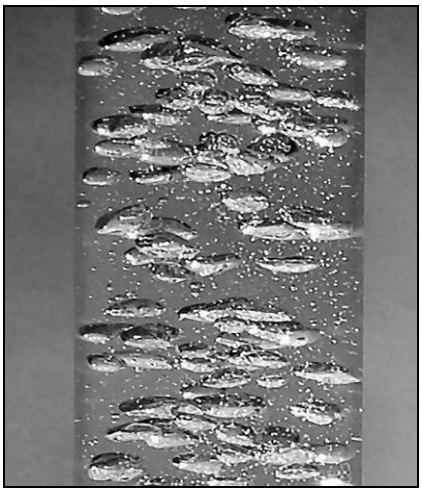
U_G = 17.0 cm/s

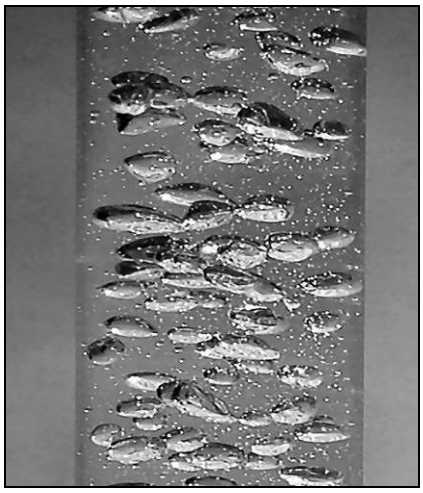
U_G = 18.0 cm/s

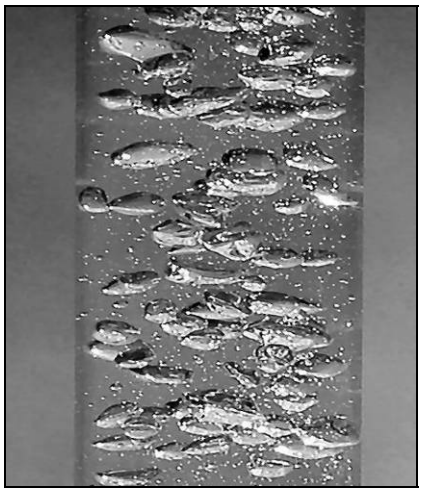
U_G = 19.0 cm/s

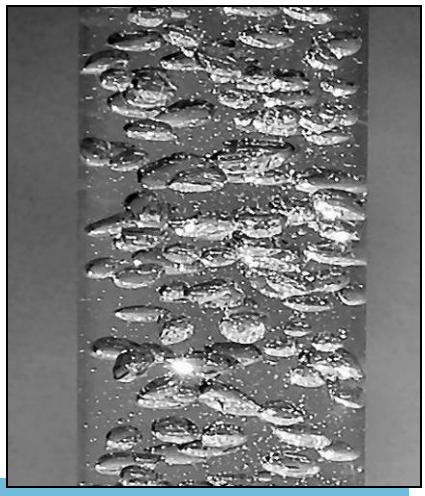

Test Conditions:
A = 0.62%
Closed Vent Mode
Lower Horizontal Connector

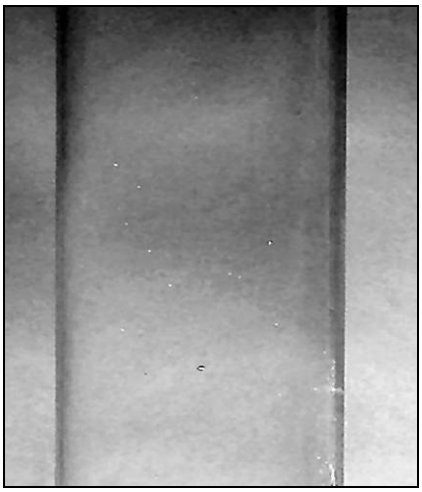
U_G = 0.5 cm/s

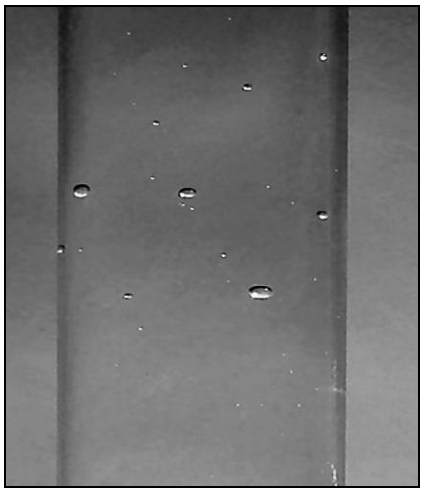
U_G = 1.0 cm/s

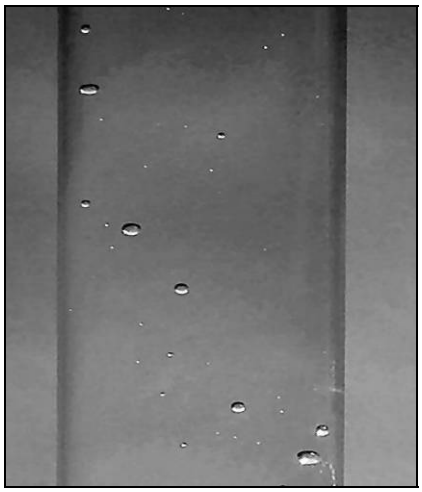
U_G = 1.5 cm/s

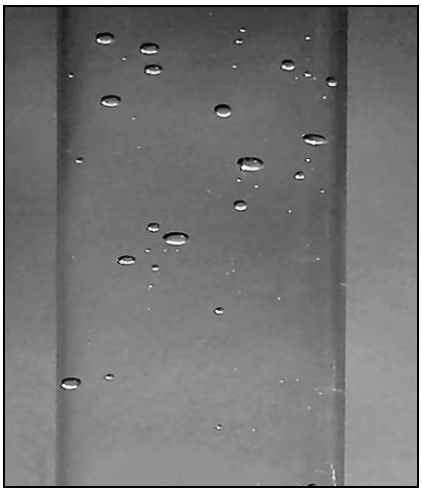
U_G = 2.0 cm/s

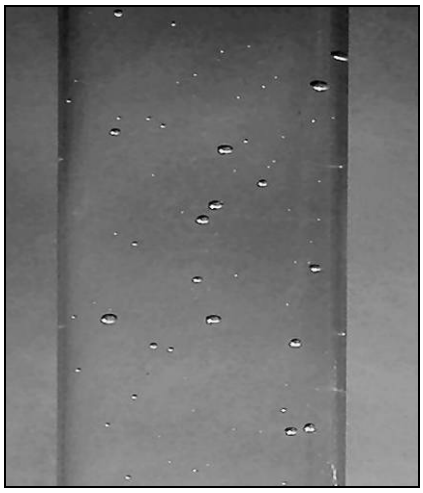
U_G = 2.5 cm/s

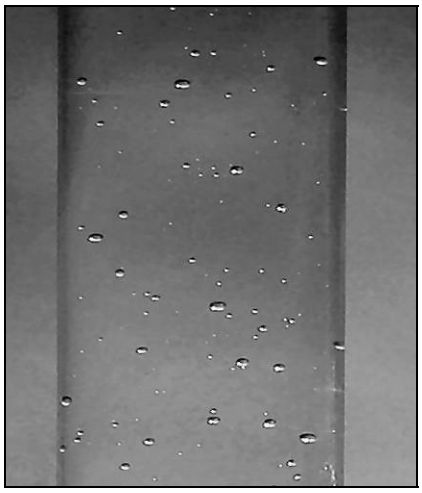
U_G = 3.0 cm/s

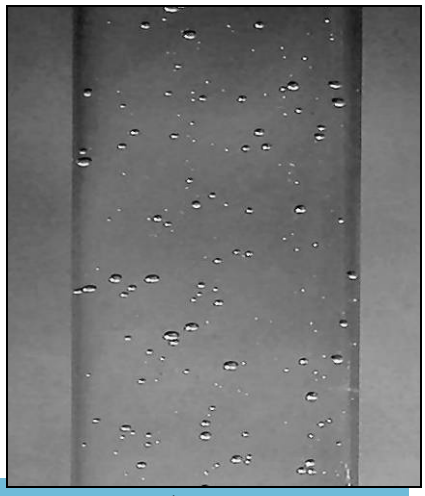
U_G = 3.5 cm/s

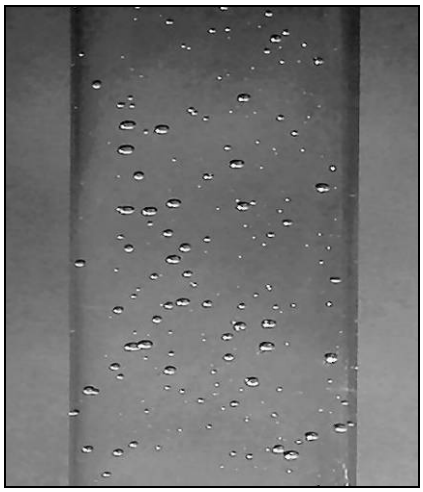
U_G = 4.0 cm/s

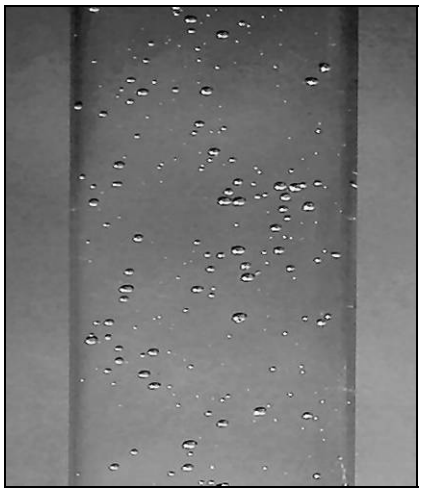
U_G = 4.5 cm/s

Test Conditions:
A = 0.62%
Closed Vent Mode
Lower Horizontal Connector

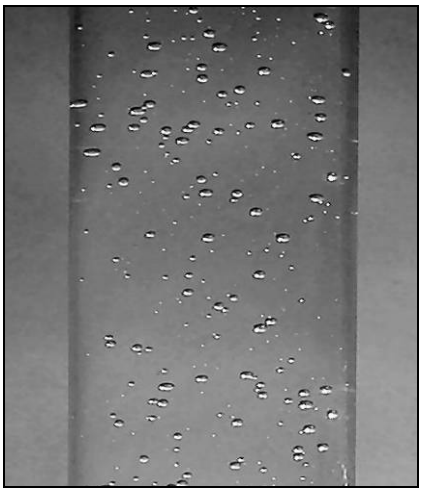
U_G = 5.0 cm/s

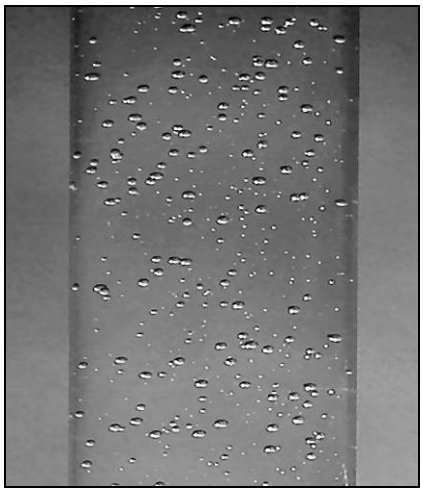
U_G = 6.0 cm/s

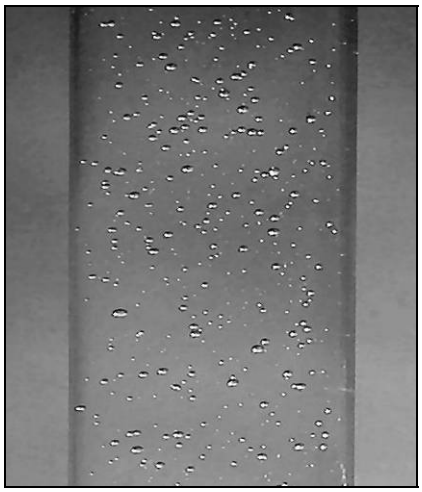
U_G = 7.0 cm/s

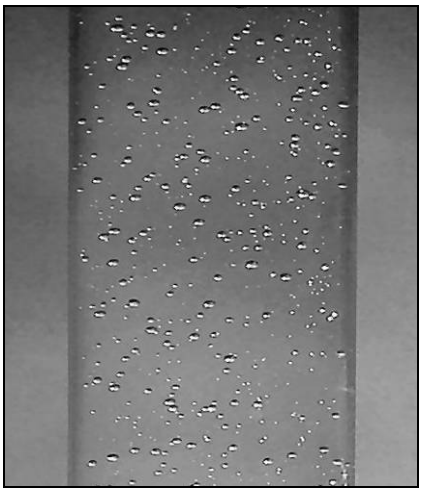
U_G = 8.0 cm/s

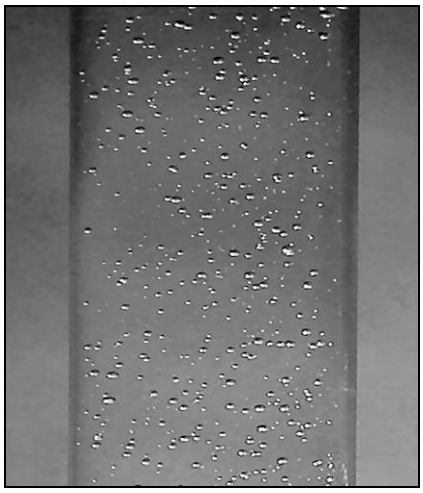
U_G = 9.0 cm/s

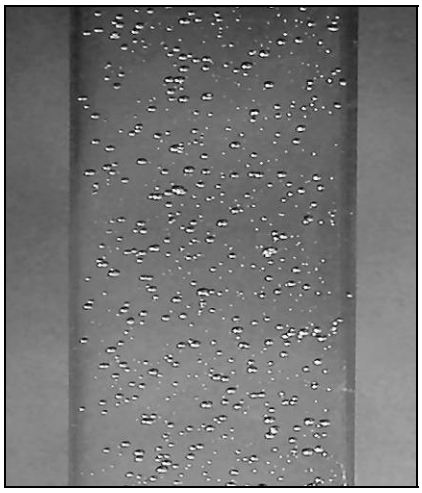
U_G = 10.0 cm/s

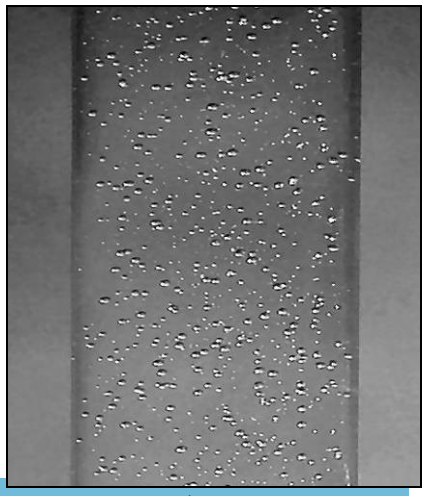
U_G = 11.0 cm/s

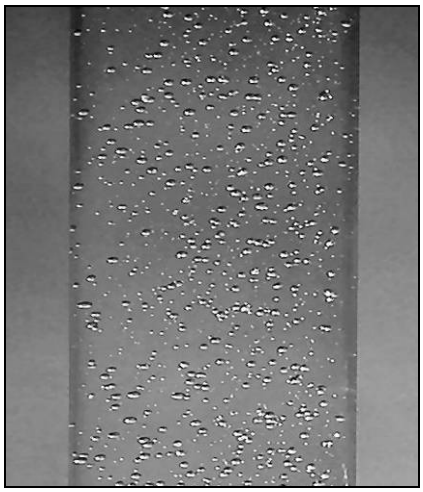
U_G = 12.0 cm/s

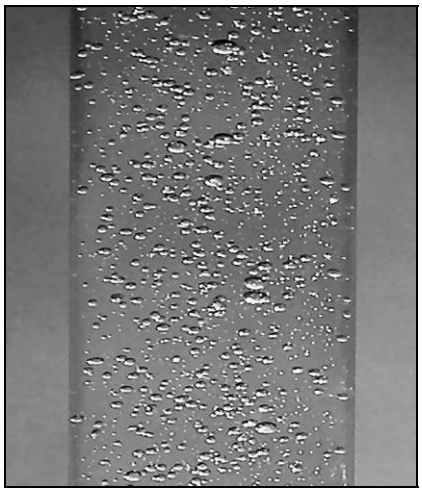
U_G = 13.0 cm/s

Test Conditions:
A = 0.62%
Closed Vent Mode
Lower Horizontal Connector

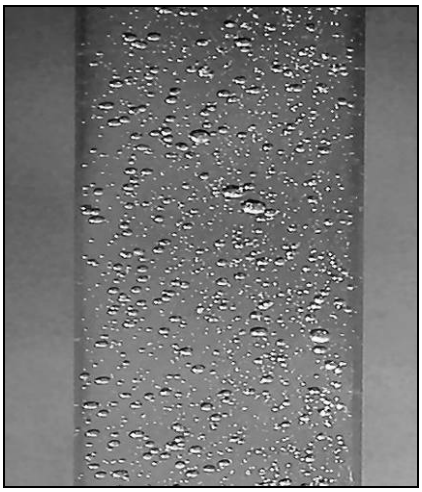
U_G = 14.0 cm/s

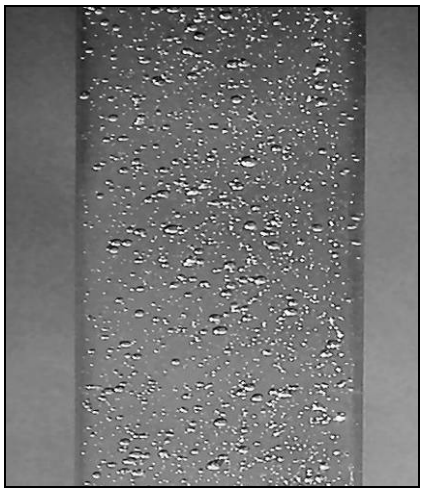
U_G = 15.0 cm/s

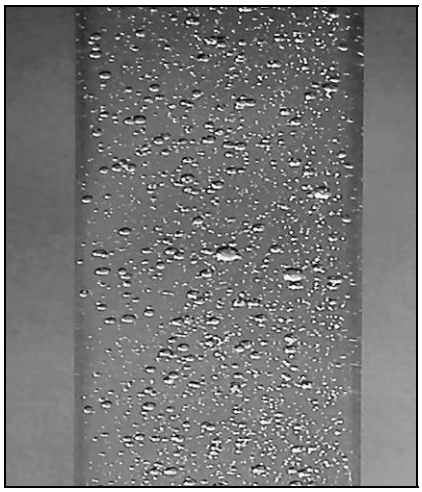
U_G = 16.0 cm/s

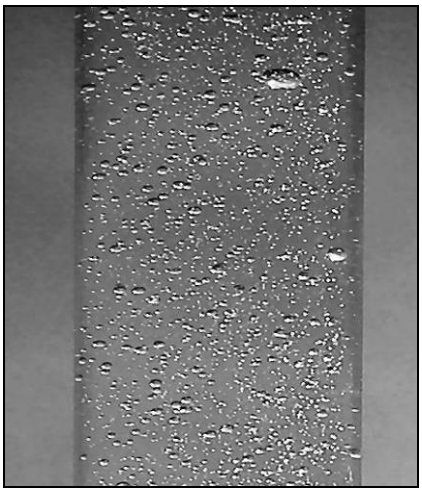
U_G = 17.0 cm/s

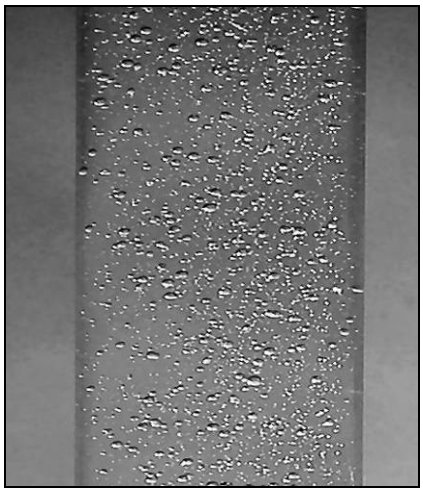
U_G = 18.0 cm/s

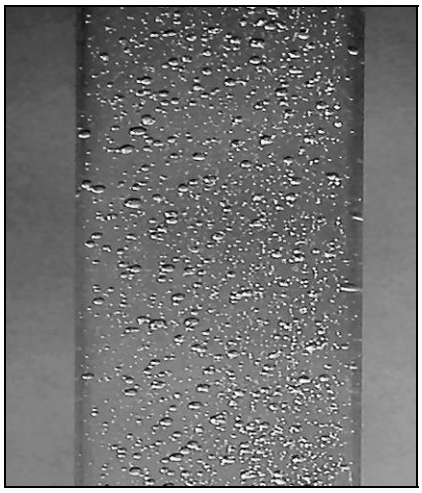
U_G = 19.0 cm/s

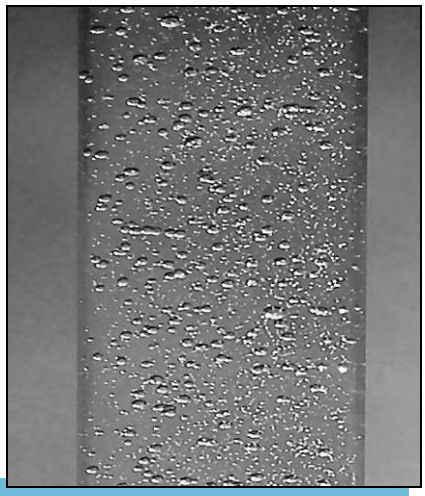

Test Conditions:
A = 0.99%
Open Vent Mode
Lower Horizontal Connector

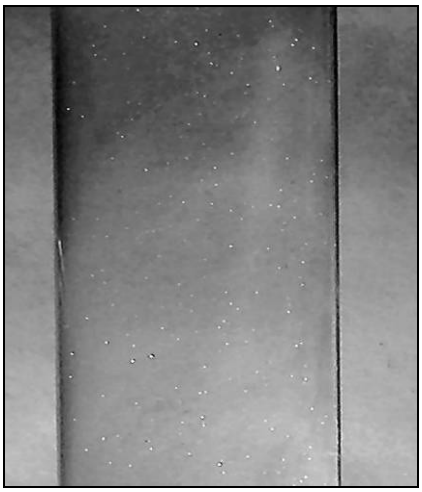
U_G = 0.5 cm/s

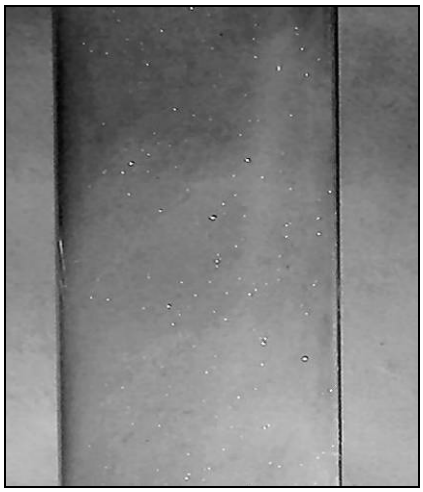
U_G = 1.0 cm/s

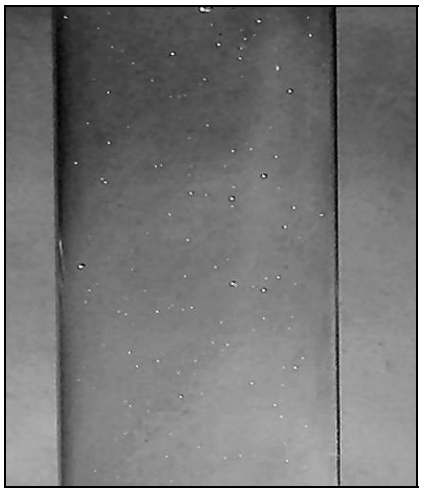
U_G = 1.5 cm/s

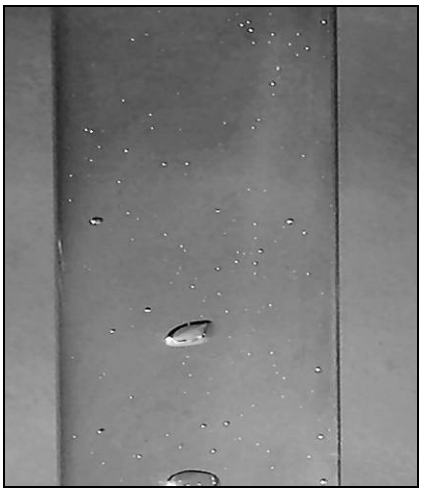
U_G = 2.0 cm/s

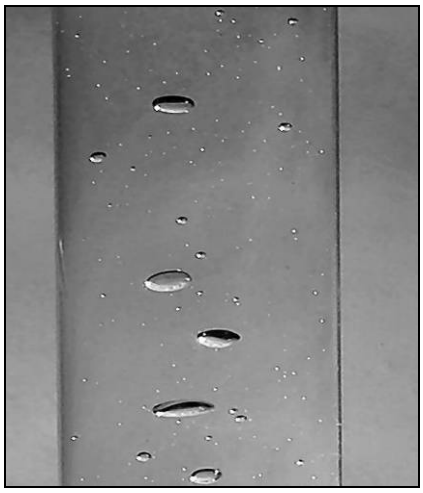
U_G = 2.5 cm/s


U_G = 3.0 cm/s

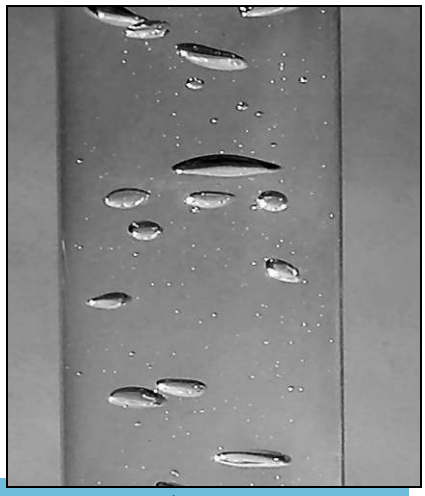
U_G = 3.5 cm/s

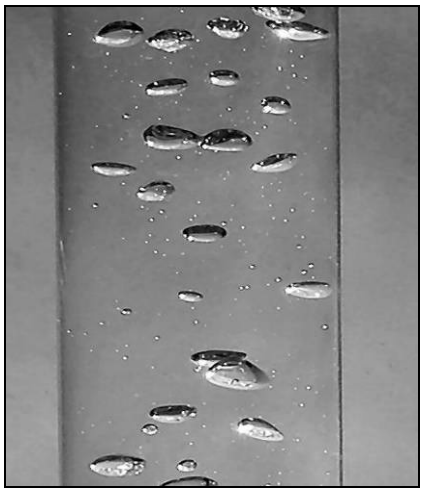
U_G = 4.0 cm/s

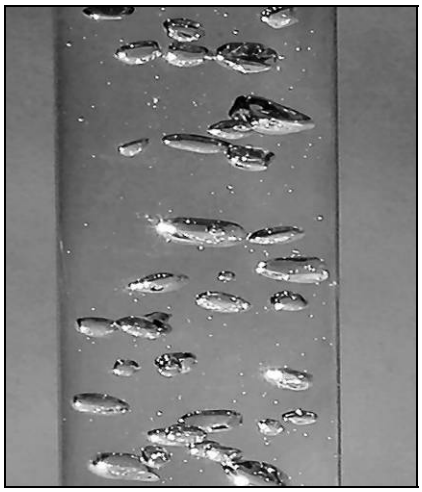
U_G = 4.5 cm/s

Test Conditions:
A = 0.99%
Open Vent Mode
Lower Horizontal Connector

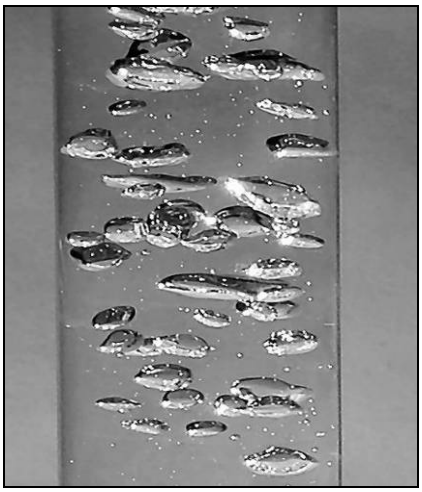
U_G = 5.0 cm/s

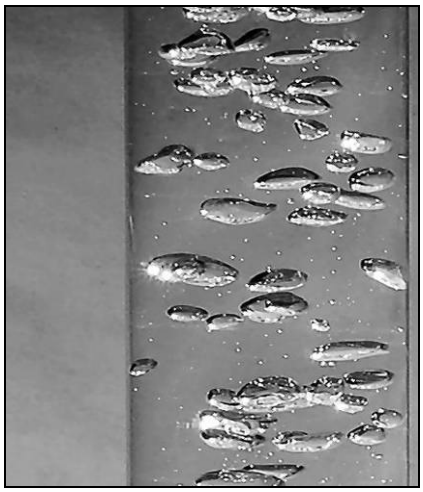
U_G = 6.0 cm/s

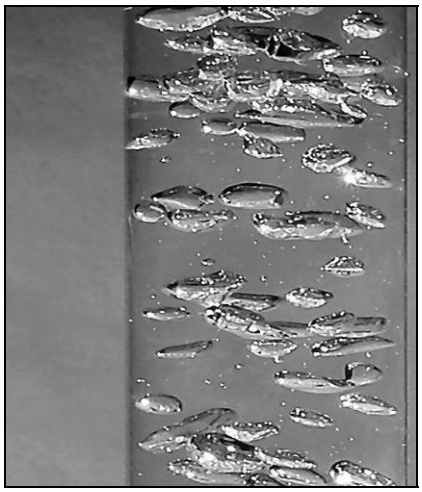
U_G = 7.0 cm/s

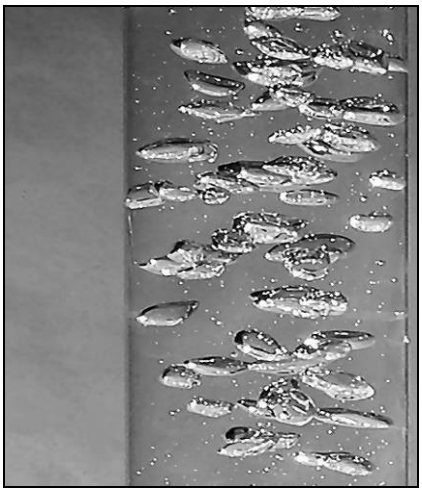
U_G = 8.0 cm/s

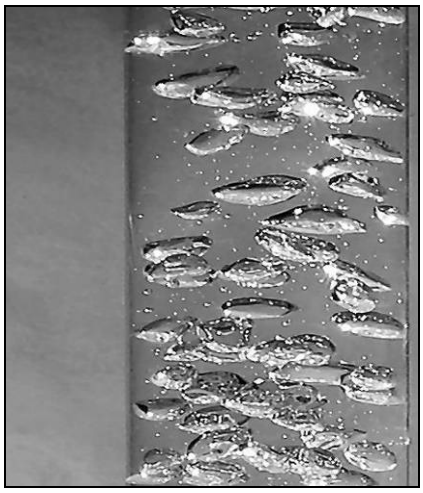
U_G = 9.0 cm/s

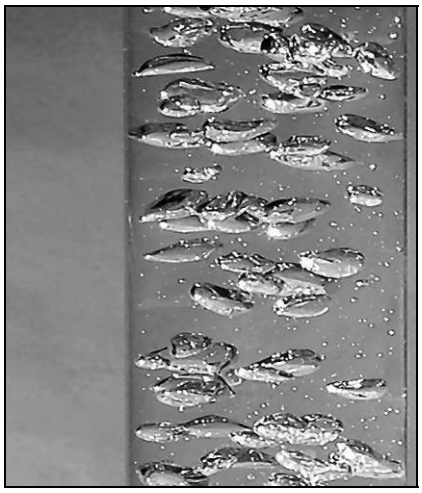
U_G = 10.0 cm/s

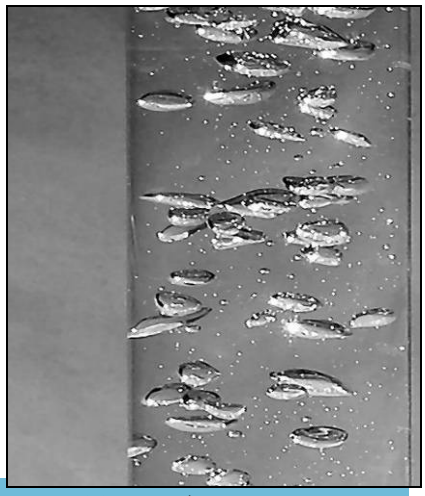
U_G = 11.0 cm/s


U_G = 12.0 cm/s

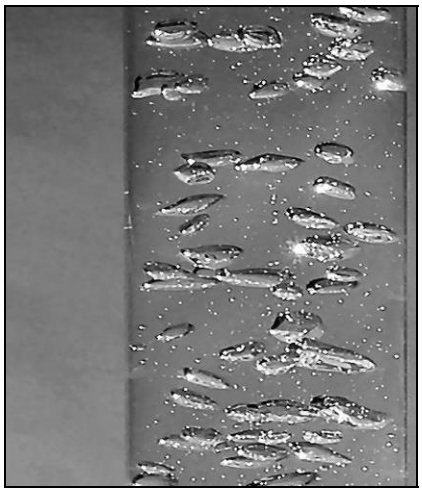
U_G = 13.0 cm/s

Test Conditions:
A = 0.99%
Open Vent Mode
Lower Horizontal Connector


U_G = 14.0 cm/s


U_G = 15.0 cm/s


U_G = 16.0 cm/s

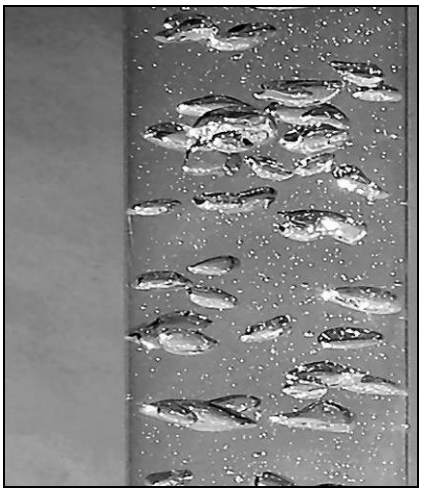
U_G = 17.0 cm/s


U_G = 18.0 cm/s

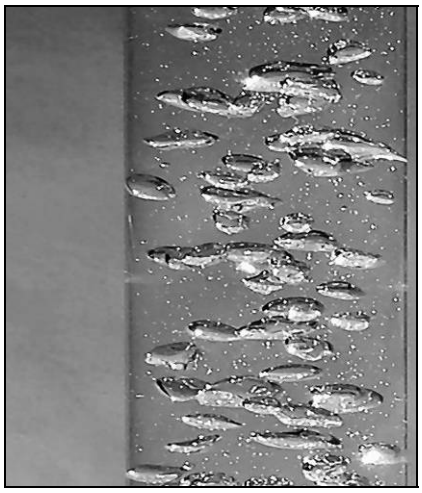
U_G = 19.0 cm/s

Test Conditions:
A = 0.99%
Closed Vent Mode
Lower Horizontal Connector

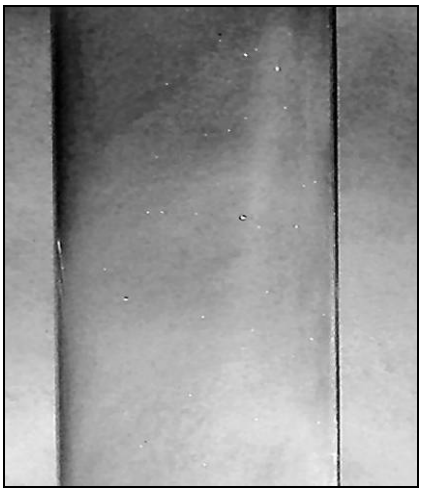
U_G = 0.5 cm/s

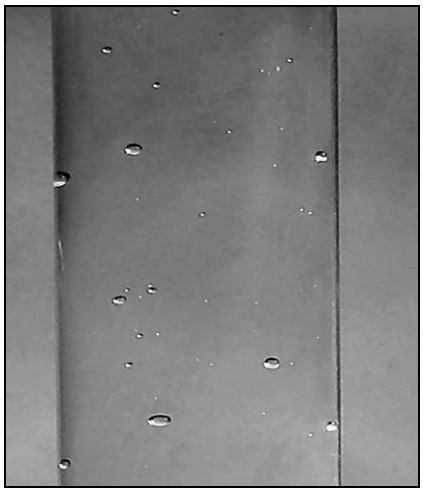
U_G = 1.0 cm/s

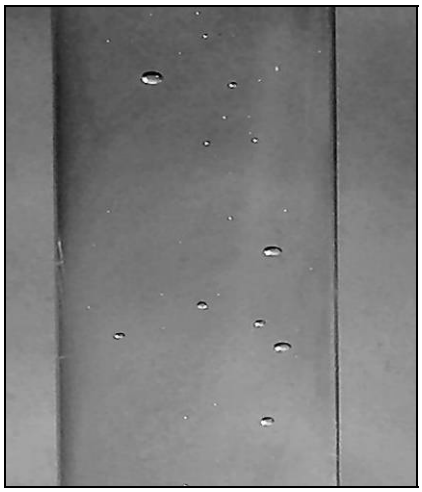
U_G = 1.5 cm/s

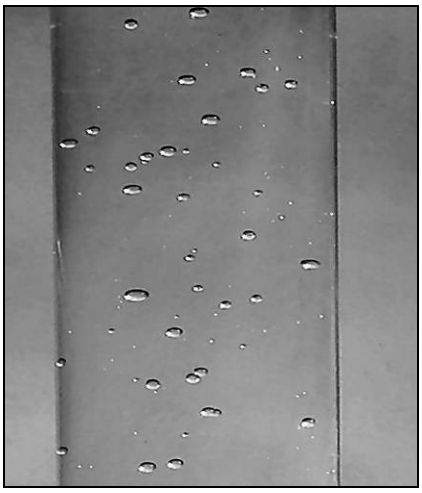
U_G = 2.0 cm/s

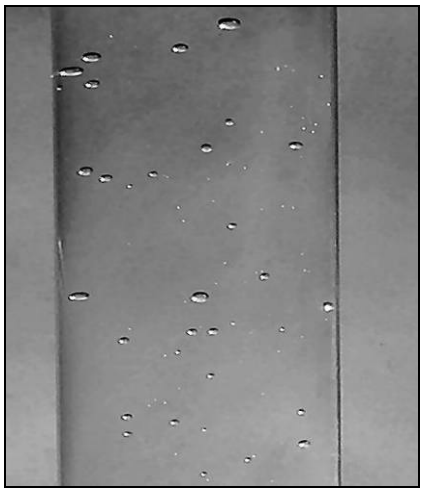
U_G = 2.5 cm/s

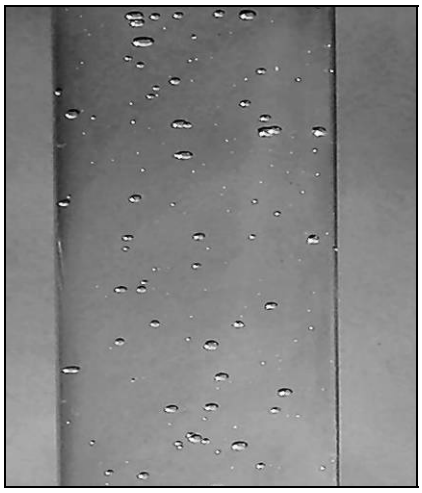
U_G = 3.0 cm/s

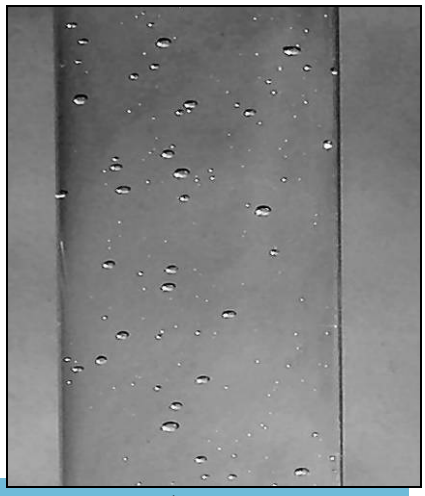
U_G = 3.5 cm/s

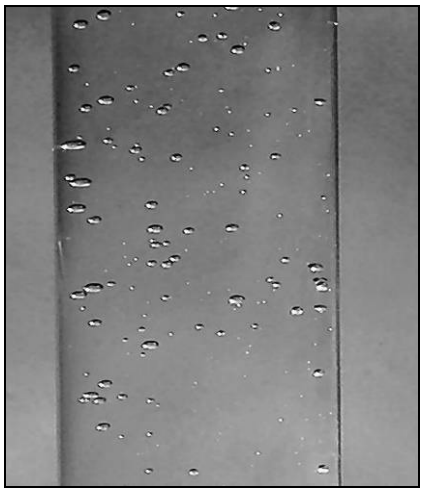
U_G = 4.0 cm/s

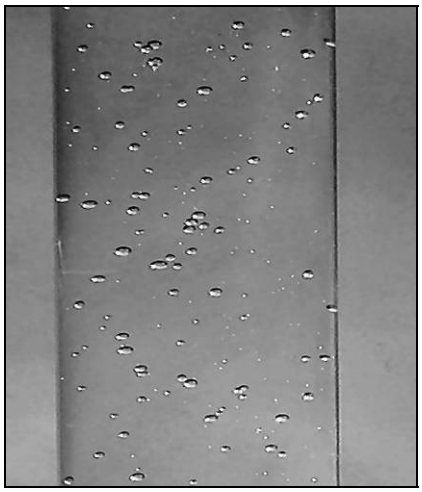
U_G = 4.5 cm/s

Test Conditions:
A = 0.99%
Closed Vent Mode
Lower Horizontal Connector


U_G = 5.0 cm/s


U_G = 6.0 cm/s

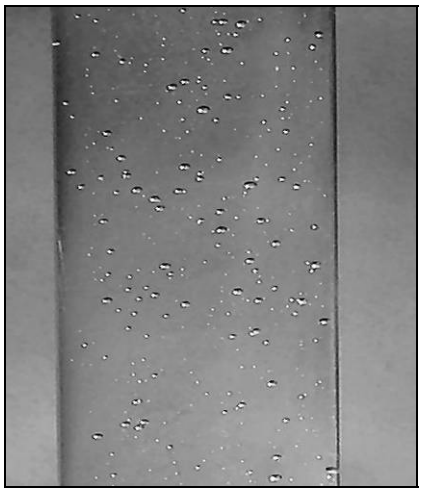
U_G = 7.0 cm/s

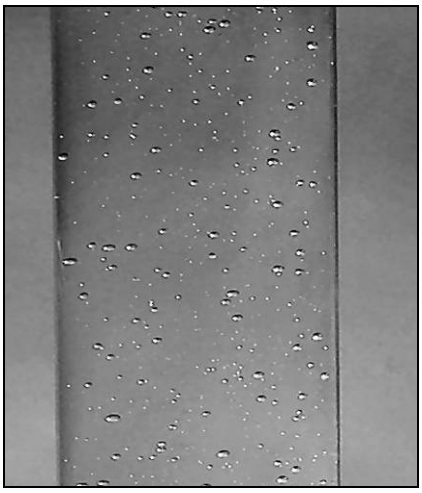
U_G = 8.0 cm/s

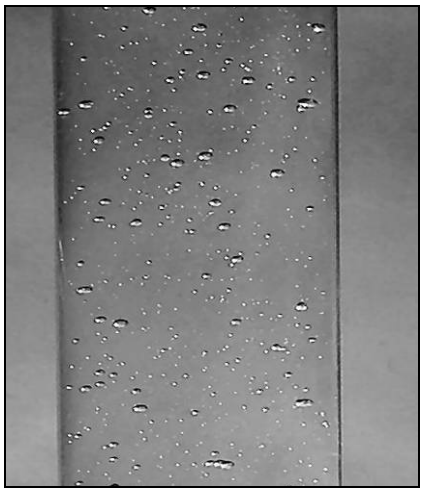
U_G = 9.0 cm/s

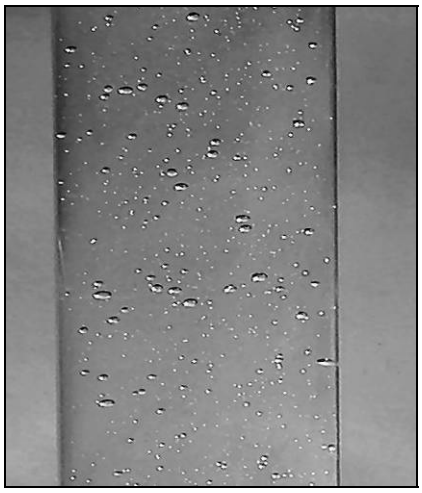
U_G = 10.0 cm/s

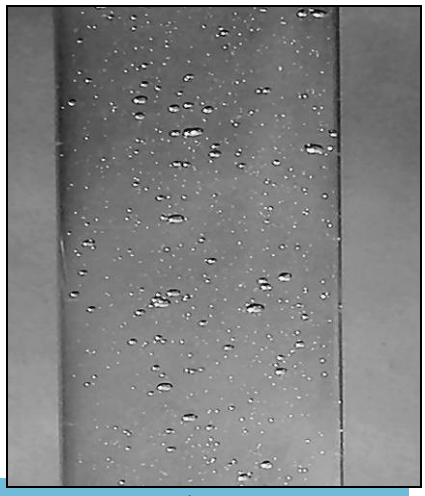
U_G = 11.0 cm/s

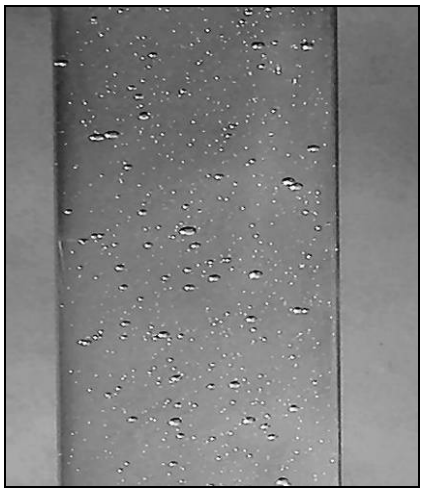
U_G = 12.0 cm/s

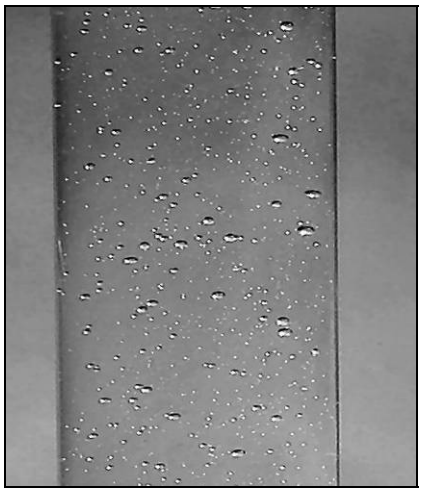
U_G = 13.0 cm/s

Test Conditions:
A = 0.99%
Closed Vent Mode
Lower Horizontal Connector

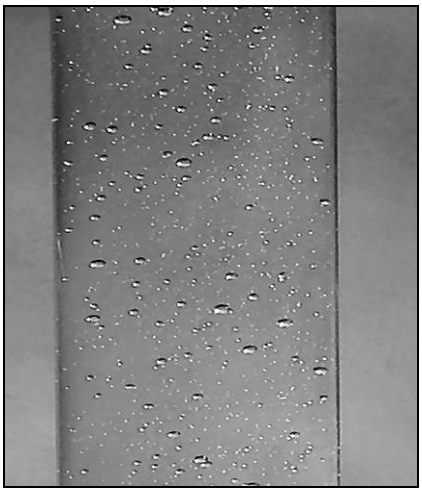
U_G = 14.0 cm/s

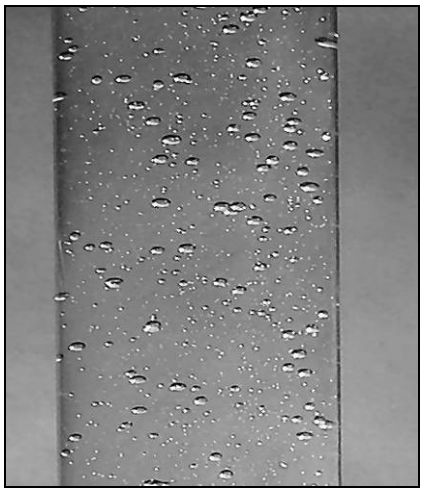
U_G = 15.0 cm/s

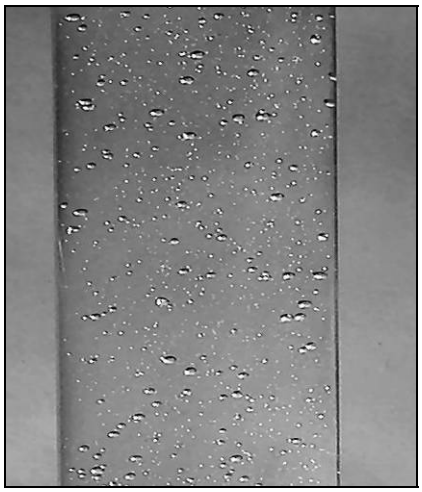
U_G = 16.0 cm/s

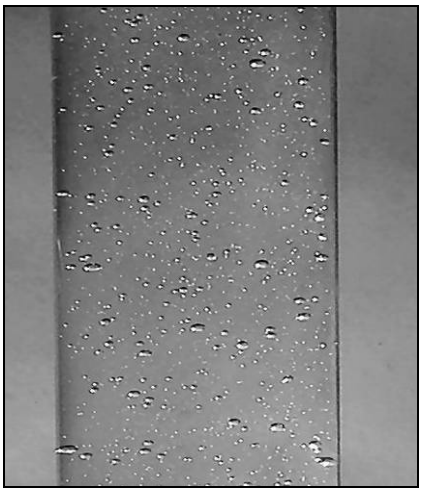
U_G = 17.0 cm/s


U_G = 18.0 cm/s

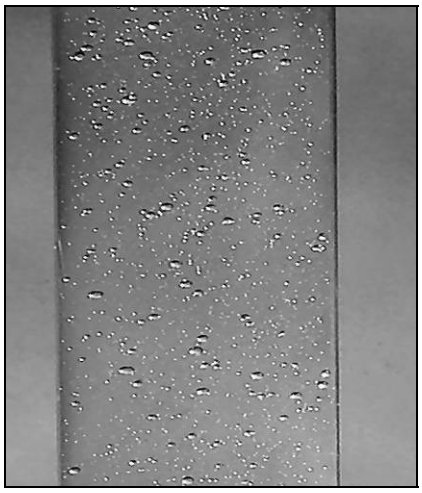
U_G = 19.0 cm/s

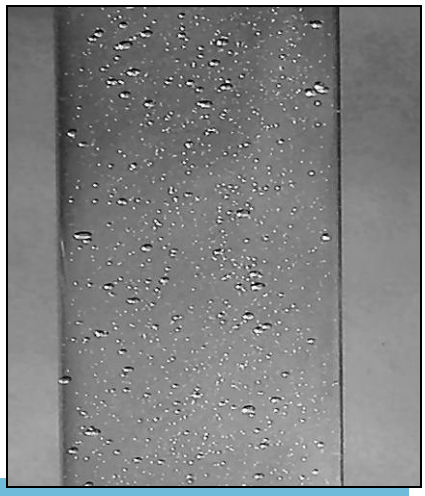

Test Conditions:
A = 2.22%
Open Vent Mode
Lower Horizontal Connector

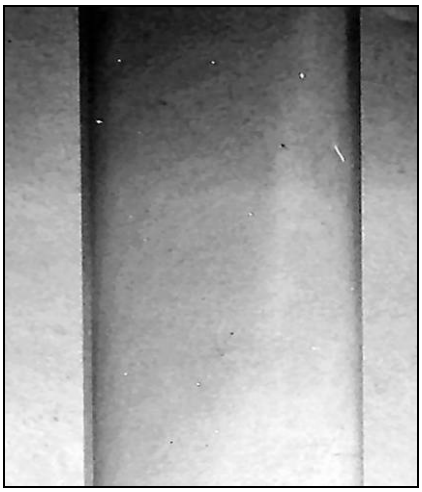
U_G = 0.5 cm/s

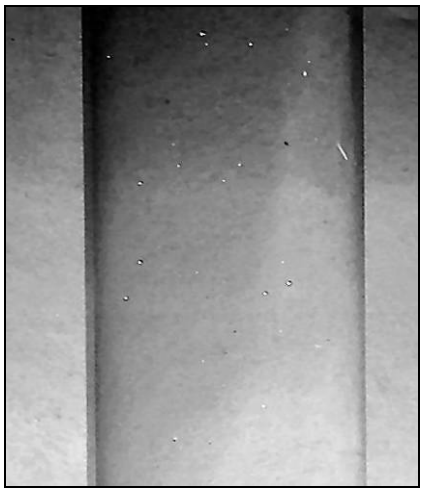
U_G = 1.0 cm/s

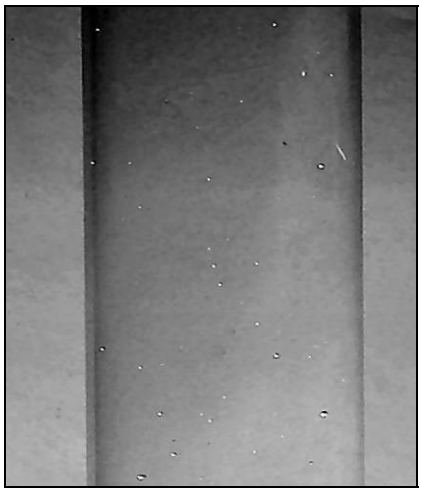
U_G = 1.5 cm/s

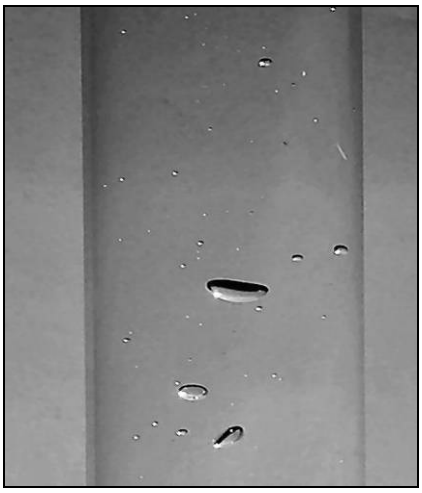
U_G = 2.0 cm/s

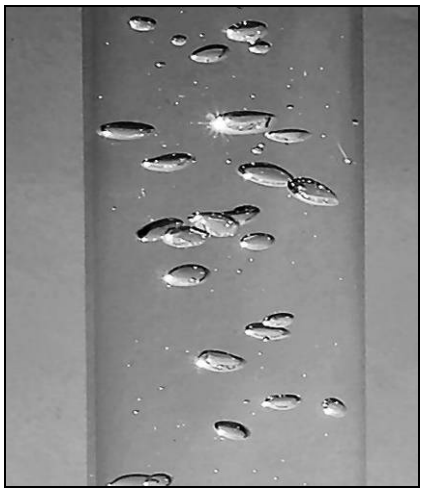
U_G = 2.5 cm/s

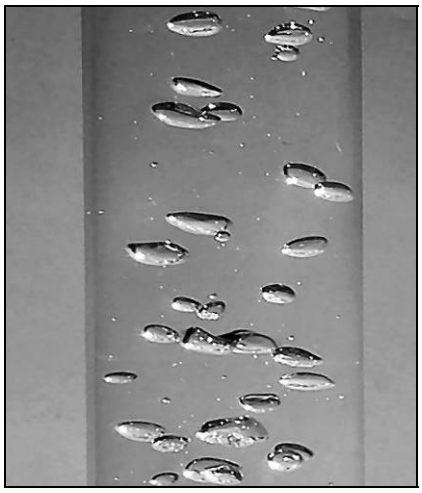
U_G = 3.0 cm/s

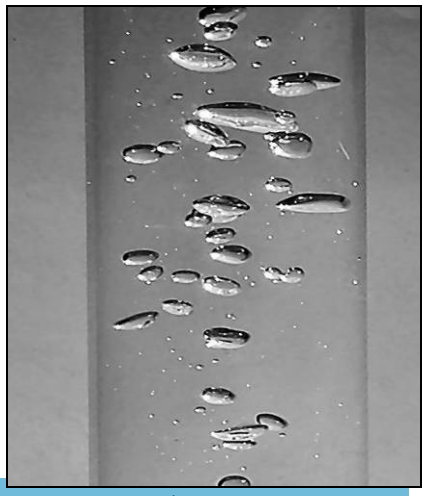
U_G = 3.5 cm/s

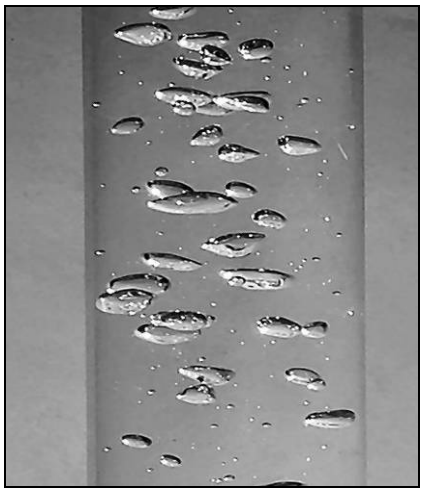
U_G = 4.0 cm/s

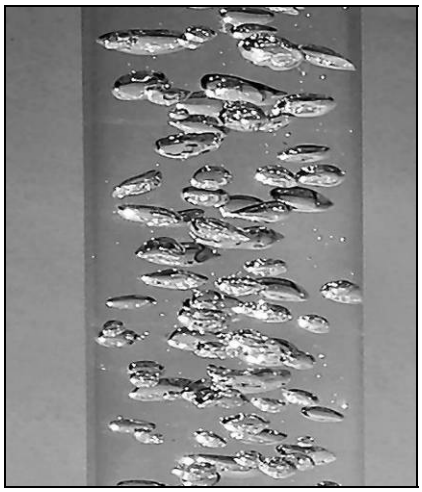
U_G = 4.5 cm/s

Test Conditions:
A = 2.22%
Open Vent Mode
Lower Horizontal Connector

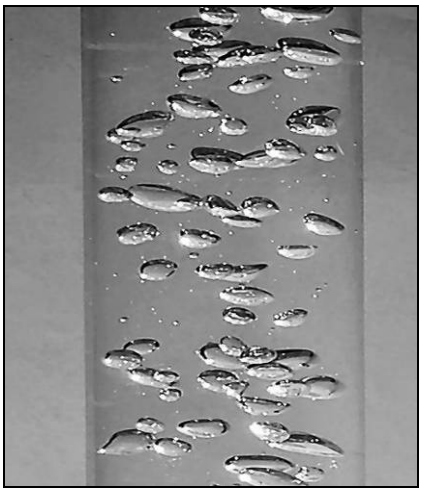
U_G = 5.0 cm/s

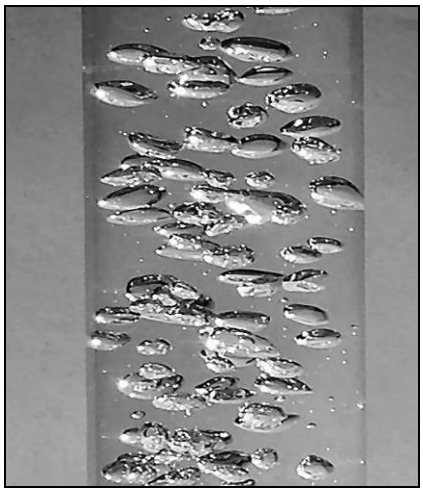
U_G = 6.0 cm/s

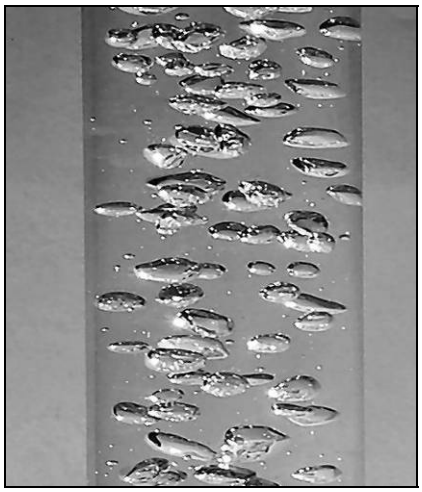
U_G = 7.0 cm/s

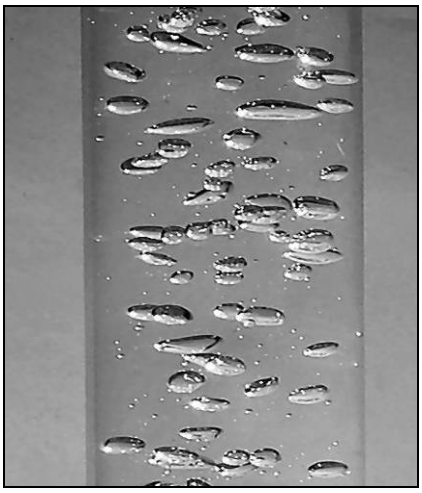
U_G = 8.0 cm/s

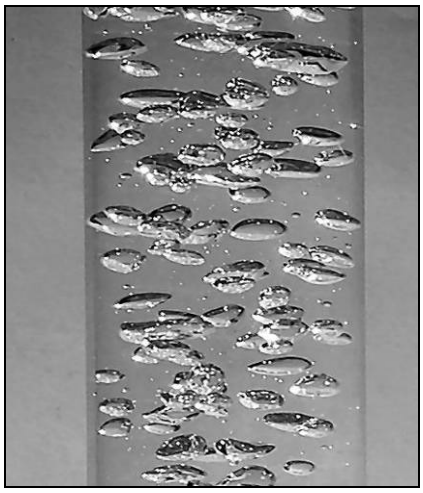
U_G = 9.0 cm/s

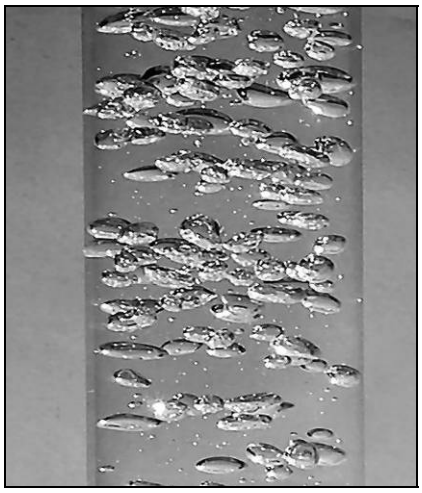
U_G = 10.0 cm/s

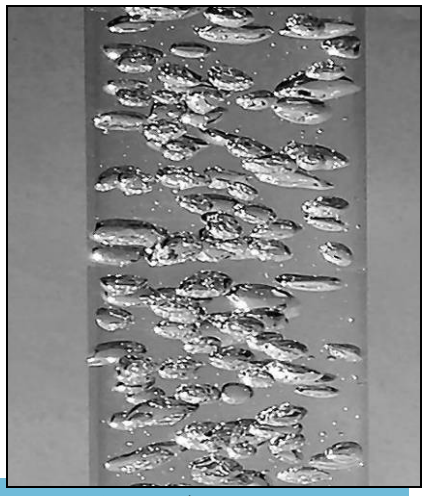
U_G = 11.0 cm/s

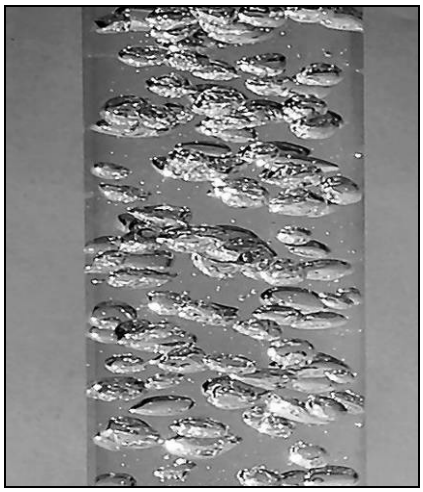
U_G = 12.0 cm/s

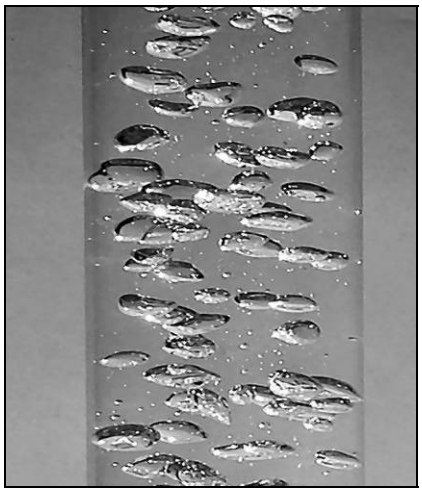
U_G = 13.0 cm/s

Test Conditions:
A = 2.22%
Open Vent Mode
Lower Horizontal Connector

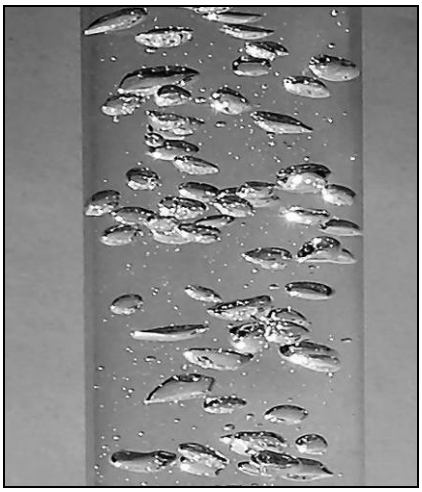
U_G = 14.0 cm/s

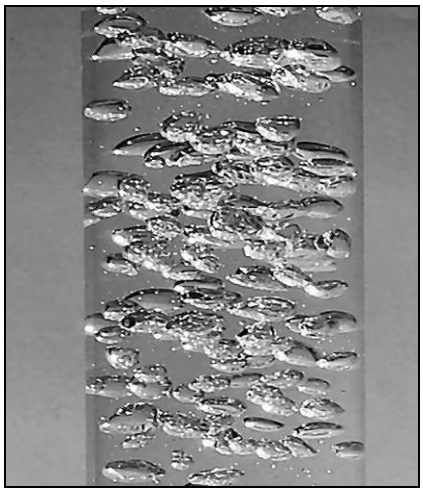
U_G = 15.0 cm/s

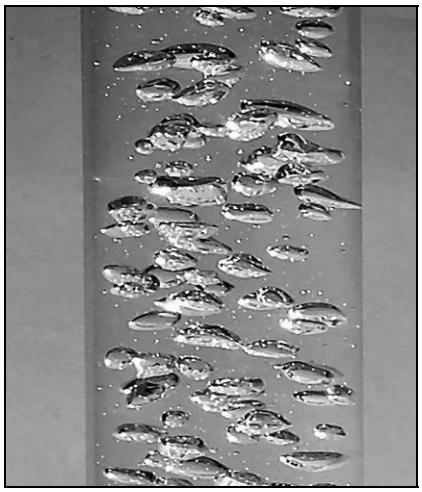
U_G = 16.0 cm/s

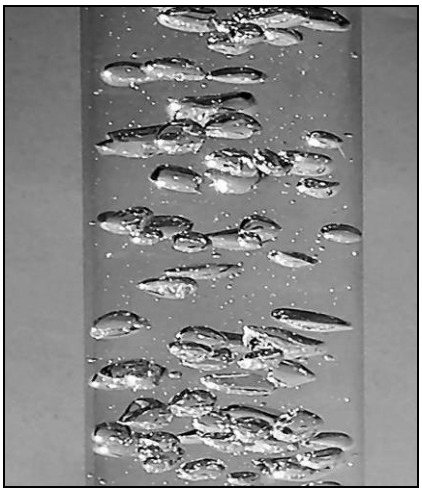
U_G = 17.0 cm/s

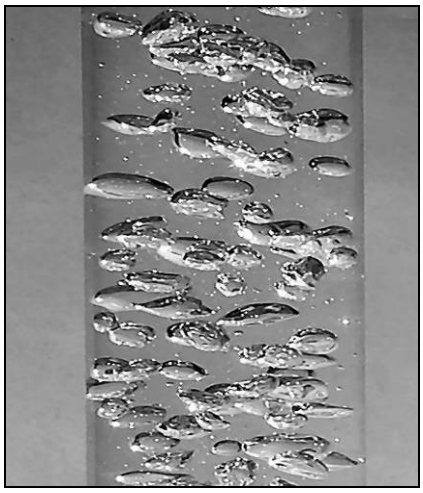
U_G = 18.0 cm/s

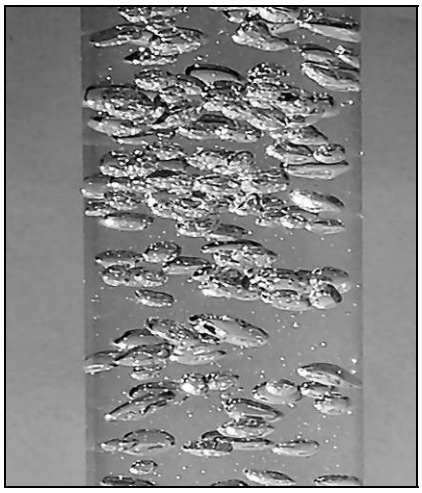
U_G = 19.0 cm/s

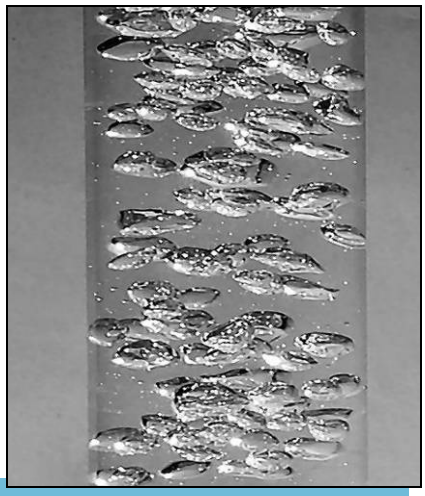

Test Conditions:
A = 2.22%
Closed Vent Mode
Lower Horizontal Connector

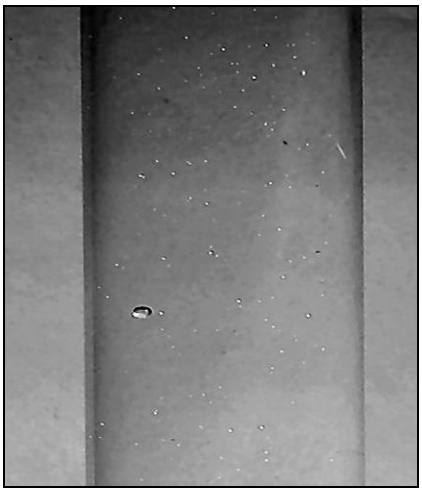
U_G = 0.5 cm/s

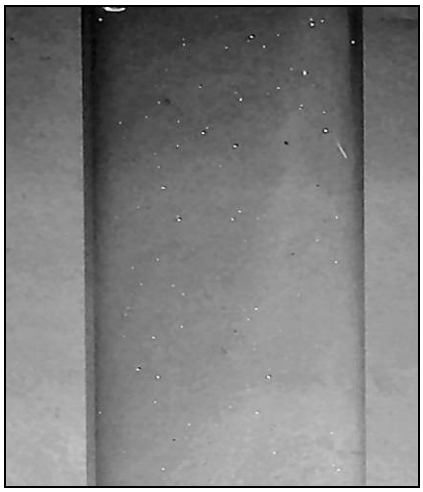
U_G = 1.0 cm/s

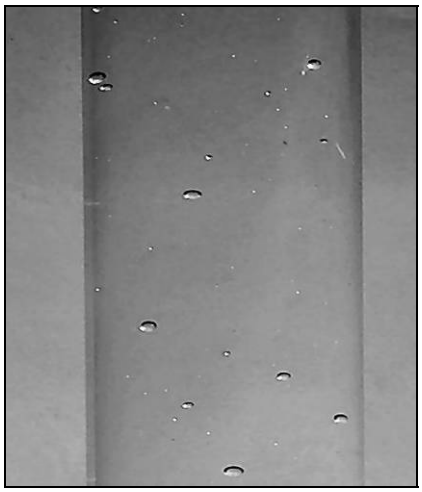
U_G = 1.5 cm/s

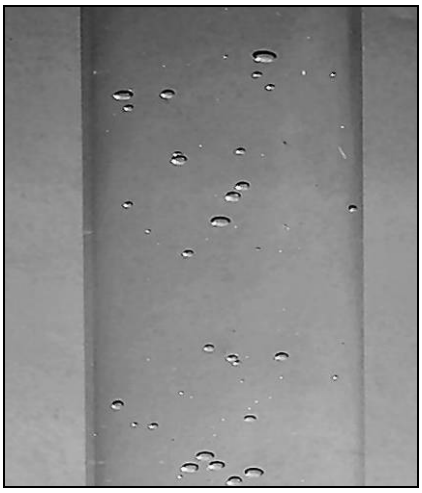
U_G = 2.0 cm/s

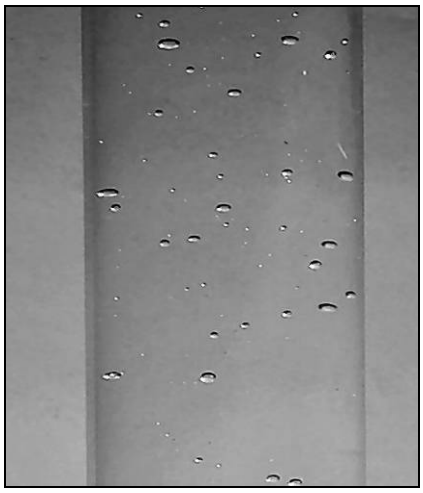
U_G = 2.5 cm/s

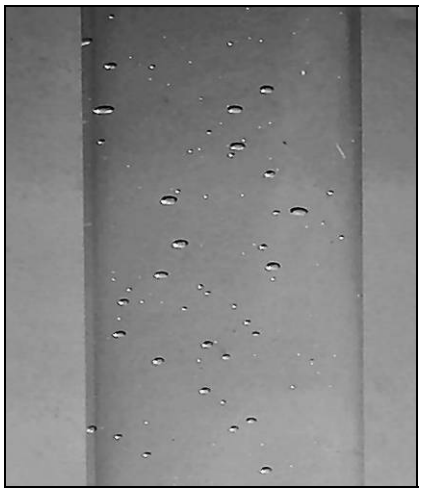
U_G = 3.0 cm/s

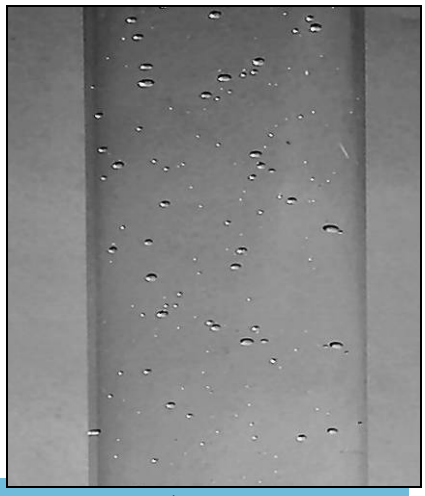
U_G = 3.5 cm/s

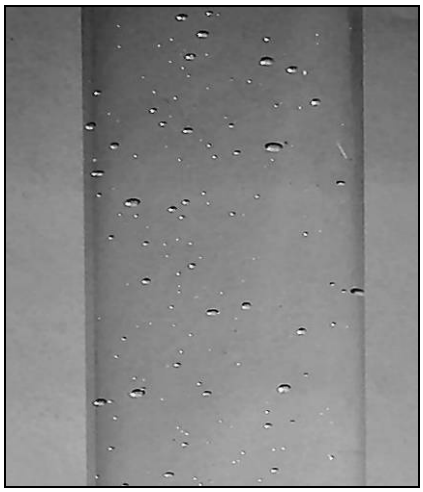
U_G = 4.0 cm/s

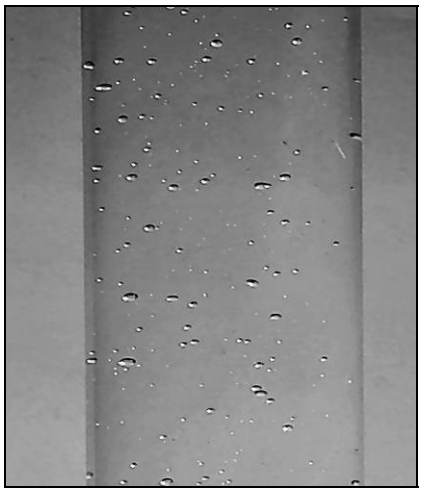
U_G = 4.5 cm/s

Test Conditions:
A = 2.22%
Closed Vent Mode
Lower Horizontal Connector

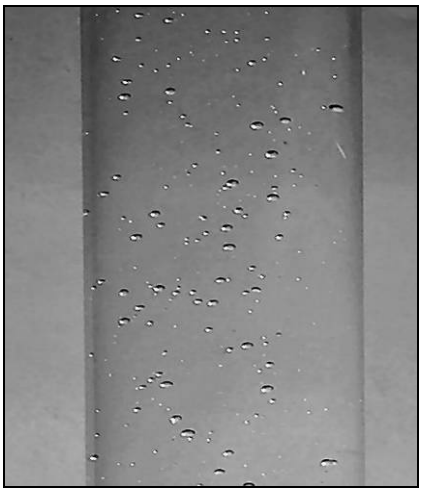
U_G = 5.0 cm/s

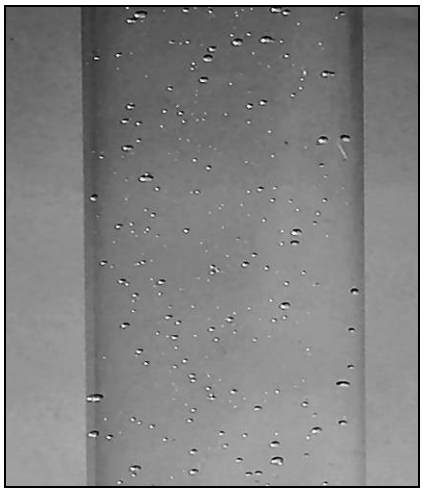
U_G = 6.0 cm/s

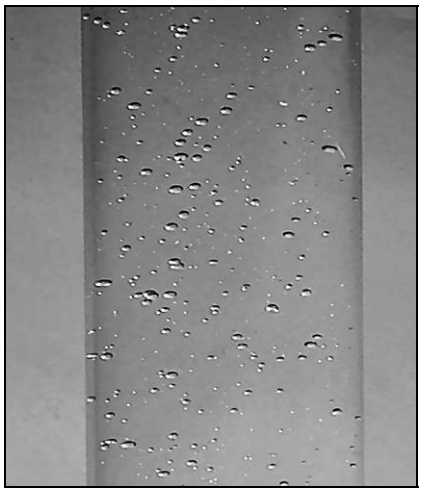
U_G = 7.0 cm/s

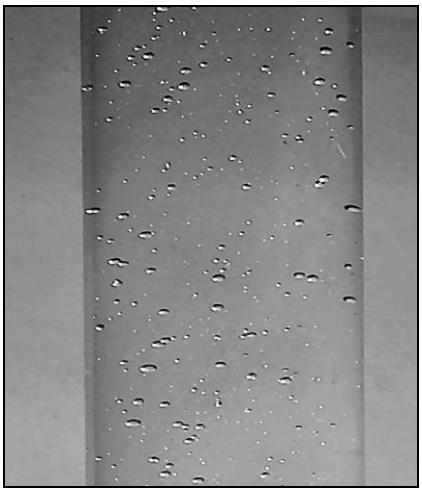
U_G = 8.0 cm/s

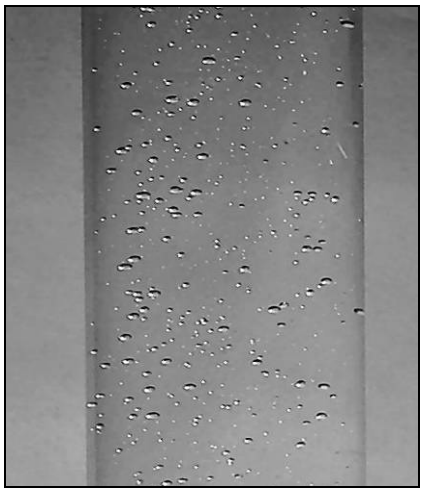
U_G = 9.0 cm/s

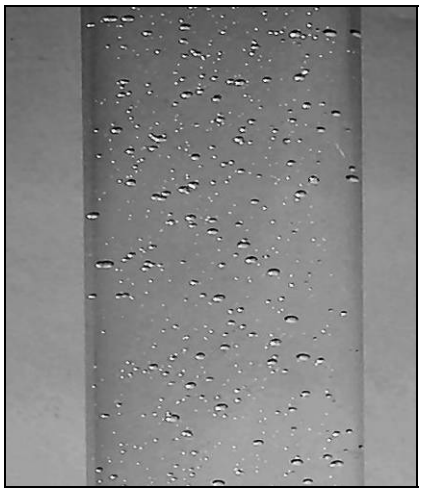
U_G = 10.0 cm/s

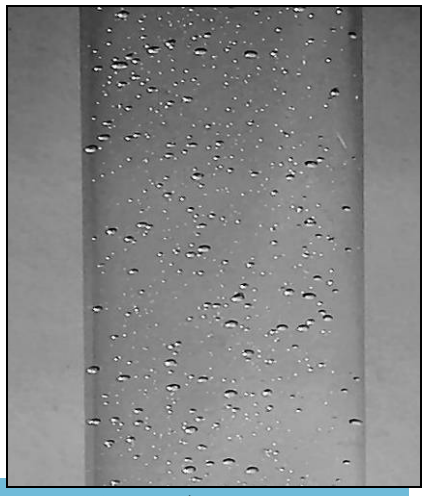
U_G = 11.0 cm/s

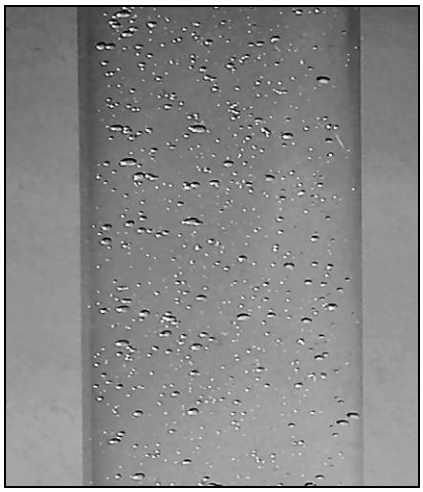
U_G = 12.0 cm/s

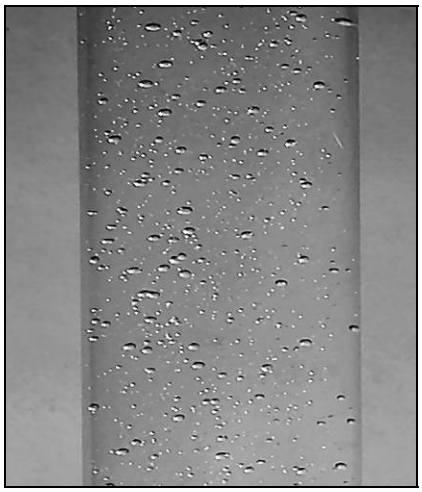
U_G = 13.0 cm/s

Test Conditions:
A = 2.22%
Closed Vent Mode
Lower Horizontal Connector

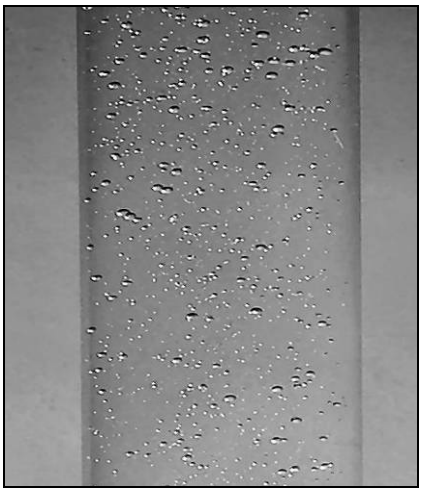
U_G = 14.0 cm/s

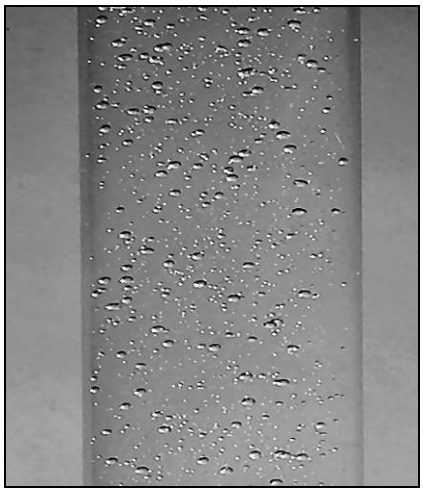
U_G = 15.0 cm/s

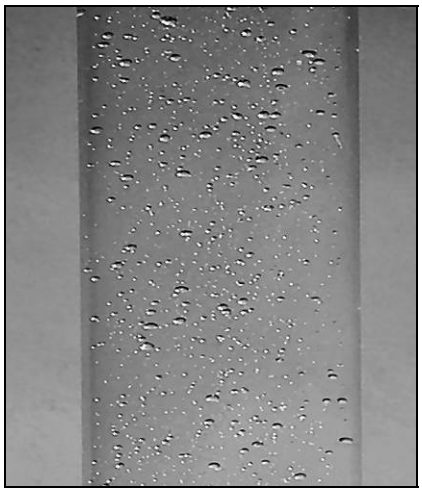
U_G = 16.0 cm/s

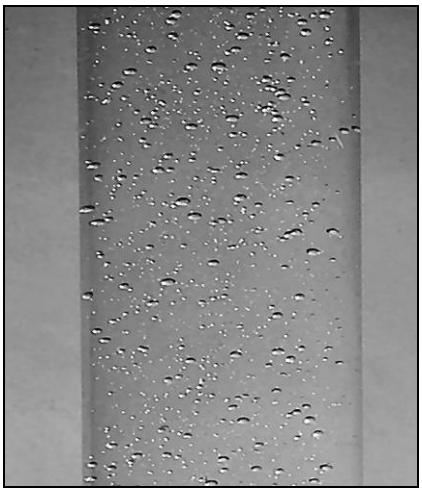
U_G = 17.0 cm/s

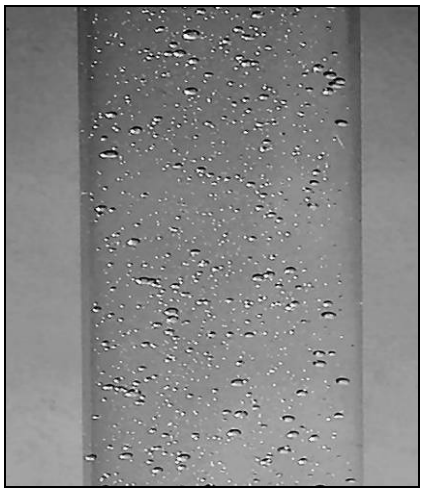
U_G = 18.0 cm/s

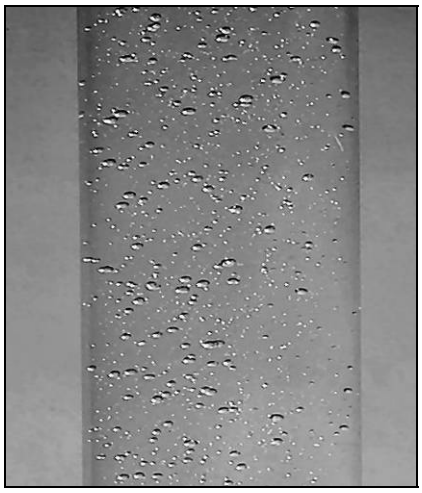
U_G = 19.0 cm/s

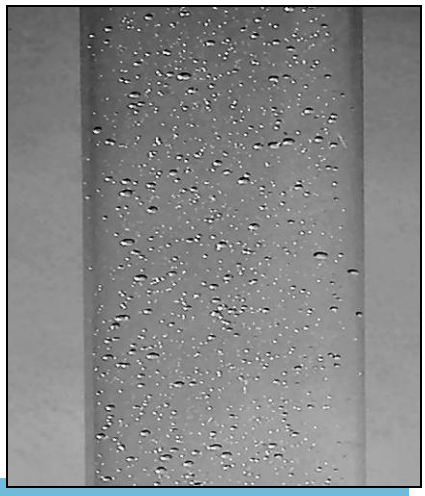

APPENDIX C:

HYDRODYNAMIC DATA

Appendix C contains a summary of the EALR hydrodynamic data collected during this study. Included in these tables are the superficial gas velocity, riser and downcomer (where applicable) gas holdup, downcomer linear liquid velocity, and calculated riser superficial liquid velocity data. The data is first presented for the tap water condition followed by the deionized water, potassium chloride solution, and nitrosomonas solution conditions.

Test Conditions:
Tap Water
A = 0.62%
Open Vent Mode

Target Superficial Gas Velocity	Measured Superficial Gas Velocity				Measured Riser Gas Holdup				Measured Downcomer Gas Holdup				Measured Downcomer Linear Liquid Velocity				Calculated Riser Superficial Liquid Velocity			
	Test #1	Test #2	Test #3	Avg	Test #1	Test #2	Test #3	Avg	Test #1	Test #2	Test #3	Avg	Test #1	Test #2	Test #3	Avg	Test #1	Test #2	Test #3	Avg*
(cm/s)	(cm/s)	(cm/s)	(cm/s)	(cm/s)	(-)	(-)	(-)	(-)	(-)	(-)	(-)	(-)	(cm/s)	(cm/s)	(cm/s)	(cm/s)	(cm/s)	(cm/s)	(cm/s)	(cm/s)
0.5	0.50	0.54	0.52	**0.52**	0.010	0.006	0.005	**0.007**	0.002	0.002	0.002	**0.002**	25.98	29.91	29.47	**28.46**	1.62	1.87	1.84	**1.74**
1.0	1.04	1.04	1.08	**1.05**	0.024	0.020	0.021	**0.022**	0.004	0.003	0.003	**0.003**	39.73	38.82	40.29	**39.61**	2.47	2.42	2.51	**2.41**
1.5	1.54	1.48	1.49	**1.50**	0.037	0.031	0.033	**0.034**	0.005	0.005	0.005	**0.005**	46.54	45.70	45.50	**45.91**	2.90	2.84	2.83	**2.91**
2.0	2.00	2.00	1.97	**1.99**	0.053	0.052	0.049	**0.051**	0.009	0.009	0.009	**0.009**	53.22	53.28	51.86	**52.79**	3.30	3.30	3.21	**3.27**
2.5	2.47	2.50	2.50	**2.49**	0.069	0.070	0.066	**0.068**	0.015	0.016	0.016	**0.016**	57.05	56.65	56.47	**56.72**	3.51	3.48	3.47	**3.47**
3.0	3.02	2.99	3.07	**3.03**	0.086	0.081	0.084	**0.084**	0.024	0.025	0.024	**0.024**	59.66	57.82	58.91	**58.80**	3.64	3.52	3.59	**3.58**
3.5	3.53	3.51	3.52	**3.52**	0.101	0.099	0.098	**0.099**	0.030	0.034	0.031	**0.032**	60.56	59.23	59.95	**59.91**	3.67	3.58	3.63	**3.61**
4.0	4.00	4.01	4.02	**4.01**	0.116	0.115	0.113	**0.115**	0.041	0.045	0.043	**0.043**	60.86	59.28	59.38	**59.84**	3.65	3.54	3.55	**3.59**
4.5	4.44	4.49	4.51	**4.48**	0.128	0.131	0.125	**0.128**	0.055	0.056	0.053	**0.055**	60.23	60.43	59.63	**60.10**	3.56	3.57	3.53	**3.53**
5.0	5.00	4.97	4.98	**4.99**	0.143	0.142	0.136	**0.140**	0.066	0.063	0.062	**0.064**	59.69	60.25	59.07	**59.67**	3.48	3.53	3.46	**3.44**
6.0	6.00	5.99	5.92	**5.97**	0.166	0.165	0.161	**0.164**	0.074	0.070	0.070	**0.071**	55.87	54.30	54.15	**54.77**	3.23	3.15	3.15	**3.23**
7.0	7.02	7.00	6.99	**7.00**	0.188	0.179	0.177	**0.181**	0.084	0.079	0.078	**0.080**	52.57	52.25	52.02	**52.28**	3.01	3.01	3.00	**3.00**
8.0	8.02	8.00	7.98	**8.00**	0.201	0.200	0.194	**0.198**	0.083	0.086	0.085	**0.085**	49.87	49.20	50.30	**49.79**	2.86	2.81	2.88	**2.80**
9.0	8.98	9.05	8.98	**9.00**	0.219	0.216	0.208	**0.214**	0.087	0.087	0.082	**0.085**	44.92	45.62	45.93	**45.49**	2.56	2.60	2.63	**2.65**
10.0	10.05	10.00	10.06	**10.04**	0.229	0.225	0.219	**0.224**	0.086	0.082	0.086	**0.085**	44.50	43.51	43.49	**43.84**	2.54	2.50	2.48	**2.54**
11.0	11.02	11.09	11.03	**11.05**	0.233	0.229	0.221	**0.228**	0.086	0.086	0.086	**0.086**	44.27	43.84	44.05	**44.05**	2.53	2.51	2.52	**2.47**
12.0	11.99	12.01	11.95	**11.98**	0.209	0.230	0.218	**0.224**	0.085	0.085	0.086	**0.085**	43.08	43.04	42.20	**42.77**	2.46	2.46	2.41	**2.43**
13.0	13.01	13.03	13.01	**13.01**	0.187	0.228	0.227	**0.228**	0.085	0.081	0.083	**0.083**	42.36	41.65	41.57	**41.86**	2.42	2.39	2.38	**2.40**
14.0	14.01	13.95	13.99	**13.98**	0.223	0.218	0.222	**0.221**	0.080	0.083	0.081	**0.081**	41.41	41.33	41.39	**41.38**	2.38	2.37	2.38	**2.38**
15.0	14.97	14.98	14.98	**14.97**	0.221	0.235	0.223	**0.226**	0.080	0.085	0.080	**0.082**	40.90	40.52	40.46	**40.62**	2.35	2.32	2.33	**2.35**
16.0	16.00	15.99	15.95	**15.98**	0.229	0.232	0.229	**0.230**	0.083	0.084	0.084	**0.084**	40.93	41.13	40.24	**40.77**	2.34	2.35	2.30	**2.33**
17.0	16.96	16.97	17.03	**16.99**	0.236	0.232	0.229	**0.232**	0.088	0.087	-	**0.087**	40.71	40.29	40.85	**40.62**	2.32	2.30	-	**2.31**
18.0	17.91	18.06	18.03	**18.00**	0.233	0.235	0.233	**0.234**	-	0.086	0.088	**0.087**	41.76	40.31	39.82	**40.63**	-	2.30	2.27	**2.31**
19.0	19.04	18.96	18.98	**18.99**	0.227	0.241	0.237	**0.235**	0.086	0.085	0.093	**0.088**	40.05	40.31	39.42	**39.92**	2.29	2.30	2.24	**2.30**
20.0	20.00	19.97	20.08	**20.02**	0.243	0.243	0.240	**0.242**	0.091	0.083	0.093	**0.089**	39.49	39.80	40.47	**39.92**	2.24	2.28	2.29	**2.27**

* Average riser superficial liquid velocities were calculated by applying a 6th order polynomial to the raw data.

Test Conditions:
Tap Water
A = 0.62%
Closed Vent Mode

Target Superficial Gas Velocity	Measured Superficial Gas Velocity				Measured Riser Gas Holdup				Closed Vent Mode - Downcomer Linear Liquid Velocity				Closed Vent Mode - Riser Superficial Liquid Velocity			
	Test #1	Test #2	Test #3	Avg	Test #1	Test #2	Test #3	Avg	Test #1	Test #2	Test #3	Avg	Test #1	Test #2	Test #3	Avg*
(cm/s)	(cm/s)	(cm/s)	(cm/s)	(cm/s)	(-)	(-)	(-)	(-)	(cm/s)	(cm/s)	(cm/s)	(cm/s)	(cm/s)	(cm/s)	(cm/s)	(cm/s)
0.5	0.52	0.51	0.52	**0.52**	0.005	0.002	0.001	**0.003**	21.72	21.53	21.49	**21.58**	1.36	1.35	1.34	**1.35**
1.0	1.04	1.03	1.05	**1.04**	0.023	0.017	0.018	**0.019**	19.91	20.30	20.21	**20.14**	1.24	1.27	1.26	**1.27**
1.5	1.52	1.51	1.51	**1.51**	0.035	0.031	0.032	**0.033**	18.58	19.26	19.26	**19.03**	1.16	1.20	1.20	**1.19**
2.0	2.06	2.04	2.04	**2.05**	0.057	0.051	0.051	**0.053**	18.03	18.18	18.40	**18.20**	1.13	1.14	1.15	**1.12**
2.5	2.52	2.50	2.52	**2.51**	0.073	0.072	0.068	**0.071**	17.12	16.58	17.06	**16.92**	1.07	1.04	1.07	**1.06**
3.0	3.02	3.01	3.01	**3.01**	0.091	0.089	0.088	**0.089**	16.08	15.32	15.82	**15.74**	1.01	0.96	0.99	**1.00**
3.5	3.52	3.49	3.54	**3.51**	0.107	0.103	0.105	**0.105**	14.95	14.97	15.40	**15.11**	0.93	0.94	0.96	**0.95**
4.0	4.05	4.03	4.03	**4.04**	0.124	0.120	0.121	**0.122**	14.14	14.52	15.00	**14.55**	0.88	0.91	0.94	**0.91**
4.5	4.51	4.49	4.49	**4.50**	0.138	0.136	0.128	**0.134**	13.99	13.37	14.00	**13.78**	0.87	0.84	0.87	**0.86**
5.0	5.01	5.00	5.01	**5.01**	0.150	0.152	0.151	**0.151**	13.29	13.24	13.23	**13.25**	0.83	0.83	0.83	**0.83**
6.0	6.01	6.01	6.02	**6.01**	0.180	0.177	0.176	**0.178**	12.63	12.29	12.38	**12.43**	0.79	0.77	0.77	**0.78**
7.0	6.99	7.01	7.00	**7.00**	0.198	0.195	0.193	**0.195**	12.14	12.03	12.29	**12.16**	0.76	0.75	0.77	**0.75**
8.0	8.03	8.01	8.02	**8.02**	0.213	0.213	0.210	**0.212**	12.25	12.06	11.97	**12.09**	0.77	0.75	0.75	**0.74**
9.0	9.01	9.05	9.04	**9.03**	0.227	0.226	0.225	**0.226**	12.44	11.49	12.00	**11.98**	0.78	0.72	0.75	**0.76**
10.0	10.03	10.04	10.03	**10.03**	0.234	0.237	0.233	**0.235**	13.29	12.14	12.16	**12.53**	0.83	0.76	0.76	**0.80**
11.0	11.04	11.05	11.00	**11.03**	0.241	0.243	0.241	**0.242**	13.56	12.87	12.86	**13.10**	0.85	0.80	0.80	**0.84**
12.0	12.01	12.00	12.05	**12.02**	0.239	0.245	0.239	**0.241**	14.68	13.91	14.35	**14.31**	0.92	0.87	0.90	**0.88**
13.0	12.98	13.01	13.02	**13.00**	0.236	0.238	0.241	**0.238**	14.96	15.57	15.05	**15.19**	0.93	0.97	0.94	**0.92**
14.0	14.04	14.06	14.08	**14.06**	0.239	0.239	0.237	**0.238**	15.49	15.06	15.14	**15.23**	0.97	0.94	0.95	**0.95**
15.0	15.05	15.01	15.03	**15.03**	0.239	0.237	0.235	**0.237**	14.96	15.80	15.18	**15.31**	0.93	0.99	0.95	**0.96**
16.0	16.07	16.05	16.05	**16.06**	0.237	0.235	0.235	**0.236**	14.97	15.54	15.43	**15.31**	0.94	0.97	0.96	**0.97**
17.0	17.01	17.03	17.06	**17.03**	0.238	0.239	0.238	**0.238**	15.64	15.66	15.55	**15.62**	0.98	0.98	0.97	**0.97**
18.0	18.06	18.05	18.03	**18.05**	0.242	0.243	0.241	**0.242**	15.30	16.01	15.25	**15.52**	0.96	1.00	0.95	**0.97**
19.0	19.02	19.04	19.07	**19.04**	0.244	0.241	0.242	**0.242**	15.34	15.38	15.62	**15.45**	0.96	0.96	0.98	**0.97**
20.0	20.04	20.09	20.06	**20.06**	0.245	0.240	0.246	**0.244**	15.58	15.55	15.40	**15.51**	0.97	0.97	0.96	**0.97**

* Average riser superficial liquid velocities were calculated by applying a 6th order polynomial to the raw data.

Test Conditions:
Tap Water
A = 0.62%
Bubble Column Mode

Target Superficial Gas Velocity	Measured Superficial Gas Velocity				Measured Riser Gas Holdup			
	Test #1	Test #2	Test #3	Avg	Test #1	Test #2	Test #3	Avg
(cm/s)	(cm/s)	(cm/s)	(cm/s)	(cm/s)	(-)	(-)	(-)	(-)
0.5	0.54	0.52	0.52	**0.52**	0.000	0.010	0.006	**0.005**
1.0	1.03	1.04	0.99	**1.02**	0.017	0.025	0.019	**0.020**
1.5	1.51	1.52	1.51	**1.51**	0.035	0.038	0.034	**0.036**
2.0	2.01	2.02	2.00	**2.01**	0.053	0.058	0.052	**0.054**
2.5	2.52	2.52	2.47	**2.50**	0.070	0.077	0.068	**0.072**
3.0	3.05	3.05	3.07	**3.05**	0.087	0.095	0.088	**0.090**
3.5	3.52	3.52	3.49	**3.51**	0.105	0.111	0.103	**0.106**
4.0	4.04	4.02	4.02	**4.02**	0.118	0.127	0.118	**0.121**
4.5	4.55	4.52	4.50	**4.52**	0.128	0.144	0.132	**0.135**
5.0	5.03	5.02	4.94	**5.00**	0.142	0.156	0.144	**0.147**
6.0	6.04	6.04	6.01	**6.03**	0.165	0.173	0.169	**0.169**
7.0	7.01	7.03	6.97	**7.00**	0.190	0.192	0.185	**0.189**
8.0	8.04	8.05	8.02	**8.04**	0.194	0.212	0.200	**0.202**
9.0	9.03	9.04	8.95	**9.01**	0.217	0.223	0.214	**0.218**
10.0	10.06	10.01	9.97	**10.01**	0.226	0.233	0.220	**0.226**
11.0	11.01	11.03	11.09	**11.06**	0.219	0.237	0.232	**0.235**
12.0	12.00	12.03	12.01	**12.01**	0.229	0.240	0.228	**0.232**
13.0	13.05	13.05	13.10	**13.07**	0.210	0.228	0.226	**0.227**
14.0	14.03	14.03	14.00	**14.02**	0.229	0.232	0.220	**0.227**
15.0	15.03	15.02	14.99	**15.01**	0.221	0.232	0.223	**0.225**
16.0	16.04	16.04	15.91	**16.00**	0.222	0.233	0.226	**0.227**
17.0	16.99	17.04	16.92	**16.98**	0.215	0.233	0.224	**0.229**
18.0	17.99	18.02	17.95	**17.99**	0.230	0.236	0.227	**0.231**
19.0	19.01	19.02	18.97	**19.00**	0.232	0.239	0.232	**0.234**
20.0	20.04	20.00	20.07	**20.04**	0.234	0.240	0.233	**0.236**

Test Conditions:
Tap Water
A = 0.99%
Open Vent Mode

Target Superficial Gas Velocity	Measured Superficial Gas Velocity				Measured Riser Gas Holdup				Measured Downcomer Gas Holdup				Measured Downcomer Linear Liquid Velocity				Calculated Riser Superficial Liquid Velocity			
	Test #1	Test #2	Test #3	Avg	Test #1	Test #2	Test #3	Avg	Test #1	Test #2	Test #3	Avg	Test #1	Test #2	Test #3	Avg	Test #1	Test #2	Test #3	Avg*
(cm/s)	(cm/s)	(cm/s)	(cm/s)	(cm/s)	(-)	(-)	(-)	(-)	(-)	(-)	(-)	(-)	(cm/s)	(cm/s)	(cm/s)	(cm/s)	(cm/s)	(cm/s)	(cm/s)	(cm/s)
0.5	0.55	0.54	0.54	**0.54**	0.003	0.000	-0.001	**0.001**	0.001	0.002	0.002	**0.002**	30.34	33.14	32.51	**31.99**	1.89	2.07	2.03	**1.96**
1.0	1.05	1.04	1.04	**1.04**	0.018	0.016	0.014	**0.016**	0.002	0.005	0.005	**0.004**	42.67	44.13	42.81	**43.20**	2.66	2.74	2.66	**2.61**
1.5	1.54	1.49	1.51	**1.51**	0.029	0.027	0.025	**0.027**	0.007	0.006	0.005	**0.006**	48.49	49.98	49.16	**49.21**	3.01	3.10	3.06	**3.10**
2.0	2.04	2.01	2.02	**2.02**	0.046	0.044	0.042	**0.044**	0.008	0.013	0.013	**0.011**	57.01	56.35	56.94	**56.77**	3.54	3.48	3.51	**3.42**
2.5	2.48	2.49	2.54	**2.50**	0.058	0.059	0.060	**0.059**	0.019	0.019	0.018	**0.019**	58.36	57.83	59.42	**58.54**	3.58	3.54	3.65	**3.61**
3.0	3.04	3.03	3.03	**3.03**	0.076	0.075	0.074	**0.075**	0.031	0.033	0.030	**0.031**	60.30	61.05	60.42	**60.59**	3.65	3.69	3.66	**3.70**
3.5	3.50	3.54	3.53	**3.52**	0.056	0.091	0.089	**0.090**	0.041	0.039	0.040	**0.040**	52.20	61.54	61.43	**61.49**	3.13	3.70	3.69	**3.72**
4.0	4.02	4.04	4.03	**4.03**	0.105	0.106	0.104	**0.105**	0.048	0.045	0.051	**0.048**	60.95	62.65	60.98	**61.53**	3.63	3.74	3.62	**3.68**
4.5	4.46	4.46	4.53	**4.48**	0.118	0.119	0.119	**0.119**	0.057	0.057	0.061	**0.058**	60.76	62.26	60.93	**61.32**	3.58	3.67	3.58	**3.61**
5.0	5.01	5.02	5.01	**5.02**	0.133	0.132	0.128	**0.131**	0.065	0.065	0.066	**0.066**	59.96	60.17	60.24	**60.12**	3.50	3.52	3.52	**3.51**
6.0	6.00	6.03	6.03	**6.02**	0.157	0.156	0.154	**0.156**	0.071	0.072	0.073	**0.072**	56.26	56.18	56.43	**56.29**	3.27	3.26	3.27	**3.28**
7.0	7.04	7.03	7.03	**7.03**	0.166	0.176	0.172	**0.171**	0.077	0.079	0.075	**0.077**	53.08	53.33	53.08	**53.16**	3.06	3.07	3.07	**3.04**
8.0	8.02	8.04	8.01	**8.02**	0.182	0.195	0.189	**0.189**	0.086	0.085	0.083	**0.085**	51.17	49.38	49.14	**49.90**	2.92	2.82	2.82	**2.83**
9.0	9.02	9.03	9.02	**9.02**	0.209	0.209	0.205	**0.208**	0.087	0.085	0.084	**0.085**	46.39	46.14	46.19	**46.24**	2.65	2.64	2.64	**2.67**
10.0	10.05	10.07	10.05	**10.05**	0.221	0.218	0.195	**0.211**	0.086	0.088	0.090	**0.088**	45.90	45.11	47.19	**46.07**	2.62	2.57	2.68	**2.56**
11.0	10.99	11.00	11.00	**11.00**	0.225	0.229	0.229	**0.228**	0.092	0.088	0.092	**0.091**	45.09	43.44	43.44	**43.99**	2.56	2.48	2.46	**2.49**
12.0	12.04	12.06	12.04	**12.05**	0.230	0.236	0.217	**0.228**	0.091	0.094	0.096	**0.094**	43.87	42.07	43.88	**43.27**	2.49	2.38	2.48	**2.46**
13.0	13.01	13.03	13.05	**13.03**	0.234	0.235	0.234	**0.234**	0.092	0.092	0.094	**0.093**	43.85	41.61	43.61	**43.02**	2.49	2.36	2.47	**2.44**
14.0	14.05	14.06	14.03	**14.05**	0.240	0.239	0.234	**0.238**	0.092	0.094	0.092	**0.093**	43.87	41.59	42.73	**42.73**	2.49	2.36	2.42	**2.43**
15.0	15.00	15.04	15.06	**15.03**	0.240	0.225	0.234	**0.233**	0.094	0.092	0.091	**0.092**	43.14	42.62	42.70	**42.82**	2.44	2.42	2.43	**2.42**
16.0	16.06	16.05	16.03	**16.04**	0.238	0.236	0.238	**0.237**	0.093	0.090	0.091	**0.091**	42.66	41.63	41.36	**41.88**	2.42	2.37	2.35	**2.40**
17.0	17.03	17.05	17.02	**17.03**	0.238	0.238	0.237	**0.238**	0.092	0.091	0.093	**0.092**	41.57	42.06	41.50	**41.71**	2.36	2.39	2.35	**2.38**
18.0	18.04	18.02	18.05	**18.04**	0.241	0.239	0.239	**0.240**	0.091	0.093	0.093	**0.092**	42.22	40.98	42.29	**41.83**	2.40	2.32	2.40	**2.35**
19.0	18.88	19.01	19.02	**18.97**	0.241	0.242	0.240	**0.241**	0.095	0.093	0.094	**0.094**	41.36	40.62	41.82	**41.27**	2.34	2.30	2.37	**2.34**
20.0	19.98	20.05	20.04	**20.02**	0.243	0.244	0.241	**0.243**	0.094	0.091	0.094	**0.093**	41.04	40.95	41.69	**41.23**	2.32	2.33	2.36	**2.34**

* Average riser superficial liquid velocities were calculated by applying a 6th order polynomial to the raw data.

Test Conditions:
Tap Water
A = 0.99%
Closed Vent Mode

Target Superficial Gas Velocity	Measured Superficial Gas Velocity				Measured Riser Gas Holdup				Closed Vent Mode - Downcomer Linear Liquid Velocity				Closed Vent Mode - Riser Superficial Liquid Velocity			
	Test #1	Test #2	Test #3	Avg	Test #1	Test #2	Test #3	Avg	Test #1	Test #2	Test #3	Avg	Test #1	Test #2	Test #3	Avg*
(cm/s)	(cm/s)	(cm/s)	(cm/s)	(cm/s)	(-)	(-)	(-)	(-)	(cm/s)	(cm/s)	(cm/s)	(cm/s)	(cm/s)	(cm/s)	(cm/s)	(cm/s)
0.5	0.53	0.54	0.50	**0.52**	0.002	0.001	-0.001	**0.001**	22.15	22.09	22.24	**22.16**	1.38	1.38	1.39	**1.39**
1.0	1.02	1.00	1.04	**1.02**	0.017	0.017	0.015	**0.016**	20.44	20.57	20.23	**20.41**	1.28	1.29	1.26	**1.29**
1.5	1.48	1.53	1.56	**1.52**	0.031	0.031	0.022	**0.028**	18.85	19.46	19.05	**19.12**	1.18	1.22	1.19	**1.20**
2.0	2.03	2.03	2.04	**2.04**	0.047	0.048	0.047	**0.047**	17.64	17.69	18.25	**17.86**	1.10	1.11	1.14	**1.12**
2.5	2.50	2.53	2.54	**2.52**	0.064	0.068	0.065	**0.066**	17.25	17.32	16.88	**17.15**	1.08	1.08	1.06	**1.06**
3.0	2.97	3.01	2.99	**2.99**	0.083	0.083	0.083	**0.083**	15.86	15.56	16.50	**15.97**	0.99	0.97	1.03	**1.00**
3.5	3.49	3.50	3.54	**3.51**	0.095	0.097	0.100	**0.097**	15.03	15.13	14.85	**15.00**	0.94	0.95	0.93	**0.94**
4.0	4.01	4.05	4.00	**4.02**	0.111	0.116	0.114	**0.114**	14.20	14.23	14.20	**14.21**	0.89	0.89	0.89	**0.89**
4.5	4.52	4.46	4.47	**4.49**	0.129	0.124	0.131	**0.128**	13.28	13.49	13.50	**13.42**	0.83	0.84	0.84	**0.85**
5.0	5.00	4.95	5.02	**4.99**	0.142	0.143	0.143	**0.143**	13.30	13.09	13.15	**13.18**	0.83	0.82	0.82	**0.82**
6.0	5.99	5.98	6.03	**6.00**	0.168	0.165	0.162	**0.165**	12.01	12.15	11.81	**11.99**	0.75	0.76	0.74	**0.76**
7.0	6.99	7.04	7.04	**7.02**	0.187	0.189	0.188	**0.188**	11.88	11.87	11.70	**11.82**	0.74	0.74	0.73	**0.73**
8.0	8.06	7.99	8.04	**8.03**	0.207	0.203	0.206	**0.205**	11.92	12.02	11.76	**11.90**	0.74	0.75	0.74	**0.72**
9.0	9.00	9.03	9.03	**9.02**	0.222	0.219	0.218	**0.220**	11.82	12.13	11.85	**11.94**	0.74	0.76	0.74	**0.74**
10.0	9.99	10.03	10.01	**10.01**	0.231	0.224	0.220	**0.225**	12.16	12.07	13.27	**12.50**	0.76	0.75	0.83	**0.77**
11.0	11.03	11.03	11.06	**11.04**	0.238	0.238	0.238	**0.238**	13.25	13.11	12.85	**13.07**	0.83	0.82	0.80	**0.81**
12.0	11.99	12.03	12.05	**12.02**	0.246	0.245	0.246	**0.246**	13.74	14.05	13.52	**13.77**	0.86	0.88	0.84	**0.86**
13.0	13.02	12.98	13.02	**13.01**	0.245	0.243	0.247	**0.245**	15.31	14.82	14.79	**14.97**	0.96	0.93	0.92	**0.91**
14.0	14.01	14.02	14.04	**14.02**	0.237	0.245	0.244	**0.242**	15.28	15.13	15.01	**15.14**	0.96	0.95	0.94	**0.95**
15.0	15.03	15.05	15.02	**15.03**	0.237	0.245	0.244	**0.242**	15.94	15.38	15.86	**15.73**	1.00	0.96	0.99	**0.98**
16.0	15.95	16.05	16.03	**16.01**	0.246	0.243	0.242	**0.244**	15.95	15.48	15.59	**15.67**	1.00	0.97	0.97	**0.99**
17.0	17.07	17.00	16.96	**17.01**	0.245	0.244	0.244	**0.244**	15.58	15.49	15.89	**15.65**	0.97	0.97	0.99	**0.99**
18.0	18.05	18.03	17.96	**18.01**	0.248	0.247	0.246	**0.247**	16.18	16.08	15.78	**16.01**	1.01	1.01	0.99	**0.99**
19.0	19.01	19.06	19.07	**19.05**	0.248	0.247	0.249	**0.248**	16.06	15.71	15.60	**15.79**	1.00	0.98	0.98	**0.98**
20.0	19.93	20.04	20.05	**20.01**	0.249	0.247	0.246	**0.247**	15.86	15.70	16.23	**15.93**	0.99	0.98	1.01	**0.99**

* Average riser superficial liquid velocities were calculated by applying a 6th order polynomial to the raw data.

Test Conditions:
Tap Water
A = 0.99%
Bubble Column Mode

Target Superficial Gas Velocity	Measured Superficial Gas Velocity				Measured Riser Gas Holdup			
	Test #1	Test #2	Test #3	Avg	Test #1	Test #2	Test #3	Avg
(cm/s)	(cm/s)	(cm/s)	(cm/s)	(cm/s)	(-)	(-)	(-)	(-)
0.5	0.55	0.57	0.52	**0.55**	0.007	0.007	0.003	**0.006**
1.0	1.01	1.01	1.07	**1.03**	0.022	0.021	0.022	**0.022**
1.5	1.51	1.50	1.55	**1.52**	0.036	0.034	0.036	**0.035**
2.0	2.03	2.04	2.01	**2.03**	0.053	0.058	0.053	**0.055**
2.5	2.55	2.51	2.51	**2.52**	0.073	0.075	0.070	**0.073**
3.0	3.00	2.97	3.03	**3.00**	0.089	0.088	0.091	**0.089**
3.5	3.51	3.49	3.49	**3.50**	0.108	0.109	0.104	**0.107**
4.0	4.00	3.99	4.00	**4.00**	0.120	0.124	0.120	**0.121**
4.5	4.49	4.54	4.48	**4.50**	0.139	0.143	0.137	**0.140**
5.0	5.04	5.00	4.99	**5.01**	0.149	0.155	0.144	**0.149**
6.0	5.98	6.00	6.05	**6.01**	0.176	0.180	0.170	**0.175**
7.0	7.07	7.07	7.02	**7.05**	0.198	0.200	0.182	**0.193**
8.0	8.09	8.00	8.01	**8.03**	0.212	0.211	0.207	**0.210**
9.0	9.03	9.04	9.02	**9.03**	0.225	0.228	0.225	**0.226**
10.0	10.00	10.05	9.98	**10.01**	0.235	0.242	0.230	**0.236**
11.0	11.00	10.98	10.97	**10.98**	0.246	0.244	0.240	**0.243**
12.0	12.01	12.04	12.10	**12.05**	0.250	0.253	0.249	**0.251**
13.0	12.99	13.02	13.03	**13.01**	0.247	0.255	0.255	**0.252**
14.0	14.06	14.05	13.99	**14.03**	0.258	0.255	0.252	**0.255**
15.0	15.02	15.03	15.03	**15.03**	0.257	0.253	0.252	**0.254**
16.0	16.02	16.02	16.00	**16.02**	0.249	0.254	0.247	**0.250**
17.0	16.97	17.02	16.98	**16.99**	0.246	0.251	0.246	**0.248**
18.0	18.00	18.00	18.05	**18.01**	0.250	0.253	0.249	**0.251**
19.0	19.04	19.05	19.03	**19.04**	0.252	0.244	0.249	**0.248**
20.0	19.98	19.98	20.04	**20.00**	0.254	0.249	0.253	**0.252**

Test Conditions:
Tap Water
A = 2.22%
Open Vent Mode

Target Superficial Gas Velocity	Measured Superficial Gas Velocity				Measured Riser Gas Holdup				Measured Downcomer Gas Holdup				Measured Downcomer Linear Liquid Velocity				Calculated Riser Superficial Liquid Velocity			
	Test #1	Test #2	Test #3	Avg	Test #1	Test #2	Test #3	Avg	Test #1	Test #2	Test #3	Avg	Test #1	Test #2	Test #3	Avg	Test #1	Test #2	Test #3	Avg*
(cm/s)	(cm/s)	(cm/s)	(cm/s)	(cm/s)	(-)	(-)	(-)	(-)	(-)	(-)	(-)	(-)	(cm/s)	(cm/s)	(cm/s)	(cm/s)	(cm/s)	(cm/s)	(cm/s)	(cm/s)
0.5	0.52	0.52	0.50	**0.51**	0.005	0.006	0.005	**0.005**	0.004	0.003	0.004	**0.004**	31.57	31.88	32.59	**32.01**	1.96	1.99	2.03	**2.01**
1.0	1.05	1.03	1.03	**1.04**	0.021	0.022	0.021	**0.021**	0.006	0.005	0.006	**0.006**	42.55	43.05	43.35	**42.98**	2.64	2.68	2.69	**2.60**
1.5	1.53	1.51	1.51	**1.52**	0.033	0.032	0.030	**0.032**	0.007	0.007	0.008	**0.007**	49.22	48.12	48.63	**48.66**	3.05	2.99	3.02	**3.05**
2.0	2.00	2.00	2.02	**2.01**	0.047	0.045	0.047	**0.046**	0.012	0.012	0.012	**0.012**	54.04	54.19	54.59	**54.27**	3.34	3.35	3.37	**3.35**
2.5	2.51	2.53	2.49	**2.51**	0.063	0.065	0.061	**0.063**	0.018	0.019	0.017	**0.018**	57.23	58.63	56.28	**57.38**	3.51	3.60	3.46	**3.52**
3.0	3.03	3.01	3.03	**3.02**	0.077	0.075	0.076	**0.076**	0.025	0.026	0.027	**0.026**	59.08	60.17	59.23	**59.49**	3.60	3.66	3.60	**3.61**
3.5	3.51	3.51	3.47	**3.49**	0.092	0.093	0.090	**0.092**	0.038	0.038	0.036	**0.037**	60.49	59.45	60.73	**60.22**	3.64	3.57	3.66	**3.63**
4.0	4.01	3.98	4.03	**4.01**	0.106	0.107	0.106	**0.106**	0.045	0.048	0.048	**0.047**	61.09	61.43	59.05	**60.52**	3.65	3.66	3.51	**3.61**
4.5	4.50	4.50	4.54	**4.51**	0.117	0.120	0.119	**0.119**	0.056	0.056	0.058	**0.057**	60.07	59.45	59.08	**59.53**	3.54	3.51	3.48	**3.54**
5.0	5.01	5.00	5.00	**5.00**	0.128	0.130	0.130	**0.129**	0.063	0.065	0.062	**0.064**	60.55	58.95	59.14	**59.55**	3.54	3.44	3.47	**3.46**
6.0	6.04	6.03	5.98	**6.02**	0.150	0.144	0.151	**0.148**	0.072	0.071	0.070	**0.071**	55.65	55.12	56.56	**55.78**	3.23	3.20	3.29	**3.24**
7.0	7.09	6.98	7.04	**7.03**	0.170	0.163	0.170	**0.168**	0.077	0.077	0.077	**0.077**	51.27	51.70	52.62	**51.87**	2.96	2.98	3.03	**3.00**
8.0	8.05	8.01	7.98	**8.01**	0.171	0.178	0.180	**0.176**	0.079	0.078	0.078	**0.079**	48.17	49.45	49.37	**49.00**	2.77	2.85	2.84	**2.79**
9.0	9.04	9.06	9.03	**9.04**	0.190	0.197	0.196	**0.194**	0.081	0.079	0.082	**0.080**	44.39	43.64	44.40	**44.15**	2.55	2.51	2.55	**2.62**
10.0	10.03	10.00	10.00	**10.01**	0.204	0.190	0.205	**0.200**	0.082	0.084	0.085	**0.084**	43.62	44.33	43.61	**43.85**	2.50	2.54	2.49	**2.49**
11.0	11.05	11.00	11.02	**11.02**	0.207	0.209	0.211	**0.209**	0.084	0.083	0.086	**0.084**	42.09	42.34	42.22	**42.22**	2.41	2.43	2.41	**2.40**
12.0	12.03	12.03	12.01	**12.02**	0.217	0.217	0.219	**0.218**	0.087	0.085	0.088	**0.087**	41.23	40.67	40.53	**40.81**	2.35	2.32	2.31	**2.35**
13.0	13.01	13.06	12.99	**13.02**	0.228	0.225	0.214	**0.222**	0.088	0.089	0.091	**0.089**	41.45	41.24	41.91	**41.53**	2.36	2.35	2.38	**2.33**
14.0	14.00	14.07	13.96	**14.01**	0.233	0.229	0.233	**0.232**	0.090	0.089	0.090	**0.090**	39.52	40.22	40.66	**40.13**	2.25	2.29	2.31	**2.32**
15.0	15.08	15.00	15.02	**15.03**	0.238	0.238	0.225	**0.234**	0.091	0.093	0.090	**0.091**	40.75	41.43	41.08	**41.09**	2.32	2.35	2.34	**2.32**
16.0	16.05	16.03	16.05	**16.04**	0.239	0.243	0.243	**0.242**	0.093	0.093	0.093	**0.093**	40.65	40.76	40.71	**40.71**	2.30	2.31	2.31	**2.32**
17.0	17.03	17.05	17.08	**17.05**	0.248	0.244	0.250	**0.247**	0.094	0.092	0.092	**0.093**	40.89	40.85	40.44	**40.73**	2.32	2.32	2.29	**2.31**
18.0	18.05	18.05	18.07	**18.06**	0.252	0.242	0.253	**0.249**	0.093	0.093	0.093	**0.093**	40.93	40.68	40.63	**40.75**	2.32	2.31	2.30	**2.31**
19.0	19.05	19.07	19.04	**19.05**	0.253	0.257	0.254	**0.255**	0.092	0.095	0.094	**0.094**	39.77	41.60	42.13	**41.17**	2.26	2.35	2.39	**2.31**
20.0	20.04	20.07	19.98	**20.03**	0.256	0.255	0.258	**0.256**	0.093	0.092	0.096	**0.094**	41.24	40.75	39.86	**40.62**	2.34	2.31	2.25	**2.31**

* Average riser superficial liquid velocities were calculated by applying a 6th order polynomial to the raw data.

Test Conditions:
Tap Water
A = 2.22%
Closed Vent Mode

Target Superficial Gas Velocity	Measured Superficial Gas Velocity				Measured Riser Gas Holdup				Closed Vent Mode - Downcomer Linear Liquid Velocity				Closed Vent Mode - Riser Superficial Liquid Velocity			
	Test #1	Test #2	Test #3	Avg	Test #1	Test #2	Test #3	Avg	Test #1	Test #2	Test #3	Avg	Test #1	Test #2	Test #3	Avg*
(cm/s)	(cm/s)	(cm/s)	(cm/s)	(cm/s)	(-)	(-)	(-)	(-)	(cm/s)	(cm/s)	(cm/s)	(cm/s)	(cm/s)	(cm/s)	(cm/s)	(cm/s)
0.5	0.51	0.53	0.50	**0.52**	0.005	0.004	0.005	**0.005**	21.85	21.93	21.14	**21.64**	1.37	1.37	1.32	**1.34**
1.0	1.04	1.03	1.03	**1.04**	0.024	0.025	0.024	**0.024**	20.00	19.57	19.23	**19.60**	1.25	1.22	1.20	**1.25**
1.5	1.52	1.51	1.51	**1.51**	0.034	0.034	0.033	**0.034**	18.36	18.00	18.51	**18.29**	1.15	1.12	1.16	**1.16**
2.0	2.03	2.01	2.03	**2.03**	0.054	0.054	0.052	**0.053**	17.38	17.31	17.74	**17.47**	1.09	1.08	1.11	**1.08**
2.5	2.50	2.51	2.50	**2.50**	0.062	0.068	0.070	**0.067**	16.67	16.66	16.42	**16.58**	1.04	1.04	1.03	**1.02**
3.0	3.03	3.02	2.99	**3.01**	0.080	0.084	0.084	**0.083**	15.17	15.02	15.57	**15.25**	0.95	0.94	0.97	**0.96**
3.5	3.54	3.49	3.49	**3.51**	0.101	0.094	0.102	**0.099**	14.39	14.84	14.68	**14.64**	0.90	0.93	0.92	**0.91**
4.0	4.03	4.00	4.05	**4.03**	0.115	0.116	0.116	**0.116**	13.73	13.65	13.89	**13.76**	0.86	0.85	0.87	**0.87**
4.5	4.53	4.51	4.52	**4.52**	0.130	0.130	0.129	**0.130**	13.41	13.49	13.43	**13.44**	0.84	0.84	0.84	**0.84**
5.0	5.00	5.01	5.04	**5.02**	0.140	0.140	0.140	**0.140**	13.29	13.15	13.21	**13.22**	0.83	0.82	0.83	**0.81**
6.0	5.98	6.03	6.03	**6.01**	0.165	0.162	0.162	**0.163**	12.24	12.67	12.54	**12.48**	0.76	0.79	0.78	**0.79**
7.0	7.03	6.99	7.04	**7.02**	0.182	0.178	0.181	**0.180**	12.29	11.96	12.16	**12.14**	0.77	0.75	0.76	**0.78**
8.0	7.99	8.04	7.99	**8.01**	0.191	0.195	0.194	**0.193**	12.49	13.10	12.56	**12.72**	0.78	0.82	0.79	**0.79**
9.0	9.06	9.03	9.02	**9.04**	0.206	0.206	0.204	**0.205**	13.44	13.19	13.18	**13.27**	0.84	0.82	0.82	**0.81**
10.0	9.97	10.03	10.07	**10.02**	0.213	0.212	0.214	**0.213**	13.50	13.63	13.74	**13.62**	0.84	0.85	0.86	**0.84**
11.0	11.06	11.03	11.01	**11.03**	0.215	0.222	0.219	**0.219**	13.98	14.21	14.21	**14.13**	0.87	0.89	0.89	**0.88**
12.0	12.01	11.98	11.99	**11.99**	0.229	0.230	0.233	**0.231**	14.50	14.32	14.29	**14.37**	0.91	0.90	0.89	**0.91**
13.0	12.99	13.02	12.95	**12.99**	0.235	0.239	0.239	**0.238**	14.33	15.24	14.51	**14.69**	0.90	0.95	0.91	**0.93**
14.0	13.98	14.08	14.06	**14.04**	0.242	0.244	0.245	**0.244**	15.57	15.55	15.03	**15.38**	0.97	0.97	0.94	**0.96**
15.0	15.06	15.03	15.06	**15.05**	0.250	0.248	0.250	**0.249**	15.89	15.49	15.55	**15.64**	0.99	0.97	0.97	**0.97**
16.0	16.06	16.01	16.02	**16.03**	0.255	0.251	0.257	**0.254**	16.10	16.08	15.97	**16.05**	1.01	1.01	1.00	**0.99**
17.0	17.03	17.00	17.04	**17.02**	0.256	0.259	0.260	**0.258**	15.87	16.41	15.71	**16.00**	0.99	1.03	0.98	**1.01**
18.0	18.02	18.07	18.00	**18.03**	0.264	0.257	0.264	**0.262**	17.07	15.89	16.27	**16.41**	1.07	0.99	1.02	**1.02**
19.0	19.04	19.08	19.09	**19.07**	0.271	0.259	0.269	**0.266**	16.84	16.11	16.89	**16.61**	1.05	1.01	1.06	**1.04**
20.0	20.05	20.03	20.06	**20.05**	0.263	0.269	0.270	**0.267**	16.85	16.65	16.79	**16.76**	1.05	1.04	1.05	**1.05**

* Average riser superficial liquid velocities were calculated by applying a 6th order polynomial to the raw data.

Test Conditions:
Tap Water
A = 2.22%
Bubble Column Mode

Target Superficial Gas Velocity	Measured Superficial Gas Velocity				Measured Riser Gas Holdup			
	Test #1	Test #2	Test #3	Avg	Test #1	Test #2	Test #3	Avg
(cm/s)	(cm/s)	(cm/s)	(cm/s)	(cm/s)	(-)	(-)	(-)	(-)
0.5	0.57	0.51	0.50	**0.53**	0.000	0.004	0.005	**0.003**
1.0	1.06	0.99	1.03	**1.02**	0.022	0.019	0.021	**0.021**
1.5	1.55	1.52	1.49	**1.52**	0.036	0.035	0.035	**0.035**
2.0	2.05	2.04	2.01	**2.03**	0.055	0.055	0.053	**0.054**
2.5	2.55	2.52	2.51	**2.53**	0.062	0.072	0.071	**0.068**
3.0	3.02	2.99	3.01	**3.01**	0.091	0.088	0.087	**0.089**
3.5	3.51	3.53	3.54	**3.53**	0.107	0.104	0.105	**0.105**
4.0	4.04	4.00	4.00	**4.01**	0.106	0.118	0.118	**0.114**
4.5	4.51	4.50	4.54	**4.52**	0.138	0.134	0.134	**0.135**
5.0	5.02	4.99	5.01	**5.01**	0.150	0.143	0.143	**0.145**
6.0	6.01	6.01	6.00	**6.01**	0.161	0.168	0.169	**0.166**
7.0	7.04	7.04	7.02	**7.03**	0.187	0.185	0.184	**0.185**
8.0	8.02	8.10	8.07	**8.06**	0.200	0.201	0.198	**0.200**
9.0	9.11	9.07	9.01	**9.06**	0.209	0.211	0.207	**0.209**
10.0	10.02	9.98	9.97	**9.99**	0.204	0.217	0.213	**0.215**
11.0	10.99	11.04	11.06	**11.03**	0.228	0.228	0.228	**0.228**
12.0	12.04	11.97	12.02	**12.01**	0.237	0.234	0.236	**0.236**
13.0	13.08	12.99	13.07	**13.05**	0.243	0.236	0.243	**0.241**
14.0	13.99	13.94	13.96	**13.96**	0.247	0.247	0.234	**0.243**
15.0	15.04	14.92	15.03	**15.00**	0.252	0.250	0.252	**0.251**
16.0	16.04	16.03	16.10	**16.06**	0.248	0.258	0.256	**0.257**
17.0	17.00	17.04	17.01	**17.02**	0.262	0.262	0.258	**0.261**
18.0	18.02	18.03	18.05	**18.03**	0.264	0.264	0.264	**0.264**
19.0	19.02	19.00	19.03	**19.02**	0.269	0.267	0.269	**0.268**
20.0	20.02	20.03	20.03	**20.03**	0.269	0.272	0.270	**0.270**

Test Conditions:
DI Water
A = 0.62%
Open Vent Mode

Target Superficial Gas Velocity	Measured Superficial Gas Velocity				Measured Riser Gas Holdup				Measured Downcomer Gas Holdup				Measured Downcomer Linear Liquid Velocity				Calculated Riser Superficial Liquid Velocity			
	Test #1	Test #2	Test #3	Avg	Test #1	Test #2	Test #3	Avg	Test #1	Test #2	Test #3	Avg	Test #1	Test #2	Test #3	Avg	Test #1	Test #2	Test #3	Avg*
(cm/s)	(cm/s)	(cm/s)	(cm/s)	(cm/s)	(-)	(-)	(-)	(-)	(-)	(-)	(-)	(-)	(cm/s)	(cm/s)	(cm/s)	(cm/s)	(cm/s)	(cm/s)	(cm/s)	(cm/s)
0.5	0.524	0.534	0.525	**0.528**	0.022	0.023	0.022	**0.023**	0.005	0.007	0.008	**0.007**	31.40	28.23	31.86	**30.50**	1.95	1.75	1.98	**1.89**
2.0	2.009	2.030	2.057	**2.032**	0.065	0.065	0.064	**0.065**	0.008	0.015	0.016	**0.013**	53.57	54.46	53.66	**53.90**	3.32	3.35	3.30	**3.32**
4.0	3.997	4.056	4.052	**4.035**	0.124	0.124	0.125	**0.124**	0.041	0.049	0.049	**0.046**	59.94	60.61	61.89	**60.81**	3.59	3.60	3.68	**3.62**
6.0	6.046	5.999	6.020	**6.021**	0.172	0.170	0.169	**0.170**	0.065	0.065	0.068	**0.066**	53.91	54.05	55.80	**54.59**	3.15	3.16	3.25	**3.19**
8.0	8.069	8.071	8.069	**8.070**	0.201	0.198	0.197	**0.199**	0.085	0.084	0.084	**0.084**	53.36	53.20	-	**53.28**	3.05	3.05	-	**3.05**
10.0	10.078	10.025	10.020	**10.041**	0.222	0.219	0.218	**0.219**	0.088	0.094	0.096	**0.093**	49.94	49.14	50.66	**49.91**	2.85	2.78	2.86	**2.83**
12.0	12.021	12.051	12.054	**12.042**	0.232	0.233	0.233	**0.233**	0.088	0.092	0.094	**0.091**	43.95	44.44	48.81	**45.73**	2.51	2.52	2.76	**2.60**
14.0	14.040	14.107	14.066	**14.071**	0.233	0.234	0.232	**0.233**	0.084	0.085	0.084	**0.084**	44.99	43.92	46.21	**45.04**	2.58	2.51	2.65	**2.58**
16.0	16.064	16.110	16.072	**16.082**	0.230	0.230	0.230	**0.230**	0.080	0.081	0.082	**0.081**	42.42	43.46	44.31	**43.40**	2.44	2.50	2.54	**2.49**
18.0	18.082	18.118	18.055	**18.085**	0.226	0.233	0.235	**0.231**	0.072	0.078	0.082	**0.077**	42.26	42.51	43.18	**42.65**	2.45	2.45	2.48	**2.46**
20.0	20.074	20.084	20.080	**20.080**	0.242	0.242	0.240	**0.241**	0.081	0.083	0.084	**0.083**	39.97	43.15	42.20	**41.77**	2.30	2.47	2.42	**2.40**

Test Conditions:
DI Water
A = 0.62%
Closed Vent Mode

Target Superficial Gas Velocity	Measured Superficial Gas Velocity				Measured Riser Gas Holdup				Measured Downcomer Linear Liquid Velocity				Calculated Riser Superficial Liquid Velocity			
	Test #1	Test #2	Test #3	Avg	Test #1	Test #2	Test #3	Avg	Test #1	Test #2	Test #3	Avg	Test #1	Test #2	Test #3	Avg*
(cm/s)	(cm/s)	(cm/s)	(cm/s)	(cm/s)	(-)	(-)	(-)	(-)	(cm/s)	(cm/s)	(cm/s)	(cm/s)	(cm/s)	(cm/s)	(cm/s)	(cm/s)
0.5	0.563	0.522	0.509	**0.531**	0.025	0.026	0.025	**0.025**	19.40	18.77	18.57	**18.91**	1.21	1.17	1.16	**1.18**
2.0	2.009	2.055	2.030	**2.031**	0.070	0.071	0.071	**0.071**	16.37	16.44	16.65	**16.49**	1.02	1.03	1.04	**1.03**
4.0	4.058	-	4.034	**4.046**	0.134	0.137	0.135	**0.135**	14.08	13.32	12.46	**13.29**	0.88	0.83	0.78	**0.83**
6.0	-	5.982	5.974	**5.978**	0.184	0.185	0.185	**0.185**	-	12.07	12.97	**12.52**	-	0.75	0.81	**0.78**
8.0	8.006	8.012	8.116	**8.045**	0.213	0.212	0.211	**0.212**	11.79	12.90	12.39	**12.36**	0.74	0.81	0.77	**0.77**
10.0	10.027	10.031	10.025	**10.028**	0.238	0.234	0.236	**0.236**	12.85	13.17	12.75	**12.92**	0.80	0.82	0.80	**0.81**
12.0	12.021	12.040	12.002	**12.021**	-	0.247	0.243	**0.245**	-	14.08	13.88	**13.98**	-	0.88	0.87	**0.87**
14.0	13.951	14.001	14.023	**13.991**	0.246	0.246	0.243	**0.245**	14.57	14.83	15.16	**14.85**	0.91	0.93	0.95	**0.93**
16.0	16.024	15.963	16.012	**16.000**	-	0.242	0.241	**0.241**	-	15.18	14.31	**14.74**	-	0.95	0.89	**0.92**
18.0	18.033	17.974	17.996	**18.001**	0.228	0.242	0.240	**0.237**	13.97	14.89	14.23	**14.36**	0.87	0.93	0.89	**0.90**
20.0	20.016	19.979	19.971	**19.988**	0.238	0.248	0.248	**0.245**	15.14	14.88	15.66	**15.23**	0.95	0.93	0.98	**0.95**

Test Conditions:
DI Water
A = 0.62%
Bubble Column Mode

Target Superficial Gas Velocity	Measured Superficial Gas Velocity				Measured Riser Gas Holdup			
	Test #1	Test #2	Test #3	Avg	Test #1	Test #2	Test #3	Avg
(cm/s)	(cm/s)	(cm/s)	(cm/s)	(cm/s)	(-)	(-)	(-)	(-)
0.5	0.563	0.522	0.509	**0.531**	0.026	0.020	0.019	**0.022**
2.0	2.009	2.055	2.030	**2.031**	0.073	0.069	0.069	**0.070**
4.0	4.058	-	4.034	**4.046**	0.140	0.135	0.134	**0.136**
6.0	-	5.982	5.974	**5.978**	0.187	0.184	0.182	**0.185**
8.0	8.006	8.012	8.116	**8.045**	0.216	0.209	0.210	**0.212**
10.0	10.027	10.031	10.025	**10.028**	0.238	0.232	0.231	**0.234**
12.0	12.021	12.040	12.002	**12.021**	0.251	0.247	0.242	**0.247**
14.0	13.951	14.001	14.023	**13.991**	0.250	0.245	0.244	**0.246**
16.0	16.024	15.963	16.012	**16.000**	0.239	0.243	0.240	**0.241**
18.0	18.033	17.974	17.996	**18.001**	0.242	0.241	0.240	**0.241**
20.0	20.016	19.979	19.971	**19.988**	0.256	0.245	0.245	**0.248**

Test Conditions:
DI Water
A = 0.99%
Open Vent Mode

Target Superficial Gas Velocity	Measured Superficial Gas Velocity				Measured Riser Gas Holdup				Measured Downcomer Gas Holdup				Measured Downcomer Linear Liquid Velocity				Calculated Riser Superficial Liquid Velocity			
	Test #1	Test #2	Test #3	Avg	Test #1	Test #2	Test #3	Avg	Test #1	Test #2	Test #3	Avg	Test #1	Test #2	Test #3	Avg	Test #1	Test #2	Test #3	Avg*
(cm/s)	(cm/s)	(cm/s)	(cm/s)	(cm/s)	(-)	(-)	(-)	(-)	(-)	(-)	(-)	(-)	(cm/s)	(cm/s)	(cm/s)	(cm/s)	(cm/s)	(cm/s)	(cm/s)	(cm/s)
0.5	0.495	0.493	0.485	**0.491**	0.024	0.027	0.027	**0.026**	0.002	0.006	0.004	**0.004**	30.47	31.72	30.47	**30.89**	1.90	1.97	1.90	**1.92**
2.0	1.996	2.005	2.016	**2.006**	0.067	0.067	0.066	**0.067**	-0.003	0.000	0.006	**0.001**	54.86	53.59	53.68	**54.05**	3.44	3.35	3.34	**3.37**
4.0	3.972	3.989	4.005	**3.989**	0.129	0.130	0.130	**0.130**	0.047	0.048	0.045	**0.047**	59.03	59.71	61.00	**59.91**	3.52	3.55	3.64	**3.57**
6.0	5.970	5.964	5.964	**5.966**	0.180	0.177	0.178	**0.179**	0.067	0.065	0.064	**0.065**	54.94	55.45	56.04	**55.48**	3.20	3.24	3.28	**3.24**
8.0	8.015	7.997	8.050	**8.021**	0.189	0.202	0.202	**0.198**	-	0.080	0.079	**0.080**	53.17	53.42	53.57	**53.39**	-	3.07	3.08	**3.07**
10.0	10.038	10.052	10.086	**10.059**	-	0.229	0.229	**0.229**	0.084	0.093	0.093	**0.090**	51.18	49.10	50.10	**50.13**	2.93	2.78	2.84	**2.85**
12.0	11.984	11.972	12.029	**11.995**	-	0.244	0.245	**0.244**	-	0.092	0.091	**0.091**	46.84	47.79	47.44	**47.35**	-	2.71	2.70	**2.69**
14.0	14.013	14.010	14.055	**14.026**	0.255	0.257	0.254	**0.256**	0.089	0.089	0.085	**0.088**	46.57	46.11	47.00	**46.56**	2.65	2.63	2.69	**2.66**
16.0	16.092	15.964	15.975	**16.010**	0.251	0.255	0.253	**0.253**	0.079	0.081	0.077	**0.079**	43.93	43.36	44.47	**43.92**	2.53	2.49	2.57	**2.53**
18.0	17.989	18.023	18.043	**18.018**	0.245	0.251	0.255	**0.251**	0.070	0.072	0.072	**0.071**	43.70	42.04	44.14	**43.29**	2.54	2.44	2.56	**2.51**
20.0	19.981	19.978	20.072	**20.010**	0.258	0.259	0.258	**0.258**	0.073	0.073	0.070	**0.072**	41.61	41.30	41.01	**41.31**	2.41	2.39	2.38	**2.40**

Test Conditions:
DI Water
A = 2.22%
Open Vent Mode

Target Superficial Gas Velocity	Measured Superficial Gas Velocity				Measured Riser Gas Holdup				Measured Downcomer Gas Holdup				Measured Downcomer Linear Liquid Velocity				Calculated Riser Superficial Liquid Velocity			
	Test #1	Test #2	Test #3	Avg	Test #1	Test #2	Test #3	Avg	Test #1	Test #2	Test #3	Avg	Test #1	Test #2	Test #3	Avg	Test #1	Test #2	Test #3	Avg*
(cm/s)	(cm/s)	(cm/s)	(cm/s)	(cm/s)	(-)	(-)	(-)	(-)	(-)	(-)	(-)	(-)	(cm/s)	(cm/s)	(cm/s)	(cm/s)	(cm/s)	(cm/s)	(cm/s)	(cm/s)
0.5	0.529	0.493	0.527	**0.516**	0.026	0.025	0.026	**0.026**	-0.001	0.003	0.008	**0.003**	32.19	31.74	32.72	**32.21**	2.01	1.98	2.03	**2.01**
2.0	1.996	2.005	2.016	**2.006**	0.067	0.067	0.066	**0.067**	0.007	0.010	0.016	**0.011**	54.81	54.50	53.68	**54.33**	3.40	3.37	3.30	**3.36**
4.0	4.036	3.973	4.000	**4.003**	0.125	0.122	0.122	**0.123**	0.042	0.042	0.045	**0.043**	59.17	59.01	59.74	**59.31**	3.54	3.53	3.57	**3.55**
6.0	5.954	5.952	5.987	**5.964**	0.166	0.165	0.163	**0.165**	0.056	0.060	0.064	**0.060**	55.83	55.38	55.56	**55.59**	3.30	3.25	3.25	**3.27**
8.0	8.105	7.983	8.054	**8.047**	0.189	0.181	0.187	**0.185**	0.069	0.100	0.073	**0.081**	52.70	51.08	53.64	**52.47**	3.07	2.87	3.11	**3.02**
10.0	10.011	10.060	10.051	**10.041**	0.209	0.207	0.207	**0.208**	0.077	0.078	0.083	**0.079**	50.53	49.22	50.89	**50.21**	2.91	2.84	2.92	**2.89**
12.0	12.016	12.039	12.013	**12.023**	0.220	0.221	0.222	**0.221**	0.076	0.079	0.085	**0.080**	46.59	46.68	46.17	**46.48**	2.69	2.69	2.64	**2.67**
14.0	14.007	14.078	14.017	**14.034**	0.233	0.239	0.236	**0.236**	0.076	0.080	0.084	**0.080**	44.01	45.49	43.41	**44.30**	2.54	2.61	2.49	**2.55**
16.0	15.978	16.012	16.081	**16.024**	0.246	0.243	0.246	**0.245**	0.078	0.078	0.086	**0.081**	42.20	43.18	44.85	**43.41**	2.43	2.49	2.56	**2.49**
18.0	18.079	17.986	17.961	**18.009**	0.257	0.250	0.250	**0.252**	0.080	0.081	0.082	**0.081**	42.56	43.89	44.67	**43.71**	2.45	2.52	2.56	**2.51**
20.0	19.908	20.038	19.967	**19.971**	0.258	0.260	0.259	**0.259**	0.077	0.080	0.084	**0.080**	42.20	44.80	41.45	**42.82**	2.43	2.58	2.37	**2.46**

Test Conditions:
KCl Solution
A = 0.62%
Open Vent Mode

Target Superficial Gas Velocity	Measured Superficial Gas Velocity				Measured Riser Gas Holdup				Measured Downcomer Gas Holdup				Measured Downcomer Linear Liquid Velocity				Calculated Riser Superficial Liquid Velocity			
	Test #1	Test #2	Test #3	Avg	Test #1	Test #2	Test #3	Avg	Test #1	Test #2	Test #3	Avg	Test #1	Test #2	Test #3	Avg	Test #1	Test #2	Test #3	Avg*
(cm/s)	(cm/s)	(cm/s)	(cm/s)	(cm/s)	(-)	(-)	(-)	(-)	(-)	(-)	(-)	(-)	(cm/s)	(cm/s)	(cm/s)	(cm/s)	(cm/s)	(cm/s)	(cm/s)	(cm/s)
0.5	0.486	0.498	0.537	**0.507**	0.026	0.027	0.028	**0.027**	0.002	0.003	0.005	**0.004**	32.36	30.35	31.74	**31.48**	2.02	1.89	1.97	**1.96**
2.0	2.011	2.025	2.029	**2.022**	0.071	0.073	0.073	**0.072**	0.012	0.014	0.015	**0.014**	51.82	52.65	53.34	**52.60**	3.20	3.24	3.28	**3.24**
4.0	3.999	3.985	3.980	**3.988**	0.144	0.141	0.141	**0.142**	0.066	0.062	0.063	**0.064**	53.68	-	54.37	**54.03**	3.13	-	3.19	**3.16**
6.0	5.993	5.989	5.975	**5.986**	0.210	0.210	0.212	**0.211**	0.103	0.101	0.107	**0.104**	50.53	49.67	48.74	**49.65**	2.83	2.79	2.72	**2.78**
8.0	8.042	8.006	8.031	**8.026**	0.238	0.238	0.240	**0.239**	0.126	0.128	0.135	**0.130**	45.06	44.25	42.88	**44.06**	2.46	2.41	2.32	**2.40**
10.0	9.977	9.997	10.025	**10.000**	0.262	0.263	0.262	**0.263**	0.152	0.141	0.149	**0.147**	38.74	38.65	38.73	**38.71**	2.05	2.07	2.06	**2.06**
12.0	12.046	12.045	12.019	**12.037**	-	0.276	0.273	**0.275**	-	0.149	0.149	**0.149**	-	38.92	39.53	**39.22**	-	2.07	2.10	**2.09**
14.0	14.008	14.030	14.001	**14.013**	0.282	0.284	0.283	**0.283**	0.146	0.147	0.147	**0.147**	39.40	39.87	39.53	**39.60**	2.10	2.13	2.11	**2.11**
16.0	16.010	16.059	16.040	**16.036**	0.268	0.269	0.272	**0.270**	0.109	0.110	0.116	**0.112**	41.89	41.73	40.04	**41.22**	2.33	2.32	2.21	**2.29**
18.0	18.031	18.019	18.045	**18.032**	0.270	0.265	0.268	**0.268**	0.103	0.098	0.101	**0.101**	40.87	41.45	40.01	**40.78**	2.29	2.34	2.25	**2.29**
20.0	20.055	20.050	20.110	**20.071**	0.274	0.272	0.272	**0.272**	0.098	0.099	0.095	**0.098**	39.01	39.52	39.15	**39.23**	2.20	2.23	2.21	**2.21**

Test Conditions:
Nitrosomonas Solution
A = 0.62%
Open Vent Mode

Target Superficial Gas Velocity	Measured Superficial Gas Velocity				Measured Riser Gas Holdup				Measured Downcomer Gas Holdup				Measured Downcomer Linear Liquid Velocity				Calculated Riser Superficial Liquid Velocity			
	Test #1	Test #2	Test #3	Avg	Test #1	Test #2	Test #3	Avg	Test #1	Test #2	Test #3	Avg	Test #1	Test #2	Test #3	Avg	Test #1	Test #2	Test #3	Avg*
(cm/s)	(cm/s)	(cm/s)	(cm/s)	(cm/s)	(-)	(-)	(-)	(-)	(-)	(-)	(-)	(-)	(cm/s)	(cm/s)	(cm/s)	(cm/s)	(cm/s)	(cm/s)	(cm/s)	(cm/s)
0.5	0.507	0.511	0.506	**0.508**	0.026	0.033	0.033	**0.030**	-0.005	0.007	0.012	**0.005**	31.39	31.36	31.54	**31.43**	1.97	1.95	1.95	**1.96**
2.0	1.972	1.987	1.998	**1.986**	0.071	0.074	0.077	**0.074**	0.005	0.011	0.019	**0.012**	52.87	52.71	53.48	**53.02**	3.29	3.26	3.28	**3.28**
4.0	3.995	4.032	4.007	**4.012**	0.136	0.142	0.143	**0.140**	0.044	0.053	0.061	**0.053**	60.28	58.37	58.91	**59.19**	3.60	3.45	3.46	**3.50**
6.0	5.996	5.999	5.996	**5.997**	0.209	0.206	0.210	**0.208**	0.093	0.095	0.098	**0.095**	49.74	50.66	49.28	**49.89**	2.82	2.87	2.78	**2.82**
8.0	8.039	8.020	8.038	**8.032**	0.229	0.231	0.247	**0.235**	0.108	0.116	0.141	**0.122**	46.68	47.35	41.19	**45.08**	2.60	2.62	2.21	**2.47**
10.0	10.010	10.029	10.077	**10.039**	0.265	0.265	0.277	**0.269**	0.142	0.153	0.162	**0.152**	37.21	37.99	38.02	**37.74**	2.00	2.01	1.99	**2.00**
12.0	12.032	12.006	12.007	**12.015**	0.278	0.286	0.278	**0.281**	0.138	0.169	0.148	**0.152**	43.59	42.05	42.74	**42.80**	2.35	2.18	2.28	**2.27**
14.0	14.115	13.976	14.011	**14.034**	0.287	0.283	0.284	**0.285**	0.141	0.143	0.143	**0.142**	46.65	42.97	39.81	**43.14**	2.50	2.30	2.13	**2.31**
16.0	16.031	16.042	16.078	**16.050**	0.279	0.278	0.270	**0.276**	0.116	0.122	0.116	**0.118**	45.96	40.92	40.86	**42.58**	2.54	2.25	2.26	**2.35**
18.0	18.010	17.999	17.984	**17.997**	0.272	0.273	0.276	**0.274**	0.095	0.112	0.117	**0.109**	41.66	41.23	39.71	**40.87**	2.36	2.29	2.19	**2.27**
20.0	20.062	20.036	20.050	**20.049**	0.282	0.273	0.279	**0.278**	0.119	0.111	0.119	**0.116**	39.98	40.72	40.00	**40.23**	2.20	2.26	2.20	**2.22**

APPENDIX D:

GAS-LIQUID MASS TRANSFER DATA

Appendix D contains a summary of the EALR oxygen and carbon monoxide gas-liquid mass transfer data collected during this study. Included in these tables are the oxygen gas-liquid mass transfer rate data measured when the liquid phase in the EALR was sparged with air, carbon monoxide, and nitrogen using the extended dynamic gassing out method and carbon monoxide gas-liquid mass transfer rate data measured when the liquid phase was sparged with air and carbon monoxide using the basic dynamic gassing out method. The data is first presented for the deionized water condition followed by the potassium chloride solution, the nitrosomonas solution, and the deionized water with surfactant conditions.

Test Conditions:

DI Water — Open Vent Mode

A = 0.62% — U_G = 0.5 cm/s

Oxygen Mass Transfer Data							
Test	Inlet Gas	Gas Velocity (cm/s)	Temperature (ºC)	k_La (1/s)	C_o (% of Sat)	C_∞ (% of Sat)	τ_e (s)
#1	Nitrogen	0.51	19.9	0.0071	98.8	-2.0	4.37
#2	Nitrogen	0.57	20.2	0.0084	99.4	-0.9	3.00
#3	Nitrogen	0.55	20.1	0.0077	99.2	-1.3	4.86
#1	Air	0.54	20.1	0.0083	0.5	101.0	2.53
#2	Air	0.52	20.3	0.0079	0.4	101.0	2.36
#3	Air	0.55	20.1	0.0076	0.3	101.2	1.75
#1	Carbon Monoxide	0.51	20.2	0.0072	99.3	-1.9	4.77
#2	Carbon Monoxide	0.51	20.4	0.0076	99.3	-1.4	4.31
#3	Carbon Monoxide	0.54	20.3	0.0078	99.0	-1.3	4.25
#1	Air	0.54	20.3	0.0084	0.7	101.4	1.77
#2	Air	0.52	20.5	0.0079	0.5	101.1	2.43
#3	Air	0.50	20.4	0.0077	0.7	101.2	2.34
Average		**0.53**	**20.2**	**0.0078**	**-**	**-**	**3.23**

Test Conditions:

DI Water — Open Vent Mode

A = 0.62% — U_G = 2.0 cm/s

Oxygen Mass Transfer Data							
Test	Inlet Gas	Gas Velocity (cm/s)	Temperature (ºC)	k_La (1/s)	C_o (% of Sat)	C_∞ (% of Sat)	τ_e (s)
#1	Nitrogen	2.02	20.6	0.0252	99.9	0.0	2.46
#2	Nitrogen	2.04	19.9	0.0257	99.3	0.0	2.25
#3	Nitrogen	2.08	19.3	0.0253	99.9	0.0	2.63
#1	Air	2.01	20.7	0.0255	0.6	99.9	1.84
#2	Air	2.02	19.9	0.0258	0.5	99.9	1.79
#3	Air	2.08	19.3	0.0263	-0.1	100.3	2.82
#1	Carbon Monoxide	2.00	20.7	0.0249	100.0	-0.1	2.50
#2	Carbon Monoxide	2.06	20.0	0.0260	99.5	0.0	2.03
#3	Carbon Monoxide	2.08	19.5	0.0252	99.6	0.0	2.44
#1	Air	2.01	20.8	0.0252	0.4	100.0	2.06
#2	Air	2.01	20.1	0.0256	-0.4	99.9	1.67
#3	Air	2.03	19.6	0.0264	0.4	100.4	2.55
Average		**2.04**	**20.0**	**0.0256**	**-**	**-**	**2.25**

Carbon Monoxide Mass Transfer Data						
Test	Inlet Gas	Gas Velocity (cm/s)	Temperature (ºC)	k_La (1/s)	C_o (% of Sat)	C_∞ (% of Sat)
#1	Carbon Monoxide	2.00	20.7	0.0230	0.0	100.9
#2	Carbon Monoxide	2.06	20.0	0.0253	0.0	99.0
#3	Carbon Monoxide	2.08	19.5	0.0274	0.0	98.9
Average		**2.05**	**20.1**	**0.0252**	**-**	**-**

Test Conditions:

DI Water — Open Vent Mode

A = 0.62% — U_G = 4.0 cm/s

Oxygen Mass Transfer Data							
Test	Inlet Gas	Gas Velocity (cm/s)	Temperature (ºC)	k_La (1/s)	C_o (% of Sat)	C_∞ (% of Sat)	τ_e (s)
#1	Nitrogen	4.00	19.9	0.0553	100.0	0.0	2.61
#2	Nitrogen	4.06	20.0	0.0571	99.3	0.1	2.37
#3	Nitrogen	3.99	20.1	0.0576	99.2	0.0	3.18
#1	Air	3.99	20.0	0.0567	0.2	99.9	3.29
#2	Air	4.00	19.9	0.0583	1.1	99.9	2.33
#3	Air	3.99	20.1	0.0571	0.9	99.8	2.50
#1	Carbon Monoxide	4.00	20.1	0.0569	99.3	0.1	2.87
#2	Carbon Monoxide	3.99	20.0	0.0578	99.7	0.1	2.39
#3	Carbon Monoxide	4.06	20.1	0.0570	98.9	0.0	2.55
#1	Air	3.99	20.1	0.0560	0.8	99.9	2.32
#2	Air	4.00	20.1	0.0584	0.7	100.1	2.55
#3	Air	4.05	20.1	0.0575	0.3	99.9	2.69
Average		**4.01**	**20.0**	**0.0571**	**-**	**-**	**2.64**

Test Conditions:

DI Water — Open Vent Mode

A = 0.62% — U_G = 6.0 cm/s

Oxygen Mass Transfer Data							
Test	Inlet Gas	Gas Velocity (cm/s)	Temperature (ºC)	k_La (1/s)	C_o (% of Sat)	C_∞ (% of Sat)	τ_e (s)
#1	Nitrogen	6.06	20.1	0.0837	99.8	0.2	2.96
#2	Nitrogen	6.01	19.9	0.0865	101.1	0.2	4.47
#3	Nitrogen	6.03	20.3	0.0868	100.8	0.1	3.22
#1	Air	6.03	20.2	0.0861	0.4	100.1	3.06
#2	Air	5.99	19.9	0.0867	0.6	100.0	3.19
#3	Air	6.03	20.3	0.0929	0.7	100.5	3.09
#1	Carbon Monoxide	6.05	20.2	0.0833	100.1	0.1	3.10
#2	Carbon Monoxide	6.00	20.0	-	104.9	0.3	8.55
#3	Carbon Monoxide	6.01	20.4	0.0887	99.6	0.1	3.72
#1	Air	6.04	20.3	0.0865	-0.2	99.9	3.19
#2	Air	6.00	20.0	0.0868	0.6	100.4	2.95
#3	Air	6.02	20.5	0.0892	-0.7	100.2	3.09
Average		**6.02**	**20.2**	**0.0870**	**-**	**-**	**3.72**

Carbon Monoxide Mass Transfer Data						
Test	Inlet Gas	Gas Velocity (cm/s)	Temperature (ºC)	k_La (1/s)	C_o (% of Sat)	C_∞ (% of Sat)
#1	Carbon Monoxide	6.05	20.2	0.0774	0.0	102.1
#2	Carbon Monoxide	6.00	20.0	0.0898	0.0	98.8
#3	Carbon Monoxide	6.01	20.4	0.0788	0.0	102.8
Average		**6.02**	**20.2**	**0.0820**	**-**	**-**

Test Conditions:

DI Water — Open Vent Mode

A = 0.62% — U_G = 8.0 cm/s

Oxygen Mass Transfer Data							
Test	Inlet Gas	Gas Velocity (cm/s)	Temperature (ºC)	k_La (1/s)	C_o (% of Sat)	C_∞ (% of Sat)	τ_e (s)
#1	Nitrogen	8.07	20.2	0.1119	100.6	0.2	3.78
#2	Nitrogen	8.09	19.8	0.1085	99.9	0.2	3.11
#3	Nitrogen	8.08	20.2	0.1067	100.0	0.1	2.88
#1	Air	8.08	20.2	0.1080	0.4	100.1	2.90
#2	Air	8.06	19.8	0.1083	0.7	100.0	2.58
#3	Air	8.08	20.2	0.1067	0.4	99.9	2.65
#1	Carbon Monoxide	8.05	20.2	0.1075	99.7	0.1	3.58
#2	Carbon Monoxide	8.08	19.8	0.1093	99.4	0.1	3.07
#3	Carbon Monoxide	8.08	20.3	0.1066	99.4	0.1	2.61
#1	Air	8.09	20.3	0.1068	-0.5	99.8	3.07
#2	Air	8.05	19.9	0.1089	1.9	100.0	2.51
#3	Air	8.06	20.3	0.1114	-0.8	100.0	3.22
Average		**8.07**	**20.1**	**0.1084**	**-**	**-**	**3.00**

Test Conditions:

DI Water — Open Vent Mode

A = 0.62% — U_G = 10.0 cm/s

Oxygen Mass Transfer Data							
Test	Inlet Gas	Gas Velocity (cm/s)	Temperature (ºC)	k_La (1/s)	C_o (% of Sat)	C_∞ (% of Sat)	τ_e (s)
#1	Nitrogen	9.99	20.0	0.1356	101.2	0.2	3.71
#2	Nitrogen	10.05	20.0	0.1252	99.3	0.1	2.58
#3	Nitrogen	9.92	20.3	0.1254	99.6	0.2	2.94
#1	Air	10.16	20.1	0.1233	1.1	99.9	2.33
#2	Air	10.03	19.9	0.1233	0.0	100.0	2.32
#3	Air	9.92	20.3	0.1323	1.3	100.5	3.05
#1	Carbon Monoxide	10.00	20.1	0.1229	99.8	0.1	2.83
#2	Carbon Monoxide	9.99	19.9	0.1283	99.5	0.1	3.15
#3	Carbon Monoxide	10.06	20.4	0.1275	99.8	0.1	3.05
#1	Air	10.16	20.1	0.1190	0.0	99.9	2.08
#2	Air	10.03	19.9	0.1229	-1.3	99.7	2.68
#3	Air	10.06	20.4	0.1357	-0.4	100.1	3.10
Average		**10.03**	**20.1**	**0.1268**	**-**	**-**	**2.82**

Carbon Monoxide Mass Transfer Data						
Test	Inlet Gas	Gas Velocity (cm/s)	Temperature (ºC)	k_La (1/s)	C_o (% of Sat)	C_∞ (% of Sat)
#1	Carbon Monoxide	10.00	20.1	0.1304	0.0	98.8
#2	Carbon Monoxide	9.99	19.9	0.1217	0.0	98.7
#3	Carbon Monoxide	10.06	20.4	0.1213	0.0	95.9
Average		**10.01**	**20.1**	**0.1244**	**-**	**-**

Test Conditions:

DI Water — Open Vent Mode

A = 0.62% — U_G = 12.0 cm/s

Oxygen Mass Transfer Data							
Test	Inlet Gas	Gas Velocity (cm/s)	Temperature (ºC)	k_La (1/s)	C_o (% of Sat)	C_∞ (% of Sat)	τ_e (s)
#1	Nitrogen	12.00	19.7	0.1164	99.0	0.3	2.30
#2	Nitrogen	12.02	19.9	0.1187	100.6	0.2	2.77
#3	Nitrogen	12.02	20.5	0.1319	101.1	0.2	2.35
#1	Air	12.03	19.7	0.1140	1.0	100.2	1.90
#2	Air	12.07	19.9	0.1315	0.6	100.1	3.32
#3	Air	12.02	20.5	0.1272	0.7	100.1	2.43
#1	Carbon Monoxide	12.02	19.7	0.1168	99.6	0.2	2.68
#2	Carbon Monoxide	12.05	19.9	0.1278	100.8	0.2	3.70
#3	Carbon Monoxide	12.03	20.5	0.1311	98.7	0.2	2.25
#1	Air	12.03	19.7	0.1157	-0.2	100.2	2.11
#2	Air	12.05	19.9	0.1279	-0.3	100.1	2.71
#3	Air	12.09	20.5	0.1350	0.3	99.9	2.47
Average		**12.04**	**20.0**	**0.1245**	**-**	**-**	**2.58**

Test Conditions:

DI Water — Open Vent Mode

A = 0.62% — U_G = 14.0 cm/s

Oxygen Mass Transfer Data							
Test	Inlet Gas	Gas Velocity (cm/s)	Temperature (ºC)	k_La (1/s)	C_o (% of Sat)	C_∞ (% of Sat)	τ_e (s)
#1	Nitrogen	14.01	20.3	0.1126	100.1	0.1	2.50
#2	Nitrogen	14.12	19.6	0.1202	100.5	0.2	2.69
#3	Nitrogen	14.05	20.2	0.1231	100.2	0.2	2.45
#1	Air	14.08	20.3	0.1182	0.4	99.8	2.24
#2	Air	14.07	19.6	0.1185	0.1	99.8	1.66
#3	Air	14.05	20.2	0.1197	0.2	100.0	1.86
#1	Carbon Monoxide	14.06	20.2	0.1184	99.5	0.1	3.08
#2	Carbon Monoxide	14.16	19.6	0.1171	100.1	0.1	2.24
#3	Carbon Monoxide	14.04	20.2	0.1173	100.4	0.1	2.23
#1	Air	14.01	20.2	0.1191	-0.4	100.1	2.67
#2	Air	14.08	19.6	0.1222	0.0	99.6	2.29
#3	Air	14.10	20.2	0.1189	0.3	100.0	2.16
Average		**14.07**	**20.0**	**0.1188**	**-**	**-**	**2.34**

Carbon Monoxide Mass Transfer Data						
Test	Inlet Gas	Gas Velocity (cm/s)	Temperature (ºC)	k_La (1/s)	C_o (% of Sat)	C_∞ (% of Sat)
#1	Carbon Monoxide	14.06	20.2	0.1272	0.0	100.2
#2	Carbon Monoxide	14.16	19.6	0.1098	0.0	100.5
#3	Carbon Monoxide	14.04	20.2	0.1219	0.0	99.3
Average		**14.09**	**20.0**	**0.1196**	**-**	**-**

Test Conditions:

DI Water — Open Vent Mode

A = 0.62% — U_G = 16.0 cm/s

Oxygen Mass Transfer Data							
Test	Inlet Gas	Gas Velocity (cm/s)	Temperature (ºC)	k_La (1/s)	C_o (% of Sat)	C_∞ (% of Sat)	τ_e (s)
#1	Nitrogen	16.04	20.2	0.1213	99.6	0.1	2.79
#2	Nitrogen	16.09	20.1	0.1265	98.8	0.2	3.27
#3	Nitrogen	16.06	20.3	0.1237	99.8	0.1	2.51
#1	Air	16.10	20.2	0.1276	0.0	99.9	3.00
#2	Air	16.27	20.1	0.1166	1.1	99.9	1.87
#3	Air	16.06	20.3	0.1258	0.3	100.3	2.07
#1	Carbon Monoxide	16.08	20.2	0.1204	99.6	0.1	2.85
#2	Carbon Monoxide	16.08	20.1	0.1232	100.1	0.1	2.45
#3	Carbon Monoxide	16.05	20.3	0.1238	100.3	0.1	2.68
#1	Air	16.03	20.2	0.1207	0.2	100.0	2.31
#2	Air	16.00	20.1	0.1195	0.2	100.0	2.18
#3	Air	16.07	20.3	0.1322	0.0	100.2	2.35
Average		**16.08**	**20.2**	**0.1234**	**-**	**-**	**2.53**

Test Conditions:

DI Water — Open Vent Mode

A = 0.62% — U_G = 18.0 cm/s

Oxygen Mass Transfer Data							
Test	Inlet Gas	Gas Velocity (cm/s)	Temperature (ºC)	k_La (1/s)	C_o (% of Sat)	C_∞ (% of Sat)	τ_e (s)
#1	Nitrogen	18.04	20.0	-	99.2	0.1	2.53
#2	Nitrogen	18.08	20.3	0.1256	99.8	0.2	2.61
#3	Nitrogen	18.02	20.2	0.1267	99.2	0.2	2.88
#1	Air	18.08	20.0	0.1102	-0.5	99.8	2.41
#2	Air	18.15	20.3	0.1267	-0.9	99.7	2.17
#3	Air	18.02	20.2	0.1289	-0.7	100.0	2.67
#1	Carbon Monoxide	18.09	20.0	-	100.4	0.1	2.41
#2	Carbon Monoxide	18.06	20.2	0.1264	99.5	0.1	2.59
#3	Carbon Monoxide	18.05	20.1	0.1278	99.4	0.2	2.96
#1	Air	18.11	19.9	-	0.3	100.0	2.01
#2	Air	18.17	20.2	0.1255	1.0	99.8	2.07
#3	Air	18.08	20.1	0.1280	0.7	100.1	2.93
Average		**18.08**	**20.1**	**0.1251**	**-**	**-**	**2.52**

Test Conditions:

DI Water — Open Vent Mode

A = 0.62% — U_G = 20.0 cm/s

Oxygen Mass Transfer Data							
Test	Inlet Gas	Gas Velocity (cm/s)	Temperature (ºC)	k_La (1/s)	C_o (% of Sat)	C_∞ (% of Sat)	τ_e (s)
#1	Nitrogen	20.02	20.5	0.1322	100.6	0.2	3.68
#2	Nitrogen	20.09	20.8	-	99.5	0.1	2.72
#3	Nitrogen	20.03	20.2	0.1314	99.7	0.1	2.56
#1	Air	20.09	20.5	0.1344	0.4	99.9	2.76
#2	Air	20.10	20.8	-	0.0	99.8	2.63
#3	Air	20.03	20.2	0.1379	1.1	100.0	2.43
#1	Carbon Monoxide	20.05	20.5	0.1314	100.8	0.2	3.50
#2	Carbon Monoxide	20.07	20.7	-	101.1	0.2	3.00
#3	Carbon Monoxide	20.04	20.1	0.1354	99.5	0.1	2.65
#1	Air	20.13	20.5	0.1301	0.6	100.2	2.86
#2	Air	20.07	20.6	0.1342	0.2	99.9	2.28
#3	Air	20.14	20.1	-	-0.2	100.3	2.72
Average		**20.07**	**20.4**	**0.1334**	**-**	**-**	**2.81**

Test Conditions:

DI Water — Closed Vent Mode

A = 0.62% — U_G = 0.5 cm/s

Oxygen Mass Transfer Data							
Test	Inlet Gas	Gas Velocity (cm/s)	Temperature (ºC)	k_La (1/s)	C_o (% of Sat)	C_∞ (% of Sat)	τ_e (s)
#1	Nitrogen	0.53	20.2	0.0077	99.3	-1.3	5.81
#2	Nitrogen	0.54	20.4	0.0084	99.6	-0.8	3.09
#3	Nitrogen	0.54	19.6	0.0081	99.5	-1.0	4.15
#1	Air	0.52	20.3	0.0088	0.7	100.8	2.71
#2	Air	0.54	20.5	0.0082	0.5	100.7	2.60
#3	Air	0.50	19.8	0.0080	0.8	101.4	3.14
#1	Carbon Monoxide	0.53	20.4	0.0076	99.2	-1.4	5.62
#2	Carbon Monoxide	0.54	20.6	0.0084	99.3	-0.8	3.46
#3	Carbon Monoxide	0.54	19.9	0.0080	99.4	-1.2	3.00
#1	Air	0.52	20.5	0.0089	1.0	101.0	2.66
#2	Air	0.54	20.7	0.0084	0.3	100.6	2.05
#3	Air	0.50	20.0	0.0089	1.0	101.7	5.67
Average		**0.53**	**20.2**	**0.0083**	**-**	**-**	**3.66**

Test Conditions:

DI Water — Closed Vent Mode

A = 0.62% — U_G = 2.0 cm/s

Oxygen Mass Transfer Data							
Test	Inlet Gas	Gas Velocity (cm/s)	Temperature (ºC)	k_La (1/s)	C_o (% of Sat)	C_∞ (% of Sat)	τ_e (s)
#1	Nitrogen	2.06	20.0	0.0275	100.0	0.2	2.29
#2	Nitrogen	2.02	19.5	0.0289	99.9	0.3	2.36
#3	Nitrogen	2.03	19.6	0.0277	99.6	0.1	3.73
#1	Air	2.07	20.1	0.0286	-0.3	99.6	1.95
#2	Air	2.02	19.6	0.0298	0.0	100.3	2.49
#3	Air	2.01	19.7	-	4.9	103.9	0.00
#1	Carbon Monoxide	2.04	20.1	0.0276	100.2	0.2	2.76
#2	Carbon Monoxide	2.04	19.6	0.0300	99.6	0.1	2.51
#3	Carbon Monoxide	2.03	19.7	-	98.6	-0.8	21.24
#1	Air	2.07	20.2	0.0282	0.2	99.6	1.64
#2	Air	2.02	19.7	0.0291	-0.2	100.2	1.99
#3	Air	2.02	19.8	-	-1.2	102.1	30.16
Average		**2.04**	**19.8**	**0.0286**	**-**	**-**	**6.09**

Carbon Monoxide Mass Transfer Data						
Test	Inlet Gas	Gas Velocity (cm/s)	Temperature (ºC)	k_La (1/s)	C_o (% of Sat)	C_∞ (% of Sat)
#1	Carbon Monoxide	2.04	20.1	0.0270	0.0	99.0
#2	Carbon Monoxide	2.04	19.6	0.0265	0.0	98.7
#3	Carbon Monoxide	2.03	19.7	0.0279	0.0	98.2
Average		**2.04**	**19.8**	**0.0272**	**-**	**-**

Test Conditions:

DI Water — Closed Vent Mode

A = 0.62% — U_G = 4.0 cm/s

Oxygen Mass Transfer Data							
Test	Inlet Gas	Gas Velocity (cm/s)	Temperature (ºC)	k_La (1/s)	C_o (% of Sat)	C_∞ (% of Sat)	τ_e (s)
#1	Nitrogen	4.02	19.6	0.0612	99.6	0.2	2.76
#2	Nitrogen	4.07	20.7	0.0667	80.0	0.2	0.53
#3	Nitrogen	4.02	19.7	0.0687	100.4	-0.3	4.36
#1	Air	4.03	19.7	0.0657	0.7	99.8	3.34
#2	Air	4.00	20.7	0.0647	19.6	99.8	0.01
#3	Air	4.00	19.7	0.0686	-0.1	100.4	3.26
#1	Carbon Monoxide	4.02	19.7	0.0622	90.1	0.2	2.67
#2	Carbon Monoxide	4.07	20.7	0.0678	87.0	0.2	0.85
#3	Carbon Monoxide	4.02	19.7	0.0668	100.2	-0.4	3.46
#1	Air	4.04	19.8	0.0676	0.1	99.4	3.48
#2	Air	4.00	20.8	0.0645	14.3	99.7	0.19
#3	Air	3.99	19.7	0.0701	0.5	100.4	3.52
Average		**4.02**	**20.0**	**0.0662**	**-**	**-**	**2.37**

Test Conditions:

DI Water — Closed Vent Mode

A = 0.62% — U_G = 6.0 cm/s

Oxygen Mass Transfer Data							
Test	Inlet Gas	Gas Velocity (cm/s)	Temperature (ºC)	k_La (1/s)	C_o (% of Sat)	C_∞ (% of Sat)	τ_e (s)
#1	Nitrogen	6.09	19.5	0.0973	99.9	0.2	3.39
#2	Nitrogen	5.97	19.3	0.0972	101.3	0.3	4.83
#3	Nitrogen	5.98	19.7	0.0989	99.6	0.2	3.58
#1	Air	6.02	19.5	0.0934	-0.2	99.8	3.25
#2	Air	5.95	19.3	0.1099	0.1	100.5	4.33
#3	Air	5.98	19.8	0.1111	-0.1	100.7	3.80
#1	Carbon Monoxide	5.94	19.6	0.0939	99.2	0.2	3.26
#2	Carbon Monoxide	6.02	19.3	0.0904	99.6	0.2	3.20
#3	Carbon Monoxide	5.95	19.8	0.1031	100.1	0.1	3.92
#1	Air	6.02	19.7	0.0918	-0.7	99.5	3.14
#2	Air	5.95	19.4	0.0961	-0.7	100.1	3.78
#3	Air	6.09	19.9	0.1012	-0.3	100.0	3.43
Average		**6.00**	**19.6**	**0.0987**	**-**	**-**	**3.66**

Carbon Monoxide Mass Transfer Data						
Test	Inlet Gas	Gas Velocity (cm/s)	Temperature (ºC)	k_La (1/s)	C_o (% of Sat)	C_∞ (% of Sat)
#1	Carbon Monoxide	5.94	19.6	0.0793	0.0	95.1
#2	Carbon Monoxide	6.02	19.3	0.0802	0.0	97.8
#3	Carbon Monoxide	5.95	19.8	0.0791	0.0	98.5
Average		**5.97**	**19.6**	**0.0795**	**-**	**-**

Test Conditions:

DI Water — Closed Vent Mode

A = 0.62% — U_G = 8.0 cm/s

Oxygen Mass Transfer Data							
Test	Inlet Gas	Gas Velocity (cm/s)	Temperature (ºC)	k_La (1/s)	C_o (% of Sat)	C_∞ (% of Sat)	τ_e (s)
#1	Nitrogen	8.02	20.2	0.1207	100.8	0.3	4.22
#2	Nitrogen	8.09	19.1	0.1188	100.2	0.3	4.13
#3	Nitrogen	7.98	19.7	0.1367	100.2	0.3	4.34
#1	Air	8.02	20.2	0.1345	0.7	100.3	3.84
#2	Air	8.09	19.1	0.1378	-0.6	100.0	4.54
#3	Air	7.95	19.7	0.1397	0.3	100.0	4.06
#1	Carbon Monoxide	8.03	20.2	0.1187	100.5	0.3	3.98
#2	Carbon Monoxide	8.09	19.2	0.1151	100.7	0.3	3.66
#3	Carbon Monoxide	7.98	19.8	0.1399	100.4	0.3	4.67
#1	Air	8.03	20.2	0.1353	0.8	100.4	3.99
#2	Air	8.11	19.2	-	-1.2	99.8	5.42
#3	Air	7.95	19.8	0.1404	0.0	100.2	3.88
Average		**8.03**	**19.7**	**0.1307**	**-**	**-**	**4.23**

Test Conditions:

DI Water — Closed Vent Mode

A = 0.62% — U_G = 10.0 cm/s

Oxygen Mass Transfer Data							
Test	Inlet Gas	Gas Velocity (cm/s)	Temperature (ºC)	k_La (1/s)	C_o (% of Sat)	C_∞ (% of Sat)	τ_e (s)
#1	Nitrogen	10.03	19.7	0.1290	99.4	0.3	3.32
#2	Nitrogen	9.99	19.6	-	103.1	0.2	5.39
#3	Nitrogen	10.05	19.7	0.1611	100.3	0.2	4.31
#1	Air	10.10	19.7	0.1361	0.7	100.1	2.72
#2	Air	10.00	19.6	0.1527	0.3	99.8	3.72
#3	Air	10.01	19.7	-	-0.5	100.4	4.91
#1	Carbon Monoxide	10.01	19.7	0.1663	104.0	0.3	6.02
#2	Carbon Monoxide	9.98	19.6	0.1554	99.1	0.0	3.58
#3	Carbon Monoxide	10.05	19.7	-	100.5	0.0	5.17
#1	Air	10.11	19.8	0.1269	-0.2	100.2	2.77
#2	Air	10.03	19.7	0.1388	-0.5	99.7	3.30
#3	Air	10.02	19.7	0.1574	-0.4	100.5	3.89
Average		**10.03**	**19.7**	**0.1471**	**-**	**-**	**4.09**

Carbon Monoxide Mass Transfer Data						
Test	Inlet Gas	Gas Velocity (cm/s)	Temperature (ºC)	k_La (1/s)	C_o (% of Sat)	C_∞ (% of Sat)
#1	Carbon Monoxide	10.01	19.7	0.1227	0.0	97.6
#2	Carbon Monoxide	9.98	19.6	0.1404	0.0	95.4
#3	Carbon Monoxide	10.05	19.7	0.1349	0.0	98.6
Average		**10.01**	**19.7**	**0.1327**	**-**	**-**

Test Conditions:

DI Water — Closed Vent Mode

A = 0.62% — U_G = 12.0 cm/s

Oxygen Mass Transfer Data							
Test	Inlet Gas	Gas Velocity (cm/s)	Temperature (ºC)	k_La (1/s)	C_o (% of Sat)	C_∞ (% of Sat)	τ_e (s)
#1	Nitrogen	12.01	19.5	-	99.3	0.1	3.05
#2	Nitrogen	11.97	19.5	0.1521	99.2	0.2	3.30
#3	Nitrogen	11.99	19.7	0.1342	99.6	0.1	2.66
#1	Air	12.06	19.6	-	0.6	99.9	2.41
#2	Air	11.97	19.6	0.1498	-0.1	99.8	2.83
#3	Air	11.99	19.7	0.1414	0.2	100.3	3.09
#1	Carbon Monoxide	12.04	19.6	-	99.6	0.1	2.93
#2	Carbon Monoxide	11.98	19.6	0.1463	100.9	0.2	3.09
#3	Carbon Monoxide	12.01	19.7	0.1391	100.1	0.2	3.01
#1	Air	12.07	19.6	-	-0.1	100.0	2.89
#2	Air	11.98	19.6	0.1544	0.6	100.1	3.24
#3	Air	12.00	19.7	0.1426	0.0	100.2	2.70
Average		**12.01**	**19.6**	**0.1450**	**-**	**-**	**2.93**

Test Conditions:

DI Water — Closed Vent Mode

A = 0.62% — U_G = 14.0 cm/s

Oxygen Mass Transfer Data							
Test	Inlet Gas	Gas Velocity (cm/s)	Temperature (ºC)	k_La (1/s)	C_o (% of Sat)	C_∞ (% of Sat)	τ_e (s)
#1	Nitrogen	14.02	19.7	0.1182	100.5	0.2	2.69
#2	Nitrogen	13.99	19.7	-	99.9	0.2	2.65
#3	Nitrogen	14.00	20.8	0.1408	100.0	0.0	3.36
#1	Air	14.05	19.7	-	0.3	100.4	2.69
#2	Air	13.95	19.7	0.1345	0.1	100.5	2.59
#3	Air	13.94	20.8	0.1292	-0.1	99.7	2.06
#1	Carbon Monoxide	14.10	19.7	-	99.8	0.2	2.19
#2	Carbon Monoxide	14.01	19.7	0.1231	99.4	0.2	2.95
#3	Carbon Monoxide	13.92	20.7	0.1337	101.3	0.0	2.30
#1	Air	14.09	19.7	-	-0.8	99.9	2.39
#2	Air	14.00	19.6	0.1243	0.5	100.1	2.71
#3	Air	13.96	20.7	0.1322	0.5	100.1	2.45
Average		**14.00**	**20.0**	**0.1295**	**-**	**-**	**2.59**

Carbon Monoxide Mass Transfer Data						
Test	Inlet Gas	Gas Velocity (cm/s)	Temperature (ºC)	k_La (1/s)	C_o (% of Sat)	C_∞ (% of Sat)
#1	Carbon Monoxide	14.10	19.7	0.1233	0.0	97.7
#2	Carbon Monoxide	14.01	19.7	0.1125	0.0	98.8
#3	Carbon Monoxide	13.92	20.7	0.1130	0.0	98.7
Average		**14.01**	**20.0**	**0.1162**	**-**	**-**

Test Conditions:

DI Water — Closed Vent Mode

A = 0.62% — U_G = 16.0 cm/s

Oxygen Mass Transfer Data							
Test	Inlet Gas	Gas Velocity (cm/s)	Temperature (ºC)	k_La (1/s)	C_o (% of Sat)	C_∞ (% of Sat)	τ_e (s)
#1	Nitrogen	15.90	20.4	-	98.3	0.0	2.78
#2	Nitrogen	15.95	19.2	0.1267	99.4	0.0	2.65
#3	Nitrogen	15.96	19.6	0.1404	100.5	0.2	3.84
#1	Air	16.02	20.4	-	0.6	99.8	2.56
#2	Air	16.01	19.3	0.1320	0.8	100.1	2.53
#3	Air	16.00	19.6	0.1350	0.9	100.2	2.50
#1	Carbon Monoxide	15.93	20.4	-	99.8	0.1	2.91
#2	Carbon Monoxide	15.96	19.3	0.1400	100.5	0.2	3.47
#3	Carbon Monoxide	15.96	19.6	0.1395	100.2	0.1	3.85
#1	Air	16.04	20.4	-	0.6	99.7	2.26
#2	Air	16.01	19.3	0.1340	0.0	100.0	2.89
#3	Air	16.01	19.6	0.1344	0.6	100.5	2.36
Average		**15.98**	**19.8**	**0.1353**	**-**	**-**	**2.88**

Test Conditions:

DI Water — Closed Vent Mode

A = 0.62% — U_G = 18.0 cm/s

Oxygen Mass Transfer Data							
Test	Inlet Gas	Gas Velocity (cm/s)	Temperature (ºC)	k_La (1/s)	C_o (% of Sat)	C_∞ (% of Sat)	τ_e (s)
#1	Nitrogen	18.02	19.2	0.1162	99.8	0.1	2.72
#2	Nitrogen	18.05	19.1	-	99.5	0.2	2.67
#3	Nitrogen	17.95	19.9	0.1255	40.0	-1.4	0.11
#1	Air	18.02	19.2	0.1253	1.1	99.9	2.83
#2	Air	18.09	19.1	0.1351	0.9	100.3	3.26
#3	Air	17.99	20.0	0.1351	64.6	101.0	0.05
#1	Carbon Monoxide	18.06	19.2	0.1217	100.4	0.2	3.12
#2	Carbon Monoxide	18.05	19.0	0.1191	99.2	0.2	2.92
#3	Carbon Monoxide	17.95	20.0	0.1295	41.9	-1.2	0.03
#1	Air	18.05	19.2	0.1310	0.0	99.9	3.44
#2	Air	18.12	19.1	0.1305	0.3	100.3	2.85
#3	Air	18.00	20.0	0.1309	65.7	101.1	0.22
Average		**18.03**	**19.4**	**0.1273**	**-**	**-**	**2.02**

Test Conditions:

DI Water — Closed Vent Mode

A = 0.62% — U_G = 20.0 cm/s

Oxygen Mass Transfer Data							
Test	Inlet Gas	Gas Velocity (cm/s)	Temperature (ºC)	k_La (1/s)	C_o (% of Sat)	C_∞ (% of Sat)	τ_e (s)
#1	Nitrogen	19.98	19.2	0.1240	98.3	0.1	2.47
#2	Nitrogen	20.04	19.5	0.1217	99.5	0.2	2.74
#3	Nitrogen	19.98	20.0	0.1394	99.7	0.1	2.83
#1	Air	20.05	19.2	0.1331	1.8	100.0	2.83
#2	Air	20.11	19.5	0.1384	0.1	100.4	2.67
#3	Air	19.97	20.0	0.1366	0.1	99.7	3.09
#1	Carbon Monoxide	19.96	19.2	0.1358	100.6	0.2	3.39
#2	Carbon Monoxide	20.08	19.5	0.1266	100.5	0.2	3.21
#3	Carbon Monoxide	20.03	20.0	0.1363	98.8	0.1	2.58
#1	Air	20.09	19.2	0.1357	-0.3	100.0	2.79
#2	Air	20.14	19.4	0.1391	0.2	100.4	2.75
#3	Air	19.99	20.0	0.1348	1.0	99.7	2.73
Average		**20.04**	**19.6**	**0.1335**	**-**	**-**	**2.84**

Test Conditions:

DI Water — Bubble Column Mode

A = 0.62% — U_G = 0.5 cm/s

Oxygen Mass Transfer Data							
Test	Inlet Gas	Gas Velocity (cm/s)	Temperature (ºC)	k_La (1/s)	C_o (% of Sat)	C_∞ (% of Sat)	τ_e (s)
#1	Nitrogen	0.57	20.2	0.0094	99.4	-0.3	3.40
#2	Nitrogen	0.53	19.6	0.0088	99.2	-0.6	3.49
#3	Nitrogen	0.51	19.9	0.0084	99.4	-0.7	4.97
#1	Air	0.56	20.3	0.0094	0.5	100.3	3.04
#2	Air	0.51	19.7	0.0087	0.7	100.7	3.28
#3	Air	0.50	20.0	0.0083	0.5	100.7	2.74
#1	Carbon Monoxide	0.57	20.4	0.0096	99.4	-0.3	3.53
#2	Carbon Monoxide	0.53	19.8	0.0089	99.5	-0.6	4.90
#3	Carbon Monoxide	0.51	20.2	0.0085	99.5	-0.7	4.01
#1	Air	0.56	20.5	0.0094	0.2	100.2	2.47
#2	Air	0.51	19.9	0.0088	0.6	100.5	3.02
#3	Air	0.51	20.3	0.0082	0.4	101.0	3.00
Average		**0.53**	**20.1**	**0.0089**	**-**	**-**	**3.49**

Test Conditions:

DI Water — Bubble Column Mode

A = 0.62% — U_G = 2.0 cm/s

Oxygen Mass Transfer Data							
Test	Inlet Gas	Gas Velocity (cm/s)	Temperature (ºC)	k_La (1/s)	C_o (% of Sat)	C_∞ (% of Sat)	τ_e (s)
#1	Nitrogen	2.03	20.1	0.0329	100.7	0.2	3.14
#2	Nitrogen	2.09	20.4	0.0328	99.7	0.1	3.50
#3	Nitrogen	2.09	20.8	0.0331	99.6	0.2	2.28
#1	Air	2.00	20.1	0.0325	0.2	99.7	2.68
#2	Air	2.02	20.5	0.0319	0.1	99.9	3.55
#3	Air	2.01	20.8	0.0318	0.4	99.7	2.16
#1	Carbon Monoxide	2.01	20.2	0.0325	99.5	0.2	2.28
#2	Carbon Monoxide	2.09	20.5	0.0330	99.7	0.1	3.64
#3	Carbon Monoxide	2.01	20.8	0.0314	99.6	0.2	2.79
#1	Air	2.00	20.2	0.0314	-0.2	99.8	2.09
#2	Air	2.02	20.5	0.0313	-0.3	100.0	3.13
#3	Air	2.02	20.9	0.0319	0.4	99.8	2.21
Average		**2.03**	**20.5**	**0.0322**	**-**	**-**	**2.79**

Carbon Monoxide Mass Transfer Data						
Test	Inlet Gas	Gas Velocity (cm/s)	Temperature (ºC)	k_La (1/s)	C_o (% of Sat)	C_∞ (% of Sat)
#1	Carbon Monoxide	2.01	20.2	0.0323	0.0	97.7
#2	Carbon Monoxide	2.09	20.5	0.0313	0.0	99.4
#3	Carbon Monoxide	2.01	20.8	0.0258	0.0	99.7
Average		**2.04**	**20.5**	**0.0298**	**-**	**-**

Test Conditions:

DI Water — Bubble Column Mode

A = 0.62% — U_G = 4.0 cm/s

Oxygen Mass Transfer Data							
Test	Inlet Gas	Gas Velocity (cm/s)	Temperature (ºC)	k_La (1/s)	C_o (% of Sat)	C_∞ (% of Sat)	τ_e (s)
#1	Nitrogen	4.04	20.5	0.0731	100.6	0.2	3.42
#2	Nitrogen	0.38	19.6	0.0697	99.6	0.1	3.77
#3	Nitrogen	4.05	22.8	0.0734	99.7	0.2	2.65
#1	Air	4.03	20.5	0.0738	-0.1	99.8	3.42
#2	Air	0.38	19.7	0.0709	1.1	102.9	3.98
#3	Air	4.01	22.8	0.0785	-1.5	100.0	3.54
#1	Carbon Monoxide	4.15	20.5	-	110.1	-0.3	11.22
#2	Carbon Monoxide	0.38	19.7	0.0717	100.5	0.2	4.36
#3	Carbon Monoxide	4.06	22.8	0.0749	99.5	0.2	3.18
#1	Air	4.02	20.5	0.0714	-0.7	99.9	3.14
#2	Air	0.38	19.8	0.0713	0.2	99.8	4.35
#3	Air	4.02	22.8	0.0769	1.2	100.1	2.96
Average		**2.82**	**21.0**	**0.0732**	**-**	**-**	**4.17**

Test Conditions:

DI Water — Bubble Column Mode

A = 0.62% — U_G = 6.0 cm/s

Oxygen Mass Transfer Data							
Test	Inlet Gas	Gas Velocity (cm/s)	Temperature (ºC)	k_La (1/s)	C_o (% of Sat)	C_∞ (% of Sat)	τ_e (s)
#1	Nitrogen	0.41	20.2	0.1133	100.0	0.1	3.88
#2	Nitrogen	6.00	20.2	0.1024	98.7	0.1	3.35
#3	Nitrogen	5.99	20.4	0.1038	99.4	0.2	2.85
#1	Air	0.41	20.2	0.1127	0.3	99.8	3.61
#2	Air	5.94	20.2	0.1040	0.6	99.9	3.82
#3	Air	5.95	20.4	0.1123	0.5	99.9	3.60
#1	Carbon Monoxide	0.41	20.2	0.1167	100.1	0.2	4.32
#2	Carbon Monoxide	6.03	20.2	0.1079	99.6	0.1	4.05
#3	Carbon Monoxide	6.00	20.4	0.1057	99.2	0.1	3.19
#1	Air	0.41	20.2	0.1117	0.5	99.8	3.93
#2	Air	5.97	20.2	0.1005	0.6	99.7	3.61
#3	Air	5.95	20.4	0.1054	0.7	99.8	3.10
Average		**4.12**	**20.3**	**0.1080**	**-**	**-**	**3.61**

Carbon Monoxide Mass Transfer Data						
Test	Inlet Gas	Gas Velocity (cm/s)	Temperature (ºC)	k_La (1/s)	C_o (% of Sat)	C_∞ (% of Sat)
#1	Carbon Monoxide	0.41	20.2	0.0873	0.0	100.7
#2	Carbon Monoxide	6.03	20.2	0.0821	0.0	100.8
#3	Carbon Monoxide	6.00	20.4	0.0825	0.0	100.2
Average		**4.14**	**20.3**	**0.0839**	**-**	**-**

Test Conditions:

DI Water — Bubble Column Mode

A = 0.62% — U_G = 8.0 cm/s

Oxygen Mass Transfer Data							
Test	Inlet Gas	Gas Velocity (cm/s)	Temperature (ºC)	k_La (1/s)	C_o (% of Sat)	C_∞ (% of Sat)	τ_e (s)
#1	Nitrogen	8.03	20.0	-	100.6	0.1	4.61
#2	Nitrogen	8.03	20.2	0.1305	99.3	0.2	3.85
#3	Nitrogen	8.16	20.2	0.1321	99.8	0.2	2.92
#1	Air	7.96	20.1	0.1408	0.4	99.9	3.96
#2	Air	7.99	20.2	0.1261	-0.7	99.7	3.43
#3	Air	8.08	20.1	0.1325	1.5	100.3	2.86
#1	Carbon Monoxide	8.05	20.1	0.1461	100.2	0.1	4.09
#2	Carbon Monoxide	8.05	20.2	0.1262	99.0	0.1	3.52
#3	Carbon Monoxide	8.16	20.1	0.1285	99.4	0.0	2.81
#1	Air	7.98	20.1	0.1384	-0.1	99.9	3.49
#2	Air	7.99	20.2	0.1252	1.2	99.7	3.29
#3	Air	8.07	20.1	-	0.0	99.6	3.95
Average		**8.04**	**20.1**	**0.1327**	**-**	**-**	**3.56**

Test Conditions:

DI Water — Bubble Column Mode

A = 0.62% — U_G = 10.0 cm/s

Oxygen Mass Transfer Data							
Test	Inlet Gas	Gas Velocity (cm/s)	Temperature (ºC)	k_La (1/s)	C_o (% of Sat)	C_∞ (% of Sat)	τ_e (s)
#1	Nitrogen	10.07	20.2	-	98.3	0.2	3.50
#2	Nitrogen	10.05	20.1	0.1464	100.5	0.2	3.44
#3	Nitrogen	10.04	20.4	0.1462	99.6	0.2	3.26
#1	Air	9.99	20.2	-	-0.2	99.9	3.28
#2	Air	10.02	20.1	0.1432	0.4	99.7	3.23
#3	Air	10.01	20.4	0.1434	0.7	99.9	3.20
#1	Carbon Monoxide	10.04	20.2	-	100.1	0.1	3.39
#2	Carbon Monoxide	10.03	20.2	0.1481	99.8	0.1	3.49
#3	Carbon Monoxide	10.04	20.4	0.1506	100.0	0.2	3.71
#1	Air	10.01	20.3	0.1545	-0.4	99.8	3.19
#2	Air	10.02	20.2	0.1363	0.5	99.6	2.98
#3	Air	10.02	20.4	0.1449	-0.4	99.6	3.44
Average		**10.03**	**20.3**	**0.1460**	**-**	**-**	**3.34**

Carbon Monoxide Mass Transfer Data						
Test	Inlet Gas	Gas Velocity (cm/s)	Temperature (ºC)	k_La (1/s)	C_o (% of Sat)	C_∞ (% of Sat)
#1	Carbon Monoxide	10.04	20.2	0.1180	0.0	97.9
#2	Carbon Monoxide	10.03	20.2	0.1192	0.0	97.5
#3	Carbon Monoxide	10.04	20.4	0.1125	0.0	100.2
Average		**10.04**	**20.3**	**0.1166**	**-**	**-**

Test Conditions:

DI Water — Bubble Column Mode

A = 0.62% — U_G = 12.0 cm/s

Oxygen Mass Transfer Data							
Test	Inlet Gas	Gas Velocity (cm/s)	Temperature (ºC)	k_La (1/s)	C_o (% of Sat)	C_∞ (% of Sat)	τ_e (s)
#1	Nitrogen	12.01	20.2	0.1524	100.1	0.1	2.38
#2	Nitrogen	12.03	20.3	0.1511	100.4	0.2	3.46
#3	Nitrogen	11.98	20.9	0.1360	99.3	0.2	2.11
#1	Air	12.03	20.2	0.1568	-0.9	99.9	2.48
#2	Air	12.04	20.3	0.1419	-0.7	99.8	2.45
#3	Air	12.00	20.9	0.1482	0.0	99.6	2.38
#1	Carbon Monoxide	12.02	20.1	0.1508	99.4	0.1	2.28
#2	Carbon Monoxide	12.04	20.3	0.1476	101.0	0.2	3.48
#3	Carbon Monoxide	12.00	20.8	0.1422	101.6	0.2	2.56
#1	Air	12.03	20.1	0.1559	0.8	99.7	2.29
#2	Air	12.05	20.2	0.1411	-1.1	99.9	2.55
#3	Air	12.02	20.8	0.1459	-0.2	99.8	1.93
Average		**12.02**	**20.4**	**0.1475**	**-**	**-**	**2.53**

Test Conditions:

DI Water — Bubble Column Mode

A = 0.62% — U_G = 14.0 cm/s

Oxygen Mass Transfer Data							
Test	Inlet Gas	Gas Velocity (cm/s)	Temperature (ºC)	k_La (1/s)	C_o (% of Sat)	C_∞ (% of Sat)	τ_e (s)
#1	Nitrogen	14.03	19.9	0.1476	100.6	0.1	3.56
#2	Nitrogen	14.01	20.0	0.1324	99.4	0.1	3.14
#3	Nitrogen	14.04	20.6	0.1360	100.3	0.1	2.37
#1	Air	13.96	19.9	0.1338	1.3	100.0	2.45
#2	Air	13.99	20.0	0.1282	-0.6	99.8	2.24
#3	Air	14.04	20.6	0.1473	0.5	100.1	2.18
#1	Carbon Monoxide	13.81	19.8	0.1382	99.5	0.0	2.22
#2	Carbon Monoxide	14.01	20.0	0.1368	99.5	0.1	3.16
#3	Carbon Monoxide	13.94	20.6	-	100.4	0.2	3.43
#1	Air	14.00	19.8	0.1363	0.6	99.9	2.48
#2	Air	13.99	19.9	0.1271	0.5	99.6	2.52
#3	Air	14.06	20.5	0.1437	0.4	100.1	2.08
Average		**13.99**	**20.1**	**0.1370**	**-**	**-**	**2.65**

Carbon Monoxide Mass Transfer Data						
Test	Inlet Gas	Gas Velocity (cm/s)	Temperature (ºC)	k_La (1/s)	C_o (% of Sat)	C_∞ (% of Sat)
#1	Carbon Monoxide	13.81	19.8	0.1148	0.0	102.7
#2	Carbon Monoxide	14.01	20.0	0.1206	0.0	99.0
#3	Carbon Monoxide	13.94	20.6	-	0.0	100.1
Average		**13.92**	**20.1**	**0.1177**	**-**	**-**

Test Conditions:

DI Water — Bubble Column Mode

A = 0.62% — U_G = 16.0 cm/s

Oxygen Mass Transfer Data							
Test	Inlet Gas	Gas Velocity (cm/s)	Temperature (ºC)	k_La (1/s)	C_o (% of Sat)	C_∞ (% of Sat)	τ_e (s)
#1	Nitrogen	16.03	20.7	0.1289	100.3	0.1	2.50
#2	Nitrogen	15.93	20.1	0.1318	100.3	0.1	3.15
#3	Nitrogen	15.99	20.1	0.1365	100.3	0.1	2.16
#1	Air	15.99	20.6	0.1274	0.5	100.0	1.87
#2	Air	15.98	20.0	0.1305	-0.4	100.0	2.91
#3	Air	16.02	20.1	0.1460	0.9	99.5	2.78
#1	Carbon Monoxide	16.06	20.6	0.1311	99.7	0.1	2.51
#2	Carbon Monoxide	15.94	20.0	0.1379	101.7	0.2	3.60
#3	Carbon Monoxide	16.01	20.1	-	138.0	0.1	7.10
#1	Air	16.01	20.6	0.1308	-0.1	99.9	2.32
#2	Air	16.00	19.9	0.1287	0.1	99.9	2.50
#3	Air	16.03	20.1	0.1351	0.9	100.4	1.90
Average		**16.00**	**20.2**	**0.1332**	**-**	**-**	**2.94**

Test Conditions:

DI Water — Bubble Column Mode

A = 0.62% — U_G = 18.0 cm/s

Oxygen Mass Transfer Data							
Test	Inlet Gas	Gas Velocity (cm/s)	Temperature (ºC)	k_La (1/s)	C_o (% of Sat)	C_∞ (% of Sat)	τ_e (s)
#1	Nitrogen	18.05	20.4	0.1255	99.7	0.0	2.11
#2	Nitrogen	17.96	20.1	0.1284	99.2	0.1	2.88
#3	Nitrogen	18.02	20.4	0.1387	100.0	0.0	2.49
#1	Air	18.00	20.4	0.1429	1.5	99.8	2.86
#2	Air	17.96	20.1	0.1356	0.5	99.9	3.27
#3	Air	17.99	20.4	0.1412	0.6	99.8	2.20
#1	Carbon Monoxide	18.06	20.3	-	103.3	0.2	4.69
#2	Carbon Monoxide	17.99	20.0	0.1347	99.9	0.1	3.27
#3	Carbon Monoxide	18.04	20.3	0.1375	100.2	0.1	2.58
#1	Air	18.03	20.2	0.1353	0.4	99.9	2.44
#2	Air	17.99	19.9	0.1288	1.2	99.9	2.54
#3	Air	17.94	20.2	-	-0.5	99.7	2.63
Average		**18.00**	**20.2**	**0.1349**	**-**	**-**	**2.83**

Test Conditions:

DI Water — Bubble Column Mode

A = 0.62% — U_G = 20.0 cm/s

Oxygen Mass Transfer Data							
Test	Inlet Gas	Gas Velocity (cm/s)	Temperature (ºC)	k_La (1/s)	C_o (% of Sat)	C_∞ (% of Sat)	τ_e (s)
#1	Nitrogen	20.01	20.0	0.1410	99.0	0.1	2.43
#2	Nitrogen	19.97	19.8	0.1355	99.5	0.1	3.02
#3	Nitrogen	19.95	20.1	-	108.0	-0.2	5.87
#1	Air	20.01	20.0	0.1485	-0.5	99.9	2.90
#2	Air	19.98	19.7	0.1345	0.3	99.7	2.70
#3	Air	19.97	20.0	0.1514	-0.4	99.8	2.34
#1	Carbon Monoxide	20.02	19.9	0.1447	99.4	0.1	2.97
#2	Carbon Monoxide	19.97	19.6	0.1351	99.9	0.1	3.24
#3	Carbon Monoxide	19.96	20.0	0.1497	101.8	0.1	3.16
#1	Air	20.03	19.9	-	-0.3	99.8	3.56
#2	Air	19.99	19.6	0.1412	0.6	99.7	3.15
#3	Air	20.00	19.9	0.1445	1.3	100.1	2.07
Average		**19.99**	**19.9**	**0.1426**	**-**	**-**	**3.12**

Test Conditions:

DI Water — Open Vent Mode

A = 0.99% — U_G = 0.5 cm/s

Oxygen Mass Transfer Data							
Test	Inlet Gas	Gas Velocity (cm/s)	Temperature (ºC)	k_La (1/s)	C_o (% of Sat)	C_∞ (% of Sat)	τ_e (s)
#1	Nitrogen	0.50	19.9	0.0070	98.9	-2.1	4.36
#2	Nitrogen	0.55	20.1	0.0080	99.6	-1.1	4.08
#3	Nitrogen	0.50	20.5	0.0077	99.5	-1.5	4.34
#1	Air	0.49	20.0	0.0069	0.5	102.2	2.61
#2	Air	0.50	20.2	0.0076	0.3	101.3	1.53
#3	Air	0.47	20.5	0.0076	0.6	101.4	2.62
#1	Carbon Monoxide	0.50	20.2	0.0070	99.5	-2.1	3.98
#2	Carbon Monoxide	0.43	20.4	0.0069	99.1	-2.3	5.68
#3	Carbon Monoxide	0.50	20.6	0.0078	99.3	-1.3	4.14
#1	Air	0.49	20.4	0.0069	0.4	102.0	0.10
#2	Air	0.50	20.5	0.0078	0.5	101.2	1.60
#3	Air	0.47	20.7	0.0076	0.5	101.3	2.53
Average		**0.49**	**20.3**	**0.0074**	**-**	**-**	**3.13**

Test Conditions:

DI Water — Open Vent Mode

A = 0.99% — U_G = 2.0 cm/s

Oxygen Mass Transfer Data							
Test	Inlet Gas	Gas Velocity (cm/s)	Temperature (ºC)	k_La (1/s)	C_o (% of Sat)	C_∞ (% of Sat)	τ_e (s)
#1	Nitrogen	1.98	20.1	0.0253	99.9	0.0	2.17
#2	Nitrogen	2.00	21.1	0.0271	99.4	0.1	2.25
#3	Nitrogen	1.97	20.9	0.0261	99.7	0.0	1.68
#1	Air	1.99	20.2	0.0257	0.8	100.0	1.25
#2	Air	1.98	21.1	0.0268	0.7	100.0	0.98
#3	Air	1.98	20.9	0.0265	0.6	99.8	1.18
#1	Carbon Monoxide	2.01	20.2	0.0257	99.8	0.0	1.78
#2	Carbon Monoxide	2.02	21.2	0.0270	99.5	0.0	2.08
#3	Carbon Monoxide	2.01	20.9	0.0266	99.0	0.0	2.06
#1	Air	1.99	20.3	0.0258	1.1	100.0	1.17
#2	Air	1.98	21.2	0.0262	0.3	99.9	0.90
#3	Air	1.98	21.0	0.0267	0.2	100.1	1.13
Average		**1.99**	**20.8**	**0.0263**	**-**	**-**	**1.55**

Carbon Monoxide Mass Transfer Data						
Test	Inlet Gas	Gas Velocity (cm/s)	Temperature (ºC)	k_La (1/s)	C_o (% of Sat)	C_∞ (% of Sat)
#1	Carbon Monoxide	2.01	20.2	0.0279	0.0	99.9
#2	Carbon Monoxide	2.02	21.2	0.0268	0.0	100.3
#3	Carbon Monoxide	2.01	20.9	0.0294	0.0	99.3
Average		**2.01**	**20.8**	**0.0281**	**-**	**-**

Test Conditions:

DI Water — Open Vent Mode

A = 0.99% — U_G = 4.0 cm/s

Oxygen Mass Transfer Data							
Test	Inlet Gas	Gas Velocity (cm/s)	Temperature (ºC)	k_La (1/s)	C_o (% of Sat)	C_∞ (% of Sat)	τ_e (s)
#1	Nitrogen	3.99	20.4	0.0574	100.1	0.1	2.28
#2	Nitrogen	3.99	20.5	0.0576	98.8	-1.2	1.67
#3	Nitrogen	4.03	20.2	0.0584	99.8	0.1	2.14
#1	Air	3.95	20.4	0.0578	-0.2	99.8	2.23
#2	Air	4.00	20.6	0.0589	0.1	100.9	2.22
#3	Air	3.98	20.2	0.0595	0.0	99.9	2.46
#1	Carbon Monoxide	3.99	20.5	0.0573	100.4	0.0	1.74
#2	Carbon Monoxide	3.98	20.6	0.0592	99.4	-1.0	2.35
#3	Carbon Monoxide	4.03	20.2	0.0582	100.4	0.0	2.23
#1	Air	3.95	20.5	0.0567	0.7	99.8	2.06
#2	Air	3.99	20.6	0.0594	0.4	101.0	2.13
#3	Air	3.98	20.3	0.0595	0.2	99.9	2.30
Average		**3.99**	**20.4**	**0.0583**	**-**	**-**	**2.15**

Test Conditions:

DI Water — Open Vent Mode

A = 0.99% — U_G = 6.0 cm/s

Oxygen Mass Transfer Data							
Test	Inlet Gas	Gas Velocity (cm/s)	Temperature (ºC)	k_La (1/s)	C_o (% of Sat)	C_∞ (% of Sat)	τ_e (s)
#1	Nitrogen	5.96	20.5	0.0873	99.8	0.0	2.13
#2	Nitrogen	5.98	20.4	0.0878	99.5	0.1	2.64
#3	Nitrogen	5.94	20.6	0.0888	101.2	0.2	2.43
#1	Air	6.01	20.5	0.0916	0.4	99.8	2.47
#2	Air	5.96	20.5	0.0897	0.6	99.8	2.26
#3	Air	5.95	20.6	0.0880	0.7	100.0	1.86
#1	Carbon Monoxide	5.90	20.5	0.0868	98.5	0.0	2.33
#2	Carbon Monoxide	5.94	20.5	0.0877	99.9	0.1	2.25
#3	Carbon Monoxide	6.02	20.6	0.0887	99.0	0.1	2.13
#1	Air	6.01	20.5	0.0909	-0.3	99.9	2.43
#2	Air	5.97	20.5	0.0866	0.2	100.0	1.97
#3	Air	5.95	20.7	0.0876	-0.1	99.8	2.12
Average		**5.97**	**20.5**	**0.0885**	**-**	**-**	**2.25**

Carbon Monoxide Mass Transfer Data						
Test	Inlet Gas	Gas Velocity (cm/s)	Temperature (ºC)	k_La (1/s)	C_o (% of Sat)	C_∞ (% of Sat)
#1	Carbon Monoxide	5.90	20.5	0.0893	0.0	99.2
#2	Carbon Monoxide	5.94	20.5	0.0890	0.0	99.2
#3	Carbon Monoxide	6.02	20.6	0.0869	0.0	100.6
Average		**5.95**	**20.5**	**0.0884**	**-**	**-**

Test Conditions:

DI Water — Open Vent Mode

A = 0.99% — U_G = 8.0 cm/s

Oxygen Mass Transfer Data							
Test	Inlet Gas	Gas Velocity (cm/s)	Temperature (ºC)	k_La (1/s)	C_o (% of Sat)	C_∞ (% of Sat)	τ_e (s)
#1	Nitrogen	8.01	20.0	0.1045	101.2	0.2	2.59
#2	Nitrogen	7.98	20.5	0.1066	99.8	0.1	2.22
#3	Nitrogen	8.09	20.8	0.1267	197.8	-0.2	7.90
#1	Air	8.03	20.0	0.1029	-0.7	99.8	1.96
#2	Air	8.00	20.5	0.1103	0.9	99.8	2.63
#3	Air	8.04	20.9	0.1103	1.4	100.0	2.19
#1	Carbon Monoxide	8.00	20.0	0.0992	99.7	0.1	1.83
#2	Carbon Monoxide	7.99	20.6	0.1109	102.2	0.3	3.26
#3	Carbon Monoxide	8.03	20.8	0.1077	100.1	0.1	2.07
#1	Air	8.02	20.1	0.1053	0.3	99.9	2.32
#2	Air	8.01	20.6	0.1117	-0.3	100.0	2.71
#3	Air	8.04	20.8	0.1090	2.4	100.0	2.21
Average		**8.02**	**20.5**	**0.1087**	**-**	**-**	**2.82**

Test Conditions:

DI Water — Open Vent Mode

A = 0.99% — U_G = 10.0 cm/s

Oxygen Mass Transfer Data							
Test	Inlet Gas	Gas Velocity (cm/s)	Temperature (ºC)	k_La (1/s)	C_o (% of Sat)	C_∞ (% of Sat)	τ_e (s)
#1	Nitrogen	10.00	20.6	0.1041	100.0	0.1	1.69
#2	Nitrogen	10.01	20.6	0.1296	99.3	0.1	2.24
#3	Nitrogen	10.02	21.1	0.1297	100.5	0.1	2.73
#1	Air	10.05	20.6	0.1104	1.3	100.0	1.78
#2	Air	10.05	20.7	0.1341	0.0	99.7	2.09
#3	Air	10.07	21.1	0.1331	1.4	100.1	2.52
#1	Carbon Monoxide	10.04	20.6	0.1108	100.6	0.2	2.26
#2	Carbon Monoxide	10.08	20.7	0.1264	97.0	0.0	1.94
#3	Carbon Monoxide	10.14	21.1	0.1321	98.6	0.2	2.14
#1	Air	10.07	20.6	0.1089	-0.3	99.9	1.94
#2	Air	10.07	20.7	0.1266	0.2	99.8	2.20
#3	Air	10.12	21.1	0.1349	1.6	99.8	2.32
Average		**10.06**	**20.8**	**0.1234**	**-**	**-**	**2.15**

Carbon Monoxide Mass Transfer Data						
Test	Inlet Gas	Gas Velocity (cm/s)	Temperature (ºC)	k_La (1/s)	C_o (% of Sat)	C_∞ (% of Sat)
#1	Carbon Monoxide	10.04	20.6	0.1157	0.0	100.6
#2	Carbon Monoxide	10.08	20.7	0.1230	0.0	100.1
#3	Carbon Monoxide	10.14	21.1	0.1320	0.0	99.0
Average		**10.09**	**20.8**	**0.1236**	**-**	**-**

Test Conditions:

DI Water — Open Vent Mode

A = 0.99% — U_G = 12.0 cm/s

Oxygen Mass Transfer Data							
Test	Inlet Gas	Gas Velocity (cm/s)	Temperature (ºC)	k_La (1/s)	C_o (% of Sat)	C_∞ (% of Sat)	τ_e (s)
#1	Nitrogen	11.95	20.1	0.1162	99.3	0.0	1.61
#2	Nitrogen	12.04	20.2	0.1565	216.6	-0.1	6.39
#3	Nitrogen	12.00	20.3	0.1270	99.0	-0.3	2.10
#1	Air	11.95	20.1	0.1286	-0.5	100.1	2.14
#2	Air	11.90	20.2	0.1364	0.7	99.9	2.07
#3	Air	12.03	20.3	0.1460	0.2	99.6	2.49
#1	Carbon Monoxide	12.07	20.2	0.1173	100.8	-0.7	1.34
#2	Carbon Monoxide	12.05	20.2	0.1433	100.9	0.2	2.20
#3	Carbon Monoxide	12.03	20.3	0.1352	99.4	0.0	2.03
#1	Air	11.97	20.2	0.1568	-0.1	116.0	3.06
#2	Air	11.90	20.2	0.1352	-0.3	100.0	1.98
#3	Air	12.05	20.3	0.1465	-0.4	100.0	2.18
Average		**11.99**	**20.2**	**0.1371**	**-**	**-**	**2.47**

Test Conditions:

DI Water — Open Vent Mode

A = 0.99% — U_G = 14.0 cm/s

Oxygen Mass Transfer Data							
Test	Inlet Gas	Gas Velocity (cm/s)	Temperature (ºC)	k_La (1/s)	C_o (% of Sat)	C_∞ (% of Sat)	τ_e (s)
#1	Nitrogen	13.99	20.6	0.1408	101.2	0.2	2.07
#2	Nitrogen	14.04	20.3	0.1488	100.8	0.2	2.39
#3	Nitrogen	14.03	20.4	0.1367	100.7	0.1	2.05
#1	Air	14.02	20.5	0.1373	-0.2	99.8	1.85
#2	Air	14.01	20.3	0.1426	-0.1	100.0	1.63
#3	Air	14.07	20.4	0.1399	-1.0	100.0	2.12
#1	Carbon Monoxide	13.99	20.5	0.1398	100.5	0.2	1.93
#2	Carbon Monoxide	13.98	20.3	0.1496	100.0	0.2	2.25
#3	Carbon Monoxide	14.04	20.4	0.1399	101.5	0.2	2.00
#1	Air	14.06	20.5	0.1384	1.1	99.6	1.81
#2	Air	14.02	20.3	0.1378	-0.5	99.7	1.89
#3	Air	14.08	20.4	0.1426	-1.1	99.8	2.41
Average		**14.03**	**20.4**	**0.1412**	**-**	**-**	**2.03**

Carbon Monoxide Mass Transfer Data						
Test	Inlet Gas	Gas Velocity (cm/s)	Temperature (ºC)	k_La (1/s)	C_o (% of Sat)	C_∞ (% of Sat)
#1	Carbon Monoxide	13.99	20.5	0.1315	0.0	100.1
#2	Carbon Monoxide	13.98	20.3	0.1327	0.0	101.1
#3	Carbon Monoxide	14.04	20.4	0.1336	0.0	100.7
Average		**14.00**	**20.4**	**0.1326**	**-**	**-**

Test Conditions:

DI Water — Open Vent Mode

A = 0.99% — U_G = 16.0 cm/s

Oxygen Mass Transfer Data							
Test	Inlet Gas	Gas Velocity (cm/s)	Temperature (ºC)	k_La (1/s)	C_o (% of Sat)	C_∞ (% of Sat)	τ_e (s)
#1	Nitrogen	16.09	20.7	0.1565	172.8	0.0	6.40
#2	Nitrogen	15.97	20.7	0.1379	102.8	0.2	2.69
#3	Nitrogen	15.97	20.3	0.1411	98.1	0.1	2.48
#1	Air	16.07	20.7	0.1527	-50.9	99.7	6.55
#2	Air	15.94	20.8	0.1440	0.0	99.7	2.18
#3	Air	15.97	20.4	0.1470	-1.0	99.5	2.47
#1	Carbon Monoxide	16.11	20.7	0.1310	101.1	0.4	1.41
#2	Carbon Monoxide	15.99	20.8	0.1351	100.2	0.2	1.76
#3	Carbon Monoxide	15.99	20.4	0.1346	100.5	-0.1	1.92
#1	Air	16.10	20.7	0.1171	0.1	100.0	1.55
#2	Air	15.95	20.8	0.1362	1.1	99.6	1.55
#3	Air	15.98	20.4	0.1439	-0.2	99.7	2.04
Average		**16.01**	**20.6**	**0.1398**	**-**	**-**	**2.75**

Test Conditions:

DI Water — Open Vent Mode

A = 0.99% — U_G = 18.0 cm/s

Oxygen Mass Transfer Data							
Test	Inlet Gas	Gas Velocity (cm/s)	Temperature (ºC)	k_La (1/s)	C_o (% of Sat)	C_∞ (% of Sat)	τ_e (s)
#1	Nitrogen	17.92	20.1	0.1554	103.2	0.3	4.12
#2	Nitrogen	18.02	20.8	0.1275	99.4	-0.2	1.89
#3	Nitrogen	18.02	21.4	0.1400	99.1	-0.1	1.90
#1	Air	18.00	20.1	0.1410	0.0	99.6	2.25
#2	Air	18.00	20.8	0.1349	-0.5	100.1	1.76
#3	Air	18.04	21.4	0.1383	1.7	100.0	1.39
#1	Carbon Monoxide	18.01	20.1	0.1362	101.1	0.2	1.83
#2	Carbon Monoxide	18.03	20.8	0.1338	99.5	0.0	1.99
#3	Carbon Monoxide	18.05	21.4	0.1471	100.8	0.0	2.57
#1	Air	18.02	20.0	0.1350	-0.9	100.0	1.79
#2	Air	18.04	20.7	0.1354	-0.5	100.2	1.86
#3	Air	18.06	21.4	0.1442	-0.3	99.5	1.80
Average		**18.02**	**20.7**	**0.1391**	**-**	**-**	**2.10**

Test Conditions:

DI Water — Open Vent Mode

A = 0.99% — U_G = 20.0 cm/s

Oxygen Mass Transfer Data							
Test	Inlet Gas	Gas Velocity (cm/s)	Temperature (ºC)	k_La (1/s)	C_o (% of Sat)	C_∞ (% of Sat)	τ_e (s)
#1	Nitrogen	19.94	21.0	0.1438	99.2	0.2	2.10
#2	Nitrogen	19.95	20.7	0.1417	100.8	0.1	1.97
#3	Nitrogen	20.06	20.2	0.1416	100.0	0.0	2.16
#1	Air	20.00	21.0	0.1343	-0.1	99.5	2.07
#2	Air	20.00	20.7	0.1393	0.1	99.9	1.86
#3	Air	20.07	20.2	0.1479	-1.0	99.9	2.20
#1	Carbon Monoxide	19.97	21.0	0.1485	100.4	0.1	2.16
#2	Carbon Monoxide	19.97	20.7	0.1555	100.4	0.3	2.87
#3	Carbon Monoxide	20.04	20.2	0.1448	99.3	0.1	2.13
#1	Air	20.01	21.0	0.1395	-1.0	99.8	2.47
#2	Air	19.99	20.7	0.1454	0.4	100.0	2.15
#3	Air	20.12	20.2	0.1537	-0.5	100.1	2.64
Average		**20.01**	**20.6**	**0.1447**	**-**	**-**	**2.23**

Test Conditions:

DI Water — Open Vent Mode

A = 2.22% — U_G = 0.5 cm/s

Oxygen Mass Transfer Data							
Test	Inlet Gas	Gas Velocity (cm/s)	Temperature (ºC)	k_La (1/s)	C_o (% of Sat)	C_∞ (% of Sat)	τ_e (s)
#1	Nitrogen	0.53	20.3	0.0078	99.4	-1.2	3.81
#2	Nitrogen	0.49	20.3	0.0074	98.9	-1.6	4.09
#3	Nitrogen	0.52	20.4	0.0079	99.6	-1.2	5.08
#1	Air	0.53	20.4	0.0080	99.5	-1.1	3.29
#2	Air	0.50	20.4	0.0076	99.2	-1.4	4.32
#3	Air	0.53	20.5	0.0081	99.3	-1.1	4.59
#1	Carbon Monoxide	0.53	20.5	0.0079	99.2	-1.1	2.98
#2	Carbon Monoxide	0.49	20.5	0.0074	99.4	-1.6	4.41
#3	Carbon Monoxide	0.52	20.6	0.0080	99.4	-1.2	4.38
#1	Air	0.53	20.6	0.0079	0.7	101.0	0.71
#2	Air	0.50	20.6	0.0077	0.7	101.1	1.81
#3	Air	0.53	20.7	0.0082	0.2	100.9	2.21
Average		**0.52**	**20.5**	**0.0078**	**-**	**-**	**3.47**

Test Conditions:

DI Water — Open Vent Mode

A = 2.22% — U_G = 2.0 cm/s

Oxygen Mass Transfer Data							
Test	Inlet Gas	Gas Velocity (cm/s)	Temperature (ºC)	k_La (1/s)	C_o (% of Sat)	C_∞ (% of Sat)	τ_e (s)
#1	Nitrogen	1.99	20.0	0.0256	99.8	0.0	1.95
#2	Nitrogen	2.01	20.2	0.0267	100.0	0.1	1.92
#3	Nitrogen	2.03	19.8	0.0252	99.4	0.0	1.29
#1	Air	1.99	20.0	0.0258	1.0	99.8	1.62
#2	Air	1.99	20.2	0.0263	0.7	100.1	1.59
#3	Air	2.01	19.8	0.0255	0.5	99.8	1.20
#1	Carbon Monoxide	2.01	20.1	0.0259	99.7	-0.1	2.01
#2	Carbon Monoxide	2.03	20.3	0.0269	99.8	0.0	1.97
#3	Carbon Monoxide	2.01	19.9	0.0254	99.6	0.0	1.83
#1	Air	1.99	20.1	0.0255	0.6	100.0	1.20
#2	Air	1.99	20.3	0.0263	-0.1	99.9	1.22
#3	Air	2.01	20.0	0.0252	0.2	100.2	1.38
Average		**2.01**	**20.1**	**0.0259**	**-**	**-**	**1.60**

Carbon Monoxide Mass Transfer Data						
Test	Inlet Gas	Gas Velocity (cm/s)	Temperature (ºC)	k_La (1/s)	C_o (% of Sat)	C_∞ (% of Sat)
#1	Carbon Monoxide	2.01	20.1	0.0250	0.0	99.4
#2	Carbon Monoxide	2.03	20.3	0.0254	0.0	99.9
#3	Carbon Monoxide	2.01	19.9	0.0257	0.0	100.9
Average		**2.02**	**20.1**	**0.0254**	**-**	**-**

Test Conditions:

DI Water — Open Vent Mode

A = 2.22% — U_G = 4.0 cm/s

Oxygen Mass Transfer Data							
Test	Inlet Gas	Gas Velocity (cm/s)	Temperature (ºC)	k_La (1/s)	C_o (% of Sat)	C_∞ (% of Sat)	τ_e (s)
#1	Nitrogen	4.01	20.1	0.0563	99.9	0.0	2.00
#2	Nitrogen	3.97	20.4	0.0554	100.2	0.1	2.05
#3	Nitrogen	3.99	19.9	0.0552	100.1	0.1	2.40
#1	Air	3.99	20.2	0.0573	0.2	100.1	2.11
#2	Air	3.98	20.4	0.0576	-0.6	99.9	2.38
#3	Air	4.01	20.0	0.0567	0.1	100.1	2.63
#1	Carbon Monoxide	4.09	20.2	0.0589	98.9	0.1	2.07
#2	Carbon Monoxide	3.97	20.5	0.0555	100.6	0.1	2.07
#3	Carbon Monoxide	3.99	20.0	0.0556	100.8	0.1	2.48
#1	Air	4.06	20.3	0.0582	-0.2	99.8	2.18
#2	Air	3.98	20.5	0.0572	0.2	100.0	2.23
#3	Air	4.01	20.1	0.0564	0.2	100.0	2.30
Average		**4.00**	**20.2**	**0.0567**	**-**	**-**	**2.24**

Test Conditions:

DI Water — Open Vent Mode

A = 2.22% — U_G = 6.0 cm/s

Oxygen Mass Transfer Data							
Test	Inlet Gas	Gas Velocity (cm/s)	Temperature (ºC)	k_La (1/s)	C_o (% of Sat)	C_∞ (% of Sat)	τ_e (s)
#1	Nitrogen	5.93	20.8	0.0810	100.6	0.0	2.05
#2	Nitrogen	5.94	20.3	0.0815	100.0	0.1	1.85
#3	Nitrogen	6.00	20.2	0.0826	99.8	0.2	2.35
#1	Air	5.97	20.8	0.0840	-0.4	99.9	2.32
#2	Air	5.94	20.3	0.0841	-0.5	99.9	2.16
#3	Air	5.97	20.3	0.0821	0.0	100.0	2.18
#1	Carbon Monoxide	5.96	20.8	0.0822	100.2	0.0	2.50
#2	Carbon Monoxide	5.99	20.4	0.0871	101.6	0.2	2.81
#3	Carbon Monoxide	6.00	20.3	0.0840	99.5	0.2	2.30
#1	Air	5.97	20.8	0.0824	0.4	99.8	1.79
#2	Air	5.93	20.4	0.0818	0.6	100.0	1.96
#3	Air	5.97	20.3	0.0800	0.1	99.8	1.39
Average		**5.96**	**20.5**	**0.0827**	**-**	**-**	**2.14**

Carbon Monoxide Mass Transfer Data						
Test	Inlet Gas	Gas Velocity (cm/s)	Temperature (ºC)	k_La (1/s)	C_o (% of Sat)	C_∞ (% of Sat)
#1	Carbon Monoxide	5.96	20.8	0.0818	0.0	98.0
#2	Carbon Monoxide	5.99	20.4	0.0825	0.0	98.5
#3	Carbon Monoxide	6.00	20.3	0.0815	0.0	99.2
Average		**5.98**	**20.5**	**0.0819**	**-**	**-**

Test Conditions:

DI Water — Open Vent Mode

A = 2.22% — U_G = 8.0 cm/s

Oxygen Mass Transfer Data							
Test	Inlet Gas	Gas Velocity (cm/s)	Temperature (ºC)	k_La (1/s)	C_o (% of Sat)	C_∞ (% of Sat)	τ_e (s)
#1	Nitrogen	8.12	20.3	0.0985	99.4	0.1	2.00
#2	Nitrogen	7.99	19.4	0.0986	102.3	0.3	2.89
#3	Nitrogen	8.05	19.8	0.0947	99.7	0.0	1.92
#1	Air	8.08	20.3	0.1013	0.1	99.8	2.47
#2	Air	7.97	19.4	0.0909	0.2	100.0	2.15
#3	Air	8.07	19.8	0.0945	-0.5	100.0	1.85
#1	Carbon Monoxide	8.13	20.3	0.0990	100.1	0.1	2.05
#2	Carbon Monoxide	7.99	19.5	0.0908	99.1	0.0	1.80
#3	Carbon Monoxide	8.03	19.9	0.0989	100.2	0.2	2.73
#1	Air	8.09	20.3	0.1003	1.7	99.8	1.89
#2	Air	7.98	19.5	0.0965	1.5	99.9	2.09
#3	Air	8.06	19.9	0.1022	0.7	99.7	2.47
Average		**8.05**	**19.9**	**0.0972**	**-**	**-**	**2.19**

Test Conditions:

DI Water — Open Vent Mode

A = 2.22% — U_G = 10.0 cm/s

Oxygen Mass Transfer Data							
Test	Inlet Gas	Gas Velocity (cm/s)	Temperature (ºC)	k_La (1/s)	C_o (% of Sat)	C_∞ (% of Sat)	τ_e (s)
#1	Nitrogen	9.93	20.4	0.1112	99.3	-0.2	2.31
#2	Nitrogen	10.04	20.8	0.1083	100.2	0.2	1.88
#3	Nitrogen	10.03	20.3	0.1047	99.2	0.0	1.62
#1	Air	10.00	20.4	0.1122	-0.9	99.9	2.40
#2	Air	10.08	20.8	0.1157	-1.9	99.9	2.14
#3	Air	10.05	20.3	0.1176	-0.8	99.8	2.65
#1	Carbon Monoxide	10.07	20.4	0.1154	99.4	-0.1	2.57
#2	Carbon Monoxide	10.03	20.8	0.1122	100.5	0.1	2.57
#3	Carbon Monoxide	10.06	20.3	0.1099	98.6	0.1	2.02
#1	Air	10.04	20.4	0.1119	-1.3	100.0	1.95
#2	Air	10.09	20.8	0.1111	-0.7	100.2	2.22
#3	Air	10.06	20.3	0.1075	-0.1	99.8	2.07
Average		**10.04**	**20.5**	**0.1115**	**-**	**-**	**2.20**

Carbon Monoxide Mass Transfer Data						
Test	Inlet Gas	Gas Velocity (cm/s)	Temperature (ºC)	k_La (1/s)	C_o (% of Sat)	C_∞ (% of Sat)
#1	Carbon Monoxide	10.07	20.4	0.1091	0.0	99.2
#2	Carbon Monoxide	10.03	20.8	0.1125	0.0	98.7
#3	Carbon Monoxide	10.06	20.3	0.1141	0.0	98.7
Average		**10.06**	**20.5**	**0.1119**	**-**	**-**

Test Conditions:

DI Water — Open Vent Mode

A = 2.22% — U_G = 12.0 cm/s

Oxygen Mass Transfer Data							
Test	Inlet Gas	Gas Velocity (cm/s)	Temperature (ºC)	k_La (1/s)	C_o (% of Sat)	C_∞ (% of Sat)	τ_e (s)
#1	Nitrogen	12.02	20.1	0.1144	98.9	0.2	1.21
#2	Nitrogen	11.99	20.5	0.1205	100.7	0.2	2.30
#3	Nitrogen	11.98	20.1	0.1118	100.1	0.1	2.19
#1	Air	12.00	20.1	0.1141	1.7	99.9	1.90
#2	Air	12.08	20.5	0.1213	-0.2	100.0	1.67
#3	Air	12.03	20.1	0.1171	-0.7	100.0	2.39
#1	Carbon Monoxide	12.03	20.1	0.1112	99.7	0.0	1.93
#2	Carbon Monoxide	12.00	20.6	0.1175	100.5	0.1	2.10
#3	Carbon Monoxide	11.99	20.1	0.1187	100.1	0.1	2.35
#1	Air	12.01	20.2	0.1198	1.1	100.0	1.93
#2	Air	12.09	20.6	0.1180	1.2	99.9	1.92
#3	Air	12.04	20.1	0.1240	0.9	99.8	2.50
Average		**12.02**	**20.3**	**0.1174**	**-**	**-**	**2.03**

Test Conditions:

DI Water — Open Vent Mode

A = 2.22% — U_G = 14.0 cm/s

Oxygen Mass Transfer Data							
Test	Inlet Gas	Gas Velocity (cm/s)	Temperature (ºC)	k_La (1/s)	C_o (% of Sat)	C_∞ (% of Sat)	τ_e (s)
#1	Nitrogen	14.00	20.2	0.1243	101.4	0.2	2.44
#2	Nitrogen	14.03	20.2	0.1215	99.2	0.1	1.81
#3	Nitrogen	14.08	20.1	0.1259	101.2	0.1	2.20
#1	Air	14.07	20.2	0.1248	-0.8	100.0	2.37
#2	Air	14.08	20.2	0.1296	0.6	100.0	2.17
#3	Air	14.03	20.1	0.1286	-0.4	99.7	1.82
#1	Carbon Monoxide	13.88	20.2	0.1287	100.0	0.2	2.44
#2	Carbon Monoxide	14.11	20.2	0.1297	99.5	0.1	2.16
#3	Carbon Monoxide	13.92	20.1	0.1235	100.1	0.1	1.59
#1	Air	14.08	20.2	0.1254	0.1	100.2	1.88
#2	Air	14.10	20.2	0.1270	0.2	99.9	1.78
#3	Air	14.04	20.1	0.1292	-0.1	100.2	2.33
Average		**14.03**	**20.2**	**0.1265**	**-**	**-**	**2.08**

Carbon Monoxide Mass Transfer Data						
Test	Inlet Gas	Gas Velocity (cm/s)	Temperature (ºC)	k_La (1/s)	C_o (% of Sat)	C_∞ (% of Sat)
#1	Carbon Monoxide	13.88	20.2	0.1358	0.0	100.0
#2	Carbon Monoxide	14.11	20.2	0.1299	0.0	99.3
#3	Carbon Monoxide	13.92	20.1	0.1277	0.0	100.3
Average		**13.97**	**20.2**	**0.1311**	**-**	**-**

Test Conditions:

DI Water — Open Vent Mode

A = 2.22% — U_G = 16.0 cm/s

Oxygen Mass Transfer Data							
Test	Inlet Gas	Gas Velocity (cm/s)	Temperature (ºC)	k_La (1/s)	C_o (% of Sat)	C_∞ (% of Sat)	τ_e (s)
#1	Nitrogen	15.96	20.6	0.1480	104.4	0.2	4.15
#2	Nitrogen	15.93	20.5	0.1307	100.9	0.2	2.26
#3	Nitrogen	16.08	20.2	0.1361	101.4	0.2	3.21
#1	Air	15.97	20.6	0.1330	0.8	100.0	1.65
#2	Air	16.03	20.5	0.1437	-0.1	99.8	2.39
#3	Air	16.06	20.2	0.1359	-1.6	99.9	2.23
#1	Carbon Monoxide	16.01	20.6	0.1324	100.3	0.1	2.06
#2	Carbon Monoxide	16.04	20.5	0.1368	99.9	0.2	2.57
#3	Carbon Monoxide	16.11	20.2	0.1363	100.3	0.2	2.38
#1	Air	15.97	20.6	0.1401	0.0	100.3	2.43
#2	Air	16.05	20.5	0.1406	-1.1	100.0	2.33
#3	Air	16.08	20.1	0.1328	-0.5	100.2	2.35
Average		**16.02**	**20.4**	**0.1372**	**-**	**-**	**2.50**

Test Conditions:

DI Water — Open Vent Mode

A = 2.22% — U_G = 18.0 cm/s

Oxygen Mass Transfer Data							
Test	Inlet Gas	Gas Velocity (cm/s)	Temperature (ºC)	k_La (1/s)	C_o (% of Sat)	C_∞ (% of Sat)	τ_e (s)
#1	Nitrogen	18.05	19.6	0.1359	100.1	0.1	2.35
#2	Nitrogen	17.99	20.5	0.1375	100.3	0.0	2.21
#3	Nitrogen	17.95	20.5	0.1392	99.0	0.1	2.21
#1	Air	18.07	19.6	0.1403	-1.1	100.0	2.22
#2	Air	17.98	20.6	0.1492	-1.0	99.6	2.84
#3	Air	17.95	20.5	0.1433	-0.9	99.9	2.43
#1	Carbon Monoxide	18.11	19.6	0.1330	98.5	0.1	1.71
#2	Carbon Monoxide	17.99	20.6	0.1329	100.1	0.0	1.82
#3	Carbon Monoxide	17.98	20.5	0.1410	99.6	0.0	2.31
#1	Air	18.09	19.5	0.1320	-0.1	99.6	1.88
#2	Air	17.99	20.6	0.1453	0.6	99.8	2.06
#3	Air	17.96	20.5	0.1437	-0.9	99.9	2.14
Average		**18.01**	**20.2**	**0.1395**	**-**	**-**	**2.18**

Test Conditions:

DI Water — Open Vent Mode

A = 2.22% — U_G = 20.0 cm/s

Oxygen Mass Transfer Data							
Test	Inlet Gas	Gas Velocity (cm/s)	Temperature (ºC)	k_La (1/s)	C_o (% of Sat)	C_∞ (% of Sat)	τ_e (s)
#1	Nitrogen	19.95	20.0	0.1375	99.6	0.1	2.25
#2	Nitrogen	19.97	20.3	0.1372	99.2	-0.1	2.21
#3	Nitrogen	19.81	20.3	0.1466	97.8	0.1	2.37
#1	Air	19.88	20.1	0.1570	-0.9	100.0	2.98
#2	Air	20.07	20.3	0.1525	0.5	100.1	2.13
#3	Air	19.99	20.3	0.1377	0.0	99.9	1.63
#1	Carbon Monoxide	19.93	20.1	0.1450	101.5	0.2	2.49
#2	Carbon Monoxide	20.02	20.3	0.1436	100.4	0.0	2.35
#3	Carbon Monoxide	20.04	20.3	0.1525	100.1	0.2	2.59
#1	Air	19.88	20.1	0.1544	-0.2	99.9	2.12
#2	Air	20.09	20.3	0.1547	-0.2	100.2	2.42
#3	Air	20.02	20.3	0.1594	0.6	99.8	2.42
Average		**19.97**	**20.2**	**0.1482**	**-**	**-**	**2.33**

Test Conditions:

KCl Solution — Open Vent Mode

A = 0.62% — U_G = 0.5 cm/s

Oxygen Mass Transfer Data							
Test	Inlet Gas	Gas Velocity (cm/s)	Temperature (ºC)	k_La (1/s)	C_o (% of Sat)	C_∞ (% of Sat)	τ_e (s)
#1	Nitrogen	0.49	19.7	0.0073	99.3	-1.9	6.06
#2	Nitrogen	0.50	20.3	0.0079	99.4	-1.3	4.23
#3	Nitrogen	0.54	20.2	0.0083	99.0	-1.1	4.11
#1	Air	0.48	19.8	0.0073	0.6	101.7	2.61
#2	Air	0.50	20.4	0.0080	0.3	101.1	1.30
#3	Air	0.54	20.4	0.0085	0.4	100.7	1.97
#1	Carbon Monoxide	0.49	20.0	0.0075	99.3	-1.6	5.08
#2	Carbon Monoxide	0.50	20.5	0.0080	98.9	-1.2	4.48
#3	Carbon Monoxide	0.54	20.5	0.0085	99.3	-0.9	5.15
#1	Air	0.48	20.1	0.0075	0.5	101.3	3.21
#2	Air	0.50	20.6	0.0081	0.5	100.8	1.02
#3	Air	0.54	20.6	0.0085	0.3	100.7	2.13
Average		**0.51**	**20.3**	**0.0080**	**-**	**-**	**3.45**

Test Conditions:

KCl Solution — Open Vent Mode

A = 0.62% — U_G = 2.0 cm/s

Oxygen Mass Transfer Data							
Test	Inlet Gas	Gas Velocity (cm/s)	Temperature (ºC)	k_La (1/s)	C_o (% of Sat)	C_∞ (% of Sat)	τ_e (s)
#1	Nitrogen	2.03	20.1	0.0282	99.4	0.0	1.60
#2	Nitrogen	2.03	19.9	0.0281	99.2	0.0	1.81
#3	Nitrogen	2.03	19.5	0.0282	98.7	0.1	1.89
#1	Air	1.99	20.2	0.0281	0.4	100.1	1.53
#2	Air	2.02	19.9	0.0294	0.0	100.0	1.88
#3	Air	2.03	19.6	0.0287	0.0	100.1	1.83
#1	Carbon Monoxide	2.03	20.2	0.0285	100.0	0.0	2.59
#2	Carbon Monoxide	2.02	20.0	0.0287	99.3	0.2	1.49
#3	Carbon Monoxide	2.02	19.7	0.0287	99.5	0.1	1.79
#1	Air	1.99	20.3	0.0274	-0.6	99.7	1.93
#2	Air	2.03	20.1	0.0288	0.5	99.7	1.17
#3	Air	2.03	19.8	0.0291	0.6	99.9	1.54
Average		**2.02**	**19.9**	**0.0285**	**-**	**-**	**1.75**

Carbon Monoxide Mass Transfer Data						
Test	Inlet Gas	Gas Velocity (cm/s)	Temperature (ºC)	k_La (1/s)	C_o (% of Sat)	C_∞ (% of Sat)
#1	Carbon Monoxide	2.03	20.2	0.0299	0.0	100.8
#2	Carbon Monoxide	2.02	20.0	0.0312	0.0	100.7
#3	Carbon Monoxide	2.02	19.7	0.0283	0.0	100.0
Average		**2.02**	**20.0**	**0.0298**	**-**	**-**

Test Conditions:

KCl Solution — Open Vent Mode

A = 0.62% — U_G = 4.0 cm/s

Oxygen Mass Transfer Data							
Test	Inlet Gas	Gas Velocity (cm/s)	Temperature (ºC)	k_La (1/s)	C_o (% of Sat)	C_∞ (% of Sat)	τ_e (s)
#1	Nitrogen	4.02	20.7	0.0670	99.5	0.1	2.24
#2	Nitrogen	3.98	19.7	0.0632	99.3	0.2	1.86
#3	Nitrogen	3.97	20.3	0.0641	99.3	0.0	2.64
#1	Air	3.98	20.7	0.0714	0.3	100.2	3.48
#2	Air	3.98	19.7	0.0671	0.3	99.9	2.72
#3	Air	3.99	20.3	0.0672	-0.2	99.8	2.46
#1	Carbon Monoxide	4.02	20.7	0.0689	99.3	0.1	2.25
#2	Carbon Monoxide	3.99	19.8	0.0684	100.6	0.1	3.36
#3	Carbon Monoxide	3.97	20.3	0.0677	99.6	0.1	2.83
#1	Air	3.98	20.7	0.0692	-0.1	99.6	2.53
#2	Air	3.98	19.8	0.0685	2.2	99.9	2.35
#3	Air	3.99	20.4	0.0689	0.0	100.0	2.79
Average		**3.99**	**20.3**	**0.0676**	**-**	**-**	**2.63**

Test Conditions:

KCl Solution — Open Vent Mode

A = 0.62% — U_G = 6.0 cm/s

Oxygen Mass Transfer Data							
Test	Inlet Gas	Gas Velocity (cm/s)	Temperature (ºC)	k_La (1/s)	C_o (% of Sat)	C_∞ (% of Sat)	τ_e (s)
#1	Nitrogen	6.01	20.4	0.1042	99.6	0.2	3.13
#2	Nitrogen	5.98	20.3	0.1050	98.9	0.1	2.15
#3	Nitrogen	5.98	19.5	0.1037	98.7	0.2	2.17
#1	Air	6.02	20.5	0.1016	0.3	100.0	2.49
#2	Air	5.99	20.3	0.1092	0.5	99.9	2.77
#3	Air	5.97	19.6	0.1084	0.4	99.5	3.17
#1	Carbon Monoxide	5.93	20.5	0.1020	99.4	0.1	2.39
#2	Carbon Monoxide	6.00	20.3	0.1095	101.0	0.2	2.68
#3	Carbon Monoxide	5.97	19.7	0.1070	102.5	0.1	3.67
#1	Air	6.01	20.5	0.1024	1.1	99.8	2.17
#2	Air	5.99	20.4	-	-0.6	99.9	3.35
#3	Air	5.97	19.7	0.1028	-0.9	99.6	2.23
Average		**5.99**	**20.2**	**0.1051**	**-**	**-**	**2.70**

Carbon Monoxide Mass Transfer Data						
Test	Inlet Gas	Gas Velocity (cm/s)	Temperature (ºC)	k_La (1/s)	C_o (% of Sat)	C_∞ (% of Sat)
#1	Carbon Monoxide	5.93	20.5	0.1084	0.0	102.3
#2	Carbon Monoxide	6.00	20.3	0.0956	0.0	101.6
#3	Carbon Monoxide	5.97	19.7	0.1041	0.0	99.8
Average		**5.97**	**20.2**	**0.1027**	**-**	**-**

Test Conditions:

KCl Solution — Open Vent Mode

A = 0.62% — U_G = 8.0 cm/s

Oxygen Mass Transfer Data							
Test	Inlet Gas	Gas Velocity (cm/s)	Temperature (ºC)	k_La (1/s)	C_o (% of Sat)	C_∞ (% of Sat)	τ_e (s)
#1	Nitrogen	8.04	20.5	-	100.9	0.1	2.58
#2	Nitrogen	8.01	19.9	0.1247	100.1	0.2	2.79
#3	Nitrogen	8.01	20.1	0.1218	99.2	0.1	2.67
#1	Air	8.02	20.5	0.1211	0.8	99.6	2.13
#2	Air	7.99	19.9	-	-0.8	100.0	1.78
#3	Air	8.05	20.0	0.1227	-0.6	99.8	2.05
#1	Carbon Monoxide	8.09	20.5	0.1221	99.9	0.1	2.31
#2	Carbon Monoxide	8.03	19.9	0.1269	100.5	0.1	2.25
#3	Carbon Monoxide	8.02	20.2	0.1208	100.5	0.1	2.03
#1	Air	8.02	20.5	0.1255	-1.2	99.7	2.60
#2	Air	7.99	20.0	0.1205	0.9	100.0	2.19
#3	Air	8.05	20.1	0.1343	-0.8	99.9	2.87
Average		**8.03**	**20.2**	**0.1240**	**-**	**-**	**2.35**

Test Conditions:

KCl Solution — Open Vent Mode

A = 0.62% — U_G = 10.0 cm/s

Oxygen Mass Transfer Data							
Test	Inlet Gas	Gas Velocity (cm/s)	Temperature (ºC)	k_La (1/s)	C_o (% of Sat)	C_∞ (% of Sat)	τ_e (s)
#1	Nitrogen	10.02	19.7	0.1634	100.0	0.2	3.22
#2	Nitrogen	10.02	19.3	0.1447	99.8	0.2	2.40
#3	Nitrogen	10.00	20.2	0.1403	99.9	0.1	1.86
#1	Air	9.98	19.7	0.1417	-0.4	99.8	1.86
#2	Air	9.96	19.4	0.1554	-0.6	99.8	2.67
#3	Air	10.03	20.3	0.1497	2.8	99.8	2.36
#1	Carbon Monoxide	9.92	19.7	0.1559	100.2	0.3	2.87
#2	Carbon Monoxide	10.00	19.4	0.1441	98.4	-0.1	2.16
#3	Carbon Monoxide	10.01	20.2	0.1609	101.1	0.2	3.22
#1	Air	9.99	19.7	0.1482	-0.2	99.9	2.62
#2	Air	10.00	19.4	0.1462	0.6	99.8	2.46
#3	Air	10.05	20.3	0.1405	1.1	99.7	2.32
Average		**10.00**	**19.8**	**0.1493**	**-**	**-**	**2.50**

Carbon Monoxide Mass Transfer Data						
Test	Inlet Gas	Gas Velocity (cm/s)	Temperature (ºC)	k_La (1/s)	C_o (% of Sat)	C_∞ (% of Sat)
#1	Carbon Monoxide	9.92	19.7	0.1550	0.0	101.1
#2	Carbon Monoxide	10.00	19.4	0.1426	0.0	101.2
#3	Carbon Monoxide	10.01	20.2	0.1547	0.0	100.5
Average		**9.98**	**19.8**	**0.1508**	**-**	**-**

Test Conditions:

KCl Solution — Open Vent Mode

A = 0.62% — U_G = 12.0 cm/s

Oxygen Mass Transfer Data							
Test	Inlet Gas	Gas Velocity (cm/s)	Temperature (ºC)	k_La (1/s)	C_o (% of Sat)	C_∞ (% of Sat)	τ_e (s)
#1	Nitrogen	12.03	20.2	-	102.3	0.2	2.97
#2	Nitrogen	12.03	19.9	0.1777	101.3	0.3	3.01
#3	Nitrogen	12.00	20.1	0.1704	100.9	0.2	2.58
#1	Air	12.05	20.3	0.1521	-1.1	99.9	2.39
#2	Air	12.05	19.9	0.1915	-0.7	100.0	3.18
#3	Air	12.03	20.2	0.1598	1.8	100.0	2.26
#1	Carbon Monoxide	12.05	20.2	0.1414	99.5	0.1	2.38
#2	Carbon Monoxide	12.05	20.0	0.1671	99.4	0.2	2.23
#3	Carbon Monoxide	12.02	20.0	0.1658	99.0	0.1	2.40
#1	Air	12.06	20.2	0.1505	-0.4	99.7	1.99
#2	Air	12.05	20.0	0.1976	0.0	99.9	3.35
#3	Air	12.03	20.1	0.1876	-0.2	99.8	3.09
Average		**12.04**	**20.1**	**0.1692**	**-**	**-**	**2.65**

Test Conditions:

KCl Solution — Open Vent Mode

A = 0.62% — U_G = 14.0 cm/s

Oxygen Mass Transfer Data							
Test	Inlet Gas	Gas Velocity (cm/s)	Temperature (ºC)	k_La (1/s)	C_o (% of Sat)	C_∞ (% of Sat)	τ_e (s)
#1	Nitrogen	14.02	20.2	0.1860	101.6	0.3	2.94
#2	Nitrogen	14.05	20.1	0.1721	101.0	0.2	2.17
#3	Nitrogen	14.01	20.3	0.1664	99.9	0.2	2.14
#1	Air	14.01	20.2	0.1745	-1.3	99.7	2.08
#2	Air	14.02	20.1	0.1666	-0.9	99.7	1.72
#3	Air	13.99	20.3	0.1860	0.5	99.6	2.79
#1	Carbon Monoxide	13.99	20.2	0.1846	100.7	0.3	2.75
#2	Carbon Monoxide	14.00	20.1	0.1976	102.5	0.3	3.36
#3	Carbon Monoxide	14.00	20.3	0.1795	99.8	0.3	2.50
#1	Air	14.02	20.2	0.1603	-0.3	99.9	1.83
#2	Air	14.04	20.1	0.1810	-0.7	99.6	2.38
#3	Air	14.00	20.3	0.1653	-0.6	99.6	2.42
Average		**14.01**	**20.2**	**0.1767**	**-**	**-**	**2.42**

Carbon Monoxide Mass Transfer Data						
Test	Inlet Gas	Gas Velocity (cm/s)	Temperature (ºC)	k_La (1/s)	C_o (% of Sat)	C_∞ (% of Sat)
#1	Carbon Monoxide	13.99	20.2	0.1555	0.0	98.2
#2	Carbon Monoxide	14.00	20.1	0.1816	0.0	98.3
#3	Carbon Monoxide	14.00	20.3	0.1810	0.0	100.0
Average		**14.00**	**20.2**	**0.1727**	**-**	**-**

Test Conditions:

KCl Solution — Open Vent Mode

A = 0.62% — U_G = 16.0 cm/s

Oxygen Mass Transfer Data							
Test	Inlet Gas	Gas Velocity (cm/s)	Temperature (ºC)	k_La (1/s)	C_o (% of Sat)	C_∞ (% of Sat)	τ_e (s)
#1	Nitrogen	16.00	20.1	0.1710	100.6	0.3	3.01
#2	Nitrogen	16.01	19.8	-	101.6	0.4	3.92
#3	Nitrogen	16.01	20.2	0.1593	100.7	0.2	2.26
#1	Air	16.02	20.2	0.1661	1.4	99.8	2.21
#2	Air	16.08	19.8	0.1631	0.5	99.9	1.85
#3	Air	16.01	20.2	0.1763	1.1	99.6	2.50
#1	Carbon Monoxide	16.00	20.1	0.1631	99.3	0.2	2.35
#2	Carbon Monoxide	16.09	19.8	0.1770	101.2	0.3	2.81
#3	Carbon Monoxide	16.05	20.2	0.1749	99.9	0.2	2.23
#1	Air	16.05	20.1	0.1725	-0.7	100.1	2.05
#2	Air	16.09	19.8	0.1681	-1.1	99.5	1.94
#3	Air	16.02	20.2	0.1679	-0.1	100.0	1.93
Average		**16.04**	**20.1**	**0.1690**	**-**	**-**	**2.42**

Test Conditions:

KCl Solution — Open Vent Mode

A = 0.62% — U_G = 18.0 cm/s

Oxygen Mass Transfer Data							
Test	Inlet Gas	Gas Velocity (cm/s)	Temperature (ºC)	k_La (1/s)	C_o (% of Sat)	C_∞ (% of Sat)	τ_e (s)
#1	Nitrogen	17.98	20.4	0.1645	99.9	0.3	2.09
#2	Nitrogen	17.98	20.2	0.1727	100.7	0.3	2.87
#3	Nitrogen	18.06	20.1	0.1638	100.0	0.3	2.53
#1	Air	18.05	20.4	0.1599	-0.1	99.9	1.66
#2	Air	18.01	20.2	0.1704	0.6	99.8	2.20
#3	Air	18.02	20.1	0.1622	0.4	100.0	2.22
#1	Carbon Monoxide	18.04	20.4	0.1894	100.7	0.4	3.16
#2	Carbon Monoxide	18.05	20.2	0.1679	101.8	0.3	2.34
#3	Carbon Monoxide	18.06	20.1	0.1760	101.3	0.3	2.83
#1	Air	18.06	20.4	0.1717	0.1	99.9	2.42
#2	Air	18.04	20.2	0.1802	-0.1	99.7	2.50
#3	Air	18.03	20.1	0.1763	0.9	99.7	2.62
Average		**18.03**	**20.3**	**0.1712**	**-**	**-**	**2.45**

Test Conditions:

KCl Solution — Open Vent Mode

A = 0.62% — U_G = 20.0 cm/s

Oxygen Mass Transfer Data							
Test	Inlet Gas	Gas Velocity (cm/s)	Temperature (ºC)	k_La (1/s)	C_o (% of Sat)	C_∞ (% of Sat)	τ_e (s)
#1	Nitrogen	20.00	20.5	-	100.8	0.4	4.04
#2	Nitrogen	20.05	20.1	0.1713	101.3	0.2	2.34
#3	Nitrogen	20.06	20.2	-	123.7	0.2	5.90
#1	Air	20.07	20.5	0.1947	0.8	99.5	2.76
#2	Air	20.06	20.1	0.1770	1.2	99.6	2.09
#3	Air	20.13	20.2	0.1877	-0.8	99.6	2.78
#1	Carbon Monoxide	20.06	20.4	0.1768	100.2	0.2	2.51
#2	Carbon Monoxide	20.01	20.1	0.1753	100.3	0.3	2.35
#3	Carbon Monoxide	20.09	20.2	0.1814	100.8	0.2	2.56
#1	Air	20.10	20.4	0.1751	-0.8	99.7	2.36
#2	Air	20.08	20.1	0.1769	-0.3	100.0	2.17
#3	Air	20.16	20.2	0.1837	-0.7	99.6	2.57
Average		**20.07**	**20.2**	**0.1800**	**-**	**-**	**2.87**

Test Conditions:

Nitrosomonas Solution — Open Vent Mode

A = 0.62% — U_G = 0.5 cm/s

Oxygen Mass Transfer Data							
Test	Inlet Gas	Gas Velocity (cm/s)	Temperature (ºC)	k_La (1/s)	C_o (% of Sat)	C_∞ (% of Sat)	τ_e (s)
#1	Nitrogen	0.51	19.8	0.0076	99.4	-1.4	3.39
#2	Nitrogen	0.52	20.1	0.0077	99.5	-1.4	4.14
#3	Nitrogen	0.50	19.9	0.0077	99.8	-1.4	4.48
#1	Air	0.51	20.0	0.0077	98.9	-1.3	2.90
#2	Air	0.50	20.3	0.0080	98.9	-1.1	3.22
#3	Air	0.51	20.0	0.0080	99.5	-1.2	5.41
#1	Carbon Monoxide	0.51	20.1	0.0077	98.9	-1.3	4.28
#2	Carbon Monoxide	0.52	20.4	0.0078	99.2	-1.2	3.00
#3	Carbon Monoxide	0.50	20.0	0.0078	99.3	-1.2	2.68
#1	Air	0.51	20.2	0.0077	0.7	101.3	2.51
#2	Air	0.50	20.6	0.0078	0.6	101.1	2.26
#3	Air	0.51	20.2	0.0081	0.4	100.9	1.59
Average		**0.51**	**20.1**	**0.0078**	**-**	**-**	**3.32**

Test Conditions:

Nitrosomonas Solution — Open Vent Mode

A = 0.62% — U_G = 2.0 cm/s

Oxygen Mass Transfer Data							
Test	Inlet Gas	Gas Velocity (cm/s)	Temperature (ºC)	k_La (1/s)	C_o (% of Sat)	C_∞ (% of Sat)	τ_e (s)
#1	Nitrogen	1.98	20.3	0.0255	99.5	0.1	1.90
#2	Nitrogen	2.01	20.4	0.0262	99.6	0.1	2.12
#3	Nitrogen	2.00	20.0	0.0280	100.1	0.1	2.06
#1	Air	1.96	20.4	0.0255	0.4	99.8	1.23
#2	Air	1.96	20.4	0.0283	1.0	100.6	2.48
#3	Air	1.99	20.1	0.0281	0.5	99.8	1.82
#1	Carbon Monoxide	1.99	20.4	0.0275	102.2	0.1	8.58
#2	Carbon Monoxide	2.01	20.4	0.0265	99.6	0.0	1.88
#3	Carbon Monoxide	2.02	20.1	0.0284	100.0	0.0	2.03
#1	Air	1.96	20.5	0.0259	0.1	100.0	0.99
#2	Air	1.96	20.4	0.0279	0.4	100.2	1.67
#3	Air	1.99	20.3	0.0281	0.8	102.0	1.41
Average		**1.99**	**20.3**	**0.0272**	**-**	**-**	**2.35**

Carbon Monoxide Mass Transfer Data						
Test	Inlet Gas	Gas Velocity (cm/s)	Temperature (ºC)	k_La (1/s)	C_o (% of Sat)	C_∞ (% of Sat)
#1	Carbon Monoxide	1.99	20.4	0.0255	0.0	103.1
#2	Carbon Monoxide	2.01	20.4	0.0257	0.0	103.2
#3	Carbon Monoxide	2.02	20.1	0.0286	0.0	101.8
Average		**2.01**	**20.3**	**0.0266**	**-**	**-**

Test Conditions:

Nitrosomonas Solution — Open Vent Mode

A = 0.62% — U_G = 4.0 cm/s

Oxygen Mass Transfer Data							
Test	Inlet Gas	Gas Velocity (cm/s)	Temperature (ºC)	k_La (1/s)	C_o (% of Sat)	C_∞ (% of Sat)	τ_e (s)
#1	Nitrogen	3.98	20.4	0.0607	100.9	0.0	3.00
#2	Nitrogen	4.04	19.6	0.0608	98.7	0.1	2.26
#3	Nitrogen	4.02	20.2	0.0636	100.5	0.1	2.74
#1	Air	4.01	20.4	0.0631	-0.3	99.7	2.54
#2	Air	4.02	19.6	0.0652	0.3	100.0	2.53
#3	Air	3.99	20.2	0.0634	1.2	99.8	2.13
#1	Carbon Monoxide	3.99	20.4	0.0645	99.7	0.0	2.66
#2	Carbon Monoxide	4.05	19.9	0.0633	98.7	0.1	1.96
#3	Carbon Monoxide	4.03	20.2	-	135.0	0.1	14.94
#1	Air	4.01	20.5	0.0641	-0.3	99.9	2.51
#2	Air	4.02	19.9	0.0673	0.3	99.9	2.47
#3	Air	3.99	20.3	0.0642	-0.3	100.3	2.16
Average		**4.01**	**20.1**	**0.0637**	**-**	**-**	**3.49**

Carbon Monoxide Mass Transfer Data						
Test	Inlet Gas	Gas Velocity (cm/s)	Temperature (ºC)	k_La (1/s)	C_o (% of Sat)	C_∞ (% of Sat)
#1	Carbon Monoxide	3.99	20.4	0.0678	0.0	99.8
#2	Carbon Monoxide	4.05	19.9	0.0667	0.0	99.9
#3	Carbon Monoxide	4.03	20.2	0.0723	0.0	98.9
Average		**4.02**	**20.2**	**0.0689**	**-**	**-**

Test Conditions:

Nitrosomonas Solution — Open Vent Mode

A = 0.62% — U_G = 6.0 cm/s

Oxygen Mass Transfer Data							
Test	Inlet Gas	Gas Velocity (cm/s)	Temperature (ºC)	k_La (1/s)	C_o (% of Sat)	C_∞ (% of Sat)	τ_e (s)
#1	Nitrogen	5.99	20.1	0.0985	98.9	0.2	2.54
#2	Nitrogen	5.99	21.0	0.1069	100.8	0.2	2.94
#3	Nitrogen	6.00	20.5	0.1003	99.9	0.1	2.62
#1	Air	5.98	20.2	0.0992	-1.2	99.9	2.86
#2	Air	5.98	21.1	0.1078	1.1	99.6	2.10
#3	Air	6.01	20.5	0.1002	0.3	99.8	2.22
#1	Carbon Monoxide	6.04	20.2	0.0986	100.6	0.1	1.89
#2	Carbon Monoxide	6.04	21.1	0.1038	100.1	0.1	2.58
#3	Carbon Monoxide	5.97	20.5	0.1047	100.9	0.2	2.49
#1	Air	5.98	20.2	0.1138	111.7	-0.6	8.78
#2	Air	5.98	21.1	0.1054	99.3	0.2	2.57
#3	Air	6.01	20.5	0.1026	100.9	0.2	2.46
Average		**6.00**	**20.6**	**0.1035**	**-**	**-**	**3.00**

Carbon Monoxide Mass Transfer Data						
Test	Inlet Gas	Gas Velocity (cm/s)	Temperature (ºC)	k_La (1/s)	C_o (% of Sat)	C_∞ (% of Sat)
#1	Carbon Monoxide	6.04	20.2	0.1059	0.0	100.5
#2	Carbon Monoxide	6.04	21.1	0.0944	0.0	100.9
#3	Carbon Monoxide	5.97	20.5	0.0934	0.0	101.3
Average		**6.02**	**20.6**	**0.0979**	**-**	**-**

Test Conditions:

Nitrosomonas Solution — Open Vent Mode

A = 0.62% — U_G = 8.0 cm/s

Oxygen Mass Transfer Data							
Test	Inlet Gas	Gas Velocity (cm/s)	Temperature (ºC)	k_La (1/s)	C_o (% of Sat)	C_∞ (% of Sat)	τ_e (s)
#1	Nitrogen	8.02	20.4	0.1207	99.0	-0.3	2.79
#2	Nitrogen	8.01	20.3	0.1207	101.2	0.2	2.95
#3	Nitrogen	8.04	19.9	0.1210	100.3	0.1	2.33
#1	Air	8.05	20.4	0.1294	0.4	100.1	2.99
#2	Air	8.02	20.3	0.1352	0.4	99.7	3.34
#3	Air	8.03	19.9	0.1296	0.2	100.1	2.24
#1	Carbon Monoxide	8.03	20.4	0.1150	99.7	-0.6	2.17
#2	Carbon Monoxide	8.03	20.3	0.1168	99.3	0.1	2.02
#3	Carbon Monoxide	8.04	19.9	0.1267	99.3	0.2	2.72
#1	Air	8.06	20.4	0.1256	0.2	100.0	2.55
#2	Air	8.02	20.4	0.1270	-0.8	99.9	2.83
#3	Air	8.04	19.9	0.1259	0.5	100.0	2.16
Average		**8.03**	**20.2**	**0.1245**	**-**	**-**	**2.59**

Test Conditions:

Nitrosomonas Solution — Open Vent Mode

A = 0.62% — U_G = 10.0 cm/s

Oxygen Mass Transfer Data							
Test	Inlet Gas	Gas Velocity (cm/s)	Temperature (ºC)	k_La (1/s)	C_o (% of Sat)	C_∞ (% of Sat)	τ_e (s)
#1	Nitrogen	9.95	20.2	0.1443	98.7	-0.1	2.52
#2	Nitrogen	9.99	20.3	0.1417	98.7	0.3	2.53
#3	Nitrogen	10.07	20.0	0.1414	97.3	0.2	2.04
#1	Air	10.02	20.2	0.1531	1.0	100.0	2.30
#2	Air	10.03	20.3	0.1605	-0.1	100.2	3.14
#3	Air	10.06	20.0	0.1455	-0.3	100.2	2.54
#1	Carbon Monoxide	10.02	20.2	0.1733	101.2	0.3	3.92
#2	Carbon Monoxide	10.04	20.3	0.1559	100.2	0.1	3.16
#3	Carbon Monoxide	10.11	19.9	0.1431	98.9	0.1	2.45
#1	Air	10.05	20.2	0.1616	1.4	99.8	3.22
#2	Air	10.05	20.3	0.1490	0.7	99.9	2.16
#3	Air	10.06	19.9	0.1468	2.3	99.8	2.44
Average		**10.04**	**20.1**	**0.1514**	**-**	**-**	**2.70**

Carbon Monoxide Mass Transfer Data						
Test	Inlet Gas	Gas Velocity (cm/s)	Temperature (ºC)	k_La (1/s)	C_o (% of Sat)	C_∞ (% of Sat)
#1	Carbon Monoxide	10.02	20.2	0.1704	0.0	99.9
#2	Carbon Monoxide	10.04	20.3	0.1715	0.0	100.5
#3	Carbon Monoxide	10.11	19.9	0.1770	0.0	100.8
Average		**10.06**	**20.1**	**0.1730**	**-**	**-**

Test Conditions:

Nitrosomonas Solution — Open Vent Mode

A = 0.62% — U_G = 12.0 cm/s

Oxygen Mass Transfer Data							
Test	Inlet Gas	Gas Velocity (cm/s)	Temperature (ºC)	k_La (1/s)	C_o (% of Sat)	C_∞ (% of Sat)	τ_e (s)
#1	Nitrogen	11.98	20.3	0.1844	102.1	0.4	3.79
#2	Nitrogen	12.02	19.6	0.1616	100.2	0.1	2.34
#3	Nitrogen	11.96	19.6	0.1737	98.3	0.2	2.89
#1	Air	12.06	20.3	0.1664	-0.7	100.1	2.56
#2	Air	12.01	19.7	0.1567	-1.4	99.8	2.03
#3	Air	12.03	19.6	-	1.3	99.7	4.37
#1	Carbon Monoxide	12.02	20.3	0.1800	101.1	0.2	3.19
#2	Carbon Monoxide	11.97	19.7	0.1548	100.0	0.0	2.18
#3	Carbon Monoxide	12.00	19.7	0.1783	100.8	0.2	2.92
#1	Air	12.06	20.3	0.1799	-0.2	100.0	3.12
#2	Air	12.02	19.7	0.1529	1.3	99.8	1.75
#3	Air	12.04	19.7	-	-0.8	99.8	4.33
Average		**12.02**	**19.9**	**0.1689**	**-**	**-**	**2.96**

Test Conditions:

Nitrosomonas Solution — Open Vent Mode

A = 0.62% — U_G = 14.0 cm/s

Oxygen Mass Transfer Data							
Test	Inlet Gas	Gas Velocity (cm/s)	Temperature (ºC)	k_La (1/s)	C_o (% of Sat)	C_∞ (% of Sat)	τ_e (s)
#1	Nitrogen	14.07	20.1	0.1634	99.8	0.2	1.71
#2	Nitrogen	14.02	20.3	0.1739	101.5	0.2	2.55
#3	Nitrogen	14.06	20.3	0.1708	99.3	0.2	2.26
#1	Air	14.17	20.2	0.1864	-0.2	99.7	2.50
#2	Air	13.99	20.3	0.1852	0.3	99.8	2.35
#3	Air	13.99	20.3	0.1764	0.7	99.8	1.83
#1	Carbon Monoxide	14.11	20.2	0.1712	97.3	0.2	2.21
#2	Carbon Monoxide	13.89	20.3	0.1859	99.8	0.3	2.80
#3	Carbon Monoxide	13.97	20.3	0.1790	100.6	0.2	2.69
#1	Air	14.11	20.2	0.1668	-2.0	99.8	2.12
#2	Air	14.01	20.3	0.1784	-0.9	100.0	2.18
#3	Air	14.02	20.3	0.1892	-0.8	99.7	2.59
Average		**14.03**	**20.3**	**0.1772**	**-**	**-**	**2.31**

Carbon Monoxide Mass Transfer Data						
Test	Inlet Gas	Gas Velocity (cm/s)	Temperature (ºC)	k_La (1/s)	C_o (% of Sat)	C_∞ (% of Sat)
#1	Carbon Monoxide	14.11	20.2	0.1616	0.0	100.1
#2	Carbon Monoxide	13.89	20.3	0.1821	0.0	100.3
#3	Carbon Monoxide	13.97	20.3	0.1897	0.0	98.9
Average		**13.99**	**20.3**	**0.1778**	**-**	**-**

Test Conditions:

Nitrosomonas Solution — Open Vent Mode

A = 0.62% — U_G = 16.0 cm/s

Oxygen Mass Transfer Data							
Test	Inlet Gas	Gas Velocity (cm/s)	Temperature (ºC)	k_La (1/s)	C_o (% of Sat)	C_∞ (% of Sat)	τ_e (s)
#1	Nitrogen	16.00	19.8	0.1746	100.4	0.2	2.36
#2	Nitrogen	16.07	20.5	0.1805	100.9	0.3	2.52
#3	Nitrogen	16.07	20.7	0.1565	100.6	0.2	2.09
#1	Air	16.03	19.8	0.1735	0.6	99.9	1.91
#2	Air	16.02	20.5	0.1944	0.1	99.8	2.79
#3	Air	16.12	20.7	0.1763	-0.8	99.8	2.21
#1	Carbon Monoxide	16.07	19.9	0.1892	100.4	0.2	2.82
#2	Carbon Monoxide	16.06	20.5	0.1776	97.6	0.2	2.05
#3	Carbon Monoxide	16.04	20.7	0.1720	100.5	0.2	2.37
#1	Air	16.03	19.9	0.1900	-0.4	99.6	2.56
#2	Air	16.02	20.6	-	-0.3	100.1	4.00
#3	Air	16.08	20.7	0.1851	0.0	99.9	2.48
Average		**16.05**	**20.4**	**0.1791**	**-**	**-**	**2.51**

Test Conditions:

Nitrosomonas Solution — Open Vent Mode

A = 0.62% — U_G = 18.0 cm/s

Oxygen Mass Transfer Data							
Test	Inlet Gas	Gas Velocity (cm/s)	Temperature (ºC)	k_La (1/s)	C_o (% of Sat)	C_∞ (% of Sat)	τ_e (s)
#1	Nitrogen	18.00	19.9	-	101.2	0.1	2.23
#2	Nitrogen	18.02	20.2	-	99.4	0.1	2.01
#3	Nitrogen	17.95	20.0	0.1705	100.7	0.1	2.33
#1	Air	18.01	20.0	0.1941	-0.1	99.5	3.13
#2	Air	17.98	20.2	0.2093	-1.4	99.4	3.32
#3	Air	18.00	19.9	0.1912	0.1	99.8	2.47
#1	Carbon Monoxide	18.02	19.9	-	99.9	0.0	2.03
#2	Carbon Monoxide	18.00	20.1	0.1803	100.9	0.3	2.39
#3	Carbon Monoxide	17.96	19.9	0.1851	100.4	0.3	2.59
#1	Air	18.07	19.9	0.1882	-1.6	100.0	2.84
#2	Air	18.00	20.1	0.1700	0.9	99.8	1.94
#3	Air	18.02	19.9	0.1933	-1.2	99.8	2.85
Average		**18.00**	**20.0**	**0.1869**	**-**	**-**	**2.51**

Test Conditions:

Nitrosomonas Solution

A = 0.62%

Open Vent Mode

U_G = 20.0 cm/s

Oxygen Mass Transfer Data							
Test	Inlet Gas	Gas Velocity (cm/s)	Temperature (ºC)	k_La (1/s)	C_o (% of Sat)	C_∞ (% of Sat)	τ_e (s)
#1	Nitrogen	20.04	20.2	0.1920	100.1	0.2	3.12
#2	Nitrogen	20.00	20.4	0.1778	100.5	0.3	2.75
#3	Nitrogen	20.04	20.0	-	102.3	0.3	5.52
#1	Air	20.15	20.2	0.1888	-0.6	99.9	2.35
#2	Air	20.05	20.4	0.1685	0.1	100.1	2.02
#3	Air	20.09	20.1	0.1849	-0.3	99.8	2.20
#1	Carbon Monoxide	20.00	20.2	0.1957	102.0	0.4	2.99
#2	Carbon Monoxide	20.05	20.4	0.1842	101.6	0.3	2.54
#3	Carbon Monoxide	20.07	20.0	0.1825	99.9	0.2	2.50
#1	Air	20.07	20.2	-	-0.5	99.7	3.93
#2	Air	20.05	20.4	0.2091	0.1	99.6	2.94
#3	Air	20.00	20.0	0.1888	1.8	99.8	2.60
Average		**20.05**	**20.2**	**0.1872**	**-**	**-**	**2.96**

Test Conditions:

DI Water w/ Surfactant — Open Vent Mode

A = 0.62% — U_G = 0.5 cm/s

Oxygen Mass Transfer Data							
Test	Inlet Gas	Gas Velocity (cm/s)	Temperature (ºC)	k_La (1/s)	C_o (% of Sat)	C_∞ (% of Sat)	τ_e (s)
#1	Nitrogen	0.52	20.8	0.0050	98.8	0.0	4.36
#2	Nitrogen	0.52	20.5	0.0052	98.6	0.0	5.33
#3	Nitrogen	0.52	20.7	0.0052	98.5	-0.1	4.69
#1	Air	0.52	20.8	0.0050	0.6	99.5	3.82
#2	Air	0.52	20.5	0.0052	0.9	100.0	6.51
#3	Air	0.52	20.7	0.0048	0.4	99.0	1.69
#1	Carbon Monoxide	0.52	20.8	0.0050	98.6	-0.1	4.53
#2	Carbon Monoxide	0.52	20.5	0.0051	99.2	-0.2	3.17
#3	Carbon Monoxide	0.52	20.7	0.0051	98.6	-0.1	4.63
#1	Air	0.52	20.8	0.0053	1.3	99.9	6.52
#2	Air	0.52	20.5	0.0053	0.8	99.7	5.48
#3	Air	0.52	20.7	0.0050	0.9	99.3	2.03
Average		**0.52**	**20.7**	**0.0051**	**-**	**-**	**4.40**

Carbon Monoxide Mass Transfer Data						
Test	Inlet Gas	Gas Velocity (cm/s)	Temperature (ºC)	k_La (1/s)	C_o (% of Sat)	C_∞ (% of Sat)
#1	Carbon Monoxide	0.52	20.8	0.0056	-12.7	96.0
#2	Carbon Monoxide	0.52	20.5	0.0056	-8.2	97.7
#3	Carbon Monoxide	0.52	20.7	0.0060	-13.0	100.1
Average		**0.52**	**20.7**	**0.0057**	**-**	**-**

Test Conditions:

DI Water w/ Surfactant — Open Vent Mode

A = 0.62% — U_G = 2.0 cm/s

Oxygen Mass Transfer Data							
Test	Inlet Gas	Gas Velocity (cm/s)	Temperature (ºC)	k_La (1/s)	C_o (% of Sat)	C_∞ (% of Sat)	τ_e (s)
#1	Nitrogen	2.06	20.6	0.0112	99.4	0.1	2.37
#2	Nitrogen	2.06	20.3	0.0113	99.0	0.0	2.04
#3	Nitrogen	2.06	19.9	0.0112	98.7	0.0	2.15
#1	Air	2.06	20.6	0.0110	0.4	99.1	0.95
#2	Air	2.06	20.3	0.0112	0.5	99.5	1.27
#3	Air	2.06	19.9	0.0110	0.5	99.6	1.27
#1	Carbon Monoxide	2.06	20.6	0.0115	98.9	0.0	2.29
#2	Carbon Monoxide	2.06	20.3	0.0116	101.7	0.1	8.15
#3	Carbon Monoxide	2.06	19.9	0.0114	99.1	0.0	2.06
#1	Air	2.06	20.6	0.0117	0.8	99.5	1.91
#2	Air	2.06	20.3	0.0114	0.6	99.6	1.92
#3	Air	2.06	19.9	0.0112	0.9	99.7	1.55
Average		**2.06**	**20.3**	**0.0113**	**-**	**-**	**2.33**

Carbon Monoxide Mass Transfer Data						
Test	Inlet Gas	Gas Velocity (cm/s)	Temperature (ºC)	k_La (1/s)	C_o (% of Sat)	C_∞ (% of Sat)
#1	Carbon Monoxide	2.06	20.6	0.0134	-15.3	105.3
#2	Carbon Monoxide	2.06	20.3	0.0115	6.6	104.6
#3	Carbon Monoxide	2.06	19.9	0.0133	-9.9	105.1
Average		**2.06**	**20.3**	**0.0127**	**-**	**-**

Test Conditions:

DI Water w/ Surfactant — Open Vent Mode

A = 0.62% — U_G = 4.0 cm/s

Oxygen Mass Transfer Data							
Test	Inlet Gas	Gas Velocity (cm/s)	Temperature (ºC)	k_La (1/s)	C_o (% of Sat)	C_∞ (% of Sat)	τ_e (s)
#1	Nitrogen	4.02	19.6	0.0193	98.7	0.0	2.47
#2	Nitrogen	4.01	20.2	0.0194	99.3	0.0	2.85
#3	Nitrogen	4.00	20.4	0.0194	99.0	0.1	2.95
#1	Air	4.02	19.6	0.0203	0.9	99.8	2.11
#2	Air	4.01	20.2	0.0207	0.8	100.1	1.86
#3	Air	4.00	20.4	0.0206	0.8	100.0	1.69
#1	Carbon Monoxide	4.02	19.6	0.0207	98.5	-0.5	2.80
#2	Carbon Monoxide	4.01	20.2	0.0209	98.2	-0.4	2.78
#3	Carbon Monoxide	4.00	20.4	0.0245	103.3	-0.1	9.78
#1	Air	4.02	19.6	0.0197	1.2	100.0	2.39
#2	Air	4.01	20.2	0.0201	0.7	100.4	2.32
#3	Air	4.00	20.4	0.0204	0.7	100.1	1.96
Average		**4.01**	**20.1**	**0.0205**	**-**	**-**	**3.00**

Carbon Monoxide Mass Transfer Data						
Test	Inlet Gas	Gas Velocity (cm/s)	Temperature (ºC)	k_La (1/s)	C_o (% of Sat)	C_∞ (% of Sat)
#1	Carbon Monoxide	4.02	19.6	0.0253	-18.3	96.2
#2	Carbon Monoxide	4.01	20.2	0.0219	-10.4	100.3
#3	Carbon Monoxide	4.00	20.4	0.0250	-19.7	100.4
Average		**4.01**	**20.1**	**0.0241**	**-**	**-**

Test Conditions:

DI Water w/ Surfactant — Open Vent Mode

A = 0.62% — U_G = 6.0 cm/s

Oxygen Mass Transfer Data							
Test	Inlet Gas	Gas Velocity (cm/s)	Temperature (ºC)	k_La (1/s)	C_o (% of Sat)	C_∞ (% of Sat)	τ_e (s)
#1	Nitrogen	6.00	19.5	0.0279	98.9	0.1	2.18
#2	Nitrogen	5.99	20.0	0.0281	98.9	0.0	2.64
#3	Nitrogen	5.97	20.3	0.0287	99.1	0.0	2.03
#1	Air	6.00	19.5	0.0273	1.2	99.3	2.11
#2	Air	5.99	20.0	0.0280	1.4	99.8	1.98
#3	Air	5.97	20.3	0.0284	0.9	99.9	2.54
#1	Carbon Monoxide	6.00	19.5	0.0284	99.0	0.1	2.00
#2	Carbon Monoxide	5.99	20.0	0.0288	99.2	0.0	2.35
#3	Carbon Monoxide	5.97	20.3	0.0289	99.0	0.0	2.14
#1	Air	6.00	19.5	0.0280	1.0	99.9	1.91
#2	Air	5.99	20.0	0.0283	1.5	99.8	1.90
#3	Air	5.97	20.3	0.0285	0.9	99.8	1.93
Average		**5.99**	**19.9**	**0.0283**	**-**	**-**	**2.14**

Carbon Monoxide Mass Transfer Data						
Test	Inlet Gas	Gas Velocity (cm/s)	Temperature (ºC)	k_La (1/s)	C_o (% of Sat)	C_∞ (% of Sat)
#1	Carbon Monoxide	6.00	19.5	0.0298	0.1	101.4
#2	Carbon Monoxide	5.99	20.0	0.0275	-6.5	101.9
#3	Carbon Monoxide	5.97	20.3	0.0287	-5.3	100.5
Average		**5.99**	**19.9**	**0.0287**	**-**	**-**

Test Conditions:

DI Water w/ Surfactant — Open Vent Mode

A = 0.62% — U_G = 8.0 cm/s

Oxygen Mass Transfer Data							
Test	Inlet Gas	Gas Velocity (cm/s)	Temperature (ºC)	k_La (1/s)	C_o (% of Sat)	C_∞ (% of Sat)	τ_e (s)
#1	Nitrogen	8.02	20.1	0.0377	99.3	0.0	1.92
#2	Nitrogen	8.02	20.2	0.0384	99.3	0.0	1.92
#3	Nitrogen	7.99	20.1	0.0384	99.1	0.1	2.08
#1	Air	8.02	20.1	0.0376	1.1	99.7	2.22
#2	Air	8.02	20.2	0.0397	1.3	100.3	2.36
#3	Air	7.99	20.1	0.0392	0.9	100.0	1.81
#1	Carbon Monoxide	8.02	20.1	0.0387	98.6	0.0	2.35
#2	Carbon Monoxide	8.02	20.2	0.0394	99.0	0.0	2.17
#3	Carbon Monoxide	7.99	20.1	0.0390	99.1	0.0	1.89
#1	Air	8.02	20.1	0.0381	0.8	100.1	2.41
#2	Air	8.02	20.2	0.0404	0.7	100.2	2.29
#3	Air	7.99	20.1	0.0395	0.9	100.0	1.48
Average		**8.01**	**20.1**	**0.0388**	**-**	**-**	**2.08**

Carbon Monoxide Mass Transfer Data						
Test	Inlet Gas	Gas Velocity (cm/s)	Temperature (ºC)	k_La (1/s)	C_o (% of Sat)	C_∞ (% of Sat)
#1	Carbon Monoxide	8.02	20.1	0.0489	-26.5	99.0
#2	Carbon Monoxide	8.02	20.2	0.0421	-3.2	102.2
#3	Carbon Monoxide	7.99	20.1	-	-	-
Average		**8.01**	**20.1**	**0.0455**	**-**	**-**

Test Conditions:

DI Water w/ Surfactant — Open Vent Mode

A = 0.62% — U_G = 12.0 cm/s

Oxygen Mass Transfer Data							
Test	Inlet Gas	Gas Velocity (cm/s)	Temperature (ºC)	k_La (1/s)	C_o (% of Sat)	C_∞ (% of Sat)	τ_e (s)
#1	Nitrogen	11.95	20.1	0.0550	99.2	0.0	1.59
#2	Nitrogen	11.98	19.8	0.0533	98.7	0.0	1.45
#3	Nitrogen	11.95	19.3	0.0530	98.5	0.0	1.79
#1	Air	11.95	20.1	0.0556	2.0	100.1	1.83
#2	Air	11.98	19.8	0.0547	0.5	100.0	1.26
#3	Air	11.95	19.3	0.0549	1.0	100.0	1.65
#1	Carbon Monoxide	11.95	20.1	0.0550	98.6	0.0	1.72
#2	Carbon Monoxide	11.98	19.8	0.0554	98.7	0.0	1.91
#3	Carbon Monoxide	11.95	19.3	0.0554	99.3	0.0	1.81
#1	Air	11.95	20.1	0.0552	1.1	100.0	1.72
#2	Air	11.98	19.8	0.0552	0.8	99.9	1.43
#3	Air	11.95	19.3	0.0557	0.9	100.2	2.11
Average		**11.96**	**19.7**	**0.0549**	**-**	**-**	**1.69**

Carbon Monoxide Mass Transfer Data						
Test	Inlet Gas	Gas Velocity (cm/s)	Temperature (ºC)	k_La (1/s)	C_o (% of Sat)	C_∞ (% of Sat)
#1	Carbon Monoxide	11.95	20.1	0.0449	5.4	108.6
#2	Carbon Monoxide	11.98	19.8	0.0747	-33.5	95.8
#3	Carbon Monoxide	11.95	19.3	0.0682	-28.1	98.8
Average		**11.96**	**19.7**	**0.0626**	**-**	**-**

Test Conditions:

DI Water w/ Surfactant — Open Vent Mode

A = 0.62% — U_G = 16.0 cm/s

Oxygen Mass Transfer Data							
Test	Inlet Gas	Gas Velocity (cm/s)	Temperature (ºC)	k_La (1/s)	C_o (% of Sat)	C_∞ (% of Sat)	τ_e (s)
#1	Nitrogen	16.03	19.9	0.0690	98.7	0.0	1.68
#2	Nitrogen	15.99	20.2	0.0695	99.5	0.4	1.78
#3	Nitrogen	16.06	19.7	0.0713	99.2	0.1	2.03
#1	Air	16.03	19.9	0.0750	1.3	100.4	1.76
#2	Air	15.99	20.2	0.0707	1.3	99.7	1.28
#3	Air	16.06	19.7	0.0727	1.9	99.7	1.82
#1	Carbon Monoxide	16.03	19.9	0.0707	98.9	0.0	1.53
#2	Carbon Monoxide	15.99	20.2	0.0706	99.1	0.2	1.82
#3	Carbon Monoxide	16.06	19.7	0.0725	99.2	0.1	1.82
#1	Air	16.03	19.9	0.0726	0.4	100.3	1.76
#2	Air	15.99	20.2	0.0716	1.4	99.7	1.30
#3	Air	16.06	19.7	0.0727	6.4	99.9	2.64
Average		**16.03**	**19.9**	**0.0716**	**-**	**-**	**1.77**

Carbon Monoxide Mass Transfer Data						
Test	Inlet Gas	Gas Velocity (cm/s)	Temperature (ºC)	k_La (1/s)	C_o (% of Sat)	C_∞ (% of Sat)
#1	Carbon Monoxide	16.03	19.9	0.0741	-14.7	103.3
#2	Carbon Monoxide	15.99	20.2	0.0871	-23.9	96.7
#3	Carbon Monoxide	16.06	19.7	0.0814	-21.1	98.8
Average		**16.03**	**19.9**	**0.0808**	**-**	**-**

Test Conditions:

DI Water w/ Surfactant — Open Vent Mode

A = 0.62% — U_G = 20.0 cm/s

Oxygen Mass Transfer Data							
Test	Inlet Gas	Gas Velocity (cm/s)	Temperature (ºC)	k_La (1/s)	C_o (% of Sat)	C_∞ (% of Sat)	τ_e (s)
#1	Nitrogen	19.47	19.3	0.0829	99.0	0.0	1.57
#2	Nitrogen	20.09	19.6	0.0837	98.6	0.0	1.47
#3	Nitrogen	20.04	19.9	0.0829	98.6	0.0	2.04
#1	Air	19.47	19.3	0.0872	1.7	100.1	1.96
#2	Air	20.09	19.6	0.0856	1.7	100.2	1.29
#3	Air	20.04	19.9	0.0883	1.8	100.9	2.06
#1	Carbon Monoxide	19.47	19.3	0.0833	99.2	0.0	1.64
#2	Carbon Monoxide	20.09	19.6	0.0867	99.0	0.0	2.14
#3	Carbon Monoxide	20.04	19.9	0.0844	99.0	0.0	1.94
#1	Air	19.47	19.3	0.0862	1.1	100.2	1.67
#2	Air	20.09	19.6	0.0867	1.3	100.2	1.75
#3	Air	20.04	19.9	0.0856	1.4	100.3	1.85
Average		**19.87**	**19.6**	**0.0853**	**-**	**-**	**1.78**

Carbon Monoxide Mass Transfer Data						
Test	Inlet Gas	Gas Velocity (cm/s)	Temperature (ºC)	k_La (1/s)	C_o (% of Sat)	C_∞ (% of Sat)
#1	Carbon Monoxide	19.47	19.3	0.0937	-26.7	102.6
#2	Carbon Monoxide	20.09	19.6	0.0890	-28.7	105.0
#3	Carbon Monoxide	20.04	19.9	0.1044	-33.0	99.9
Average		**19.87**	**19.6**	**0.0957**	**-**	**-**

Test Conditions:

DI Water w/ Surfactant — Closed Vent Mode

A = 0.62% — U_G = 0.5 cm/s

Oxygen Mass Transfer Data							
Test	Inlet Gas	Gas Velocity (cm/s)	Temperature (ºC)	k_La (1/s)	C_o (% of Sat)	C_∞ (% of Sat)	τ_e (s)
#1	Nitrogen	0.48	21.0	0.0058	99.2	0.0	6.52
#2	Nitrogen	0.50	20.5	0.0055	99.6	0.0	0.10
#3	Nitrogen	0.50	21.4	0.0058	99.0	0.1	2.93
#1	Air	0.48	21.0	0.0059	0.8	99.6	6.24
#2	Air	0.50	20.5	0.0055	0.6	99.5	3.14
#3	Air	0.50	21.4	0.0058	0.4	99.3	2.30
#1	Carbon Monoxide	0.48	21.0	0.0062	99.5	0.0	5.64
#2	Carbon Monoxide	0.50	20.5	0.0056	99.4	0.0	4.44
#3	Carbon Monoxide	0.50	21.4	0.0059	99.4	0.1	4.50
#1	Air	0.48	21.0	0.0059	0.5	99.8	3.66
#2	Air	0.50	20.5	0.0056	0.7	99.8	3.09
#3	Air	0.50	21.4	0.0059	0.6	99.5	2.80
Average		**0.49**	**21.0**	**0.0058**	**-**	**-**	**3.78**

Carbon Monoxide Mass Transfer Data						
Test	Inlet Gas	Gas Velocity (cm/s)	Temperature (ºC)	k_La (1/s)	C_o (% of Sat)	C_∞ (% of Sat)
#1	Carbon Monoxide	0.48	21.0	0.0058	-4.6	104.3
#2	Carbon Monoxide	0.50	20.5	0.0062	-13.1	98.2
#3	Carbon Monoxide	0.50	21.4	0.0060	-10.0	101.1
Average		**0.49**	**21.0**	**0.0060**	**-**	**-**

Test Conditions:

DI Water w/ Surfactant — Closed Vent Mode

A = 0.62% — U_G = 2.0 cm/s

Oxygen Mass Transfer Data							
Test	Inlet Gas	Gas Velocity (cm/s)	Temperature (ºC)	k_La (1/s)	C_o (% of Sat)	C_∞ (% of Sat)	τ_e (s)
#1	Nitrogen	2.01	20.7	0.0135	99.6	0.1	2.13
#2	Nitrogen	2.02	20.3	0.0131	99.4	0.1	1.23
#3	Nitrogen	2.01	20.7	0.0124	99.5	0.1	1.15
#1	Air	2.01	20.7	0.0133	0.4	99.5	1.64
#2	Air	2.02	20.3	0.0133	0.6	99.6	1.80
#3	Air	2.01	20.7	0.0124	0.6	99.7	1.96
#1	Carbon Monoxide	2.01	20.7	0.0134	93.3	0.1	8.33
#2	Carbon Monoxide	2.02	20.3	0.0131	99.5	0.1	1.76
#3	Carbon Monoxide	2.01	20.7	0.0123	99.5	0.1	1.16
#1	Air	2.01	20.7	0.0134	0.8	99.5	1.88
#2	Air	2.02	20.3	0.0124	3.7	99.2	0.00
#3	Air	2.01	20.7	0.0123	0.7	99.8	2.14
Average		**2.01**	**20.6**	**0.0129**	**-**	**-**	**2.10**

Carbon Monoxide Mass Transfer Data						
Test	Inlet Gas	Gas Velocity (cm/s)	Temperature (ºC)	k_La (1/s)	C_o (% of Sat)	C_∞ (% of Sat)
#1	Carbon Monoxide	2.01	20.7	0.0142	-1.9	101.4
#2	Carbon Monoxide	2.02	20.3	0.0130	-7.5	106.7
#3	Carbon Monoxide	2.01	20.7	0.0107	-1.0	101.1
Average		**2.01**	**20.6**	**0.0126**	**-**	**-**

Test Conditions:

DI Water w/ Surfactant — Closed Vent Mode

A = 0.62% — U_G = 4.0 cm/s

Oxygen Mass Transfer Data							
Test	Inlet Gas	Gas Velocity (cm/s)	Temperature (ºC)	k_La (1/s)	C_o (% of Sat)	C_∞ (% of Sat)	τ_e (s)
#1	Nitrogen	3.99	19.6	0.0205	99.4	0.1	2.27
#2	Nitrogen	4.04	19.7	0.0206	99.6	0.1	1.77
#3	Nitrogen	3.99	20.6	0.0205	99.1	0.1	1.83
#1	Air	3.99	19.6	0.0202	0.8	99.8	1.90
#2	Air	4.04	19.7	0.0205	0.4	99.4	1.75
#3	Air	3.99	20.6	0.0205	0.7	99.6	2.09
#1	Carbon Monoxide	3.99	19.6	0.0207	99.3	0.1	2.45
#2	Carbon Monoxide	4.04	19.7	0.0204	99.8	0.0	0.48
#3	Carbon Monoxide	3.99	20.6	0.0207	99.6	0.1	2.10
#1	Air	3.99	19.6	0.0204	0.5	99.7	1.41
#2	Air	4.04	19.7	0.0208	0.4	99.7	1.29
#3	Air	3.99	20.6	0.0203	0.4	99.7	1.60
Average		**4.01**	**20.0**	**0.0205**	**-**	**-**	**1.75**

Carbon Monoxide Mass Transfer Data						
Test	Inlet Gas	Gas Velocity (cm/s)	Temperature (ºC)	k_La (1/s)	C_o (% of Sat)	C_∞ (% of Sat)
#1	Carbon Monoxide	3.99	19.6	0.0229	-16.4	99.7
#2	Carbon Monoxide	4.04	19.7	0.0235	-17.3	99.7
#3	Carbon Monoxide	3.99	20.6	0.0213	-15.6	103.3
Average		**4.01**	**20.0**	**0.0226**	**-**	**-**

Test Conditions:

DI Water w/ Surfactant — Closed Vent Mode

A = 0.62% — U_G = 6.0 cm/s

Oxygen Mass Transfer Data							
Test	Inlet Gas	Gas Velocity (cm/s)	Temperature (ºC)	k_La (1/s)	C_o (% of Sat)	C_∞ (% of Sat)	τ_e (s)
#1	Nitrogen	5.96	20.1	0.0290	98.9	0.1	1.56
#2	Nitrogen	5.97	20.0	0.0287	99.0	0.1	2.17
#3	Nitrogen	5.98	19.8	0.0289	99.6	0.1	2.60
#1	Air	5.96	20.1	0.0290	1.1	99.8	1.84
#2	Air	5.97	20.0	0.0289	0.6	99.8	2.27
#3	Air	5.98	19.8	0.0297	0.6	99.9	2.18
#1	Carbon Monoxide	5.96	20.1	0.0294	98.9	0.0	2.10
#2	Carbon Monoxide	5.97	20.0	0.0292	99.1	0.0	2.17
#3	Carbon Monoxide	5.98	19.8	0.0292	99.3	0.1	2.18
#1	Air	5.96	20.1	0.0287	0.7	100.1	1.34
#2	Air	5.97	20.0	0.0284	0.7	99.7	1.69
#3	Air	5.98	19.8	0.0299	0.6	99.9	1.92
Average		**5.97**	**20.0**	**0.0291**	**-**	**-**	**2.00**

Carbon Monoxide Mass Transfer Data						
Test	Inlet Gas	Gas Velocity (cm/s)	Temperature (ºC)	k_La (1/s)	C_o (% of Sat)	C_∞ (% of Sat)
#1	Carbon Monoxide	5.96	20.1	0.0338	-20.0	102.4
#2	Carbon Monoxide	5.97	20.0	0.0306	-9.7	100.9
#3	Carbon Monoxide	5.98	19.8	0.0411	-42.4	98.8
Average		**5.97**	**20.0**	**0.0352**	**-**	**-**

Test Conditions:

DI Water w/ Surfactant — Closed Vent Mode

A = 0.62% — U_G = 8.0 cm/s

Oxygen Mass Transfer Data							
Test	Inlet Gas	Gas Velocity (cm/s)	Temperature (ºC)	k_La (1/s)	C_o (% of Sat)	C_∞ (% of Sat)	τ_e (s)
#1	Nitrogen	8.08	20.1	0.0368	99.2	0.1	2.21
#2	Nitrogen	8.01	19.8	0.0361	99.0	0.1	2.07
#3	Nitrogen	7.98	19.8	0.0365	98.7	0.1	2.78
#1	Air	8.08	20.1	0.0373	0.4	99.9	2.15
#2	Air	8.01	19.8	0.0368	0.9	99.8	1.71
#3	Air	7.98	19.8	0.0374	1.2	99.4	1.90
#1	Carbon Monoxide	8.08	20.1	0.0367	99.2	0.1	2.00
#2	Carbon Monoxide	8.01	19.8	0.0367	98.8	0.1	2.67
#3	Carbon Monoxide	7.98	19.8	0.0368	98.7	0.1	2.18
#1	Air	8.08	20.1	0.0369	0.6	99.7	1.79
#2	Air	8.01	19.8	0.0354	0.3	99.7	0.85
#3	Air	7.98	19.8	0.0373	0.6	99.9	2.28
Average		**8.02**	**19.9**	**0.0367**	**-**	**-**	**2.05**

Carbon Monoxide Mass Transfer Data						
Test	Inlet Gas	Gas Velocity (cm/s)	Temperature (ºC)	k_La (1/s)	C_o (% of Sat)	C_∞ (% of Sat)
#1	Carbon Monoxide	8.08	20.1	0.0409	-19.4	100.3
#2	Carbon Monoxide	8.01	19.8	0.0432	-24.5	101.8
#3	Carbon Monoxide	7.98	19.8	0.0456	-24.5	100.6
Average		**8.02**	**19.9**	**0.0432**	**-**	**-**

Test Conditions:

DI Water w/ Surfactant — Closed Vent Mode

A = 0.62% — U_G = 12.0 cm/s

Oxygen Mass Transfer Data							
Test	Inlet Gas	Gas Velocity (cm/s)	Temperature (ºC)	k_La (1/s)	C_o (% of Sat)	C_∞ (% of Sat)	τ_e (s)
#1	Nitrogen	12.03	19.6	0.0547	98.2	0.1	1.81
#2	Nitrogen	11.91	19.5	0.0583	99.2	0.1	1.90
#3	Nitrogen	11.94	19.3	0.0606	99.0	0.1	1.97
#1	Air	12.03	19.6	0.0568	0.0	99.7	1.66
#2	Air	11.91	19.5	0.0631	0.2	99.8	2.14
#3	Air	11.94	19.3	0.0634	-0.3	99.1	1.33
#1	Carbon Monoxide	12.03	19.6	0.0554	98.1	0.1	1.90
#2	Carbon Monoxide	11.91	19.5	0.0569	707.6	0.0	1.90
#3	Carbon Monoxide	11.94	19.3	0.0625	98.8	0.1	2.09
#1	Air	12.03	19.6	0.0595	0.6	100.0	2.23
#2	Air	11.91	19.5	0.0622	0.7	99.9	1.72
#3	Air	11.94	19.3	0.0635	0.2	98.7	1.54
Average		**11.96**	**19.5**	**0.0598**	**-**	**-**	**1.85**

Carbon Monoxide Mass Transfer Data						
Test	Inlet Gas	Gas Velocity (cm/s)	Temperature (ºC)	k_La (1/s)	C_o (% of Sat)	C_∞ (% of Sat)
#1	Carbon Monoxide	12.03	19.6	0.0649	-31.1	99.8
#2	Carbon Monoxide	11.91	19.5	0.0607	-26.4	101.9
#3	Carbon Monoxide	11.94	19.3	0.0845	-37.1	96.2
Average		**11.96**	**19.5**	**0.0701**	**-**	**-**

Test Conditions:

DI Water w/ Surfactant — Closed Vent Mode

A = 0.62% — U_G = 16.0 cm/s

Oxygen Mass Transfer Data							
Test	Inlet Gas	Gas Velocity (cm/s)	Temperature (ºC)	k_La (1/s)	C_o (% of Sat)	C_∞ (% of Sat)	τ_e (s)
#1	Nitrogen	16.06	19.3	0.1049	109.5	0.0	9.53
#2	Nitrogen	16.06	19.7	0.0657	98.9	0.1	2.00
#3	Nitrogen	16.12	19.7	0.0640	99.6	0.1	2.00
#1	Air	16.06	19.3	0.0631	99.2	0.2	1.72
#2	Air	16.06	19.7	0.0929	1.4	100.6	2.26
#3	Air	16.12	19.7	0.0695	1.3	100.3	1.77
#1	Carbon Monoxide	16.06	19.3	0.0661	1.2	100.2	1.74
#2	Carbon Monoxide	16.06	19.7	0.0683	1.0	100.0	2.17
#3	Carbon Monoxide	16.12	19.7	0.0784	99.5	0.1	2.04
#1	Air	16.06	19.3	0.0674	102.4	0.1	3.51
#2	Air	16.06	19.7	0.0635	99.1	0.1	1.72
#3	Air	16.12	19.7	0.0646	99.3	0.2	1.97
Average		**16.08**	**19.6**	**0.0724**	**-**	**-**	**2.70**

Carbon Monoxide Mass Transfer Data						
Test	Inlet Gas	Gas Velocity (cm/s)	Temperature (ºC)	k_La (1/s)	C_o (% of Sat)	C_∞ (% of Sat)
#1	Carbon Monoxide	16.06	19.3	0.0684	-7.4	100.4
#2	Carbon Monoxide	16.06	19.7	0.0779	-6.7	99.6
#3	Carbon Monoxide	16.12	19.7	0.0000	0.0	0.0
Average		**16.08**	**19.6**	**0.0488**	**-**	**-**

Test Conditions:

DI Water w/ Surfactant — Closed Vent Mode

A = 0.62% — U_G = 20.0 cm/s

Oxygen Mass Transfer Data							
Test	Inlet Gas	Gas Velocity (cm/s)	Temperature (ºC)	k_La (1/s)	C_o (% of Sat)	C_∞ (% of Sat)	τ_e (s)
#1	Nitrogen	19.99	19.9	0.0749	98.7	0.1	1.85
#2	Nitrogen	19.96	19.9	0.0744	99.1	0.1	1.77
#3	Nitrogen	19.93	19.8	0.0786	99.9	0.1	4.43
#1	Air	19.99	19.9	0.0812	1.7	100.2	2.02
#2	Air	19.96	19.9	0.0799	0.9	100.3	2.07
#3	Air	19.93	19.8	0.0783	1.0	100.0	1.86
#1	Carbon Monoxide	19.99	19.9	0.0759	99.1	0.0	2.12
#2	Carbon Monoxide	19.96	19.9	0.0749	99.9	0.1	1.92
#3	Carbon Monoxide	19.93	19.8	0.0755	99.1	0.1	1.79
#1	Air	19.99	19.9	0.0779	1.0	100.3	2.15
#2	Air	19.96	19.9	0.0777	1.4	100.2	1.92
#3	Air	19.93	19.8	0.0769	0.4	100.2	1.66
Average		**19.96**	**19.9**	**0.0772**	**-**	**-**	**2.13**

Carbon Monoxide Mass Transfer Data						
Test	Inlet Gas	Gas Velocity (cm/s)	Temperature (ºC)	k_La (1/s)	C_o (% of Sat)	C_∞ (% of Sat)
#1	Carbon Monoxide	19.99	19.9	0.0728	-3.5	99.6
#2	Carbon Monoxide	19.96	19.9	0.0685	-2.2	98.7
#3	Carbon Monoxide	19.93	19.8	0.0791	-4.6	96.1
Average		**19.96**	**19.9**	**0.0735**	**-**	**-**

Test Conditions:

DI Water w/ Surfactant — Bubble Column Mode

A = 0.62% — U_G = 0.5 cm/s

Oxygen Mass Transfer Data							
Test	Inlet Gas	Gas Velocity (cm/s)	Temperature (ºC)	k_La (1/s)	C_o (% of Sat)	C_∞ (% of Sat)	τ_e (s)
#1	Nitrogen	0.52	20.5	0.0054	113.9	-0.1	0.00
#2	Nitrogen	0.52	20.5	0.0057	98.6	0.1	7.37
#3	Nitrogen	0.53	20.6	0.0062	98.5	0.0	6.71
#1	Air	0.52	20.5	0.0060	1.2	99.8	7.15
#2	Air	0.52	20.5	0.0058	1.0	99.8	6.94
#3	Air	0.53	20.6	0.0064	1.4	99.4	5.50
#1	Carbon Monoxide	0.52	20.5	0.0058	98.2	0.1	7.92
#2	Carbon Monoxide	0.52	20.5	0.0057	104.1	0.0	14.18
#3	Carbon Monoxide	0.53	20.6	0.0062	103.1	0.0	15.64
#1	Air	0.52	20.5	0.0059	1.1	100.0	5.32
#2	Air	0.52	20.5	0.0064	1.4	100.0	5.53
#3	Air	0.53	20.6	-	-	-	-
Average		**0.52**	**20.5**	**0.0060**	**-**	**-**	**7.48**

Carbon Monoxide Mass Transfer Data						
Test	Inlet Gas	Gas Velocity (cm/s)	Temperature (ºC)	k_La (1/s)	C_o (% of Sat)	C_∞ (% of Sat)
#1	Carbon Monoxide	0.52	20.5	0.0070	-18.9	104.1
#2	Carbon Monoxide	0.52	20.5	0.0068	-14.2	103.6
#3	Carbon Monoxide	0.53	20.6	0.0070	-12.7	101.8
Average		**0.52**	**20.5**	**0.0069**	**-**	**-**

Test Conditions:

DI Water w/ Surfactant — Bubble Column Mode

A = 0.62% — U_G = 2.0 cm/s

Oxygen Mass Transfer Data							
Test	Inlet Gas	Gas Velocity (cm/s)	Temperature (ºC)	k_La (1/s)	C_o (% of Sat)	C_∞ (% of Sat)	τ_e (s)
#1	Nitrogen	2.02	20.1	0.0142	99.3	0.0	3.91
#2	Nitrogen	2.02	19.9	0.0144	98.9	0.1	3.29
#3	Nitrogen	2.02	20.1	0.0145	99.2	0.0	3.50
#1	Air	2.02	20.1	0.0152	1.2	99.4	3.91
#2	Air	2.02	19.9	0.0155	1.7	100.0	4.64
#3	Air	2.02	20.1	0.0159	1.3	100.2	4.94
#1	Carbon Monoxide	2.02	20.1	0.0145	98.8	0.0	3.54
#2	Carbon Monoxide	2.02	19.9	0.0149	99.2	0.0	3.84
#3	Carbon Monoxide	2.02	20.1	0.0150	98.7	0.0	4.14
#1	Air	2.02	20.1	0.0148	0.5	99.7	2.63
#2	Air	2.02	19.9	0.0158	1.4	100.1	5.25
#3	Air	2.02	20.1	0.0156	2.0	101.0	4.52
Average		**2.02**	**20.0**	**0.0150**	**-**	**-**	**4.01**

Carbon Monoxide Mass Transfer Data						
Test	Inlet Gas	Gas Velocity (cm/s)	Temperature (ºC)	k_La (1/s)	C_o (% of Sat)	C_∞ (% of Sat)
#1	Carbon Monoxide	2.02	20.1	0.0141	-2.9	105.1
#2	Carbon Monoxide	2.02	19.9	0.0151	0.2	101.7
#3	Carbon Monoxide	2.02	20.1	0.0136	-1.3	103.6
Average		**2.02**	**20.0**	**0.0143**	**-**	**-**

Test Conditions:

DI Water w/ Surfactant — Bubble Column Mode

A = 0.62% — U_G = 4.0 cm/s

Oxygen Mass Transfer Data							
Test	Inlet Gas	Gas Velocity (cm/s)	Temperature (ºC)	k_La (1/s)	C_o (% of Sat)	C_∞ (% of Sat)	τ_e (s)
#1	Nitrogen	4.02	20.2	0.0274	98.4	0.1	3.34
#2	Nitrogen	3.99	20.1	0.0284	98.6	0.1	3.86
#3	Nitrogen	4.03	19.8	0.0287	100.2	0.1	1.75
#1	Air	4.02	20.2	0.0301	1.2	101.5	3.90
#2	Air	3.99	20.1	0.0317	1.5	102.7	4.13
#3	Air	4.03	19.8	0.0317	1.3	101.6	4.21
#1	Carbon Monoxide	4.02	20.2	0.0281	98.6	0.0	2.89
#2	Carbon Monoxide	3.99	20.1	0.0297	98.7	0.0	3.45
#3	Carbon Monoxide	4.03	19.8	0.0300	98.7	0.1	3.27
#1	Air	4.02	20.2	0.0303	1.9	102.8	4.32
#2	Air	3.99	20.1	0.0311	1.8	102.6	4.40
#3	Air	4.03	19.8	0.0317	2.0	102.2	4.36
Average		**4.01**	**20.0**	**0.0299**	**-**	**-**	**3.66**

Carbon Monoxide Mass Transfer Data						
Test	Inlet Gas	Gas Velocity (cm/s)	Temperature (ºC)	k_La (1/s)	C_o (% of Sat)	C_∞ (% of Sat)
#1	Carbon Monoxide	4.02	20.2	0.0317	-20.3	102.1
#2	Carbon Monoxide	3.99	20.1	0.0289	-5.1	101.2
#3	Carbon Monoxide	4.03	19.8	0.0322	-17.3	100.9
Average		**4.01**	**20.0**	**0.0309**	**-**	**-**

Test Conditions:

DI Water w/ Surfactant — Bubble Column Mode

A = 0.62% — U_G = 6.0 cm/s

Oxygen Mass Transfer Data							
Test	Inlet Gas	Gas Velocity (cm/s)	Temperature (ºC)	k_La (1/s)	C_o (% of Sat)	C_∞ (% of Sat)	τ_e (s)
#1	Nitrogen	5.97	20.0	0.0406	99.0	0.1	3.24
#2	Nitrogen	5.98	19.9	0.0326	98.7	0.1	4.03
#3	Nitrogen	5.98	19.6	0.0305	99.1	0.3	2.77
#1	Air	5.97	20.0	0.0442	1.9	102.1	4.16
#2	Air	5.98	19.9	0.0382	1.6	100.0	4.26
#3	Air	5.98	19.6	0.0307	0.9	99.7	2.55
#1	Carbon Monoxide	5.97	20.0	0.0415	99.2	0.1	3.15
#2	Carbon Monoxide	5.98	19.9	0.0331	98.7	0.1	3.17
#3	Carbon Monoxide	5.98	19.6	0.0309	98.9	0.2	2.32
#1	Air	5.97	20.0	0.0443	1.6	102.5	4.18
#2	Air	5.98	19.9	0.0361	1.0	100.0	3.44
#3	Air	5.98	19.6	0.0313	0.9	99.7	2.15
Average		**5.98**	**19.8**	**0.0362**	**-**	**-**	**3.28**

Carbon Monoxide Mass Transfer Data						
Test	Inlet Gas	Gas Velocity (cm/s)	Temperature (ºC)	k_La (1/s)	C_o (% of Sat)	C_∞ (% of Sat)
#1	Carbon Monoxide	5.97	20.0	0.0389	-1.3	98.4
#2	Carbon Monoxide	5.98	19.9	0.0301	-0.7	106.3
#3	Carbon Monoxide	5.98	19.6	0.0297	-1.8	105.1
Average		**5.98**	**19.8**	**0.0329**	**-**	**-**

Test Conditions:

DI Water w/ Surfactant — Bubble Column Mode

A = 0.62% — U_G = 8.0 cm/s

Oxygen Mass Transfer Data							
Test	Inlet Gas	Gas Velocity (cm/s)	Temperature (ºC)	k_La (1/s)	C_o (% of Sat)	C_∞ (% of Sat)	τ_e (s)
#1	Nitrogen	8.02	20.0	0.0395	98.7	0.2	2.38
#2	Nitrogen	8.02	19.8	0.0395	98.3	0.1	2.61
#3	Nitrogen	8.02	19.9	0.0393	98.6	0.1	2.96
#1	Air	8.02	20.0	0.0397	1.4	99.9	2.33
#2	Air	8.02	19.8	0.0395	0.5	99.9	2.41
#3	Air	8.02	19.9	0.0393	1.1	99.8	2.37
#1	Carbon Monoxide	8.02	20.0	0.0399	99.1	0.1	2.49
#2	Carbon Monoxide	8.02	19.8	0.0399	98.9	0.1	2.90
#3	Carbon Monoxide	8.02	19.9	0.0396	98.9	0.1	2.64
#1	Air	8.02	20.0	0.0392	1.1	99.7	2.24
#2	Air	8.02	19.8	0.0390	1.1	99.7	2.18
#3	Air	8.02	19.9	0.0391	1.2	99.9	2.55
Average		**8.02**	**19.9**	**0.0395**	**-**	**-**	**2.51**

Carbon Monoxide Mass Transfer Data						
Test	Inlet Gas	Gas Velocity (cm/s)	Temperature (ºC)	k_La (1/s)	C_o (% of Sat)	C_∞ (% of Sat)
#1	Carbon Monoxide	8.02	20.0	0.0436	-24.6	100.9
#2	Carbon Monoxide	8.02	19.8	0.0477	-24.2	101.1
#3	Carbon Monoxide	8.02	19.9	0.0459	-23.8	99.2
Average		**8.02**	**19.9**	**0.0457**	**-**	**-**

Test Conditions:

DI Water w/ Surfactant — Bubble Column Mode

A = 0.62% — U_G = 12.0 cm/s

Oxygen Mass Transfer Data							
Test	Inlet Gas	Gas Velocity (cm/s)	Temperature (ºC)	k_La (1/s)	C_o (% of Sat)	C_∞ (% of Sat)	τ_e (s)
#1	Nitrogen	12.00	20.1	0.0554	98.6	0.1	2.97
#2	Nitrogen	11.99	19.8	0.0559	97.9	0.1	2.66
#3	Nitrogen	12.01	19.9	0.0560	98.3	0.1	2.78
#1	Air	12.00	20.1	0.0570	1.2	100.1	2.80
#2	Air	11.99	19.8	0.0572	1.3	100.1	2.85
#3	Air	12.01	19.9	0.0580	2.0	100.0	3.30
#1	Carbon Monoxide	12.00	20.1	0.0567	98.2	0.0	3.00
#2	Carbon Monoxide	11.99	19.8	0.0567	98.3	0.0	3.17
#3	Carbon Monoxide	12.01	19.9	0.0571	98.6	0.0	3.17
#1	Air	12.00	20.1	0.0549	1.5	100.2	2.44
#2	Air	11.99	19.8	0.0558	1.0	100.2	2.89
#3	Air	12.01	19.9	0.0568	1.6	100.1	2.88
Average		**12.00**	**19.9**	**0.0565**	**-**	**-**	**2.91**

Carbon Monoxide Mass Transfer Data						
Test	Inlet Gas	Gas Velocity (cm/s)	Temperature (ºC)	k_La (1/s)	C_o (% of Sat)	C_∞ (% of Sat)
#1	Carbon Monoxide	12.00	20.1	0.0473	0.4	105.2
#2	Carbon Monoxide	11.99	19.8	0.1063	-326.7	100.1
#3	Carbon Monoxide	12.01	19.9	0.0734	-39.0	99.1
Average		**12.00**	**19.9**	**0.0756**	**-**	**-**

Test Conditions:

DI Water w/ Surfactant — Bubble Column Mode

A = 0.62% — U_G = 16.0 cm/s

Oxygen Mass Transfer Data							
Test	Inlet Gas	Gas Velocity (cm/s)	Temperature (ºC)	k_La (1/s)	C_o (% of Sat)	C_∞ (% of Sat)	τ_e (s)
#1	Nitrogen	15.87	19.3	0.0692	98.9	0.1	3.07
#2	Nitrogen	15.89	20.0	0.0685	98.5	0.1	3.10
#3	Nitrogen	15.90	19.7	0.0688	98.6	0.1	3.34
#1	Air	15.87	19.3	0.0721	1.9	99.9	2.74
#2	Air	15.89	20.0	0.0736	1.5	102.1	2.68
#3	Air	15.90	19.7	0.0747	1.7	102.4	3.02
#1	Carbon Monoxide	15.87	19.3	0.0715	99.1	0.0	3.17
#2	Carbon Monoxide	15.89	20.0	0.0719	98.6	-0.2	3.36
#3	Carbon Monoxide	15.90	19.7	0.0733	98.3	-0.2	3.50
#1	Air	15.87	19.3	0.0699	1.2	100.3	2.47
#2	Air	15.89	20.0	0.0668	1.5	101.4	2.70
#3	Air	15.90	19.7	0.0677	1.8	102.2	2.60
Average		**15.89**	**19.7**	**0.0707**	**-**	**-**	**2.98**

Carbon Monoxide Mass Transfer Data						
Test	Inlet Gas	Gas Velocity (cm/s)	Temperature (ºC)	k_La (1/s)	C_o (% of Sat)	C_∞ (% of Sat)
#1	Carbon Monoxide	15.87	19.3	0.0763	-15.2	101.1
#2	Carbon Monoxide	15.89	20.0	0.0727	-17.4	101.7
#3	Carbon Monoxide	15.90	19.7	0.0806	-26.9	99.4
Average		**15.89**	**19.7**	**0.0765**	**-**	**-**

Test Conditions:

DI Water w/ Surfactant — Bubble Column Mode

A = 0.62% — U_G = 20.0 cm/s

Oxygen Mass Transfer Data							
Test	Inlet Gas	Gas Velocity (cm/s)	Temperature (ºC)	k_La (1/s)	C_o (% of Sat)	C_∞ (% of Sat)	τ_e (s)
#1	Nitrogen	19.99	19.8	0.0826	99.1	0.4	1.92
#2	Nitrogen	19.97	19.1	0.0847	98.1	0.1	2.35
#3	Nitrogen	20.00	19.8	0.0890	98.9	0.1	2.43
#1	Air	19.99	19.8	0.0856	1.4	99.9	1.97
#2	Air	19.97	19.1	0.0898	1.5	100.1	2.53
#3	Air	20.00	19.8	0.0892	1.3	100.2	2.12
#1	Carbon Monoxide	19.99	19.8	0.0835	99.0	0.1	2.27
#2	Carbon Monoxide	19.97	19.1	0.0850	98.6	0.1	2.38
#3	Carbon Monoxide	20.00	19.8	0.0892	97.9	0.1	2.37
#1	Air	19.99	19.8	0.0861	1.7	99.9	2.30
#2	Air	19.97	19.1	0.0870	1.3	100.2	2.51
#3	Air	20.00	19.8	0.0904	1.4	100.1	2.21
Average		**19.99**	**19.6**	**0.0868**	**-**	**-**	**2.28**

Carbon Monoxide Mass Transfer Data						
Test	Inlet Gas	Gas Velocity (cm/s)	Temperature (ºC)	k_La (1/s)	C_o (% of Sat)	C_∞ (% of Sat)
#1	Carbon Monoxide	19.99	19.8	0.0818	-19.2	100.8
#2	Carbon Monoxide	19.97	19.1	0.0972	-22.2	96.8
#3	Carbon Monoxide	20.00	19.8	0.0889	-6.3	101.3
Average		**19.99**	**19.6**	**0.0893**	**-**	**-**